1

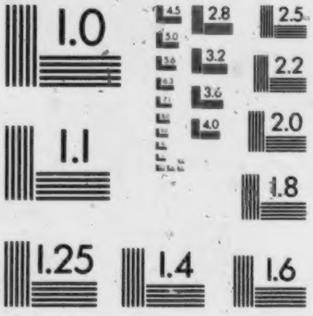
1.0
4.5
5.0
5.6
6.3
2.8
3.2
3.6
4.0
2.5
2.2
2.0
1.1
1.8
1.25
1.4
1.6

National Library of Canada
Bibliothèque nationale du Canada

Canadian Theses Service
Service des thèses canadiennes

Ottawa, Canada
K1A 0N4

NOTICE

The quality of this microform is heavily dependent upon the quality of the original thesis submitted for microfilming. Every effort has been made to ensure the highest quality of reproduction possible.

If pages are missing, contact the university which granted the degree.

Some pages may have indistinct print especially if the original pages were typed with a poor typewriter ribbon or if the university sent us an inferior photocopy.

Previously copyrighted materials (journal articles, published tests, etc.) are not filmed.

Reproduction in full or in part of this microform is governed by the Canadian Copyright Act, R.S.C. 1970, c. C-30.

AVIS

La qualité de cette microforme dépend grandement de la qualité de la thèse soumise au microfilmage. Nous avons tout fait pour assurer une qualité supérieure de reproduction.

S'il manque des pages, veuillez communiquer avec l'université qui a conféré le grade.

La qualité d'impression de certaines pages peut laisser à désirer, surtout si les pages originales ont été dactylographiées à l'aide d'un ruban usé ou si l'université nous a fait parvenir une photocopie de qualité inférieure.

Les documents qui font déjà l'objet d'un droit d'auteur (articles de revue, tests publiés, etc.) ne sont pas microfilmés.

La reproduction, même partielle, de cette microforme est soumise à la Loi canadienne sur le droit d'auteur, SRC 1970, c. C-30.

NL-339 (r. 88/04)

Canada

THE UNIVERSITY OF ALBERTA

DEVELOPMENT AND CHARACTERIZATION OF DIRECT SAMPLE INSERTION DEVICES FOR INDUCTIVELY COUPLED PLASMAS

by

VASSILIOS KARANASSIOS of STERGIOS

©

A THESIS

SUBMITTED TO THE FACULTY OF GRADUATE STUDIES AND RESEARCH

IN PARTIAL FULFILMENT OF THE REQUIREMENTS FOR THE DEGREE

OF DOCTOR OF PHILOSOPHY

DEPARTMENT OF CHEMISTRY

EDMONTON, ALBERTA

FALL 1988

Permission has been granted to the National Library of Canada to microfilm this thesis and to lend or sell copies of the film.

The author (copyright owner) has reserved other publication rights, and neither the thesis nor extensive extracts from it may be printed or otherwise reproduced without his/her written permission.

L'autorisation a été accordée à la Bibliothèque nationale du Canada de microfilmer cette thèse et de prêter ou de vendre des exemplaires du film.

L'auteur (titulaire du droit d'auteur) se réserve les autres droits de publication; ni la thèse ni de longs extraits de celle-ci ne doivent être imprimés ou autrement reproduits sans son autorisation écrite.

ISBN 0-315-45781-3

University of Alberta
Edmonton

Canada T6G 2G2

Department of Chemistry
Faculty of Science

E3-43 Chemistry Building East, Telephone (403) 432-3254

Edmonton, Oct. 6, 1988

I hereby provide permission to Vassilios Karanassios of Stergios to include the following material in his thesis entitled *"Development and Characterization of Direct Sample Insertion Devices for Inductively Coupled Plasmas"*.

1. V. Karanassios and G. Horlick, *"Spectral Characteristics of a New Spectrometer Design for Atomic Emission Spectroscopy"*, Appl. Spectrosc., **40**, 813-821 (1986)
2. V. Karanassios and G. Horlick, *"Human Processor Interface for ICP-AES: Concepts and Implementation"*, Appl. Spectrosc., **41**, 360-380 (1987)
3. V. Karanassios and G. Horlick, *"New Design Concepts for Direct Reader Measurement Electronics"*, Appl. Spectrosc., **42**, 961-972 (1988)

Yours sincerely

Gary Horlick

Prof. Gary Horlick

THE UNIVERSITY OF ALBERTA

RELEASE FORM

NAME OF AUTHOR: VASSILIOS KARANASSIOS of STERGIOS

TITLE OF THESIS: DEVELOPMENT AND CHARACTERIZATION OF DIRECT SAMPLE INSERTION DEVICES FOR INDUCTIVELY COUPLED PLASMAS

DEGREE FOR WHICH THESIS WAS PRESENTED: Ph.D.

YEAR THIS DEGREE GRANTED: 1988

Permission is hereby granted to THE UNIVERSITY OF ALBERTA LIBRARY to reproduce single copies of this thesis and to lend or sell such copies for private, scholarly or scientific research purposes only.

The author reserves other publication rights, and neither the thesis nor extensive extracts from it may be printed or otherwise reproduced without the author's written permission.

Vassili Karanassios
(Student's signature)

Permanent address:
1 KRESTALY STR
SERRES 621 00
GREECE

Date: July 1988

TO IMAGINE IS EVERYTHING.

Albert Einstein

THE UNIVERSITY OF ALBERTA

FACULTY OF GRADUATE STUDIES AND RESEARCH

The undersigned certify that they have read, and recommend to the Faculty of Graduate Studies and Research for acceptance, a thesis entitled DEVELOPMENT AND CHARACTERIZATION OF DIRECT SAMPLE INSERTION DEVICES FOR INDUCTIVELY COUPLED PLASMAS submitted by VASSILIOS KARANASSIOS OF STERGIOS in partial fulfilment of the requirements for the degree of DOCTOR OF PHILOSOPHY.

Gary Horlick

G. Horlick, Supervisor

James A. Plambeck

J.A. Plambeck

D.J. Harrison

A Kalantar

A. Kalantar

H.P. Baltes

Date: July 22, 1988

J.A. Holcombe, External Examiner

ΣΤΟΥΣ ΓΟΝΕΙΣ ΜΟΥ

and

to all those who made this possible

ABSTRACT

Undoubtedly, the most important current limitation of the ICP arises from sample introduction. A particularly attractive method involves the use of Direct Sample Insertion Devices (DSIDs). In these, the sample is placed into or onto a probe, for example, a graphite cup or a wire-loop, with subsequent introduction of the sample carrying probe into the plasma. The advantages offered by a DSID for ICP-AES include increased sample introduction efficiency and an inherent ability to handle µl volumes of liquids and mg quantities of powders/solids with little or no sample pretreatment. In addition to these, a host of benefits arise from coupling a DSID to ICP-MS. Among these are considerable reductions in spectroscopic and non-spectroscopic interference. The basic goal of this thesis is to extend the analytical capability and utility of the ICP by developing and characterizing DSIDs for ICP-AES and ICP-MS.

In order to handle the transient signals generated by the DSID, a measurement system for ICP-AES capable of handling peak-like signals was developed. This system was subsequently used to establish the characteristics of the device. Because poor results were obtained for carbide forming elements, chemical modification was used to improve the vaporization characteristics of such analytes. Automated addition of reagents into the sample carrying probe gives

rise to the concepts of the sample carrying probe as a 'crucible' in which *in situ* chemical processing of samples takes place and of the DSID, not as a mere sample introduction system, but as an intelligent sample processor for the ICP. These concepts were applied to the development of a computer controlled DSID for ICP-MS. This system was subsequently used in order to establish ICP-MS-DSID interference effects.

In terms of data acquisition and control systems, a multiprocessor approach was taken throughout, the *instrument metaphor* concept was invented, a unique Human Processor Interface (HPI) was developed for ICP-AES and the concept of *simulating virtual reality* was developed for the ICP-MS DSID.

ACKNOWLEDGEMENTS

I wish to thank Professor Gary Horlick for all he has taught me, shared with me, for the opportunities he has given me and for, among other things, what he has *"perturbed"* me to learn and inspired me to do. His guidance in academic matters and his understanding of personal matters has been invaluable.

Special thanks are extended to Dr. Elizabeth Stubley for help and encouragement during the initial stages of this study and to Greg King for his constant supply of Macintosh trivia, valuable technical information and development tools.

The expert advice and technical support of the staff of the electronics-, glass- and machine-shop is deeply appreciated. Tony's (Raymond Anthony Walford) mechanical talents were vital to the construction of the ICP-MS-DSID and his contribution is gratefully acknowledged.

The Department of Chemistry is to be thanked for awarding teaching and research fellowships throughout this work. Support from ARL Inc., in the form of donation of a direct reading spectrometer and from PRA Inc., for the use of their pre-prototype SPS-10 spectrometer is appreciated.

Finally, I wish to express my sincere appreciation στους γονεις μου, στον Νικο, την Αγγελα και τη Μαρια και τον Νικο Κοκκινη και σε συγγενεις and to close friends for their contributions and their support.

TABLE OF CONTENTS

CHAPTER PAGE

1. A REVIEW OF DIRECT SAMPLE INSERTION DEVICES FOR INDUCTIVELY COUPLED PLASMAS 1
    A. The ICP 2
    B. Sample Introduction Systems for the ICP 5
        B.1 Pneumatic Nebulization 6
        B.2 Alternatives to Pneumatic Nebulization 9
        C. Direct Sample Insertion Devices............ 10
        C.1 Basic Experimental set-up for a DSID 57
            C.1.1 DSID Designs and their Attributes 57
            C.1.2 ICP and Instrumentation 67
        C.2 Optimization 71
        C.3 Survey Results 72
        C.4 Performance Characteristics 74
        C.5 Applications 76
        C.6 Advantages, Limitations and Criticisms ... 77
    D. Thesis Objectives and Approach............... 80
    REFERENCES 85

2. A COMPUTER-CONTROLLED DIRECT SAMPLE INSERTION DEVICE FOR ICP-AES 95
    A. Introduction................................ 96

B. Instrumentation 102
B.1 ICP, Spectrometer and Operating Conditions 102
B.2 Direct Sample Insertion Device 103
B.3 Readout and Control Electronics 111
B.4 Data Acquisition 116
C. Software 123
D. Conclusions 156
REFERENCES 158

3. CHARACTERIZATION OF A DIRECT SAMPLE INSERTION DEVICE FOR ICP-AES 163
A. Introduction 164
B. Experimental 167
C. Results and Discussion 172
C.1 Survey of Analyte Emission Temporal Behavior 172
C.2 Volatility Sequence 175
C.3 DSID Design Attributes 179
C.3.1 Cup Insertion Position 180
C.3.2 Cup Insertion Speed 183
C.4 Probe Attributes and Applied Forward Power 192
C.4.1 Electrode Geometry and Power 196
C.4.2 Electrode Composition 213
C.5 Performance Characteristics 217

D. Conclusions 222
REFERENCES 227

4. THE APPLICATION OF CHEMICAL MODIFICATION TO A DIRECT SAMPLE INSERTION DEVICE FOR ICP-AES 231
A. Introduction 232
B. Experimental 236
C. Results and Discussion 238
  C.1 Multielement Solution Residues 238
    C.1.1 Survey Results 238
    C.1.2 Analyte Chemical Modification 242
    C.1.3 Characterization of NaF Chemical Modification 249
  C.2 Powdered Samples 257
D. Conclusions 261
REFERENCES 262

5. HUMAN PROCESSOR INTERFACE FOR ICP-AES: CONCEPTS AND IMPLEMENTATION 265
A. Introduction 266
B. Human Processor Interface Concepts 271
  B.1 Graphics 271
  B.2 The Desk Top Metaphor 273
  B.3 The Apple Macintosh 274
C. Instrument User Interface Considerations 277

D. ICP-AES Instrument User Interface............ 282
   D.1 The Instrument User Interface 282
   D.2 Parameter Readout and Control 290
   D.3 Spectral Data base Access and Display 303
   D.4 Help and Explain Files 314
   D.5 Communication to System Support Programs.............................. 320
E. Conclusions................................ 324
REFERENCES 325

6. DEVELOPMENT OF A COMPUTER-CONTROLLED DIRECT SAMPLE INSERTION DEVICE FOR ICP-MS 328

A. Introduction............................... 329
B. Instrumentation............................ 336
   B.1 ICP-MS, Computer Systems and Operating Conditions 336
   B.2 DSID 343
   B.3 Data Acquisition Considerations 361
   B.4 Software 364
      B.4.1 For Serial Transfers and DSID Control 367
      B.4.2 Simulating Virtual Reality 371
C. Basic Response............................. 373
D. Conclusions................................ 377
REFERENCES 383

7. SPECTRAL AND MATRIX INTERFERENCE EFFECTS USING A DSID FOR ICP-MS 387

A. Introduction................................ 388

B. Experimental................................ 390

C. Spectroscopic Interference Effects........... 391

C.1 Background Spectral Features of ICP-MS ... 391

C.1.1 Wet and Dry Plasma Background Spectra 393

C.1.1.1 Distiled Water Background Spectra 395

C.1.1.2 Dry Plasma Background Spectra 403

C.1.1.3 Comparison of Background Spectral Features 416

C.1.1.4 Summary and Conclusions 422

C.1.2 Probe Background Spectra 425

C.1.2.1 Graphite Electrodes 426

C.1.2.2 Mo Cups 430

C.1.2.3 Ta Cups 436

C.1.2.4 W Wire-loop 440

C.1.2.5 Summary and Conclusions 445

C.2 Oxides, Hydroxides and Doubly-charged Species 449

C.3 Solvent-induced Background Species 459

D. Non-spectroscopic Interference Effects....... 463

E. Conclusions 468
REFERENCES 471

8. CONCLUDING REMARKS 473
A. Summary 474
B. The Concept of Processors in Spectrochemical Instrumentation 479
C. Integration: Imagineering the Next Generation Analytical Instrumentation 483
REFERENCES 488

APPENDIX A. NEW DESIGN CONCEPTS FOR DIRECT READER MEASUREMENT ELECTRONICS 489

APPENDIX B. ICP-MS-DSID BLUEPRINTS 516

APPENDIX C. ICP-MS PARAMETER SET UTILIZED FOR THE ACQUISITION OF TRANSIENT SIGNALS 533

APPENDIX D. SPECTRAL CHARACTERISTICS OF A NEW SPECTROMETER DESIGN FOR ATOMIC EMISSION SPECTROSCOPY 535

APPENDIX E. DEVELOPMENT SYSTEMS AND PROGRAMMING ENVIRONMENTS UTILIZED 569

LIST OF TABLES

TABLE PAGE
1-1. Research groups and their DSID-related work... 14
1-2. DSID designs and their attributes............ 18
1-3. ICP and instrumentation...................... 24
1-4. Optimization................................. 29
1-5. Survey results............................... 32
1-6. Performance characteristics.................. 40
1-7. Applications................................. 51
3-1. Experimental parameters and design attributes affecting the analytical performance characteristics of a DSID for ICP-AES......... 166
3-2. Instrumentation and typical operating conditions......................... 169
3-3. Comparison of detection limits and %RSDs...... 219
4-1. Melting and boiling points of oxides and carbides......................... 241
4-2. Detection limits and %RSDs with and without the addition of a chemical modifier........... 253
5-1. Microcomputer selection criteria............. 269
5-2. Main program active areas.................... 286

6-1. Ion lens voltage settings........................ 342

7-1. Types of interference effects in ICP-MS....... 389

7-2. Typical solvent-induced background species.... 394

7-3. Background species arising from a wet and dry plasma................................ 400

7-4. Background species eliminated from a wet plasma when using a dry plasma and an extended torch............................. 423

7-5. Probe-induced background species.............. 446

A-1. Truth table for 74154, 4-line-to-16-line decoder/demultiplexer........................ 509

A-2. Truth table for 74155, 2-line-to-4-line decoder/demultiplexer........................ 511

A-3. Truth table for 74138, 3-line-to-8-line decoder/demultiplexer........................ 512

C-1. Sciex® Elan parameter set used for the acquisition of transient signals.............. 534

D-1. Preliminary technical specifications for the SPS-10 Simultaneous Plasma Spectrometer....... 539

D-2. Mask Specifications........................... 543

E-1. Development systems and programming environments utilized...................................... 570

LIST OF FIGURES

FIGURE PAGE

1-1. Illustration of a typical torch configuration for a vertical DSID for ICP-AES. Dimensions in mm 11

1-2. Block diagram of a typical experimental set-up for an ICP-DISD 56

1-3. Generic block diagram of the essential hardware required for a vertical, cup-based DSID 58

1-4. Typical examples of sample carrying probes employed. (a)Flat-top graphite electrode; (b) undercut dc arc graphite electrode; (c) undercut dc arc graphite electrode fitted with a boiler cup (c) and a lid (d); (e) narrow undercut dc arc electrode; (f) long undercut dc arc graphite electrode; (g) flat-top graphite electrode fitted with a metal cup; (h) wire-loop. Dimensions in inches 60

1-5. Top view of a horizontal DSID for ICP-MS 61

1-6. Illustration of a vertical DSID for ICP-AES (see Reference 69 for more details) 64

1-7. Typical examples of analyte emission temporal behavior for 10 ng of: (a) Cd; (b) Cu; (c) Mn and (d) Zn measured using long undercut electrodes (Figure 1-4f) and with an applied forward power of 1.25 kW 66

1-8. Block diagram for the measurement electronics required for: (a) steady state signals and (b) transient signals 70

2-1. Block diagram of the experimental set-up of a DSID for ICP-AES 97

2-2. Sample tray, sample holder assembly (i.e., Vespel® plug, quartz stem and probe) and probe types (Left: flat-top electrode fitted with a metal cup; center: long undercut graphite electrode; right: wire-loop) 98

2-3. Illustration sample holder insertion. (Diagram not to scale) 106

2-4. Solenoid valve configuration for sample holder retraction 107

2-5. Block diagram of motor driver and support electronics 109

2-6. DSID controller and step measuring electronics 113

2-7. Typical analyte emission temporal behavior 114

2-8. Analyte emission temporal behavior for 25 ng Cu. (a) Long undercut graphite electrode; (b) Ta metal cup; (c) W metal cup; and (d) W wire-loop 115

2-9. Block diagram of direct reader measurement electronics for steady state signals (i.e., continuous sample aspiration via pneumatic nebulization) 117

2-10. Block diagram of direct reader measurement electronics for transient signals.............. 119

2-11. A four channel measurement electronics subsystem for the DISD and the IBM PC............. 121

2-12. Block diagram of the software package developed for the DSID.......................... 125

2-13. Main program main menu............................ 127

2-14. Menu shown upon selection of initialize electrode from main menu (a); power supply diagnostics, power supplies at fault (b); power supply diagnostics, proper voltages detected on the power supplies (c)............ 128

2-15. DSID and data acquisition module menu and parameters. (a) DISD control menu upon entry; (b) DISD control menu, item 6 disabled; (c) electrode handling and data acquisition parameters; (d) DSID control menu with no disabled items.................................. 130

2-16. Screen dump of a typical four-window split-screen, C1 stands for channel 1, C2 for channel 2, C3 for channel 3 and C4 for channel 4.. 132

2-17. Typical messages displayed after appropriate function key selection (Figure 2-16)............ 134

2-18. (a) Parameter and (b) electronic notebook files.................... 137

2-19. Screen dump of a two-window split-screen........ 140

2-20. Spectral interference of Cu on Zn, see text for details....................................... 142

2-21. Peak assignment and identification during a post-processing session, see text for details... 145

2-22. Peak-area integration, see text for details..... 147

2-23. Smoothing and integration of a low-level Cd signals. (a) Original signal; (b) smoothed signal; (c) peak-area integration; (d) pedestal subtracted peak after integration...... 149

2-24. (a) Subtract channels menu; (b) error message; (c) warning; (d) electronic notebook file for subtracted channels............................. 152

2-25. Screen dump of subtracted Al temporal behavior, see text for details.................. 153

2-26. (a) Main program help menu and (b) initialize data disk example................................ 155

3-1. Illustration (not to scale) of the DSID utilized in this work. Sample carrying probes shown (left to right): metal cups (left); long undercut graphite electrodes (center, the cup is inserted into a water cooled torch supported by an air cooled torch assembly); wire-loop (right) 168

3-2. Typical temporal behavior for Ag, Cd, Co, Cr, Cu, Fe, Mn, Mg, Si, Sn, Ni and Zn acquired using long undercut graphite electrodes, a regular drive insertion mode and an applied forward power of 2.00 kW (other operating conditions as in Table 3-2) 173

3-3. Appearance time *versus* element of interest (i.e., volatility sequence) 176

3-4. Signal-to-background ratio (SBR) for Cd, Cr, Cu and Mn determined form multielement solution residues for different cup positions (i.e., distance form the top of the sample carrying cup to TOLC) for long undercut graphite electrodes, a regular drive insertion mode and at 1.25 kW (other operating conditions as in Table 3-2) 182

3-5. The effect of insertion speed on Cu and Cr background signals (324.75 nm and 205.55 nm lines respectively) for long undercut graphite electrodes and 1.25 kW (other operating conditions as in Table 3-2) for: (a) Cu channel, blank electrode, regular drive insertion mode; (b) Cr channel, blank electrode, regular drive insertion mode; (c) Cu channel, blank electrode, one-shot insertion mode; and (d) Cr channel, blank electrode, one-shot insertion mode. All channels saturate at 10 Volts 185

3-6. The effect of insertion speed on both the background and the atomic signals observed on the Zn channel (213.86 nm line) for long undercut graphite electrodes, a regular drive insertion mode and 1.25 kW (other operating conditions as in Table 3-2) for: (a) Zn channel, blank electrode, background signal; and (b) Zn channel, 1 ng Zn 188

3-7. The effect of insertion speed on the Cd atomic signal for long undercut graphite electrodes and 1.25 kW (other operating conditions as in Table 3-2) for: (a) Cd channel, 1 ng Cd, regular drive insertion; and (b) Cd channel, 1 ng Cd, direct drive insertion 190

3-8. Graphite electrode geometries employed (dimensions in inches). (a) HPND+ 4000; (b) HPND+ 4004; (c) HPND+ 4021 'Regular' and (d) HPND+ 4021 'Long Undercut' 197

3-9. Analyte emission temporal behavior for 1 µg Sn, long undercut graphite electrodes, and power settings from 1.25 kW to 2.00 kW in increments of 250 Watts for: (a) 1.25 kW; (b) 1.50 kW; (c) 1.75 kW and (d) 2.00 kW (other operating conditions as in Table 3-2) 198

3-10. The effect of applied forward power (1.25 kW to 2.00 kW in increments of 250 Watts) on the appearance time of Ag, Cd, Co, Cu, Fe, Ni, Sn and Zn for: (a) HPND+ 4000; (b) HPND+ 4004; (c) HPND+ 4021 'Regular' and (d) HPND+ 4021

'Long Undercut' (other operating conditions as in Table 3-2) 199

3-11. The effect of electrode geometry and power on analyte emission temporal behavior of 100 ng Zn for: (a) 1.25 kW; (b) 1.50 kW; (c) 1.75 kW and (d) 2.00 kW (other operating conditions as in Table 3-2). Electrodes: 4000 (HPND+ 4000, Figure 3-8a); 4004 (HPND+ 4004, Figure 3-8b); 4021 R (HPND+ 4021 'Regular', Figure 3-8c); 4021 L (HPND+ 4021 'Long Undercut', Figure 3-8d). Temporal behavior was scaled with respect to the peak intensity of the 4021 L electrode at 2.00 kW (d) 201

3-12. The effect of electrode geometry and power on analyte emission temporal behavior of 100 ng Cu for: (a) 1.25 kW; (b) 1.50 kW; (c) 1.75 kW and (d) 2.00 kW (other operating conditions as in Table 3-2). Electrodes: 4000 (HPND+ 4000, Figure 3-8a); 4004 (HPND+ 4004, Figure 3-8b); 4021 R (HPND+ 4021 'Regular', Figure 3-8d); 4021 L (HPND+ 4021 'Long Undercut', Figure 3-8d). Temporal behavior was scaled with respect to the peak intensity of the 4021 L electrode at 2.00 kW (d) 202

3-13. The effect of electrode geometry and power on analyte emission temporal behavior of 1 μg Sn for: (a) 1.25 kW; (b) 1.50 kW; (c) 1.75 kW and (d) 2.00 kW (other operating conditions as in Table 3-2). Electrodes: 4000 (HPND+ 4000, Figure 3-8a); 4004 (HPND+ 4004, Figure 3-8b); 4021 R (HPND+ 4021 'Regular', Figure 3-8c); 4021 L (HPND+ 4021 'Long Undercut', Figure 3-

8d). Temporal behavior was scaled with respect to the peak intensity of the 4021 L electrode at 2.00 kW (d) 203

3-14. The effect of electrode geometry and power on analyte emission temporal behavior of 1 μg Ni for: (a) 1.25 kW; (b) 1.50 kW; (c) 1.75 kW and (d) 2.00 kW (other operating conditions as in Table 3-2). Electrodes: 4000 (HPND+ 4000, Figure 8a); 4004 (HPND+ 4004, Figure 3-8b); 4021 R (HPND+ 4021 'Regular', Figure 3-8c); 4021 L (HPND+ 4021 'Long Undercut', Figure 3-8d). Temporal behavior was scaled with respect to the peak intensity of the 4021 L electrode at 2.00 kW (d) 204

3-15. The effect of electrode geometry and power on the peak heights of: (a) 100 ng Cd; (b) 100 ng Zn; (c) 100 ng; (d) 1 μg Cu; (e) 1 μg Sn; (f) 1 μg Ni; (g) 1 μg Fe and (h) 1 μg Co.
-□- 4000, -◆- 4004, -■- 4021 Regular, -▲- 4021 Long Undercut
.... 205

3-16. The effect of electrode geometry and power on the peak areas of: (a) 100 ng Cd; (b) 100 ng Zn; (c) 100 ng; (d) 1 μg Cu; (e) 1 μg Sn; (f) 1 μg Ni; (g) 1 μg Fe and (h) 1 μg Co.
-□- 4000, -◆- 4004, -■- 4021 Regular, -▲- 4021 Long Undercut
.... 206

3-17. The effect of electrode geometry and power on the signal-to-background ratio (SBR) for: (a) 100 ng Cd; (b) 100 ng Zn; (c) 100 ng; (d) 1 μg Cu; (e) 1 μg Sn; (f) 1 μg Ni; (g) 1 μg Fe and (h) 1 μg Co.
-□- 4000, -◆- 4004, -■- 4021 Regular, -▲- 4021 Long Undercut
....212

3-18. The effect of cup composition on the temporal behavior of Cu, Cd, Cr and Ni (50, 100, 250 and 500 ng respectively) at 1.25 kW (other operating conditions as in Table 3-2), for: (a) Cd and Cu using Ta cups; (b) Cr and Ni using Ta cups; (c) Cd and Cu using W cups; (d) Cr and Ni using W cups; (e) Cd and Cu using long undercut graphite electrodes; and (f) Cr and Ni using long undercut graphite electrodes (Figure 3-8d). Temporal behavior for Cd and Cu was scaled with respect to the peak intensity of Cd for the Ta cup, that for Ni and Cr was scaled with respect to Ni and W cup............215

3-19. Analyte emission temporal behavior for Cd and Mn (100 pg each) at 2.00 kW, long undercut graphite electrodes and a one-shot insertion mode (other other operating conditions as in Table 3-2).................................. 220

3-20. Calibration curves for Ag, Cd, Cu and Mg (with slopes of the log-log plots of 1.04, 1.04, 1.00 and 0.996 respectively) constructed form multielement solution residues using long undercut graphite electrodes and a regular drive insertion mode (other operating conditions as in Table 3-2) 223

3-21. Illustration of a proposed 'next generation' DSID 226

4-1. Typical temporal emission behavior for: (a) water blank and 250 ng Al; (b) water blank and 250 ng Ca; (c) water blank and 250 ng Sr; (d) water blank and 250 ng Zr. The full scale intensity is 4096 239

4-2. Typical temporal emission behavior for: (a) 10 µl of 0.25 M KCl blank and 10 µl of 0.25 M KCl on 250 ng of Al; (b) 10 µl of 0.25 M KF blank and 10 µl of 0.25 M KF on 250 ng of Al; (c) 10 µl of 0.25 M NaCl blank and 10 µl of 0.25 M NaCl on 250 ng of Al; (d) 10 µl of NaF blank and 10 µl of 0.25 M NaF on 250 ng of Al. The full scale intensity is 4096 245

4-3. Typical temporal emission behavior for: (a) 10 µl of 0.25 M KCl blank and 10 µl of 0.25 M KCl on 250 ng of Ca; (b) 10 µl of 0.25 M KF blank and 10 µl of 0.25 M KF on 250 ng of Ca; (c) 10 µl of 0.25 M NaCl blank and 10 µl of 0.25 M NaCl on 250 ng of Ca; (d) 10 µl of NaF blank and 10 µl of 0.25 M NaF on 250 ng of Ca. The full scale intensity is 4096 246

4-4. Typical temporal emission behavior for: (a) 10 µl of 0.25 M KCl blank and 10 µl of 0.25 M KCl on 250 ng of Sr; (b) 10 µl of 0.25 M KF blank and 10 µl of 0.25 M KF on 250 ng of Sr; (c) 10 µl of 0.25 M NaCl blank and 10 µl of

0.25 M NaCl on 250 ng of Sr; (d) 10 µl of NaF blank and 10 µl of 0.25 M NaF on 250 ng of Sr. The full scale intensity is 4096................ 247

4-5. Typical temporal emission behavior for: (a) 10 µl of 0.25 M KCl blank and 10 µl of 0.25 M KCl on 250 ng of Zr; (b) 10 µl of 0.25 M KF blank and 10 µl of 0.25 M KF on 250 ng of Zr; (c) 10 µl of 0.25 M NaCl blank and 10 µl of 0.25 M NaCl on 250 ng of Zr; (d) 10 µl of NaF blank and 10 µl of 0.25 M NaF on 250 ng of Zr. The full scale intensity is 4096................ 248

4-6. The effect of NaF concentration (10 µl injection) on the signal-to-background ratio (SBR) of Al, Ca and Zr......................... 250

4-7. The effect of a 10 µl injection of 0.25 M NaF on the temporal emission behavior of Al, Ca, Sr and Zr for: (a) 10 µl of 0.25 M NaF blank and 10 µl of 0.25 M NaF on 250 ng of Al; (b) 10 µl of 0.25 M NaF blank and 10 µl of 0.25 M NaF on 250 ng of Ca; (c) 10 µl of 0.25 M NaF blank and 10 µl of 0.25 M NaF on 250 ng of Sr and (d) 10 µl of 0.25 M NaF blank and 10 µl of 0.25 M NaF on 250 ng of Zr. The full scale intensity is 4096................................ 251

4-8. The effect of a 10 µl injection of 0.25 M NaF on the temporal emission behavior of Ag, Cd and Zn for: (a) water blank and 10 µl of 0.25 M NaF on 10 ng Ag; (b) 10 µl of 0.25 M NaF blank and 10 µl of 0.25 M NaF on 10 ng Ag; (c) water blank and 10 µl of 0.25 M NaF on 10 ng Cd; (d) 10 µl of 0.25 M NaF blank and 10 µl of

0.25 M NaF on 10 ng Cd; (e) water blank and 10 µl of 0.25 M NaF on 10 ng Zn; (f) 10 µl of 0.25 M NaF blank and 10 µl of 0.25 M NaF on 10 ng Zn 254

4-9. Calibration curves from multielement solution residues of Al, Ca and Zr with a 10 µl addition of 0.25 M NaF for (a) Al (slope: 0.96); (d) Ca (slope: 0.96) and (c) Zr (slope: 1.03) 256

4-10. The effect of NaF concentration (25 µl injection) on the signal-to-background ratio (SBR) of B in 2 mg $CaSO_4$ 259

4-11. Calibration curves for B in 2 mg $CaSO_4$ with a 25 µl injection of 0.5 M NaF: (a) standard additions method; (b) from synthetic standards (slope: 0.98) 260

5-1. Block diagram of a dual processor based inductively coupled plasma atomic emission spectrometer (ICP-AES) 270

5-2. Instrument metaphor for the ICP-AES 280

5-3. Examples of first level windows accessible by clicking on the instrument metaphor (a) at location A (b), location J (c), and location B (d) 284

5-4. Examples of second level windows accessible by clicking on the RF generator window (a) at location A (b), location E (c), and location F (d) 287

5-5. (a) The Macintosh window accessed by clicking on location M of Figure 3a, (b) the Macintosh pull down menu, (c) and (d) are secondary windows accessible from the Macintosh pull down menu 289

5-6. Examples of second level windows (Monitor Off) accessible by clicking on the Plasma Box window (a) at location A (b), location K (c) and location B (d) 291

5-7. The ICP pull down menu (see text for discussion) 292

5-8. Examples of second level windows (Monitor On) accessible by clicking on the plasma Box window (Figure 6a) at location B (a), location D (d), location J (c) and location I (d) 294

5-9. The window display for "Monitor All" selected from the ICP menu 296

5-10. (a) The main screen display and (b-e) menu bar options and selections when "Set parameters" is selected from the ICP pull down menu. (f) Window display when "Frequently used" is selected from the "Plasma" pull down menu, (g) Plasma Box window for "Set Parameters" program 298

5-11. Examples of secondary windows for the Plasma Box window (Figure 10g) of the "Set Parameters" program accessed by clicking locations A (a), B (b), C (c), and E (d) 300

5-12. (a) Secondary window for setting coolant flow rate, (b) Alert window indication a potential problem and (d) History window giving last 9 settings 302

5-13. The instrument metaphor (a) with first level windows accessible by clicking the polychromator at locations A (b), B (c) and C (d) 304

5-14. The alert window (a) telling the user to load the Element Info program (b) in order to access the periodic table data (c). The alert window (d) indicating inactivity of graphic areas under the new program. Selections with the new "Elements" pull down menu associated with the periodic table window (e, f, g) 305

5-15. The periodic table window (a) with general information (b), Interference, (c) and Operating conditions (d) windows for Zn......... 308

5-16. The periodic table window (a) with General Information, (b) Interference (c) and Operating Conditions (d) windows for Cu......... 310

5-17. The General Information windows for Y (a) and Sb (b). The Interference and Operating Conditions windows for Y (b) and Sb (d)......... 312

5-18. (a) The periodic table window, (b) general Information window for Ar, (c) Interference or Operating Conditions window for Ar, (d) and window for La (marked 57-71 on the periodic table) 313

5-19. (a) Pull down menu to access Help and Explain files. (b) Explain files "Mini Finder" window for the ICP main program, (c) profile explain file, (d) Specifications explain file........... 316

5-20. Mini Finder window for Help files of Element Info program. (b) Ar 317-367 help file, (c) Op Conds help file and (d) Interference help file...................... 317

5-21. Examples of Explain files available in the Element Info program............................. 319

5-22. Pull down menu structure for the complete instrument user interface....................... 321

5-23. (a) The "Transfer" menu help file, (b) the "External" menu help file, (c) Launcher window after choosing "Launcher" from the "Apple" menu (Figure 22a), and (d) Mini Finder.......... 323

6-1 . Block diagram of the experimental set-up of a DSID for ICP-MS................................ 331

6-2. Sample carrying probes employed in this work. (a) long undercut graphite electrode; (b) long undercut graphite electrode fitted with a metal cup; (c) wire-loop........................ 334

6-3. Typical analyte temporal behavior............... 335

6-4. Schematic illustration of alignment device...... 338

6-5. Top view of the direct sample insertion device (x, y is the plane of the drawing, the z-axis is perpendicular to the drawing)............... 340

6-6. Three dimensional view of the DSID (not to scale)....................................... 344

6-7. Three dimensional view of the torch support assembly (not to scale)........................ 346

6-8. Schematic illustration of the 'DSID' torch...... 348

6-9. Top view of the shutter, (a) open and (b) closed.. 349

6-10. Top view of the sliding platform (x- and y-axis define the plane of the page, the z-axis is perpendicular to the drawing)............... 351

6-11. Schematic illustration of the probe assembly support, (a) probe assembly positioned vertically; (b) probe assembly positioned horizontally.................................. 352

6-12. Front view of sliding platform (probe assembly support is not shown for clarity, dimensions in cm).. 353

6-13. Schematic illustration of probe assembly at: (a) home position; (b) an intermediate state and (c) the horizontal position................ 357

6-14. Schematic illustration of probe insertion....... 359

6-15. Typical temporal behavior for Cu and Zn (10 ng each) as transferred to the Macintosh at 1200 baud... 362

6-16. Pull-down menu structure........................ 365

6-17. An example of a hierarchical menu............... 369

6-18. Typical temporal behavior for Cu and Zn (10 ng each) as transferred to the Macintosh at 9600 baud... 370

6-19. Number of data points per second per number of masses scanned. (a) one mass scanned; (b) two masses; (c) three masses and (d) four masses.... 375

6-20. The effect of central tube flow rate on intensity as a function of power and sampling depth for: (a) 10 ng Mg; (b) 10 ng Mn; (c) 10 ng Zn.. 376

6-21. Typical analyte temporal behavior from long undercut graphite electrodes, a 10 mm sampling depth and 1.50 kW power for 1 ng of: (a) Mg; (b) Mn and (c) Zn.............................. 378

6-22. Background spectrum for a graphite electrode (low resolution scan, 10 mm sampling depth, 1.25 kW)....................................... 379

6-23. Background spectrum for a Mo cup (low resolution scan, 10 mm sampling depth, 1.25 kW) 380

6-24. Background spectrum for a Ta cup (low resolution scan, 10 mm sampling depth, 1.25 kW) 381

6-25. Background spectrum for a W wire-loop (low resolution scan, 10 mm sampling depth, 1.25 kW) 392

7-1. Illustration of the DSID torch with its extension in place 396

7-2. Background spectra for a wet plasma, high resolution scan, sampling depth 15 mm, mass range 1-45 amu 397

7-3. Background spectra for a wet plasma, high resolution scan, sampling depth 15 mm, mass range 40-85 amu 405

7-4. Background spectra for a dry plasma, high resolution scan, sampling depth 15 mm, mass range 10-40 amu 406

7-5. Background spectra for a dry plasma, high resolution scan, sampling depth 15 mm, mass range 40-75 amu 411

7-6. Background spectra for a dry plasma, high resolution scan, sampling depth 10 mm, mass range 10-40 amu 412

7-7. Background spectra for a dry plasma, high resolution scan, sampling depth 10 mm, mass range 40-75 amu 414

7-8. Background spectra for a dry plasma, extended torch, high resolution scan, sampling depth 10 mm, mass range 10-45 amu 415

7-9. Background spectra for a dry plasma, extended torch, high resolution scan, sampling depth 10 mm, mass range 40-75 amu 417

7-10. Background spectra, mass range 10-40 amu for: (a) wet plasma (15 mm); (b) Dry plasma (15 mm);(c) Dry plasma (10 mm); (d) Dry plasma, extended torch 418

7-11. Background spectra, mass range 40-75 amu for: (a) wet plasma (15 mm); (b) Dry plasma (15 mm); c) Dry plasma (10 mm); (d) Dry plasma, extended torch 420

7-12. Bar graph background spectra, mass range 12-38 amu. (a) Wet plasma, sampling depth 15 mm; (b) Dry plasma, extended torch 421

7-13. Bar graph background spectra, mass range 42-75 amu. (a) Wet plasma, sampling depth 15 mm; (b) Dry plasma, extended torch 424

7-14. Bar graph background spectra (logarithmic scale intensity axis) for the wet plasma (sampling depth 15 mm) and the dry plasma (extended torch) for: (a) mass range 12-42 amu and (b) mass range 42-75 amu 427

7-15. High resolution background spectrum of a 'blank' long undercut graphite electrode, mass range 1-40 amu 428

7-16. High resolution background spectrum of a 'blank' long undercut graphite electrode, mass range 40-85 amu. Note scale expansion in (c) 431

7-17. Low resolution background spectrum for a Mo cup, mass range 1-40 amu 432

7-18. Low resolution background spectrum for a Mo cup, mass range 40-85 amu 433

7-19. Low resolution background spectrum for a Mo cup, mass range 80-140 amu. Note scale expansion 434

7-20. Low resolution background spectrum for a Mo cup,mass range 140-210 amu 437

7-21. Low resolution background spectrum for a Ta cup, mass range 1-40 amu 438

7-22. Low resolution background spectrum for a Ta cup, mass range 40-85 amu 439

7-23. Low resolution background spectrum for a Ta cup. (a) Mass range 80-160 amu, scale expanded; (b) Mass range 160-210 amu; (c) Mass range 160-210, note scale expansion 441

7-24. Low resolution background spectrum for a W wire-loop, mass range 1-40 amu 442

7-25. Low resolution background spectrum for a W wire-loop, mass range 40-85 amu 443

7-26. Low resolution background spectrum for a W wire-loop, mass range 80-140 amu 444

7-27. Low resolution background spectrum for a W wire-loop, mass range 140-205 amu 453

7-28. Temporal behavior arising form 1 μg Ba for: (a) $^{138}Ba^{+}$; (b) $^{138}Ba^{16}O^{+}$; (c) $^{138}Ba^{2+}$; and (d) $^{138}Ba^{16}OH^{+}$ 455

7-29. Temporal behavior after addition of 10 μl of 0.25 M of NaF on the dried solution residue of the previously run electrode (Figure 2-28). (a) $^{138}Ba^{+}$; (b) $^{138}Ba^{16}O^{+}$; (c) $^{138}Ba^{2+}$ and (d) $^{138}Ba^{16}OH^{+}$ 457

7-30. Temporal behavior arising from 10 μl of 0.25 M NaF for: (a) $^{138}Ba^{+}$; (b) $^{138}Ba^{16}O^{+}$; (c) $^{138}Ba^{2+}$ and (d) $^{138}Ba^{16}OH^{+}$ 458

7-31. Temporal behavior arising form 1 μg of Ce, for $^{140}Ce^{+}$, $^{140}Ce^{16}O^{+}$ and $^{140}Ce^{2+}$ (a), (c) and (d); and after addition of 10 μl of 0.25 M NaF into a previously inserted electrode and upon re-insertion for $^{140}Ce^{+}$, $^{140}Ce^{16}O^{+}$ and $^{140}Ce^{2+}$, (b), (d) and (f) 461

7-32. Effect of $^{35}Cl^{16}O^{+}$ on $^{51}V^{+}$ determinations. Blank long undercut graphite electrode, $^{51}V^{+}$ (a) and $^{35}Cl^{+}$ (c); 10 μg of NaCl, $^{51}V^{+}$ (b) and $^{35}Cl^{+}$ (c) 462

7-33. Effect of $^{35}Cl^{16}O^+$ on $^{51}V^+$ determinations. After injection of 0.1 μg of V, $^{51}V^+$ (a) and $^{35}Cl^+$ (c); after addition of 10 μl of 0.25 M NaF and electrode re-insertion, $^{51}V^+$ (b) and $^{35}Cl^+$ (d) 465

7-34. The effect of Zn on U. 50 ng of Zn, $^{64}Zn^+$ (a) and $^{238}U^+$ (b); 50 ng of Zn and 10 μg of U, $^{64}Zn^+$ (c) and $^{238}U^+$ (d); after addition of 10 μl of 0.25 M NaF and electrode re-insertion, $^{64}Zn^+$ (e) and $^{238}U^+$ (f) 467

7-35. Same as Figure 7-34 without scale expansion..... 491

8-1. Illustration of a proposed 'next generation' DSID for ICP-MS.................................. 478

8-2. Block diagram of an atomic spectrochemical measurement system............................. 481

8-3. Concept diagram illustrating a 'next generation' analytical instrumentation.......... 485

8-4. Illustration of a spectrochemical answer machine....................................... 486

A-1. Optical configuration of a typical Paschen-Runge mount direct reading spectrometer......... 491

A-2. Block diagram of a typical readout system for a conventional direct reading spectrometer..... 492

A-3. Block diagram of a multichannel measurement system for a direct reading spectrometer based on i/f converters and a series of single channel frequency meters 494

A-4. Block diagram of a single measurement channel... 497

A-5. Circuit diagram for a single measurement channel 498

A-6. Simplified circuit diagram for the Microflex 65 bus to single channel system interface logic. LDB is the Local Data Bus, LAD is the Local Address Bus and LCB is the Local Control Bus, see text for discussion 503

A-7. Functional block diagram of the single channel system with the relocatable partial address decoding scheme 505

A-8. Simplified block diagram of the relocatable, switch configurable address decoding scheme..... 507

A-9. Circuit diagram of the address decoding scheme utilized in the single channel system. DAB is the Decoded Address Bus, see text for discussion 508

A-10. Photograph of the single channel system. The LEDs are Light Emitting Diodes, the 8253s are the programmable timer/counter chips, the 6522 VIA (Versatile Interface Adapter) is a digital I/O integrated circuit, the 74LS138 is a 3-line-to-8-line decoder/demultiplexer, the 74LS155 is a 2-line-to-4-line decoder/demultiplexer, the 74154 is a 4-line-to-16-line decoder/demultiplexer, S-1 is the first switch bank, S-2 is the second switch bank, the 74LS640 is an octal bus transceiver, the 74LS240s are octal buffers/line drivers, and the discrete transistor is a PNP 3393. The dimensions of the card are (LxW):6.5 v 3.9 in (164 v 100 mm) 513

B-1. Top view of DSID-base (see Figure C-2 for more details) 517

B-2. Top view of DSID-base (complements dimensions shown in Figure C-1) 518

B-3. Bottom view of DSID-base 519

B-4. Three-dimensional view of DSID- and of plexiglass-base 520

B-5. Lead screw support 521

B-6. Top view of sliding platform (dimensions in cm) 522

B-7. Top view of plasma box 523

B-8. Top view of plexiglass-base 524

B-9. Top view of plexiglass-base with the torch support in place 525

B-10. Side view of plexiglass-base with the torch support in place 526

B-11. Side view of torch, torch support and shutter... 527

B-12. Three-dimensional illustration of shutter....... 528

B-13. Top view of torch support assembly (with torch and shutter in place) on top of the plasma box.. 529

B-14. Side view of torch support brace................ 530

B-15. Front view of torch brace...................... 531

B-16. Top view of torch support assembly on DSID-base.. 532

D-1. Simplified schematic diagram of the optical design of the SPS-10 Simultaneous Plasma Spectrometer.................................. 540

D-2. Schematic diagram of pre-disperser selection mask.. 542

D-3. Schematic diagram of instrument spectral operation..................................... 545

D-4. Mask-out/mask-in spectra for Cu................ 548

D-5. Mask-out/mask-in spectra for Fe................ 549

D-6. Mask-out/mask-in spectra for Ti................ 551

D-7. Spectra for Mo indicating source of leakage lines (see text for discussion)................. 552

D-8. Spectra for Si indicating sources of leakage lines (see text for discussion 554

D-9. Mask-out/mask-in spectra for multielement solution (10 ppm Al, Cr, Fe, Mo, Ni, Si; 1 ppm Cu, Mg, Ti) 555

D-10. Mask-out single element spectra composite with mask-in multielement spectrum.................. 557

D-11. Multielement bar graph spectrum................ 558

D-12. Mask-out/mask-in spectra for V................. 560

D-13. Superimposition of V and multielement bar graph spectra................................. 561

D-14. Mask-out/mask-in spectra for Co................ 562

D-15. Superimposition of Co and multielement bar graph spectra................................. 563

CHAPTER 1

A REVIEW OF DIRECT SAMPLE INSERTION DEVICES FOR INDUCTIVELY COUPLED PLASMAS

A. The Inductively Coupled Plasma

Of the various plasma sources utilized in atomic spectroscopy [1-3], for example, the inductively coupled plasma (ICP), the direct current plasma (DCP) and the microwave induced plasma (MIP), the ICP [4-13] is the most widely used. Being credited with the revitalization of atomic emission spectroscopy, it can be considered as one of the most important developments in analytical atomic spectrometry in the last 25 or so years. Moreover, a true alternative to ICPs has not yet emerged.

Since the introduction of a commercial ICP instrument for atomic emission spectrometry (AES) in 1974 [12], the interest in ICPs has been growing steadily. According to an estimate [14], there are about 30 vendors of ICP-based instrumentation world-wide, the number of installed units is approximately 6000 and is *"increasing at a rate of approximately 400/year, which in recent years has represented a percentage growth rate higher than any other analytical instrument"* [13]. The areas in which the ICP has been applied are very diverse [15-16], ranging from industrial [17], geological [18], environmental [19], and biological/clinical [20] materials to agricultural [21] and organic and petroleum products [22].

In addition to its use as a source for Atomic Emission Spectrometry, the ICP also has been used as an atom reservoir for both atomic absorption spectrometry (AAS) [23, 24] and atomic fluorescence spectrometry (AFS) [4, 25, 26] and as an ion source for mass spectrometry (MS) [27-30] and ICP-AFS and ICP-MS instrumentation is currently commercially available. The success the ICP enjoys can be attributed to its desirable characteristics (i.e., wide linear dynamic range, relative freedom from interference effects, acceptable accuracy and good precision, low detection limits, which are in the ppb range for ICP-AES and sub-ppb range for ICP-MS for some elements, and an inherent capability for simultaneous determinations); these are hardly worth elaborating on as they have become standard textbook material. And although the capabilities of the ICP are not unlimited, its characteristics approach those of an 'ideal' source for atomic spectroscopy.

The wide acceptance of the ICP, as exemplified by the range of applications reported and the key current trend of AAS users in replacing their aging AAS instruments with modern, low-cost ICPs, is a clear indication of not only the success but also of the maturity of the technique. To use Laitinen's analogy of the *"seven ages of an analytical method"* [31] and applied to the ICP, (i.e., conception of the idea; design and construction of working prototypes and experimental verification of the principles involved; development of instrumentation and evaluation of performance characteristics and figures-of-merit; fundamental studies and design and construction of improved instrumentation;

standardization of methods and operating conditions, general acceptance and attainment of maturity, automation; application to new and old problems and in depth understanding of the scientific principles; old age and senescence), the ICP has reached the general acceptance stage and, therefore, a stage of relative maturity.

Does this mean that its analytical figures-of-merit cannot be further improved? In spite of its wide acceptance, applicability and maturity, there remain two basic areas in which further progress would improve the already impressive performance characteristics of the ICP. First, from a fundamental-studies point of view, a thorough understanding of excitation mechanisms and of the physical and chemical processes taking place in the plasma discharge is required in order to *"ensure optimized analytical performance"* [32] or to yield *"better ICP instrumentation"* [33]. Fundamental studies, however, frequently constitute a distant objective. Second, and from the more immediate and practical point of view, sample introduction and the almost exclusive use of liquid samples is the most important current limitation of the ICP; the capability of the ICP for the direct analysis (i.e., little or no sample pre-treatment) of powdered/solid samples has not yet been either fully exploited or fully developed.

Of the two possible alternatives and due to the importance of sample introduction, the practical route has been taken in this thesis: the basic goal is to extend the analytical capability and utility of the ICP by investigating, developing and implementing means of overcoming its key practical limitations with respect to sample introduction. The results of this investigation will form the basis for a proposed intelligent sample processor for the ICP. Toward the end of this thesis, the scope of this research will be further extended and the concept of an intelligent sample processor for the ICP will be used as a spring board for yet another proposal attempting to blue print intelligent instrumentation. Before proceeding, however, a literature review of sample introduction systems for the ICP is warranted. From this, the impetus of this work is expected to emerge.

B. Sample Introduction Systems for the ICP

Because a sample introduction sub-system provides the essential link between the sample and the ICP, it can be considered as a key sub-system in any plasma-based instrumentation. Ironically, sample introduction is also a major stumbling block in preventing the ICP from attaining its full potential. According to Barnes [34], "*The precision, reliability, sensitivity and speed of ICP-AES is more often than not limited by the technique employed for sample introduction or preparation*". Undoubtedly, the same arguments apply to ICP-MS and ICP-AFS.

A key requirement for the successful utilization of a sample introduction system in ICP spectrometry is that of the sample matching the sample introduction system. In terms of samples, three basic types can be distinguished: liquids (i.e., natural and industrial waters, geological and biological fluids); powders/solids (i.e., those of biological, botanical, geological and metallurgical origin) and gases (i.e., combustion and pyrolysis products). In terms of sample introduction systems, samples can be introduced into the ICP either as gases (i.e., hydride generation) or as liquids (i.e., pneumatic nebulization) or as powders/solids (direct sample injection or insertion).

B.1 Pneumatic Nebulization

The desirable characteristics of pneumatic nebulization of liquid samples make it the most popular means of sample introduction into the ICP, it is almost exclusively used in routine analysis. Included in these are: relatively good stability; simplicity in design and operation; and, with the exception of ultrasonic nebulization, rapid change over and no memory effects. The disadvantages include nebulizer blockage at high salt concentrations, the requirement for solution samples and volumes greater than 1 ml and drift [35, 36, 37]. The poor efficiency (typically less than 3%) is, perhaps, the most important drawback of pneumatic nebulization. Put otherwise, 97% of a hard earned sample literally 'goes down the drain'. It comes as no surprise then why sample introduction systems have been termed the *"Achilles' heel"* of atomic spectroscopy [35].

Pneumatic nebulization systems also suffer from a host of limitations. For example, they have been designed to handle only liquid samples. This can be thought of as a 'virtue' when analyzing liquid samples and as a 'vice' when the analysis of powdered/solid samples is considered. Because a great deal of samples naturally occur as powders or solids, these must be first quantitatively converted to liquids before they can be introduced into the ICP via pneumatic nebulization. By dissolving the sample (assuming proper sampling procedures), the sample becomes homogenized. This, in turn provides a reliable estimate of the composition of the bulk. And even though bulk composition is important, there is an increasing need for localization of elemental composition in solid samples (i.e., dopants in Si wafers, microelectronic devices). Moreover, from the time the sample is dissolved, some information about the analyte (i.e., oxidation state, chemical form, localized composition) and the matrix is lost, to paraphrase an old adage 'by homogenizing you loose intelligence'.

Because sample dissolution also results in sample dilution, trace elements may fall below the range of acceptable concentration levels for determination with the ICP. This necessitates a pre-concentration step prior to analysis. As the number of steps increases, sample preparation procedures become more complicated; as more reagents are added to the sample, the risk for contamination also increases. However, as ICP detection limits approach sub-ppb levels (i.e., ICP-MS), contamination is becoming an increasingly important consideration: even highly purified acids, matrix modifiers and solvents may contain elemental concentrations above this level.

There is little doubt that as sample preparation procedures become more tedious, involved and complicated, they also become error-prone, labour-intensive and time-consuming. Because the speed of analysis offered by many ICP-instrumentation systems is orders of magnitude faster than the best available sample preparation procedures, the need to automate sample preparation becomes readily apparent. However, multi-step sample preparation procedures do not easily lend themselves to automation. This could be the reason why automation of sample preparation of liquid samples from powders/solids has been slow in coming, even with the recent advances in robotics.

In addition, there are cases in which a limited sample quantity is available, for example, samples of archeological, biological, biochemical, environmental, forensic and planetary origin. In other cases, even when a large sample quantity is available, a conversion to a solution may result in small volumes after separation. Clearly, continuous aspiration of small solution volumes via pneumatic nebulization (typically requiring 1-3 ml/min) is unrealistic.

In summary, and in spite of the advantages and the popularity of conventional pneumatic nebulization, *"to day no one can deny that the nebulizer system is the weakest link in an ICP"* [36]. Therefore, an alternative sample introduction system is required.

B.2 Alternatives to Pneumatic Nebulization

Several attempts to minimize or eliminate some of the limitations of pneumatic nebulization have been made, comprehensive reviews and book chapters abound in the literature. To summarize [35, 38-42]: sample introduction of μl volumes of solutions via FIA-like methods or thermosprays; injection of powders with the help of mechanical agitation devices or fluidized beds; chemical derivatization (i.e., hydride generation) devices; and slurry atomization devices have been developed and characterized. The most important disadvantage of these sample introduction schemes is their limited applicability to certain types of samples and, for the most part, for samples with simple matrices. Alternatively, atomic vapors generated electrothermally (i.e., by heating carbon rods, furnaces or wires), or via arc and spark atomization or via laser ablation have been injected into ICPs. In these, the atomic vapor is generated externally to the ICP and is carried into the plasma discharge typically by means of tubing and an argon stream. Perhaps the most important disadvantage of vapor generating devices is condensation on the walls of the tube and complex instrumentation. Due to their limitations, none of these devices described above has been accepted as a true alternative sample introduction system for the ICP.

Undoubtedly, the analytical capability and utility of the ICP would be greatly extended if µl volumes of liquid samples and mg quantities of powdered/solid samples could be directly introduced (i.e., with 100% efficiency) into the plasma with little or no sample pre-treatment. The direct sample insertion device (DSID) fits in this realm. Therefore, a closer look at the relevant literature is warranted.

C. Direct Sample Insertion Devices

In the direct sample introduction technique (DSIT), reminiscent of both Reed's initial application of crystal growth in the plasma [43] and of the dc arc [44, 45] and as its name implies, the sample is inserted directly into the source. And although the term 'direct sample insertion' has been used for a variety of techniques and systems, the working definition of a direct sample insertion device in which the sample is placed into or onto a probe, with subsequent introduction of the sample carrying probe into the plasma, as shown in Figure 1-1, will be used throughout.

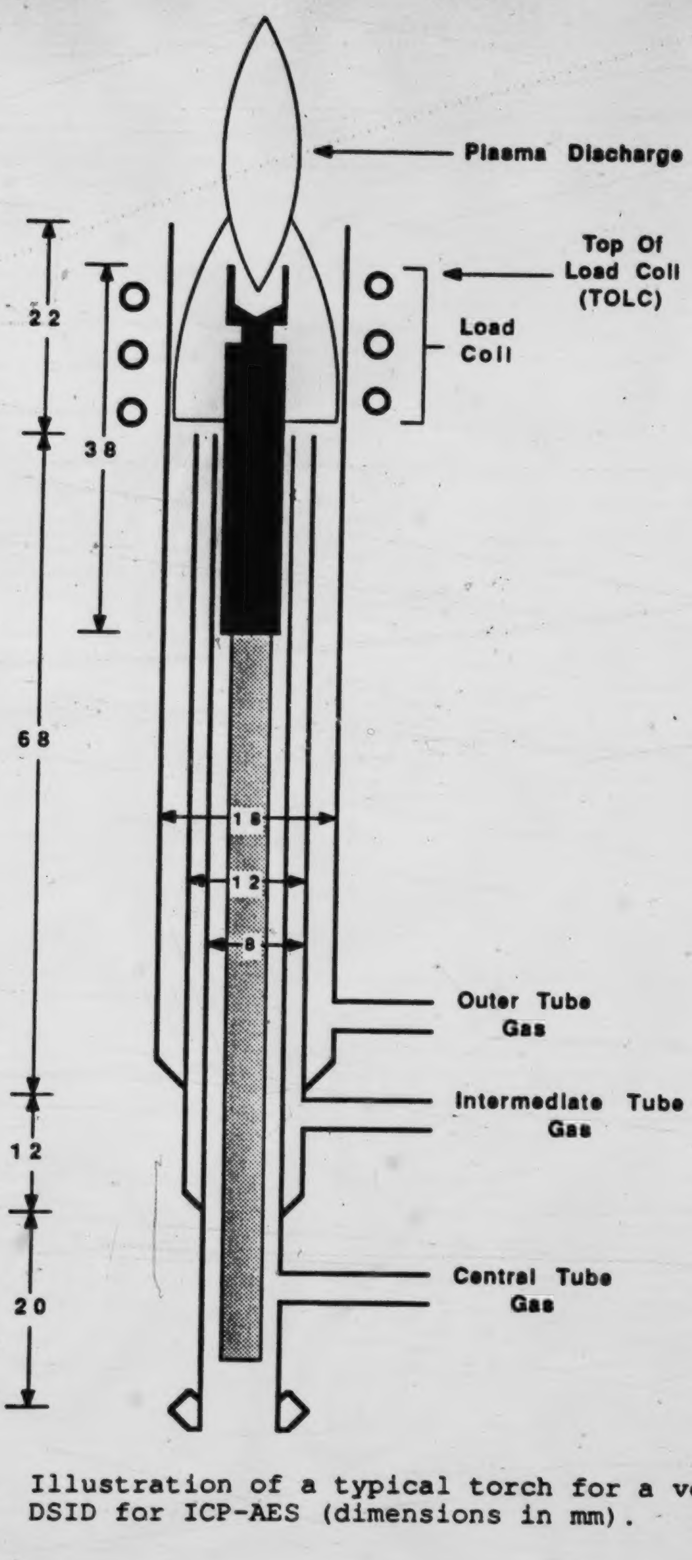
Plasma Discharge
Top Of Load Coil (TOLC)
Load Coil
22
38
68
16
12
8
Outer Tube Gas
Intermediate Tube Gas
12
20
Central Tube Gas

Figure 1-1. Illustration of a typical torch for a vertical DSID for ICP-AES (dimensions in mm).

From a historical perspective, an early attempt to design an 'electrothermal-like' device as the means to directly introduce samples into a low power ICP dates back to 1969 [46]. In this design, 30 µl of sample were placed on a graphite support that was held (by means of a Ta support) at the same level as the lower turns of the load coil of a 40 MHz, 200 W inductively coupled plasma. The sample was evaporated by means of ohmic heating from the graphite support and was subsequently excited by the ICP. Using this system, detection limits for 15 elements from solution samples were determined spectrographically. And although determinations from powders and melts were suggested, no further work was reported.

In 1979, Salin and Horlick [47] reported the use of a conventional undercut dc arc electrode as the means to introduce mg quantities of powders/solids and µl volumes of liquid samples into a medium power (<2.5 kW) ICP and coined the term DSID. An interrupted plasma operation (the ICP had to be re-ignited for each electrode insertion) was, perhaps, the most important disadvantage of their manually driven DSID. At about the same time, Sommer and Ohls [48] reported on the development of a DSID, dubbed the SET (sample elevator technique), and achieved continuous plasma operation. In their device, a version of which is commercially available from Kontron (Kontron Instruments Gmbh, Div. of Spectralanalytic, Oskar-v. Miller-Strasse 1, D-8057, Eching bei

München, FDR), a graphite cup is pneumatically driven into a 3 kW Argon-Nitrogen mixed-gas plasma.

Since then, DSIDs appear to have reached both a 'critical mass' and a state of 'relative maturity'. In addition to the discussions included in reviews [42, 49] and in book chapters [40-41], a number of papers dealing with DSIDs have been published [50-84]. Furthermore, DSIDs are being studied in a number of laboratories around the world (Table 1-1) and are being developed for both ICP-AES [63, 65-81, 84] and ICP-MS [64, 82]. For the purposes of this review, a fair amount of detailed information has been gathered and is presented in tabular form (Tables 1-2 to 1-7). The tabular presentation format was chosen because details and nuances that would otherwise be impossible to present can now be included. Thus, the interested reader is provided with a more complete 'picture' of the work done on DSIDs. The contents of Tables 1-2 to 1-7 are self-explanatory. However, the contents of Table 1-1 deserve special mention.

Listed in this table are the research groups involved in the development, characterization and application of DSIDs. The principal investigator (or group leader) shown in the first column of Table 1-1 is the *"author to whom correspondence should be addressed"*. Where this information or other pertinent data (i.e., conference proceedings) were not available, the first author or the first common author was

Table 1-1. Research groups and their DSID-related work.

Group	Author(s)	Title	Objective(s)	Year	Ref
Bastiaans (USA)	E.R. Prack and G.J. Bastiaans	Metal speciation by evolved gas/inductively coupled plasma emission spectrometry.	To evaluate the applicability of the DSID as an evolved gas analysis system for the speciation of solid inorganic compounds (i.e., mixtures of vanadium and lead salts and oxides).	1983	50
Broekaert (FDR)	G. Zaray, J.A.C. Broekaert, and F. Leis	The use of direct sample insertion into an Argon/Nitrogen ICP for emission spectrometry I. Optimization of the technique and application to the analysis of Aluminum oxide.	To investigate the analytical performance of a DSID with a high power (i.e., 3 kW) argon/nitrogen ICP and to optimize it for the analysis of volatile elements in Aluminium oxide using a variety of volatilization enhancing agents.	1988	51
Broekaert (FDR)	G. Zaray, P. Burba, J.A.C. Broekaert and F. Leis	The use of direct sample insertion into an Argon/Nitrogen ICP for emission spectrometry II. Determination of trace elements in high-purity Aluminium by preconcentration on cellulose and their subsequent insertion into the ICP.	To determine trace elements (i.e., Cu, Cr, Fe, Mn and Pb) in high purity Aluminum by preconcentration on cellulose collectors.	1988	52
Haraguchi (Japan)	H. Haraguchi, M. Abdullah, T. Hasegawa, M. Kurosawa and K. Fuwa	Inductively coupled plasma atomic emission spectrometry utilizing a direct graphite cup insertion technique.	To design a mechanical DSID for a continuously operating ICP and to overcome the limitations of other designs.	1984	53
Haraguchi (Japan)	M. Abdullah, K. Fuwa and H. Haraguchi	Simultaneous multielement analysis of microliter volumes of solution samples by inductively coupled plasma-atomic emission spectrometry utilizing a graphite cup direct insertion technique.	To investigate the feasibility of performing simultaneous multielement analysis of µl volumes of solution samples; to establish compromise conditions for 15 elements, to determine LODs and %RSDs for these elements and to to apply the method for the analysis of spinach and orchard leaves.	1984	54
Haraguchi (Japan)	M. Abdullah and H. Haraguchi	Computer controlled graphite cup direct insertion device for the analysis of plant samples by inductively coupled plasma atomic emission spectrometry.	To develop a computer controlled DSID and apply it for the analysis of powdered plant samples; to test it with a series of SRMs; to determine LODs and %RSDs for 18 elements; and to investigate the effect of ashing time on powdered botanical samples.	1985	55
Haraguchi (Japan)	M. Abdullah, K. Fuwa and H. Haraguchi	Electrochemical preconcentration of trace elements for simultaneous multielement determination by inductively coupled plasma-atomic emission spectrometry utilizing a graphite cup direct-insertion technique.	To preconcentrate and separate trace elements from artificial sea water by controlled potential cathodic deposition inside a graphite cup. A teflon cell was designed for this purpose.	1987	56
Horlick (Canada)	E.D. Salin and G. Horlick	Direct sample insertion device for inductively coupled plasma emission spectrometry.	To design a sample introduction system that allows the direct insertion of small amounts of samples (powders/solids or dessolvated liquids) into the plasma. This is the first description of a DSID for ICP-AES.	1979	57
Horlick (Canada)	W.E. Pettit and G. Horlick	An automated direct sample insertion system for the inductively coupled plasma.	To design an automated means of changing and running a series of sample carrying cups with computer controlled drying, ashing and atomization cycles. Also to briefly characterize the analytical performance characteristics of the device.	1986	58

Table 1-1. Continued.

Group	Author(s)	Title	Objective(s)	Year	Ref
Horlick (Canada)	Y. Shao and G. Horlick	Performance of a direct sample insertion system for the inductively coupled plasma.	To design a mechanical DSID for precise cup positioning in the plasma torch and to establish its performance characteristics.	1986	59
Horlick (Canada)	V. Karanassios and G. Horlick	Human Processor Interface for ICP-EAS: concepts and implementation.	To develop a dual-processor system for the computerization of a DSID for ICP-AES. In this, one proccesor does data acquisition and control whereas the other does 'information processing'. A unique human processor interface (HPI) implementing the 'instrument metaphor concept' was developed for this purpose.	1987	60
Horlick (Canada)	V. Karanassios and G. Horlick	A computer-controlled direct sample insertion device for ICP-AES.	To develop: an automated DSID capable of handling a variety of sample carrying probes; control electronics; a readout electronics sub-system capable of digitazing DSID-generated transient signals in high-speed; and DSID-specific software for control, data acquisition, display and processing.	1988	61
Horlick (Canada)	V. Karanassios, G. Horlick and M. Abdullah	Characterization of a direct sample insertion device for ICP-AES.	To assess analyte emission behavior in the time domain, to isolate the design attributes affecting analytical performance characteristics; to get some preliminary results on the analytical figures-of-merit of the device; and to use these findings as the basis for a proposed 'next generation' DSID.	1988	62
Horlick (Canada)	V. Karanassios, M. Abdullah and G. Horlick	The application of chemical modification to a direct sample insertion device for ICP-AES.	To investigate volatilization enhancement of difficult to volatilize elements via the addition of chemical modifiers (i.e., KCl, KF, NaCl, NaF) in a graphite cup from both multielement solution residues and powdered samples and to demonstrate the concept of in situ sample processing in the cup.	1988	63
Horlick (Canada)	V. Karanassios and G. Horlick	Development and characterization of a direct sample insertion device for ICP-MS.	To develop an automated DSID capable of handling a variety of sample carrying probes for a Sciex-Elan ICP-MS system and to establish some of its performance characteristics.	1988	64
Kirkbright (UK)	G.F. Kirkbright and S.J. Walton	Optical emission spectrometry with an inductively coupled radiofrequency argon plasma source and direct sample introduction from a graphite rod.	To develop a method for the direct insertion of small sample volumes into a low power, continuously operating ICP.	1982	65
Kirkbright (UK)	G.F. Kirkbright and Z. Li-Xing	Volatilization of some elements from a graphite rod direct sample insertion device into an inductively coupled argon plasma for optical emission spectrometry.	To investigate the analytical performance of a graphite rod DSID and to use 0.1 % Freon (in the central tube of the torch) as a volatilization enhancing agent.	1982	66
Kirkbright (UK)	Z. Li-Xing, G.F. Kirkbright, M.J. Cope and J.M. Watson	A microprocessor controlled graphite rod direct sample insertion device for inductively coupled plasma optical emission spectrometry.	To develop a stepper motor, microcomputer controlled DSID.	1983	67

Table 1-1. Continued.

Group	Author(s)	Title	Objective(s)	Year	Ref
Kirkbright (UK)	N.W. Barnett, M.J. Cope, G.F. Kirkbright and A.A.H. Taobi	Design consideration and temperature determination of an automated graphite furnance cup system used for direct sample insertion for ICP optical emission spectrometry.	To investigate the effect of probe geometry on final and equilibrium probe temperatures.	1984	68
Lorber (Israel)	A. Lorber and Z. Goldbart	Convenient method for the determination of trace elements in solid samples using an inductively coupled plasma.	To design a horizontally operated DSID and using it to demonstrate the applicability of the carrier distillation method in powdered uranium oxide samples.	1985	69
Lorber (Israel)	I.B. Brenner, A. Lorber and Z. Goldbart	Trace elemental analysis of geological materials by direct solids insertion of a graphite cup into the inductively coupled plasma.	To document interference effects with a horizontally operated DSID from powdered silicate samples.	1987	70
MacLeod (UK)	C.W. McLeod, P.A. Clarke and D.J. Mowthorpe	Simultaneous determination of volatile trace elements in nickel-base alloys using a direct insertion probe and inductively coupled plasma emission spectrometry.	To extend the capability of the DSID for the determination of volatile elements in Ni-base alloys and to determine if sufficiently high temperatures are being reached in order to melt the metal chips.	1986	71
Ohls (FDR)	D. Sommer and K. Ohls	Direkte probeneinführung in ein stabil brennendes, induktiv gekoppeltes plasma.	The development of the Sample Elevator Technique (SET) for a high power (i.e., 3 kW) argon/nitrogen ICP.	1980	72
Ohls (FDR)	K. Ohls and D. Sommer	Analysis of liquid, solid and gaseous samples using a high power Nitrogen/Argon plasma.	The development of the Sample Elevator Technique (SET) for a high power (i.e., 3 kW) argon/nitrogen ICP.	1981	73
Ohls (FDR)	K. Ohls	Die bestimmung kleiner cadmium-anteile in verschiedenen materialien durch festprobeneinsatz bei ICP- und flammenloser atomabsortionsspektrometrie.	To demonstrate the applicablity of the DSID (dubbed SET) for the determination of Cd in biological samples and in minerals. Solid samples were also analyzed using electrothermal AAS.	1984	74
Page (India)	A.G. Page, K.H. Madraswala, S.V. Godbole, M.J. Kulkarni, V.S. Mallapurkar and B.D. Joshi	Carrier distillation-ICAP approach for trace metal assay of Uranium oxide powder.	To modify and apply the dc arc carrier distillation method on an ICP-DSID for the selective volatilization of Cd, Cu, K, Na, Ni and Pb from Uranium oxide powder using 5% AgCl as a carrier.	1983	75
Page (India)	A.G. Page, S.V. Godbole, K.H. Madraswala, M.J. Kulkarni, V.S. Mallapurkar and B.D. Joshi	Selective volatilization of trace metals from refractory solids into an inductively coupled plasma.	To extend the previously developed carrier distillation method for the determination of B, Be, Cd, Co, Cr, Cu, Fe, K, Li, Mn, Na, Ni and Pb in powder Uranium oxide samples.	1984	76

Table 1-1. Continued.

Group	Author(s)	Title	Objective(s)	Year	Ref
Salin (Canada)	E.D. Salin and M.M. Habib	Electrochemical preconcentration and separation for elemental analysis by inductively coupled plasma emission spectrometry.	To use electrochemical preconcentration by cathodic deposition onto a graphite cup before insertion into the ICP as the means of achieving low detection limits and separation from difficult matrices.	1984	77
Salin (Canada)	E.D. Salin and R.L.A. Sing	Microsample liquid analysis with a wire-loop direct sample insertion technique in an inductively coupled plasma.	To investigate the possibility of analyzing small solution volumes via a wire-loop DSID, and to report some preliminary performance characteristics of the device.	1984	78
Salin (Canada)	M.M. Habib and E.D. Salin	Controlled potential electrolysis coupled with a direct sample insertion device for multielement determination of Heavy metals by inductively coupled plasma-atomic emission spectrometry.	To preconcentrate samples by cathodic deposition onto a graphite cup prior to insertion in the ICP for the simultaneous determination of Cu, Pb, Cd, Zn, Ni and Co from difficult matrices.	1985	79
Salin (Canada)	C.V. Monasterios, A.M. Jones and E.D. Salin	Determination of Cu and Zn in human head hair by inductively coupled plasma atomic emission spectrometry with a direct sample insertion device.	To demonstrate the direct analysis (i.e., minimal sample pre-treatment) of trace elements in human hair with a graphite cup DSID.	1986	80
Salin (Canada)	R.L.A. Sing and E.D. Salin	Evaluation of the wire loop direct insertion technique for ICP-AES and ICP-MS.	To compare the analytical performance characterstics of a wire-loop DSID for both ICP-AES and ICP-MS.	1986	81
Salin (Canada)	D.W. Boomer, M. Powell, R.L.A. Sing and E.D. Salin	Application of a wire loop sample insertion device for inductively coupled mass spectrometry.	To describe a wire-loop DSID for a Sciex Elan ICP-MS system and to briefly compare its performance characteristics with those obtained from an ICP-AES wire-loop DSID.	1986	82
Salin (Canada)	T.W. Williams and E.D. Salin	Hazards of a naive approach to detection limits with transient signals.	To point out some statistical errors that can be made when dealing with transient signals.	1988	83
Umemoto (Japan)	M. Umemoto and M. Kubota	Determination of arsenic and antimony in iron and steels by inductively coupled plasma-atomic emission spectrometry using a graphite cup direct insertion device.	The determination of As and Sb in dissolved iron and steel samples.	1987	84

Table 1-2. DSID designs and their attributes.

Group	DSID Type	Probe(s)	Insertion	Torch	DSID description	Dry/Ash	Year	Ref
Bastiaans (Prack & Bastiaans)	Vertical/ Graphite cup	Conventional dc arc undercut electrodes.	Mechanical, computer controlled. Electrodes are inserted axially into the torch.	Modified Fassel-type (demountable) with a central channel.	An initial manual insertion is followed by a computer controlled insertion. The plasma extinguished in order to run new samples/electrodes.	External (electrode/cup position is computer controlled).	1983	50
Broekaert (Zaray, Broekaert, Leis)	Vertical/ Graphite cup	Graphite cups were machined out of graphite rods. These were used with and without lids with a hole allowing the release of analyte vapor release.	Using a reversible dc motor.	Modified Greenfield-type.	Graphite cup, dc motor driven DSID. The speed of insertion can be varied between 10 and 80 mm/s.	External.	1988	51
Broekaert (Zaray, Burba, Broekaert & Leis)	Vertical/ Graphite cup	Graphite cups were machined out of graphite rods. These were used with and without lids.	Using a reversible dc motor.	Modified Greenfield-type.	Graphite cup, dc motor driven DSID. The speed of insertion can be varied between 10 and 80 mm/s.	External.	1988	52
Haraguchi (Haraguchi, Abdullah, Hasegawa, Kurosawa & Fuwa)	Vertical/ Graphite cup	Graphite rods. ID: 2-5 mm, Depth: 2 mm. Pre-burned 5 times prior to use.	Manual. The graphite probes are inserted axially into the torch.	Modified Fassel-type with a central tube. Central tube gas: Ar (0.1 L/min).	The final electrode position is controlled by a Teflon insulating handle. The plasma is sustained with the bottom of the torch open.	Not used. Samples dried with an IR lamp.	1984	53
Haraguchi (Abdullah, Fuwa & Haraguchi)	Vertical/ Graphite cup	Graphite rods. ID: 3 mm, Depth: 1.6 mm. These were treated with HCl for 24 hours, washed with distilled water, dried at 110 °C for 3 hours & preburned 5 times prior to use.	Manual. The graphite probes are inserted axially into the torch.	Modified Fassel-type with a central tube. Central tube gas: Ar (0.1 L/min).	The final electrode position is controlled by a Teflon insulating handle. The plasma is sustained with the bottom of the torch open.	Drying at 38-32 mm below TOLC for about 150 sec. Ashing at 32-35 mm below TOLC for about 15 sec.	1984	54
Haraguchi (Abdullah & Haraguchi)	Vertical/ Graphite Cup	Graphite rods. ID: 3 mm, Depth: 1.6 mm. These were treated as described above prior to their use. A lid was also used.	Mechanical, computer controlled. Electrodes are inserted axially into the torch.	Modified Fassel with a central tube. Central tube gas: Ar (0.1 L/min).	Automated. Electrode insertion and its final insertion position are computer controlled. A stepper motor/timing belt combination forms the basis of the drive mechanism. The stepper motor controller communicates with the controlling microcomputer (an NEC PC-2001) via an RS232 serial interface.	Ashing at 11 ± 1 mm below TOLC for about 6 min.	1985	55

Table 1-2. Continued.

Group	DSID Type	Probe(s)	Insertion	Torch	DSID description	Dry/Ash	Year	Ref
Haraguchi (Abdullah, Fuwa & Haraguchi)	Vertical/ Graphite cup	Graphite; ID: 3 mm; OD: 4.1 mm; Depth: 1.6 mm.	Mechanical, computer controlled. The probes are inserted axially into the torch.	Modified Fassel-type with a central tube. Central tube gas: Ar (0.1 L/min).	Automated. Electrode insertion its final insertion position are computer controlled. A stepper motor/timing belt combination forms the basis of the drive mechanism. The stepper motor controller communicates with the controlling microcomputer (an NEC PC-2001) via an RS232 serial interface.	Ashing at 29-25 mm below TOLC.	1985	56
Horlick (Salin & Horlick)	Vertical/ Graphite cup	Conventional dc arc undercut with boiler cups.	Manual. The graphite electrodes are inserted axially into the torch.	Modified Fassel-type with a central tube. A central tube gas was not used.	A lead screw-based drive mechanism was used for electrode insertion. The plasma was extinguished in order to run new samples/electrodes.	External.	1979	57
Horlick (Pettit & Horlick)	Vertical/ Graphite cup	Conventional undercut dc arc graphite electrodes and Mo, Ta and W cups (only the undercut is metal).	Pneumatic & mechanical, µC controlled. The probes are inserted axially into the torch.	Laboratory constructed, water-cooled, with no central tube and non-standard dimensions. The torch is supported by an air cooled torch assembly.	This automated system handles up to 24 electrodes (placed in a sample tray) in an sequential fashion. Sample tray, electrode insertion and final insertion position are computer controlled (DEC PDP 11 minicomputer).	In situ drying, dessolvation and ashing before atomization.	1986	58
Horlick (Shao & Horlick)	Vertical/ Graphite cup	Conventional undercut dc arc undercut electrodes. OD: 3.5, 4.5 and 6 mm.	Mechanical, computer controlled. The electrodes are inserted axially into the torch.	Modified Fassel-type with a central tube. Central tube gas: He (0.4 L/min).	Automated. Electrode insertion and its final insertion position are computer controlled (standard ARL-supplied, DEC PDP 11 minicomputer). A reversible motor/lead screw combination forms the basis of the electrode drive mechanism.	External using a hot plate (80-90 °C for 5-10 min).	1986	59
Horlick (Karanassios & Horlick)	Vertical/ Graphite cup & wire-loop	A variety of conventional undercut dc arc graphite electrodes, special electrode geometries, metal cups and a W wire-loop.	Pneumatic & mechanical, µC controlled. The probes are inserted axially into the torch.	Laboratory constructed, water-cooled, with no central tube and non-standard dimensions. The torch is supported by an air cooled torch assembly.	This pneumatically and mechanically driven DSID can handle a variety of sample carrying probes (placed in a sample tray) in an automated fashion. Sample tray, probe insertion and final insertion position are computer controlled (IBM PC microcomputer).	External using either a hot plate or an IR-lamp.	1988	61
Horlick (Karanassios, Horlick & Abdullah)	Vertical/ Graphite cup & wire-loop	A variety of conventional undercut dc arc graphite electrodes, special electrode geometries, metal cups and a W wire-loop.	Pneumatic & mechanical, µC controlled. The probes are inserted axially into the torch.	Laboratory constructed, water-cooled, with no central tube and non-standard dimensions. The torch is supported by an air cooled torch assembly.	This pneumatically and mechanically driven DSID can handle a variety of sample carrying probes (placed in a sample tray) in an automated fashion. Sample tray, probe insertion and final insertion position are computer controlled (IBM PC microcomputer).	External using either a hot plate or an IR-lamp.	1988	62

Table 1-2. Continued.

Group	DSID Type	Probe(s)	Insertion	Torch	DSID description	Dry/Ash	Year	Ref
Horlick (Karanassios, Abdullah & Horlick)	Vertical/ Graphite cup & wire-loop	A variety of conventional undercut dc arc graphite electrodes, special electrode geometries, metal cups and a W wire-loop.	Pneumatic & mechanical, µC controlled. The probes are inserted axially into the torch.	Laboratory constructed, water-cooled, with no central tube and non-standard dimensions. The torch is supported by an air cooled torch assembly.	This pneumatically and mechanically driven DSID can handle a variety of sample carrying probes (placed in a sample tray) in an automated fashion. Sample tray, probe insertion and final insertion position are computer controlled (IBM PC microcomputer).	External using either a hot plate or an IR-lamp.	1988	63
Horlick (Karanassios & Horlick)	Horizontal/ Vertical/ Graphite cup & wire-loop	A variety of conventional undercut dc arc graphite electrodes, special electrode geometries, metal cups and a W wire-loop.	Mechanical, µC controlled. The probes are inserted axially into the torch.	Modified Fassel-type with a central tube. Central tube gas: Ar (variable flow rate).	An automated, stepper-motor and lead-srew driven. An Apple II+ microcomputer was used for DSID control, a standard Sciex Elan multibus based system was used for data acquisition and control. An Apple Macintosh was used as a front end processor.	External using either a hot plate or an IR-lamp.	1988	64
Kirkbright (Kirkbright & Walton)	Vertical/ Graphite rod	Graphite rods forming flat top electrodes.	Manual, the graphite probes are inserted axially into the torch.	Demountable, modified Fassel-type with a central tube. Central gas: Ar 0 L/min, best SBR at 0.2 L/min, but it was difficult to run the plasma.	The DSID consists of a rod attatched to an insulating handle. An adjustable stop controls the position of the rod in the plasma.	External using a heat gun. Initial attempts to use the plasma to dessolvate aqueous solutions were not successful.	1982	65
Kirkbright (Kirkbright & Li-Xing)	Vertical/ Graphite rod	Graphite rods forming flat top electrodes.	Manual, the graphite probes are inserted axially into the torch.	Demountable, modified Fassel-type with a central tube. Central gas: Ar/Freon mixture, 0-0.95 L/min.	It consists of a rod attatched to an insulating handle. An adjustable stop controls the position of the rod in the plasma.	External using a heat gun.	1982	66
Kirkbright (Li-Xing, Kirkbright, Cope & Watson)	Vertical/ Graphite rod	Graphite rods forming flat top electrodes.	Mechanical, computer controlled. The probes are inserted axially into the torch.	Demountable, modified Fassel-type with a central tube. Central tube gas: Ar, 0.1-1.0 L/min.	Automated. Electrode insertion and its final insertion position are computer controlled. A microcomputer (PET 2001-16NBS) and a stepper-motor (200 steps per revolution) driven lead-screw serve this function. The cup is attached on top of the graphite rod.	Computer controlled. Reflected power initially increases to about 100 W then decreases and, upon dessolvation, it remains at <3 W.	1983	67
Kirkbright (Barnett, Cope, Kirkbright & Taobi)	Vertical/ Graphite rods/cups of different geometry	Four different electrode/cup geometries were investigated with respect to heating rates and maximum attainable temperatures.	Mechanical, computer controlled. The probes are inserted axially into the torch.	Demountable, modified Fassel-type with a central tube.	On this automated system, electrode insertion and its final insertion position in the torch are computer controlled. A microcomputer (PET 2001-16NBS) and a stepper-motor (200 steps per revolution) driven lead-screw are used. The cup is attached on top of the graphite rod.	Computer controlled.	1984	68

Table 1-2. Continued.

Group	DSID Type	Probe(s)	Insertion	Torch	DSID description	Dry/Ash	Year	Ref
Lorber (Lorber & Goldbart)	Horizontal/ Graphite cup	Conventional dc arc graphite electrodes.	Manual, the graphite electrodes are inserted transversely to the torch.	Conventional Fassel-type (same as that used for pneumatic nebulization).	Horizontal, the sample carrying cups are inserted transversely to the torch at about 8-mm above the top of the load coil (TOLC).	Not used (not needed, solid inorganic samples).	1985	69
Lorber (Brenner, Lorber & Goldbart)	Horizontal/ Graphite cup	Conventional dc arc graphite electrodes.	Manual, the graphite electrodes are inserted transversely to the torch.	Conventional Fassel-type (same as that used for pneumatic nebulization).	Horizontal, the sample carrying cups are inserted transversely to the torch at about 6-mm above the top of the load coil (TOLC).	Not used (not needed, solid inorganic samples).	1987	70
McLeod (Mcleod, Clarke & Mowthorpe)	Vertical/ Graphite cup	Home made, OD: 3-mm ID: 2-mm and 7-mm in length.	Electro-mechanical (car aerial). The electrodes are inserted axially into the torch.	Modified Fassel-type with a central channel but with no central tube gas flow.	A car aerial supported by a laboratory jack and a dc power supply drive this DSID. A mechanical stop defines the final insertion position of the cup in the plasma.	External.	1986	71
Ohls (Sommer & Ohls)	Vertical/ Graphite cup	Graphite cup supported by a glossy carbon support and a quartz stem.	Pneumatic, the graphite electrodes are inserted axially into the torch.	Greenfield-type with no central tube.	It handles one electrode at a time. The electrodes are pneumatically driven into a high power (3 KW), Argon/Nitrogen ICP. Conference report.	External.	1980	72
Ohls (Sommer & Ohls)	Vertical/ Graphite cup	Graphite cup supported by a glossy carbon support and a quartz stem.	Pneumatic, the graphite electrodes are inserted axially into the torch.	Greenfield-type with no central tube.	It handles one electrode at a time. The electrodes are pneumatically driven into a high power (3 KW), Argon/Nitrogen ICP.	External.	1981	73
Ohls (Ohls & Sommer)	Vertical/ Graphite cup	Graphite cup supported by a glossy carbon support and a quartz stem.	Pneumatic, the electrodes are inserted axially into the torch.	Greenfield type with no central tube.	It handles one electrode at a time. The electrodes are pneumatically driven into a high power (3 KW), Argon/Nitrogen ICP.	????	1984	74

Table 1-2. Continued.

Group	DSID Type	Probe(s)	Insertion	Torch	DSID description	Dry/Ash	Year	Ref
Page (Page, Madraswala, Godbole, Kulkarni, Mallapurkar & Joshi)	Vertical/ Graphite cup	Standard carrier distillation electrodes (Scribner-Müllin), 0.125" in diameter.	Manual, the electrodes are inserted axially into the torch.	Modified Fassel-type with no central tube. The bottom of the central tube was converted into an electrode supporting facility.	One electrode at a time is manually spring-loaded into a continuously running ICP.	Externalusing an IR lamp.	**1983**	**75**
Page (Page, Godbole, Madraswala, Kulkarni, Mallapurkar & Joshi)	Vertical/ Graphite cup	Scribner-Müllin electrodes fitted with a home-made lid that has a 1 mm diameter hole to allow analyte vapor release.	Manual, the electrodes are inserted axially into the torch.	Modified Fassel-type with no central tube. The bottom of the central tube was converted into an electrode supporting facility.	One electrode at a time is manually spring loaded into a continuously running ICP.	External using an IR lamp.	**1984**	**76**
Salin (Salin & Habib)	Vertical/ Graphite cup	Conventional undercut dc arc graphite electrodes were used as working electrodes in a controlled potential electrolysis cell.	Manual, the graphite electrodes are inserted axially into the torch.	Modified Fassel-type with no central tube. The central tube was replaced with a movable quartz tube that provides electrode support.	One electrode at a time, placed on top of a lead screw, is manually inserted into the ICP. The plasma is extinguished in order to run a new sample or a new electrode. The objective was electrochemical sample preconcentration and separation, rather than the design and characterization of a DSID.	In situ (underneath the plasma), under computer control.	**1984**	**77**
Salin (Salin & Sing)	Vertical/ Wire-loop	A W wire (4-cm in length, 0.46-mm in diameter forming two, 2 mm in diameter loops onto which 10 µl of sample is deposited) was used instead of graphite electordes.	Manual/ Pneumatic. The wire-loop is inserted axially into the torch.	Modified Fassel-type with no central tube. The central tube was replaced with a movable quartz tube that provides support to the probe assembly.	The wire-loop, powered by an independant Ar cylinder, is pneumatically driven into the ICP. Pneumatic insertion was chosen because it provides fast insertion. A series of movable mechanical stops are used in order to program the drying and atomization cycles. Manually removing the drying mechanical stop triggers data acquisition.	An in situ (i.e., underneath the plasma) drying cycle was used.	**1984**	**78**
Salin (Habib & Salin)	Vertical/ Graphite cup	Conventional undercut dc arc.	Manual, the sample carrying probes are inserted axially into the torch.	Modified Fassel-type with no central tube. The central tube was replaced with a movable quartz tube that provides support to the electrode assembly.	An electrode, placed on top of a lead screw, is manually inserted into the ICP. The plasma is extinguished in order to run new samples or electrodes. The objective was electrochemical sample preconcentration and separation, rather than the design and characterization of a DSID.	Drying inside the plasma torch with the plasma off and 30 Watts of applied forward power for 1 min.	**1985**	**79**
Salin (Monasterios, Jones & Salin)	Vertical/ Graphite Cup	Conventional undercut dc arc graphite electodes and graphite electrodes with deep craters. Boiler cups, reportedly decreasing the heating rate of the electrode, were also used.	Manual, the electrodes are inserted axially into the torch.	Modified Fassel-type with no central tube. The central tube was replaced with a movable quartz tube that provides support to the electrode assembly.	An electrode, placed on top of a lead screw, is manually inserted into the ICP. The plasma extinguished in order to run new samples/electrodes.	External.	**1986**	**80**

Table 1-2. Continued.

Group	DSID Type	Probe(s)	Insertion	Torch	DSID description	Dry/Ash	Year	Ref
Salin (Sing & Salin)	Vertical or Horizontal/ Wire-loop	W or Ta wire-loop.	Pneumatic or stepper-motor driven. The wire-loop is inserted axially into the torch.	Modified Fassel-type with no central tube. The central tube was replaced with a movable quartz tube that provides support to the electrode assembly.	The wire-loop, powered by an independent Ar cylinder, is pneumatically driven into the ICP. The DSID can be either pneumatically or stepper-motor controlled. The wire-loop ICP-MS-DSID, is operated horizontally, manual or vaccum retraction is used.	????	1986	81
Salin (Boomer, Powell, Sing & Salin)	Horizontal/ Wire-loop	W wire-loop.	Pneumatic, the electrodes are inserted axially into the torch.	????	The wire-loop, powered by an independent Ar cylinder, is pneumatically driven into the ICP.	An in situ (i.e., underneath the plasma) drying cycle was used.	1986	82
Umemoto (Umemoto & Kubota)	Vertical/ Graphite cup	Graphite electrodes. ID: 3-mm; 3.5-mm deep; 0.2-mm wall; machined out of graphite rods.	Manual, the graphite electrodes are inserted axially into the torch.	Modified Fassel-type with a central channel but no central tube gas.	The cup position is adjusted by rotating a screw stopper. The plasma is extinguished in order to run new samples/electrodes.	Drying inside the plasma torch for 30 sec @ 200 W with the plasma off.	1987	84

Table 1-3. ICP and Instrumentation.

Group	Power	ICP and Spectrometer	Readout electronics	Software	Year	Ref
Bastiaans (Prack & Bastiaans)	1.25 kW	A Plasma Therm HFP-1500 D RF generator equipped with an MN 1500 E matching network, a PT 1500 matching box and a SPEX 0.5-m Czerny-Turner monochromator.	DEC PDP 11/34 minicomputer.	Not mentioned.	**1983**	**50**
Broekaert (Zaray, Broekaert, Leis)	3.0 kW	An 10 kW, FS-10 (Kontron-Linn) 27.12 MHz free-running ICP equipped with a Greenfield-type torch; a computer-controlled, 0.9-m Czerny-Turner monochromator and a 1-m, Paschen-Runge polychromator.	An Intel 88/25 single board microcomputer (based on an Intel 8088 CPU) front-ended with a 12-bit ADC.	Not mentioned.	**1986**	**51**
Broekaert (Zaray, Burba, Broekaert & Leis)	3.0 kW	An 10-kW, FS-10 (Kontron-Linn) 27.12 MHz free-running ICP equipped with a Greenfield-type torch; a computer-controlled, 0.9-m Czerny-Turner monochromator and a 1-m, Paschen-Runge polychromator.	An Intel 88/25 single board microcomputer (based on an Intel 8088 CPU) front-ended with a 12-bit ADC.	Not mentioned.	**1988**	**52**
Haraguchi (Haraguchi, Abdullah, Hasegawa, Kurosawa & Fuwa)	Optimum at 0.9 kW (varied from 0.7 to 1.5 kW in increments of 200 Watts)	A Jarrell-Ash (Plasma AutoComp Mk II) plasma spectrometer was used. This system consists of a 2.5 kW, 27.12 MHz Plasma Therm RF generator, a Paschen-Runge, 0.75-m direct reading spectrometer and a Jarrell-Ash (model 82-00) 0.5-m, Ebert monochromator.	A high speed current amplifier (Keithley model 427) and a chart recorder were utilized.	No description.	**1984**	**53**
Haraguchi (Abdullah, Fuwa & Haraguchi)	Optimum at 0.95 kW (varied from 0.7 to 1.4 kW in increments of 200 Watts)	A Jarrell-Ash (Plasma AutoComp Mk II) plasma spectrometer was used. This system consists of a 2.5 kW, 27.12 MHz Plasma Therm RF generator, a Paschen-Runge, 0.75-m direct reading spectrometer and a Jarrell-Ash (model 82-00) 0.5-m, Ebert monochromator.	A high speed current amplifier (Keithley model 427) and a chart recorder were utilized.	No description.	**1984**	**54**
Haraguchi (Abdullah, Fuwa & Haraguchi)	1.2 kW	A Jarrell-Ash (Plasma AutoComp Mk II) plasma spectrometer was used. This system consists of a 2.5 kW, 27.12 MHz Plasma Therm RF generator, a Paschen-Runge, 0.75-m direct reading spectrometer and a Jarrell-Ash (model 82-00) 0.5-m Ebert monochromator.	A high speed current amplifier (Keithley model 427) and a chart recorder were utilized.	Designed for DSID automation and control but not for data processing or data display.	**1985**	**55**
Haraguchi (Abdullah, Fuwa & Haraguchi)	0.95 kW	A Jarrell-Ash (Plasma AutoComp Mk II) plasma spectrometer was used. This system consists of a 2.5 kW, 27.12 MHz Plasma Therm RF generator, a Paschen-Runge, 0.75-m direct reading spectrometer and a Jarrell-Ash (model 82-00) 0.5-m Ebert monochromator.	A high speed current amplifier (Keithley model 427) and a chart recorder were utilized.	Designed for DSID automation and control but not for data processing or data display.	**1985**	**56**

Table 1-3. Continued.

Group	Power	ICP and Spectrometer	Readout electronics	Software	Year	Ref
Horlick (Salin & Horlick)	2.0 kW	A 2.5 KW, 27.12 MHz, Plasma Therm RF generator and a diode array spectrometer mounted on a McPherson 0.35-m Czerny-Turner monochromator equipped with a single PMT channel were used. A Baush & Lomb 2 m dual-grating spectrograph with a photographic plate attatchment (for SA-1 plates) was also utilized.	PDP 8/e minicomputer front-ended with a 10-bit ADC. An oscilloscope/chart recorder was used for signal display/registration.	No description.	1979	57
Horlick (Pettit & Horlick)	2.0 kW	A 2.5 KW, 27.12 MHz, Plasma Therm RF generator and a computer controlled diode array spectrometer mounted on a McPherson 0.35-m Czerny-Turner scanning monochromator with a single photomultiplier tube channel were used.	DEC PDP 11 minicomputer front-ended with a 10-bit ADC. A CRT was used for signal display.	No description.	1986	58
Horlick (Shao & Horlick)	1.2 or 1.5 kW (varied from 1.2 to 1.9 kW)	An ARL 34000 ICP spectrometer system was utilized. This system consists of a 2.0 KW, 27.12 MHz Plasma Therm RF generator and a 34-channel polychromator.	DEC PDP 11 minicomputer and standard ARL elecctronics. A common integration time (40 sec) was used for all channels. A high speed current amplifier and a chart recorder as also used. Readout electronics & signal processing are singled out as areas in need of further development.	Not mentioned.	1986	59
Horlick (Karanassios & Horlick)	1.25 kW	A continuously operating 17.12 MHz Ar ICP was fitted with a computer controlled, vertically operated, pneumatically and mechanically driven DSID capable of handling up to 24 sample carrying probes in an automated fashion and it was coupled to a 1-m, 29 channel polychromator. Plasma, DSID and direct reader were mounted on an optical rail bed.	A four-channel readout electronics sub-system was developed around a bank of operational amplifiers, a Data Translation DT2801 data acquisition board and an IBM PC microcomputer.	Extensive. The window-based software package developed for the IBM PC is described in detail.	1988	61
Horlick (Karanassios & Horlick)	1.25 - 2.0 kW in increments of 250 Watts	A continuously operating 17.12 MHz Ar ICP was fitted with a computer controlled, vertically operated, pneumatically and mechanically driven DSID capable of handling up to 24 sample carrying probes in an automated fashion and it was coupled to a 1-m, 29 channel polychromator. Plasma, DSID and direct reader were mounted on an optical rail bed.	A four-channel readout electronics sub-system was developed around a bank of operational amplifiers, a Data Translation DT2801 data acquisition board and an IBM PC. Data were serially transferred to an Apple Macintosh (front-end processor) for further processing.	No description. They have utilized the software package (previously developed) for the IBM PC.	1988	62
Horlick (Karanassios, Abdullah & Horlick)	1.25 kW	A continuously operating 17.12 MHz Ar ICP was fitted with a computer controlled, vertically operated, pneumatically and mechanically driven DSID capable of handling up to 24 sample carrying probes in an automated fashion and it was coupled to a 1-m, 29 channel polychromator. Plasma, DSID and direct reader were mounted on an optical rail bed.	A four-channel readout electronics sub-system was developed around a bank of operational amplifiers, a Data Translation DT2801 data acquisition board and an IBM PC. The acquired data were serially transferred to an Apple Macintosh (front-end processor) for further processing.	No description. They have utilized the software package (previously developed) for the IBM PC.	1988	63
Horlick (Karanassios & Horlick)	1.25 or 1.5 kW	A Sciex-Elan ICP-MS system was utilized.	The multibus-based microcomputer of the Sciex Elan ICP-MS system does data acquisition. The acquired data are serially transferred (in high speed) to an Apple Macintosh microcomputer for further processing.	Developed for the Macintosh, it supports high speed transfers and implements the virtual reality concept.	1988	64

Table 1-3. Continued.

Group	Power	ICP and Spectrometer	Readout electronics	Software	Year	Ref
Kirkbright (Kirkbright & Walton)	Optimum at 1.0 kW (varied form 0.6 to 1.3 kW in increments of 100 Watts)	A 1.5 KW, 27.12 MHz, Plasma Therm RF generator and a single-channel, 1-m grating monochromator (Monospek 1000, Rank Hilger) were used.	Both a slow and a fast response chart recorder and a digital storage oscilloscope were used.	No description.	1982	65
Kirkbright (Kirkbright & Li-Xing)	Optimum power was element dependent (varied from 0.8 to 1.0 kW)	A 1.5 KW, 27.12 MHz, Plasma Therm RF generator and a single-channel, 1-m grating monochromator (Monospek 1000, Rank Hilger) were used.	A fast response chart recorder was used.	No description.	1982	66
Kirkbright (Li-Xing, Kirkbright, Cope & Watson)	1.0 kW	A 1.5 KW, 27.12 MHz, Plasma Therm RF generator and a single-channel, 1-m grating monochromator (SPEX industries) were used.	A fast response chart recorder was used.	No description.	1983	67
Kirkbright (Barnett, Cope, Kirkbright & Taobi)	1.0 kW (??)	A 1.5 KW, 27.12 MHz, Plasma Therm RF generator and a single-channel, 1-m grating monochromator (SPEX industries) were used.	A fast response chart recorder was used.	No description.	1984	68
Lorber (Lorber & Goldbart)	1.4 kW	A 2.5 KW, 27.12 MHz Plasma Therm RF generator and a Jobin Yvon JY48P, 48-channel direct reading spectrometer was used.	Standard JY48P electronics and microcomputer.	No description.	1985	69
Lorber (Brenner, Lorber & Goldbart)	1.25 and 2.0 kW	A 2.5 KW, 27.12 MHz Plasma Therm RF generator and a Jobin Yvon JY48P, 48-channel direct reading spectrometer was used.	Standard JY48P electronics and microcomputer.	No description.	1987	70
McLeod (Mcleod, Clarke & Mowthorpe)	1.0 kW typical (varied from 0.8 to 1.8 kW in increments of 200 Watts)	A Jarrell-Ash ICAP 9000 direct reading spectrometer was used.	Standard Jarrell-Ash ICAP 9000 electronics and an Apple II microcomputer.	Standard ICAP 9000 software for data acquisition and display.	1986	71

Table 1-3. Continued.

Group	Power	ICP and Spectrometer	Readout electronics	Software	Year	Ref
Ohle (Sommer & Ohle)	3.0	A <4.5 KW (max 7.0 kW), 27.12+/- 0.11 MHz, free running, Kontron/Linn RF generator was used. Both, a simultaneous (1.5 m, ARL 15000) and a sequential (0.6 m, Labtest V25) spectrometer were utilized.	No information available, conference report.	Not mentioned.	1980	72
Ohle (Ohle & Sommer)	3.0	A <4.5 KW (max 7.0 kW), 27.12+/- 0.11 MHz, free running, Kontron/Linn RF generator was used. Both, a simultaneous (1.5 m, ARL 15000) and a sequential (0.6 m, Labtest V25) spectrometer were utilized.	Microcomputer controlled data acquisition. "... a microcomputer was included which obtained, transferred and printed data".	Not mentioned.	1981	73
Ohle (Ohle)	3.0	A <4.5 KW (max 7.0 kW), 27.12+/- 0.11 MHz, free running, Kontron/Linn RF generator was used . Both, a simultaneous and a sequential spectrometer were utilized.	Microcomputer controlled data acquisition.	Not mentioned.	1984	74
Page (Page, Madraswala, Godbole, Kulkarni, Mallapurkar & Joshi)	1.08 kW	A 2.5 KW, 27.12 MHz RF generator supplied with a Jarrell-Ash, Atom Comp 1000, 0.75-m (48 channels and an N+1 channel) direct reading spectrometer.	DEC PDP 11/23 minicomputer and standard Jarrell-Ash electronics.	No description.	1983	75
Page (Page, Godbole, Madraswala, Kulkarni, Mallapurkar & Joshi)	1.4 kW	A 2.5 KW, 27.12 MHz RF generator supplied with a Jarrell-Ash, Atom Comp 1000, 0.75-m (48 channels and an N+1 channel) direct reading spectrometer.	DEC PDP 11/23 minicomputer and standard Jarrell-Ash electronics.	No description.	1984	76
Salin (Salin & Habib)	2.0 kW	A 2.5 KW, 27.12 MHz Plasma Therm RF generator and a Jarell-Ash, 0.5-m Ebert monochromator, with a single photomultiplier tube (1P28) channel were used.	A strip chart recorder or an 8-bit ADC interfaced to an AIM 65 microcomputer were utilized.	Very brief mention. A program written in BASIC was used for peak height and peak area calculations.	1984	77
Salin (Salin & Sing)	1.75 kW	A 2.5 KW, 27.12 MHz Plasma Therm RF generator and a Jarell-Ash, 0.5-m Ebert monochromator, with a single photomultiplier tube (1P28) channel were used.	A strip chart recorder or an 8-bit ADC interfaced to an AIM 65 microcomputer were utilized.	Very brief mention. A program written in BASIC was used for peak height and peak area calculations.	1984	78

Table 1-3. Continued.

Group	Power	ICP and Spectrometer	Readout electronics	Software	Year	Ref
Salin (Habib & Salin)	2.0 kW	A 2.5 KW, 27.12 MHz Plasma Therm RF generator and a Jarell-Ash, 0.5-m Ebert monochromator, with a single photomultiplier tube (1P28) channel were used.	A strip chart recorder or an 8-bit ADC interfaced to an AIM 65 microcomputer were utilized.	Very brief mention. A program written in BASIC was used for peak height and peak area calculations.	1985	79
Salin (Monasterios, Jones & Salin)	2.0 kW	A 2.5 KW, 27.12 MHz Plasma Therm RF generator and a Jarell Ash, 0.5-m Ebert monochromator were used.	A strip chart recorder or a 12-bit ADC interfaced to an AIM 65 microcomputer. The data were then transferred to an S-100 bus-based microcomputer (Z80 CPU), for further processing.	Brief mention. The S100 μC performs data processing and display. Software examples are not shown.	1986	80
Salin (Sing & Salin)	?	A 2.5 KW, 27.12 MHz Plasma Therm RF generator and a Jarell-Ash, 0.5-m Ebert monochromator, with a single photomultiplier tube (1P28) channel were used for the AES work. A SCIEX-Elan (model 250) mass spectrometry system was utilized for mass spectrometric detection.	A strip chart recorder or a 12-bit ADC interfaced to an AIM 65 microcomputer. The data are transferred to a Z80, S-100 bus-based microcomputer, for further processing. Unmodified Sciex Elan electronics and a Multibus-based microcomputer were used with the ICP-MS system.	According to the authors, software is important because peak half widths are in the order of 100's of milliseconds.	1986	81
Salin (Boomer, Powell, Sing & Salin)	Optimum at 0.95 kW	A 2.5 KW, 27.12 MHz Plasma Therm RF generator supplied with a SCIEX-Elan (model 250) mass spectrometry system were used.	Unmodified Sciex-Elan electronics and a Multibus-based microcomputer were used for the ICP-MS work.	An important consideration due to the transient signals generated by the wire-loop system. No further description.	1986	82
Umemoto (Umemoto & Kubota)	1.4 and 1.6 kW (varier from 1.0 to 1.8 in increments of 200 Watts)	A 2.5 KW, 27.12 MHz Kyoto Konen RF generator and a 0.8-m, scanning, computer controlled, echelle monochromator (Kyoto Konen model UOP-1 Mark II) were used.	Lock-in amplifier and a chart recorder.	No description.	1987	84

Table 1-4. Optimization.

Group	Optimization	Year	Ref
Broekaert (Zaray, Broekaert, Leis)	Electrode geometry, size, insertion position and plasma observation height were optimized with dryed solution residues of Cu, Sr and Zn. The optimum cup insertion position was found to be the "0-mm" position (i.e., TOLC).	1988	51
Haraguchi (Haraguchi, Abdullah, Hasegawa, Kurosawa & Fuwa)	Simplex with a univariate search was applied on the following parameters: cup insertion position relative to TOLC, depth of recess in the cup, RF power (defined as Forward minus Reflected), observation height, lateral plasma viewing position, and outer tube- and intermediate tube-gas flow rates. These parameters were optimized for maximum SBR of the Mn II 256.7 nm line (utilizing a 5 µl, 50 ppb Mn solution). The final conditions represent a compromise between all optimized variables, as follows: graphite cup (ID: 2.5-mm; depth: 2-mm); cup position (4-mm above TOLC); RF power (0.9 KW); observation height (16-mm above TOLC); lateral viewing position (plasma center); outer tube-gas flow rate (17 L/min Ar); and intermediate tube-gas flow rate (1.4 L/min Ar).	1984	53
Haraguchi (Abdullah, Fuwa & Haraguchi)	Simplex with a univariate search was applied on the following parameters: cup insertion position relative to TOLC, RF power (defined as Forward minus Reflected), observation height, and outer tube- and intermediate tube-gas flow rates. These parameters were optimized for maximum SBR of Co, Cr, Cu, Mg, Mn, Na, Ni & Pb lines (utilizing 10 µl injections of a 1 ppm multielement solution). The final conditions represent a compromise between all optimized variables, and were as follows: cup position (2-mm above TOLC); RF power (0.95 KW); observation height (16-mm above TOLC); lateral viewing position (plasma center); outer tube-gas flow (17 L/min of Ar); intermediate tube gas-flow (1.4 L/min of Ar); and central tube-gas flow (0.1 L/min of Ar). From their results (numurous figures shown) it was concluded that SBRs were element dependent. Optimization of the parameters of the drying and ashing cycles was also performed for solution samples.	1984	54
Haraguchi (Abdullah & Haraguchi)	The operating conditions for direct analysis of plant samples were optimized for maximum SBR of the Mn II 257.6 nm line, utilizing 2 mgs of Orchard leaves (NBS-SRM 1571). This line was chosen as it represents all 'hard' and 'soft' lines in the ICP. The optimum conditions were as follows: Cup position (2.2-mm above TOLC); RF power (1.2 KW); observation height (14-mm above TOLC); lateral viewing position (plasma center); outer tube-gas flow (17 L/min of Ar); intermediate tube-gas flow (0.6 L/min of Ar); and central tube-gas flow (0.1 L/min of Ar). Optimization of ashing parameters for 4 mg of plant samples was also performed, an optimum cup height of 11±1 mm below the body of the plasma and an optimum 5-6 min time was reported.	1985	55
Haraguchi (Abdullah, Fuwa & Haraguchi)	Of electrolysis parameters.	1985	56
Horlick (Shao & Horlick)	The effect of cup insertion position on peak heights was investigated for several elements. Their results indicate that peak intensities are strongly dependent on cup insertion position, "with a 1-mm difference resulting in a 10% signal change" for some elements. The degree of change, however, it was found to be element dependent. For example, as cup insertion position inceases (from 2 mm below TOLC to 6 mm above TOLC) peak heights decrease for As, Pb & Sn; they increase for Li; and the peak height remains relatively constant for Ag. The observation height for these experiments was fixed at 15-mm above the load coil, and according to the authors, a sub-optimal readout electronics sub-system was utilized.	1986	57

Table 1-4. Continued.

Group	Optimization	Year	Ref
Horlick (Karanassios, Horlick & Abdullah)	Optimization of cup insertion position with respect to SBRs for dryed solution residues of Cr, Mn, Cu and Cd. The "0-mm" position (i.e., TOLC) was found to be the optimum insertion position. In terms of an optimum cup geometry, a 'long undercut' graphite electrode was found to give the best SBRs for most elements tested.	1988	62
Horlick (Karanassios & Horlick)	In contrast with the results reported for conventional pneumatic nebulizer systems, the central tube flow rate (i.e., nebulizer flow rate) was found to have very little effect on analyte emission temporal behavior.	1988	63
Kirkbright (Kirkbright & Walton)	Simplex with a univariate search was applied on the following parameters: cup insertion position relative to TOLC, RF power (defined as Forward minus Reflected), observation height, rod height, outer tube and intermediate tube gas flow rates. These parameters were optimized (utilizing 5 µl injections of a 100 ppb Mn solution) for maximum SBR of the Mn II 256.7 nm line. A lateral scan of the plasma revealed that the best lateral observation position is in the center of the plasma. A central tube gas flow rate of 0.2 L/min produced the best SBRs, however, a difficulty was experienced in sustaining the plasma.	1982	65
Kirkbright (Kirkbright & Li-Xing)	Simplex with a univariate search was applied on the following parameters: cup insertion position relative to TOLC, RF power (defined as Forward minus Reflected), observation height, rod height, outer tube gas flow rate, intermediate tube gas flow rate and central tube gas flow rate. These parameters were optimized (utilizing 5 µl injections of a multielement solution) for maximum SBR of Ag, B, Cr, Cu, Mo, Ti, U, Zn & Zr. The cup insertion position was found to be element dependent, optimum cup positions ranging form 3 mm below TOLC (for Zn) to 6 mm above TOLC for Cr were reported. (Plasma observation height and forward power were also varied).	1982	66
Kirkbright (Li-Xing, Kirkbright, Cope & Watson)	The effect of plasma operating parameters on the optimal rod position for the dessolvation of aqueous solutions underneath the plasma was studied. Outer tube- and intermediate tube-gas flow rates were found to have little effect on the optimal rod position, however, a central tube-gas flow rate and forward power were found to exert considerable influence.	1983	67
Kirkbright (Barnett, Cope, Kirkbright & Taobi)	The objective was to establish the optimum electrode geometry that produces the fastest heating rate and to document the effect of electrode geometry on analyte emission temporal behavior.	1984	68

Table 1-4. Continued.

Group	Optimization	Year	Ref
Page (Page, Madraswala, Godbole, Kulkarni, Mallapurkar & Joshi)	Their goal was to optimize the background subtracted analyte signal intensities of volatile elements in Uranium oxide. An optimum RF power of 1.08 KW; an outer tube-gas flow rate of 22 L/min; an intermediate tube-gas flow of 0.6 L/min; an observation height of 6 mm above TOLC; and a lateral viewing position of 1.5-mm off axis were reported.	1983	75
Page (Page, Godbole, Madraswala, Kulkarni, Mallapurkar & Joshi)	Optimized for maximum ICP response (although the term 'response' was not defined) for: cup insertion position; sample size; outer tube- and intermediate tube-gas flow rates; integration time; observation height; lateral viewing position and forward power. A modified Simplex method was applied for the optimization of: observation height; lateral viewing position and forward power. These were optimized for maximum Boron 'response'. Their results are summarized as follows: outer tube-gas flow rate (22 L/min); intermediate tube-gas flow rate (1 L/min); sample size (100 mg); forward power (1.4 KW); reflected power (<20W); observation height (15-mm above TOLC); lateral viewing position (plasma center); cup insertion position (0-mm avove TOLC). According to the authors, these settings gave "....very high signal to blank ratio for all analyte elements".	1984	76
Salin (Salin & Sing)	The optimum operating conditions for Cu (from solution residues) were established for two parameters: observation height and final insertion position of the wire-loop. The best response (?) was achieved when the wire-loop was inserted at 2-mm below TOLC and by observing the center of the plasma.	1984	78
Salin (Habib & Salin)	Optimization of sample drying time.	1985	79
Salin (Boomer, Powell, Sing & Salin)	Univariate search was performed in order to optimize the SBR of a Mn solution. The following results were obtained: orifice distance (-1 mm form the tip of the plume); insertion distance (9-mm from TOLC); plasma power (0.95 KW); outer tube-gas flow (14 L/min); intermediate tube-gas flow (2.0 L/min); central tube-gas flow rate (0.75 L/min); ion optics (BBA -6.1 V); ion optics (BBB/photon stop +4.7 V); ion optics (BBC -9.1 V); ion optics (ring lens -6.9 V).	1986	82
Umemoto (Umemoto & Kubota)	Optimized for As and Sb (with respect to SBRs) for applied forward power and cup insertion position.	1987	84

Table 1-5. Survey results.

Group	Samples	Temporal	Modification	Power Studies	Temperature	Year	Ref
Bastiaans (Prack & Bastiaans)	Solids (oxides diluted with graphite)	Several examples are shown for mixtures of Pb & V salts and oxides.	No data	No data	A thermocouple was used for temperatures of <1000 °C, for temperatures of >1000 °C oxides and chlorides were used. Cup temperature was estimated to be 1800 °C.	1983	50
Broekaert (Zaray, Broekaert, Lele)	Liquids and solids (Al oxide powder)	Shown for Al, Cu, Mg and Zn form 2.5 mg of Aluminium oxide; form 2.5 mg Aluminium oxide plus 2.5 mg graphite; and form 2.5 mg Aluminium oxide plus 2.5 mg graphite plus PTFE. Also shown for Al, Cu, Mg and Zn from 10 mg Aluminum oxide plus 10 mg graphite and for Zn (both signal and background) from Aluminium oxide and graphite (5 mg each). Ti emission was not observed unless a thermochemical reagent was used.	The effect of Ammonium chloride, Silver chloride, Barium fluoride and PTFE on Ti temporal emission behavior was investigated.	No data	Estimated to be about 3000°C utilizing metal strips.	1987	51
Broekaert (Zaray, Burba, Broekaert & Lele)	Solids	Shown for Mn, Cu and Pb from 5 mg of HYPHAN-cellulose and for Fe with and without the addition of HCl.	Addition of HCl on dryed solution residues of Fe produces peaks with a shorter appearance time, the Fe signal returnes to its pre-insertion value after 24 s.	No data	No data	1988	52
Haraguchi (Haraguchi, Abdullah, Hasegawa, Kurosawa & Fuwa)	Liquids	Shown for solution samples of Cr, Mn, Ni, Pb & Zn (under optimized conditions).	No data	Power (kW) vs SBR for a 5 µl injection of 50 ppb Mn solution is shown.	No data	1984	53

Table 1-5. Continued.

Group	Samples	Temporal	Modification	Power Studies	Temperature	Year	Ref
Haraguchi (Abdullah, Fuwa & Haraguchi)	Liquids and digested powdered botanicals	Shown for solution samples of Al (1.0 ppm), Cd (0.1 ppm), Co (0.5 ppm), Cr (0.1 ppm), Fe (.01 ppm), Mg (0.1 ppm), Mn (0.1 ppm) & Pb (0.5 ppm) at 1.1 KW. The emission signal for Cd and Pb is not well resolved from the change in background due to cup insertion. Carbide forming elements (i.e., B, La, Sr, Ti, Zr and Y) could not be determined.	No data	Power (kW) vs SBR is shown for Cd, Co, Cr, Cu, Mg, Mn, Ni, Pb & Zn from a multielemnt solution and for powers from 0.7 to 1.4 kW in increments of 100 Watts. Power was found to exert a considerable influence on SBRs and to be element dependent. Optimium power for Co, Mg & Pb was at 0.7 kW; for Ni at >1.1 kW. The optimium power for most elements was found to be at 0.95 kW.	No data	1984	54
Haraguchi (Abdullah & Haraguchi)	Liquids and powdered botanicals	Shown for Mn in orchard leaves (4 mg of NBS SRM 1571) and for Cd & Pb in tomatoe leaves, (4 mg of NBS SRM 1573) @ 1.2 kW. Carbide forming elements (i.e., Al, B, Ca, La and Sr) could not be determined.	Significant enhancements in sensitivity were observed for carbide forming elements (i.e., Ba, La, Sr and Ti) when high salt (i.e., NaCl, KCl) concentrations were used. Supressions were observed for Ba, La and Sr when Calcium chloride and Magnesium chloride were used.	No data	Estimated using 1 to 3 mg of powdered samples of Co, Cu, Fe & Ti. The cup temperature was estimated to be at about 3200 °C.	1985	55
Haraguchi (Abdullah, Fuwa & Haraguchi)	Aqueous (artificial sea wate, matrix NaCl, KCl & MgCl2)	No data	No data	No data	No data	1987	56
Horlick (Salin & Horlick)	Liquids and solids (SPEX G, 49 element standard and powdered coal and botanicals)	Shown for 5 µl of 1 ppm Zn and Cd. From these results it was concluded that "...this sampling system will require extensive characterization in the time domain".	No data	No data	No data	1979	57

Table 1-5. Continued.

Group	Samples	Temporal	Modification	Power Studies	Temperature	Year	Ref
Horlick, (Pettit & Horlick)	Liquids and powders (coal and botanicals)	Time resolved spectra for solution samples of Cd, In, Mn, Ni & Zn (diode array system); temporal behavior for Cd, In, Mn, Ni & Zn (PMT system, an Argon-Oxygen mixed-gas plasma and graphite cups) and temporal behavior for Ni & Zn with metal cups (i.e., Ta, Mo & W) and an Argon-Hydrogen mixed-gas plasma are shown.	The effect of 1-6% Oxygen on the temporal behavior of Cd, In, Mn, Ni & Zn with graphite cups and of 1% Hydrogen on Cd, In, Ni & Zn with metal cups is shown. In general, mixed-gases enhance signal intensities, the peak-like signals get sharper and appear faster. With Hydrogen, metal cups remain clean and re-usable for hundreds of times.	No data	No data	**1986**	**58**
Horlick (Shao & Horlick)	Aqueous, digested botanicals and solids (SPEX G and TS-6 oxide standards.	Shown for solutions of Ag, As, Cr, Cu & Sb and for Cu solutions in cups of 3-, 4.5- and 6-mm OD. Also, temporal behavior (registered on a chart recorder) for a 20 pg of Ag, Cd, & Zn. No signal intensity was observed for powdered samples at the 33 ppm level for Zr, V, Sn, Ba, Al, Si and K.	Preliminary results using NaF show considerable enhancements in the sensititivity of Zr, V, Sn, Ba, Al, Si and K.	In general, peak intensities for As, Cd, Cu, In, Li, Mg, Na, Pb, Sb, Mn, Sn & Zn are relatively insensitive to power. Three examples are given: Cu temporal behavior @ 1.2, 1.5 & 1.9 kW (with the same peak intensities); superimposable calibration curves for a solution of Ag; and for As from powder samples (@ 1.2 & 1.5 kW). The calibration curve for Cr shows a power dependence.	No data	**1986**	**59**
Horlick (Karanassios & Horlick)	Liquids	Shown for Ag, Co, Cu and Mn and for 25 ng of Cu solution residue for: a long undercut graphite electrode (machined out of a SPEX HPND+ 4021 electrode), a Ta metal cup, W metal cup and a W wire loop.	No data	No data	No data	**1988**	**61**
Horlick (Karanassios, Horlick & Abdullah)	Liquids	Shown for Ag, Cd, Co, Cr, Cu, Fe, Mn, Mg, Ni, Si, Sn and Zn and for Cu, Ni, Sn and Zn for four electrode types and for powers of 1.25 kW to 2.00 kW in increments of 250 Watts. Also for Cd and Mn (100 pg each) for a long undercut electrode and at 2.00 kW. Finally, for Cd, Cr, Cu and Ni for long undercut electrodes, and Ta and W metal cups. Little or no signal at all was observed for Al, Ca, Sr, Ti and Zr.	No data	The effect of power: on peak heights, peak areas and SBRs is shown for Ag, Cd, Co, Cu, Fe, Sn, Ni and Zn; and on temporal behavior is shown for Cu, Sn, Ni and Zn for four electrode geometries and powers of 1.25 kW to 2.0 kW in increments of 250 Watts. The effect of power on the appearance time of Ag, Cd, Co, Cu, Fe, Ni, Sn & Zn and for four electrode types is also shown.	No data	**1988**	**62**

Table 1-5. Continued.

Group	Samples	Temporal	Modification	Power Studies	Temperature	Year	Ref
Horlick (Karanassios, Abdullah & Horlick)	Liquids and solids (powdered Calcium sulfate)	Shown for water blank and for Al, Ca, Sr & Zr. Also, for Al with KCl, KF, NaCl and NaF; for Zr with KCl, KF, NaCl and NaF; and for Al, Ca, Sr, Ti and Zr with NaF.	KCl, KF, NaCl and NaF were used as volatilization enhancing agents. These were applied on both liquid and powdered samples. Considerable enhancements in sensitivity and the analytical figures-of-merit were reported with the use of NaF which was subsequently used for the determination of B in Calcium sulfate.	No data	No data	1988	63
Horlick (Karanassios & Horlick)	Liquids	Shown for Cu, Mg, Mn and Zn form graphite cups, Ta and W metal cups; and a W wire-loop. Emission intensity for U was not observed, this was attributed to carbide formation.	NaF was used as a volatilization enhancing agent.	Shown for Cu, Mg, Mn and Zn form graphite cups, Ta and W metal cups; and a W wire-loop at 1.25 kW and 1.5 kW.	No data	1988	64
Kirkbright (Kirkbright & Walton)	Liquids	Shown for solution samples of Cd, Co, Mn, Ni & Pb (0.5 ng each) and Fe (5.0 ng).	No data	Power (kW) vs SBR for 5 µl of 50 ppm solution of Mn (257.6 nm line) for power settings of 0.6 to 1.3 kW in increments of 100 Watts, the optimum power was found to be at about 1.0 kW.	No data	1982	65
Kirkbright (Kirkbright & Li-Xing)	Liquids	An emission signal was not observed unless Freon was used.	An Argon/Freon (0.1%) mixture was used as the central tube gas. Freon was used as a volatilization enhancing agent, significant improvements (i.e., a 100-fold enhancement in the sensitivity of Ti, U and Zr) were observed. The use of Freon was also found to improve precision.	No temporal data, but studied as part of the optimization procedure. The optimum power setting were as follows: Ag (760 W); B (855 W); Cr (740 W); Cu (775 W); Mo (800 W); Ti (710 W); U (800 W); Zn (970 W) and Zr (900 W). The heating rate and the final temperature of the graphite rod were found to be power dependent.	The outer surface of the graphite rod was estimated to be at about 4000 °C.	1982	66

Table 1-5. Continued.

Group	Samples	Temporal	Modification	Power Studies	Temperature	Year	Ref
Kirkbright (Li-Xing, Kirkbright, Cope & Watson)	Liquids.	No data	No data	No data	The effect of cup position during the drying and ashing cycles was investigated.	1983	67
Kirkbright (Barnett, Cope, Kirkbright & Taobi)	Liquids	Shown for solution samples of Cr, Mn, Ni & Pb for four graphite electrode geometries. Peak heights and temporal behavior was found to be electrode geometry dependent.	No data	No data	Measured using a radiation thermometer for four electrode geometries. Equilibrium temperatures of about 1800 °C (attained after 3 to 8 s) were measured.	1984	68
Lorber (Lorber & Goldbart)	Liquids and solids (Uraniom oxide)	Not shown, although temporal behavior for several elements is described.	Matrix modification with AgCl/NaF (5/3 m/m). A 2% concentration of the carrier was mixed with the matrix.	No data	Measured at the center of the cup using an optical pyrometer. Temperatures of 1600 °C @ 1.2 kW and of 2050 °C @ 2.2 kW were reported.	1985	69
Lorber (Brenner, Lorber & Goldbart)	SRM silicates.	Not shown, but a volatilization sequence for a wide range of volatile elements in glasses and synthetic standards with and without graphite at two power settings (1.25 kW and 2.0 kW) is shown instead.	No data, however, samples were mixed with graphite.	SBR vs volatilization time of silicate glass for Zn and Cd without graphite at 1.25 kW and 2.0 kW and for Zn and Cd with graphite (1 part sample & 5 parts graphite) at 1.25 and 2.0 kW are shown.	No data	1987	70

Table 1-5. Continued.

Group	Samples	Temporal	Modification	Power Studies	Temperature	Year	Ref
McLeod (Mcleod, Clarke & Mowthorpe)	Liquids and solids (Ni-base alloys)	Shown for Mg & Pb (injections of 5 µl of 1 ppm solution) and for solid samples (5 mg of alloy BAS 346) @ 0.8 to 1.8 kW (in 200 Watt increments). Also, for Al, Co, Cr & Ni from solid ssamples (5 mg of alloy BAS 346) @ 1.0, 1.4 & 1.8 kW. Different temporal behavior was observed for the same element from solution residues and from solid samples. Emission was not observed for Mo and Ti for solution residues and for As and Se from Ni-base alloys.	No data	Signal, background and SBR for Cd, Mg, Pb & Zn aqueous solutions (1 ppm, 5 µl injections) and from 5 mg of brass samples are shown. Similar trends in SBRs were observed for both sample types. Applied forward power influences temporal behavior. An increase in emission intensity was observed with an increase in power.	Confirmation of previous reports (??) with 5 mg alloy chips.	1986	71
Ohle (Ohle Sommer)		Shown for 10 µl of solution samples of Te, Pb and Ni; discussed for As, Hg, Cd and Tl.	No data	No data, a free-running 3.0 kW Argon-Nitrogen mixed-gas plasma was used.	Estimated to be about 3000 °C.	1980	73
Ohle (Ohle)		No data	No data	No data, a free-running 3.0 kW Argon-Nitrogen mixed-gas plasma was used.	No data	1984	74
Page (Page, Madraswala, Godbole, Kulkarni, Mallapurkar & Joshi)	Liquids and solids (Uranium oxide SRM)	No data	Application of the carrier distillation method using AgCl as carrier.	No data	No data	1983	75

Table 1-5. Continued.

Group	Samples	Temporal	Modification	Power Studies	Temperature	Year	Ref
Page (Page, Godbole, Madraswala, Kulkarni, Mallapurkar & Joshi)	Solids (Uranium oxide)	Shown for solid samples of B, Fe & Li , with and without a lid. The lid was found to have a considerable effect on analyte emission temporal behavior of the elements tested.	Application of the carrier distillation method using AgCl as carrier.	No data	Estimated to be at about 1800 °C.	1984	76
Salin (Salin & Habib)	Liquids	Shown for a solution of Cu.	No data	No data	No data	1984	77
Salin (Salin & Sing)	Liquids	Raw signal, background and net signals are shown for a solution of Cu. A raw signal for Cu in the presence of high salt concentrations (0.1% Ca) is also shown.	No data	No data	Not data	1984	78
Salin (Habib & Salin)	Aqueous (artificial sea water)	Not shown, but the temporal behavior of Co in an Argon and an Argon-Oxygen mixed-gas ICP was briefly discussed.	Oxygen was used in the outer tube of the torch.	No data	No data	1985	79

Table 1-5. Continued.

Group	Samples	Temporal	Modification	Power Studies	Temperature	Year	Ref
Salin (Monasterios, Jones & Salin)	Solids (human hair)	Shown for a Cu solution (50 µl of 0.5 ppm) and for Cu in 0.542 mg of human hair. Also for a Zn solution (50 µl of 1.0 ppm) and for Zn in 0.186 mg of human hair.	No data	No data	No data	1986	80
Salin (Sing & Salin)	Liquids	No data	No data	No data	No data	1986	81
Salin (Boomer, Powell, Sing & Salin)	Liquids	Shown for a Cu solution (10 ppb, 10 µl injection) for both ICP-AES and ICP-MS.	No data	No data	No data	1986	82
Umemoto (Umemoto & Kubota)	Liquids and solids (dissolved iron and steel)	Shown for a solution of As for power settings of 1.2, 1.4, 1.6 and 1.8 kW.	No data	A power of 1.6 kW was used for As. Also, SBRs were found to decrease as power increased from 1.2 to 1.8 kW.	Estimated using 10 mg of 100 mesh Pt and Ti. Based on the boiling points of these elements, a cup temperature of about 3600 °K was proposed.	1987	84

Table 1-6. Performance characteristics.

Group	Samples	%RSD	Detection Limits	Calibration curves	Other/Comments	Year	Ref
Bastiaans (Prack & Bastiaans)	Solids (oxides diluted with graphite)	1-9% form powdered samples	No data	Although curves are not shown, quantitative data for the determination of the composition of mixtures of salts and oxides of Pd, Cd, Hg and V are presented in tabular form.	Temperature programming was accomplished by varying the insertion rate of the electrode into the plasma. A calibration curve of temperature vs cup height is also shown, a temperature of about 1800 °C (at TOLC) was estimated (by extrapolation). Advantages: simple system. Disadvantages: because some samples decompose to the same product, speciation could not be achieved. Other conclusions: sample size and cup position are important; better temperature control and finer resolution in temperature are required; chemical reactions between sample and the matrix must be considered. The use of pyrolytically coated cups or metal cups is suggested as the means to avoid carbide formation.	1983	50
Broekaert (Zaray, Broekaert & Leis)	Liquids and Solids (Al oxide powder)	6-8% from powdered samples.	Reported for Cd, Cu, Mg, Ti and Zn.	Shown for Zn from solution residues (from peak height and peak area measurements) and from Aluminium oxide plus graphite (from peak height and peak area measurement); for Cd, Cu and Mg from aluminum oxide plus graphite (peak area measurement); and for Ti from aluminum oxide plus graphite plus PTFE (peak area measurement). Non-linear calibration curves were constructed when peak height measurements were used, linear calibration curves obtained from peak area measurements.	Temporal behavior of Ti from 10 mg Aluminum oxide plus 9 mg of graphite plus 1 mg of AgCl or Ammonium Chloride or PTFE is also shown. The effect of cup mass and geometry with and without the use of boiler cups was briefly investigated using solution residues of Cu, Sr and Zn; a small change in the net signal intensity was observed when a lid was used, however, background intensities decreased by a factor of 1.3 (Zn 213.8 nm) and 2.3 (Cu 324.7 nm) when a lid was used. Spectral scans between 200 nm and 500 nm with and without insertion of graphite cup were also obtained, when the cup was inserted a decrease in the intensity of N2 plus band and an increase in the intensity of the CN bands was observed.	1987	51
Broekaert (Zaray, Burba, Broekaert & Leis)	Solids	No data	Reported for Cr and Mn with sorption on HYPHAN (1-(2-hydroxyphenylazo) 2-napthol)) cellulose and for Cu, Fe and Pb with sorption on HMDC (hexamethylene dithio carbamate) cellulose.	Shown for Cu, Fe and Pb (obtained with preconcentration on HMD-cellulose) and for Mn and Cr (obtained with preconcentration on HYPHAN-cellulose). A procedure for the preparation of matrix matched standards is also given.	The evaporation of Fe was investigated with a radiotracer. To minimize impurities, graphite cups were pre-burned for 15 s, the samples were ashed in situ (10 mm below the plasma). HCl was added as a volatilization enhancing agent. A method for the preconcentration of trace elements in HMD-cellulose is also described The technique developed was applied to the analysis of Cu, Fe, Cr and Mn in high purity Aluminium.	1988	52

Table 1-6. Continued.

Group	Samples	%RSD	Detection Limits	Calibration curves	Other/Comments	Year	Ref
Haraguchi (Haraguchi, Abdullah, Hasegawa, Kurosawa & Fuwa)	Liquids	4.1-12% (from solution samples) measured from both peak areas & heights. Peak heights gave poorer results than peak areas.	Reported for aqueous solutions of Mn, Zn, Pb, Cr & Ni determined from peak height and peak area measurements. Results (in pg) from peak area measurements: Mn (8.4); Zn (180); Pb (58); Cr (97); Ni (148). Results (in pg) from peak height measurement : Mn (4); Zn (18), Pb (105).	Not shown, a linear dynamic range of 4.0-5.7 orders of magnitude is reported.	Optimization for each individual element, the use of more sensitive lines, and automation using a stepper motor are suggested as the means to improve the analytical figures of merit of the device.	1984	53
Haraguchi (Abdullah, Fuwa & Haraguchi)	Liquids and digested powdered botanicals	1.9-12% (for solution samples)	Determined using a 10 µl injection of a multielement standard solution, their results (in ng) are as follows: Al(1.03); Ca (5.96); Cd (0.013); Co (0.098); Cr (7.1); Cu (0.14); Fe (0.81); K (1.81); Mg (0.15); Mn (0.043); Na (5.67); Ni (0.18); P (0.64); Pb (0.063); Zn (0.12). Cup impurities were found to affect LODs of Al, Ca, Fe, K & Na.	Curves are not shown, but analytical results for spinach (NBS-SRM 1570) and orchard leaves (NBS-SRM 1571) are given, their results are in good agreement with the NBS certified values.	Results for: SBR vs rod height; SBR vs Power (0.7-1.4); SBR vs observation height; and emission intensity vs ashing time are also given. The effect of 1 M acids (i.e., Hydrochloric, Perchloric, Nitric, Sulfuric) on the emission intensity of Al, Ca, Cd, Co, Cr, Cu, Fe, K, Mg, Mn, Na, Ni, P, Pb & Zn (2 ppm) was investigated; Perchloric supressed signals for Cd, Co, Cr, Cu, Fe, Na, Ni, P, Pb & Zn; Sulfuric supressed signals for Ca, Co, Cr, Cu, Fe, K, Mg & Mn; little or no effect was observed for Hydrochloric and Nitric acids. Graphite cups were found to be reusable for 10 to 30 times depending on analyte and concentration; cup porocity was found to affect precision; memory effects were caused by carbide forming elements. The use of pyrolytically or Zr coated cups and a µC-controlled DSID were suggested as a means to improve the analytical figures of merit of the device.	1984	54
Haraguchi (Abdullah & Haraguchi)	Liquids and powdered botanicals	2.6-26% (in cellulose matrix). The high values are for carbide formers (Ba, Ca & Sr). For most elements was less than 13%.	Reported for solid samples in cellulose matrix (in ng) for: Al (26), As (10), B (46.4), Ba (40), Be (8.6), Ca (139), Cd (3.28), Co (1.3), Cr (1.58), Cu (1.06), Fe (19.1), K (167), La (135), Mg (9.82), Mn (2.16), Na (76), Ni (2.1), P (29.6), Pb (2.8), Sn (2.5), Sr (10.9), Ti (104) & Zn (3.54).	Shown for As, Mn and Pb in orchard leaves (NBS SRM 1571), spinach (NBS SRM 1570), tomato leaves (NBS SRM 1573), pine needles (NBS SRM 1575) & pepperbush samples (NIES SRM no. 1). Also, analytical results for As, Cd, Cr, Cu, Fe, K, Mg, Mn, Na, Ni, P, Pb & Zn in orchard leaves (2-mg) using a cellulose standard and matrix matching. Al, B, Ca & Sr could not be determined due to carbide formation.	Effect of ashing time on emission intensity of As, Cd, P, Pb and Zn (in 2 mg of pepperbush samples and 11±1 mm below the plasma body): a 5 min ashing time was adequate for all samples, a little sample loss was observed for Zn. Matrix effects: the effect of 2% Ca, K, Mg & Na (as Chlorides) on the emission intensities of Al, As, B, Ba, Be, Ca, Cd, Co, Cr, Cu, Fe, K, La, Mg, Mn, Na, Ni, P, Pb, Sn, Sr, Ti & Zn was investigated, matrix matching was found to be important, especially for the analysis of botanicals containing high concentrations of Ca, K, Mg & Na. Memory effects were also observed. Carbide forming elements, such as, Al, Ca, B and Sr could not be determined. In order to avoid memory effects, the cups were washed with HCl and pre-burned for several times. The use of a graphite lid prevented sample loss, with a 4 min pre-burn time lid contamination was negligible.	1985	55

Table 1-6. Continued.

Group	Samples	%RSD	Detection Limits	Calibration curves	Other/Comments	Year	Ref
Haraguchi (Abdullah, Fuwa & Haraguchi)	Aqueous (artificial sea water, matrix NaCl, KCl & MgCl2)	2.3-11% (after pre-concentration)	Reported for Cd, Co, Cr, Cu, Mn, Ni, Pb & Zn with preconcentration (in the pg/ml range) and without preconcentration (in the ng/ml range).	No curves are shown, however, linear dynamic range of 4 to 5 orders of magnitude was reported.	Cathodic deposition (by controlled potential electrolysis) of Cd, Co, Cr, Cu, Mn, Ni, Pb & Zn inside a graphite cup (using a new cell design) was performed in order to separate (and preconcentrate) these elements from artificial sea water. Preconcentration factors of: 30 (for Cr), 102 (for Pb), 173 (for Mn), 188 (for Zn), 211 (for Ni), 288 (for Cd), 300 (for Co) and 328 (for Cu) were reported.	1987	56
Horlick (Salin & Horlick)	Liquids and solids (SPEX G-7 standard and powdered coal and botanicals)	15% for Zn solution samples).	0.1 ng for Zn (in graphite). A comparison of ICP-DSID and the dc arc using Spex G standards produced essentially equivalent LODs for Ag, Be, Cd, Cr, Fe, Mg, Mn, Sd and Sn. The ICP-DSID was better for As, Bi, Cu, Ga, In, Na, Pb, Tl and Zn whereas the dc arc was better for B, Ca, Ge, Mo, Ti and V. Co, Nb and Ni was detected only by the dc arc; Hg, P and Sr only by the ICP-DSID.	Shown for Zn in powdered samples with a graphite matrix. Analytical results for direct analysis of coal (NBS-SRM 1632) and orchard leaves (NBS-SRM 1571). The most sensitive line for some elements was not utilized due to spectrometer limitations. A semiquantitative comparison (31 elements compared) of dc arc and ICP-DSID using SPEX G-7 standards is also included. A 0.1% Indium was used as an internal standard.	The use of boiler cups provided a more reproducible time behavior. This is the first paper on a graphite cup DSID.	1979	57
Horlick (Pettit & Horlick)	Liquids and powders (coal and botanicals)	1.8 to 4.5% (from aqueous solutions, a W metal cup and a 1% Hydrogen Argon mixed-gas plasma).	Reported (in pg) for: Zn (18), Cd (21), Pb (440) & Ni (900); using aqueous standards, a W cup and an Argon/Hydrogen mixed-gas plasma.	Shown for Zn in powdered samples of: subbituminous coal (NBS-SRM 1635); orchard leaves (NBS-SRM 1571); spinach (NBS-SRM 1570); coal (NBS-SRM 1632); tomato leaves (NBS-SRM 1573); coal fly ash (NBS-SRM 1633), with an Argon Oxygen mixed-gas plasma and a graphite cup. Their results indicate that direct analysis, without any sample pre-treatment, can be performed for volatile elements. Perhaps the most important characteristic is the relative independence of calibration curves of powdered botanicals from the matrix.	In summary, metal cups (i.e., Ta, Mo & W) and graphite cups with boiler cups; a mixed-gas plasma; automation of changing and running a series of samples, computer control of drying, ashing and atomization were used. In addition, the direct analysis of powdered samples was performed. Future: robotics and in situ sample pre-treatment. The temporal behavior of Ni & Zn from solid samples and graphite cups, metal (i.e., Mo, Ta) cups and that of 1 ng Zn with a W cup and an Argon/Hydrogen mixed gas plasma are also shown. Metal cups were found to exert a significant influence on analyte emission temporal behavior.	1986	58

Table 1-6. Continued.

Group	Samples	%RSD	Detection Limits	Calibration curves	Other/Comments	Year	Ref
Horlick (Shao & Horlick)	Aqueous and digested botanicals. Also, SPEX G and TS-6 oxide (Si and Al) standards.	For 16 elements and 3-, 4.5- and 6-mm diameter electrode sizes for solution samples and for powdered samples. For more details see comments.	Reported for 4.5-mm and 6-mm OD graphite cups (in ng): Ag (.17 & 0.11), As (.5 & , .37) Cd (.03 & .17), Cr (3.1 & .25), Cu (33.6 & 5.8), Ge (0.7 & .47), In (1.2 & 2.5), K (0.3 & .48), Li (0.3 & .06), Mg (3.5 & .85), Mn (0.1 & .23), Na (136.8 & 2.7), Pb (0.4 & 6), Sb (1.2 & 1.14), Sn (3.5) and Zn (0.2 & 3.3) in solution and Ag, As, Ge, In, Li, Pb, Sb, Sn & Zn in powdered samples.	Although shown only for Ag, linear curves were constructed from multielement solution residues for As, Cu, In, Li, Mg, Na, Pb, Sb, Cd, Mn, Sn and Zn; Al, B, Be, Ca, Fe, Mo, Ni, Si, Sr, Ti, V & Zn(?) had non-linear calibration curves. An explanation for the non-linearity is also given, "these elements are, in general, difficult to volatilize and/or strong carbide formers". Also shown are curves for Ag, As, Ge, Li, In, Pb, Sb, Sn & Zn from powdered samples, and a curve for As in Si dioxide, Al oxide and Graphite. Analytical results for digested pine needles (NBS SRM 1575) are also given.	The effect of cup insertion position on the temporal emission intensities of Ag, As, Li, Pb and Sn was also investigated. %RSDs (for solution samples): 2.8-16.5% for 3-mm OD electrodes, 1.8-7.2% for 4.5-mm OD electrodes and 2.9-10.6 % for 6-mm OD electrodes. The 4.5-mm OD electrode shows the best overall %RSD (3.3%). %RSDs for powdered samples: 2.8% to 16.6% with an average of 7%. Helium was used as the central tube gas in order to minimize filament formation upon electrode retraction. Temporal behavior (chart recorder tracing) for a 20 pg of Ag, Cd, & Zn demonstrates the detection capability of the technique. Future work includes the design of a high speed data acquisition sub-system and a stepper motor driven DSID. Electrode impurities were found to affect the LODs of Cr, Cu, Mg, Pb & Zn.	1986	59
Horlick (Karanassios & Horlick)	Liquids	No data	No data	No data	Temporal behavior was used as a means to resolve spectral interference in the time domain, the case of the spectral interference of Cu (213.851 nm line) on Zn (213.856 nm line) is shown, the case of Ni (213.828 nm line) on Zn (213.856 nm line) is discussed. Their system is capable of handling different probe types interchangeably. A readout electronics sub-system capable of digitizing transient signals in real-time, and DSID-specific software are also discussed. This sub-system was subsequently used in order to assess analyte emission behavior in the time domain and to characterize the DSID.	1988	61
Horlick (Karanassios, Horlick & Abdullah)	Liquids	4.5%-18.1%, poor precision attributed to electrode impurities.	Determined from multielement solution residues, and are reported (in ng) for: Ag (1.8), Cd (0.5), Cr (8.7), Cu (0.1), Mg (3.6), Mn (0.1), Ni (41.6) and Zn (0.4).	Shown for Ag, Cd, Cu and Mg (form multielemnt solution residues). Fe, Co, Cr, Ni and Zn had non-linear calibration curves. The non-linearity of the Fe, Co, Cr and Ni calibration curves was attributed to carbide formation, that observed for Zn was attributed to electrode impurities.	The effect of insertion speed on the background signals was tested for Ag, Cd, Co, Cu, Fe, Sn, Ni and Zn; the results shown are only those for Cu and Cr. Also, the effect of insertion speed on both the background change and the analyte signal (1 ng Zn) is shown. The effect of insertion speed was investigated for Ag, Cd, Co, Cu, Fe, Sn, Ni and Zn, it shown only for 1 ng Cd. Little or no signal was observed for Al, Ca, Sr, Ti and Zr; solutions to this problem are proposed. Electrode geometry was found to exert a considerable influence on analyte emission temporal behavior and the analytical figures-of-merit of the device. Based on the findings presented in this work, a 'next generation DSID' (i.e., an intelligent sample procesor for the ICP) is proposed.	1988	62

Table 1-6. Continued.

Group	Samples	%RSD	Detection Limits	Calibration curves	Other/Comments	Year	Ref
Horlick (Karanassios, Abdullah & Horlick)	Mostly liquids with a brief discussion of inorganic powdered samples.	5.1%-18.6% (with NaF) and 9.7%-22.9% (without NaF).	Determined from multielement solution residues with the addition of NaF, and are reported (in ng) for: Al (0.7), B (9.6), Ca (5.2), Co (1.3), Fe (1.5), Sr (0.03), Ti (0.8) and Zr (0.4); and without the addition of NaF for: Al (457), B (not detected at 1000 ng), Ca (602), Co (4.3), Fe (2.7), Sr (46.3), Ti (not detected at 5000 ng) and Zr (not detected at 2500 ng).	Shown for Al, Ca and Zr (from multielement solution residues and addition of NaF). Also, for B from powdered samples with the addition of NaF volatilization enhancing agent.	It demonstrates the concept of in situ (i.e., in the sample carrying cup) chemical processing of samples. In the future, extention of this method for the determination of impurities in metals, alloys and the new types materials is proposed. The findings of the previous reports are to be used as the basis for the design of a DSID for an ICP-MS system.	1988	63
Horlick (Karanassios & Horlick)	Liquids	No data	No data	No data	The advantages offered by a dry ICP in terms of oxide and background species formation formation are demonstrated. In addition, background spectra for graphite, Ta and W metal cups, and a W wire-loop are also shown. Volatilization enhancement and chemical modification via NaF addition in the sample carrying cup was also investigated. Carbide formation is used in order to reduce or eliminate MS matrix effects (i.e., the effect of 1000 ppm U on 100 ppb Zn).	1988	64
Kirkbright (Kirkbright & Walton)	Liquids	5-11% (from solution samples), depending on the physical condition of the rod.	Reported (in pg) for solution residues of Cd (19.5), Co (20.5), Cu (20), Fe (39), Mn (6), Ni (63.5) & Pb (35).	No data	Preliminary results using a wire-loop system (0.25 mm W wire), show a 25 ms rise time for 0.5 ng of Mn, a storage oscilloscope was used in order to record analyte emission temporal behavior. In the future, and in order to improve precision, the use of pyrolytic graphite, programmed ashing before atomization, and of higher plasma powers (important for refractory elements) is proposed.	1982	65

Table 1-6. Continued.

Group	Samples	%RSD	Detection Limits	Calibration curves	Other/Comments	Year	Ref
Kirkbright (Kirkbright & Li-Xing)	Liquids	7-12.5% (from solution samples). Precision improves when an Ar-Freon mixed-gas plasma is used.	Reported (in ng) for solution residues of Ag (0.0018 ng), B (1.3 ng), Cr (0.020 ng), Cu (0.0073 ng), Mo (1.0 ng), Ti (0.89 ng), U (1.9 ng), Zn (0.004 ng) and Zr (1.1 ng) using Ar-Freon as a central tube gas. Freon was found to improve LODs (also given for Ar only as a central tube gas), especially for carbide forming elements.	For solution sample residues of Ag, Cr, Cu & Zn without a central tube gas and B, Mo, Ti, U & Zr with Argon-Freon (0.1 %) as a central tube gas.	An interesting demonstration of volatilization enhancement via the addition of halocarbons in the plasma gases.	1982	66
Kirkbright (Li-Xing, Kirkbright, Cope & Watson)	Liquids	Seven replicas of a 50 ppb injection of a Mn solution are shown. Typical 2%.	No data	No data	The effect of operating parameters (i.e., outer tube-, intermediate tube- and central tube-gas flow rates and power) on the drying and ashing cycles (using Mn in a 5% glucose solution) was investigated. Optimum drying, ashing and atomization time and cup position for the determination of Mn in a 5% glucose solution are also discussed. A flow rate of 0.1 L/min in the central tube helps avoid extinguish the plasma during the drying cycle. Future work: solid samples (i.e., semiconductors, soils, biological materials). The use of a µC not only for DSID control but for automatic treatment of the results is also proposed.	1983	67
Kirkbright (Barnett, Cope, Kirkbright & Taobi)	Liquids	1-14% (from solution sample residues), depending on electrode geometry.	Reported for solution sample residues of Cr, Mn, Ni, & Pb for four electrode geometries. Depending on electrode geometry, LODs differed by as much as an order of magnitude.	No data	Depending on element and electrode geometry, some signals were not well resolved form the background change. RSDs (peak height determinations) show no clear dependence on cup geometry. Surface characteristics are important, the use of pyrolytically coated cups with boiler cups is recommended. The development of electrodes with reproducible geometries and surface characteristics by a commercial manufacturers is suggested. Future work includes temperature measurements inside the cup and the use of active atmosheres (as the means to improve sensitivities).	1984	68

Table 1-6. Continued.

Group	Samples	%RSD	Detection Limits	Calibration curves	Other/Comments	Year	Ref
Lorber (Lorber & Goldbart)	Liquids and powders (Uranium Oxide)	4-12% for analytes (with the exception of Sb, Co, Mg & Cu) and 5-15% for blanks (with the exception of Si & Mg)	Determined in solid samples of Uranium oxide containing Al, B, Ba, Bi, Cd, Co, Cr, Cu, Fe, Mg, Mn, Mo, Nb, Ni, Pb, Sb, Si, Sn, Sr, Ti, V & Zn. Detection limits for an ICP-DSID, an ICP-DSID utilizing the carrier distillation method, an ETV-ICP and an ICP equipped with a conventional pneumatic nebulizer system are also shown and compared.	No data	No memory effects were observed. Sample throughput was better than one sample per minute. SBRs and %RSDs for Al, B, Ba, Bi, Cd, Co, Cr, Cu, Fe, Mg, Mn, Mo, Nb, Ni, Pb, Sb, Si, Sn, Sr, Ti, V & Zn are also given. Advantages: high sample throughput, the ICP can be used for both liquids and solids, it doesn't require any specialized equipment. The first demonstration of a horizontal DSID for ICP-AES.	1985	69
Lorber (Brenner, Lorber & Goldbart)	SRM silicates	No data	No data	Shown for Cu in a variety of SRMs.	The horizontal DSID for ICP-AES previously developed was used in this work. A matrix dependent volatilization rate was observed. The volatilization rate of "involatile" elements was found to be lower than that observed for the dc arc. Also, "there appears to be little advantage in the use of the direct insertion technique and ICP-AES for multi-trace element analysis of diverse geological materials. However, this technique does possess an advantage; it can be adapted readily to most ICP-AES instrumentation and complements analysis using conventional solution nebulization".	1987	70
McLeod (Mcleod, Clarke & Mowthorpe)	Liquids and solids (Ni-base alloys)	1-7% (from solution sample residues) and 6-14% (form solid samples).	Reported for As, Cd, Mg, Pb, Se & Zn in Ni-base alloys. A comparison of detection limits between ETA-AA, HHCD-ES is also included.	Shown for Cd, Mg, Pb & Zn from a multielement solution and certified (CRM BAS 345, CRM BAS 346 & SRM 898) and non certified materials (CT4, NT4 & TTR2). Analytical results based either on solution or solid standards are also given. Peak area integration allowed them to use aqueous, non-matrix matched standards for the analysis of Ni-base alloys, thus, demonstrating a relative independence of calibration from matrix.	Double peaks frequently appear for some elements, especially for solid samples. An increase in emission intensities was observed with an increase in power. In general, a correlation between analyte volatility and the maximum electrode temperature was not observed except in the case of solution residues. Future work involves the determination of volatile elements in a range of alloy and high purity materials.	1986	71

Table 1-6. Continued.

Group	Samples	%RSD	Detection Limits	Calibration curves	Other/Comments	Year	Ref
Ohls (Sommer & Ohls)	Liquids and solids	No data	Detection limits better by as much as an order of magnitude than those obtained with an ICP equipped with a conventional pneumatic nebulization system are reported.	No data	Proceedings of the International winter conference, San Juan, Puerto Rico, Jan. 7-11, 1980, Paper 78. The first paper from Germany on the Sample Elevator technique (SET). "...thus the known techniques of cup electrodes used in arc emission spectrography have to tested for the ICP method again" "...SET will become more important in the future to solve special problems of trace analysis" A high power, Argon-Nitrogen mixed-gas plasma was used.	1981	72
Ohls (Ohls & Sommer)	Liquids and powderes/solids	According to the authors, %RSDs seldom exceeded 5% and almost never 10%.	Reported for As, Cr, Zn, Pb, Co, Ni, B, Mn, Fe, Mg, Mo, Si, Al, V, Ca, Cu, La, Ti and Zr from solution samples utilizing both the sequential and the multichannel spectrometers. Also, detection limits are for the same elements with a 9000 ppm Fe matrix. Detection limits for solid samples (steel)are reported for: Mn, Al, Co, Cu, Si and Ni.	Shown for Ni and Cu (5 mg alloy steel samples). Also, for B in lubricating oils.	Graphite cups were used with and without lids. The background spectrum (190-500 nm) of a blank cup is also shown.	1980	73
Page (Page, Madraswala, Godbole, Kulkarni, Mallapurkar & Joshi)	Liquids and powders (Uranium Oxide SRMs)	2-9% (for powdered samples).	Reported for Cd, Cu, K, Na, Ni & Pb in Uranium oxide.	Shown for Cd and Cu in Uranium matrix. Analytical results for Cd, Cu, K, Na, Ni & Pb in an NBL-SRM Uranium oxide are also included, these are in good agreement with the certified values. The sensitivity results for these elements show that the carrier distillation method gives results that are two orders of magnitude better than those obtained with aqueous nebulization.	Analysis of seven standards with the carrier distillation method for Cd, Cu, K, Na, Ni & Pb. Their results were reported to be in good agreement with the certified values, except for the high and low concentrations. "...the detection limits and senstivities obtained here are comparable or better than those in dc arc." Future work: to extend the method to other refractory nuclear materials.	1983	75

Table 1-6. Continued.

Group	Samples	%RSD	Detection Limits	Calibration curves	Other/Comments	Year	Ref
Page (Page, Godbole, Madraswala, Kulkarni, Mallapurkar & Joshi)	Powdered Uranium Oxide.	6-20% (for powdered samples with and without a lid).	Reported for B, Be,Cd, Co,Cr, Cu, Mn, Ni, Pb, Li, Na, Fe & K in powdered samples using the carrier distillation method.	No curves are shown, however, analytical results for B, Be, Cd, Co, Cr, Cu, Mn, Ni, Pb, Li, Na, Fe & K in spiked samples of Uranium oxide are included.	Graphite electrodes with and without a lid are compared. Their results show that SBRs improved for most elements with the use of a graphite lid. The precision obtained was better than that of the dc arc. No U emission was observed. Due to its advantages, namely that of higher sensitivity and precision than the dc arc, in the future, the authors anticipate to apply the method to other refractory materials.	1984	76
Salin (Salin & Habib)	Liquids	<3% via electro-chemical deposition on the cup, conventional DSID about 12%. The observed improvent is attributed to a more regular deposition.	Reported for a solution of Cu. The detection limit depends on the deposition time.	Signal intensity vs deposition time for Cu. A calibration curve for Cu is described but not shown.	Controlled potential electrolysis using a conventional dc arc electrode as a working electrode. An Argon-Oxygen mixed-gas plasma (Oxygen was mixed in the outer tube of the torch, a flow rate of 1.7 L/min was used). Limitations: it requires large solution volumes, the exterior surface of the electrode is coated. Drying was accomplished by heating the electrode with the ICP turned off and an applied forward power of 30 W. In the future, the use of a flow through cell is proposed.	1984	77
Salin (Salin & Sing)	Liquids	<5%	Cu: 0.2 ppb (2 pg) and Zn: 0.08 ppb (0.8 pg). The authors claim that their results are 50-100 better than those reported in the literature.	Not shown but a calibration curve for Cu (linear over 4 orders of magnitude) is described.	Improved LODs were obtained because the dryed sample is completely vaporized in 0.1 s, this produces a transient atom population which is 40 times higher than with conventional nebulization. High salt concentrations (i.e., 0.1% Ca solution) were used in order to demonstrate matrix effects, further studies are required. Because peak heights were found to be matrix dependent whereas peak areas were not, peak-area integration was used for calibration purposes. Temporal resolution as the means to alleviate spectral interference effects was demonstrated using W (213.815 nm) and Zn (213.856 nm) as examples. Quantitative vaporization was attained in as little as 100 msec. The readout electronics sub-system utilized allowed background subtraction.	1984	78

Table 1-6. Continued.

Group	Samples	%RSD	Detection Limits	Calibration curves	Other/Comments	Year	Ref
Salin (Habib & Salin)	Aqueous (artificial sea water).	3%	Reported for aqueous solutions of Cd, Co, Cu, Ni, Pb & Zn and a 5 min electrolysis time.	Not shown, although a Cu in sea water calibration curve is briefly described.	Three pre-concentration methods were used; predeposition, codeposition and a HMDE. High salt concentrations (i.e., 0.1% Ca solution) were used to demonstrate matrix effects. The rate of volatilization was found to be matrix dependent, further studies are required. Oxygen was used in the outer tube (1.4 L/min), Cd and Zn were determined in an Oxygen-free plasma. The effect of deposition time was investigated, an improvement by a factor of 17 and 13 in the detection limits of Cu and Ni was realized by increasing the deposition time from 5 min to 120 min. Signal-to-Noise ratio versus Cu concentration and the effect of drying time on the signal intensity of Cu are also shown.	1985	79
Salin (Monasterios, Jones & Salin)	Solids (human hair).	An average of 9% was obtained using aqueous solutions.	Reported for aqueous samples of As, Cd, Cu, Hg, Pb & Zn. Also, it was estimated for human hair using liquid samples.	Analytical results for Cu and Zn with various methods (i.e., ICP-DSID, ICP & Flame Atomic Absorption) are reported. Aqueous standards provide a close but not an exact match for the analysis of human hair.	A comparison between FAA, ICP, ICP DSID is reported. Direct analysis of hair without sample digestion in 'deep crater' graphite electrodes is described. Boiler cups produced broader peaks of lower intensity. The standards addition method in which liquid standards are directly added on the sample in the sample carying cup did not work as expected. According to the authors, more work remains to be done.	1986	80
Salin (Sing & Salin)	Liquids	Wire-loop-ICP-MS: <1% (short term) and <1.5% (long term).	With wire-loop-ICP-MS LODs are one to two orders of magnitude better than those obtained with conventional nebulization techniques.	No data	The half width of analyte peaks is less than 0.1 second. Both Ta and W wire-loop were used. The detection limits obtained with the wire-loop DSID are 1 to 2 orders of magnitude better than those reported with conventional pneumatic nebulizer systems. Detection limits can be further improved with the application of multiple drops on the wire-loop.	1986	81

Table 1-6. Continued.

Group	Samples	%RSD	Detection Limits	Calibration curves	Other/Comments	Year	Ref
Salin (Boomer, Powell, Sing & Salin)	Liquids	5-13% (form solution sample residues).	Reported for aqueous solution residues of Ag, As, Cd, Cu, Li, Mn & Pb. LODs obtained by an ICP-MS DISD are better by as much as a factor of 40 than those obtained with an ICP-MS system equipped with a conventional pneumatic nebulizer.	The linear dynamic range for Cd "appears to be 4 orders of magnitude".	The signal was integrated for 2 sec. The half-widths observed for the Cu peak were 700 ms and 100 ms for the ICP-EAS and the ICP-MS case respectively. SBR for Mn as a function of the distance of the sampling orifice from the tip of the plasma plume is also shown. Using this technique, oxide formation is avoided. In the future, optimization of operating parameters, matrix effects and the degree of oxide formation is proposed. In this report, the first demonstration of a wire-loop DSID for the ICP-MS is described.	1986	82
Umemoto (Umemoto & Kubota)	Liquids and solids (dissolved Iron and Steel samples).	4.5% for As in the presence of 5 ppm Fe and 3.2% for Sb in the presence of 2.5 ppm Fe.	Reported for solution sample residues of: As (45 ppb or 1.1 ng) in the presence of 5 ppm Fe and Pb (8 ppb or 0.2 ng) in the presence of 2.5 ppm of Fe.	No curves are shown, however, analytical results for As and Sb in dissolved Japanese steels (SRM JSS 172-5, 173-3, 61-3, 169-3 and NBS-SRM 361) are briefly discussed.	Dissolved steel samples were analyzed using the standard additions method. Graphite cups could be used for at least 15 times for low Fe concentrations and for 6 times for high Fe concentrations. Nitric and sulfuric acids (0.5-2.5 M) had no effect in the determination of As & Sb, however, the presence of Fe affected the peak heights of the corresponding emission signals. Matrix matching was found to be important. Peak height measurements were employed with satisfactory analytical results.	1987	84

Table 1-7. Applications.

Group	Application(s)	Elements	Year	Ref
Bastiaans (Prack & Bastiaans)	The DSID was used as an evolved gas analysis system for speciation and identification of inorganic compounds (i.e., salts and oxides).	Elemental analysis was not performed.	1983	50
Broekaert (Zaray, Broekaert & Leis)	The determination of trace elements in aluminium oxide by mixing the oxide with graphite powder (1:1) and by briquetting pellets. Titanium was determined by mixing the sample with graphite and PTFE.	Cd, Cu, Mg, Zn & Ti	1988	51
Broekaert (Zaray, Burba, Broekaert & Leis)	The determination of trace elements in high purity aluminium oxide by sorption on cellulose collectors with different chelating agents (i.e., hexamethylene-dithio-carbamate (HMDC) and 1-(2-hydroxyphenylazo)-2-napthol (Hyphan)).	Cu, Cr, Fe, Mn & Pb	1988	52
Haraguchi (Abdullah, Fuwa & Haraguchi)	The determination of trace elements in digested NBS SRM plant samples. In general, their results are in good agreement with the certified values. Calcium caused memory effects.	K, Na, Ca, Mg, P, Al, Fe, Mn, Zn, Cu, Ni, Cr, Cd, Co & Pd for NBS SRM 1570; and Ca, K, Mg, P, Fe, Al, Mn, Na, Pb, Zn, Cu, Cr, Ni, Co & Cd for NBS SRM 1571 orchard leaves.	1984	54
Haraguchi (Abdullah & Haraguchi)	The determination of trace elements in 2 mg of powdered botanicals with no sample pre-treatement. In general, the results are in good agreement with the NBS certified values.	K, Mg, P, Fe, Mn, Na, Pb, Zn, As, Cu, Cr, Ni & Cd in NBS SRM 1571 (orchard leaves)	1985	55
Haraguchi (Abdullah, Haraguchi & Fuwa)	The separation of trace metals from artificial sea water and their electrochemical preconcentration on a graphite cup prior to analysis.	Cd, Co, Cr, Cu, Mn, Ni, Pb & Zn	1987	56

Table 1-7. Continued.

Group	Application(s)	Elements	Year	Ref
Horlick (Salin & Horlick)	Analysis of samples with a predominantly organic matrix, such as coal (NBS SRM 1632) and orchard leaves (NBS SRM 1571) with no sample pre-treatement.	Cu, Fe, Mn and V	1979	57
Horlick (Pettit & Horlick)	The determination of Zn in a variety of powdered NBS SRMs, including: subitummous coal (1635), coal (1632), orchard leaves (1571), spinach (1570), tomato leaves (1573) and coal fly ash (1633) with no sample pre-treatement. A single calibration curve was used for all matrices tested.	Zn	1986	58
Horlick (Shao & Horlick)	Digested botanicals and powdered SPEX standard samples. The matrix (i.e., graphite, silicon dioxide, aluminium oxide) was found to have little effect on the analytical curves.	Ag, As, Ge, In, Li, Pb, Sb, Sn & Zn from digested pine needles (NBS SRM 1575). Also, linear calibration curves for Ag, As, Ge, Li, In, Pb, Sb, Sn & Zn from SPEX G, TS-6 silicon dioxide, TS-6 aluminium standards.	1986	59
Horlick (Karanassios, Abdullah Horlick)	Analysis of Boron in powdered calcium sulfate samples with no sample pre-treatement other than the addition of NaF (NaF acted as a volatilization enhancing agent).	B	1988	63
Lorber (Lorber & Goldbart)	The application of the carrier distillation method (using a AgCl/NaF carrier) for the determination of trace elements in Uranium oxide.	Mo, Cr, Sb, B, Zn, Pb, Ni, Bi, Cd, Ba, Co, Al, Fe, Sn,Si, Mn, Mg, V, Nb, Cu, Ti & Sr	1985	68
Lorber (Brenner, Lorber and Goldbart)	To document interference effects when a graphite cup containing a silicate sample is inserted into a horizontally operated DSID for ICP-AES.	Cu	1987	69

Table 1-7. Continued.

Group	Application(s)	Elements	Year	Ref
MacLeod (Mcleod, Clarke & Mowthorpe)	The determination of volatile elements in Ni-base alloys with no sample pre-treatement. Calibration curves were constructed using aqueous, non-matrix matched standards.	Cd, Mg, Pb & Zn	1986	71
Ohls (Ohls & Sommer)	The determination of Ni in shavings of alloy steel, the determination of Cu in steel trimings and the determination of B in lubricating oils.	Ni, Cu and B	1980	72
Ohls (Ohls)	The determination of Cd in biological samples and in oxides.	Cd	1984	74
Page (Page, Madraswala, Godbole, Kulkarni, Mallapurkar & Joshi)	The application of the carrier distillation method (using 5% AgCl as a carrier) for the selective volatilization of trace elements from uranium oxide.	Cd, Cu, K, Na, Ni & Pb	1983	75
Page (Page, Godbole, Madraswala, Kulkarni, Mallapurkar & Joshi)	The application of the carrier distillation method (using 5% AgCl as a carrier) for the selective volatilization of trace elements from high purity uranium oxide.	B, Be, Cd, Co, Cr, Cu, Fe, K, Li, Mn, Na, Ni, & Pb	1984	76
Salin (Salin & Habib)	Analysis of Cu from difficult matrices via electrochemical preconcentration on a graphite cup.	Cu	1984	77

Table 1-7. Continued.

Group	Application(s)	Elements	Year	Ref
Salin (Habib & Salin)	The analysis of Cd, Co, Cu, Ni, Pb and Zn from aqueous solutions and from synthetic seawater samples.	Cd, Co, Cu, Ni, Pb & Zn	1984	79
Salin (Monasterios, Jones & Salin)	The determination of Cu and Zn in human hair with no sample pre-treatement.	Cu & Zn	1985	80
Umemoto (Umemoto & Kubota)	The determination of As and Sb in dissolved iron and steel samples.	As & Sb	1987	84

arbitrarily chosen as the group leader. The name of the group leader was subsequently used to sort out the entries of this table and present them in alphabetical order. This format was chosen in order to simplify comparisons of the work done by different groups. In an attempt to more closely follow the development of DSIDs and the evolution of ideas within a research group, the title of the publication and the objectives of the work are also listed in Table 1-1. In addition, publications originating from the same research group are listed in chronological order, where applicable. For reasons of consistency, the same presentation format was used throughout (Tables 1-1 to 1-7). Because these tables are part of a comprehensive review article (manuscript in preparation), some of the work reported in this thesis has also been included in them.

Even though this review can be considered as a DSID resource inventory, it was also compiled in order to assess the current status of the DSIT and in an attempt to establish future research directions. A great deal of the work presented in this thesis has literally dropped-out of these tables. Some original results have also been included in order to support a hypothesis or illustrate a point. This review initially focuses on the basic experimental set-up required for a DSID (Figure 1-2). As a result, the building blocks shown in Figure 1-2 will be examined in some detail in what follows.

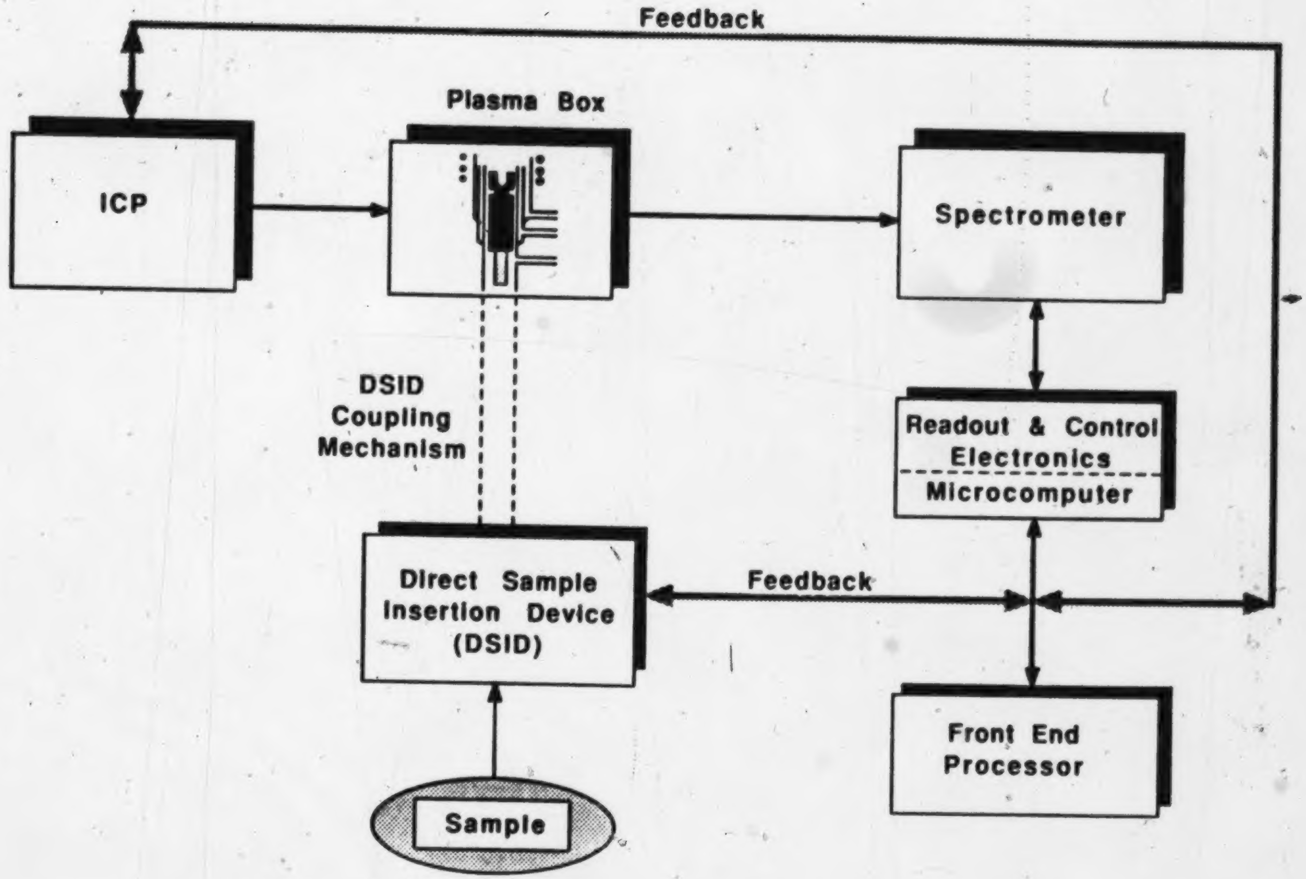
Feedback
ICP
Plasma Box
Spectrometer
DSID
Coupling
Mechanism
Readout & Control
Electronics
Microcomputer
Direct Sample
Insertion Device
(DSID)
Feedback
Front End
Processor
Sample

Figure 1-2. Block diagram of a typical set up for an ICP-DISD.

C.1 Basic Experimental Set Up

The basic experimental set-up required for a direct sample insertion device is shown, in block diagram form, in Figure 1-2. Five basic building blocks can be distinguished: the DSID; the ICP (RF generator and plasma box); the spectrometer; the readout and control electronics; and the front end processor. The measurement end (i.e, readout and control electronics and front end processor) has been broken into two parts to indicate both functionality and actual implementation. The merits of a dual processor system are discussed elsewhere [60, 85]. At the heart of the system shown in Figure 1-2 is the DSID itself.

C.1.1 DSID Designs and their Attributes

A generic block diagram illustrating the essential hardware required for a vertical, cup-based DSID is shown in Figure 1-3 and actual systems are summarized in Table 1-2. A DSID typically consists of: a sample carrying probe, a dc arc undercut electrode is shown in this case; a torch; and a drive assembly (i.e., probe assembly and drive mechanism). The mechanical stops shown in Figure 1-3 indicate functionality rather an actual implementation, the current trend is toward the design of computer controlled stepper motor driven DSIDs.

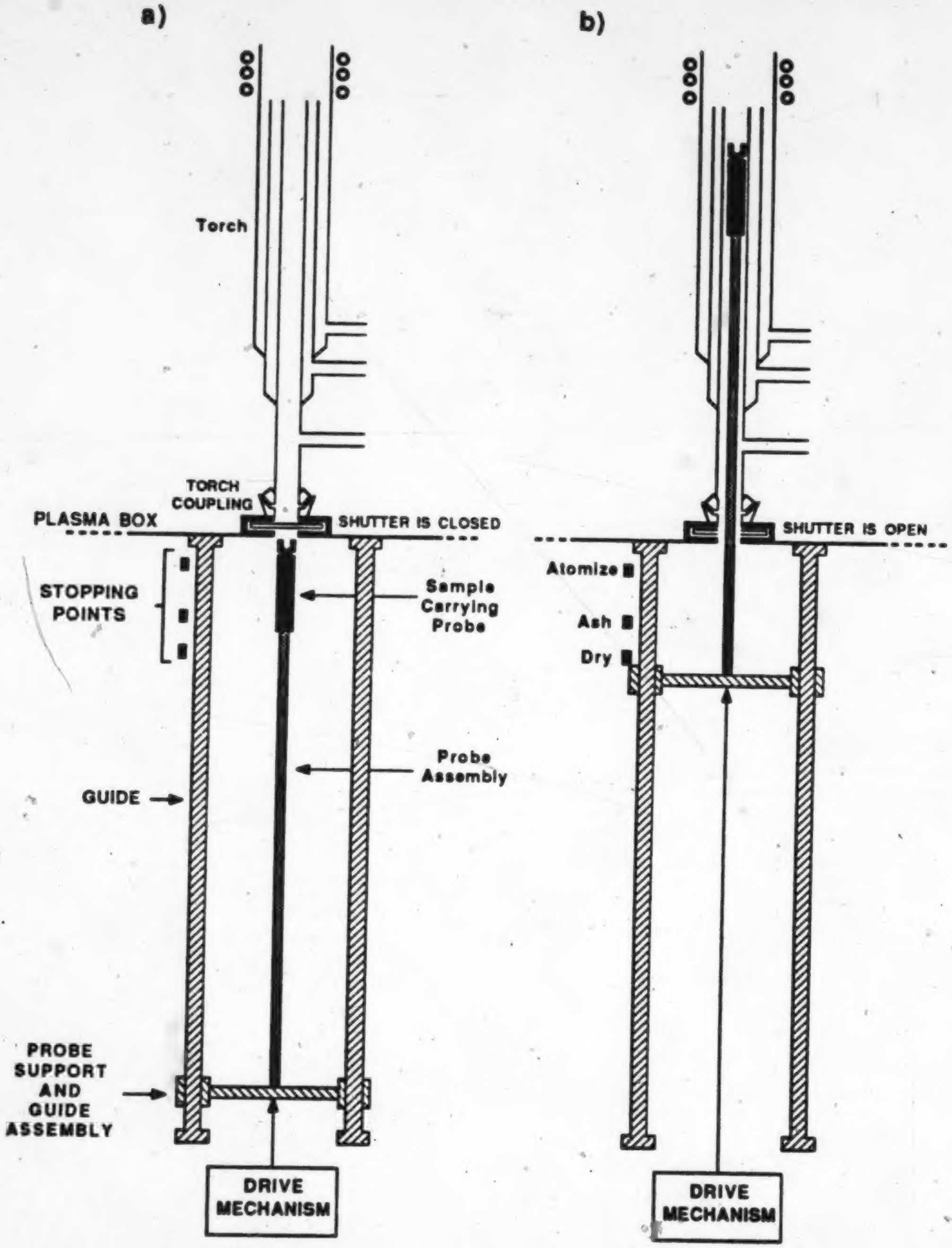
a)
Torch
TORCH COUPLING
PLASMA BOX
SHUTTER IS CLOSED
STOPPING POINTS
Sample Carrying Probe
Probe Assembly
GUIDE
PROBE SUPPORT AND GUIDE ASSEMBLY
DRIVE MECHANISM
b)
SHUTTER IS OPEN
Atomize
Ash
Dry
DRIVE MECHANISM

Figure 1-3. Generic block diagram of the essential hardware required for a vertical, cup-based DSID.

In general, DSIDs can be classified according to the type of sample probe they utilize as cup-based, as rod-based and as wire-loop-based (Table 1-2). Typical examples of sample carrying probes utilized with DSIDs are shown in Figure 1-4. Wire-loop DSIDs are mainly advocated by Salin and co-workers [78, 82]. The most important drawback of wire-loop DSIDs is their inherent inability to directly handle powdered or solid samples. DSIDs can also be classified according to their mode of operation as vertical or horizontal (Table 1-2). Vertical DSIDs, such as that shown in Figure 1-3, are most frequently utilized in ICP-AES, whereas horizontal DSIDs are exclusively utilized in ICP-MS. An example of a horizontal DSID for ICP-MS is shown in Figure 1-5.

Much like any other ICP-based measurement system, at the centre of any ICP-DSID there is a torch. And although a modified Fassel-type torch is typically employed, non-standard and Greenfield type torches have also been utilized (Table 1-2). The torch is modified by replacing the conventional injector tube (e.g., central tube) with an open quartz tube (e.g., the injector tube tip is missing). The size of the central tube varies according to design specifications: it largely depends on sample holder size. The central tube partially acts as a guide for the sample carrying probe into the torch at the beginning of an analytical run and partially helps in cooling the probe upon retraction at the end of the run. Upon retraction, the formation of a dis-

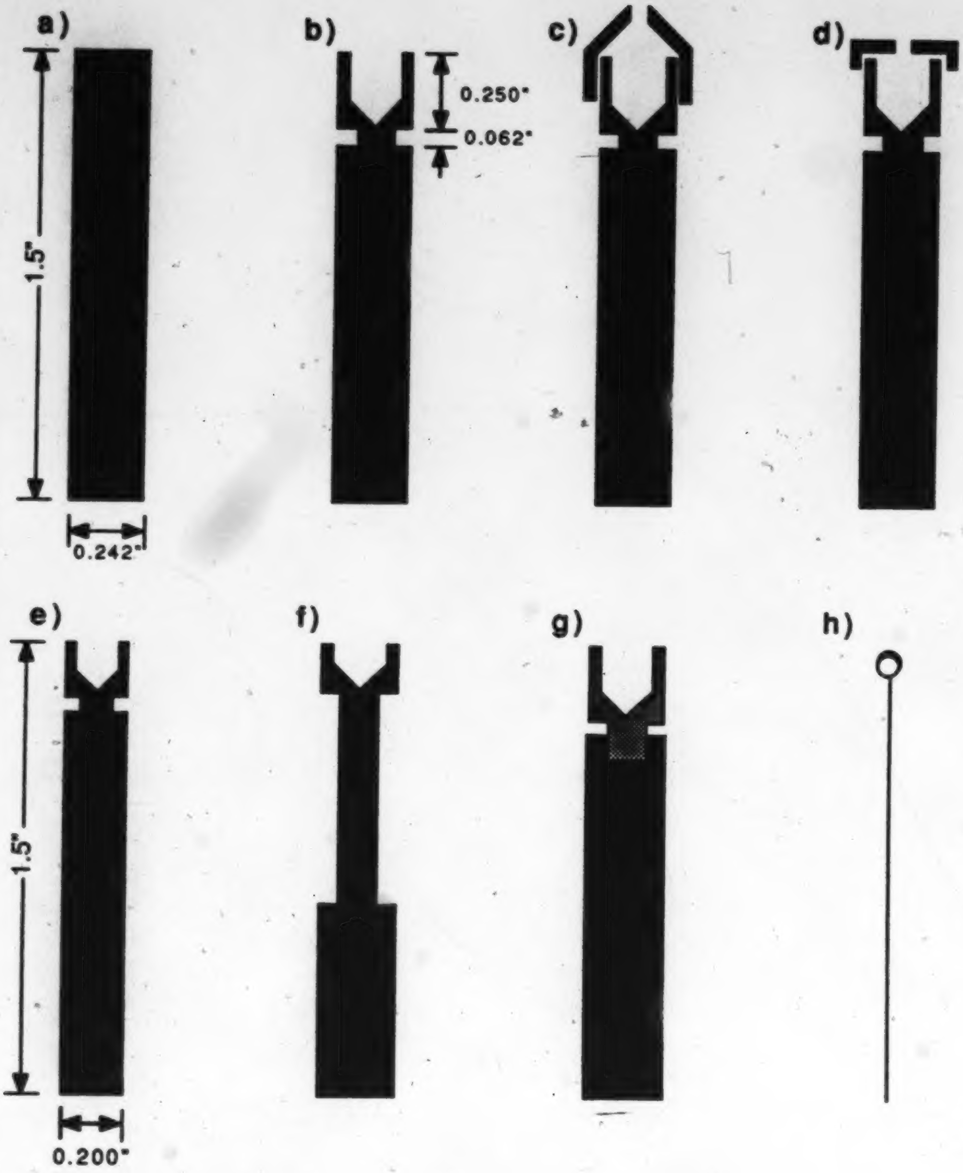

Figure 1-4. Typical examples of sample carrying probes employed. (a) Flat-top graphite electrode; (b) undercut dc arc electrode; (c) undercut dc arc electrode fitted with a boiler cup (b) and a lid (c); (e) narrow undercut dc arc electrode; (f) long undercut graphite electrode; (g) flat-top graphite electrode fitted with a metal cup; (h) wire-loop. Dimensions in inches.

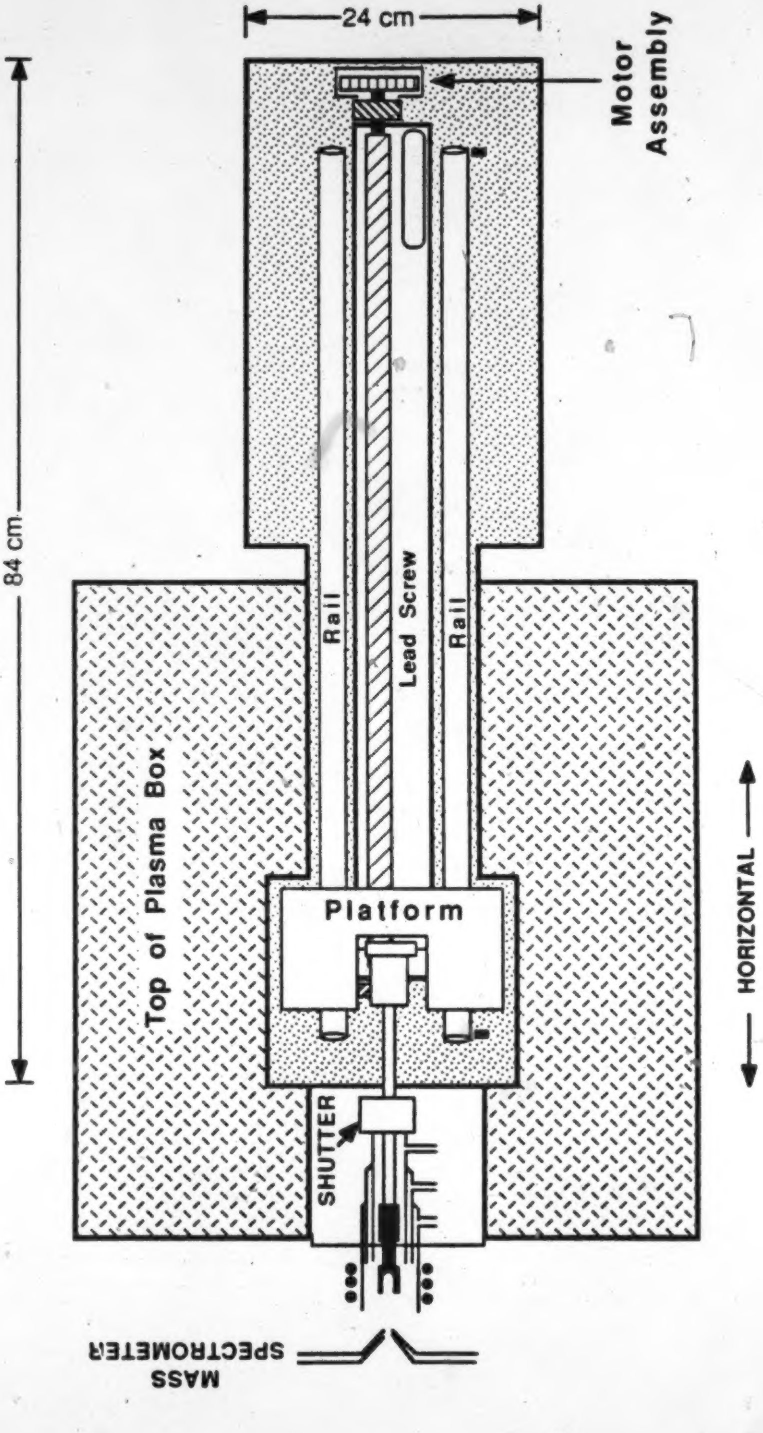
24 cm
84 cm
Motor Assembly
Rail
Lead Screw
Rail
Platform
Top of Plasma Box
HORIZONTAL
SHUTTER
MASS SPECTROMETER

Figure 1-5. Top view of a horizontal DSID for ICP-MS.

charge filament between the plasma and the probe has been reported for some systems [58, 59, 60].

The use of a central tube gas flow deserves special mention. And although it was found to be less important than in conventional pneumatic nebulizer systems, a flow rate of 0.1 l/min has been found to be essential if a dry/ash cycle is to be utilized and continuous plasma operation is to be sustained [55]. In addition, the use of a central tube gas flow (with Ar or He as the central gases) has been found to help snuff out filament formation upon probe retraction.

The torch support of most mechanical systems includes a shutter mechanism that prevents air entrainment. The shutter closes the bottom of the torch upon probe retraction, as shown in Figure 1-3a. Although the plasma can be operated with the bottom of the torch open, a shutter mechanism appears to be essential, especially if continuous operation is desirable. Because the plasma physically moves down and rests on the central tube of the torch when the bottom of the torch is open, a shutter also helps extend the life-time of the torch. In contrast with mechanical systems, a shutter mechanism is not utilized with pneumatically driven DSIDs, a pneumatic seal is established typically at the bottom of the central tube rather than the bottom of the torch.

In most designs described in the literature (Table 1-2), the electrodes are inserted axially (i.e., in parallel to the central tube) into the torch, with one exception [69, 70]. In this horizontally operated DSID for ICP-AES, the sample carrying electrodes are inserted externally to the torch and transversely through the plasma cross section, as shown in Figure 1-6.

Insertion of the sample carrying probe into the plasma can be accomplished (Table 1-2) either manually or automatically with early designs being manually driven and more recent designs automated to varying degrees. Two basic classes of automated or semi-automated designs can be further distinguished: those that are mechanically driven (i.e., reversible motor, computer/stepper motor/lead screw, computer/stepper motor/timing belt, car aerial) and those that are pneumatically driven.

Several attempts toward DSID automation have been described in the literature. As shown in Table 1-2, automated or semi-automated systems that handle a single sample carrying probe to systems capable of handling multiple sample probes in a sequential fashion have been developed. However, the final automated DSID configuration still remains elusive. Clearly, more work remains to be done in order to define the attributes of a 'next generation' DSID.

The insertion itself is accomplished either as one reproducible motion (e.g., one shot) or in a stepwise fashion utilizing either a series of mechanical stops (which can be under either manual or computer control) or via a computer-

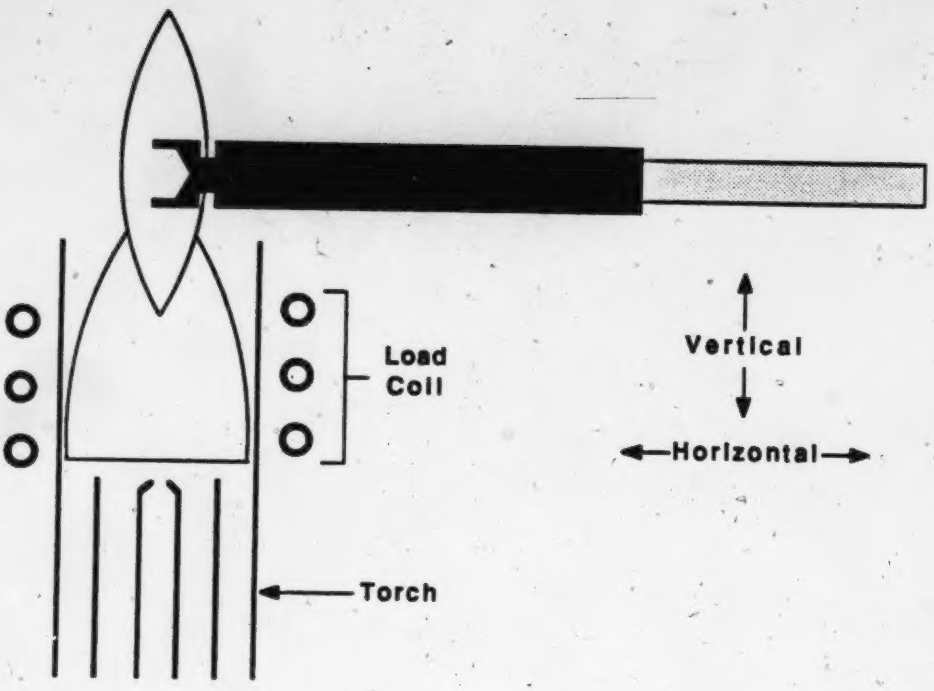
Load
Coil
Vertical
Horizontal
Torch

Figure 1-6. Illustration of a vertical DSID for ICP-AES (see Reference 69 for more details).

controlled motor. By positioning the sample holder at positions successively closer to the plasma discharge, thus taking advantage of the thermal gradient that exists underneath the plasma, sample drying and ashing can be achieved prior to atomization. These steps are analogous to the dry, ash and atomize cycles utilized in Graphite Furnace Atomic Absorption Spectrometry (GFAAS). These steps, however, may have to take on new meanings when used on DSIDs. To use the ashing step as an example, what does it accomplish when inorganic samples are analyzed? And due to the lack of O_2 and the inert nature of Ar, what does it accomplish when analysing samples with an organic matrix (i.e., powdered botanicals)? Moreover, does the analysis of samples with an organic matrix also necessitate the use of an Ar-O_2 mixed-gas plasma? Clearly, the physico-chemical processes taking place during these steps would have to be further investigated, however, detailed studies are yet to be described in the literature. As shown in Table 1-2, *in situ* drying and ashing of powdered/solid samples has been under-utilized, partly because a reasonable degree of DSID automation is required.

Because a finite amount of sample is placed into or onto the sample carrying probe, the spectral signals generated by the DSID are peak-like and transient in nature. Typical examples of analyte emission temporal behavior for a cup-based DSID are shown in Figure 1-7. These must there-

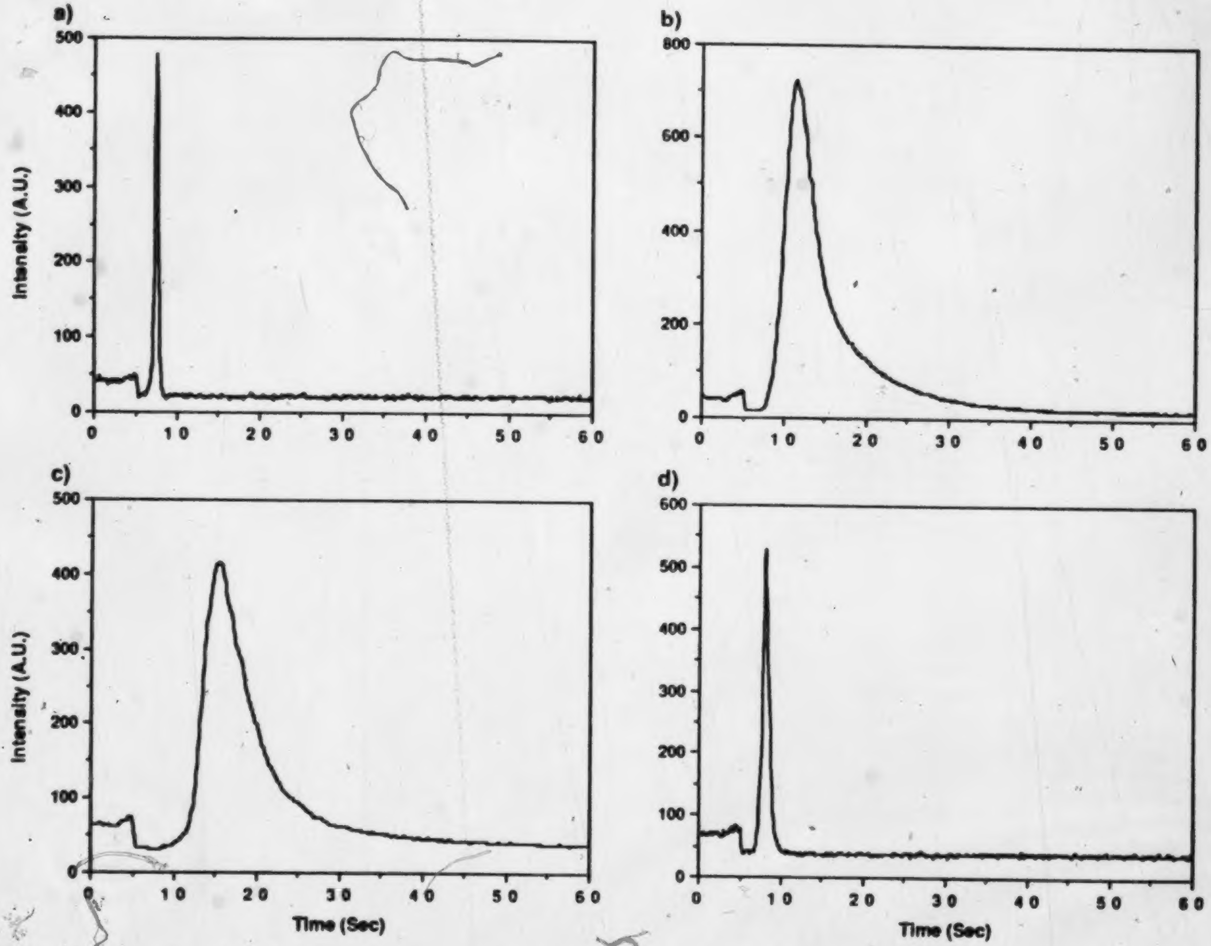

Figure 1-7. Typical examples of analyte emission temporal behavior for 10 ng of: (a) Cd; (b) Cu; (c) Mn and (d) Zn measured using long undercut electrodes (Fig. 1-4f) and with an applied forward power of 1.25 kW.

fore be digitized in real-time and acquired as time-varying intensities. With respect to Figure 1-2, analyte emission temporal behavior dictates the type of spectrometer required for multielement analysis; it determines the nature of readout electronics; and it defines the software requirements for signal acquisition, processing, display, manipulation and DSID control.

C.1.2 ICP and Instrumentation

As mentioned previously, the transient nature of signals generated by the DSID dictates the type of spectrometer required for multielement analysis by ICP-AES: it precludes the use of a monochromator or a slew-scanning spectrometer; it requires a PMT-based or an image sensor-based polychromator. And although most of the work is currently done with PMT-based spectrometers, some of the applications of DSIDs have been carried-out using diode array spectrometers (Table 1-3). Limited wavelength coverage is probably the single most important limitation of such spectrometers. The coupling of a DSID with a high resolution, echelle-based diode array spectrometer that alleviates this limitation [86, 87] appears to be only a matter of time. Such a coupling, however, is expected to place heavy demands on software.

Recently, a great deal of interest has been expressed in the use of the ICP as an ion source for mass spectrometry [27-30]. Due to the advantages of the DSID and of the capabilities of ICP-MS, the coupling of a DSID to an ICP-MS system should provide the world of analytical atomic spectroscopy with yet another acronym and, undoubtedly, a winning combination. This potential has already been recognized by Salin and co-workers who have recently reported preliminary results for a wire-loop DSID for ICP-MS [82].

In addition to the advantages offered by the DSID, an ICP-MS-DSID is expected to have additional capabilities. Consider spectroscopic interference [30, 88, 89] as an example. The absence of continuous aspiration of solvent (i.e., 1-5% aqueous acidic solutions) is expected to reduce or eliminate spectral interference due to oxide, hydroxide and background species formation (i.e., O^+, OH^+, H_2O^+, $O_2{}^+$, ArO^+, $ArOH^+$, NO^+, $NO_2{}^+$, $Cl_2{}^+$). In addition, non-spectral interference effects may also be reduced or eliminated. In these, often referred to as matrix effects [90] and simply defined as matrix induced signal changes, a high concentration of a high mass matrix element (i.e., U) results in a signal suppression of a low mass, low concentration analyte (i.e., Zn). Consider the following thought experiment involving the determination of low concentration Zn in the presence of a high concentration of U. Because U is a good carbide former, it is expected to quantitatively remain in the cup. On the other hand, because Zn is a highly volatile element, it is expected to completely volatilize. Therefore, the high mass element does not suppress the signal from the low mass element.

However, the inherently sequential nature of ICP-MS systems and the transient nature of the signals generated by the DSID necessitates new measurement schemes and DSID-specific software. And much like in AES, we come full circle again for MS: the DSID imposes new constraints on readout electronics and software.

Re-designing the readout electronics and re-writing the software appears to be a recurring theme with DSIDs. To digress for a moment, an ICP-based measurement system utilizing a conventional pneumatic nebulizer for the continuous aspiration of liquid samples into the ICP generates a steady-state signal as shown in Figs. 1-8a and 1-8b. For example, for a PMT-based ICP-AES measurement system, the signal is integrated (via analog or digital means) for a given period of time (i.e. 10 s) and the integrated value(s) (one value per channel per run) is displayed on the CRT of the controlling microprocessor [91]. The development of a readout electronics sub-system capable of handling steady-state signals fits in this niche; work done to this end has been included in Appendix A for reasons of completeness.

For a DSID, however, in order to observe analyte temporal behavior, emission intensities must be digitized in real-time and must be displayed on the CRT sometime during the course of an analysis, as shown in Figure 1-8b. This

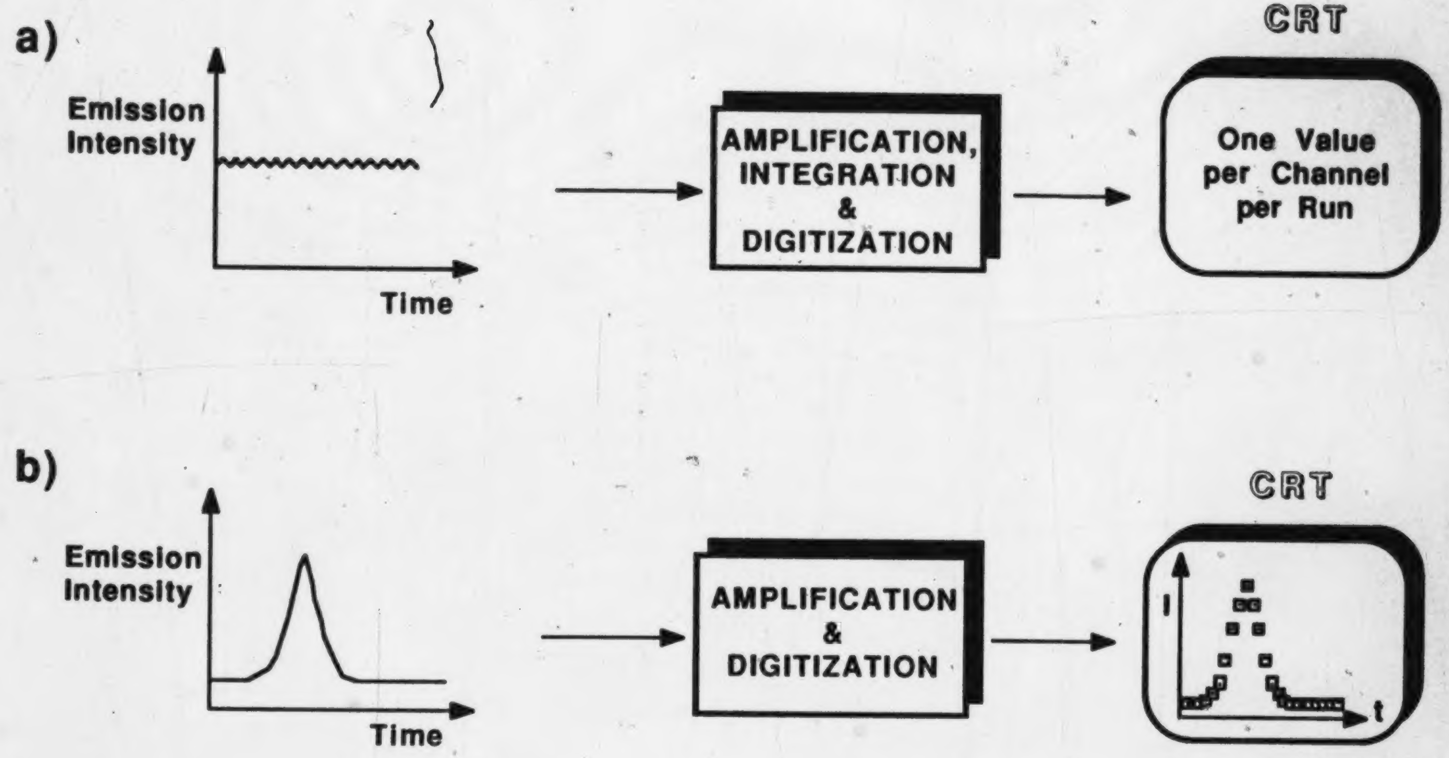
a)
Emission Intensity
Time
AMPLIFICATION, INTEGRATION & DIGITIZATION
CRT
One Value per Channel per Run
b)
Emission Intensity
Time
AMPLIFICATION & DIGITIZATION
CRT
I
t

Figure 1-8. Block diagram of the measurement electronics required for (a) steady state signals and (b) transient signals.

can be achieved by replacing the integrators with amplifiers and by digitizing the resultant signals at high speed. Clearly, new hardware and software must be developed for the DSID.

As shown in Table 1-2, the question of DSID-specific hardware has only been briefly addressed in the literature, in an age of sophisticated microcomputers a chart recorder has often been used for signal registration. And even though measurement systems capable of capturing transient signals are currently commercially available [69, 71], what is currently lacking (Table 1-2) is DSID-specific software.

C.2 Optimization

Much like any other analytical technique, the analytical figures-of-merit of the DSID can be improved by optimizing the experimental parameters affecting its performance characteristics. The questions that arise are: what are the experimental parameters affecting analyte emission temporal behavior, what is the extent of their influence on the analytical performance characteristics of the device, and what are the criteria to be used for optimization (i.e., signal-to-background ratio (SBR), signal-to-noise ratio (SNR)). As shown in Table 1-4, univariate search methods and modified Simplex techniques have been used in order to establish the best set of operating conditions. And although there is adequate information on optimization (Table 1-4), little or no information exists on the effect of DSID design attributes (i.e., probe insertion speed, sequence and geometry) on analyte and background temporal behavior and on the analytical performance characteristics of the DSID.

C.3 Survey Results

As shown in Table 1-5, analyte emission temporal behavior (i.e., intensity-versus-time) curves have been reported for a variety of sample- and probe-types. In general, probe attributes (i.e., type, geometry, composition) have been found to exert a considerable influence on analyte emission temporal behavior. As mentioned earlier, three basic classes of probe types can be distinguished: cups, rods and wire-loops. Due to thermal mass and geometrical considerations, analyte emission temporal behavior observed for wire-loops has been shown to have faster appearance times, shorter peak widths and taller peak heights than that of cups. However, with a wire-loop serving as a sample holder in an AES measurement mode, loop orientation is critical: depending on loop orientation, a different cross-section of the analyte vapor as it travels through the central channel of the plasma is viewed by the spectrometer. This can be easily corrected by designing a DSID in which the sample holder always assumes the same orientation (i.e., a mechanically driven DSID). Loop orientation is not expected to be a problem with an ICP-MS system due to the way atomic vapor is sampled by the mass spectrometer.

Looking at the literature more closely, some subtle points also begin to emerge. For example, boiler caps (Figure 1-4c) and graphite lids (Figure 1-4d) have been found to affect analyte emission temporal behavior, however, both improvements and suppressions in sensitivity have been reported. Probe composition has also been considered by many (Table 1-5). In general, carbide forming elements could not be determined when graphite electrodes were used. Several solutions to this problem have been reported, included in these are: addition of volatilization enhancing agents (i.e., NaF) in the sample carrying cup; use of mixed-gas plasmas (i.e., Ar-H_2, Ar-Freon); and use of metal cups (i.e., Ta, Mo or W) in conjunction with mixed-gas (i.e., Ar-H_2) ICPs.

Because analyte volatilization occurs due to thermal effects, the physical temperature and the heating rate of the sample carrying probe becomes an important consideration. Estimated temperatures of 1800°C to 4000°C have been reported, and depending on power, temperatures of 1600°C to 1800°C have been measured (Table 1-5). Moreover, the effect of electrode geometry on final and equilibrium temperatures and on analyte emission temporal behavior has also been investigated. The effect of power on probe temperature and on analyte emission temporal behavior has been recognized by many (Table 1-5), however, apparently contradictory results have been reported. Furthermore, the combined effect of electrode geometry and power on analyte emission temporal behavior has not been documented.

In summary, this review reveals that the effect of probe attributes (i.e., type, geometry and composition) and power on analyte emission temporal behavior is worthy of further investigation. And because the plethora of DSIDs described in the literature makes a comparison of results reported by other laboratories difficult, a DSID capable of supporting a variety of sample carrying probes may be best suited for such an investigation.

C.4 Performance Characteristics

As shown in Table 1-6, analytical figures-of-merit (i.e., %RSDs, limits of detection (LODs) and calibration curves) have been reported for a variety of sample and probe types. The results shown in Table 1-6 are, for the most part, self-explanatory.

In general, linear calibration curves have been constructed for both liquid and powdered/solid samples (mostly geological and botanical SRMs). The relative independence of calibration from matrix observed for some sample types is worth emphasizing. This was amply demonstrated for powdered botanicals [58] and for metal chips [71]. In other cases, however, matrix matching was found to be important. Undoubtedly, the construction of calibration curves for powdered/solid samples from liquid standards presents an intriguing possibility, the extent of matrix independence is worth further investigating and documenting.

The precision (%RSD) reported (Table 1-6) ranged from 1-25%, a typical value was somewhere between 5% and 10%. This is worse than the ~2% routinely achieved with conventional pneumatic nebulizer systems. Although the causes of imprecision are neither well documented nor well understood at this point, it can be suggested that: the reproducibility of injection (or weighing); the reproducibility of insertion; sample homogeneity (applicable to powdered/solid samples); the physical condition of the sample carrying probe (i.e., cup porosity); the nature of the residue remaining in the probe after drying/ashing or at the initial stages of atomization; and the matrix may provide an adequate account for the reported results. The accuracy of analytical determinations was tested using certified SRMs, in general, reasonably good agreement was found between experimental and certified values (Table 1-6).

The reported detection limits varied widely (Table 1-6), often deviating by more than an order of magnitude. The differences in instrumentation and in sample and probe types appear to be responsible for this variation. To complicate things even further, detection limits were often reported as ppm (or ppb) rather than a more appropriate unit, such as an absolute amount (i.e., ng or pg). However, suffice it to say that most LODs were in the ng to pg range, a rather significant achievement considering the size of the sample.

C.5 Applications

From the objectives of the work reported in the literature (Table 1-1) it can be concluded that the development of DSIDs has been, for the most part, 'applications driven'. Four basic types of applications have been used as the means to demonstrate their analytical capability. The modification of the classical dc arc carrier distillation technique and its application to ICP-AES-DSID was one of the early applications of the DSID, as expected. The application of a DSID for the analysis of powdered samples (i.e., oxides, powdered botanicals) has also been amply demonstrated. Electrochemical preconcentration as the means to improve detection limits (via preconcentration on graphite cups) and separation from difficult matrices (i.e., sea water) has been adequately covered. Finally, the direct analysis of metal chips is just beginning to appear. Undoubtedly, the application of DSIDs to a host of new and old analytical problems is a wide open area. In general, and although examples abound, one of the main goals for the development of DSIDs, namely, the direct analysis of solid rather than powdered samples with little or no sample pre-treatment, has yet to be full-filled.

From the range of applications and the analytical performance characteristics reviewed thus far it can be concluded that the use of DSIDs does indeed improve the analytical capability and utility of the ICP. However, in addition to their advantages revealed in this review, also revealed are some of their limitations. Advantages, limitations and some of the criticism of DSIDs are summarized in what follows.

C.6 Advantages, Limitations and Criticisms

Unlike other methods of sample introduction, no sample loss occurs when a DSID is utilized, therefore, a 100% sample introduction efficiency is realized. In addition, because sample introduction can be achieved with little or no sample pre-treatment (i.e., direct introduction of powders or solids) an added advantage is realized: that of reducing or eliminating sample preparation. The benefits of this are two-fold. First, sample preparation becomes amenable to automation and, second, the possibility for contamination is reduced or eliminated altogether.

By virtue of their design, DSIDs are capable of handling small quantities of either liquids (i.e., µl) or powdered/solid samples (i.e., mg). Therefore, multielement analysis can be performed even when limited sample quantities are available. There is a catch, however. Special attention must be paid to sample homogeneity when analyzing powdered/solid samples.

Drawing parallels between electrothermal atomization, the dc arc and the DSID is, perhaps, un-avoidable. Because the sample holder serves both as a sample container and a vaporization/atomization cell, vaporization, atomization and excitation are not easy to separate. The implications of this are two-fold: first, these steps cannot be independently optimized, and second, matrix effects may become an important consideration. Contrary to the conventional wisdom just described, a relative independence of calibration from matrix was reported in many cases. In addition, because the ICP acts as a vaporization and atomization/excitation cell, an external atomizer is not required. Thus, instrumentation is simplified and cost is reduced. The parallels mentioned above may also give rise to yet another, perhaps subtle, advantage: the large body of literature accumulated over the years for these techniques can be easily transferred and applied to the DSID.

The key limitation of graphite cup DSIDs for ICP-AES is, perhaps, that of carbide formation. (As mentioned earlier, for an ICP-MS-DSID, carbide formation may also be used to an advantage). Because a broad range of elements form carbides, the analytical figures-of-merit of the device are impaired, its applicability is limited to volatile elements and the multielement capability of the ICP is nullified.

This can be easily solved with the addition of reagents in the sample carrying cup or in the plasma-gases. Unlike many other direct sample introduction schemes, chemical modification can be easily achieved as chemical modifiers can be directly added into the sample carrying probe, thus making *in-situ* sample processing possible. Other limitations are not unlike those found in dc arc spectrometry and can be overcome by judicious choice of plasma and sample holder parameters (i.e., size, shape, composition, depth of crater and thickness).

A criticism often voiced is that for solid samples *"...analytes reach the plasma by boiling out from the matrix rather than by complete vaporization of the sample"* [49]. Depending on one's point of view and the application at hand, this can be considered as an asset rather than a liability. Isn't this the reason why the carrier distillation method (i.e., selective volatilization of trace elements) has been and still is widely used in dc arc spectroscopy? As the elements of interest 'boil-out' of the matrix whereas the matrix remains in the cup, much cleaner spectra are observed. This is particularly important for matrices with rich line-spectra, such as uranium. Not to belittle the point, the significance of selective volatilization can be appreciated by simply noting the complexity of lanthanide/actinide spectra [92]. It comes as no surprise then why one of the first and most successful applications of the

DSID for ICP-AES was the application of powdered uranium oxide samples.

Another criticism stems from the use of chemical modification, "*...the use of thermochemical reagents, as employed in dc arcs, will no doubt be discovered again*" [49]. This by no means implies that the wheel has been re-invented once more, only that there is a large body of literature from which to draw proven methodology and applied to the DSID.

The ease of transferability of dc arc and electrothermal concepts to the DSID may make the DSID more 'mature' a technique than it was initially thought to be. And from the range of applications and the analytical performance characteristics of the DSID one thing is becoming clear: the DSID may be considered a more powerful sample introduction system than it was initially perceived to be [57].

D. Thesis Objectives and Approach

Looking back at the review and the the arguments presented in this chapter, the benefits of developing and characterizing DSIDs for the ICP becomes readily apparent. It was thus decided to embark on such endeavour.

The transient nature of the signals generated by the DSID creates a need to assess analyte emission behavior in the time domain. Thus, the development of DSID specific hardware and software capable of handling transient, peak-like signals became the initial objective. This was met as described in chapter 2.

As with any analytical technique and in accord with the *"seven ages of an analytical method"* [31], the construction of working prototypes is typically followed by an evaluation of the performance characteristics of the device under consideration. However, as detailed in chapter 3, a different approach has been taken here. In this case, instead of following the well trodden path described in the literature and summarized in Table 1-4, namely that of full optimization prior to evaluating the performance characteristics of the device, it was decided to isolate the design attributes that affect analytical performance characteristics and to document their effect on the analytical figures-of-merit of the device. The benefits of this approach are two-fold. First, time and energy are not wasted in optimizing a potentially sub-optimal design. Second, when attempting to explain analyte emission temporal behavior (a simple model is also presented in chapter 3), the dangers of attributing instrumental response to physico-chemical processes taking place either in the electrode cavity or the plasma is reduced or eliminated. In order to obtain an indication of the analytical performance characteristics of the device, results documenting the analytical figures of merit of the device have also been included.

From the results presented in chapters 2 and 3, and much like those reported in the literature, it was concluded that carbide formation is a real challenge for a cup-based DSID. Carbide formation is further documented, and solutions to this problem are presented in chapter 4.

From the discussion and the arguments presented in chapters 2, 3 and 4 the concepts of the sample carrying cup as a 'crucible' in which to carry chemical reactions *in situ* (i.e., chemical modification) and that of the DSID not as a mere sample introduction system but as an intelligent sample processor for the ICP begins to emerge.

However, because the automated DSID described in chapters 2 can generate data, to borrow a phrase from the late Tomas Hirschfeld, *"a mile a minute"* and because a successful implementation of the DSID as a sample processor rests upon available processor power, an approach involving two processors, as shown in Figure 1-2, was taken. The merits of a dual processor system and of microcomputers suitable for each function are discussed in detail elsewhere [85, 93-95].

Although the problem of data acquisition and that of results presentation appear to have been adequately solved in chapter 2, as more data are being generated by successively faster measurements (i.e., an over-abundance of data generated by a fully automated ICP-AES-DSID and a 29-channel polychromator), new considerations arise. For example, what to do with the data, how to convert them to information, how to process information and, perhaps, how to turn information to knowledge.

In taking the concept of an intelligent sample processor toward intelligent ICP instrumentation also gives rise to a whole new set of questions. How to control such an instrument, how to interrogate its front end processor (although it is easy to program a computer to question the operator, the task of having the operator interrogate a computer is not as easy as it may initially appear), can the instrument be programmed to learn by monitoring operator activity or by sensing its immediate environment (i.e., self-learning), how can such an instrument be made user friendly, are but a few of these questions. In response to these requirements, the *instrument metaphor* concept was invented and a unique human processor interface (HPI) was developed and implemented on an Apple Macintosh, as described in chapter 5.

A review of HPI concepts was not included in this introduction for two reasons. Firstly, because it is adequately covered in chapter 5, it was felt that there was no need to re-phrase it and present it here. Secondly, and perhaps more importantly, it was felt that, to para-phrase an old adage, 'HPIs should not be explained, they ought to be demonstrated'.

Up to this point (chapters 2 through 5), the ICP was used in its traditional role as an atomization/ionization-excitation source for AES and the DSID was used in conjunction with ICP-AES. However, impressive detection limits are obtained by simply replacing detection of photons (i.e., ICP-AES) with mass spectrometric detection (i.e., ICP-MS). In order to tap into the advantages offered by both the DSID and the ICP-MS, it was decided to build a horizontal DSID for an ICP-MS system. The findings reported in chapters 1 to 5 and the experience gained by using the ICP-AES-DSID were used as the basis for its development and its characterization. In an attempt to merge ICP, MS, DSID and HPI, the concept of *simulating virtual reality* was developed for the ICP-MS-DSID and was implemented on an Apple Macintosh II microcomputer. The results of this investigation are reported in chapter 6 and 7.

Finally, the findings of this work, summarized in chapter 8, will be used as the basis of a blue-sky description of intelligent instrumentation.

REFERENCES

1. P.W.J.M. Boumans, *"Plasma sources other than inductively coupled plasmas"* in *'Inductively Coupled Plasma Emission Spectrometry'*, Part I, P.W.J.M. Boumans, Ed., John Wiley & Sons, New York, 1987, pp. 45-68

2. A. Montaser and D.W. Golightly, *"The significance of inductively coupled plasmas relative to other laboratory plasmas in analytical spectrometry"* in *'Inductively Coupled Plasmas in Analytical Atomic Spectroscopy'*, A. Montaser and G.W. Golightly, Eds., VCH Publishers, Inc., 1987, pp. 1-15

3. A.T. Zander, Anal. Chem., **58**, 1139A (1986)

4. P.W.J.M. Boumans, *"Inductively coupled plasmas"* in *'Inductively Coupled Plasma Emission Spectrometry'*, Part I, P.W.J.M. Boumans, Ed., John Wiley & Sons, New York, 1987, pp. 69-99

5. P.W.J.M. Boumans, *"Basic concepts and characteristics of ICP-AES"* in *'Inductively Coupled Plasma Emission Spectrometry'*, Part I, P.W.J.M. Boumans, Ed., John Wiley & Sons, New York, 1987, pp. 100-257

6. S. Greenfield, *"Common radio frequency generators, torches, and sample introduction systems"* in *'Inductively Coupled Plasmas in Analytical Atomic Spectroscopy'*, A. Montaser and G.W. Golightly, Eds., VCH Publishers, Inc., 1987, pp. 123-161

7. M. Thompson, *"Analytical performance of ICP-AES"* in *'Inductively Coupled Plasmas in Analytical Atomic Spectroscopy'*, A. Montaser and G.W. Golightly, Eds., VCH Publishers, Inc., 1987, pp. 163-198

8. V.A. Fassel, Frezenius Z. Anal. Chem., **324**, 511 (1986)

9. R.M. Barnes, Trends in Anal. Chem., **1(2)**, 51 (1981)

10. S. Greenfield, Analyst, **105**, 1032 (1980)

11. V.A. Fassel, Science, **202**, 183 (1978)

12. V.A. Fassel, Anal. Chem., **51**, 1290A (1979)

13. V.A. Fassel, Spectrochim. Acta, **40B**, 1281 (1985)

14. G.A. Mayer, Anal. Chem., **59**, 1345A (1987)

15. M.J. Thompson and J.N. Walsh, *'A hanbook of ICP Spectrometry'*, Chapman and Hall, N.Y., 1983

16. P.N. Keliher, *"An overview of analysis by ICP-AES"* in *'Inductively Coupled Plasmas in Analytical Atomic Spectroscopy'*, A. Montaser and G.W. Golightly, Eds., VCH Publishers, Inc., 1987, pp. 601-629

17. K. Ohls and D. Sommer, *"Applications: Metals and industrial materials"* in *'Inductively Coupled Plasma Emission Spectrometry'*, Part II, P.W.J.M. Boumans, Ed., John Wiley & Sons, New York, 1987, pp. 1-26

18. J. Burman, *"Applications: Geological"* in *'Inductively Coupled Plasma Emission Spectrometry'*, Part II, P.W.J.M. Boumans, Ed., John Wiley & Sons, New York, 1987, pp. 27-47

19. J. W. MacLaren, *"Applications: Environmental"* in *'Inductively Coupled Plasma Emission Spectrometry'*, Part II, P.W.J.M. Boumans, Ed., John Wiley & Sons, New York, 1987, pp. 48-64

20. F.J.M.J. Maessen, *"Applications: Biological-clinical"* in *'Inductively Coupled Plasma Emission Spectrometry'*, Part II, P.W.J.M. Boumans, Ed., John Wiley & Sons, New York, 1987, pp. 100-150

21. B.L. Sharp, *"Applications: Agriculture and food"* in *'Inductively Coupled Plasma Emission Spectrometry'*, Part II, P.W.J.M. Boumans, Ed., John Wiley & Sons, New York, 1987, pp. 65-99

22. A.W. Boorn, *"Applications: Organics"* in *'Inductively Coupled Plasma Emission Spectrometry'*, Part II, P.W.J.M. Boumans, Ed., John Wiley & Sons, New York, 1987, pp. 151-216

23. B. Maygard and F. Aeschbach, Spectrochim. Acta, **35B**, 839 (1980)

24. G. Gilson and G. Horlick, Spectrochim. Acta, **41B**, 431 (1986)

25. G. Gilson and G. Horlick, Spectrochim. Acta, **41B**, 1323 (1986)

26. N. Omenetto and J.D. Winefordner, *"Atomic fluorescence spectrometry with the ICP"* in *'Inductively Coupled Plasmas in Analytical Atomic Spectroscopy'*, A. Montaser and G.W. Golightly, Eds., VCH Publishers, Inc., 1987, pp. 323-360

27. A.L. Gray, Spectrochim. Acta, **40B**, 1525 (1985)

28. D.J. Douglas and R.S. Houk, Prog. Anal. Atom. Spectrosc., **8**, 1 (1985)

29. R.S. Houk, Anal. Chem., **58**, 97A (1986)

30. G. Horlick, S.H. Tan, M.A. Vaughan and Y. Shao, *"Inductively coupled plasma-mass spectrometry"* in *'Inductively Coupled Plasmas in Analytical Atomic Spectroscopy'*, A. Montaser and G.W. Golightly, Eds., VCH Publishers, Inc., 1987, pp. 361-398

31. H.A. Laitinen, Anal. Chem., **45**, 2305 (1973)

32. M.W. Blades, *"Excitation mechanisms and discharge characteristics-recent developments"* in *'Inductively Coupled Plasma Emission Spectrometry'*, Part II, P.W.J.M. Boumans, Ed., John Wiley & Sons, New York, 1987, pp. 387-420

33. M.W. Blades, B.L. Caughlin, Z.H. Walker and L.L. Burton, Prog. Anal. At. Spectrosc., **10**, 57 (1987)

34. R.M. Barnes, Phil. Trans. R. Soc. Lond. A **305**, 499

35. R.F. Browner and A.W. Boorn, Anal. Chem., **56**, 787A

36. A.G.T. Gustavson, *"Liquid sample introduction into plasmas"* in *'Inductively Coupled Plasmas in Analytical Atomic Spectroscopy'*, A. Montaser and G.W. Golightly, Eds., VCH Publishers, Inc., 1987, pp. 399-430

37. J.A.C. Broekaert and P.W.J.M. Boumans, *"Sample introduction techniques in ICP-AES"* in *'Inductively Coupled Plasma Emission Spectrometry'*, Part I, P.W.J.M. Boumans, Ed., John Wiley & Sons, New York, 1987, pp. 296-357

38. J.C. Van Loon, Anal. Chem., **52**, 955A (1980)

39. R.F. Browner and A.W. Boorn, Anal. Chem., **56**, 875A

40. M.W. Routh and M.W. Tikkanen, *"Introduction of solids into plasmas"* in *'Inductively Coupled Plasmas in Analytical Atomic Spectroscopy'*, A. Montaser and G.W. Golightly, Eds., VCH Publishers, Inc., 1987, pp. 431-

41. J.C. Van Loon, H. Haraguchi and K. Fuwa, *"Direct elemental analysis of solids by ICP-AES"* in *'Inductively Coupled Plasma Emission Spectrometry'*, Part II, P.W.J.M. Boumans, Ed., John Wiley & Sons, New York, 1987, pp. 217-243

42. H. Matusiewich, J. Anal. At. Spectrom., **1**, 171 (1986)

43. T.B. Reed, J. Appl. Phys., **34**, 2266 (1963)

44. P.W.J.M. Boumans, *'Theory of Spectrochemical Analysis'*, Plennum Press, NY, 1966

45. L.H. Ahrens and S.R. Taylor, *'Spectrochemical Analysis'*, Addison-Wesley, Reading, MA, 1961

46. I. Kleinmann and V. Svoboda, Anal. Chem., **41**, 1029

47. E.D. Salin and G. Horlick, Paper #564, Pittsurgh Conference on Analytical Chemistry and Applied Spectroscopy, Clevelant, OH, March 5-9, 1979

48. D. Sommer and K. Ohls, Paper presented at the A.M.S.EL/SCADEC meeting, Eihnhoven, The Netherlands, Oct. 24, 1979 as reported by: K. Ohls and D. Sommer *'Developments in Atomic Spectrochemical Analysis'*, R.M. Barnes, Ed., Hayden, London, 1981, pp. 321-336

49. B.L. Sharp, N.W. Barnett, J.C. Burridge and J.M. Ottaway, J. Anal. At. Spectrom., **1**, 121R (1986)

50. E.R. Prack and G.J. Bastiaans, Anal. Chem., **55**, 1654 (1983)

51. G. Zaray, P. Burba, J.A.C. Broekaert and F. Leis, Spectrochim. Acta, **43B**, 255 (1988)

52. G. Zaray, J.A.C. Broekaert and F. Leis, Spectrochim. Acta, **43B**, 241 (1988)

53. H. Haraguchi, M. Abdullah, T. Hasegawa and K. Fuwa, Bull. Chem. Soc. Jap., **57**, 1839 (1984)

54. M. Abdullah, K. Fuwa and H. Haraguchi, Spectrochim. Acta, **39B**, 1129 (1984)

55. M. Abdullah and H. Haraguchi, Anal. Chem., **57**, 2060 (1985)

56. M. Abdullah, K. Fuwa and H. Haraguchi, Appl. Spectrosc., **41**, 715 (1987)

57. E.D. Salin and G. Horlick, Anal. Chem., **51**, 2284

58. W.E. Pettit and G. Horlick, Spectrochim. Acta., **41B**, 699 (1986)

59. Y. Shao and G. Horlick, Appl. Spectrosc., **40**, 386

60. V. Karanassios and G. Horlick, Appl. Spectrosc., **41**, 360 (1987)

61. V. Karanassios and G. Horlick, *'A computer-controlled direct sample insertion device for ICP-AES'*, Spectrochim. Acta, (submitted)

62. V. Karanassios, G. Horlick and M. Abdullah, *'Characterization of a direct sample insertion device for ICP-AES'*, Spectrochim. Acta, (submitted)

63. V. Karanassios, M. Abdullah and G. Horlick, *'The application of chemical modification to a direct sample insertion device for ICP-AES'*, Spectrochim. Acta, (submitted)

64. V. Karanassios and G. Horlick, *'Development and characterization of a direct sample insertion device for ICP-MS'*, (in preparation)

65. G.F. Kirkbright and S.J. Walton, Analyst, **107**, 276

66. G.F. Kirkbright and Z. Li-Xing, Analyst, **107**, 617

67. Z. Li-Xing, G.F. Kirkbright, M.J. Cope and J.M. Watson, Appl. Spectrosc., **37**, 250 (1983)

68. N.W. Barnett, M.J. Cope, J.F. Kirkbright and A.A.H. Taobi, Spectrochim. Acta, **39B**, 343 (1984)

69. A. Lorber and Z. Golbard, Analyst, **110**, 155 (1983)

70. I.B. Brenner, A. Lorber and Z. Golbard, Spectrochim. Acta, **42B**, 219 (1987)

71. C.W. McLeod, P.A. Clarke and D.J. Mowthorpe, Spectrochim. Acta, **41B**, 219 (1986)

72. D. Sommer and K. Ohls, Frez. Z. Anal. Chem., **304**, 97 (1980)

73. K. Ohls and D. Sommer, in 'Developments in Atomic Spectrochemical Analysis', R.M. Barnes, Ed., Hayden, London, 1981

74. K. Ohls, Spectrochim. Acta, **39B**, 1105 (1984)

75. A.G. Page, K.H. Madraswala, S.V. Goodbole, M.J. Kulkarni, V.S. Mallapurkar and B.D. Joshi, Frez. Z. Anal. Chem., **315**, 38 (1983)

76. A.G. Page, K.H. Madraswala, S.V. Goodbole, M.J. Kulkarni, V.S. Mallapurkar and B.D. Joshi, Spectrochim. Acta, **39B**, 551 (1984)

77. E.D. Salin and M.M. Habib, Anal. Chem., **56**, 1186

78. E.D. Salin and R.L.A. Sing, Anal. Chem., **56**, 2596

79. M.M. Habib and E.D. Salin, Anal. Chem., **57**, 2055

80. C.V. Monasterios, A.M. Jones and E.D. Salin, Anal. Chem., **58**, 780 (1986)

81. R.L.A. Sing and E.D. Salin, Paper #32, 1986 Winter Conference on Plasma Spectrochemistry, Kailua-Kona, Hawaii, Jan. 2-8, 1986

82. D.W. Boomer, M. Powell, R.L.A. Sing and E.D. Salin, Anal. Chem., **58**, 975 (1986)

83. T.W. Williams and E.D. Salin, Anal. Chem., **60**, 725

84. M. Umemoto and M. Kubota, Spectrochim. Acta, **42B**, 491 (1987)

85. V. Karanassios and G. Horlick, '*Microcomputer systems for laboratory applications*', (in preparation)

86. V. Karanassios and G. Horlick, Appl. Spectrosc., **40**, 813 (1986)

87. G.M. Levy, A. Quaglia, R.E. Lazure and S.W. McGeorge, Spectrochim. Acta, **42B**, 341 (1987)

88. M.A. Vaughan and G. Horlick, Appl. Spectrosc., **40**, 434 (1986)

89. S.H. Tan and G. Horlick, Appl. Spectrsc., **40**, 445

90. S.H. Tan and G. Horlick, J. Anal. At. Spectrom., **2**, 745 (1987)

91. V. Karanassios and G. Horlick, Appl. Spectrosc., **42**, 961 (1988)

92. R.K. Winge, V.A. Fassel, V.J. Peterson and M.A. Floyd, '*Inductively Coupled Plasma Atomic Emission Specroscopy. An Atlas of Spectral Information.*',

93. V. Karanassios and G. Horlick, Talanta, **32**, 583 (1985)

94. V. Karanassios and G. Horlick, Talanta, **32**, 601 (1985)

95. V. Karanassios and G. Horlick, Talanta, **32**, 615 (1985)

CHAPTER 2

A COMPUTER-CONTROLLED DIRECT SAMPLE INSERTION DEVICE FOR ICP-AES

A. Introduction

Since the original description of a direct sample insertion device (DSID) for the inductively coupled plasma (ICP) by Salin and Horlick [1], DSIDs appear to have reached a state of relative maturity. They are being developed for both ICP-atomic emission spectrometry (ICP-AES) [1-29] and ICP-mass spectrometry (ICP-MS) [30, 31] and are being studied in a number of laboratories. In addition to the discussions included in reviews [32] and in book chapters [33, 34], a number of papers [1-31] describing their design and performance characteristics can be found in the literature. And although quite a variety of techniques and systems fall under the umbrella definition of direct sample insertion, a working definition of a DSID is, a device in which the sample is placed into or onto a probe, with subsequent introduction of the sample carrying probe into the plasma. A block diagram of a DSID is shown in Figure 2-1.

Even though a conventional undercut dc arc graphite electrode (simply referred to as 'electrode' or 'cup') is shown in Figure 2-1, special graphite electrode geometries (i.e., long undercut electrode), flat-top graphite electrodes fitted with metal cups and wire-loops have been used as sample carrying probes, as shown in Figure 2-2.

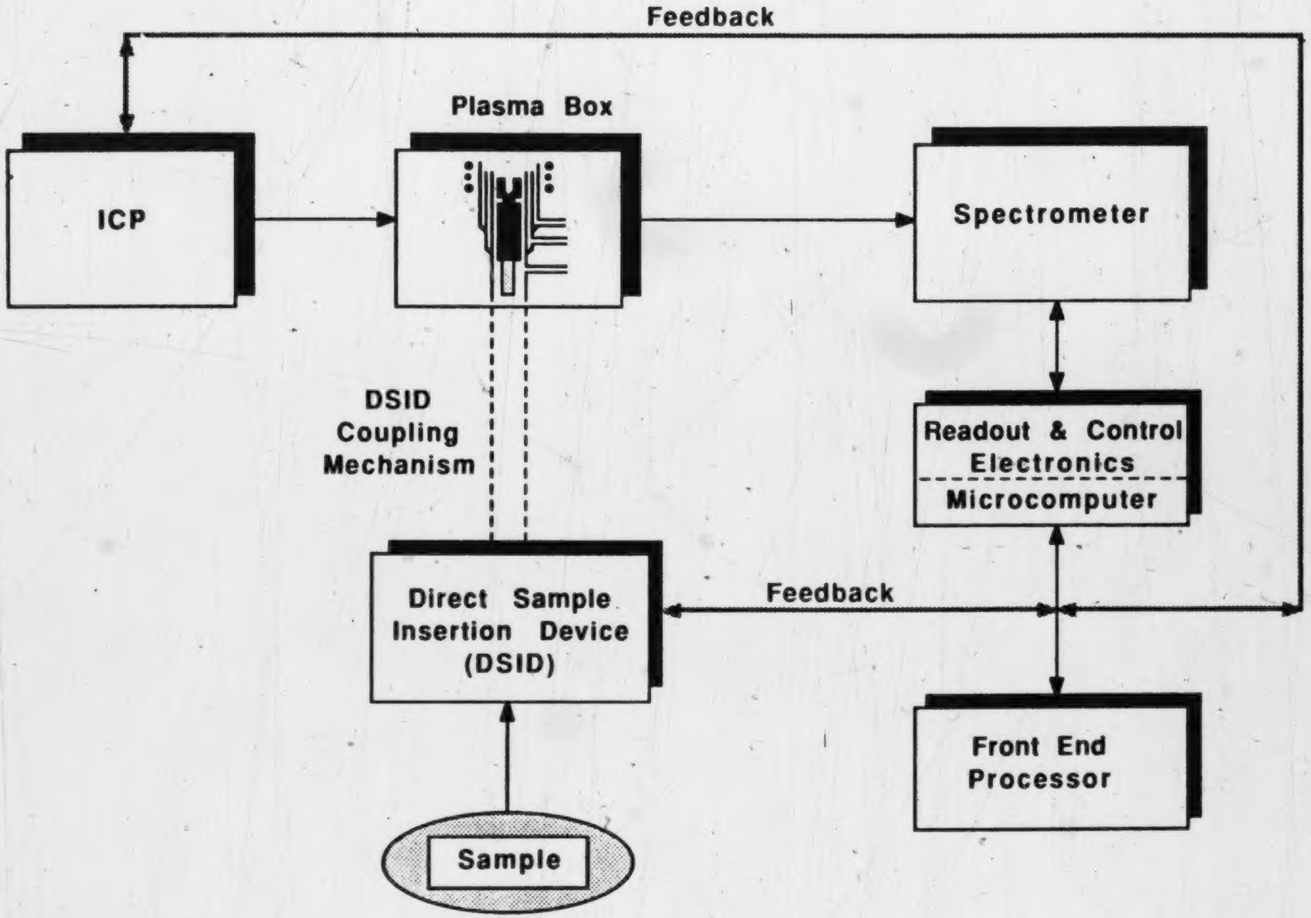
Feedback
Plasma Box
ICP
Spectrometer
DSID
Coupling
Mechanism
Readout & Control
Electronics
Microcomputer
Direct Sample
Insertion Device
(DSID)
Feedback
Front End
Processor
Sample

Figure 2-1. Block diagram of the experimental set-up of a DSID for ICP-AES.

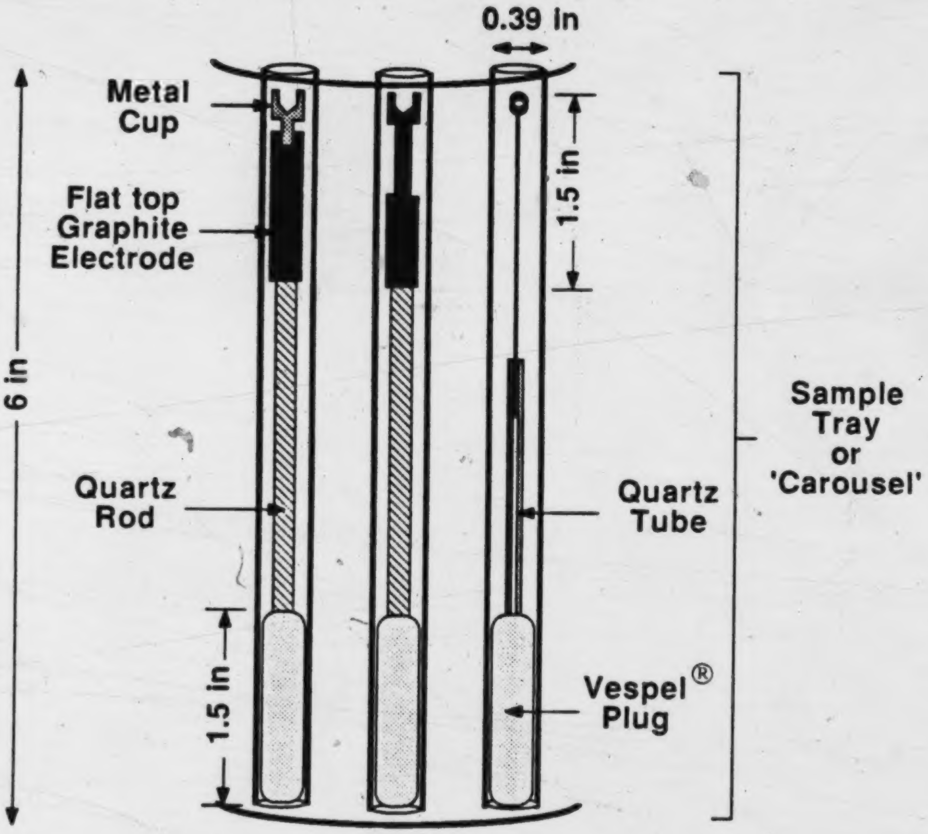
0.39 in
Metal Cup
Flat top Graphite Electrode
6 in
1.5 in
Quartz Rod
1.5 in
Quartz Tube
Vespel® Plug
Sample Tray or 'Carousel'

Figure 2-2. Sample tray, sample holder assembly (i.e., Vespel plug, quartz stem and probe) and probe types. Left: a flat-top electrode fitted with a metal cup; center: a long undercut graphite electrode; right: a wire-loop.

In general, DSIDs can be classified according to the type of sample probe utilized as graphite cup-based [1-3, 6, 7, 11-29], as graphite rod-based [4, 5, 9] and as wire-loop based [18, 30, 31]. More specifically, the probe consists of conventional undercut dc arc electrodes [1-3, 6, 7, 11-29], flat-top graphite electrodes or graphite rods serving as flat-top electrodes [4, 5, 9], flat-top graphite electrodes fitted with a metal cups (only the undercut cup is metal) [9, 28], graphite electrodes fitted with dc arc boiler cups or custom designed lids [1, 2, 6, 15, 16, 23, 26, 27] and wire-loops [18, 30, 31]. Wire-loops are mainly advocated by Salin and co-workers [18, 31]. The system described here is capable of handling graphite electrodes, special electrode geometries, metal cups and wire-loops interchangeably.

Because DSIDs can be operated either vertically (as shown in Figure 2-1) or horizontally, they can be classified accordingly as vertical or horizontal. Vertical DSIDs are mostly utilized in ICP-AES, horizontally operated systems are exclusively utilized in ICP-MS [30, 31]. In most designs described in the literature, the sample carrying probe is inserted axially into the plasma torch (i.e., in parallel to the central tube), as shown in Figure 2-1, with one possible exception [22, 23]. In this horizontally operated DSID, the electrodes are inserted externally to the torch and transversely to the plasma cross-section.

Insertion of the sample carrying probe into the plasma can be accomplished either manually [1, 4, 5, 8, 9, 15-17, 19, 20, 22, 23, 25] or automatically [2, 3, 6, 7, 10, 11, 26, 33] with early designs being manually driven and more recent designs automated to varying degrees. Two basic classes of automated or semi-automated designs can be further distinguished: those that are mechanically driven (i.e., reversible motor [26, 27], computer/stepper motor/lead screw [3, 10, 11, 25, 29], computer/stepper motor/timing belt [5, 6, 35], car aerial [24]) and those that are pneumatically driven [2, 12-14, 18, 31]. The automated, computer controlled, vertically operated, pneumatically and mechanically driven prototype DSID design described here is a modified version of that developed by Pettit and Horlick [2]. A unique feature of this system is that it can handle up to 24 sample carrying probes in an automated and uninterrupted fashion.

Because a finite amount of sample is placed into or onto the sample carrying probe, the spectral signals generated by the DSID are peak-like and transient in nature. With respect to Figure 2-1, the transient nature of analyte emission defines not only the spectrometer required for multielement analysis, but also dictates readout electronics (as transient signals need to be digitized in real-time) and software (because a number of data points must be displayed on the CRT of the controlling microprocessor in order to define analyte emission temporal behavior on the screen). These issues will be addressed in detail and the development of new readout and control electronics will be discussed.

A dual-processor system is shown in Figure 2-1, of the concept developed by Karanassios and Horlick [36]. The discussion here will be restricted to the data acquisition and control microcomputer. In this case, this microcomputer is also used as a development tool and a test-bed for new ideas and concepts. Its use in this capacity was deemed necessary, because before the dual-processor system shown in Figure 2-1 can be further developed, hardware; data acquisition, control and DSID automation software; and signal processing and control algorithms must be developed and tested. In addition, the requirements for the feedback loops shown in Figure 2-1 must be established, analyte emission temporal behavior must be understood and the analytical performance characteristics of the device must be determined. It is only then that the dual processor system can be fully developed. The concepts developed here can then be easily ported and implemented on the front-end processor.

There is little doubt that in any programmable device, software drives the hardware. The automated DSID described here is no exception. Unfortunately, software capable of handling DSID generated signals is not commercially available. It is only when DSID-specific hardware and software has been developed (with its attendant long development cycle) that the DSID can attain its potential. In response to these requirements, a user-friendly, window-based prototype software package developed for DSID automation, control and fault-diagnosis; data acquisition; signal processing; graphics display and processing; and data and information management has been developed and will be described in some detail.

B. Instrumentation

B.1 ICP, Spectrometer and Operating Conditions

The basic components of a DSID for ICP-AES are shown, in block diagram form, in Figure 2-1. The ICP utilized in this work was a Plasma Therm ICP 5000 consisting of a 27.12 MHz generator (model HFS-5000D), a matching network (model AMN-5000E) and a torch box (model PT-1). Typical running conditions were: forward power, 1.25 kW; reflected power, less than 80 W; coolant gas (Ar), 18 l/min; auxiliary (Ar), 0.6 l/min; and snuffer gas (Ar), 1 l/min. The observation height was set at 16 mm above the load coil. All measurements were taken with the top of the sample carrying probe in alignment with the top of the load coil (abbreviated as TOLC), data acquisition (t=0 s) was initiated when the sample carrying probe was in alignment with the central tube of the torch (referred as as the 'reference position'). A 'regular drive' insertion mode (explained in a later section) was used throughout. The spectrometer utilized was a one-meter, 29-channel direct reader (Paschen-Runge mount) with a 1200 grooves/mm concave grating. ICP and polychromator were set-up on a large optical rail bed, as shown in Figure 2-1 of reference 36.

Graphite rods and electrodes (SPEX Industries, Inc., Edison, NJ or Bay Carbon, Inc., Bay City, MI) were treated according to the procedure recommended by Abdullah et al. [5] and pre-burned 3 to 5 times prior to their use. All solutions were prepared by serial dilution with distiled/deionized water of 1000 ppm standard stock solution (standards for plasma emission spectroscopy, SPEX Industries Inc., Edison, NJ) of the respective element. A 10 µl volume was transferred (i.e., injected) to the sample carrying probe with an Eppendorf micropipette. Solution volumes injected into cups were dried by heating the electrodes in an aluminium holder on a hot plate prior to insertion into the plasma. Those applied onto the wire-loop were dried with an IR-lamp.

B.2 Direct Sample Insertion Device (DSID)

At the heart of the system shown in Figure 2-1 is the DSID itself, and central to it is the sample carrying probe. And although a conventional undercut dc arc graphite electrode is shown in Figure 2-1, two basic types of probes have been utilized with this system. More specifically, the probe consists of either an electrode (i.e., a long undercut dc arc graphite electrode [28] or a flat-top graphite electrode fitted with a metal cup, as shown in Figure 2-2) into which either µl volumes of liquids or mg quantities of powdered/solid samples can be placed or a wire-loop (Figure 2-2), onto which µl volumes of liquid samples can be deposited. The wire-loop consists of a W wire, 8-cm in length and 1-mm in diameter that forms two, 5-mm in diameter loops onto which the sample (typically 10 µl) is deposited. The most important drawback of this system is its inherent inability to directly handle powdered or solid samples: these must be first converted to liquids before insertion into the ICP. Metal cups (e.g., Ta and W) and flat-top graphite electrodes have been machined in our machine shop out of the corresponding metal or graphite rod. Unless otherwise stated, the use of long undercut graphite electrodes is assumed.

The probe (cup or wire-loop) is placed on top of a quartz stem (rod or tube, respectively) which, in turn, is inserted in a plastic (Vespel or Darlin) plug that provides a pneumatic seal, as shown in Figure 2-2. Metal cups used for the determination of carbide forming elements [2] will be treated as a sub-class of the graphite electrode. For reasons of brevity, probe, quartz stem and plastic plug will be henceforth referred to as the 'sample holder assembly' or 'sample holder' for short. Up to 24 sample holder assemblies can be pre-loaded on a modified, computer controlled, autosampler carousel, and are pneumatically inserted, in a sequential fashion, into the ICP for vaporization, atomization and excitation.

A more detailed diagram of the DSID is shown in Figure 2-3. The sample holder assembly is brought into insertion position (e.g., in alignment with the 'guide tube to torch') by rotating the carousel. Prior to insertion and before the sample holder assembly has been brought into insertion position, the assembly to be inserted next is purged with Ar in order to avoid air entrainment into the plasma which may be extinguished if the pre-purge is not utilized.

Insertion of the sample carrying probe into a modified, water cooled torch supported by an air cooled torch assembly is accomplished pneumatically: the 'injector gas line' and the 'snuffer line' are switched to 'on-line' and 'exhaust' respectively, as shown in Figure 2-3. Consequently, the sample holder assembly in alignment with the 'guide tube to torch' lifts off and is slowly driven into the torch. An 8 liter ballast tank is placed in series with the injector gas line in order to ensure smooth lift off and insertion. The speed of insertion depends on the applied injector gas pressure (about 4 psi); a high speed may extinguish the plasma.

Gravity is at work for sample holder retraction: the injector valve is activated, as shown in Figure 2-4, so that the injector gas is routed, through the ballast tank and the purge line (labeled purge line 1 in Figure 2-3) to pre-purge

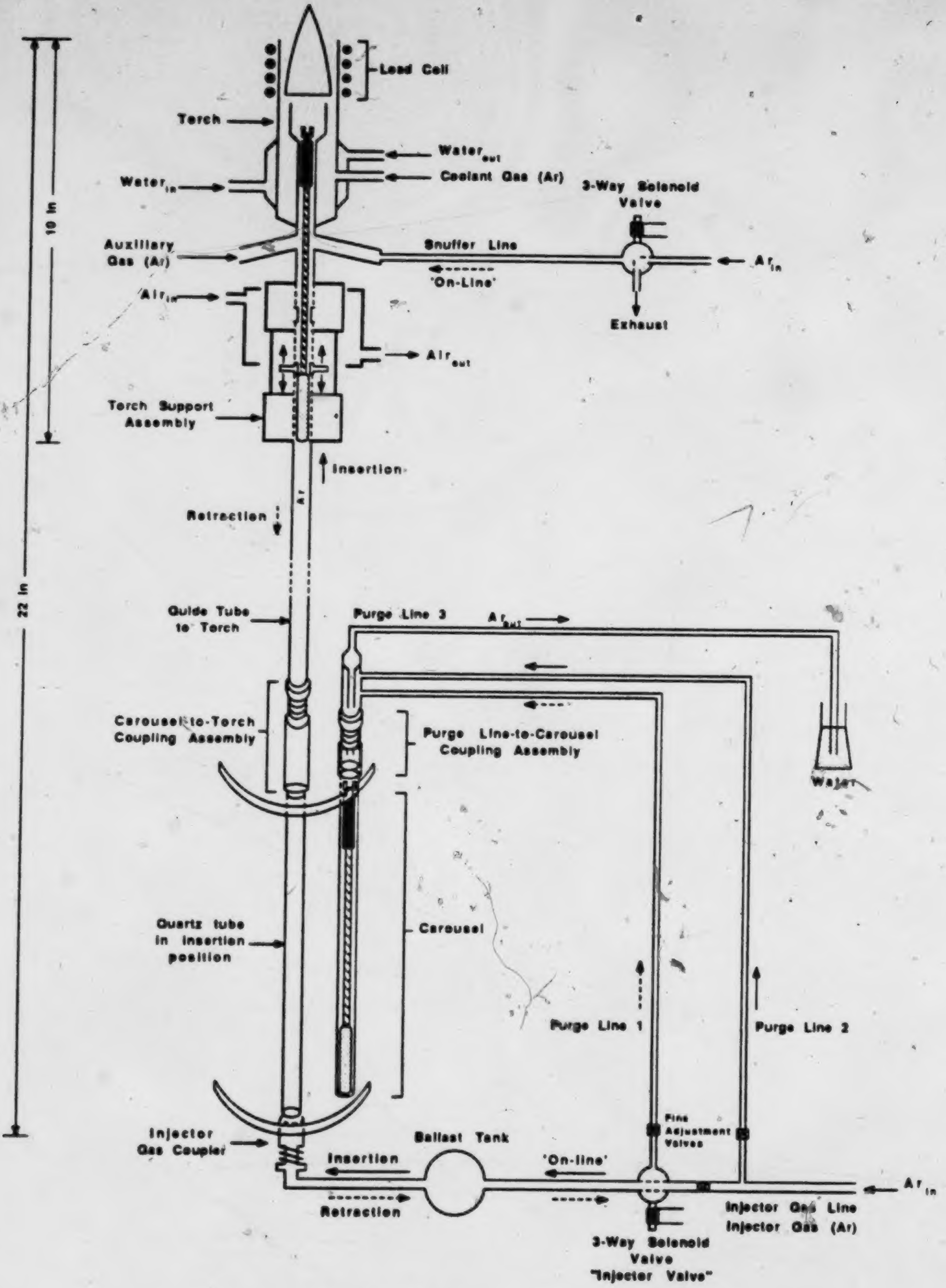
Load Coil
Torch
Water$_{out}$
Coolant Gas (Ar)
Water$_{in}$
3-Way Solenoid Valve
Auxiliary Gas (Ar)
Snuffer Line
Ar$_{in}$
'On-Line'
Exhaust
Air$_{in}$
Air$_{out}$
10 in
Torch Support Assembly
Insertion
Retraction
Ar
22 in
Guide Tube to Torch
Purge Line 3
Ar$_{out}$
Carousel-to-Torch Coupling Assembly
Purge Line-to-Carousel Coupling Assembly
Water
Quartz tube in insertion position
Carousel
Purge Line 1
Purge Line 2
Fine Adjustment Valves
Injector Gas Coupler
Ballast Tank
Insertion
'On-line'
Retraction
Ar$_{in}$
Injector Gas Line
Injector Gas (Ar)
3-Way Solenoid Valve "Injector Valve"

Figure 2-3. Illustration of sample holder insertion. (Diagram not to scale).

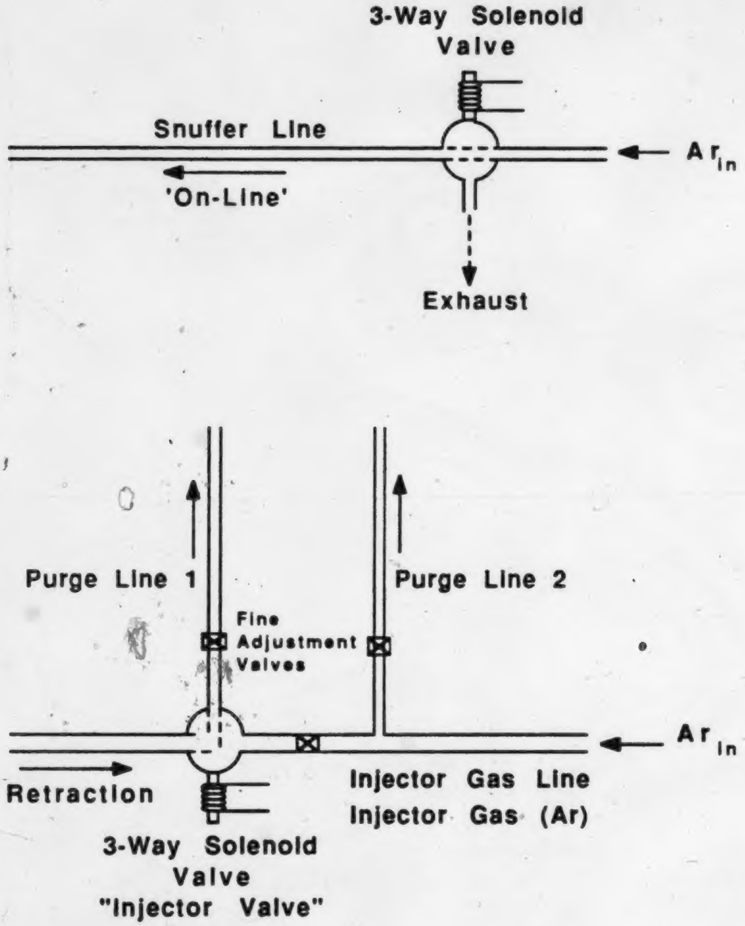
3-Way Solenoid Valve
Snuffer Line
'On-Line'
Ar$_{in}$
Exhaust
Purge Line 1
Purge Line 2
Fine Adjustment Valves
Ar$_{in}$
Retraction
Injector Gas Line
Injector Gas (Ar)
3-Way Solenoid Valve "Injector Valve"

Figure 2-4. Solenoid valve configuration for sample holder retraction.

the next electrode assembly. The ballast tank now provides a smooth retraction. The 'snuffer line', is switched form 'exhaust' to 'on-line', as shown in Figure 2-4, to snuff out any discharge filaments that form between the plasma and the sample holder, and to help maintain a stable plasma. If a snuffer gas is not utilized, the filament often follows the sample holder all the way to the carousel. All gas lines are switched via solenoid valves which are under either manual or computer control.

Precise positioning of the sample carrying probe inside the torch is required in order to obtain reproducible analytical results. The probe can be precisely positioned inside the plasma in two ways: by utilizing a 'one shot' mode in which the sample holder assembly is directly inserted (e.g., shot) into the plasma and it is stopped (by a mechanical stop) only when the top of the probe has reached TOLC (Figure 2-5), or, in a stepwise fashion (i.e., a 'regular drive' insertion mode), by stopping the sample holder assembly underneath the bottom load coil (i.e., reference position, Figure 2-5) and slowly driving it inside the plasma. Thus, the effect of insertion speed on both the atomic and the background signals can be investigated [28].

As mentioned earlier, a regular drive insertion mode has been used throughout. In this mode, by positioning the probe at positions successively closer to the plasma discharge, thereby taking advantage of the thermal gradient

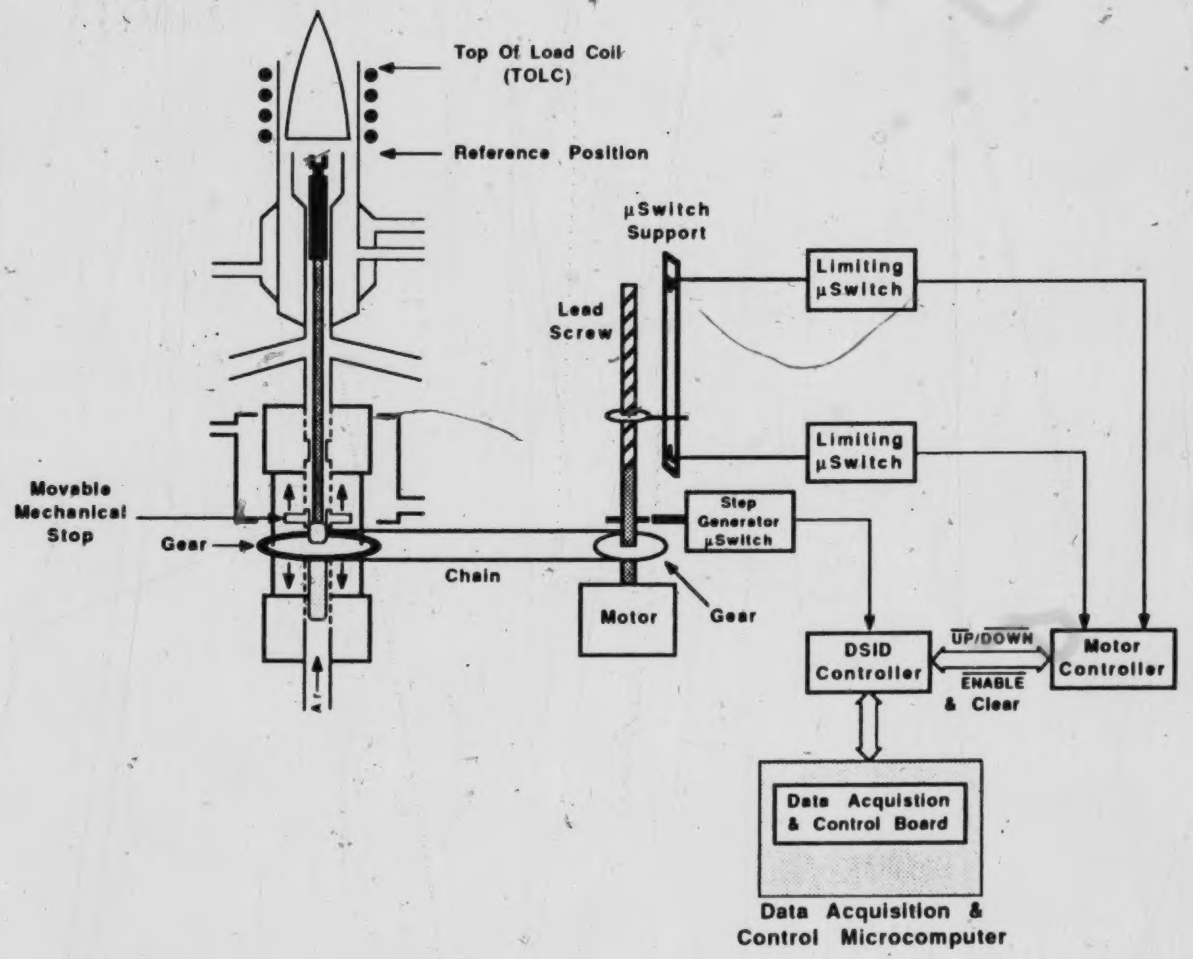
Top Of Load Coil
(TOLC)
Reference Position
μSwitch Support
Lead Screw
Limiting μSwitch
Limiting μSwitch
Step Generator μSwitch
Movable Mechanical Stop
Gear
Chain
Motor
Gear
DSID Controller
UP/DOWN
ENABLE & Clear
Motor Controller
Data Acquistion & Control Board
Data Acquisition & Control Microcomputer

Figure 2-5. Block diagram of motor driver and support electronics.

that exists underneath the plasma, *in situ* sample pretreatment (i.e., drying and ashing) can be achieved prior to atomization [2, 3, 5, 6, 10]. These steps are analogous to the dry, ash, and atomize cycles of graphite furnace atomizers. It should be noted that the plasma is extinguished upon insertion if liquid samples or powdered samples of organic origin (e.g., biological samples) are used without drying or ashing. With this system, these steps can take place either underneath the plasma or externally before loading the sample tray.

In this design, a mechanically movable stop 'catches' the sample holder, as shown in Figure 2-5. The stop uses a threaded ring operating within a threaded barrel. More details on this sub-system are presented by Pettit and Horlick [2]. The barrel is mechanically connected to a computer controlled motor, as shown in Figure 2-5. Depending on the direction of rotation, the mechanical stop and, hence, the sample holder assembly, can be reproducibly raised or lowered to any desired position within the plasma. As the motor rotates, it activates the step generator microswitch which, as its name implies, generates a train of pulses. The location of the mechanical stop, and therefore, of the probe, is monitored by the data acquisition and control microcomputer by counting the pulses generated by this microswitch. Thus, the insertion position for the dry, ash and atomize cycles can be easily and reproducibly set and monitored by the controlling microcomputer.

B.3 Readout and Control Electronics

Among the various possible alternatives [37, 38, 39], the microcomputer chosen for data acquisition and control was an IBM PC, with 640 kBytes of RAM, an AST Six Pack Plus board, a color graphics adapter, serial and printer ports and a Data Translation® (Data Translation, Inc., 100 Locke Drive, Marlborough, MA 01752) DT2801A data acquisition and control board. This board consists of a 12-bit ADC; two, 12-bit DACs (Analog Devices AD 7545), two, 8-bit I/O ports (Intel 8243), and a programmable interval timer/counter (Intel 8253, Intel Corp., 3065 Bowers Ave., Santa Clara, CA 95051). Up to 8 differential or 16 single ended analog inputs can be multiplexed and read by the ADC, thus, up to 16 polychromator channels (PMTs) can be simultaneously monitored. The ADC, capable of sustaining a 27.5 KHz data acquisition rate, is preceeded with a sample and hold amplifier; a programmable gain amplifier (PGA) supportive of 1,2,4 and 8 gains; and an analog multiplexer.

As mentioned earlier, the insertion position for drying, ashing and atomization is monitored by counting the pulses generated by the step generator microswitch. Because none of the facilities offered by the 8253 of the Data Translation board is made available to the user, an Intel

8253 programmable interval timer/counter was interfaced to the IBM PC via the digital I/O ports of this board and some support logic, as shown in Figure 2-6. Alternatively, both 8253 and support logic could be placed directly on the IBM PC bus, as it was recently demonstrated for other buses [40]. However, this option is not available to us because all slots of the IBM PC backplane bus are populated by other boards.

Differential vaporization of analyte is an important aspect of the DSID. Typical examples of analyte emission temporal behavior are shown in Figure 2-7 for Ag, Co, Cu and Mn and for 25 ng of Cu for a long undercut graphite electrode, a Ta metal-cup, a W metal-cup and a W wire-loop in Figures 2-8a, 2-8b, 2-8c and 2-8d, respectively.

Due to the temporal behavior displayed by analyte emission, analyte emission intensities must be acquired as time-varying quantities and digitized in real-time. With respect to Figure 2-1, analyte emission temporal behavior dictates the type of spectrometer required for multielement analysis, it precludes the use of a monochromator or a slew-scanning spectrometer and thus requires a PMT-based or a diode array-based direct reading spectrometer [41]; it determines the nature of the readout electronics; and it defines the software requirements for signal acquisition, display, processing and DSID control.

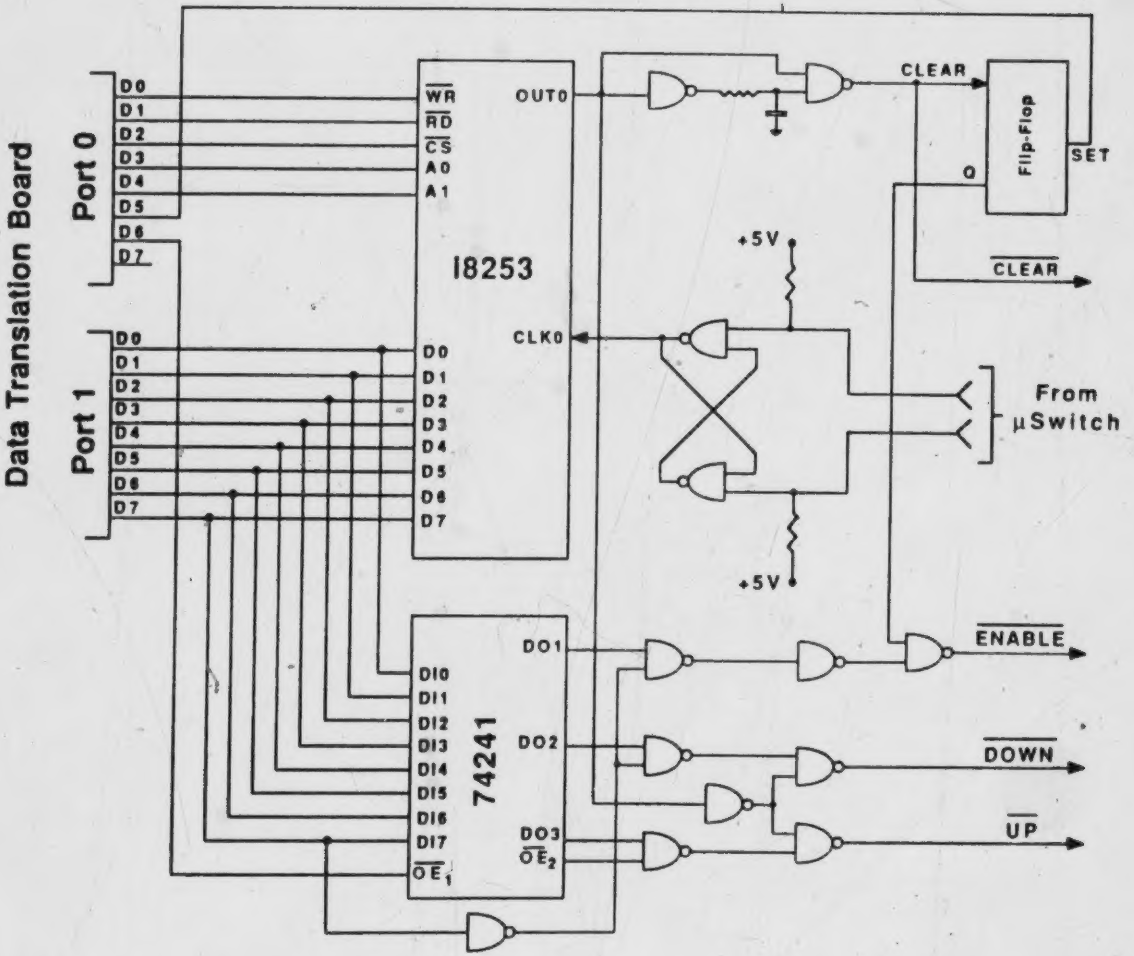
Data Translation Board
Port 0
D0
D1
D2
D3
D4
D5
D6
D7
Port 1
D0
D1
D2
D3
D4
D5
D6
D7
18253
WR
RD
CS
A0
A1
D0
D1
D2
D3
D4
D5
D6
D7
OUT0
CLK0
74241
DI0
DI1
DI2
DI3
DI4
DI5
DI6
DI7
OE1
DO1
DO2
DO3
OE2
CLEAR
Flip-Flop
Q
SET
CLEAR
+5V
+5V
From
μSwitch
ENABLE
DOWN
UP

Figure 2-6. DSID controller and step measuring electronics.

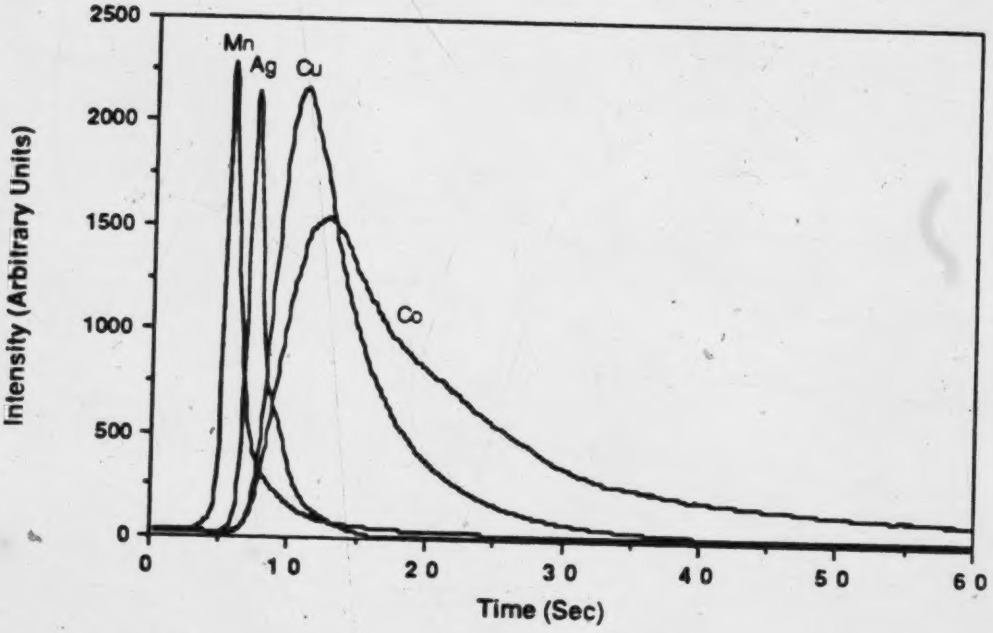

Figure 2-7. Typical analyte emission temporal behavior.

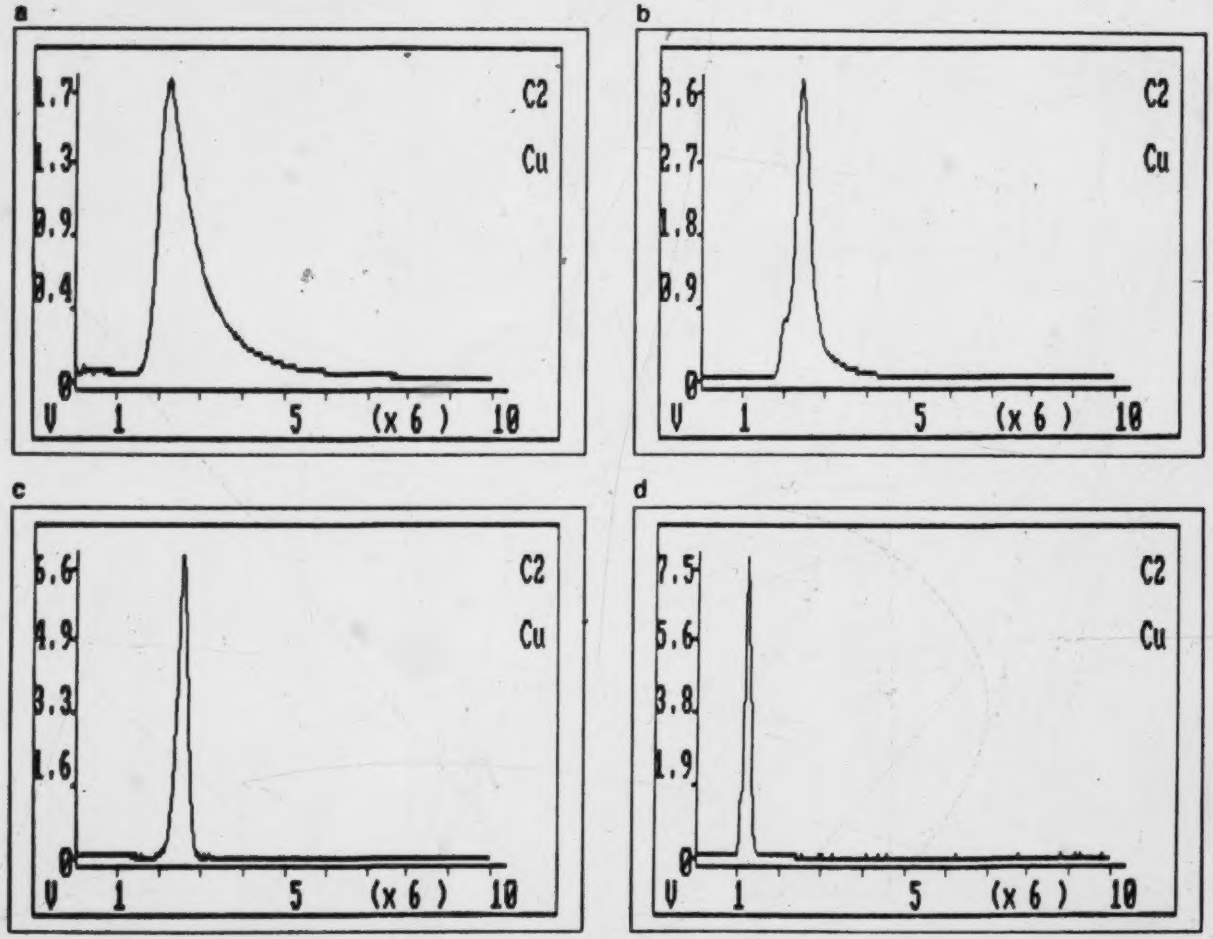

Figure 2-8. Analyte emission temporal behavior for 25 ng Cu. (a) Long undercut graphite electrode; (b) Ta metal cup; (c) W metal cup; and (d) W wire-loop.

B.4 Data Acquisition

Although the issue of DSID automation and control has been adequately addressed [2, 3, 6, 7, 10, 26, 30, 35], re-designing readout electronics and re-writing software appears to be a recurring theme with DSIDs. And even though the design of readout electronics capable of handling transient signals has been pointed out as an area in need of further development [3, 10, 35], it has only been either mentioned in passing or briefly addressed in the relevant literature [2, 3, 17, 18, 20, 33]. A current amplifier and chart recorder have often been used as the means to capture and record analyte emission temporal behavior [3, 4-11, 17-20, 25]. Furthermore, hardware capable of digitizing transient signals in real-time and appropriate signal processing, display and manipulation software are not available in commercial direct reading spectrometers. This is not surprising as pneumatic nebulization of liquid samples into the ICP is the most popular form of sample introduction into the plasma and it is used by the vast majority of ICPs in the field.

Continuous aspiration of liquid samples in the plasma generates a steady-state signal at the detector, as shown in Figure 2-9 for a PMT-based direct reading spectrometer. Because there is no need to digitize a steady-state signal in real-time, the current output of the PMTs is typically

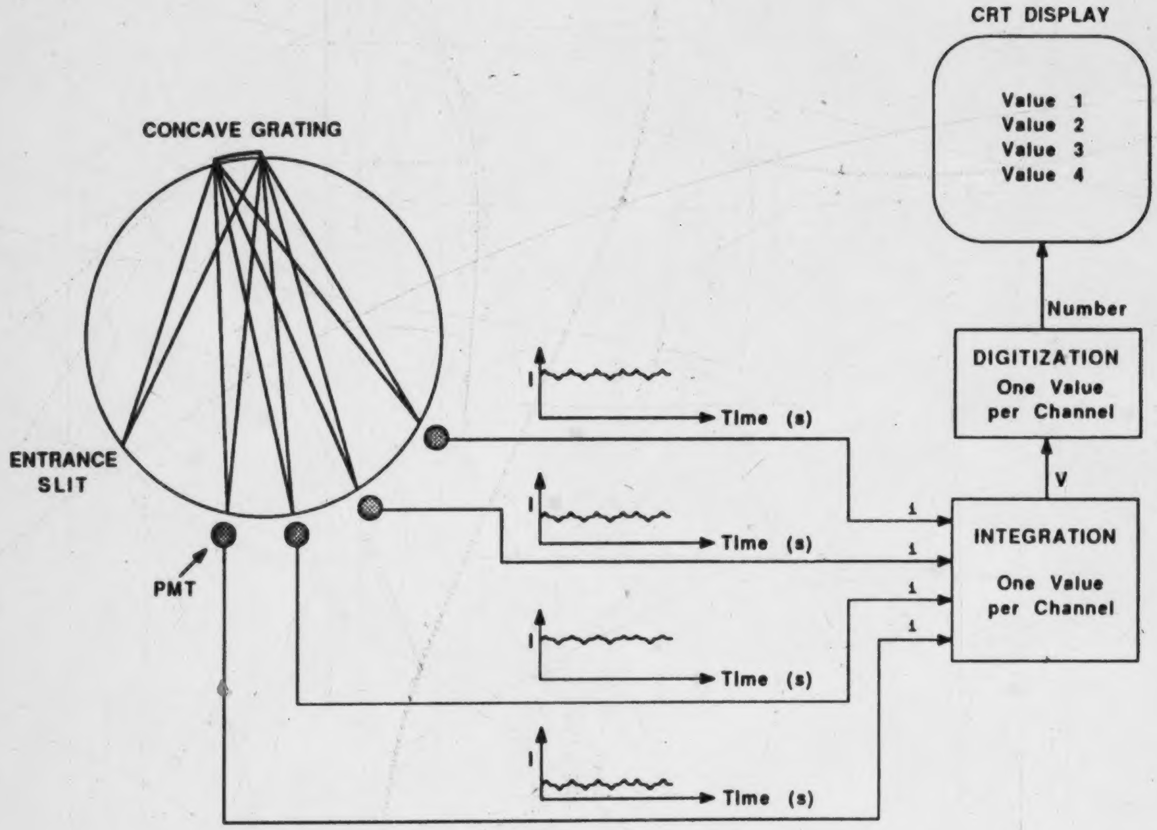
CRT DISPLAY
Value 1
Value 2
Value 3
Value 4
Number
DIGITIZATION
One Value per Channel
V
INTEGRATION
One Value per Channel
i
i
i
i
CONCAVE GRATING
ENTRANCE SLIT
PMT
I
Time (s)
I
Time (s)
I
Time (s)
I
Time (s)

Figure 2-9. Block diagram of direct reader measurement electronics for steady state signals (i.e., continuous sample aspiration via pneumatic nebulization).

integrated for a given period of time (e.g., 10 s) and an integrated value is displayed on the CRT of the controling microprocessor [40]. For a DSID, however, in order to observe analyte emission temporal behavior, emission intensities must be digitized in real-time and must be displayed on the CRT of the controlling processor some time during the course of an analytical run, as shown in Figure 2-10. In this case, analog or digital integration (Figure 2-9) is replaced with current-to-voltage conversion (Figure 2-10) and the resultant signal is digitized in real-time. Clearly, the DSID imposes new design constraints on data acquisition hardware and software.

The data acquisition rate is, perhaps, the most important criterion of these new designs, especially for multielement/multichannel applications. Several experimental parameters, because they affect analyte emission temporal behavior, also influence the choice of a data acquisition rate. Included in these are: DSID type (i.e., cup-based or wire-loop based); probe geometry and composition; probe insertion sequence, speed and final insertion position inside the plasma; applied forward power; and plasma gas composition. To complicate things even further, sample matrix and analyte volatility also affect peak widths and analyte emission temporal behavior and hence they influence the data acquisition rate. Peak widths of several seconds (Figure 2-8d) to a few hundred milliseconds have been observed here

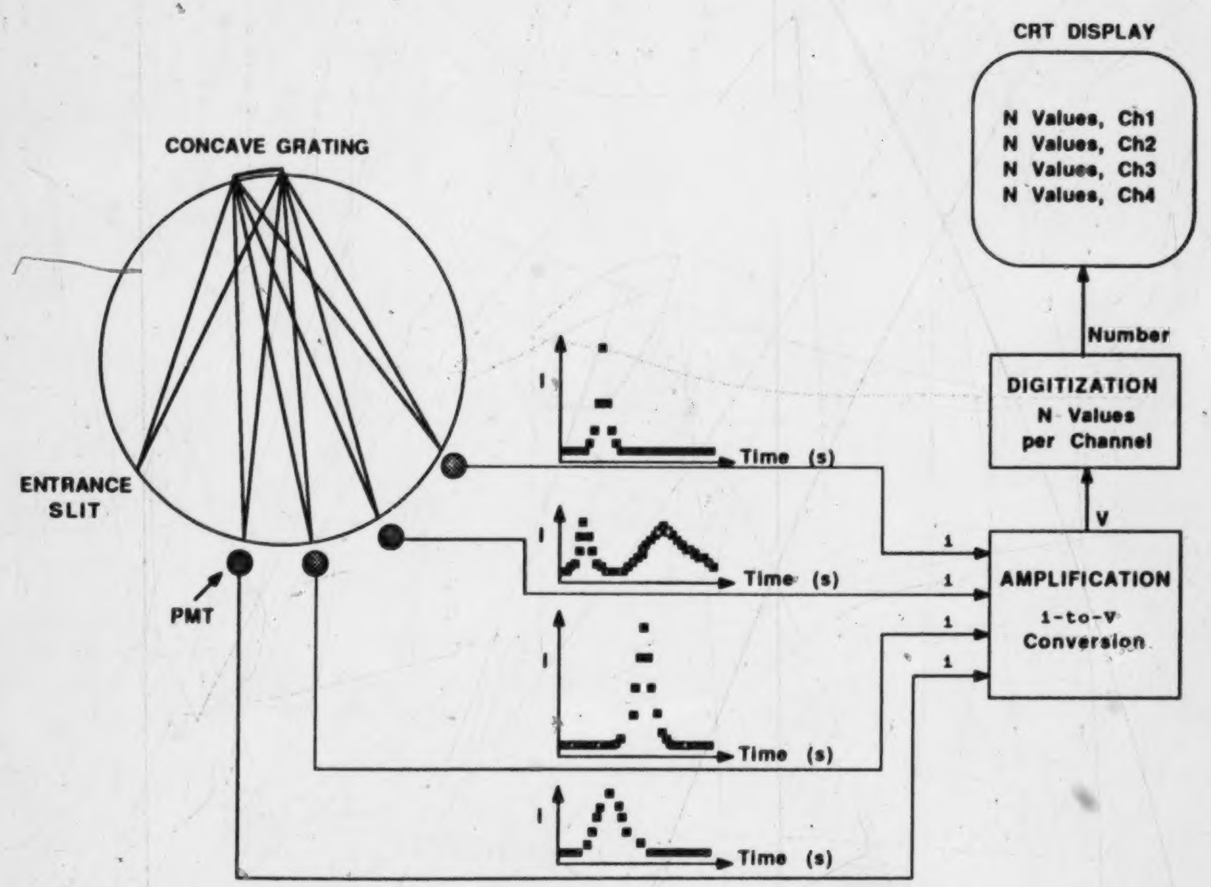
CRT DISPLAY
N Values, Ch1
N Values, Ch2
N Values, Ch3
N Values, Ch4
Number
DIGITIZATION
N Values
per Channel
V
AMPLIFICATION
i-to-V
Conversion
i
i
i
i
CONCAVE GRATING
ENTRANCE
SLIT
PMT
i
Time (s)
i
Time (s)
i
Time (s)
i
Time (s)

Figure 2-10. Block diagram of direct reader measurement electronics for transient signals.

and reported by others [18, 31]. Clearly, a data acquisition sub-system capable of sustaining a variable data acquisition rate and supportive of multiple channels and a wide bandwidth is required.

As mentioned earlier and pointed out in the literature [3], the integrating readout electronics available on most traditional polychromators are sub-optimal for the measurement of the transient signals generated by this sample introduction system. For this work, the transient signals are digitized in real-time with the aid of the Data Translation board. Any four channels of the direct reader can be simultaneously monitored by simply connecting the current output of the corresponding PMT to an Operational Amplifier (OA) input, the OA output is routed to the analog input of the Data Translation board, as shown in Figure 2-11. In order to monitor a new channel or a new set of channels, the old one(s) is simply disconnected manually from the OA and new channel(s) are connected to the appropriate OA inputs. The OAs (CDC15023, Heath Co.) were configured as current-to-voltage converters with a 10 MΩ resistor in the feedback loop and a 3 pF capacitor connected in parallel to the feedback resistor. The electronic gain of a particular PMT channel was programmed by either manually changing the applied voltage of the corresponding PMT or by replacing the resistor on the feedback loop of the OA (a 1 MΩ feedback resistor was typically used for high concentration analytes)

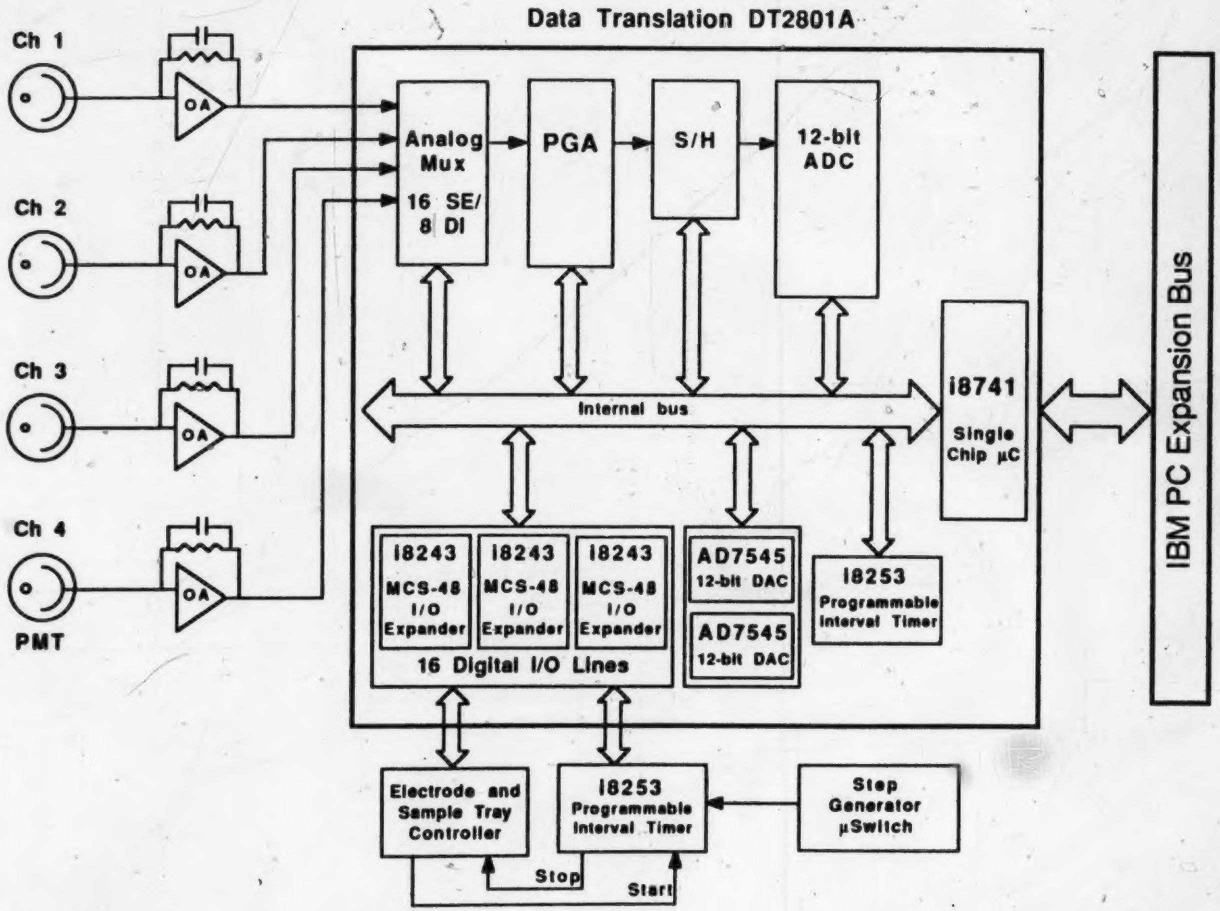
Data Translation DT2801A
Ch 1
Ch 2
Ch 3
Ch 4
PMT
OA
Analog Mux 16 SE/ 8 DI
PGA
S/H
12-bit ADC
Internal bus
i8741 Single Chip µC
IBM PC Expansion Bus
i8243 MCS-48 I/O Expander
i8243 MCS-48 I/O Expander
i8243 MCS-48 I/O Expander
16 Digital I/O Lines
AD7545 12-bit DAC
AD7545 12-bit DAC
i8253 Programmable Interval Timer
Electrode and Sample Tray Controller
i8253 Programmable Interval Timer
Step Generator µSwitch
Stop
Start

Figure 2-11. A four channel measurement electronics sub-system for the DSID and the IBM PC.

or via computer control of the programmable gain amplifier of the data acquisition and control board.

In order to handle transient, peak-like signals of quite different peak widths with a reasonable programming effort, the number of data points acquired per channel was fixed to 500 and a variable observation time and data acquisition rate were chosen. For example, for a 60 s observation time (typically used with the cup-based DSID), the data acquisition rate is 8.3 points/s (or 120 ms per data point); a 10 s observation time (typically used with the wire-loop DSID) yields a data acquisition rate of 50 points/s (20 ms/point). Depending on probe type, either an adequate number of data points is acquired, or the peak-like signals are oversampled [42]. It should be noted that with this design it takes about 13 s to drive the sample holder assembly from the bottom coil to the top coil of the 4-turn load coil of the plasma utilized in these experiments.

DSID automation and control aside, the problem of high speed data acquisition can be easily solved by purchasing a commercially available board and plugging it into the bus of the controlling microcomputer (as in this application) or by utilizing a commercially available direct reading spectrometer with a readout electronics sub-system capable of handling transient signals [22, 24]. What is currently lacking, however, is DSID-specific software, which appears to be the key to the success of a fully automated DSID.

C. Software

A Mac-like; user-friendly; menu-driven; window-based prototype software package capable of displaying multiple-, tiled- and overlapping-, text- and graphics-windows has been developed for DSID automation, control and fault-diagnosis; data acquisition; signal processing; graphics display and processing; and data and information management. Although the underlying control and signal processing algorithms are independent of user interface design, interactive graphics, on-line help, extensive error trapping, meaningful error message display, fault-diagnosis and recovery, some built-in intelligence and a DSID-specific graphics-supportive user interface make this program easy to use. In general, because the ultimate user is expected to be a non-programmer, the final utility of a program may solely rest upon the user interface it supports.

The entire software package, optimized for graphics, consists of about 10,000 lines of code (about a quarter of a million bytes of well documented source code are described here) spread over 9 program modules. These were written in a 'plain vanilla' version of the BASIC language (IBMs own BASICA). Interpreted BASIC was chosen over more modern languages (i.e., Pascal) or more exotic languages (i.e., Modula-2 or C) or even compiled BASIC because of its simplicity, the accessibility of the data acquisition and control board (via vendor provided, BASIC-callable routines), the familiarity of most researchers in the field with it, and in order to make program modules easy to modify. The price to be paid, much like in any other implementation in BASIC, is in speed and in lack of appropriate data structures and program flow-control constructs.

Modularity, independence of program modules, ease of code modification and expandability are central to this software package. These are important because hardware modifications as the DSID prototype evolves must easily be reflected in software and in order to facilitate an increased depth of understanding the analytical performance characteristics of the DSID. Modularity was implemented by making extensive use of overlays: program modules are 'chained-to' (i.e., brought into memory as executable code overlays) either form the main program or other program modules. This approach also helps overcome the 64 kByte limit imposed by BASICA. The program is structured in a hierarchical fashion by repeatedly breaking a task into sub-tasks of higher degree of detail and of lower level of abstraction. The structure of the entire software package is shown, in a block diagram form, in Figure 2-12. In order to speed up operations, both main program and program modules are loaded from a RAM disk (set-up with a batch file), thus also allowing a 'turn-key' operation.

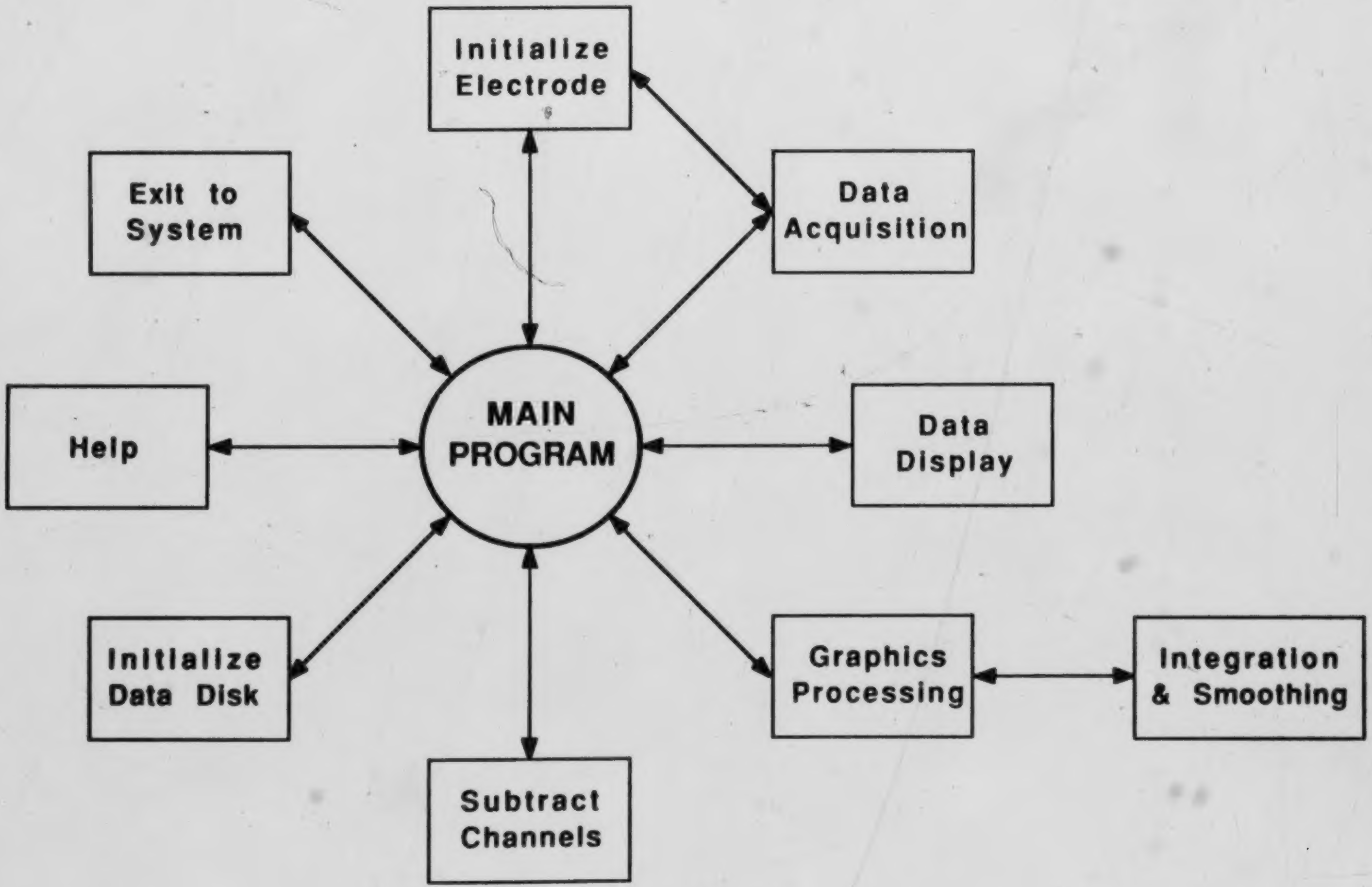
Initialize
Electrode
Exit to
System
Data
Acquisition
Help
MAIN
PROGRAM
Data
Display
Initialize
Data Disk
Graphics
Processing
Integration
& Smoothing
Subtract
Channels

Figure 2-12. Block diagram of the software package developed for the DSID.

The main menu of the main program is shown in Figure 2-13. Selecting a menu item from this menu chains-to or 'launches' (i.e., loads and executes) an overlay program module with its own menus and sub-menus. A typical example of the first level menus for an overlay module is shown in Figure 2-14a. This menu appears on the screen upon selection of item 1 (initialize electrode) of the main program menu. Throughout the entire package, the program borrows and implements the hierarchical menu concept. Menu selection is typically accomplished via a single keystroke, the user is questioned only when information is necessary, otherwise, information is either looked up in the systems data base or it is calculated.

A typical session usually begins with data acquisition (by selecting item 2 of the main menu (Figure 2-13). If 'Initialize Electrode' (item 1 of the main menu) was not previously selected, the program automatically drops into the initialize electrode module and initiates and runs a series of diagnostic tests, thus offering fault diagnosis capabilities. If, for example, the power supplies are at fault (i.e., their voltage has dropped below a given threshold level), the measured and expected voltages of the DSID interface and controller power supplies along with a diagnosis and a recommendation for appropriate corrective action are displayed on the screen, as shown in Figure 2-14b.

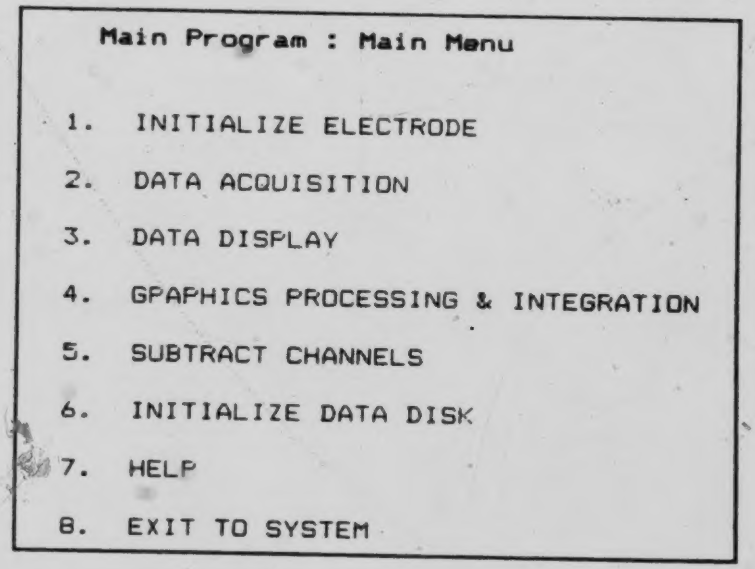

Main Program : Main Menu

1. INITIALIZE ELECTRODE
2. DATA ACQUISITION
3. DATA DISPLAY
4. GRAPHICS PROCESSING & INTEGRATION
5. SUBTRACT CHANNELS
6. INITIALIZE DATA DISK
7. HELP
8. EXIT TO SYSTEM

Figure 2-13. Main program main menu.

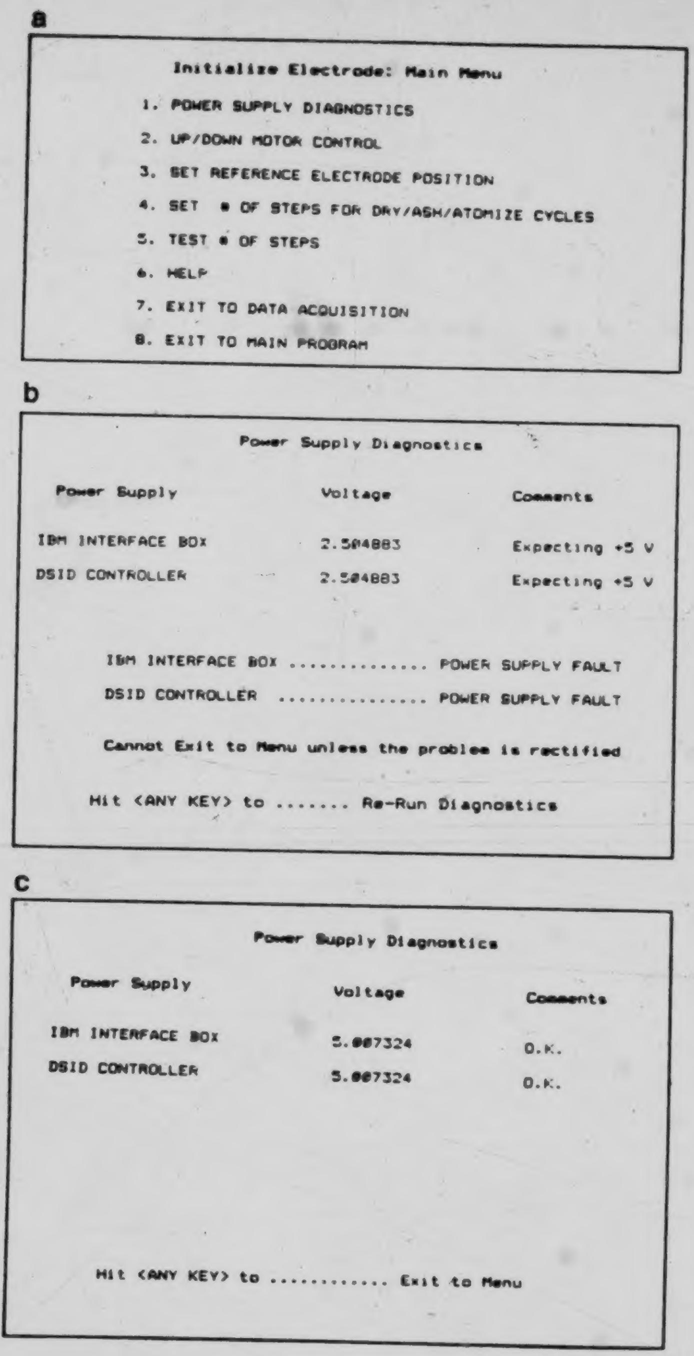

a

```
             Initialize Electrode: Main Menu

        1. POWER SUPPLY DIAGNOSTICS

        2. UP/DOWN MOTOR CONTROL

        3. SET REFERENCE ELECTRODE POSITION

        4. SET  # OF STEPS FOR DRY/ASH/ATOMIZE CYCLES

        5. TEST # OF STEPS

        6. HELP

        7. EXIT TO DATA ACQUISITION

        8. EXIT TO MAIN PROGRAM
```

b

```
                    Power Supply Diagnostics

   Power Supply                 Voltage            Comments

 IBM INTERFACE BOX              2.504883           Expecting +5 V

 DSID CONTROLLER                2.504883           Expecting +5 V


        IBM INTERFACE BOX .............. POWER SUPPLY FAULT

        DSID CONTROLLER  ............... POWER SUPPLY FAULT

        Cannot Exit to Menu unless the problem is rectified

      Hit <ANY KEY> to ....... Re-Run Diagnostics
```

c

```
                    Power Supply Diagnostics

   Power Supply                 Voltage            Comments

 IBM INTERFACE BOX              5.007324           O.K.

 DSID CONTROLLER                5.007324           O.K.




      Hit <ANY KEY> to ............ Exit to Menu
```

Figure 2-14. Menu shown upon selection of initialize electrode from main menu (a); power supply diagnostics, power supplies at fault (b); power supply diagnostics, proper voltages detected on the power supplies (c).

Fault tolerance can be implemented via redundancy, for example, by adding a power supply which operates in 'stand by' mode and is automatically switched on upon fault detection. Fault diagnosis and fault tolerance are expected to offer 'auto-repair' capabilities and reduce instrument-down time. In this case, the program will not let the user proceed unless the problem is manually rectified. If no power supply is at fault, a different set of comments appears on the screen, as shown in Figure 2-14c, and the program is allowed to exit to the main menu of this overlay module, as shown in Figure 2-14a. Its menu items are self-explanatory, for example, item 1 tests the power supplies, item 2 tests the motor, item 3 automatically finds and sets the reference position for the sample holder assembly, an so on.

At the end of a successful initialization session, the data acquisition module is loaded (via appropriate menu selections) and the user is prompted to enter, on a template that appears on the screen, the operating conditions (i.e., forward and reflected power, flow rates, polychromator channels etc) and a brief description of the sample. The main menu for the data acquisition module is shown in Figure 2-15a. And although several items are supported by it, only three are initially active. Even though this restricts the number of options available, by enforcing program flow-control, it reduces the number of trips to the instructions

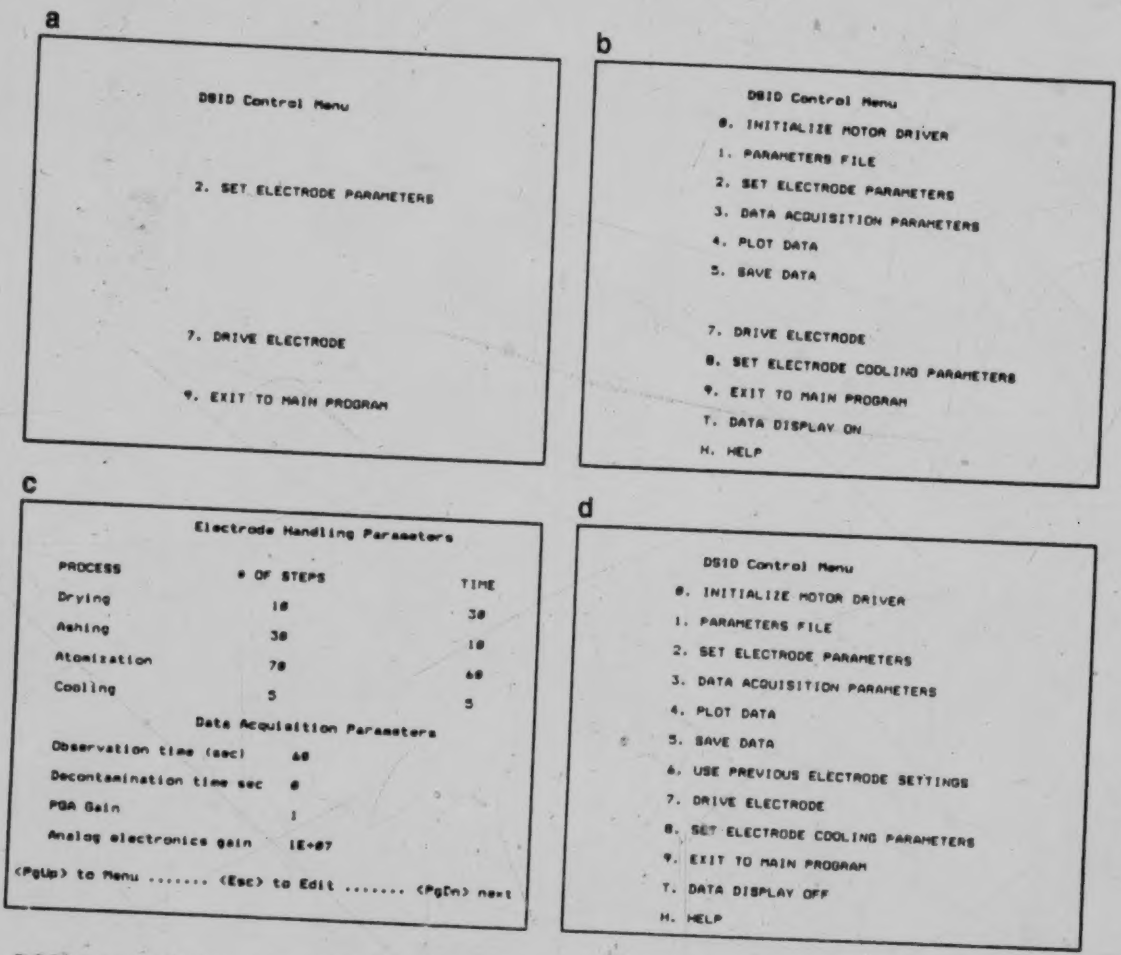
a
DSID Control Menu
2. SET ELECTRODE PARAMETERS
7. DRIVE ELECTRODE
9. EXIT TO MAIN PROGRAM
b
DSID Control Menu
0. INITIALIZE MOTOR DRIVER
1. PARAMETERS FILE
2. SET ELECTRODE PARAMETERS
3. DATA ACQUISITION PARAMETERS
4. PLOT DATA
5. SAVE DATA
7. DRIVE ELECTRODE
8. SET ELECTRODE COOLING PARAMETERS
9. EXIT TO MAIN PROGRAM
T. DATA DISPLAY ON
H. HELP
c
d
DSID Control Menu
0. INITIALIZE MOTOR DRIVER
1. PARAMETERS FILE
2. SET ELECTRODE PARAMETERS
3. DATA ACQUISITION PARAMETERS
4. PLOT DATA
5. SAVE DATA
6. USE PREVIOUS ELECTRODE SETTINGS
7. DRIVE ELECTRODE
8. SET ELECTRODE COOLING PARAMETERS
9. EXIT TO MAIN PROGRAM
T. DATA DISPLAY OFF
H. HELP

```
                 Electrode Handling Parameters

 PROCESS              # OF STEPS            TIME
 Drying                  10                  30
 Ashing                  30                  10
 Atomization             70                  60
 Cooling                 5                   5
                 Data Acquisition Parameters
 Observation time (sec)      60
 Decontamination time sec    0
 PGA Gain                    1
 Analog electronics gain     1E+07

<PgUp> to Menu ....... <Esc> to Edit ....... <PgDn> next
```

Figure 2-15. DSID and data acquisition module menu and parameters. (a) DISD control menu upon entry; (b) DISD control menu, item 6 disabled; (c) electrode handling and data acquisition parameters; (d) DSID control menu with no disabled items.

manual, as would be necessary if a large number of options were available. Program flow has been set in such a way that all required parameters are set sequentially and before data acquisition can commence. When all electrode handling parameters have been entered (and edited if necessary), all menu items but one are enabled, as shown in Figure 2-15b. When both electrode and data acquisition parameters have been correctly entered, (a typical example is shown in Figure 2-15c), then all menu items are enabled, as shown in Figure 2-15d. Some items can be toggled ON or OFF, as shown in Figures 2-15c and 2-15d respectively, for the menu item labeled T. For example, there is no need to display the data on the screen when a series of samples is run or when graphite electrodes are being 'pre-burned'. (Even if a graphite electrode has never been used, a blank insertion into the ICP is required in order to remove or 'burn-off' impurities).

It is only when all operating parameters have been entered that data can be acquired. Upon completion of an analytical run, analyte emission temporal behavior can be displayed on a four-window split-screen (i.e., tiled-windows), a typical example of which is shown in Figure 2-16. These windows are independent, each window can be thought of as a polychromator PMT-channel. What is displayed in a window is

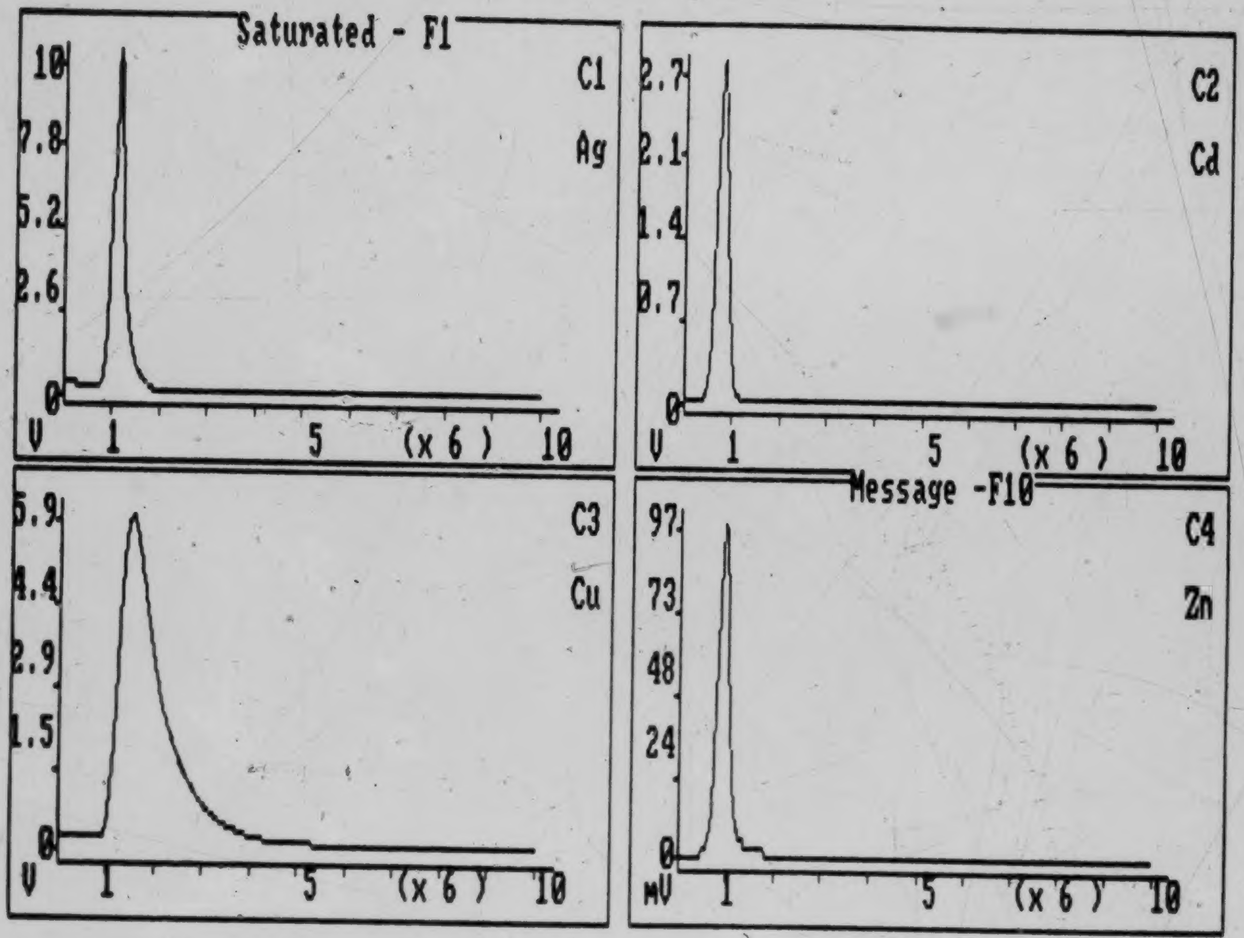
Saturated - F1
C1
Ag
10
7.8
5.2
2.6
0
V
1
5
(x 6)
10
C2
Cd
2.7
2.1
1.4
0.7
0
V
1
5
(x 6)
10
Message -F10
C3
Cu
5.9
4.4
2.9
1.5
0
V
1
5
(x 6)
10
C4
Zn
97
73
48
24
0
mV
1
5
(x 6)
10

Figure 2-16. Screen dump of a typical four-window split-screen, C1 stands for channel 1, C2 for channel 2, C3 for channel 3 and C4 for channel 4.

a graphic representation (via a series of time-lapse electronic snap-shots) of analyte emission falling on the corresponding PMT-channel. There is also some intelligence associated with each window/channel combination: if a PMT-channel is either saturated (i.e., a peak intensity greater than 10 V has been detected) or underutilized (i.e., a peak intensity of less than 100 mV has been detected) a message appears on the corresponding window frame as a window title. For example, the Ag window (channel C1) shown in Figure 2-16 is saturated (sometimes it is difficult to decide if a particular channel is saturated), there is a message pending on the underutilized Zn window (channel C4) and no title appears on either the Cd or the Cu window (channels C2 and C3 respectively), as the corresponding signals on these channels are within range. The messages can be easily retrieved by selecting the appropriate function keys as indicated in the respective window titles.

By making the appropriate function key selection, the message appearing within the frame of any saturated window (i.e., Ag window, Channel C1, Figure 2-16), makes appropriate, pre-programmed (i.e., 'canned') suggestions as to what should/could be done to rectify the situation, as shown in Figure 2-17. Thus, a one-way communication between the computer and the operator is established.

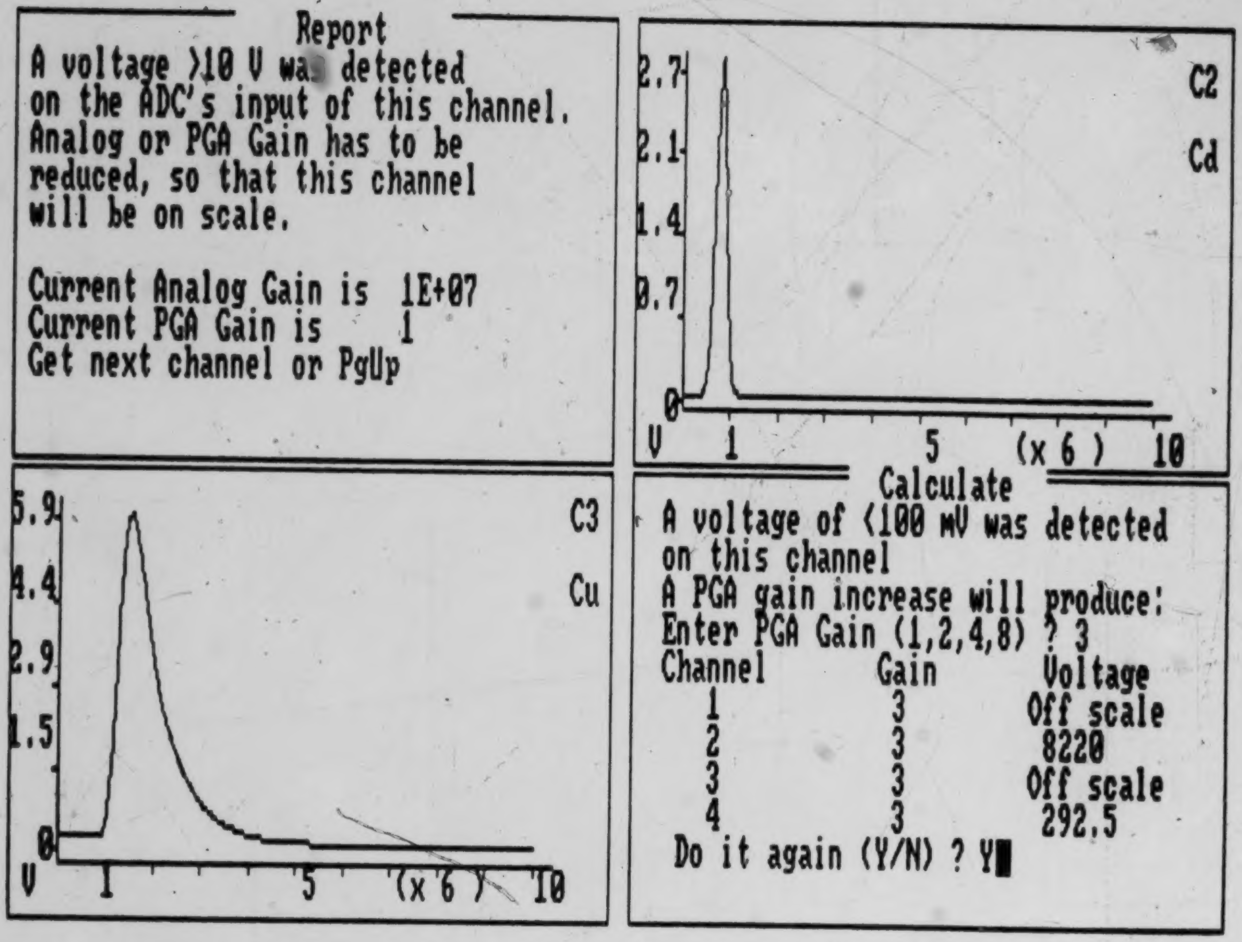

Report

```
A voltage >10 V was detected
on the ADC's input of this channel.
Analog or PGA Gain has to be
reduced, so that this channel
will be on scale.

Current Analog Gain is  1E+07
Current PGA Gain is     1
Get next channel or PgUp
```

Calculate

```
A voltage of <100 mV was detected
on this channel
A PGA gain increase will produce:
Enter PGA Gain (1,2,4,8) ? 3
Channel        Gain      Voltage
   1            3        Off scale
   2            3         8220
   3            3        Off scale
   4            3         292.5
 Do it again (Y/N) ? Y█
```

Figure 2-17. Typical messages displayed after appropriate function key selection (Fig. 2-16).

An interactive mode, in which a two-way communication is established (e.g., feedback mode), is supported by any underutilized channel (i.e., Zn window, channel C4, Figure 2-16): the program allows the operator to perform a 'what-if' experiment with the acquired signal, as shown in Figure 2-17. If the PGA gain is changed to 3 (via the keyboard), channels 1 and 3 (Ag and Cu respectively) are expected to go 'off scale', whereas the expected numerical values for channels 2 and 4 (Cd and Zn respectively) are shown. This process can be repeated, by entering a new PGA gain, until a suitable compromise solution has been found. And although not yet implemented, automating OA and PMT gains so that the signals on all channels will be within range is not hard to envision.

Taking this concept a bit further, why not also include plasma and DSID operating conditions in addition to matrix and analyte in order to automate the acquisition of optimum signals for a given sample type rather than simply bringing the observed signals 'within range'? Among the various possible alternatives, a programming paradigm that operates on objects, message-passing and constraints appears to be very appealing: a program module in which the objects themselves (i.e., DSID and plasma operating conditions, electronic gain, and matrix and analyte) are described in terms of the objects' values and/or their behavior is currently under development.

Once the data have been acquired, they can be saved on the disk. Three files are automatically saved with each analytical run: these have the same file name but, for identification purposes, they have a different extension. The first file contains the raw data (for transportability, no header file has been included). The second file, useful for data archival purposes, is dubbed the parameter file and it contains plasma and DSID operating conditions and some information about the sample, a typical example is shown in Figure 2-18a. The parameter file concept, although not new, is important here. The underlying idea behind this concept is rather simple: raw data are meaningless unless they are put within context, thus an attempt is made to give the acquired signals, if not a meaning, an identity. Because the contents of this file are derived from a series of templates that serve as place-holders for the DSID and plasma operating conditions, its structure has been defined *a priori*. Therefore, no provisions can be made for the storage of unstructured information (e.g., observations) arising during an analytical run.

However, record keeping of observations during an experiment is considered to be a key aspect of the information gathering process, the concept of the laboratory note book fits in this realm. The third file, dubbed the electronic notebook file, is a text file whose length depends only on a

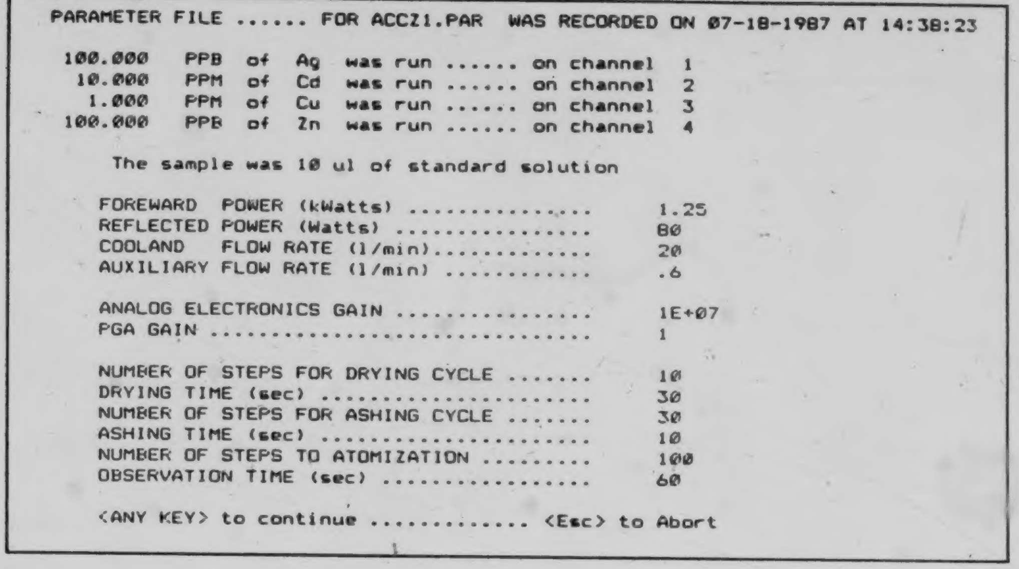

```
PARAMETER FILE ...... FOR ACCZ1.PAR  WAS RECORDED ON 07-18-1987 AT 14:38:23

 100.000   PPB  of  Ag  was run ...... on channel  1
  10.000   PPM  of  Cd  was run ...... on channel  2
   1.000   PPM  of  Cu  was run ...... on channel  3
 100.000   PPB  of  Zn  was run ...... on channel  4

     The sample was 10 ul of standard solution

    FOREWARD  POWER (kWatts) ...............      1.25
    REFLECTED POWER (Watts) ................      80
    COOLAND   FLOW RATE (l/min).............      20
    AUXILIARY FLOW RATE (l/min) ............      .6

    ANALOG ELECTRONICS GAIN ................      1E+07
    PGA GAIN ...............................      1

    NUMBER OF STEPS FOR DRYING CYCLE .......      10
    DRYING TIME (sec) ......................      30
    NUMBER OF STEPS FOR ASHING CYCLE .......      30
    ASHING TIME (sec) ......................      10
    NUMBER OF STEPS TO ATOMIZATION .........      100
    OBSERVATION TIME (sec) .................      60

    <ANY KEY> to continue ............. <Esc> to Abort
```

b

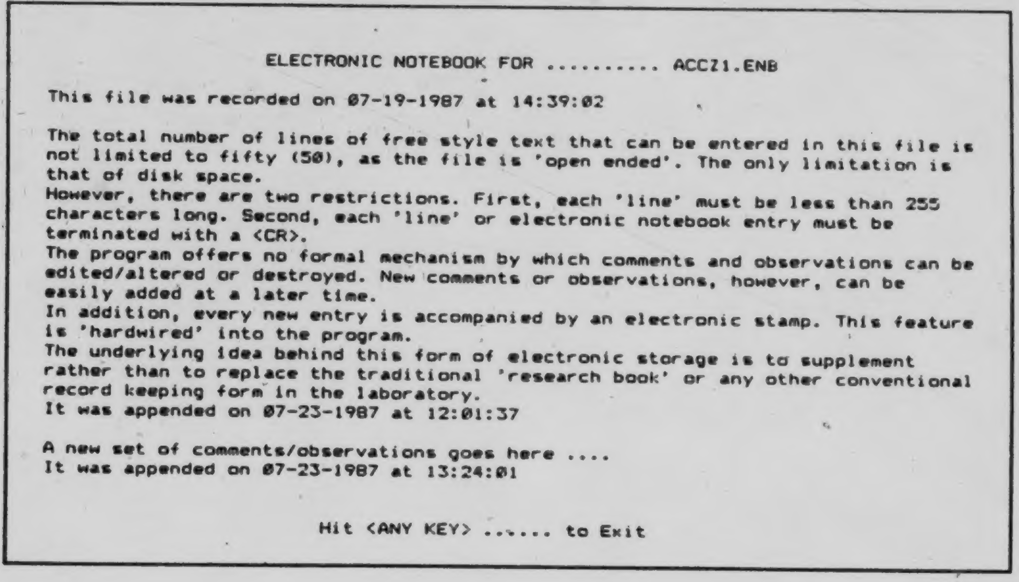

```
                    ELECTRONIC NOTEBOOK FOR .......... ACCZ1.ENB

This file was recorded on 07-19-1987 at 14:39:02

The total number of lines of free style text that can be entered in this file is
not limited to fifty (50), as the file is 'open ended'. The only limitation is
that of disk space.
However, there are two restrictions. First, each 'line' must be less than 255
characters long. Second, each 'line' or electronic notebook entry must be
terminated with a <CR>.
The program offers no formal mechanism by which comments and observations can be
edited/altered or destroyed. New comments or observations, however, can be
easily added at a later time.
In addition, every new entry is accompanied by an electronic stamp. This feature
is 'hardwired' into the program.
The underlying idea behind this form of electronic storage is to supplement
rather than to replace the traditional 'research book' or any other conventional
record keeping form in the laboratory.
It was appended on 07-23-1987 at 12:01:37

A new set of comments/observations goes here ....
It was appended on 07-23-1987 at 13:24:01


                         Hit <ANY KEY> ...... to Exit
```

Figure 2-18. (a) Parameter and (b) electronic notebook files.

available disk space. Any observations (and comments) pertinent to an analytical run can be immediately entered and recorded in an unstructured, free-styled text-form and saved on this file, rather than having to be cross-referenced at a later time. These two support files attempt to describe the data at a higher level of abstraction and convert them to information. And although more work remains to be done, the concept of information archival appears to be realizable. It should be noted that these files are meant to supplement rather than to replace traditional forms of record keeping in the laboratory.

The disk I/O routines used in this module are part of a generic sub-module developed and used throughout this program. Extensive error trapping and meaningful message display is also supported, so that program crashes are avoided, data integrity is maintained and reliability is increased. According to the approach taken thus far, namely that of describing data at a higher level of abstraction, each volume (i.e., disk) also has a header file associated with it. Contained in this file is rudimentary information about the data stored on the disk (i.e., Power Studies, Orchard Leaves etc) and creation date and time. Among other facilities supported by this module (i.e., display of disk space available, directory listing, etc), the electronic notebook can also be retrieved and displayed on the screen, an example is shown in Figure 2-18b. It is worth noting that each entry is accompanied by a time stamp (automatically inserted by the computer), as suggested by sound laboratory record keeping practices. In addition, the program provides no formal mechanism by which an inexperienced programmer can modify the parameter and electronic notebook files (an experienced programmer can always find a way).

With the fully automated DSID described here, post-processing of signals is facilitated: data gathered in an automated fashion can be processed at a later time. Selecting item 3 of the main program menu (Figure 2-13) launches another program module with its own menus and sub-menus. From within this module data can be loaded from the disk (menu not shown), and be displayed on a four-window split-screen, not shown, but similar to the one displayed immediately after data acquisition. Any two channels can be selected and can be displayed on the screen, as shown in Figure 2-19.

The two window screen is very useful for comparison of analyte emission temporal behavior. Consider Cu and Zn as an example. The direct spectral overlap of the Cu 213.851 nm line on the Zn 213.856 nm line is well documented in the literature [43-45]. And although there is a direct overlap of Cu and Zn emission in the spectral domain, their respective temporal emission intensities are separated in time, as shown in Figure 2-19.

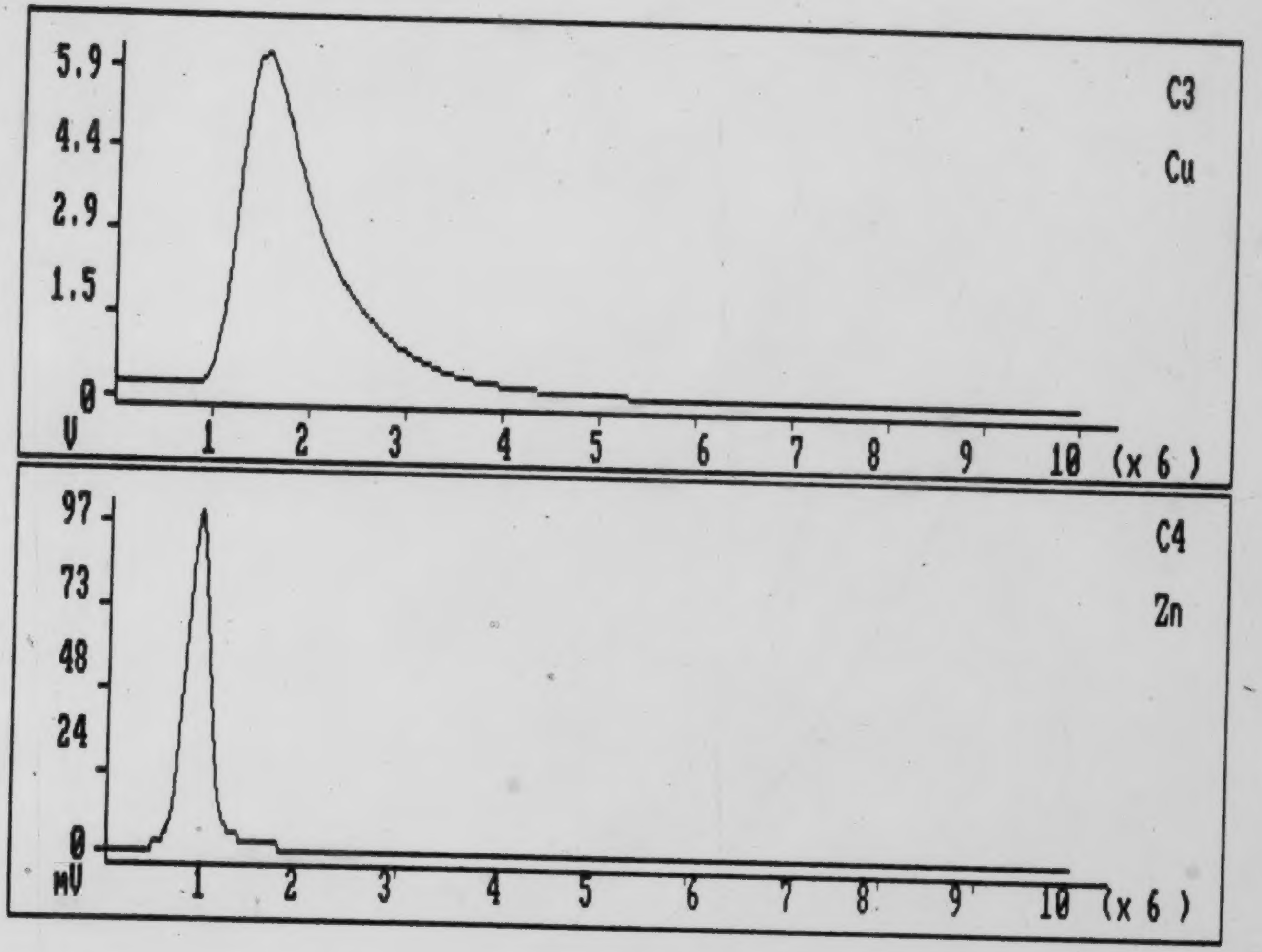
5.9
4.4
2.9
1.5
0
V
C3
Cu
1
2
3
4
5
6
7
8
9
10
(x 6)
97
73
48
24
0
mV
C4
Zn
1
2
3
4
5
6
7
8
9
10
(x 6)

Figure 2-19. Screen dump of a two-window split-screen.

It should be noted that the peak separation in time shown above can be further increased by reducing the applied forward power, thus giving rise to the feedback loop shown in Figure 2-1. By implementing this feedback loop, an added advantage is realized: computer control of the applied forward power effectively reduces to temperature programming, much like in graphite furnace spectrometry. Getting back to spectral interferences, it can be concluded that in certain cases, direct overlaps in the spectral domain can be avoided in the time domain. This interesting 'thought experiment' has been verified experimentally and is documented for the direct spectral overlap of Cu on Zn.

Analyte emission temporal behavior of both Cu and Zn PMT-channels is simultaneously observed for 60 s for: 10 µl of a 1 ppm Zn solution (Figures 2-20a and 2-20b for the Cu and Zn channels, respectively); for a 10 µl of a 100 ppm Cu solution (Figures 2-20c and 2-20d for the Cu and Zn channels, respectively); and for 10 µl of a solution containing 1 ppm Zn and 100 ppm Cu (Figures 2-20e and 2-20f for the Cu and Zn channels, respectively). When the Zn solution is run (Figures 2-20a and 2-20b), temporal emission for Cu was not observed, as expected, other than a slight change in the background (due to electrode insertion). This run also helped establish Zn analyte emission temporal behavior, a peak appearance time (defined as the time at which the maximum of the peak appears) of about 6 s was observed. When

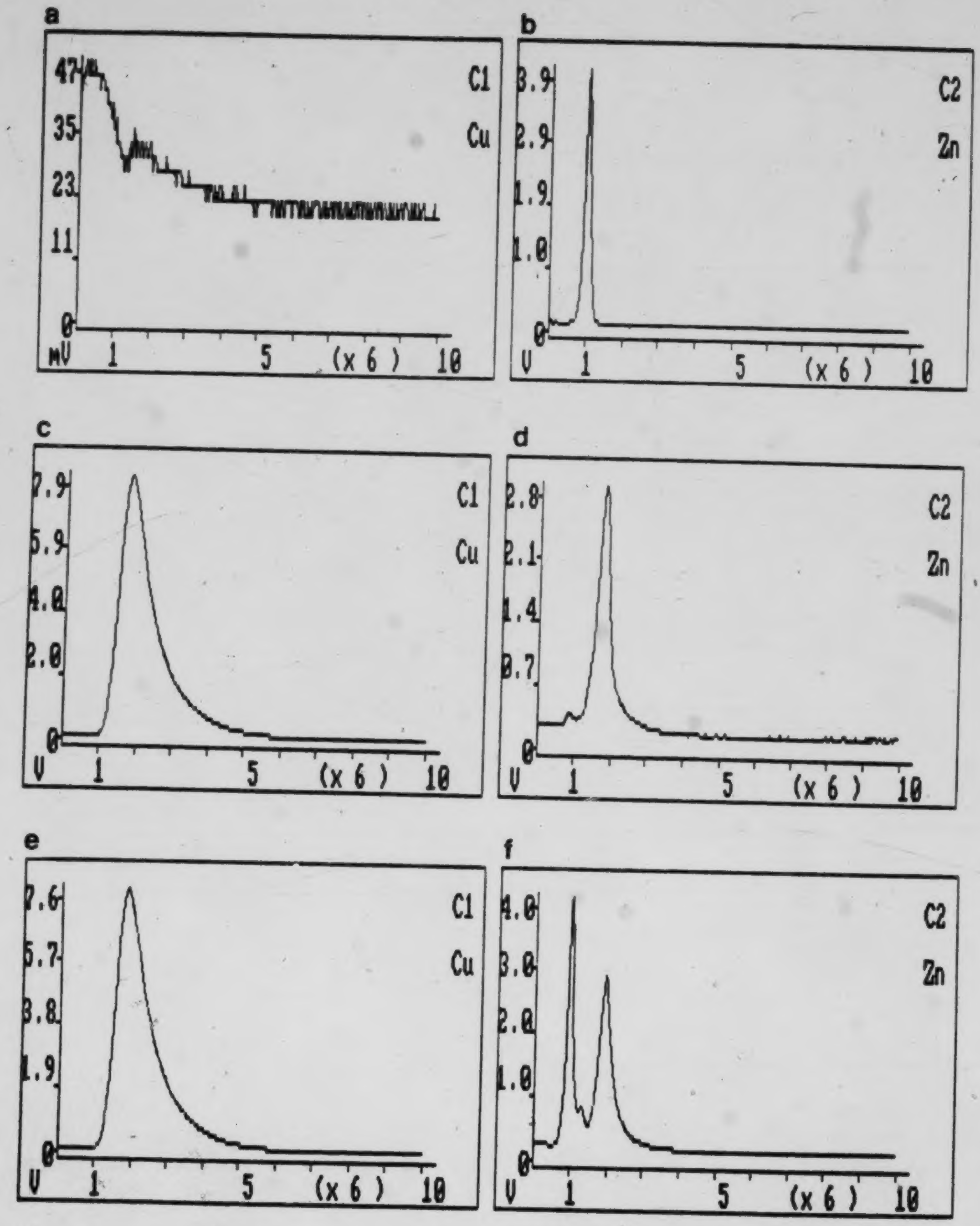

Figure 2-20. Spectral interference of Cu on Zn, see text for details.

the Cu solution is run, a signal appears on both the Cu and Zn channels (Figures 2-20c and 2-20d respectively). The peak appearance time of the Cu signal is about 10 s and that of the signal registered on the Zn channel is also about 10 s. Because no Zn has been added on the sample carrying cup and because the peak appearance time of both peaks is the same, it can be concluded that the signal registered on the Zn channel must be due to a direct spectral overlap of Cu on the Zn channel.

A comparison of the peak appearance times of the signals registered on the Zn channel when the Zn solution is run (Figure 2-20b) and that registered on the Zn channel when the Cu solution is run (Figure 2-20d) reveals that the two peaks are almost baseline resolved in time. Therefore, the two peaks must also be separated in time when a solution containing both Cu and Zn is run. Indeed, this is the case, as shown in Figure 2-20f. By comparison of the peak appearance times, the peaks shown in Figure 2-20f can be easily identified: the peak with an appearance time of about 6 s is due to Zn, the peak with an appearance time of about 10 s is due to Cu spectral interference on the Zn channel. Similarly, it can be concluded that the small peak preceding the peak registered at about 10 s on the Zn channel (Figure 2-20d) is due to electrode contamination. (Depending on the batch used, graphite electrodes may contain a considerable amount of Zn). Clearly, the direct spectral overlap of Cu on Zn can be avoided by relying on differential thermal vaporization and by taking advantage of the differences in elemental volatilities. Furthermore, by relying on differential volatilization, the direct spectral overlap of Ni (213.858 nm line) on Zn (213.856 nm line) can also be avoided. Results similar to those shown above have been observed for the direct spectral overlap of Ni on Zn.

In addition to the two-window split-screen display (Figure 2-19), windows can be overlapped as an aid to post-processing. A single window screen can be utilized, as shown in Figure 2-21a. By selecting menu item 'F2 preview', the menu changes as shown in Figure 2-21b. By selecting the second channel (menu item 'F2 CHNL #2'), the Zn channel gets selected and its contents are displayed in an overlapping window on the screen. The Cu peak can be brought to view by moving the Zn window out of the way, as shown in Figure 2-21c. Actually, this window can be moved anywhere on the screen with the use of cursor control keys, the software automatically updates and re-draws the previously overlapped portion of the screen. In this way, peak identification can be performed interactively and directly on the video screen during a post-processing session, thus reducing method development time. Once the peaks have been identified, the assignment (and possible comments) can be recorded on the electronic notebook, that now appears as an overlapping window on the screen, as shown in Fig 21d.

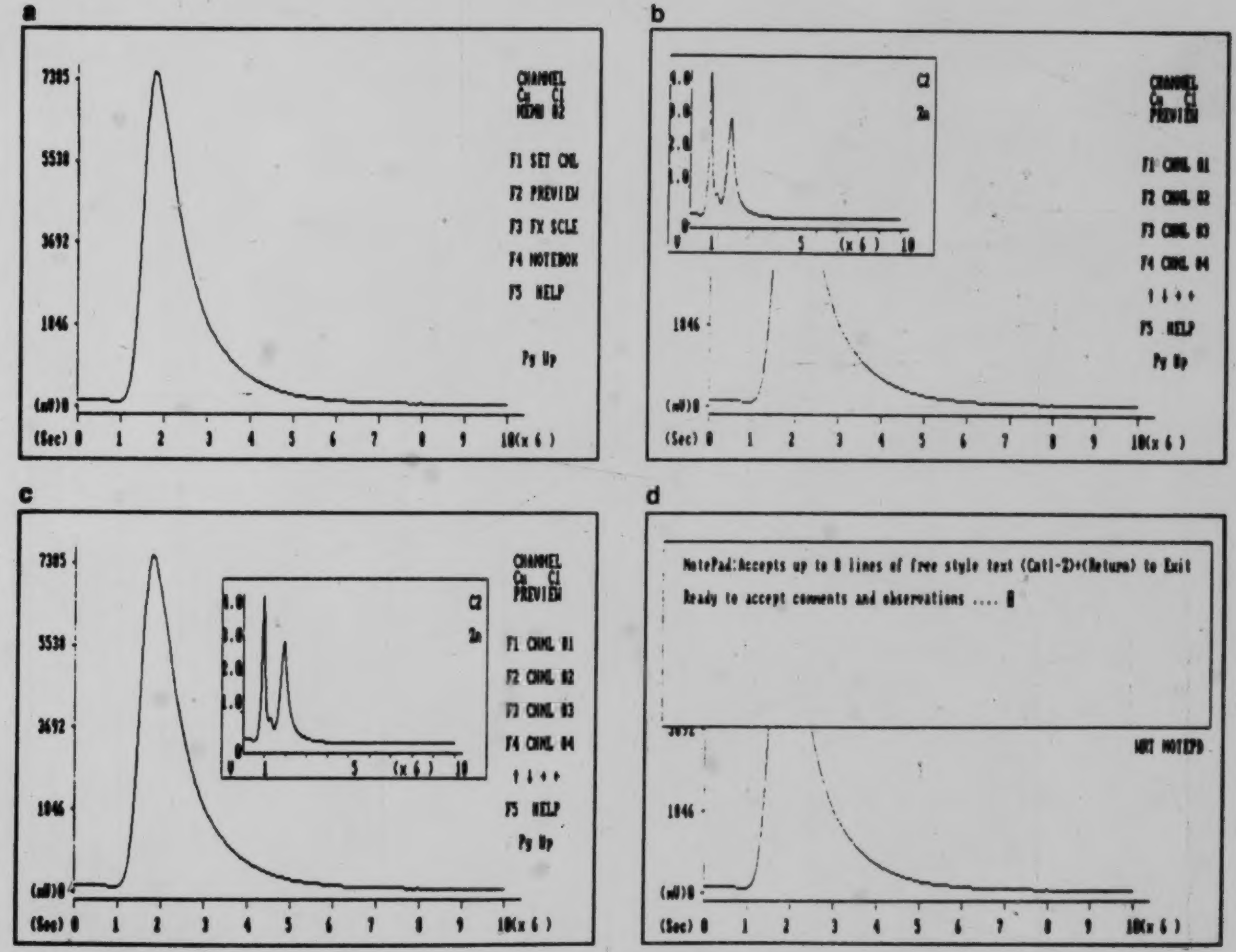
a
7385
5538
3692
1846
(mV)0
(Sec) 0 1 2 3 4 5 6 7 8 9 10(x 6)
CHANNEL
Cu C1
MENU 02
F1 SET CHL
F2 PREVIEW
F3 FX SCLE
F4 NOTEBOX
F5 HELP
Pg Up
b
4.0
3.0
2.0
1.0
0
0 1 5 (x 6) 10
C2
Zn
1846
(mV)0
(Sec) 0 1 2 3 4 5 6 7 8 9 10(x 6)
CHANNEL
Cu C1
PREVIEW
F1 CHNL 01
F2 CHNL 02
F3 CHNL 03
F4 CHNL 04
↑ ↓ ← →
F5 HELP
Pg Up
c
7385
5538
3692
1846
(mV)0
(Sec) 0 1 2 3 4 5 6 7 8 9 10(x 6)
4.0
3.0
2.0
1.0
0
0 1 5 (x 6) 10
C2
Zn
CHANNEL
Cu C1
PREVIEW
F1 CHNL 01
F2 CHNL 02
F3 CHNL 03
F4 CHNL 04
↑ ↓ ← →
F5 HELP
Pg Up
d
1846
(mV)0
(Sec) 0 1 2 3 4 5 6 7 8 9 10(x 6)
WRT NOTEPD

NotePad:Accepts up to 8 lines of free style text (Cntl-Z)+(Return) to Exit

Ready to accept comments and observations .... █

Figure 2-21. Peak assignment and identification during a post-processing session, see text for details.

The combination of hardware capable of digitizing transient signals in real-time and appropriate software enables the DSID to demonstrate its potential. For example, for the analysis of a sample containing both Cu and Zn, if the peaks were to be integrated in the way described for conventional pneumatic nebulizer sample introduction systems, the capability to temporally resolve spectral interference would have been lost and incorrect results would have been reported for Zn due to the Cu direct spectral overlap. However, in this case in order to relate analyte emission temporal behavior to concentration, peak heights rather than the more reliable estimate of peak areas must now be utilized. Peak area integration is again delegated to software.

Upon selection of item 4 of the main menu (Figure 2-13) and by making the appropriate menu selections (menus not shown) and by loading the appropriate data files (if necessary) a single window appears on the screen, as shown in Figure 2-22a. Item 5 (F9 integrate) of this menu is of interest here: upon selection, a new menu appears on the screen (Figure 2-22b) and a new program module that performs peak-area integration gets launched. But before peak integration can proceed, the integration limits (i.e., upper and lower bounds of the peak) must be set.

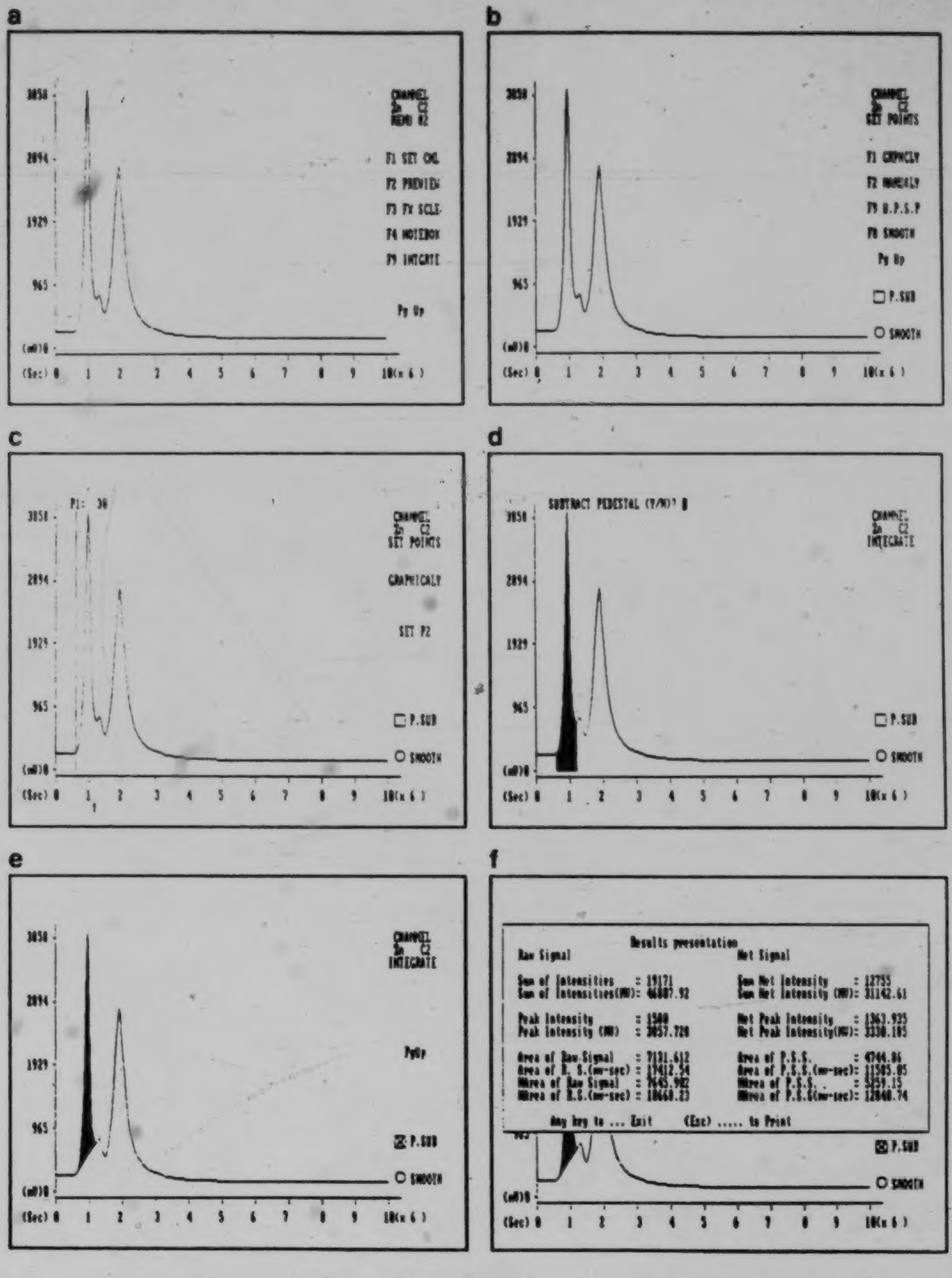
a
b
c
d
e
f
3858
2894
1929
965
(mV)0
(Sec) 0 1 2 3 4 5 6 7 8 9 10(x 6)
CHANNEL
Zn C2
MENU 02
F1 SET CHL
F2 PREVIEW
F3 FX SCLE
F4 NOTEBOX
F9 INTGRTE
Pg Up
SET POINTS
F1 GRPHCLY
F2 NUMRCLY
F9 U.P.S.P
F8 SMOOTH
☐ P.SUB
○ SMOOTH
P1: 30
GRAPHICALY
SET P2
SUBTRACT PEDESTAL (Y/N)?
INTEGRATE
PgUp
☒ P.SUB

```
                       Results presentation
Raw Signal                              Net Signal

Sum of Intensities     : 19171          Sum Net Intensity      : 12755
Sum of Intensities(MV): 46087.92        Sum Net Intensity (MV): 31142.61

Peak Intensity         : 1580           Net Peak Intensity     : 1363.935
Peak Intensity (MV)    : 3857.720       Net Peak Intensity(MV): 3330.185

Area of Raw-Signal     : 7131.612       Area of P.S.S.         : 4744.86
Area of R. S.(mv-sec) : 17412.54        Area of P.S.S.(mv-sec): 11505.05
NArea of Raw Signal    : 7645.982       NArea of P.S.S.        : 5259.15
NArea of R.S.(mv-sec) : 10660.23        NArea of P.S.S(mv-sec): 12840.74

        Any key to ... Exit      (Esc) ..... to Print
```

Figure 2-22. Peak-area integration, see text for details.

This can be done either graphically (by selecting menu item 1, F1 graphically, of the 'set points' menu, as shown in Figure 2-22b) or via the keyboard (by selecting menu item 2, F2 manually, of the same menu). The lower limit of integration can be set graphically with the aid of cursor control keys, a coarse cursor (shown as an up arrow at the bottom of Figure 2-22c) and a fine cursor (shown as a vertical line in the same figure). The upper limit of integration is set in a similar fashion. An inverse video screen animates (i.e., highlights) the peak to be integrated as it is being integrated, the final result is shown in Figure 2-20d. Based on linear extrapolation, the pedestal of the peak (i.e. background) can also be subtracted, as shown in Figure 2-20e. The result of the peak-area integration appears on the screen on yet another overlapping text window, as shown in Figure 2-20f.

Transient signals of reasonable peak intensity and area have been shown thus far. However, this may not necessarily be a faithful representation of reality in a true analytical situation: as concomitant concentration approaches the detection limit, the signals get buried in noise. A typical example of that is shown in Figure 2-23a. How does this software handle such 'low level' signals? Is the peak appearing at about 6 s real or is it an artifact? And if this peak is assumed to be real, where would the limits of integration be set?

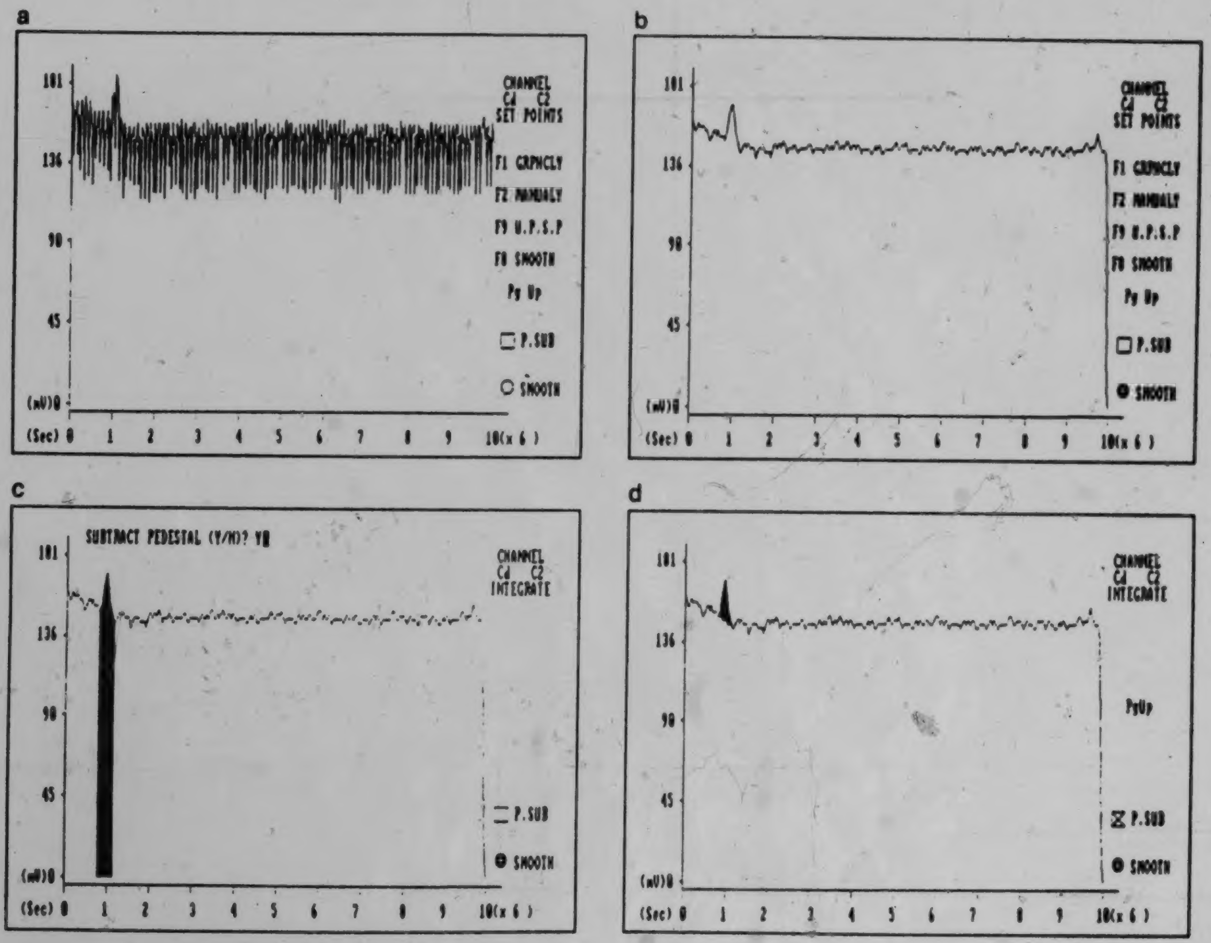

Figure 2-23. Smoothing and integration of a low-level Cd signal . (a) Original signal; (b) smoothed signal; (c) peak-area integration; (d) pedestal subtracted peak after integration.

By selecting item 4 of the 'set points' menu (F8 smooth, Figure 2-23a), the observed signal is smoothed based on a simple sliding average algorithm, the smoothed signal is shown in Figure 2-23b. Clearly, this is a well defined peak, the limits of integration can be easily set (Figure 2-23c), the peak area can be calculated as described earlier, and the pedestal it resides on can be easily subtracted (Figure 2-23d). An added advantage offered by this type of integration is that only the signal is being integrated, rather than integrating both signal and noise [3]. And assuming that linear extrapolation works (as it can be concluded by the linear calibration curves constructed with this system [28, 29]), the built-in ability to perform pedestal subtraction eliminates the need for a blank run and background subtraction.

However, there are cases in which blank subtraction may be helpful. Consider chemical modification [3, 29] as an example. With a graphite electrode as the sample carrying probe, carbide forming elements display little (i.e., Al, Sr) or no temporal emission behavior at all (i.e., Zr) unless a matrix modifier (i.e., NaF) has been added into the sample carrying cup along with the sample. And although NaF enhances emission signals considerably (over two orders of magnitude have been observed for some elements with this system and by others [3]), there is a problem: even spectroscopically pure, commercially available, five-nines NaF contains enough impurities to produce peaks of considerable intensity and area. A solution to this problem is to prepare a 'pure' matrix modifier in the laboratory, as it was demonstrated in the literature for copper fluoride dihydrate [46]. Alternatively, the signal due to a matrix modifier impurity can be subtracted out, either on a point-by-point basis or as integrated peak areas, by running a blank. Point-by-point subtraction is accomplished by selecting item 5 from the main menu (Fig 13): this launches yet another overlay module with its own menus and sub-menus.

After making the appropriate menu selections, the subtract signals menu, shown in Figure 2-24a, is displayed on the screen. Each executed step gets a check mark indicating its completion, as shown in the same figure. The program also checks various flags and parameters (stored in the parameter file) for data compatibility. For example, if an incompatibility in the operating parameters between the blank (i.e., NaF) and the sample run (i.e., analyte plus NaF) is detected, depending on the offending parameter an error or a warning is generated automatically and is displayed on the screen, as shown in Figures 2-24b and 2-24c respectively. Once the signals for the channels of interest have been subtracted, they can be plotted on the screen, as shown in Figure 2-25. The Al signal obtained from a sample run (i.e., 10 µl of 10 ppm Al solution plus 10 µl of 0.25 M NaF solution) is plotted in the Al window (Channel C1). The

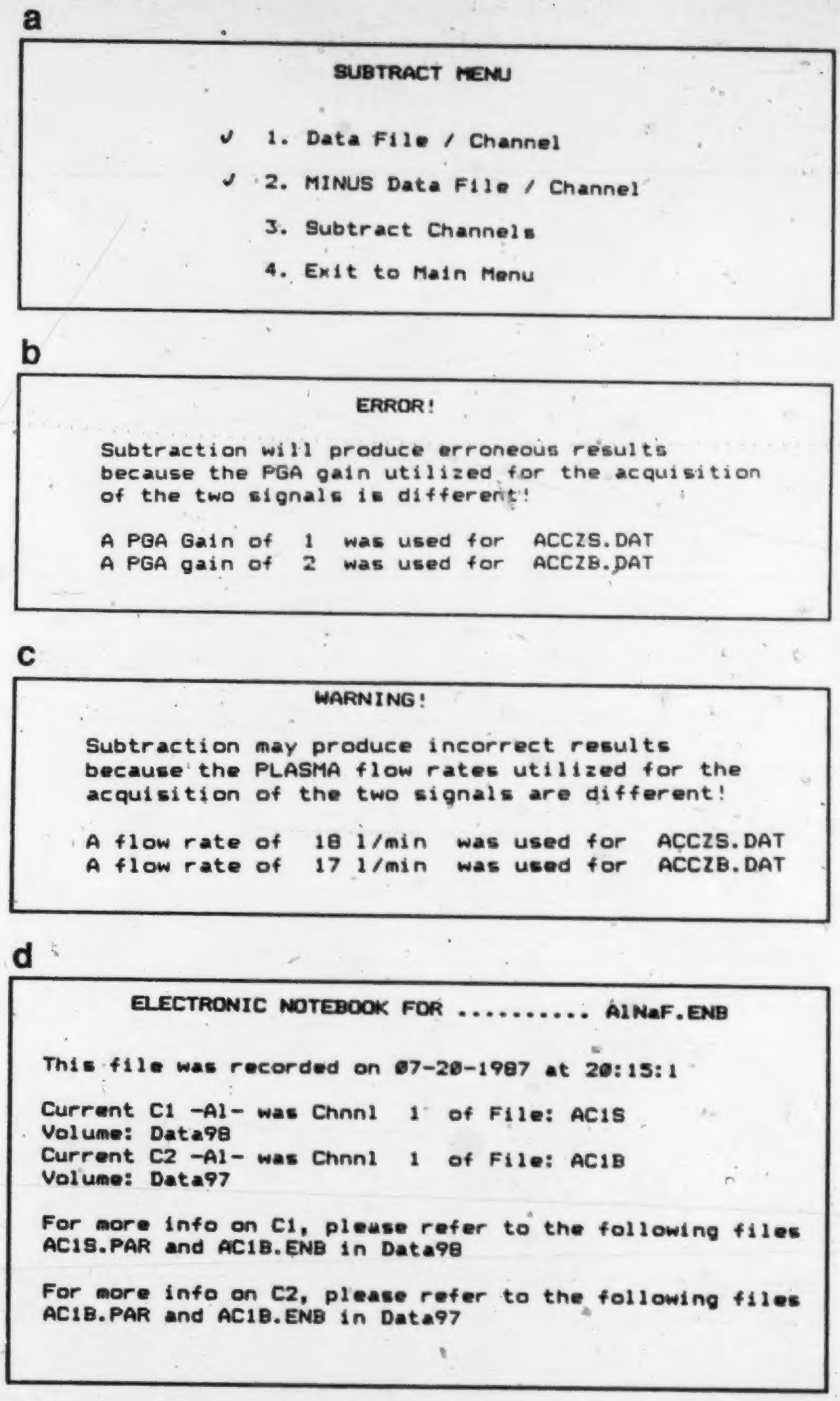

```
                    SUBTRACT MENU

          ✓  1. Data File / Channel

          ✓  2. MINUS Data File / Channel

             3. Subtract Channels

             4. Exit to Main Menu
```

```
                     ERROR!
    Subtraction will produce erroneous results
    because the PGA gain utilized for the acquisition
    of the two signals is different!

    A PGA Gain of  1  was used for  ACCZS.DAT
    A PGA gain of  2  was used for  ACCZB.DAT
```

```
                  WARNING!

   Subtraction may produce incorrect results
   because the PLASMA flow rates utilized for the
   acquisition of the two signals are different!

   A flow rate of  18 l/min  was used for  ACCZS.DAT
   A flow rate of  17 l/min  was used for  ACCZB.DAT
```

```
        ELECTRONIC NOTEBOOK FOR .......... AlNaF.ENB

  This file was recorded on 07-20-1987 at 20:15:1

  Current C1 -Al- was Chnnl  1  of File: AC1S
  Volume: Data98
  Current C2 -Al- was Chnnl  1  of File: AC1B
  Volume: Data97

  For more info on C1, please refer to the following files
  AC1S.PAR and AC1B.ENB in Data98

  For more info on C2, please refer to the following files
  AC1B.PAR and AC1B.ENB in Data97
```

Figure 2-24. (a) Subtract channels menu; (b) error message; (c) warning; (d) electronic notebook file for subtracted channels.

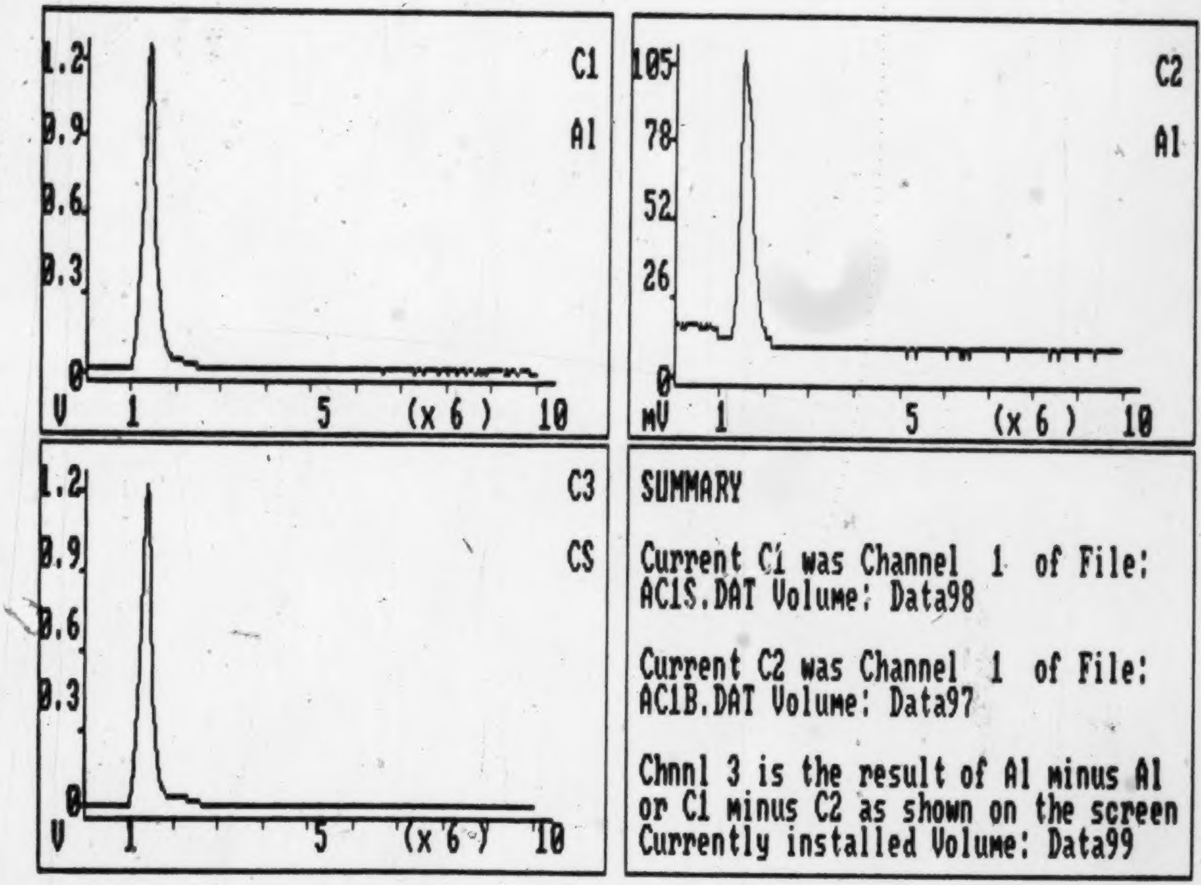
1.2
0.9
0.6
0.3
0
V
1
5
(x 6)
10
C1
A1
105
78
52
26
0
mV
1
5
(x 6)
10
C2
A1
1.2
0.9
0.6
0.3
0
V
1
5
(x 6)
10
C3
CS

```
SUMMARY

Current C1 was Channel  1  of File:
AC1S.DAT Volume: Data98

Current C2 was Channel  1  of File:
AC1B.DAT Volume: Data97

Chnnl 3 is the result of Al minus Al
or C1 minus C2 as shown on the screen
Currently installed Volume: Data99
```

Figure 2-25. Screen dump of subtracted Al temporal behavior, see text for details.

Al signal obtained from a blank run (10 µl of 0.25 M NaF solution) is plotted in the second Al window (Channel C2). The point-by-point subtracted Al signal (sample minus blank) is plotted in the Channel Subtracted (CS) window (Channel C3). The fourth window, entitled 'SUMMARY' displays housekeeping information pertinent to the subtracted signals.

If the subtracted signals are saved, a parameter file is automatically generated and saved. An appropriate message directing the user to the corresponding electronic notebook file where more information regarding the subtracted signals can be found, is also stored in this file. The electronic notebook, again automatically generated and saved, now contains information specific to the particular channels, as shown in Figure 2-24d. Thus the origin of the data under consideration can be easily established. This is how the program attempts to automate a small fraction of the information generation and gathering process.

Finally, no program can bill itself as user friendly unless it offers on-line help. The on-line help facility is invoked to explain the operating details of this software package and of the DSID. An example of the 'help' offered by the main program (accessed via item 7 of the main menu, Figure 2-13) is shown in Figure 2-26. In order to complete the discussion of all items of the main program menu, the function of item 6 of this menu is explained in Figure 2-26b.

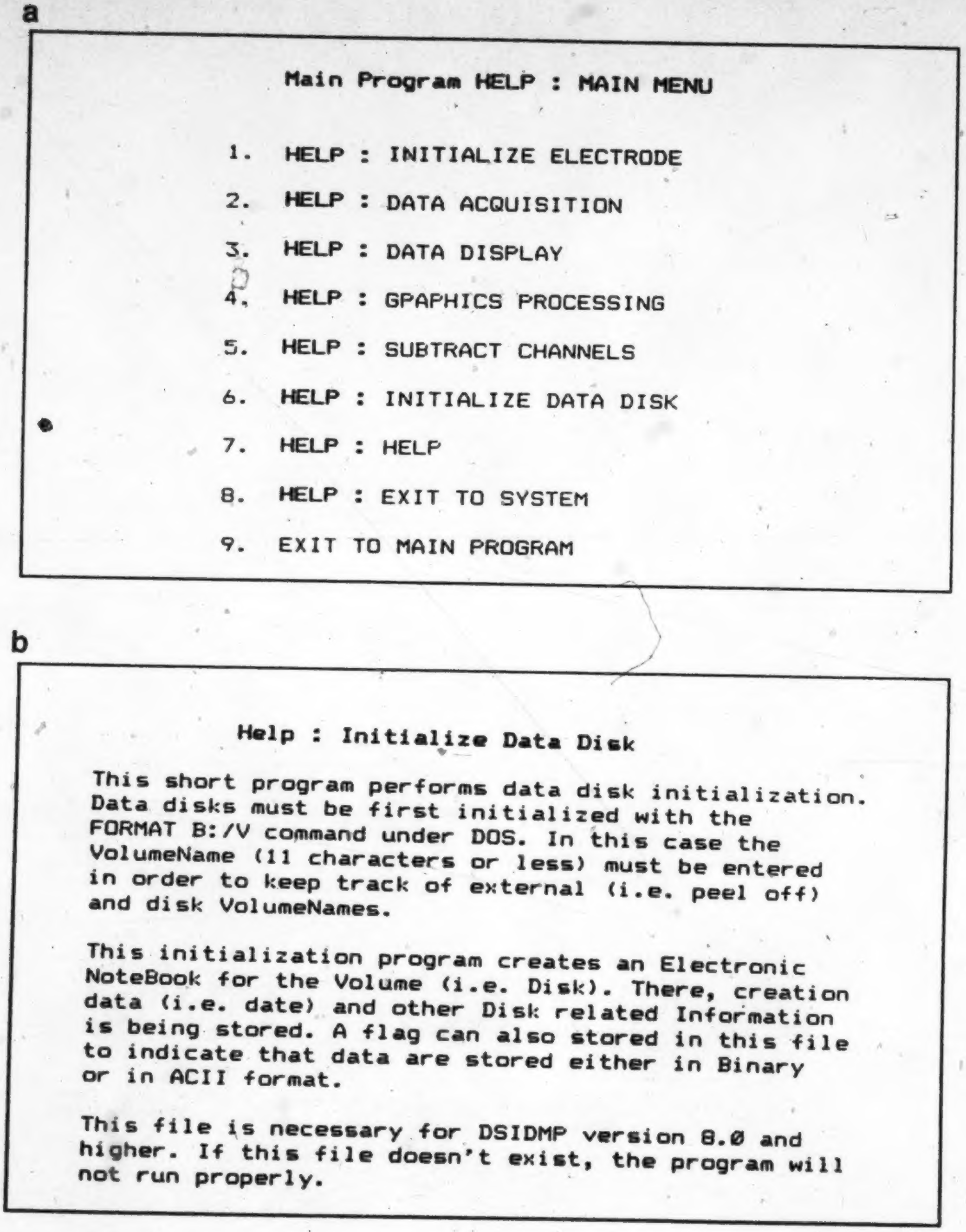

a

```
                Main Program HELP : MAIN MENU

          1.   HELP : INITIALIZE ELECTRODE

          2.   HELP : DATA ACQUISITION

          3.   HELP : DATA DISPLAY

          4.   HELP : GPAPHICS PROCESSING

          5.   HELP : SUBTRACT CHANNELS

          6.   HELP : INITIALIZE DATA DISK

          7.   HELP : HELP

          8.   HELP : EXIT TO SYSTEM

          9.   EXIT TO MAIN PROGRAM
```

b

```
             Help : Initialize Data Disk

    This short program performs data disk initialization.
    Data disks must be first initialized with the
    FORMAT B:/V command under DOS. In this case the
    VolumeName (11 characters or less) must be entered
    in order to keep track of external (i.e. peel off)
    and disk VolumeNames.

    This initialization program creates an Electronic
    NoteBook for the Volume (i.e. Disk). There, creation
    data (i.e. date) and other Disk related Information
    is being stored. A flag can also stored in this file
    to indicate that data are stored either in Binary
    or in ACII format.

    This file is necessary for DSIDMP version 8.0 and
    higher. If this file doesn't exist, the program will
    not run properly.
```

Figure 2-26. (a) Main program help menu and (b) initialize data disk example.

D. Conclusions

Developments reported in the literature over the last 10 or so years demonstrate that the DSID is a more powerful sample introduction system that it was initially perceived to be [1]. From the results presented here it can be concluded that the combination of a polychromator and of DSID-specific hardware and software offers the unique capability of assessing analyte emission temporal behavior in real-time and in an automated fashion. Due to its capabilities, this readout and control sub-system will be used in order to establish the performance characteristics of the DSID [28].

However, the automated DSID just described can generate an immense volume of data in a very short period of time. Thus, in order for the DSID to attain its full potential, machine-based intelligence and information processing capabilities become of paramount importance. Furthermore, as heavier demands are being placed on the controlling microcomputer, a fundamental limit is being rapidly exceeded: that of available processor power. In order to avoid the limitations imposed by a single processor system, a dual-processor system for the DSID described here has been developed and reported in the literature [36]. However, the key obstacle in further developing the front-end processor was lack of understanding the DSID. With this system, both cup-based and wire-loop based DSIDs can be evaluated and characterized [28, 29], and algorithms and software concepts can be rapidly tested. The concepts and ideas developed here can be easily ported to the front-end processor and, thus, the dual-processor system, shown in Figure 2-1, can be further developed.

Taking this concept a bit further, by utilizing a multi-processor environment, by implementing the *'instrument metaphor'* concept [36], by making the controlling microcomputer an integral part of readout electronics and, hence transparent to the user, and by front-ending the DSID with a robot arm (for both sample preparation and *in situ* chemical processing of the samples [29]), the DSID-robot arm combination can act both as a *'sample processor'* [47] and as an easily accessible front-end processor peripheral device capable of performing complex tasks in the laboratory. Therefore, the concept of a DSID not as a mere sample introduction system but as an intelligent sample processor for the ICP begins to emerge.

REFERENCES

1. E.D. Salin and G. Horlick, Anal. Chem., **51**, 2284 (1979)

2. W.E. Pettit and G. Horlick, Spectrochim. Acta, **41B**, 699 (1986)

3. Y. Shao and G. Horlick, Appl. Spectrosc., **40**, 386 (1986)

4. H. Haraguchi, M. Abdullah, T. Hasegawa, M. Kurosawa and K. Fuwa, Bull. Chem. Soc. Jap., **57**, 1839 (1984)

5. M. Abdullah, K. Fuwa and H. Haraguchi, Spectrochim. Acta, **39B**, 1129 (1984)

6. M. Abdullah and H. Haraguchi, Anal. Chem., **57**, 2059 (1985)

7. M. Abdullah, K. Fuwa and H. Haraguchi, Appl. Spectrosc., **41**, 715 (1987)

8. G.F. Kirkbright and S.J. Walton, Analyst, **107**, 276 (1982)

9. G.F. Kirkbright and Z. Li-Xing, Analyst, **107**, 617 (1982)

10. Z. Li-Xing, G.F. Kirkbright, M.J. Cope and J.M. Watson, Appl. Spectrosc., **37**, 250 (1983)

11. N.W. Barnett, M.J. Cope, G.F. Kirkbright and A.A.H. Taobi, Spectrochim. Acta, **39B**, 343 (1984)

12. D. Sommer and K. Ohls, Frezenius Z. Anal. Chem., **304**, 97 (1980)

13. K. Ohls and D. Sommer, in *'Developments in Atomic Spectrochemical Analysis'*, R.M. Barnes, Ed., Hayden, London, 1981, pp. 321-336

14. K. Ohls, Spectrochim. Acta, **39B**, 1105 (1984)

15. A.G. Page, K.H. Madraswala, S.V. Godbole, M.J. Kulkarni, V.S. Mallapurkar and B.D. Joshi, Frezenius Z. Anal. Chem., **315**, 38 (1983)

16. A.G. Page, S.V. Godbole, K.H. Madraswala, M.J. Kulkarni, V.S. Mallapurkar and B.D. Joshi, Spectrochim. Acta, **39B**, 551 (1984)

17. E.D. Salin and M.M. Habib, Anal. Chem., **56**, 1186 (1984)

18. E.D. Salin and R.L.A. Sing, Anal. Chem., **56**, 2596 (1984)

19. M.M. Habib and E.D. Salin, Anal. Chem., **57**, 2055 (1985)

20. C.V. Monasterios, A.M. Jones and E.D. Salin, Anal. Chem., **58**, 780 (1986)

21. E.R. Prack and G.J. Bastiaans, Anal. Chem., **55**, 1654 (1983)

22. A. Lorber and Z. Goldbart, Analyst, **110**, 155 (1983)

23. I.B. Brenner, A. Lorber and Z. Goldbart, Spectrochim. Acta, **42B**, 219 (1987)

24. C.W. McLeod, P.A. Clarke and D.J. Mowthorpe, Spectrochim. Acta, **41B**, 63 (1986)

25. M. Umemoto and M. Kubota, Spectrochim. Acta, **42B**, 491 (1987)

26. G. Zaray, J.A.C. Broekaert and F. Leis, Spectrochim. Acta, **43B**, 241 (1988)

27. G. Zaray, P. Burba, J.A.C. Broekaert and F. Leis, Spectrochim. Acta, **43B**, 255 (1988)

28. V. Karanassios, G. Horlick and M. Abdullah, *'Characterization of a direct sample insertion device for ICP-AES'*, Spectrochim. Acta, (submitted)

29. V. Karanassios, M. Abdullah and G. Horlick, *'The application of chemical modification to a direct sample insertion device for ICP-AES'*, Spectrochim. Acta, (submitted)

30. V. Karanassios and G. Horlick, *'Development and characterization of a DSID for ICP-MS'*, (in preparation)

31. D.W. Boomer, M. Powell, R.L.A. Sing and E.D. Salin, Anal. Chem., **58**, 975 (1986)

32. H. Matusiewicz, J. Anal. At. Spectrom., **1**, 171 (1986)

33. J.C. Van Loon, H. Haraguchi and K. Fuwa, *"Direct elemental analysis of solids by inductively coupled plasma emission spectrometry"* in *'Inductively Coupled Plasma Emission Spectroscopy, Part 2, Applications and Fundamentals'*, P.W.J.M. Boumans, Ed., John Wiley & Sons, New York, 1987, pp. 217-243

34. M.W. Routh and M.W. Tikkanen, *"Introduction of solids into plasmas"* in *'Inductively Coupled Plasmas in Analytical Atomic Spectrometry'*, A. Montaser and D.W. Golightly, Eds., VCH Publishers, New York, 1987, pp. 431-486

35. R.L.A. Sing and E.D. Salin, paper #32, 1986 winter conference on plasma spectrochemistry, Kailua-kona, Hawaii, Jan. 2-8, 1986

36. V. Karanassios and G. Horlick, Appl. Spectrosc., **41**, 360 (1987)

37. V. Karanassios and G. Horlick, Talanta, **32**, 583 (1985)

38. V. Karanassios and G. Horlick, Talanta, **32**, 601 (1985)

39. V. Karanassios and G. Horlick, Talanta, **32**, 615 (1985)

40. V. Karanassios and G. Horlick, *'New design concepts for direct reader measurement electronics'*, Appl. Spectrosc., (accepted)

41. V. Karanassios and G. Horlick, Appl. Spectrosc., **40**, 813 (1986)

42. P.C. Kelly and G. Horlick, Anal. Chem., **45**, 518 (1973)

43. P.W.J. Boumans, *'Line Coincidence Tables for Inductively Coupled Plasma Atomic Emission Spectrometry'*, Pergamon Press, New York, 1984, 2nd Ed.

44. I.B. Brenner and H. Eldad, ICP Info. Newsletter, **10**, 451 (1984)

45. R.K. Winge, V.A. Fassel, V.J. Peterson and M.A. Floyd, *'Inductively Coupled Plasma-Atomic Emission Spectroscopy. An Atlas of Spectral Information'*, Elsevier, New York, 1985

46. R.W. Dabeka, P. Tymchuk and D.S. Russell, Appl. Spectrosc., **34**, 43 (1980)

47. G. Horlick and V. Karanassios, Chapter for monograph on Atomic Analytical Spectrometry, J.A. Holcombe, Ed., (accepted)

CHAPTER 3

CHARACTERIZATION OF A DIRECT SAMPLE INSERTION DEVICE FOR ICP-AES

A. Introduction

Undoubtedly, conventional pneumatic nebulization of solution samples (i.e., a combination of spray chamber and a pneumatic nebulizer), is the most popular means of sample introduction into the inductively coupled plasma (ICP). However, in spite of its wide applicability, there are several shortcomings associated with this method of sample introduction. Included in these are: poor nebulization efficiency, blockage at high salt concentrations, the requirement for solution samples and volumes greater than 1 ml and drift [1, 2, 3, 4]. In order to overcome or eliminate some of these shortcomings, a number of researchers have demonstrated the feasibility of direct sample introduction into the ICP [1, 2, 5, 7, 8]. The use of: fluidized beds; slurry atomization; electrothermal vaporization; arc and spark atomization; laser ablation and direct sample insertion via graphite cups or wire-loops have all been reported. This work will focus on direct sample insertion devices (DSIDs). In these, the sample is placed into or onto a probe (i.e., a graphite electrode or a wire loop) with subsequent introduction of the sample carrying probe, typically via the central tube of the torch, into the plasma.

Recent developments in the basic DSID include automation of the device [9-16]; the design of readout electronics capable of handling transient, peak-like signals [9]; the development of DSID-specific software [9, 15]; and the development of DSIDs for ICP mass spectrometry [17, 18]. Undoubtedly, the direct sample insertion technique (DSIT) could be further refined and the analytical utility of the DSID could be greatly improved if the experimental variables affecting the analytical performance characteristics of the DSID were understood more fully. The experimental parameters affecting the performance characteristics of a DSID for ICP-AES (atomic emission spectrometry) are summarized in Table 3-1.

In a companion publication from this laboratory, the development of readout and control electronics sub-system capable of handling DSID-generated transient signals has been reported [9]. This sub-system will be used in this work in order to establish analyte emission behavior in the time domain and to assess the analytical performance characteristics of the DSID. More specifically, analyte emission temporal behavior for several elements will be surveyed, the combined effect of electrode geometry and power on analyte emission characteristics and on signal-to-background ratios (SBRs) will be investigated, and some preliminary results on the analytical figures-of-merit of the device will be reported.

Table 3-1. Experimental parameters and design attributes affecting the analytical performance characteristics of a DSID for ICP-AES.

1. **Plasma**
    - Forward power
    - Gas flow rates
    - Gas composition

2. **Spectrometer**
    - Analytical line(s) and detector attributes
    - Lateral and vertical plasma viewing position

3. **DSID design attributes**

    a. Design
    - Type (i.e., vertical, horizontal, mechanical, pneumatic)
    - Probe insertion position
    - Probe insertion speed

    b. Probe attributes
    - Type (i.e., metal or graphite cup, rod, wire-loop)
    - Composition (i.e., graphite, coated graphite, metal)
    - Geometry (i.e., size, shape, depth of crater)
    - Physical condition (i.e., surface porocity)

    c. Run-time parameters
    - Drying
        - Probe insertion position (with respect to TOLC)
        - Drying time (s)
    - Ashing
        - Probe insertion position (with respect to TOLC)
        - Ashing time (s)
    - Atomization
        - Probe insertion position (with respect to TOLC)
        - Observation time (s)
        - Integration time (s) for peak-area integration

4. **Sample**
    - Size (i.e., injected volume, sample mass)
    - Analyte concentration
    - Matrix composition

Furthermore, DSID design attributes (i.e., probe insertion speed, insertion position and composition) affecting the analytical performance characteristics of the device will be isolated and their effect will be documented. Finally, the findings of this work will be used as the basis for a proposed 'next generation' DSID for ICP-AES.

B. Experimental

The basic components of the DSID utilized in this work are shown in Figure 3-1. A 27.12 MHz Ar ICP was fitted with a computer controlled, vertically operated, pneumatically and mechanically driven DSID capable of handling up to 24 sample carrying probes in an un-interrupted and automated fashion and it was coupled to a 1-m, 29-channel polychromator. Plasma, DSID and direct reader were mounted on an in-house developed optical rail bed. The DSID and the data acquisition and control hardware and software utilized in this work have been described in detail elsewhere [9]. The instrumentation and typical operating conditions are summarized in Table 3-2. The analytical wavelengths were: Ag I 328.07, Al I 237.34, Ca II 317.93, Cd I 228.80, Co II 228.61, Cr II 205.55, Cu I 324.75, Fe II 259.94, Mg II 279.08, Mn II 257.61, Ni II 231.60, Si II 228.16, Sn II 189.99, Sr II 407.78, Zn I 213.86 and Zr II 343.82 nm.

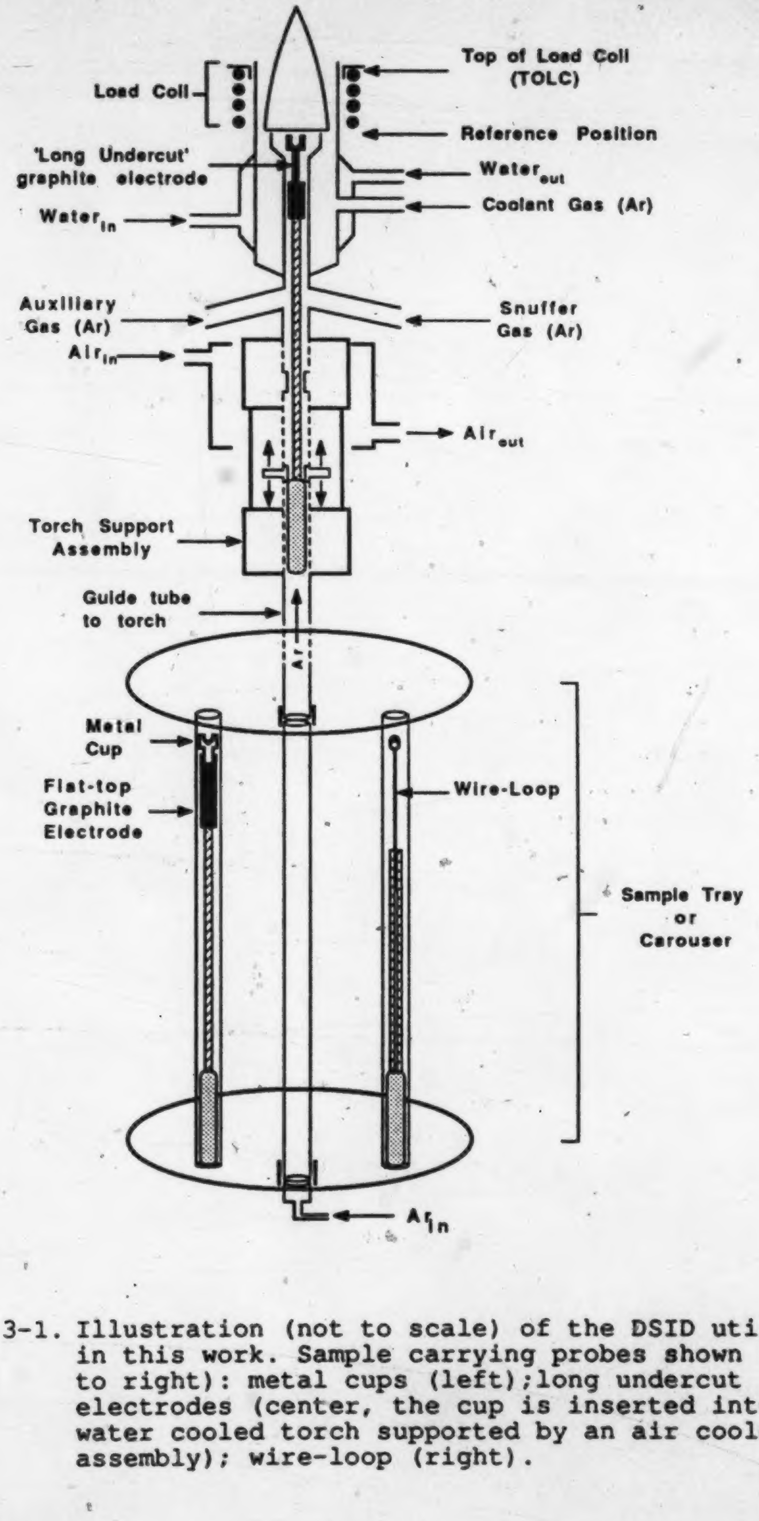
Load Coil
Top of Load Coil (TOLC)
Reference Position
'Long Undercut' graphite electrode
Water$_{out}$
Coolant Gas (Ar)
Water$_{in}$
Auxiliary Gas (Ar)
Snuffer Gas (Ar)
Air$_{in}$
Air$_{out}$
Torch Support Assembly
Guide tube to torch
Ar
Metal Cup
Flat-top Graphite Electrode
Wire-Loop
Sample Tray or Carouser
Ar$_{in}$

Figure 3-1. Illustration (not to scale) of the DSID utilized in this work. Sample carrying probes shown (left to right): metal cups (left);long undercut electrodes (center, the cup is inserted into a water cooled torch supported by an air cooled torch assembly); wire-loop (right).

Table 3-2. Instrumentation and typical operating conditions.

DSID	Prototype design (9)
Type	Vertical, pneumatic, computer-controlled
Probe types	Graphite electrodes, metal cups, wire-loops
Insertion position	Top of probe in alignment with the top load coil
Insertion mode	Regular and one-shot, see text for details
Readout electronics	Capable of capturing transient signals (9)
Amplifier	Operational Amplifier (CDC15023, Heath Co.)
Amplification mode	Current-to-Voltage conversion
ADC converter	Data Translation® DT2801A board for the IBM PC
Microcomputer	IBM PC
Software	DSID-specific, in-house developed for the IBM PC (8)
Type	Menu-driven, window-based, Mac-like, user-friendly
Functions	Automation and control, data acquisition, signal display and processing, and information management
Front-end processor	Apple Macintosh

Table 3-2. Continued.

ICP	Plasma Therm, Inc., model ICP 5000
RF Generator	Model HFS-5000D
Frequency	27.12 MHz
Max power output	5.00 kW (2.00 kW maximum power used)
Matching network	Model AMN-5000E
Torch box	Model PT-1
Torch	Water-cooled, see reference 10 for details
Forward Power	1.25-2.00 kW in increments of 250 W
Reflected Power	<80 W
Coolant gas	Ar (18 l/min at 1.25 KW, 20 l/min at 2.00 kW)
Auxiliary gas	Ar (0.6 l/min at 1.25 K), 1 l/min at 2.00 kW)
Snuffer gas	Ar (1.0 l/min at all power settings)
Observation height	16 mm above the load coil
Polychromator	ARL, Inc., Paschen-Runge mount
Focal length	1-meter
Grating	1200 grooves/mm
Slits	15 µm entrance/35 µm exit
Dispersion	0.463 nm/mm at 300 nm (2nd order)
Detector/Channels	PMT/29 (simultaneous observation of four-channels)

As previously reported [9], a variety of sample carrying probes can be used with this system. The following sample carrying probes were utilized in this work (Figure 3-1): a long undercut graphite electrode; a flat-top graphite electrode fitted with a metal cup (only the undercut cup is metal); and a wire-loop. A variety of conventional dc arc graphite electrodes were also used in this study, included in these are: HPND+ 4000, HPND+ 4004, HPND+ 4021, HPND+ 4024 or equivalent (SPEX Industries, Inc., Edison, NJ or Bay Carbon, Inc., Bay City, MI). The custom electrode geometry (dubbed a 'long undercut' electrode, Figure 3-1) was machined in our laboratory out of the corresponding graphite electrode. Similarly, metal cups (i.e., Ta or W) have been machined out of the corresponding metal rod. Unless otherwise stated, the use of a long undercut graphite electrodes (Figure 3-1), a 1.25 kW applied forward power, and a regular drive insertion mode, in which the electrode is stopped at the reference position and it is slowly driven to TOLC (Figure 3-1) is assumed.

In order to reduce the amount of impurities contained in the electrodes, commercially available graphite rods and electrodes were treated according to the procedure recommended by Abdullah et al. [19] and were pre-burned 3 to 5 times prior to their use. Graphite electrodes used with non-carbide forming analytes are re-usable for over twenty times, metal cups and wire-loops appear to be re-usable for hundreds of times.

All solutions were prepared by serial dilution with distilled/deionized water of 1000 ppm standard stock solution (standards for plasma emission spectroscopy, SPEX Industries Inc., Edison, NJ) of the respective element. A 10 µl volume was transferred (i.e., injected) to the sample carrying probe with an Eppendorf micropipette. Solution volumes injected into cups were dried by heating the electrode in an aluminium holder on a hot plate prior to insertion into the plasma, those applied onto the wire-loop were dried with an IR-lamp.

C Results and Discussion

C.1 Survey of Analyte Emission Temporal Behavior

In order to establish the nature of signals generated by this DSID, intensity-versus-time curves (i.e., analyte emission temporal behavior) were recorded for several elements with the top of the long undercut graphite electrode in alignment with the top load coil (abbreviated TOLC, Figure 3-1) and an applied plasma power of 2.00 kW. Typical results for Ag, Cd, Co, Cr, Cu, Fe, Mg, Mn, Ni, Si, Sn and Zn are shown in Figure 3-2. Unless otherwise specified, t=0 seconds (shown in Figure 3-2) is set when the probe is at the same height as the top of the central tube of the

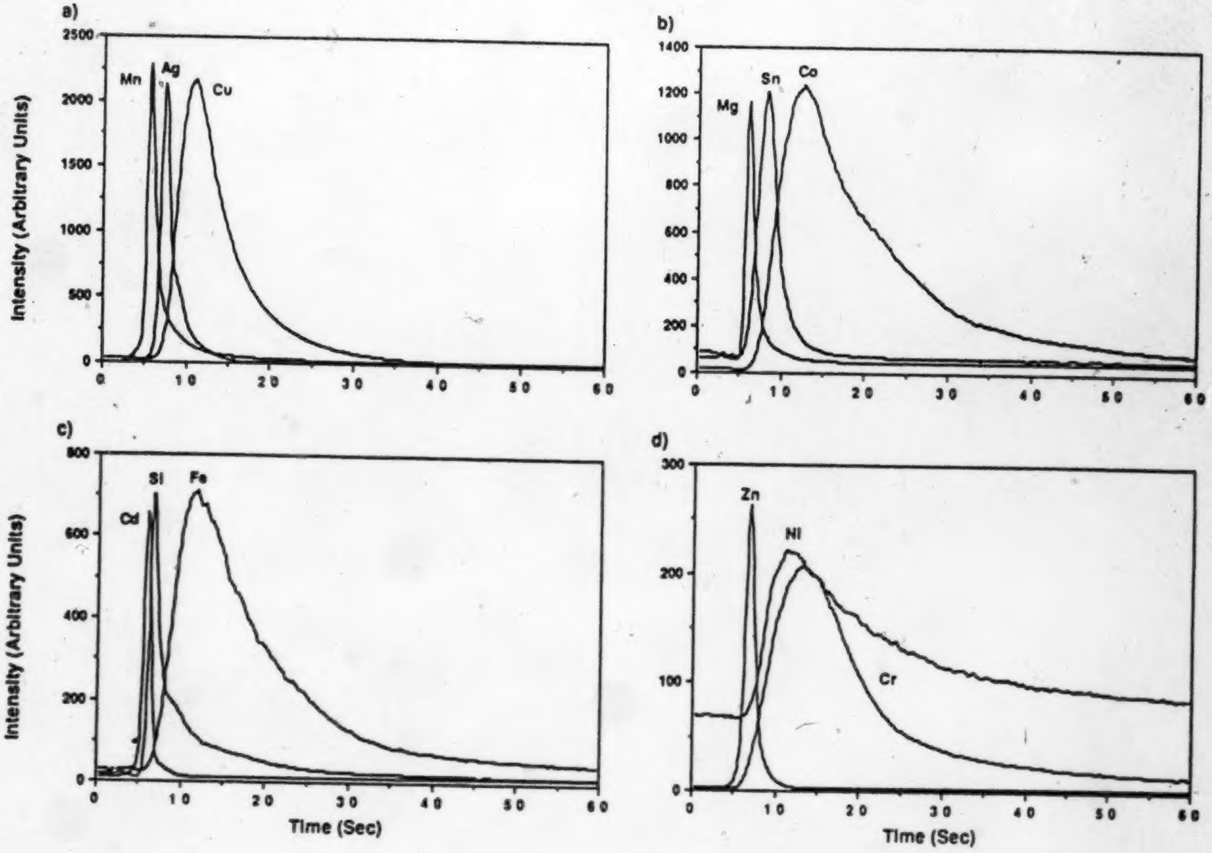

Figure 3-2. Typical temporal behavior for Ag, Cd, Co, Cr, Cu, Fe, Mn, Mg, Si, Sn, Ni and Zn acquired using long undercut graphite electrodes, a regular drive insertion mode and an applied forward power of 2.00 kW (other operating conditions as in Table 3-2).

torch (referred to as the reference position in Figure 3-1). At this point in time data acquisition is initiated and the probe is driven (using a regular drive insertion mode) to TOLC [9]. A peak appearance time (defined as the time at which the peak maximum appears) of less than 15 s was measured for all of the above elements. For Ag, Cd, Cu, Mg, Mn, Si, Sn and Zn the emission signals have a post-insertion base-line level of approximately equal magnitude of that observed during pre-insertion in less than about 35 s. However, for more difficult-to-volatilize elements (i.e., Co, Cr, Fe and Ni) the corresponding emission signals have a post-insertion base-line level which, even after 60 s, is considerably higher than the pre-insertion level. These findings are in general agreement with those reported by others [19-21]. This may be due to: the nature of the residue remaining in the cup after drying/ashing and/or during the initial stages of insertion; or to a change in the physical properties of the cup upon insertion; or both. The nature of the residue is becoming increasingly important for elements known to form refractory oxides and/or carbides, for example, only low intensity signals were observed for Sr, Ca, Al and no signal was observed for Zr and Ti.

C.2 Volatility Sequence

Based on the results of the preceding survey, a volatility sequence can be assigned as follows: Mn, Cd, Mg, Si, Zn, Ag, Sn, Cu, Ni, Fe, Co and Cr, a plot of the element of interest versus its appearance time is shown in Figure 3-3. By comparison, a different volatility sequence (i.e., As, Pb, Cd, Zn, In, Ge, Ag, Li, Na, Sb, Mn, Cu, Mg, Cr and Fe) has been reported [11]. Moreover, no correlation between the boiling point of the element of interest and it's appearance time has been found here and reported by others for solution sample residues [22] and for solid samples [23]. These observations suggest that, much like in the dc arc [24, 25], the volatility sequence does not depend on elemental volatilities alone, a more complex mechanism must be operative. This is not surprising when viewed in light of the physico-chemical processes taking place in the electrode cavity.

Drawing parallels between electrothermal vaporization techniques (ETV), the dc arc and the DSID is unavoidable. Drawing from the dc arc and electrothermal literature, and in order to understand the processes taking place in the cup and to appreciate the influence they exert on analyte emission temporal behavior, a conceptually simple model was devised. The key idea behind it is quite straightforward:

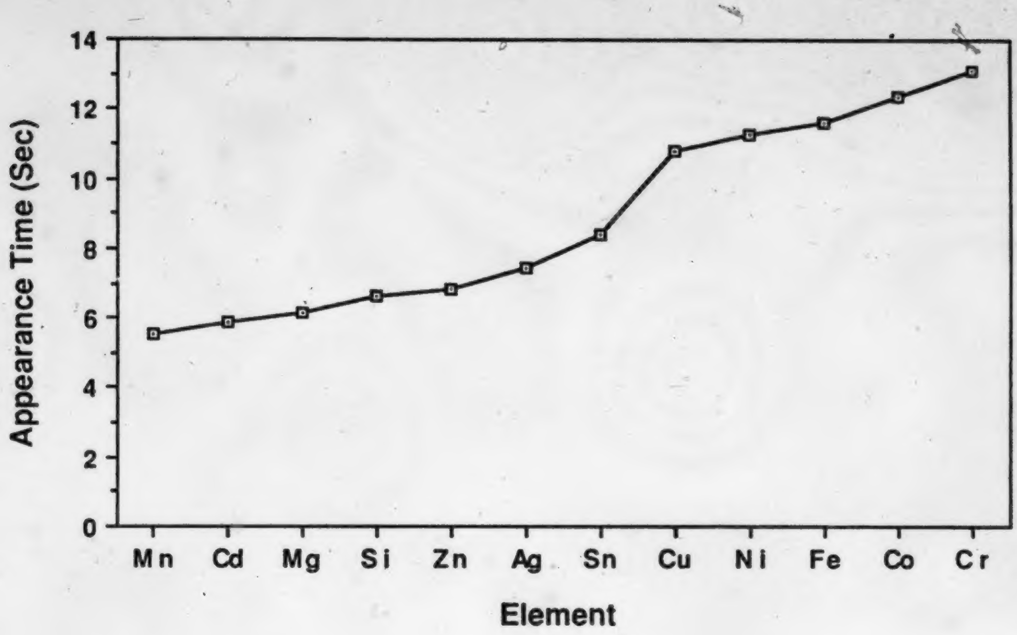

Figure 3-3. Appearance time versus element of interest (i.e., volatility sequence).

both the chemical form and, as a consequence, the physicochemical properties of the sample change due to the thermochemical processes taking place in the electrode cavity. This model is briefly outlined below by following the sample carrying cup in a stepwise fashion as it is placed underneath the discharge (i.e., reference position, Figure 3-1) and it is slowly driven to TOLC.

During the drying/ashing cycle or at the initial stages of cup insertion into the ICP, a rising cup temperature promotes thermal decomposition of an oxo-anion salt (e.g., nitrate) to an oxide. With a further increase in temperature (attained during the final stages of cup insertion or during the early stages of the atomization cycle), the oxide may react with graphite to form the corresponding carbide. Clearly, probe composition plays an important role, for example, carbide formation can be eliminated when metal cups are used. With metal cups, however, formation of intermetallic compounds also becomes an important consideration. If the final probe temperature is less than that required for oxide/carbide volatilization, no emission signal is expected from the oxo-anion salt. On the other hand, if sufficiently high temperatures are reached, quantitative volatilization is expected, regardless of chemical form of the residue remaining in the cup. Alternatively, it can also be suggested that the oxide may be reduced by graphite to metal. Furthermore, because the surface of the graphite cup can be modified by a carbide forming element during or upon final insertion into the plasma, analyte emission temporal behavior, appearance time, sensitivity and precision of non-carbide forming elements may also be affected. Therefore, a sample type dependence of analyte emission temporal behavior can also be suggested. Despite its simplicity (for example, TiO_2 reduction by graphite in a conventional furnace was found to proceed through Ti_3O_5, Ti_2O_3, TiC to Ti [26]), and its speculative nature, the model provides an attractive framework with which to explain the differences in the volatility sequence. Therefore, the concept of sample, DSID and power dependent volatility sequence, conveniently termed 'apparent volatility sequence', begins to emerge. Similar conclusions have been drawn, quite some time ago, for the dc arc: *'We should be aware, however, that the volatility of an element is not an intrinsic property but depends to a considerable degree on the environment, that is, on the presence of other substances and on the thermal conditions in the electrode cavity'* [24].

However, before any attempts can be made to understand apparent volatility and to elucidate the mechanism of atom formation, the factors that influence analyte emission temporal behavior characteristics must be identified. From the practical point of view, establishing the extent to which these factors influence temporal behavior is central to improving the analytical figures-of-merit of the device. In general, four broad categories of factors can be distinguished. Included in these are: plasma, spectrometer, DSID, and the sample itself. These are summarized in Table 3-1. And although they are listed in a linear fashion, some of them are inter-dependent. Only DISD related parameters will be considered here.

C.3 DSID Design Attributes

DSIDs can be classified in several ways according to their design attributes. For example, because DSIDs can be operated either vertically or horizontally, they can be classified accordingly as vertical or horizontal. In addition, they can also be classified according to the sample probe utilized as wire-loop, graphite-rod and as cup based. Another classification relies on the way the sample carrying probe is driven into the plasma, hence, DSIDs are classified as mechanically and a pneumatically driven. A brief review of DSID designs has been presented by Karanassios and Horlick [9]. The effect of design attributes on analyte emission temporal behavior for a computer controlled and pneumatically and mechanically driven DSID capable of handling a variety of sample probe types in an automated fashion will be presented in the following sections.

Run-time parameters refer to experimental variables (i.e., those pertaining to the drying, ashing and atomization cycles) that are either defined on a sample by sample basis or in a batch mode, and are set on the controlling microcomputer prior to analysis. With an automated DSID [9-14, 20] drying and ashing can be performed *in situ* underneath the plasma prior to atomization. Because these parameters are sample type [13, 19, 27, 28] and probe type [9, 12, 29] dependent, they will not be discussed any further.

C.3.1 Cup Insertion Position

Cup position, defined as the distance between the top of the sample carrying probe and the top load coil, has been found to exert a significant influence on both peak heights [11] and on SBRs [12-14, 19-21, 30, 31]. Depending on the element and on plasma observation height used, cup positions of 2 mm to 3 mm below TOLC [32], of 0 mm [11, 13, 31], of 2 mm [12, 14, 19-21, 32], of 4 mm [30, 32], of 6 mm [28, 34] and of 8 mm [19] above TOLC have been reported. In order to establish an optimum value for this DSID, cup insertion position was optimized with respect to SBR for four elements (i.e., Cd, Cr, Cu and Mn) with different thermochemical properties, and ion and atom emission lines covering a range of wavelengths. Analyte emission temporal behavior was recorded simultaneously for all elements and was measured for insertion positions progressively closer to TOLC (shown in Figure 3-1) at 1.25 kW. Measurements at these positions result in sharper peaks, shorter appearance times, larger integrated peak areas and lower plasma background. With the exception of Cr, SBRs peak out at TOLC (i.e., the '0 mm' position) and subsequently decrease, as shown in Figure 3-4. From these results it can be concluded that the '0 mm' insertion position (TOLC) is a good compromise for the elements tested and it will be used throughout.

Because plasma observation height is usually fixed (i.e., at 16 mm above the load coil in this case), any deviation from the final insertion position (i.e., with respect to TOLC) is also expected to affect temporal emission characteristics. A more than 10% change in peak heights for a 1 mm difference in cup insertion position has been measured here and reported by others [11] for some elements. It is worth noting that although the present drive is under computer control, the accuracy of insertion is rather low (i.e., about ±0.5 mm), due to mechanical imperfections, thus adversely affecting %RSDs.

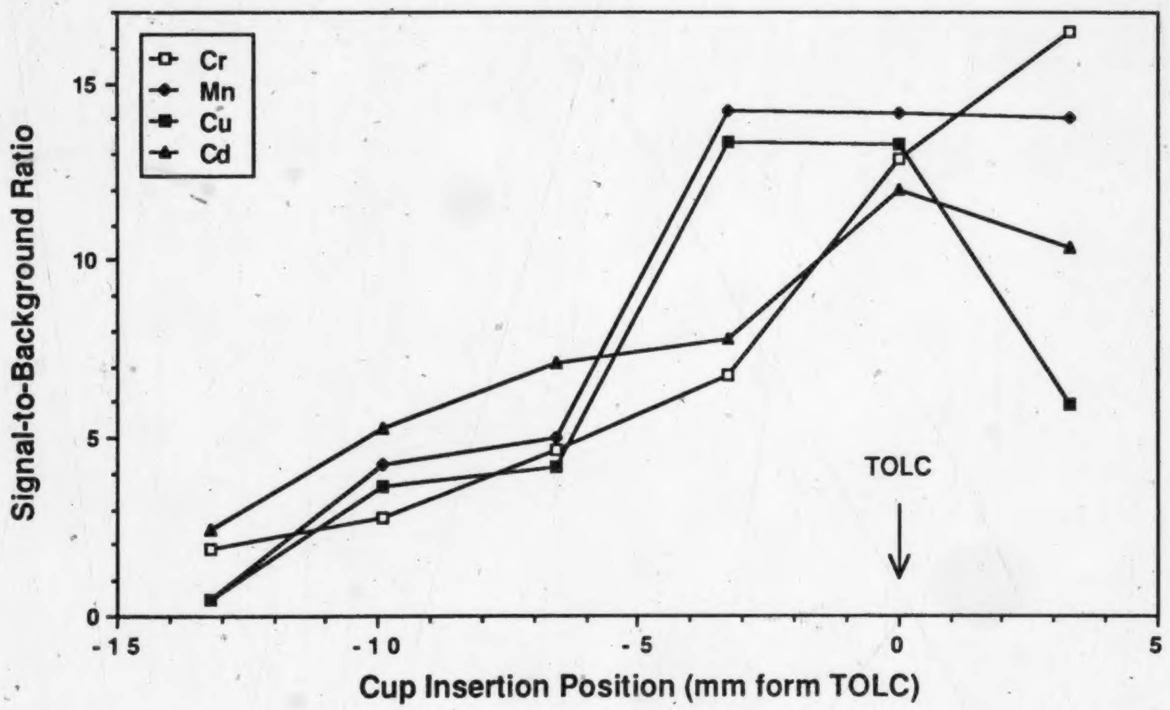

Figure 3-4. Signal-to-Background Ratio (SBR) for Cd, Cr, Cu and Mo determined from multielement solution residues for different cup positions (i.e., distance from the top of the sample carrying cup to TOLC) for long undercut electrodes, a regular drive insertion mode and at 1.25 kW (the other conditions as in Table 3-2).

C.3.2 Cup Insertion Speed

With the insertion of a foreign object (i.e., sample carrying probe) into the plasma, the discharge is disturbed, its geometry (i.e., shape and size) changes and plasma background is reduced. These effects are of a transient nature, their extent (both in magnitude and in time) depends on applied forward power, and on probe mass, geometry, composition, and insertion speed. A key question that arises is: what is the magnitude and the temporal characteristics of plasma background upon probe insertion? Also, because a high volatility analyte volatilizes during probe insertion and simultaneously with a changing background, to what extent does probe insertion speed affect analyte emission temporal behavior? The effect of probe insertion on plasma background has been investigated by Salin et al. [29] who have documented the influence wire-loop insertion has on the background of the Cu 324.75 nm and the Zn 213.86 nm lines, and by Zarray et al. [31] who have described the outcome of graphite cup insertion on the structure of the background (200 nm to 500 nm region) of an Ar-N_2 mixed-gas plasma operating at 3.00 kW. The effect of insertion speed on the background and the analyte signals is documented below.

The visual observation of plasma background reduction upon probe insertion (attributed to RF power coupling between the load coil and the sample carrying probe) has been verified experimentally and measured for two extreme cases. One in which the long undercut graphite electrode is stopped at the reference position underneath the plasma and is slowly driven to TOLC, dubbed a 'regular drive' insertion mode, and another, termed a 'one shot' insertion mode in which the electrode is directly inserted (i.e., 'shot') into the plasma and is stopped (by a mechanical stop) when the top of the electrode has reached TOLC. For all experiments described in this section, both electronics and PMT gains were at their maximum, so as to maximize the sensitivity of the corresponding PMT channel. Typical results (Cu channel), a 'blank' electrode and a 'regular drive' insertion mode are shown in Figure 3-5a. The background gradually changes and after about 13 s it attains a new steady state value. And even though the electrode begins to glow (i.e., it gets red hot), the plasma background remains relatively stable. This gradual change in background can be attributed to electrode insertion as, with the present system, it also takes about 13 s to drive the electrode from the reference position to TOLC. Therefore, it can be concluded that the change in background tracks electrode insertion, as soon as the electrode reaches TOLC the background attains its new value and remains relatively stable.

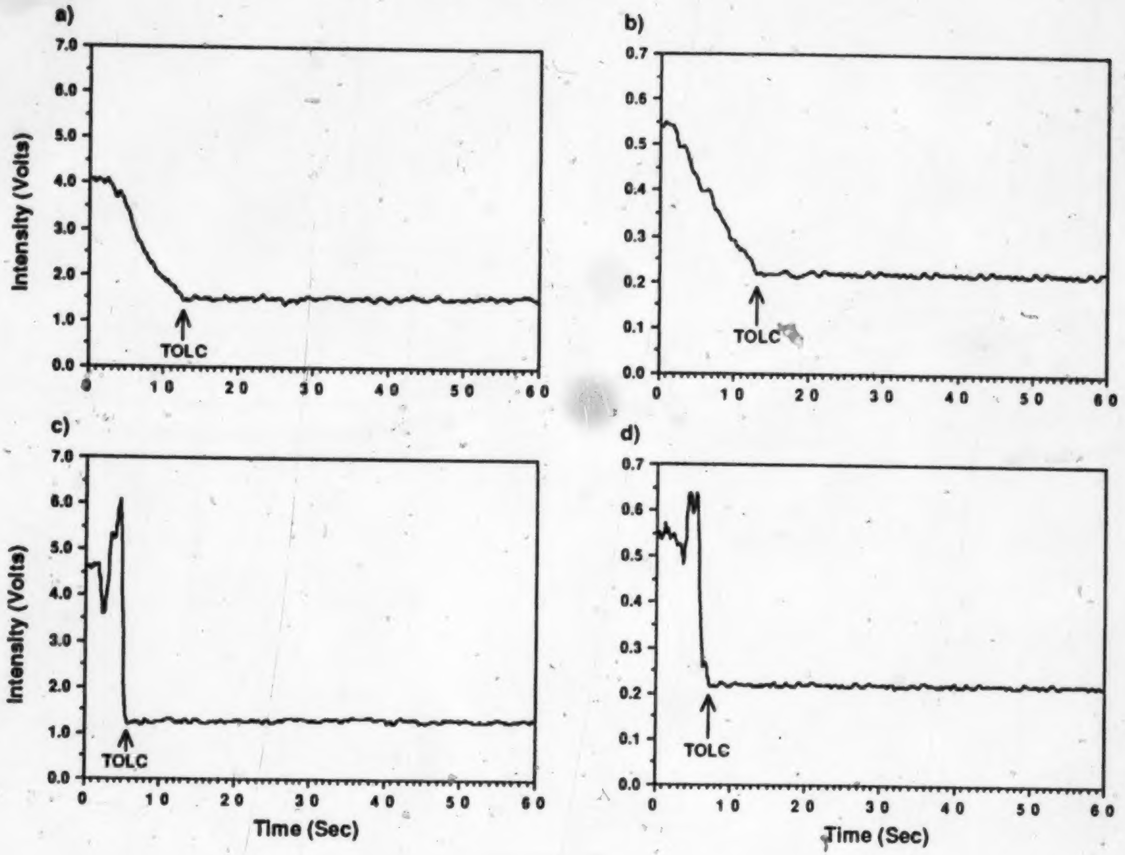

Figure 3-5. The effect of insertion speed on the Cu and Cr background signals (324.75 nm and 205.55 nm lines) for a 'blank' long undercut graphite electrode and at 1.25 kW (other operating conditions as in Table 3-2) for: a regular drive insertion mode, (a) Cu channel and (b) Cr channel; and a one-shot insertion mode, (c) Cu channel and (d) Cr channel. All channels saturate at 10 V.

Both the gradual change in background and the post-insertion background levels are reproducible for all channels tested (i.e., Cd, Co, Cr, Cu, Fe, Mn, Ni and Zn). The magnitude of the drop in background for a given power setting, however, does vary from channel to channel. This is not surprising because plasma background levels are higher at longer wavelengths (hence the choice of the Cu 324.75 nm line corresponding to the longest wavelength for all elements tested is shown in Figure 3-5a). The results of Figure 3-5a (blank electrode, Cu channel, direct drive insertion mode) show that the background level observed at the end of an insertion drops to about 25% of its pre-insertion value. For shorter wavelengths (i.e., blank electrode, direct drive insertion mode, Cr 205.55 nm line corresponding to the shortest wavelength for all elements tested) the post-insertion background level is about 40% of that observed during pre-insertion, as shown in Figure 3-5b. For all other elements/channels (i.e., Cd, Co, Fe, Mn, Ni and Zn), the drop was somewhere between 25% and 40% of the pre-insertion value depending on wavelength.

To test for the fastest attainable insertion speed, a one shot insertion mode was utilized. In this case, it takes a fraction of a second for the electrode to travel from reference to TOLC, an abrupt change of equal duration in time is observed by monitoring plasma background, as shown in Figures 3-5c and 3-5d for the Cu and Cr channels.

Much like the regular drive insertion mode, as soon as the electrode reaches TOLC, the background attains a new value and remains relatively stable. The change in magnitude of the background levels upon one shot insertion is, within experimental error, the same as that observed for the regular drive for all elements tested. And as before, the background change is of lower magnitude for shorter wavelengths. It is worth noting that unlike the direct drive, in the one shot insertion mode there is no reference point, data acquisition is initiated arbitrarily and therefore t=0 s shown in Figure 3-5c and 3-5d has no meaning as it varies from run to run. A reference point (and t=0 s) could be set by noting the sharp drop in the background signal.

In terms of analytes and for slow insertion speeds (i.e., a regular drive insertion mode), highly volatile elements, such as those with an appearance time of less than 13 s with this system, are expected to completely volatilize during electrode insertion. And because both the analyte signal and the background change simultaneously and in opposite directions, the peak-like signals are expected to reside on a sloping background. Indeed, this is the case for 1 ng Zn (chosen due to its high volatility), as shown in Figures 3-6a and 3-6b for the background and the atomic signals respectively. Similar results for Zn have been reported elsewhere [11]. From these results it can also be concluded that Zn volatilizes quantitatively

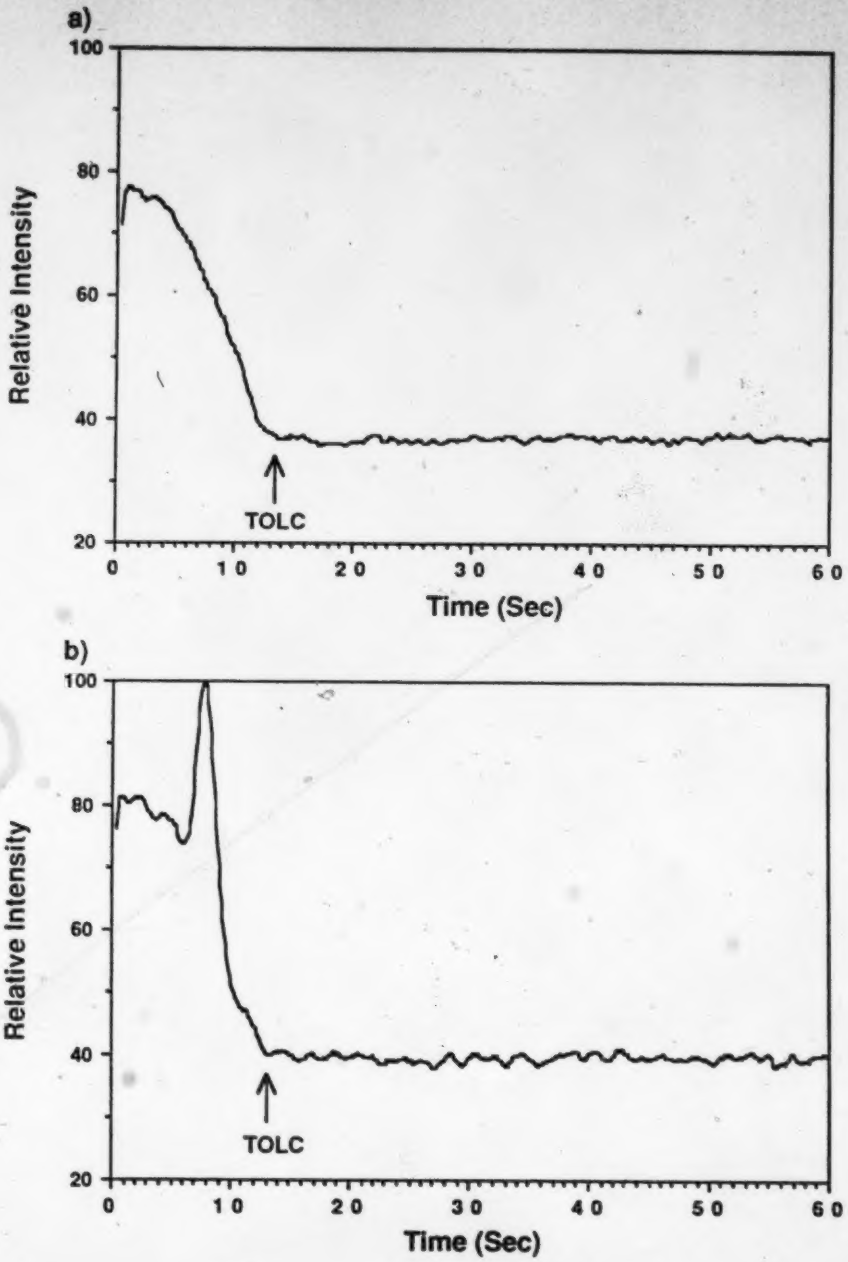

Figure 3-6. The effect of insertion speed on the background and atomic signals observed on the Zn channel (213.86 nm line) for long undercut graphite electrodes, a regular drive insertion mode and 1.25 kW (other operating conditions as in Table 3-2) for: (a) Zn channel, blank graphite electrode, background signal; and (d) Zn channel, 1 ng Zn.

well before the electrode reaches TOLC, from the peak appearance time it can be inferred that most of Zn volatilizes when the cup is at about 75% of the reference-to-TOLC distance. More volatile elements (i.e., Cd) volatilize when the electrode is even closer to the reference position, thus, some of the differences reported for the optimum cup insertion position may be explained in terms of insertion speed.

Due to the absence of a well defined central channel *viz-á-vis* a pneumatic nebulizer system, it could be argued that for a slow insertion speed, because high volatility analytes volatilize well before the cup has reached TOLC, some loss might occur as analyte vapor spreads out radially as it travels into the plasma. This, in turn, might result in poor reproducibilities. This hypothesis was tested and is documented in the following. Cadmium was chosen due to its high volatility and because it is an element for which the analyte signal has been reported to be insufficiently resolved from the abrupt change in the background observed upon probe insertion with some systems [19-21]. A 15 s observation time was chosen in this instance, the other operating conditions were kept as before.

The results for 1 ng of Cd for both the regular and the one shot insertion mode are shown in Figures 3-7a and 3-7b.

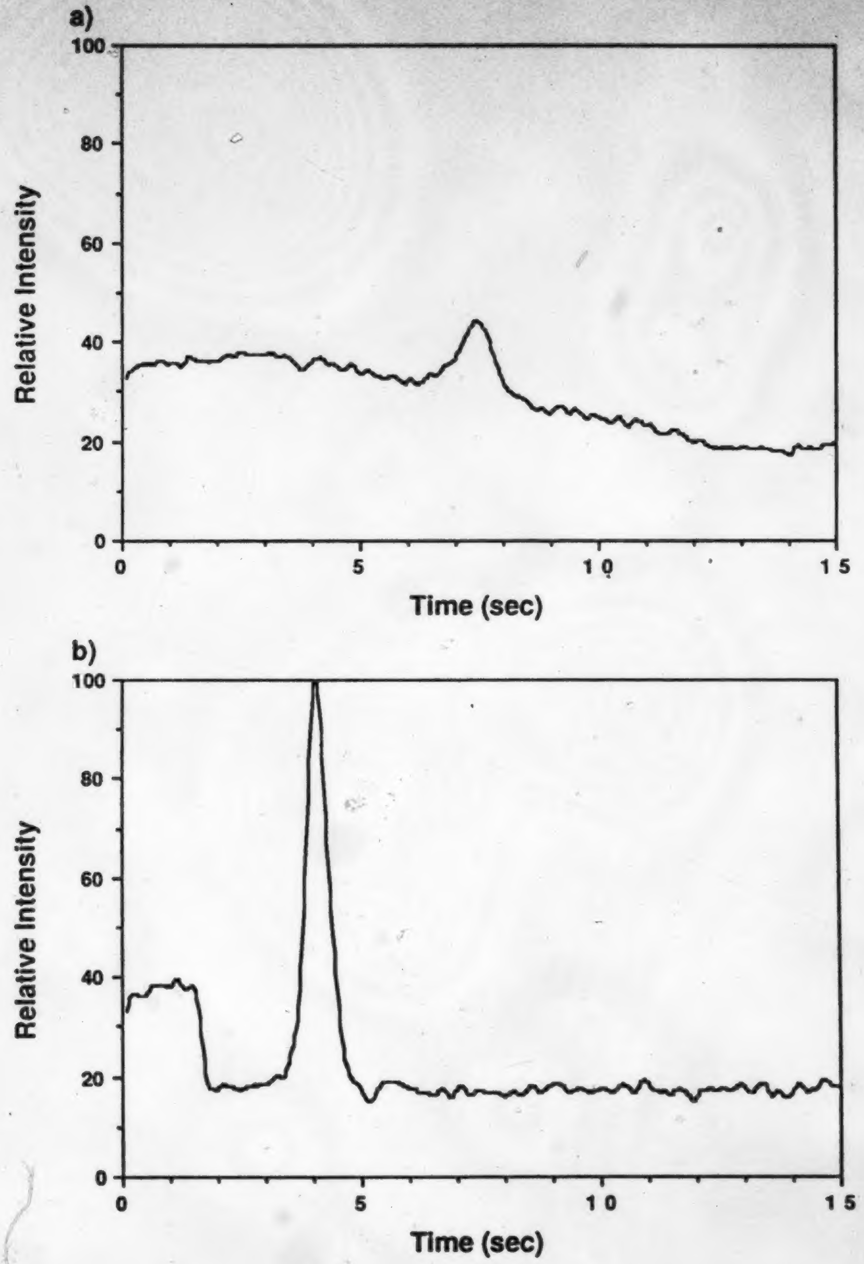

Figure 3-7. The effect of insertion speed on the Cd atomic signal for a long undercut graphite electrode and 1.25 kW (other operating conditions as in Table 3-2) for: (a) Cd channel, 1 ng Cd, regular drive insertion mode; and (d) Cd channel, 1 ng Cd, direct drive insertion mode.

The result for the direct drive insertion mode (Figure 3-7a) shows that the signal for Cd, much like that for Zn, resides on a sloping background, while the result for the one shot insertion mode (Figure 3-7b) shows that with this system and with a faster insertion speed, the analyte signal is well resolved from the change in the background level. In terms of a comparison, the one shot insertion mode results in sharper peaks and a 2.5-fold enhancement in both net peak heights and net integrated peak areas at this concentration level. The magnitude of the observed enhancement in sensitivity was found to be dependent on the volatilities of the elements tested (i.e., Cd, Co, Cr, Cu, Fe, Mn, Ni and Zn), no enhancement was observed for the elements that inherently volatilize slowly. An improvement in %RSD was also observed for Cd. A 13% RSD was observed for the regular drive case and an 8.4% RSD was observed for the one shot insertion mode (in both cases, %RSDs were calculated from the peak areas of 12 successive runs of 1 ng Cd solution residues).

The effect of a regular and a direct drive insertion mode on the background and the analyte signals was also investigated with a W wire-loop serving as the sample carrying probe. For the one shot insertion mode and for most elements tested, the atomic signals were not sufficiently resolved from the change in background indicating that, perhaps, dynamic background correction might be required for this type of DSID.

In summary, a faster insertion speed produces sharper peaks and lower %RSDs (especially for elements of high volatility), thus providing improved analytical performance. From the results presented in this section it can also be concluded that insertion speed is a parameter more critical that it was initially perceived to be and, therefore, it deserves special attention in any new DSID design. However, due to a well defined t=0 s, and unless otherwise stated, a regular drive insertion mode was used throughout this work.

C.4 Probe Attributes and Applied Forward Power

Because analyte vapor is generated by thermal volatilization, the factors affecting probe heating rate and final or equilibrium temperature must also affect analyte emission temporal behavior. A rapid heating rate of a smaller probe 'thermal time-constant' (i.e., smaller thermal mass, higher applied forward power), coupled with a probe of smaller dimensions (i.e., size and shape) is expected to result in higher sensitivities by producing a more localized and relatively higher transient analyte population in the plasma (i.e., larger analyte number densities per unit time) than a probe of larger thermal time-constant and dimensions.

However, there are limits to both probe size and applied forward power. In terms of applied forward power, 3.00 kW is the maximum power utilized with DSIDs [28, 31, 33, 34]. A maximum power of 2.00 kW was used in this work because such power levels can be easily supplied by most commercially available RF generators.

In terms of probe size, at one end there are cups, with cup size an important consideration due to capacity, sample homogeneity (of importance to powdered or solid samples) and analyte transport considerations. The effect of graphite cup size on %RSDs and detection limits has been previously reported [11]. At the other end the limiting case is the wire-loop, mainly advocated by Salin and coworkers [29, 17]. Due to its short thermal time-constant and its small dimensions, analyte emission temporal behavior observed with a wire-loop system has shorter peak appearance times, smaller peak widths and taller peak heights than conventional dc arc graphite electrodes [9, 17, 29]. A brief comparison of analyte emission temporal behavior utilizing long undercut graphite electrodes, Ta and W metal cups and W wire-loops has been presented elsewhere [9]. In this case, the main focus will be on graphite electrodes.

The effect of applied forward power on peak heights [11] and SBRs for a given probe type has been extensively documented [19-21, 23, 30], however, seemingly contradictory results have been reported. For example, Shao and

Horlick [11] using graphite cups and a sub-optimal readout electronics sub-system report that analyte emission temporal behavior was relatively insensitive to power changes for several elements. On the other hand, there seems to be a general agreement that optimum SBRs are obtained at low (i.e., less than 1.25 kW) power settings [19-21, 23, 30]. Meaningful comparisons and further generalizations, however, cannot be made because SBRs depend on applied forward power; analysis line; wavelength (plasma background increases with increasing wavelength); observation height (background intensity decreases with an increase in observation height); elemental volatility and chemical form of the element of interest; the physico-chemical properties of the matrix; reactions taking place in the cup; insertion sequence, speed and final insertion position in the plasma; plasma gas composition; probe type; and probe thermal time-constant. Undoubtedly, a combination of factors can be used in order to account for the reported results.

In addition, electrode geometry has also been found to exert a considerable influence on both appearance times and peak heights of Cr, Mn, Ni and Pb [22]. Depending on electrode geometry, equilibrium temperatures of up to 1800°C (attained after 2 to 8 s) have been measured [22]. Estimated probe temperatures of 1800°C [22, 35], of 3200°C [12], of 3600°C [30] and as high as 4000°C [32] have also been reported. Applied forward power, often defined as forward minus reflected [12, 13, 19-21, 32], has been found to affect the final or equilibrium probe temperature, for example, cup temperatures of 1600°C at 1.25 kW and of 1800°C at 2.00 kW have been measured [36].

In general, the effect of power on temporal behavior is two-fold (assuming no effect on analyte transport). First, that of ensuring quantitative volatilization, and second, that of the dependence of the spectral line on power input to the ICP. Based on conventional wisdom derived from the ICP, the dc arc and electrothermal atomization, it could be suggested that for low to medium volatility elements, an increase in power would affect both analyte volatilization and line intensity, for high volatility elements only the effect on the spectral line is important. From the practical point of view, an increase in temperature brought about by the use of special electrode geometries and higher powers is expected to yield significant enhancements in sensitivity, especially for difficult-to-volatilize elements. Clearly, the combined effect of electrode geometry and power on analyte emission temporal behavior characteristics (i.e., appearance time, peak height, peak area, SBRs) warrants further investigation.

C.4.1 Electrode Geometry and Power

Four electrode geometries, as shown in Figure 3-8, were chosen for this study. And as it has been documented in both the ICP [22] and the dc arc literature [24, 25], the length of the 'neck' of the electrode exerts a considerable influence on analyte peak shapes. Due to a reduction in mass (electrode mass was briefly described by Zarray et al. [31]), a long necked or 'long undercut' electrode (Figure 3-8), machined out of the corresponding HPND+ 4021 graphite electrode, is expected to attain a fast heating rate and a high equilibrium temperature. Others have also come to similar conclusions [22, 30].

The results obtained for 1 µg Sn and the long undercut electrode (Figure 3-8d) for power settings from 1.25 kW to 2.00 kW in 250 Watt increments, are shown in Figure 3-9. These show that an increase in power results in sharper peaks, taller peak heights and shorter appearance times. And although the magnitude of the influence an increase in power has on analyte emission temporal behavior varies considerably, similar trends have been observed for all other elements (i.e., Ag, Cd, Co, Cu, Fe, Ni and Zn) and electrode geometries tested (i.e., Figures 3-8a, 3-8b and 3-8c).

In an attempt to quantify the effect of power on the appearance time of the elements tested, the appearance time of each element is plotted against power for all electrode types (Figure 3-8), the results are shown in Figure 3-10.

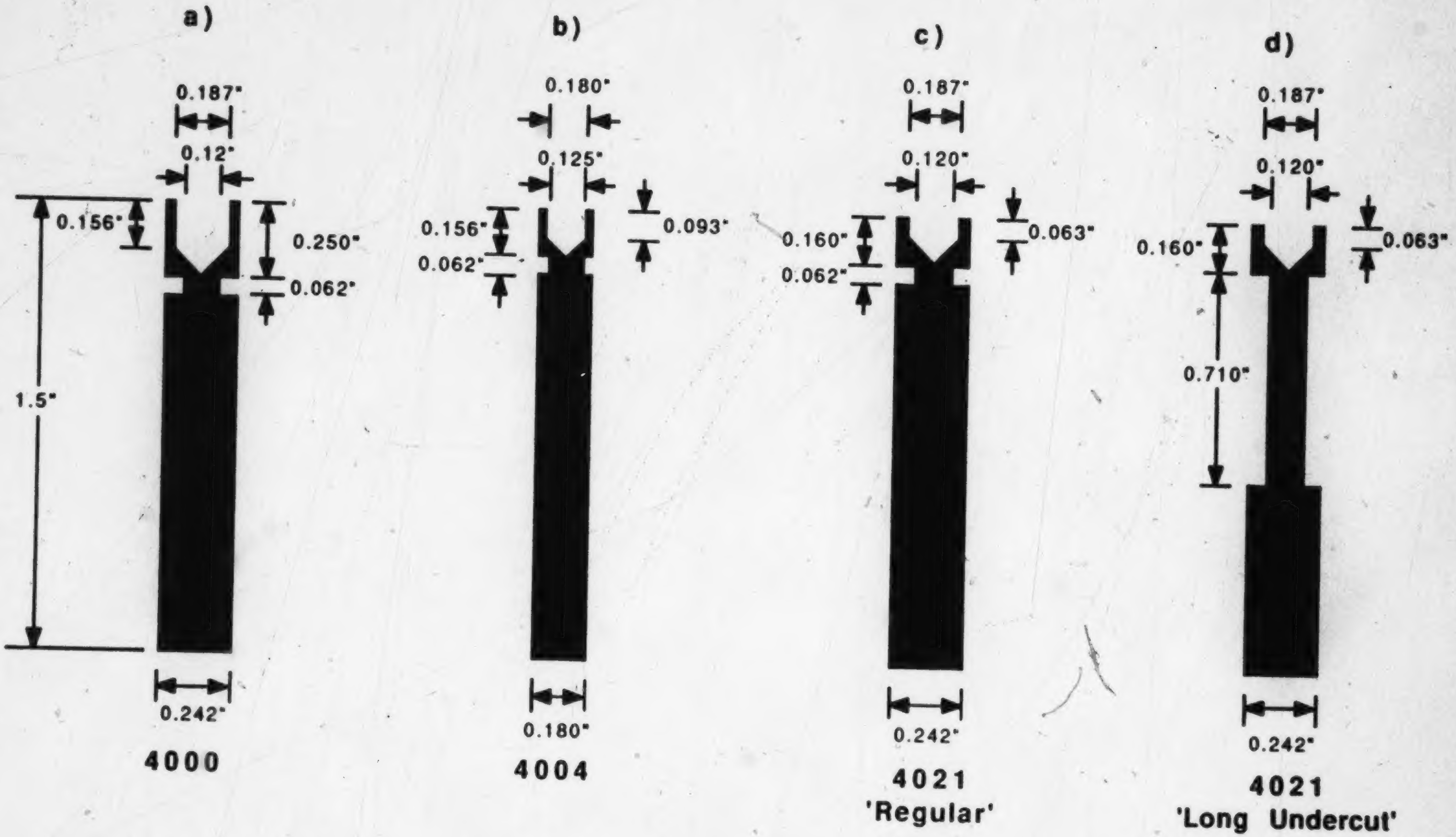
a)
0.187"
0.12"
0.156"
0.250"
0.062"
1.5"
0.242"
4000
b)
0.180"
0.125"
0.156"
0.062"
0.093"
0.180"
4004
c)
0.187"
0.120"
0.160"
0.062"
0.063"
0.242"
4021
'Regular'
d)
0.187"
0.120"
0.160"
0.063"
0.710"
0.242"
4021
'Long Undercut'

Figure 3-8. Graphite electrode geometries employed (dimensions in inches). (a) HPND+ 4000; (b) HPND+ 4004; (c) HPND+ 4021 'Regular' and (d) HPND+ 4021 'Long Undercut'

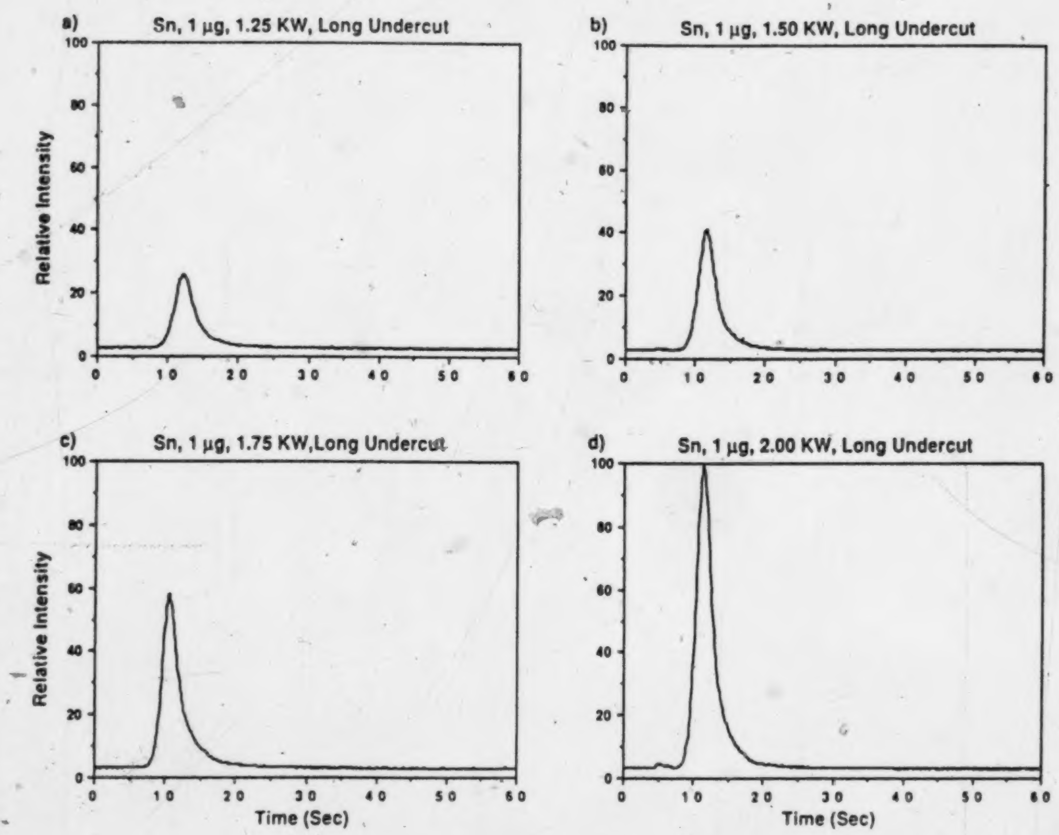

Figure 3-9. Analyte emission temporal behavior for 1 µg Sn, long undercut graphite electrodes, and power settings from 1.25 kW to 2.00 kW in increments of 250 Watts for: (a) 1.25 kW; (b) 1.50 kW; (c) 1.75 kW and (d) 2.00 kW (other operating conditions as in Table 3-2).

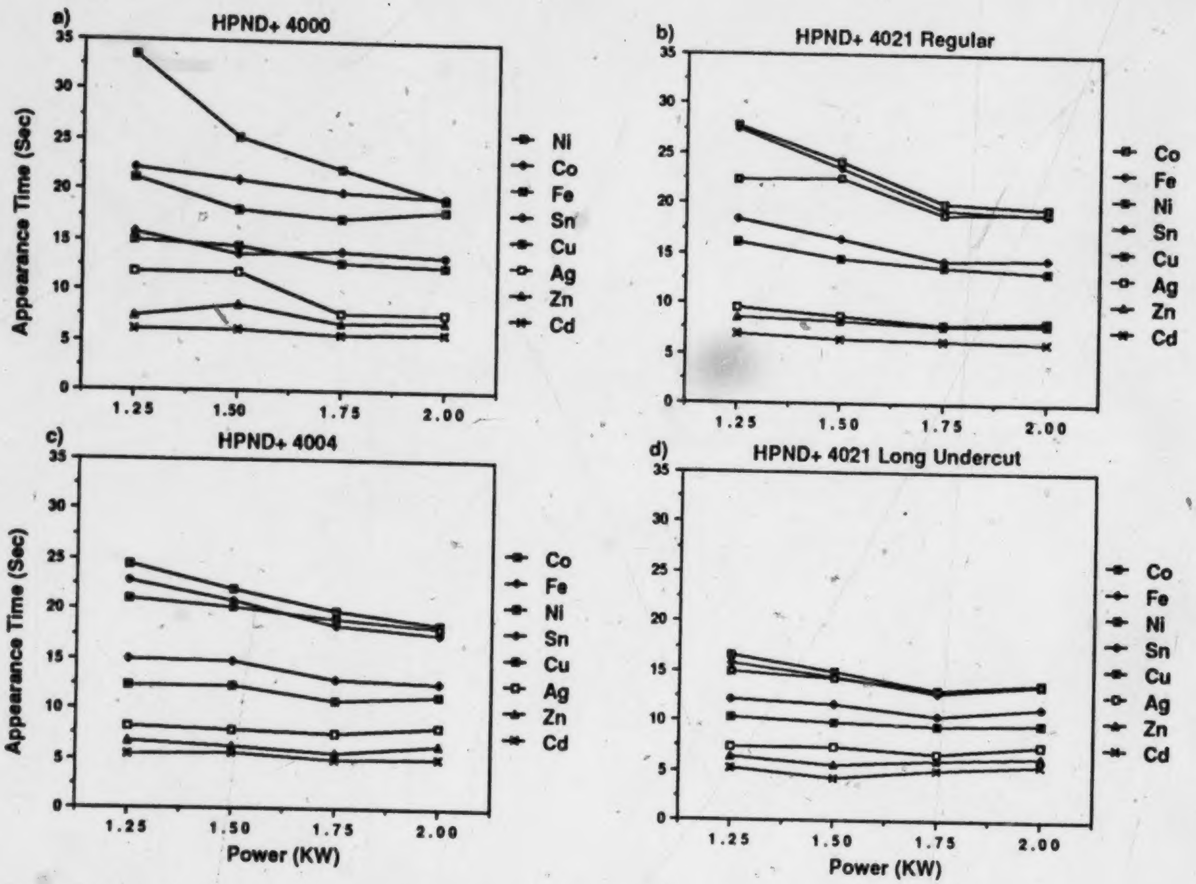

Figure 3-10. The effect of applied forward power (1.25 kW to 2.00 kW in increments of 250 Watts) on the appearance time of Ag, Cd, Co, Cu, Fe, Ni, Sn and Zn for: (a) HPND+ 4000; (b) HPND+ 4004; (c) HPND+ 4021 'Regular' and (d) HPND+ 4021 'Long Undercut' electrodes (other operating conditions as in Table 3-2).

From these data, it can be concluded that the elements tested can be grouped accordingly (much like oxides in dc arc [25]), as highly volatile (i.e., Cd, Zn and Ag), of medium volatility (i.e., Cu and Sn) and of low volatility (i.e., Ni, Fe and Co). And even though the elements group consistently for all electrode types, the volatility sequence assigned to Ni, Co and Fe for the HPND+ 4000 electrode (or simply the 4000 electrode, Figure 3-10a), is different from that observed for the other electrode types (Figures 3-10b, 3-10c and 3-10d), thus partly justifying the apparent volatility concept. In addition, the length of the appearance time is indirectly indicative of the heating rate. From the results shown in Figure 3-10 it can be inferred that the 4000 and the long undercut electrodes (Figure 3-8a and 3-8d respectively) have the longest and the shortest thermal time-constants, respectively. These observations are in general agreement with those reported by others for similar electrode types [22].

However, the key question of how the electrode types shown in Figure 3-8 inter-compare (in order to decide on an optimum electrode geometry) still remains unanswered. This question is briefly addressed below, the results are shown in Figures 3-11 to 3-16.

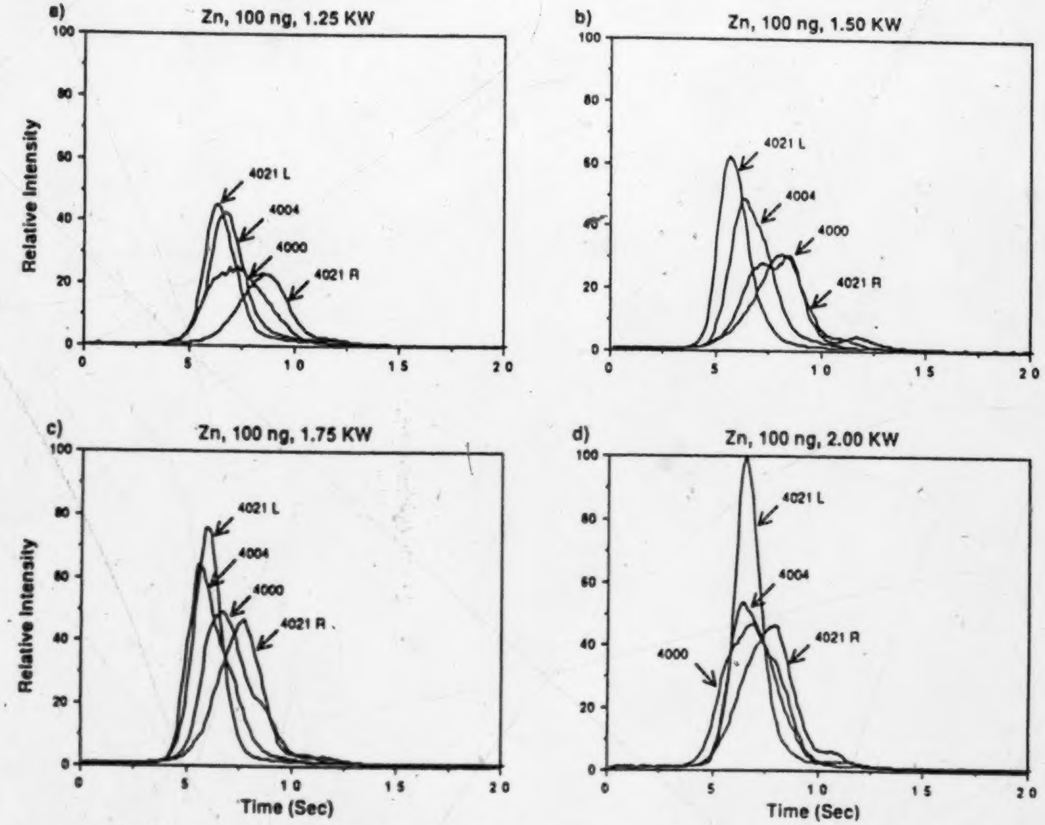

Figure 3-11. The effect of electrode geometry and power on analyte emission temporal behavior of 100 ng Zn for: (a) 1.25 kW; (b) 1.50 kW; (c) 1.75 kW and (d) 2.00 kW (other operating conditions as in Table 3-2). Electrodes: 4000 (HPND+ 4000, Fig. 8a); 4004 (HPND+ 4004, Fig. 3-8b); 4021 R (HPND+ 4021 'Regular', Fig. 3-8c); 4021 L (HPND+ 4021 'Long Undercut', Fig. 3-8d). Temporal behavior was scaled with respect to the peak intensity of the 4021 L electrode at 2.00 kW (d).

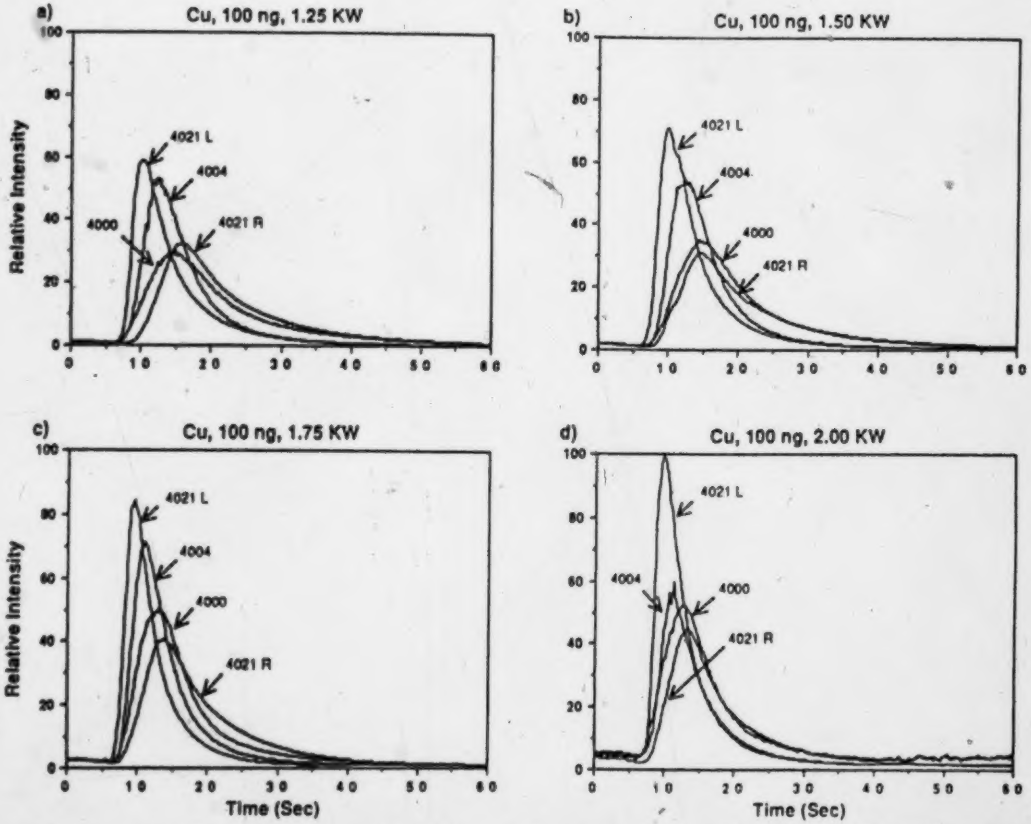

Figure 3-12. The effect of electrode geometry and power on analyte emission temporal behavior of 100 ng Cu for: (a) 1.25 kW; (b) 1.50 kW; (c) 1.75 kW and (d) 2.00 kW (other operating conditions as in Table 3-2). Electrodes: 4000 (HPND+ 4000, Fig. 3-8a); 4004 (HPND+ 4004, Fig. 3-8b); 4021 R (HPND+ 4021 'Regular', Fig. 3-8d); 4021 L (HPND+ 4021 'Long Undercut', Fig. 3-8d). Temporal behavior was scaled with respect to the peak intensity of the 4021 L electrode at 2.00 kW (d).

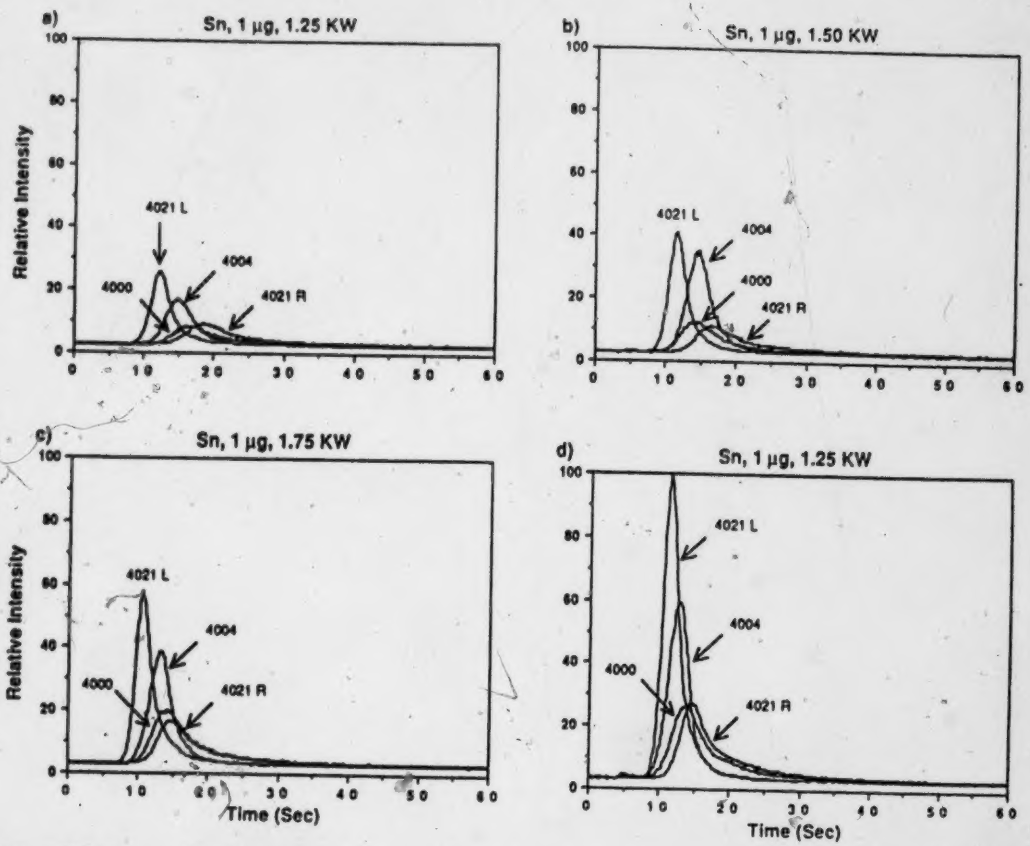

Figure 3-13. The effect of electrode geometry and power on analyte emission temporal behavior of 1 µg Sn for: (a) 1.25 kW; (b) 1.50 kW; (c) 1.75 kW and (d) 2.00 kW (other operating conditions as in Table 3-2). Electrodes: 4000 (HPND+ 4000, Fig. 8a); 4004 (HPND+ 4004, Fig. 3-8b); 4021 R (HPND+ 4021 'Regular', Fig. 3-8c); 4021 L (HPND+ 4021 'Long Undercut', Fig. 3-8d). Temporal behavior was scaled with respect to the peak intensity of the 4021 L electrode at 2.00 kW (d). 4021 L electrode at 2.00 kW (d).

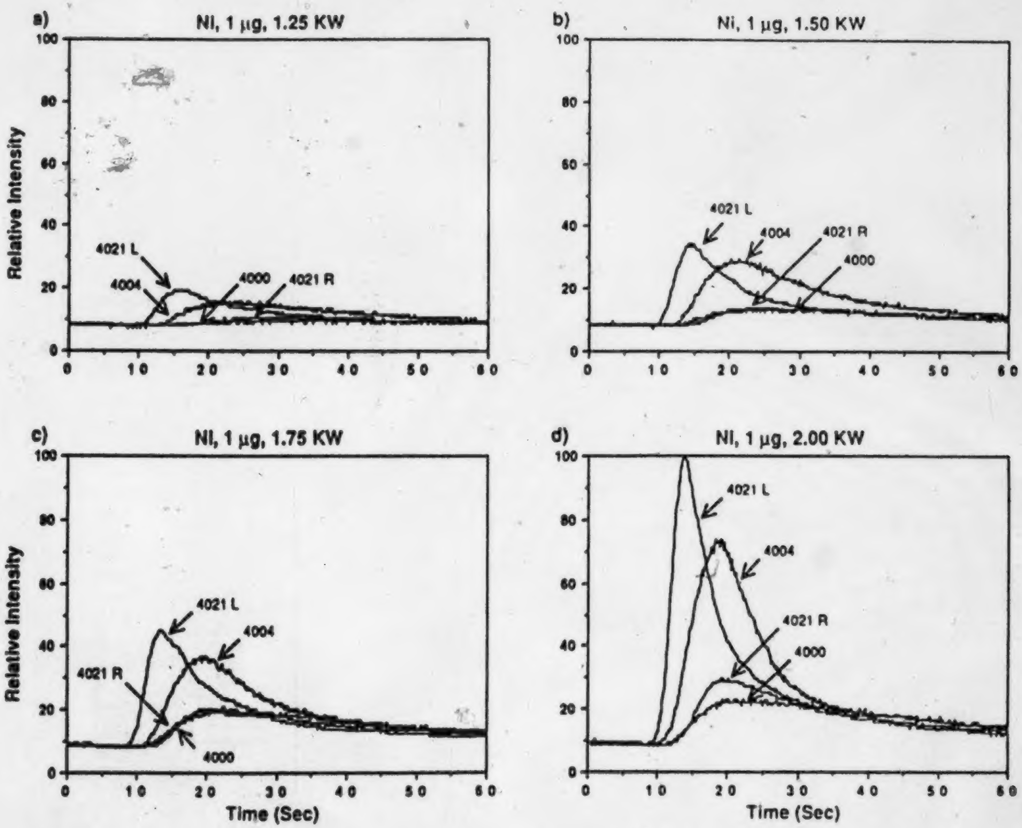

Figure 3-14. The effect of electrode geometry and power on analyte emission temporal behavior of 1 µg Ni for: (a) 1.25 kW; (b) 1.50 kW; (c) 1.75 kW and (d) 2.00 kW (other operating conditions as in Table 3-2). Electrodes: 4000 (HPND+ 4000, Fig. 8a); 4004 (HPND+ 4004, Fig. 8b); 4021 R (HPND+ 4021 'Regular', Fig. 3-8c); 4021 L (HPND+ 4021 'Long Undercut', Fig. 3-8d). Temporal behavior was scaled with respect to the peak intensity of the 4021 L electrode at 2.00 kW (d).

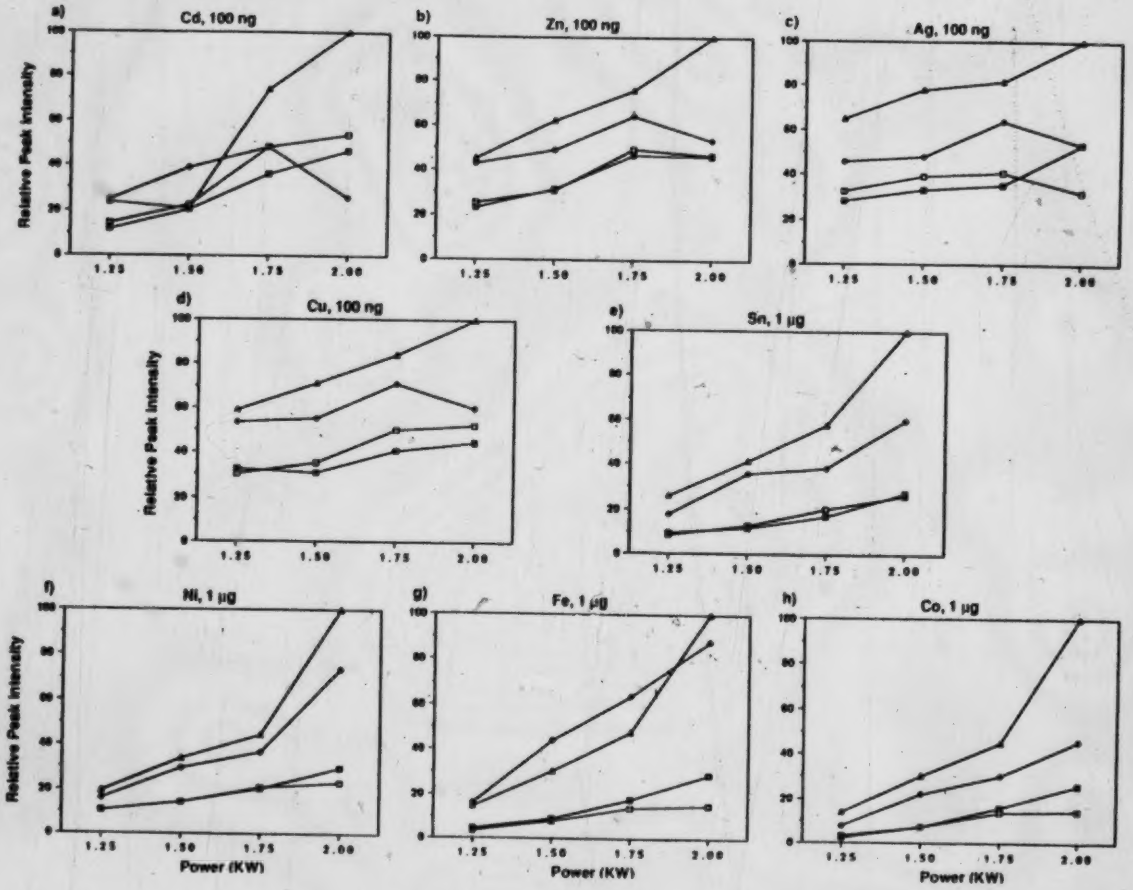

Figure 3-15. The effect of electrode geometry and power on the peak heights of: (a) 100 ng Cd; (b) 100 ng Zn; (c) 100 ng; (d) 1 µg Cu; (e) 1 µg Sn; (f) 1 µg Ni; (g) 1 µg Fe and (h) 1 µg Co.
-□- 4000, -◆- 4004, -■- 4021 Regular, -▲- 4021 Long Undercut

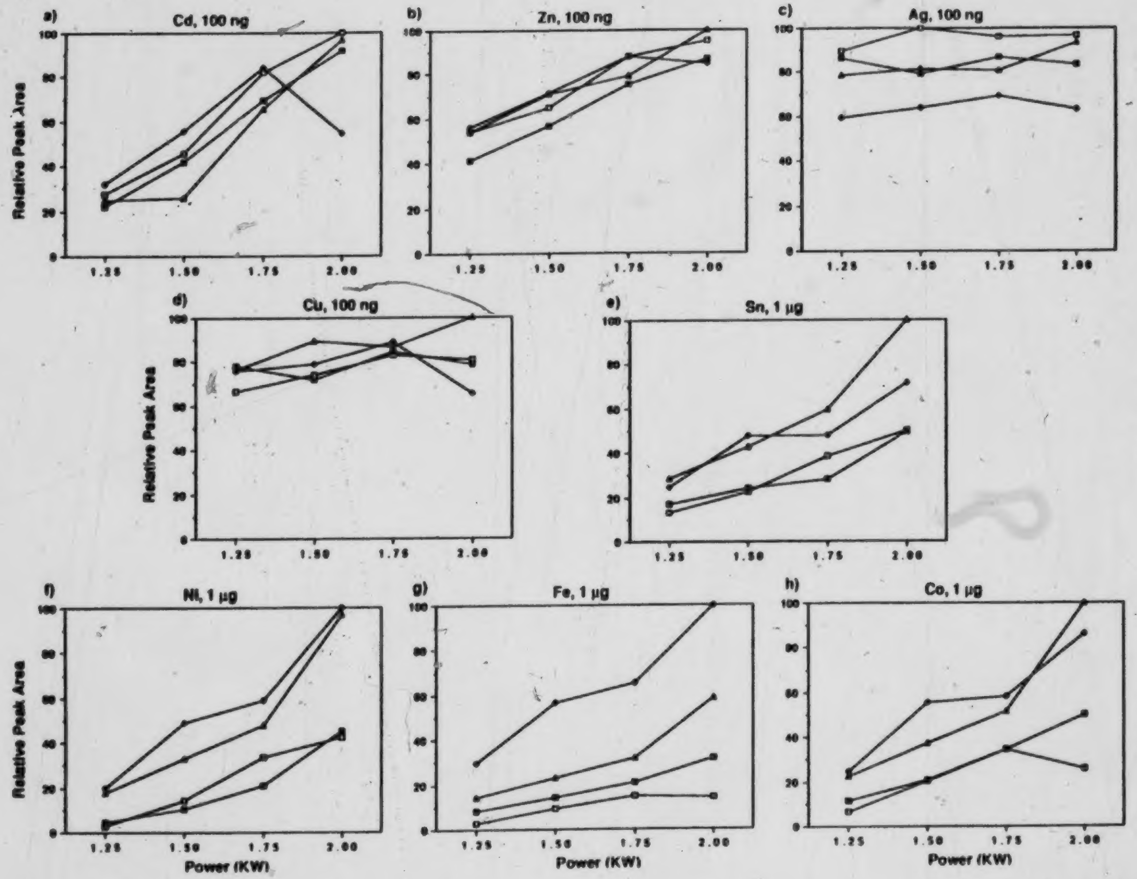

Figure 3-16. The effect of electrode geometry and power on the peak areas of: (a) 100 ng Cd; (b) 100 ng Zn; (c) 100 ng; (d) 1 µg Cu; (e) 1 µg Sn; (f) 1 µg Ni; [illegible]) 1 µg Fe and (h) 1 µg Co.
-□- 4000, -◆- 4004, -■- 4021 Regular, -▲- 4021 Long Undercut

Zinc was chosen as a typical representative of the volatile elements. The temporal behavior of 100 ng Zn for power settings ranging from 1.25 kW to 2.00 kW in increments of 250 Watts is shown in Figure 3-11. In order to increase the separation of the peak-like signals in time, a 20 s as opposed to a typical 60 s observation time was chosen for data display purposes (Figure 3-11]. Similar results have been observed for both Cd and Ag (100 ng each). The most important characteristic of these elements is an appearance time of less than 13 s for all electrode types and power settings utilized in these experiments, as shown in Figure 3-10. And although the appearance time for these elements was found to be power dependent, an insignificant dependence was observed here (Figure 3-11) and has been reported by others [23]. This suggests that even at low powers, electrode temperatures that are sufficiently high to ensure quantitative volatilization of these elements are being rapidly reached for all electrode types. The shortest appearance time, about 5 s, was observed for Cd and the long undercut electrode for the 2.00 kW power setting (Figure 3-10d). An increase in peak heights of less than 40% for Cd, Zn and Ag was observed for the 4000, 4004 and 4021 electrodes with an increase in power (i.e., 1.25 kW to 2.00 kW) as shown in Figures 3-15a, 3-15b and 3-15c. For the long undercut electrode, however, peak heights increase by about 80%, 60% and 40% for Cd, Zn and Ag respectively. With the exception of Ag (for all electrode types) and Cd (for the 4004 electrode), a continuous increase in peak areas is observed for both Cd and Zn, as shown in Figures 3-16a and 3-16b. For Ag, peak areas remain relatively constant for all electrode types and power settings (Figure 3-16c) indicating that a sufficient electrode temperature is reached for quantitative volatilization of Ag even at 1.25 kW and a relative insensitivity of the Ag I 328.07 nm line to power.

The effect of electrode geometry and power on the medium volatility elements is shown in Figure 3-12 for Cu (100 ng) and in Figure 3-13 for Sn (1 µg). With the exception of the long undercut electrode for Cu and the long undercut and 4004 electrodes for Sn, the peak heights of both Cu and Sn are relatively insensitive to power changes for a given electrode type. The appearance time of Cu and Sn is also power dependent (Figures 3-10, 3-12 and 3-13), however, unlike the results reported for Cu [11] and those observed for Ag, Cd and Zn with this system, a more substantial dependence was observed with an increase in power (Figure 3-10). The results of the effect of applied forward power and electrode type on peak heights for Cu and Sn are shown in Figure 3-15d and 3-15e. The difference in peak heights between the 2.00 kW and 1.25 kW power setting for the 4021 and 4000 electrodes is less than 20% for both Cu and Sn. For Sn and the 4004 electrode, an increase of about 45% was observed, whereas for Cu, peak heights increase up to 1.75 kW and they subsequently decrease. For the long undercut electrode, peak heights continuously increase for both Cu and Sn, by about 40% and 70% respectively. For Cu and with the exception of the long undercut electrode, peak areas, much like peak heights, increase up to 1.75 kW and they subsequently decrease, as shown in Figure 3-16d. A continuous increase in peak areas with an increase in power was observed for Sn (over 70% between the 2.00 kW and 1.25 kW power settings), as shown in Figure 3-16e.

Nickel was chosen as a typical representative of the low volatility elements tested (i.e., Co, Fe and Ni), the temporal behavior for 1 μg Ni is shown in Figure 3-14. Similar results were observed for Co and Fe. As shown in Figure 3-14a, the Ni signal at 1.25 kW and for the 4000 and 4021 electrodes is buried in noise. Thus, it can be concluded that Ni almost quantitatively remains in the cup. This results in a carryover of analyte from one determination to the next. In contrast, a considerable amount of Ni volatilizes from the long undercut electrode at 2.00 kW (Figure 3-14d), however, because the atomic signal does not reach the pre-insertion background level even after 60 s, incomplete volatilization was assumed and was verified in subsequent determinations. A substantial decrease in appearance time is observed with an increase in power (Figure

3-10), especially for the 4000 electrode (i.e., 14 s for Ni) indicating that in terms of analyte volatilization higher powers are more important for this electrode type and for these elements. The results of the effect of applied forward power and electrode geometry on the peak heights for Ni, Fe and Co are shown in Figures 3-15f, 3-15g and 3-15h respectively. An increase in power from 1.25 kW to 2.00 kW results in a less than 20% increase in the peak heights of Fe, Co and Ni for the 4000 and 4021 electrodes. A larger increase is observed for both the long undercut (i.e., over 80%) and the 4004 electrodes (i.e., over 50%) for Fe, Co and Ni indicating that higher electrode temperatures are obtained by these electrodes. Peak areas also continuously increase for all electrode types, as shown in Figures 3-16f, 3-16g and 3-16h for Ni, Fe and Co.

From the results presented in this section it can be concluded that, much like the dc arc [24, 25], electrode geometry exerts a significant influence on analyte emission temporal behavior and therefore it must be taken into account in any comparison of the analytical figures-of-merit of the DSID. For example, if peak heights are to be used as an indicator of the effect of power on analyte emission temporal behavior, little, no effect or even a reduction in peak heights may be reported depending on electrode geometry. In addition, it can be concluded that a change of electrode geometry is equivalent to an increase in power, for example, approximately equal peak heights have been observed for Sn and the long undercut electrode at 1.75 kW and the 4004 electrode at 2.00 kW, as shown in Figure 3-13.

The results of the effect of power on SBRs are shown in Figure 3-17. From these it can be concluded that optimum SBRs are also electrode dependent. For example, depending on electrode geometry, the optimum power setting for Zn (Figure 3-17b) is 1.50 kW, 1.75 kW and 2.00 kW for the 4004, 4000 and 4021 (both regular and long undercut) electrodes respectively. In general, and with the exception of Ag, optimum SBRs observed with this system are at higher plasma powers than those reported in the literature [19-21, 23, 30]. This can be attributed to the large internal diameter (i.e., 22 mm) of the torch utilized with this system [10] and the use of high plasma flow rates (Table 3-2). When the long undercut electrodes are used with a torch of smaller dimensions (i.e., 18 mm internal diameter), shorter appearance times are observed for the same element and power setting [17], thus corroborating the visual observation of a faster heating rate with a smaller torch.

In summary, it can be concluded that the long undercut electrode has the shortest thermal time-constant and it offers the best overall performance (i.e., peak heights, peak areas, SBRs) for all elements and electrodes tested. Furthermore, it can also be concluded that the combination of

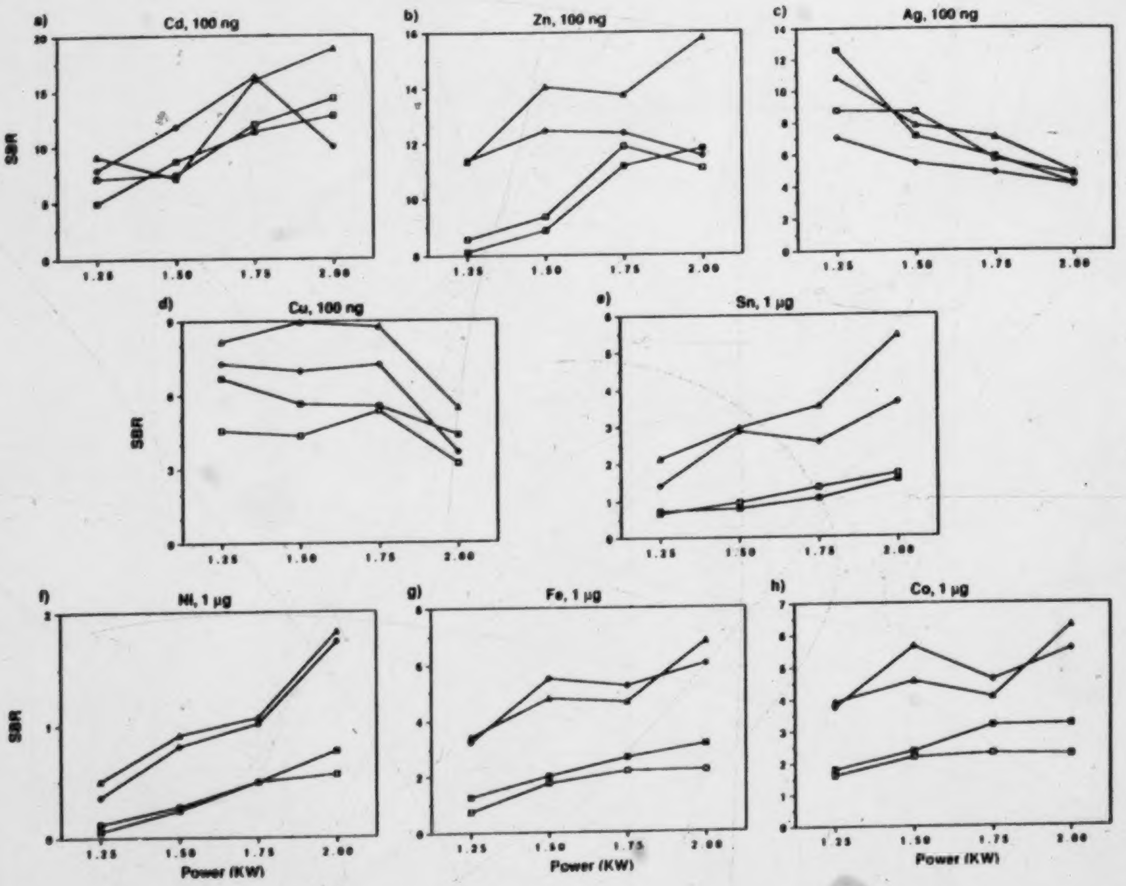

Figure 3-17. The effect of electrode geometry and power on the Signal-to-Background Ratio (SBR) for: (a) 100 ng Cd; (b) 100 ng Zn; (c) 100 ng; (d) 1 µg Cu; (e) 1 µg Sn; (f) 1 µg Ni; (g) 1 µg Fe and (h) 1 µg Co.
-□- 4000, -◆- 4004, -■- 4021 Regular, -▲- 4021 Long Undercut

high powers and special electrode geometries exerts a considerable influence on analyte emission temporal behavior and that it provides increased analytical performance for most medium to high volatility elements. It is worth noting, however, that in spite of the use of higher powers and special electrode geometries, low sensitivities are still observed for some elements (i.e., Co, Fe and Ni).

Several methods that can be easily implemented on the DSID can be proposed in order to reduce or eliminate the adverse effects of incomplete volatilization. For example, long undercut electrodes can be used in conjunction with even higher powered mixed-gas plasmas as a means to produce cup temperatures high enough to ensure quantitative volatilization. Although this approach is expected to yield significant enhancements in the sensitivity of some difficult-to-volatilize elements, poor sensitivities are expected for elements forming very high boiling point carbides (i.e., ZrC with a B.P. of 5100°C [37]). Elimination of graphite, and thus of the possibility of carbide formation, makes the use of metal cups an attractive alternative.

C.4.2 Electrode Composition

In this section, the sample carrying probe consists of a flat-top graphite electrode fitted with a metal cup (i.e., Ta or W), as shown in Figure 3-1. A high volatility (i.e., Cd), a medium volatility (i.e., Cu) and two low volatility elements (i.e., Cr and Ni) were chosen for investigation. Analyte emission temporal behavior was measured under identical operating conditions (at 1.25 kW) from multielement solution residues of Cd, Cr, Cu, and Ni (100 ng, 250 ng, 50 ng and 500 ng respectively) utilizing long undercut graphite electrodes (used as a reference) and Ta and W metal cups.

Analyte emission temporal behavior for Cd, Cu and Cr, Ni is shown respectively in Figures 3-18a and 3-18b for Ta cups; in Figures 3-18c and 3-18d for W cups; and in Figures 3-18e and 3-18f for the graphite cups. Considerable differences in temporal behavior (i.e., sharper peaks, shorter appearance times, taller peak heights) and enhancements in sensitivity were observed between the metal and the graphite cups for the low and medium volatility elements (i.e., Cd and Cu, Figures 3-18a, 3-18c and 3-18e). These findings are in general agreement with those previously reported for an Ar-H_2 mixed-gas plasma [10]. However, for the low volatility elements (i.e., Cr and Ni, Figures 3-18b, 3-18d and 3-18f) the observed sensitivities are neither as large as expected nor as significant as previously reported, again for Ar-H_2 mixed-gas plasma [10].

These observations can be explained by considering the model previously described. In this model, oxide and carbide formation was postulated but, due to the use of metal

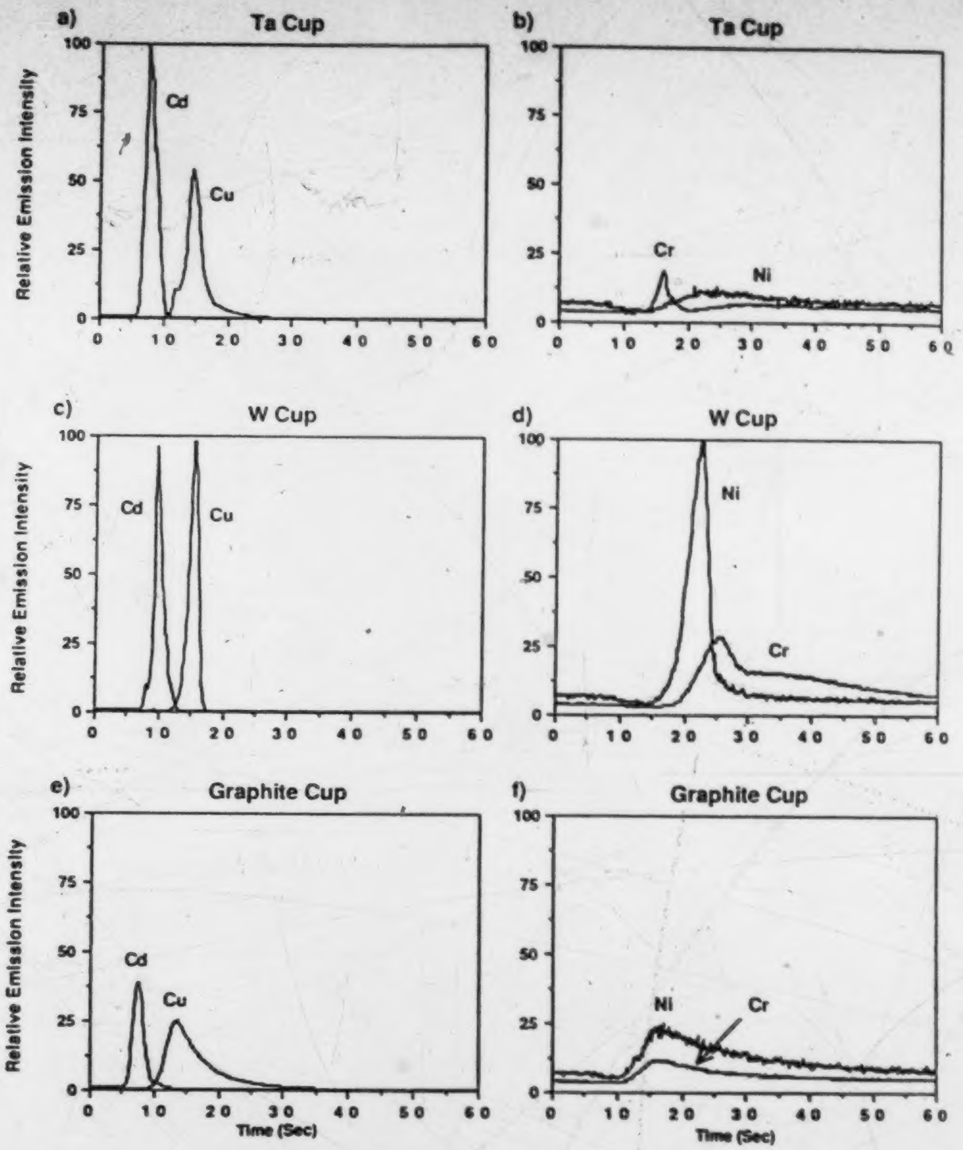

Figure 3-18. The effect of cup composition on the temporal behavior of Cu, Cd, Cr and Ni (50, 100, 250 and 500 ng respectively) at 1.25 kW (other operating conditions as in Table 3-2), for: (a) Cd and Cu using Ta cups; (b) Cr and Ni using Ta cups; (c) Cd and Cu using W cups; (d) Cr and Ni using W cups; (e) Cd and Cu using long undercut graphite electrodes; and (f) Cr and Ni using long undercut graphite electrodes (Fig. 3-8d). Temporal behavior for Cd and Cu was scaled with respect to the peak intensity of Cd for the Ta cup, that for Ni and Cr was scaled with respect to Ni and W cup.

cups, carbide formation cannot be considered as a factor. Therefore, the problem reduces to that of providing sufficient thermal energy to the sample carrying cup for oxide volatilization. However, some oxides have higher boiling points than the corresponding carbides, for example, the boiling points of Cr_3C_2 and of Cr_2O_3 are 3800°C and 4000°C respectively [37]. Therefore, the poor sensitivities shown for Cr and Ni for Ta and W cups (Figures 3-18a and 3-18b) can be attributed to oxide formation and to insufficient temperature for oxide volatilization, thus validating the original hypothesis. The increased sensitivities reported [10] for Ni and metal cups (i.e., Ta and W) with an Ar-H_2 mixed-gas plasma (H_2 was used in order to provide a reducing atmosphere and thus prevent metal cup oxidation upon sample holder retraction) cannot be explained unless the role of H_2 is also taken into account. By considering it, it could be suggested that a refractory oxide (i.e., Cr_2O_3 with a B.P. of 4000°C [37]) is reduced to the corresponding lower boiling point metal (i.e., Cr with a B.P. of ~1860°C [37]) which easily volatilizes from the cup. Similarly, it can be argued that the oxide may also be reduced to metal by the graphite. The evidence presented here for Cr and Ni (Figure 3-18f) does not support this mechanism, therefore, the original hypothesis of carbide formation must be valid for these elements.

In general, and in spite of the over-simplified and speculative nature of this model, it has been reasoned that both the chemical form and the physico-chemical properties of the element(s) of interest change due to thermochemical processes taking place in the electrode cavity. In addition, it can be suggested that probe temperature and composition, plasma atmosphere, the physico-chemical processes taking place in the electrode cavity and the nature of the residue define analyte emission characteristics. Why not then deliberately change that form to one of lower thermostability (i.e., by promoting reductions or via the addition of a chemical modifier either in the cup [11, 35, 37, 39] or in the plasma gases [32]) thus ensuring quantitative volatilization? Such an evaluation of the performance characteristics of the DSID with long undercut graphite electrodes and chemical modification is presented elsewhere [39].

C.5 Performance Characteristics

In order to establish the performance characteristics of this system, detection limits and relative standard deviations were measured and calibration curves were constructed from multielement solution residues and, unless otherwise stated, utilizing long undercut graphite electrodes, a regular drive insertion mode and an applied forward power of 1.25 kW.

The detection limits (twice the standard deviation of the background) shown in Table 3-3, were determined by running twelve consecutive water blanks and peak area integration [9]. With the exception of the results shown for Cr and Ni, detection limits are in the low- to sub-nanogram range. These results favourably compare (Table 3-3) with those reported by Shao and Horlick [11] but are poorer than those reported by Abdullah et al. [19]. With the exception of cup insertion position, no optimization of plasma or DSID operating conditions was performed prior to the determination of detection limits, the objective here was to get an indication of the analytical performance characteristics of the device rather than to obtain the best possible detection limits. When the effect of DSID design attributes is taken into account and special electrode geometries and higher powers are utilized, improved analytical performance is realized, for example, when temporal emission behavior arising from 100 pg of Cd and Mn is observed (about the detection limit reported in Table 3-3 for these elements with this system) at 2.00 kW, with maximum electronic and PMT gains, long undercut graphite electrode and a direct drive insertion mode, the results shown in Figure 3-19 are obtained. These better demonstrate the potential detection capability of this system. Further improvements in the analytical figures-of-merit of the device are anticipated by optimizing the experimental parameters shown in Table 3-1.

Table 3-3. Comparison of detection of limits and %RSDs.

Element/	**λ**	**Detection Limit (ng)**			**%RSD**		
Line	**(nm)**	**[1]**	**[2]**	**[3]**	**[1]**	**[2]**	**[3]**
Ag I	328.07	1.8	0.17	*.**	5.5	3.6	*.*
Cd I	228.80	0.5	0.03	0.013	4.5	2.9	3.5
Cr II	205.50	8.7	3.1^a	0.071	16.6	3.6	2.7
Cu I	324.75	0.1	33.6^a	0.14	4.9	7.2	5.6
Mg II	279.08	3.6	3.5^a	0.15	9.5	2.7	3.0
Mn II	257.61	0.1	0.1	0.043	8.1	1.9	3.0
Ni II	231.60	41.6	*.*	0.18	19.8	*.*	2.2
Zn I	213.86	0.4	0.2	0.12	18.1^a	3.1	5.0

a : Due to contamination
. : Not determined

[1]: This work
[2]: From reference 11 (4.5-mm graphite electrode)
[3]: From refernece 19

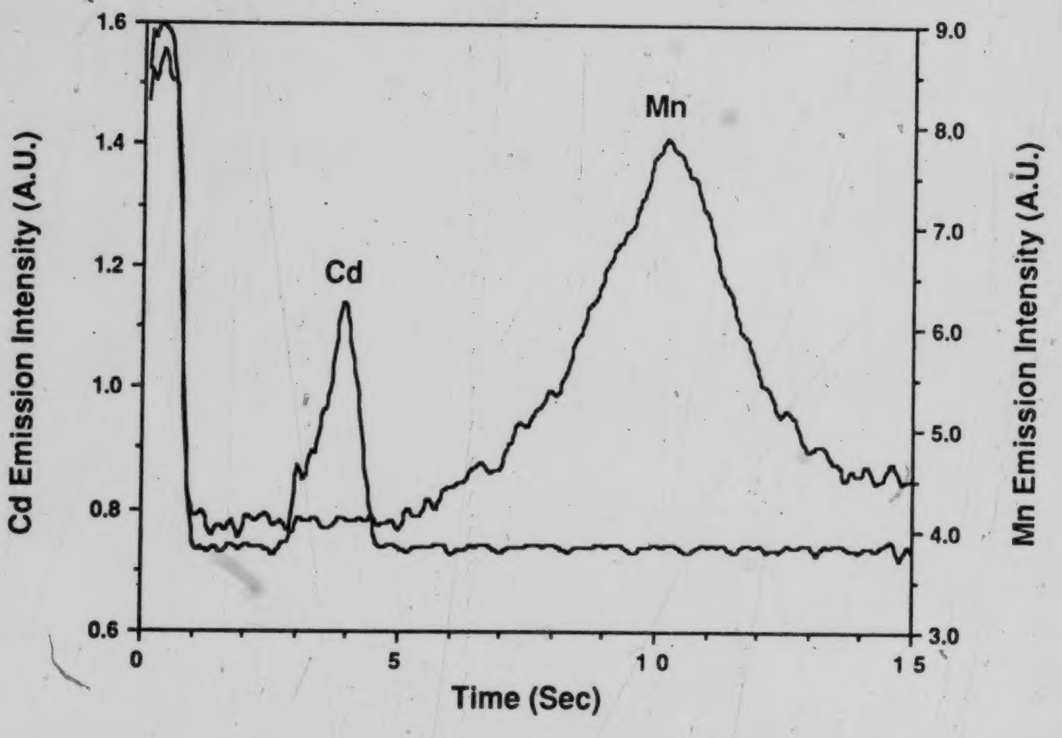

Figure 3-19. Analyte emission temporal behavior for Cd and Mn (100 pg each) at 2.00 kW, a long undercut graphite electrode and a one-shot insertion mode (other operating conditions as in Table 3-2).

However, new considerations arise as reproducibilities worsen when determinations are performed at low concentration levels. This can be attributed to analyte diffusion into the pores of the cup, the effect being more pronounced at low concentrations. This occurs because for small analyte masses a relatively larger fraction of analyte mass penetrates the pores of the graphite cup than when larger analyte masses are used. Due to an increase in cup porosity with use, new cups typically give sharper signals, improved reproducibilities (as also reported by others [21]) and offer relative freedom from memory effects. The use of pyrolytically coated cups, much like pyrolytically coated tubes in ETV spectrometry, may solve this problem.

Relative standard deviations, determined from twelve replicate runs and peak area integration are also shown in Table 3-3. The poor signal precision measured for Cr and Ni is attributed to incomplete volatilization, whereas that measured for Zn is most likely due to residual impurities in the cup. In general, %RSDs are worse than those reported by others [19], as shown in Table 3-3. This is partly due to mechanical imperfections of the insertion mechanism [10], reproducibilities are expected to improve by re-designing this mechanism.

Linear calibration curves, covering a concentration range of two to three orders of magnitude, were established from multielement solution residues for most volatile elements, typical examples for Ag, Cd, Cu and Mg are shown in Figure 3-20. Low volatility elements (i.e., Fe, Co, Cr and Ni) had non-linear calibration curves (i.e., non-unity slope of the log-log plot) due to incomplete analyte volatilization. Similar results have been reported by others [11]. The non-linearity observed in the calibration curve for Zn is attributed to residual impurities in the cup.

In general, from the results presented in this section it can be concluded that the analytical figures-of-merit of the DSID can be considerably improved by judicious choice of the experimental parameters affecting analyte emission temporal behavior and by taking into consideration the design attributes of the device.

D. Conclusions

The results presented in this study and elsewhere [9] show that the combination of a polychromator and of DSID-specific hardware and software provides the necessary means to assess background and analyte emission temporal behavior in the time domain, and offers the potential for multielement analysis from multielement solution residues. Due to the increased capability offered by this system, elucidating an atom formation mechanism also becomes possible.

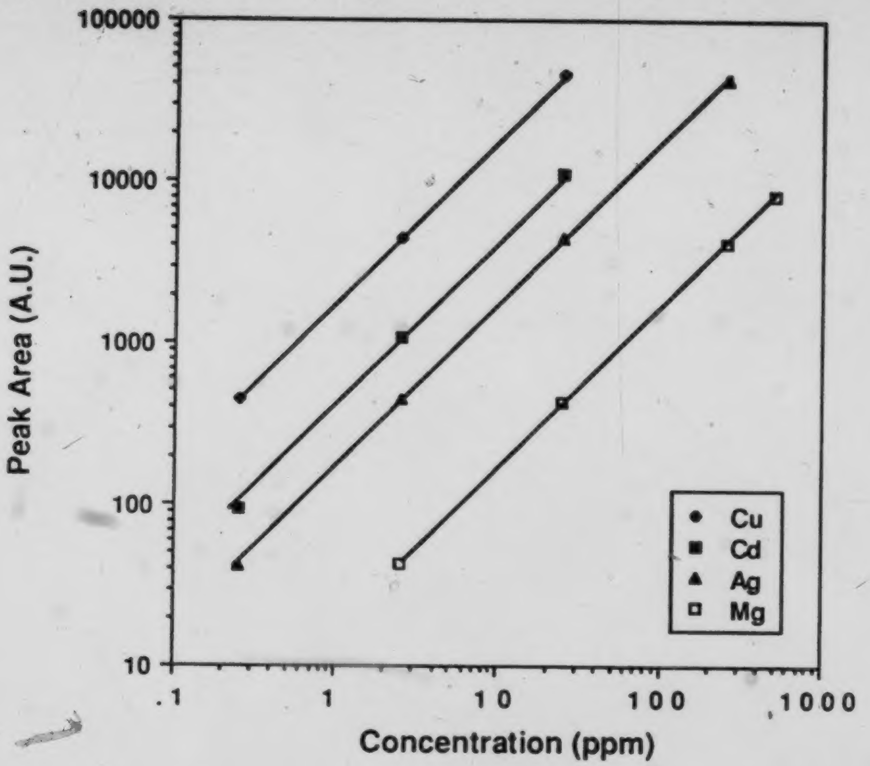

Figure 3-20. Calibration curves for Ag, Cd, Cu Mg (with slopes of the log-log plots of 1.04, 1.04, 1.00 and 0.996) constructed from multielement solution residues using long undercut graphite electrodes and a regular drive insertion mode (other operating conditions as in Table 3-2).

From the practical point of view, a host of issues must be addressed before the DSID can attain its full potential. For example, graphite cups even after pre-treatment contain significant amounts of impurities, thus adversely affecting detection limits and precision. Electrode geometry and composition have also been found to significantly affect the analytical figures-of-merit of the device. Therefore, metal cups and graphite electrodes with reproducible attributes (i.e., geometry, surface porosity) and low impurity levels are necessary for use with the ICP, especially for determinations at low concentration levels. The results presented here also demonstrate that quantitative volatilization of difficult-to-volatilize elements cannot be realized by simply increasing applied forward power or altering probe geometry and/or composition (a good carbide former is, in general, also a good oxide former), a solution involving *chemical processing* of the sample [39] may be required.

In addition, a number of DSID design attributes (i.e., insertion speed, reproducibility of insertion position and probe geometry and composition) have been isolated and have been found to exert considerable influence on analyte emission temporal behavior. Based on these findings, it can also be concluded that further improvements in the analytical figures-of-merit of the device would be realized by redesigning the DSID.

A diagram of a proposed 'next generation DSID' for ICP-AES is shown in Figure 3-21. Concept-wise, this is a computer-controlled, stepper-motor and lead-screw driven and vertically operated DSID. In order to achieve unattended operation and to facilitate automation of sample presentation, the use of a random access autosampler carousel is suggested. The robot arm, which is part of sample preparation station, also assists in the chemical processing of the samples via the addition of chemical modifiers into or onto the sample carrying probe. Thus, the overall goal of developing an intelligent sample processor for the ICP can be realized. It is worth noting that the findings presented here and elsewhere [9, 16, 39] have been used as the basis for the design of a horizontally operated, lead screw/stepper-motor driven and computer controlled DSID for an ICP-MS system [17].

Finally, with this system optimization of all the variables listed in Table 3-1 can be performed and the potential for direct analysis (i.e., no sample pre-treatment) of solid/powdered samples can be evaluated. There is clearly more to be done and these goals are being pursued in our laboratory.

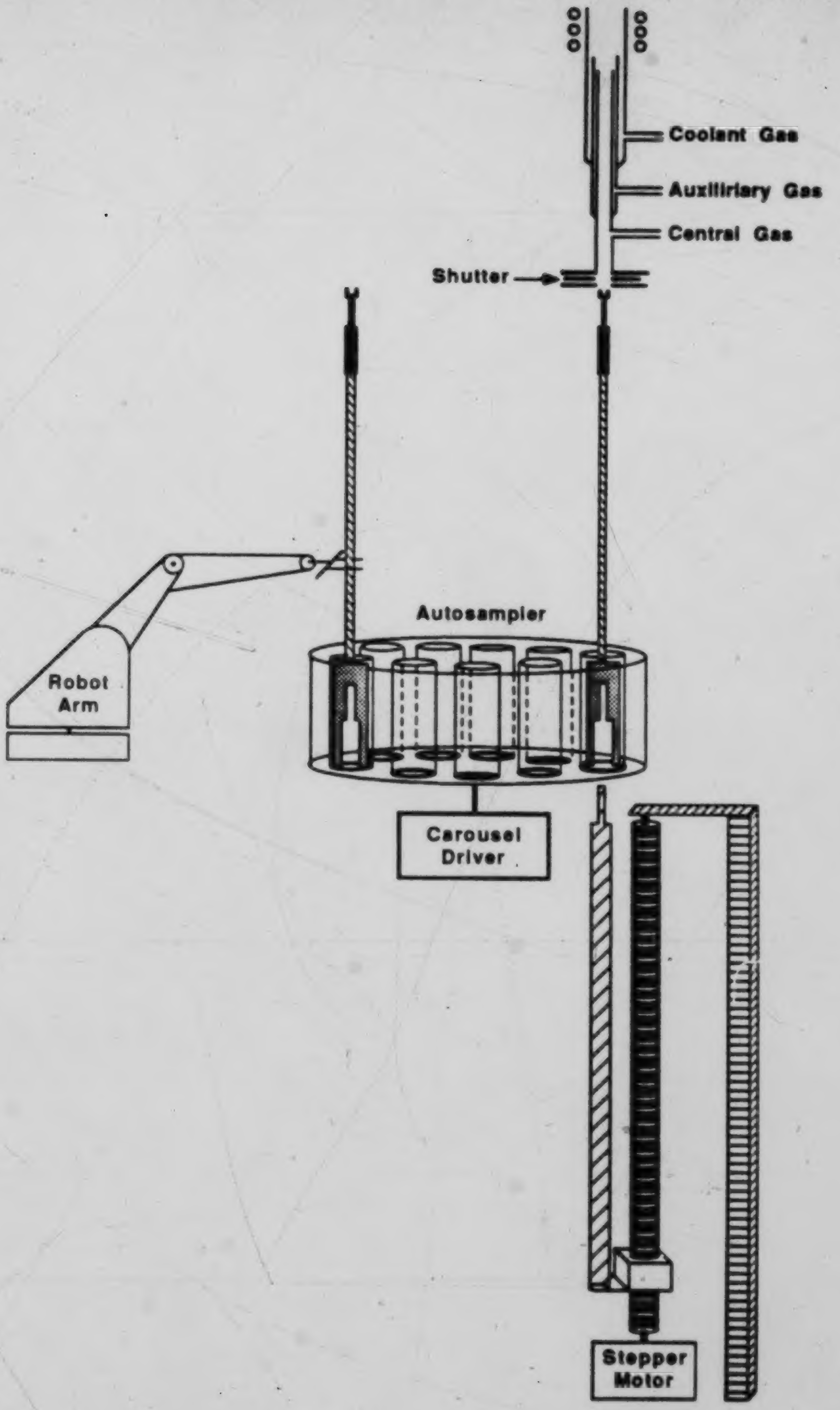
Coolant Gas
Auxilliriary Gas
Central Gas
Shutter
Autosampler
Robot Arm
Carousel Driver
Stepper Motor

Figure 3-21. Illustration of the proposed 'next generation' DSID.

REFERENCES

1. R.F. Browner and A.W. Born, Anal. Chem., **56**, 786A (1984)

2. R.F. Browner and A.W. Born, Anal. Chem., **56**, 875A (1984)

3. A.G.T. Gustavsson, *"Liquid Sample Introduction into Plasmas"*, in *'Inductively Coupled Plasmas in Analytical Atomic Spectrometry'*, A. Montaser and D.W. Golightly, Eds., VCH Publishers, Inc., N.Y., 1987, pp. 399-424

4. J.A.C. Broekaert and P.W.J.M. Boumans, *"Sample Introduction Techniques in ICP-AES"*, in *'Inductively Coupled Plasma Emission Spectrometry'*, Part I, P.W.J.M. Boumans, Ed., John Willey & Sons, N.Y., 1987, pp. 296-357

5. J.C. Van Loon, Anal. Chem., **52**, 955A (1980)

6. M.W. Routh and M.W. Tikkanen, *"Introduction of Solids into Plasmas"*, in *'Inductively Coupled Plasmas in Analytical Atomic Spectrometry'*, A. Montaser and D.W. Golightly, Eds., VCH Publishers, Inc., N.Y., 1987, pp. 431-486

7. J.C. Van Loon, H. Haraguchi and K. Fuwa, *"Direct Elemental Analysis of Solids by Inductively Coupled Plasma Emission Spectrometry"*, in *'Inductively Coupled Plasma Emission Spectrometry'*, Part II, P.W.J.M. Boumans, Ed., John Willey & Sons, N.Y., 1987, pp. 217-243

8. H. Matusiewicz, J. Anal. At. Spectrom., 1, 171 (1986)

9. V. Karanassios and G. Horlick, *'Development of a computer controlled DSID for ICP-AES'*, Spectrochim. Acta, (submitted)

10. W.E. Pettit and G. Horlick, Spectrochim. Acta, **41B**, 699

11. Y. Shao and G. Horlick, Appl. Spectrosc., **40**, 386 (1986)

12. M. Abdullah and H. Haraguchi, Anal. Chem., **57**, 2059 (1985)

13. M. Abdullah, K. Fuwa and H. Haraguchi, Appl. Spectrosc., **41**, 715 (1987)

14. Z. Li-Xing, G.F. Kirkbright, M.J. Cope and J.M. Watson, Appl. Spectrosc., **37**, 250 (1983)

15. L. Blain and E.D. Salin, paper 108, ACS book of abstracts, Third chemical congress of North America, Toronto, Canada, June, 1988

16. V. Karanassios and G. Horlick, Appl. Spectrosc., **41**, 360 (1987)

17. V.Karanassios and G. Horlick, *'Development of a computer controlled DSID for ICP-MS'*, (in preparation)

18. D.W. Boomer, M. Powell, R.L.A. Sing and E.D. Salin, Anal. Chem., **58**, 975 (1986)

19. M. Abdullah, K. Fuwa and H. Haraguchi, Spectrochim. Acta, **39B**, 1129 (1984)

20. H. Haraguchi, M. Abdullah, T. Hasegawa, M. Kurosawa and K. Fuwa, Bull. Chem. Soc. Jap., **57**, 1839 (1984)

21. G.F. Kirkbright and S.J. Walton, Analyst, **107**, 276 (1982)

22. N.W. Barnett, M.J. Cope, G.F. Kirkbright and A.A.H. Taobi, Spectrochim. Acta, **39B**, 343 (1984)

23. C.W. McLeod, P.A. Clarke and D.J. Mowthorpe, Spectrochim. Acta, **41B**, 63 (1986)

24. P.W.J.M. Boumans, '*Theory of Spectrochemical Excitation*', Hilger and Watts, London, 1966/Plennum Press, NY, 1966

25. L.H. Ahrens and S.R. Taylor, "*Spectrochemical Analysis*", Addison-Wesley, Reading, MA, 1961

26. E.K. Storms, '*The Refractory Carbides*', Academic Press, 1967

27. E.D. Salin and M.M. Habib, Anal. Chem., **56**, 1186 (1984)

28. G. Zaray, J.A.C. Broekaert and F. Leis, Spectrochim. Acta, **43B**, 241 (1988)

29. E.D. Salin and R.L.A. Sing, Anal. Chem., **56**, 2596 (1984)

30. M. Umemoto and M. Kubota, Spectrochim. Acta, **42B**, 491 (1987)

31. G. Zaray, P. Burba, J.A.C. Broekaert and F. Leis, Spectrochim. Acta, **43B**, 255 (1988)

32. G.F. Kirkbright and Z. Li-Xing, Analyst, **107**, 617 (1982)

33. D. Sommer and K. Ohls, Frez. Z. Anal. Chem., **304**, 97 (1980)

34. K. Ohls, Spectrochim. Acta, **39B**, 1105 (1984)

35. A.G. Page, S.V. Godbole, K.H. Madraswala, M.J. Kulkarni, V.S. Mallapurkar and B.D. Joshi, Spectrochim. Acta, **39B**, 551 (1984)

36. A. Lorber and Z. Goldbart, Analyst, **110**, 155 (1983)

37. CRC Handbook, 57th Edition, CRC Press, Inc., Boca Raton, Florida, 1979

38. A.G. Page, K.H. Madraswala, S.V. Godbole, M.J. Kulkarni, V.S. Mallapurkar and B.D. Joshi, Frezenius Z. Anal. Chem., **315**, 38 (1983)

39. V. Karanassios, M. Abdullah and G. Horlick, *'The application of chemical modification to a direct sample insertion device for ICP-AES'*, Spectrochim. Acta, (submitted)

CHAPTER 4

THE APPLICATION OF CHEMICAL MODIFICATION TO A DIRECT SAMPLE INSERTION DEVICE FOR ICP-AES

A. Introduction

The ability to handle small solution volumes (important for samples of biological, biochemical, environmental or forensic origin), the possibility of introducing powdered or solid samples with little or no sample pre-treatment (thus reducing or eliminating the time consuming sample preparation step) and an overall increase in sample introduction efficiency, are the basic goals in the development of direct sample insertion devices (DSIDs) for the inductively coupled plasma (ICP). In the type of DISD considered here and described elsewhere [1], the sample is placed into a modified dc arc graphite electrode or 'cup' [2] which is subsequently introduced into the plasma. By positioning the sample carrying cup at positions successively closer to the plasma, *in-situ* sample pre-treatment (i.e., drying and ashing) can be achieved prior to atomization. Taking this concept further, addition of reagents directly into the sample carrying cup offers the added advantage of *in-situ* chemical processing of the sample. Thus, the concept of the sample carrying cup as a 'crucible' in which *in situ* chemical processing (i.e., analyte or matrix chemical modification, fusion) takes place begins to emerge.

In previous investigations [2-6], the analytical performance of a DSID for ICP-AES has been reported, with results presented mostly for high to medium volatility elements from solution residues. However, poor sensitivities were observed for some difficult-to-volatilize elements when graphite cups were used [2, 4, 7]. The poor results were attributed to refractory carbide formation which results in incomplete volatilization, thus affecting sensitivity, detection limits and precision. Carbide formation also results in carryover of analyte from one determination to the next, thus causing memory effects. Therefore, despite the advantages offered by the graphite cup-based DSID, because a broad range of elements form refractory carbides, the analytical figures-of-merit of the device are impaired. Clearly, difficult-to-volatilize elements present a major challenge for the DSID. Therefore, the effect of refractory carbide formation on the analytical performance characteristics of the DSID deserves special attention.

Several methods can be used in order to solve the problem of refractory carbide formation. For example, the use of high powered plasmas in conjunction with mixed-gases and special electrode geometries [2]; utilization of metal cups [2, 3]; chemical modification via the addition of either halocarbons in the plasma gases [7] or matrix modifiers in the cup [4, 8, 9, 10]; or to borrow approaches from ETV and use pyrolytically coated [11-13], carbide coated (14 and references therein) or metal lined [15-17] cups rather than tubes can be proposed. Of these, volatilization enhancement via the addition of chemical modifiers (i.e., halides, fluorides) in the sample carrying cup was chosen for this study.

This approach was taken because of its simplicity and in order to demonstrate the concept of *in situ* chemical processing in the sample carrying cup. In this approach, the preferential formation of the corresponding high volatility halide is forced to occur by the addition of an excess of a halide containing reagent (i.e., NaF). The main function of the modifier is to alter the thermochemical properties of the sample. In general, chemical modification can be considered as a sub-set of a more general concept, namely that of chemical processing of a sample. Chemical modification may be defined as the addition of an agent (i.e., the modifier) to the sample or to the plasma in order to convert the analyte to a phase of higher thermostability or to increase the volatility of the concomitants or the analyte or to suppress matrix volatilization.

The concept of chemical modification is not new, it has been used for a number of years in both ETV techniques and in dc arc spectrometry; the approaches are easily transferable to DSIDs. For example, Page et al. [9] have suitably modified and adapted the classical dc arc carrier distillation method to the DSID. Using 5% AgCl as a matrix modifier, they have determined Cd, Cu, K, Na, Ni and Pb in powdered U_3O_8 samples. The same authors have subsequently extended and refined their method for the determination of B, Be, Cd, Co, Cr, Cu, Fe, K, Li, Mn, Na, Ni and Pb in powdered U_3O_8 samples [10]. Elalfy et al. [18], have used NH_4Cl as a volatilization enhancing agent for the determination of Fe in U_3O_8 matrix and Nickel et al. [19] have used ^{59}Fe as a radiotracer in order to study Fe retention in powdered graphite samples. The same authors [19] have also investigated Fe volatilization from an Al_2O_3-SiO_2 matrix with AgCl, NH_4Cl, BaF_2 and $CdCl_2$ as matrix modifiers. Kirkbright and Li-Xing [7] have used Freon in order to enhance analyte volatilization of carbide forming elements. Substantial improvements and sub-nanogram detection limits were reported for carbide forming elements such as B, Cr, Mo, Ti, U and Zr. Zaray et al. [8] have used NH_4Cl, AgCl, BaF_2 and PTFE as volatilization enhancing agents and have found that although no emission signal was observed for Ti in the absence of a modifier, considerable signal intensities were measured in the presence of both AgCl and PTFE. A series of halogenation reactions was proposed in order to explain the observed enhancements. Powdered PTFE was subsequently used in the determination of Cd, Mg, Cu, Zn and Ti from Al_2O_3. Finally, in a preliminary investigation, Shao and Horlick [4], utilizing NaF as a volatilization enhancing agent, have reported considerable enhancements in sensitivity for some carbide forming elements (i.e., over two orders of magnitude for Sr). From the results reported in the literature, it can be concluded that chemical modification *"is a clear indication for the future"* [4].

The aim of this study is to investigate the possibility of volatilization enhancement of difficult-to-volatilize elements from multielement solution residues via the addition of chemical modifiers in the sample carrying cup, to extend the method for the determination of carbide forming elements (i.e., B) in powdered samples and to demonstrate the concept of *in situ* sample processing.

B. Experimental

A 27.12 MHz Ar ICP (Plasma Therm ICP 5000 consisting of a 27.12 MHz generator (model HFS-5000D), a matching network (model AMN-5000E) and a torch box (model PT-1)) was fitted with a computer controlled, vertically operated, pneumatically and mechanically driven DSID capable of handling up to 24 sample carrying probes in an automated fashion and it was coupled to a 1-m, 29-channel polychromator. Typical running conditions were: forward power, 1.25 kW; reflected power, less than 80 W; coolant gas (Ar), 18 l/min; auxiliary (Ar), 0.6 l/min; and snuffer gas (Ar), 1 l/min. The observation height was set at 16 mm above the load coil. All measurements were taken with the top of the sample carrying cup in alignment with the top of the load coil, data acquisition (t=0 s) was initiated when the cup was in alignment with the central tube of the torch. A 'regular drive' insertion mode was used throughout [2]. DSID and data acquisition and control hardware and software utilized in this work has been described in detail elsewhere [1, 2]. The analytical wavelengths were: Ag I 328.07, Al I 237.34, B I 249.68, Ca II 317.93, Cd I 228.80, Co II 228.61, Fe II 259.94, Sr II 407.78, Ti II 337.28, Zn I 213.86 and Zr II 343.82 nm.

Although several probe types (i.e., graphite cups, metal cups and wire-loops) can be utilized with this system [1], long undercut graphite electrodes [2] (SPEX Industries, Inc., Edison, NJ or Bay Carbon, Inc., Bay City, MI) were exclusively utilized in this work. In order to reduce the impurities contained in them, the electrodes were treated according to the procedure recommended by Abdullah et al. [6] and pre-burned (i.e., inserted into the ICP) 3 to 5 times prior to their use. Graphite electrodes used with non-carbide forming elements are re-usable for over 20-times [2, 6], those used with carbide forming elements become re-usable after insertion into the ICP with 10 µl of 0.25 M NaF solution, then with 20 µl of concentrated HCl followed by a dry run.

All solutions were prepared by serial dilution with distilled/deionized water of 1000 ppm standard stock solution (standards for plasma emission spectroscopy, SPEX Industries, Inc., Edison, NJ) of the respective element. A 10 µl volume was transferred to the cup with an Eppendorf micropipette. Solutions transferred to cups were dried by heating the electrode in an aluminium holder on a hot plate prior to its insertion into the plasma. Analytical reagent grade chemicals were used for the preparation of aqueous solutions of the modifiers. A 10 µl volume of the modifier was added on dried solution residues, this was followed by a drying cycle and a subsequent insertion into the plasma.

C. Results and Discussion

C.1 Multielement Solution Residues

C.1.1 Survey Results

In order to establish the nature of the signals from difficult-to-volatilize elements with this system, analyte emission temporal behavior was recorded for elements known to form refractory oxides/carbides. Typical results for 250 ng of Al, Ca, Sr and Zr are shown in Figure 4-1. Low sensitivities were observed for Al and Sr (Figures 4-1a and 4-1c), the post-insertion base-line level observed even after 60 s is higher than that of pre-insertion, indicating incomplete analyte volatilization. For Ca and Zr (Figure 4-1b and 4-1c) the signal observed is indistinguishable from that observed for a water blank indicating that these elements quantitatively remain in the cup under the experimental conditions used here.

In an attempt to explain the results observed here and reported elsewhere [7], the previously described model [2] will be used. In this, it was suggested that during the drying/ashing cycle or at the initial stages of cup insertion into the plasma, an oxo-anion salt decomposes to form

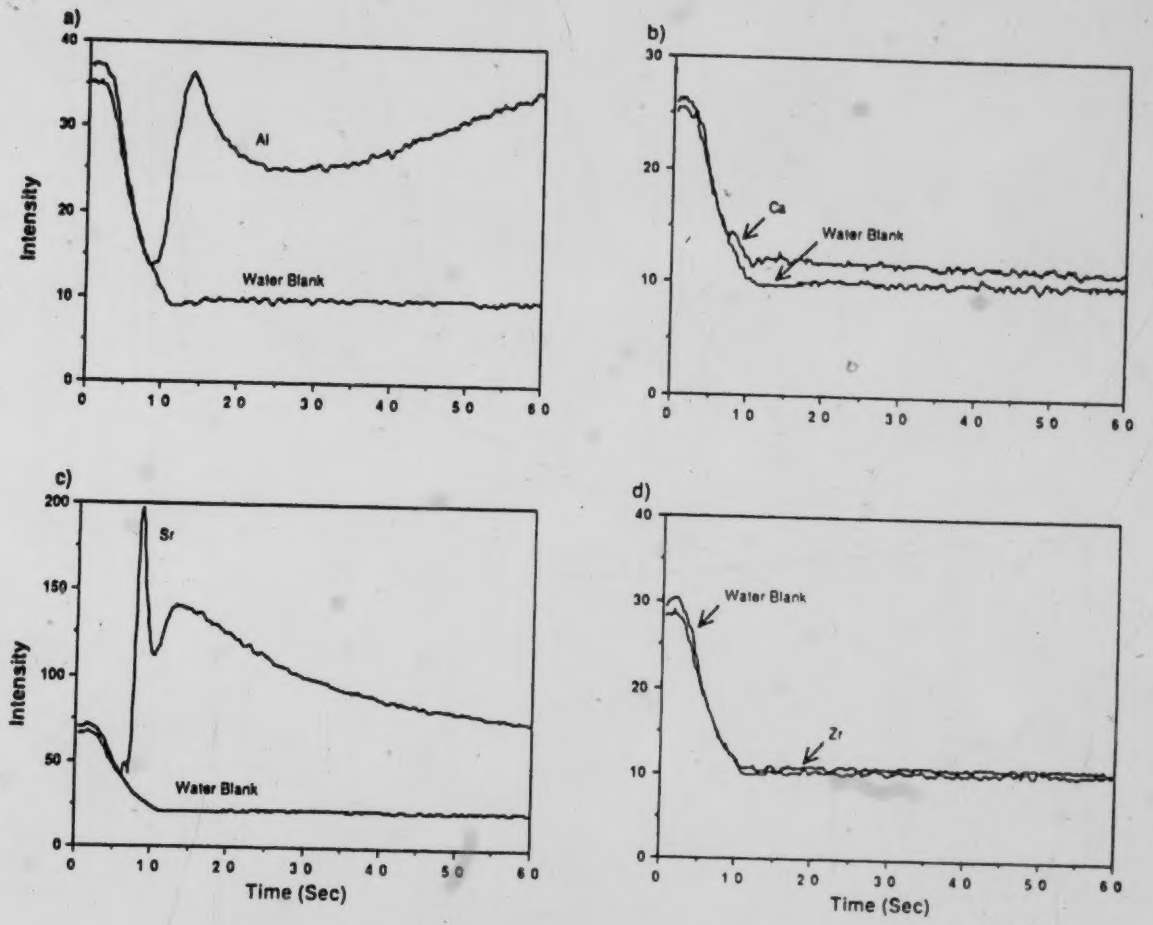

Figure 4-1. Typical temporal emission behavior for: (a) water blank and 250 ng Al; (b) water blank and 250 ng Ca; (c) water blank and 250 ng Sr; (d) water blank and 250 ng Zr. The full scale intensity is 4096.

the corresponding oxide. A further increase of cup temperature promotes either a reduction of the corresponding oxide to metal or its carbide.

Based on the thermochemical properties of the oxides and carbides of the corresponding elements (Table 4-1), and of electrode temperatures attained in the plasma (although electrode temperatures as high as 4000°C have been reported [7], temperatures of only about 1800°C have been measured [20, 21]), it can be concluded that for the 1.25 kW power setting used in these experiments, insufficient cup temperatures are reached for refractory oxide/carbide volatilization. Because Zr emission was not observed (Figure 4-1d) and due to the high boiling point of both Zr and ZrC_2 (Table 4-1), carbide formation was assumed. Because Ca emission was not observed (Figure 4-1b) and due to the low boiling point of elemental Ca and the high boiling point of CaC_2 (Table 4-1), it can be reasoned that reduction of oxide to metal is unlikely, again carbide formation was assumed. For Sr (Figure 4-1d), it can be suggested that an initial increase in temperature promotes a reduction to a lower boiling point metal (Table 4-1) with a further increase in temperature (brought about by the final cup insertion into the plasma) promoting the formation of the corresponding refractory carbide. This way, the double peak observed for the Sr signal (Figure 4-1c) can also be explained, the sharp peak

Table 4-1. Melting and Boiling points of oxides and carbides (from Ref. 25)

			OXIDE			CARBIDE		
Element	**M.P.**	**B.P.**	**Compound**	**M.P.**	**B.P.**	**Compound**	**M.P.**	**B.P.**
Al	660	2467	Al_2O_3	2072	2980	Al_4C_3	1400^a	2200^d
Ca	~840	1484	CaO	2614	2850	CaC_2	25-447^b	2300
Sr	769	1384	SrO	2420	~3000	SrC_2	>1700	....
Zr	1852	4377	ZrO_2	~2700	~5000	ZrC	3450	5100

a: Stable to b: Stable c: 2500-3000° C d: decomposes with its maximum at about 10 s can be assigned to Sr volatilization, the broad peak is possibly due to SrC_2.

The results observed for Al (Figure 4-1a) are more difficult to interpret. It could be speculated that with an increase in temperature, an oxide of lower thermostability is initially formed [22], a further increase in temperature is perhaps promoting refractory carbide formation (Table 4-1). Although it is easy to speculate, it is difficult to predict the exact nature and the chemical reactions taking place in the electrode cavity with any degree of certainty. Such information can only become available with further studies. However, it seems reasonable to infer that carbon, and probe composition in general, play a significant role. Similar conclusions have been drawn by others for DSID-ICP [2, 3, 5, 7], the dc arc [23, 24] and ETV devices [11-17]. And as mentioned earlier, chemical modification will be used to circumvent the problem of incomplete analyte volatilization.

C.1.2 Analyte Chemical Modification

The basic idea behind analyte chemical modification is rather simple. As mentioned earlier, by promoting a reaction via the deliberate addition of a modifier, a lower boiling point compound (i.e., halide, fluoride) is preferentially formed over the corresponding refractory oxide or carbide. However, the key to understanding the action of the modifier from the reaction mechanism point of view is not as easy as it may initially appear as it involves an understanding of the interaction of matrix and analyte with carbon, oxygen, the matrix, the modifier, and the plasma. It could be further suggested that the magnitude of the influence the modifier exerts on analyte emission temporal behavior largely depends on probe type, geometry and composition; on the 'sample' itself (i.e., the physico-chemical properties of matrix and analyte); and on plasma parameters (i.e., applied forward power and gas composition). These, in turn, either define or affect the physico-chemical processes taking place inside the electrode cavity and the plasma. In addition to analyte emission intensity, background levels must also be investigated in order to decide on a selection of an appropriate modifier. It can thus be concluded that it is not easy to find a modifier that works equally well for all elements and matrices for simultaneous determination by the ICP. And although the action of the modifier was briefly considered here, the choice of an appropriate modifier was mostly guided by the relevant dc arc and electrothermal literature.

In this case, concentrated solutions of KCl, KF, NaCl and NaF were considered as suitable modifiers for the simultaneous determination of Al, Ca, Sr and Zr from multielement solution residues. Due to the high boiling of Zr and of its compounds (Table 4-1), it can be concluded that Zr is difficult to volatilize, and much like in the dc arc [23], Zr volatilization from graphite cups was considered to be a real challenge.

The modifiers chosen were applied to multielement solution residues with varying degrees of success. Typical results for 250 ng of Al, Ca, Sr and Zr with KCl, KF, NaCl and NaF modifiers are shown in Figures 4-2, 4-3, 4-4 and 4-5. In general, a small enhancement in the sensitivity of Al and Ca was observed when either KCl or NaCl was used (Figures 4-2a, 4-2c and Figures 4-3a, 4-3c respectively); a large enhancement was observed for Sr (Figures 4-4a and 4-4c); whereas an enhancement was not observed for Zr (Figures 4-5a and 4-5c). And although approximately equivalent enhancements in sensitivity were observed when either KF or NaF was used with Al (Figures 4-2b and 4-2d), Ca (Figures 4-3b and 4-3d) and Sr (Figures 4-4b and 4-4d), the largest enhancement in the Zr signal was observed when NaF was used (Figure 4-5d). In addition, with KF, a high volatilization rate was observed even during the initial stages of cup insertion, and as a consequence, the plasma was frequently extinguished. This can be attributed to the formation of highly volatile $KF \cdot 2H_2O$ (B.P. 156°C [25]). Therefore, NaF was the modifier of choice and it will be used throughout.

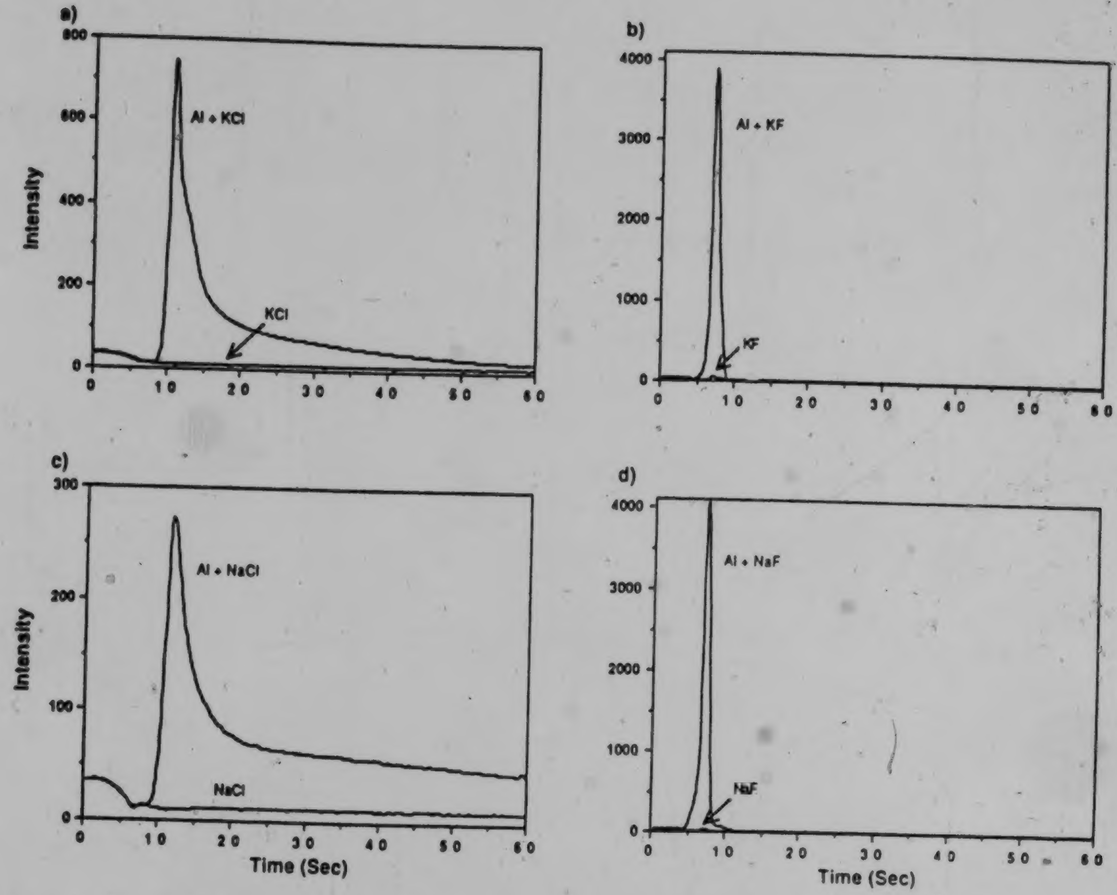

Figure 4-2. Typical temporal emission behavior for: (a) 10 µl of 0.25 M KCl blank and 10 µl of 0.25 M KCl on 250 ng of Al; (b) 10 µl of 0.25 M KF blank and 10 µl of 0.25 M KF on 250 ng of Al; (c) 10 µl of 0.25 M NaCl blank and 10 µl of 0.25 M NaCl on 250 ng of Al; (d) 10 µl of NaF blank and 10 µl of 0.25 M NaF on 250 ng of Al. The full scale intensity is 4096.

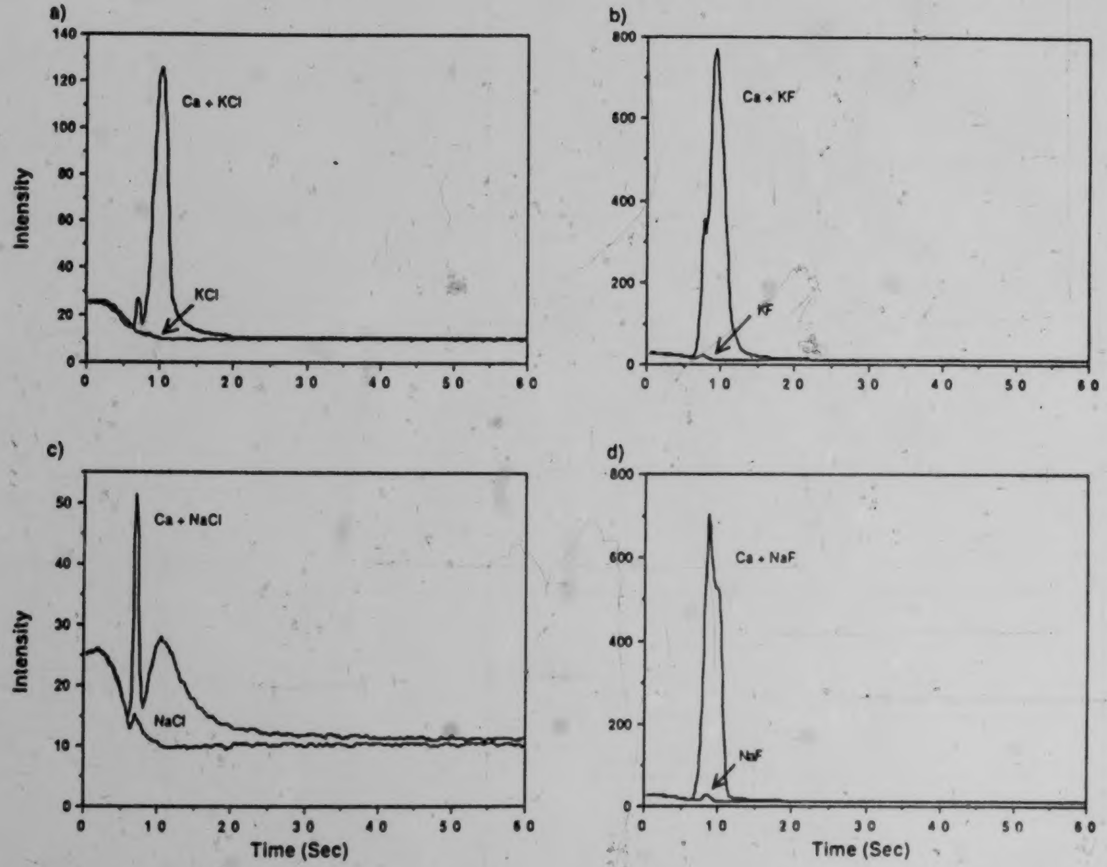

Figure 4-3. Typical temporal emission behavior for: (a) 10 µl of 0.25 M KCl blank and 10 µl of 0.25 M KCl on 250 ng of Ca; (b) 10 µl of 0.25 M KF blank and 10 µl of 0.25 M KF on 250 ng of Ca; (c) 10 µl of 0.25 M NaCl blank and 10 µl of 0.25 M NaCl on 250 ng of Ca; (d) 10 µl of NaF blank and 10 µl of 0.25 M NaF on 250 ng of Ca. The full scale intensity is 4096.

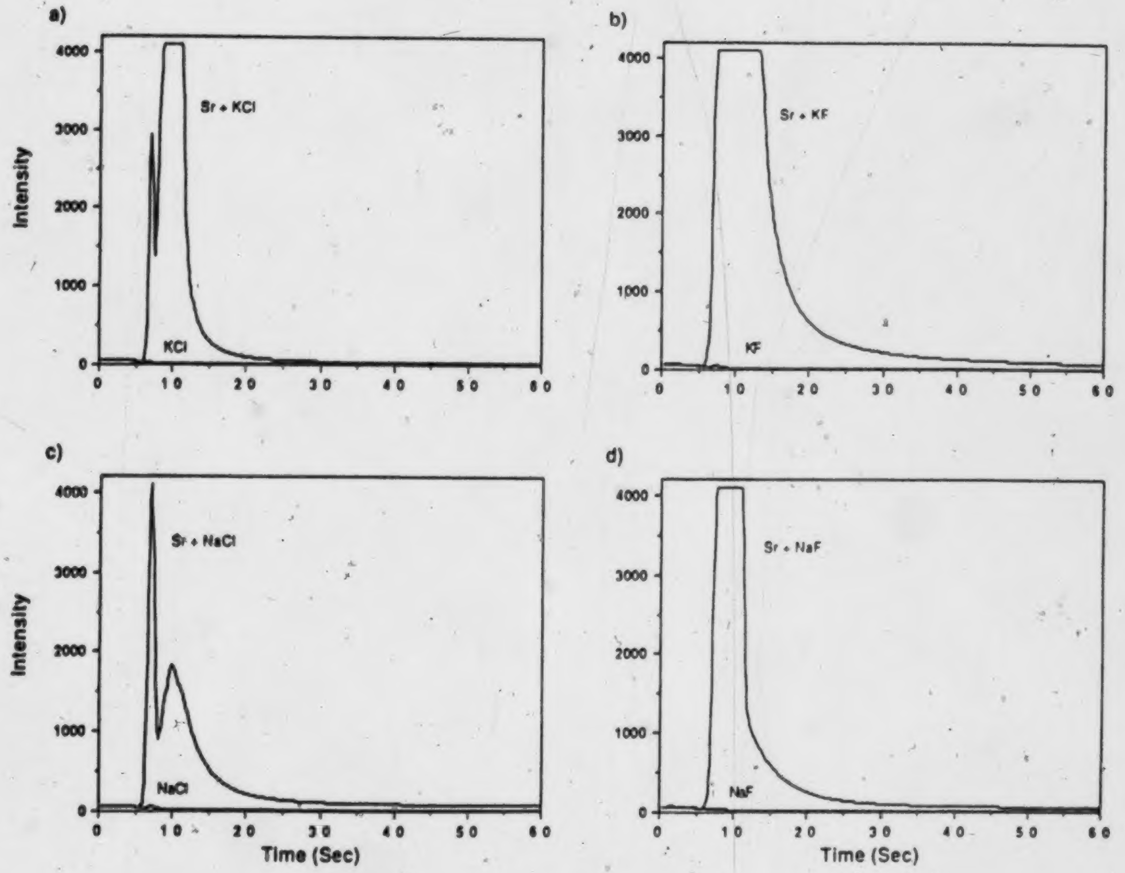

Figure 4-4. Typical temporal emission behavior for: (a) 10 µl of 0.25 M KCl blank and 10 µl of 0.25 M KCl on 250 ng of Sr; (b) 10 µl of 0.25 M KF blank and 10 µl of 0.25 M KF on 250 ng of Sr; (c) 10 µl of 0.25 M NaCl blank and 10 µl of 0.25 M NaCl on 250 ng of Sr; (d) 10 µl of NaF blank and 10 µl of 0.25 M NaF on 250 ng of Sr. The full scale intensity is 4096.

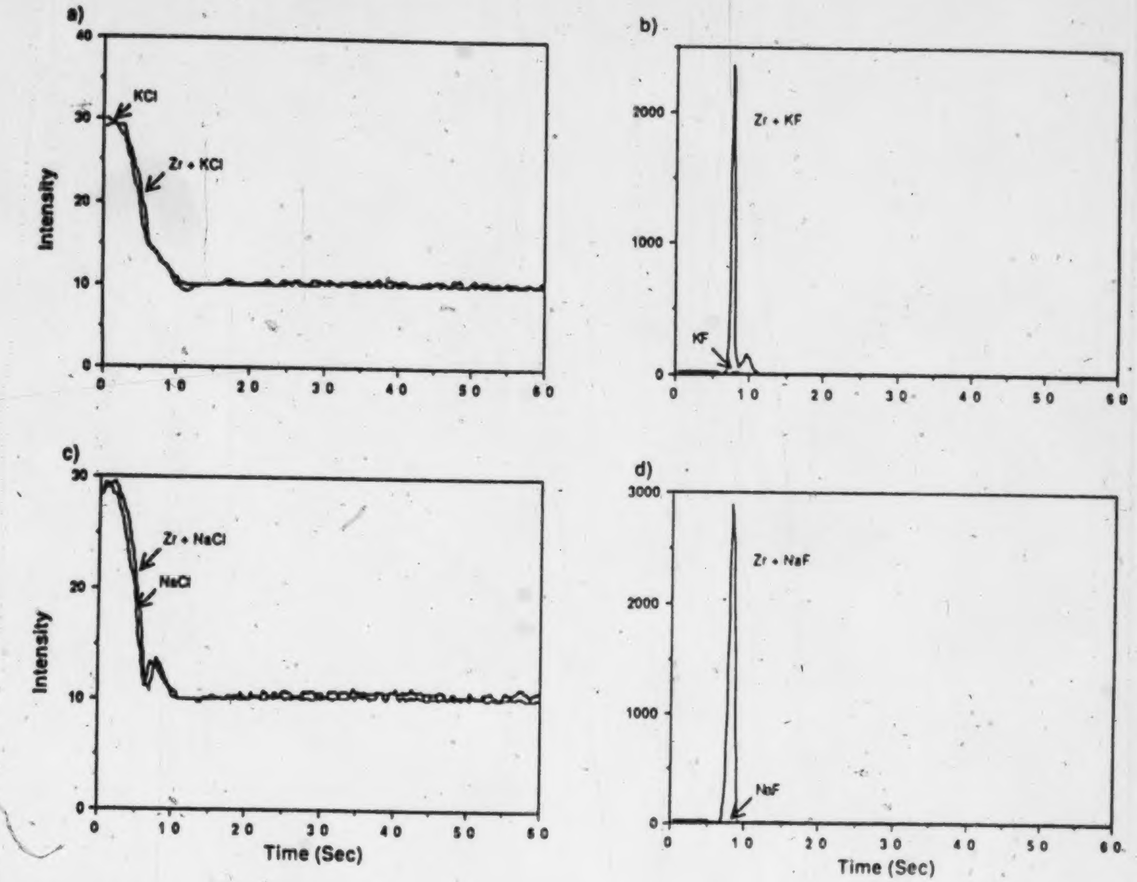

Figure 4-5. Typical temporal emission behavior for: (a) 10 µl of 0.25 M KCl blank and 10 µl of 0.25 M KCl on 250 ng of Zr; (b) 10 µl of 0.25 M KF blank and 10 µl of 0.25 M KF on 250 ng of Zr; (c) 10 µl of 0.25 M NaCl blank and 10 µl of 0.25 M NaCl on 250 ng of Zr; (d) 10 µl of NaF blank and 10 µl of 0.25 M NaF on 250 ng of Zr. The full scale intensity is 4096.

C.1.3 Characterization of NaF Chemical Modification

In order to determine the amount of NaF required for quantitative analyte conversion to the corresponding fluoride, signal-to-background ratios (SBRs) were measured for Al, Ca, and Zr for different NaF concentrations (10 µl injections), the results are shown in Figure 4-6. Initially, an increase in NaF concentration results in a steep increase in SBRs. With a further increase in the amount of NaF added in the cup, SBRs reach a maximum near 0.25 M and they subsequently decrease. From these results it can be concluded that the optimum NaF concentration is 0.25 M NaF (10 µl injection) and will be used throughout.

Typical results when 250 ng of multielement solution residues are treated with 10 µl of 0.25 M NaF are shown in Figures 4-7a, 4-7b, 4-7c and 4-7d for Al, Ca, Sr and Zr respectively. Due to its high sensitivity and at the concentration level and electronics and PMT gains utilized in these experiments, Sr saturates the corresponding PMT channel, as shown in Figure 4-5c. From the results shown in Figure 4-7 it can be concluded that considerable enhancements in the sensitivity of Al, Ca, Sr and Zr are realized by the addition of NaF.

In order to quantify the observed enhancements in sensitivity, detection limits (twice the standard deviation of the background and peak area integration) were determined by

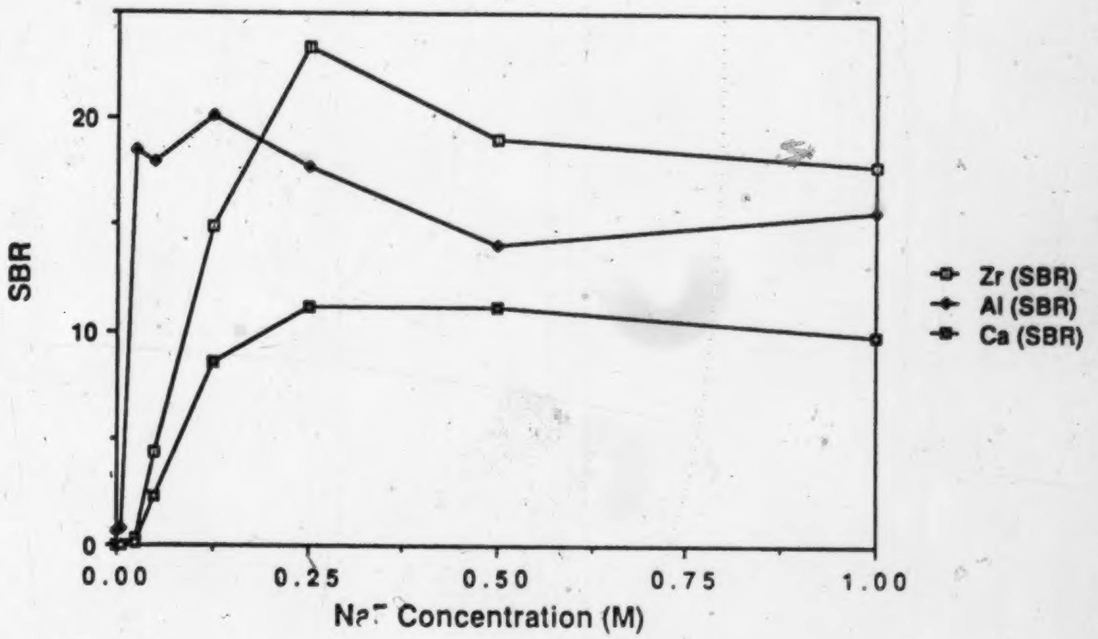

Figure 4-6. The effect of NaF concentration (10 µl injection) on the Signal-to Background Ratio (SBR) of Al, Ca and Zr.

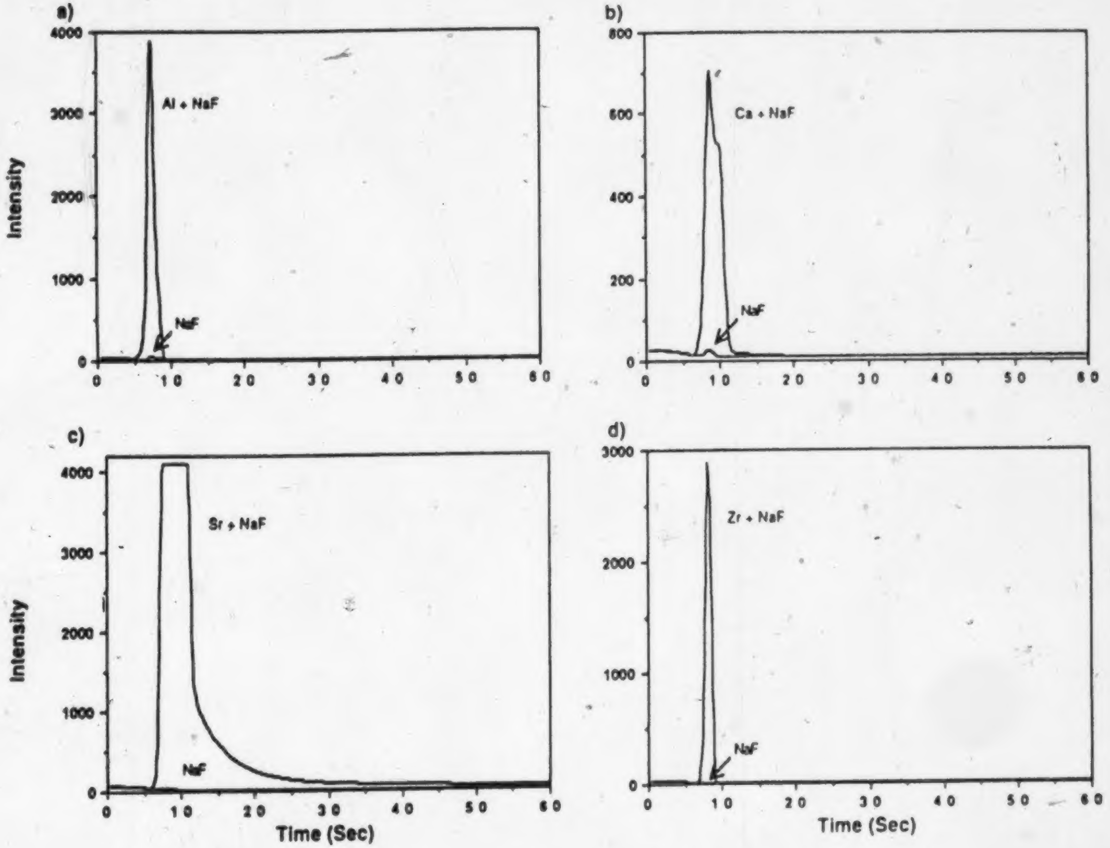

Figure 4-7. The effect of a 10 µl injection of 0.25 M NaF on the temporal emission behavior of Al, Ca, Sr and Zr for: (a) 10 µl of 0.25 M NaF blank and 10 µl of 0.25 M NaF on 250 ng of Al; (b) 10 µl of 0.25 M NaF blank and 10 µl of 0.25 M NaF on 250 ng of Ca; (c) 10 µl of 0.25 M NaF blank and 10 µl of 0.25 M NaF on 250 ng of Sr and (d) 10 µl of 0.25 M NaF blank and 10 µl of 0.25 M NaF on 250 ng of Zr. The full scale intensity is 4096.

running twelve consecutive blank runs (from either 10 µl of 0.25 M NaF blank or from a water blank) with and without the addition of NaF modifier, the results are summarized in Table 4-2. The most significant improvements in sensitivity were observed for Ti, Zr and B. For these elements, no emission signal was observed even at the 5000 ng, 2500 ng and 1000 ng levels respectively, whereas, with the addition of NaF, detection limits in the low nanogram to picogram levels have been measured here and reported by others [7], as shown in Table 4-2. The magnitude of the observed enhancement in sensitivity depends on elemental volatility and the tendency toward carbide formation. For example, as shown in Figure 4-8, the addition of 10 µl of 0.25 M NaF had little effect in the sensitivity of Ag, Cd and Zn, as expected. These findings are in general agreement with those reported by others [7]. Furthermore, the use of NaF does not only improve the sensitivity and the detection limits of the elements tested, but also their reproducibilities (calculated from 12 successive determinations and peak areas integration), as shown in Table 4-2. These results, in spite of the dissimilarity of devices and modifiers utilized, are in good agreement with those reported for Freon as a modifier [7] and are listed in Table 4-2 for convenience.

Table 4-2. Detection limits with and without the addition of a chemical modifier.

		Without modifier		With modifier		
Element/ Line	λ (nm)	LOD (ng)	%RSD	LOD (ng)	%RSD	Reference
Ti II	337.28	a	---	0.8	9.5	This work[g]
Zr II	324.82	b	---	0.4	18.6	This work[g]
B I	249.68	c	---	9.6	14.8	This work[g]
Ca II	317.93	602.0	22.8	5.2	10.7	This work[g]
Al I	237.34	457.0	22.9	0.7	5.6	This work[g]
Sr II	407.78	46.3	23.6	0.03	13.8	This work[g]
Co II	228.61	4.3	9.7	1.3	6.5	This work[g]
Fe II	259.94	2.7	9.8	1.5	5.1	This work[g]
Zr II	343.82	d	---	1.1	---	7[h]
U I	358.96	290.0	---	1.9	---	7[h]
Ti II	334.94	110.0	12.5[e]	0.89	7.5[f]	7[h]
B I	249.77	2.0	---	1.3	---	7[h]
Mo II	313.26	6.3	---	1.0	---	7[h]
Cr I	357.87	0.021	---	0.020	---	7[h]
Cu I	324.75	0.011	---	0.0073	---	7[h]
Zn I	213.86	0.004	---	0.004	---	7[h]
Ag I	328.07	0.0023	---	0.0018	---	7[h]

a: Not detected at 5000 ng
b: Not detected at 2500 ng
c: Not detected at 1000 ng
d: Not detected at 1000 ng
e: 5 μl of 1000 ppm Ti, 5 determinations
f: 5 μl of 10 ppm Ti, 5 determinations
g: NaF as a chemical modifier
h: Freon as a chemical modifier

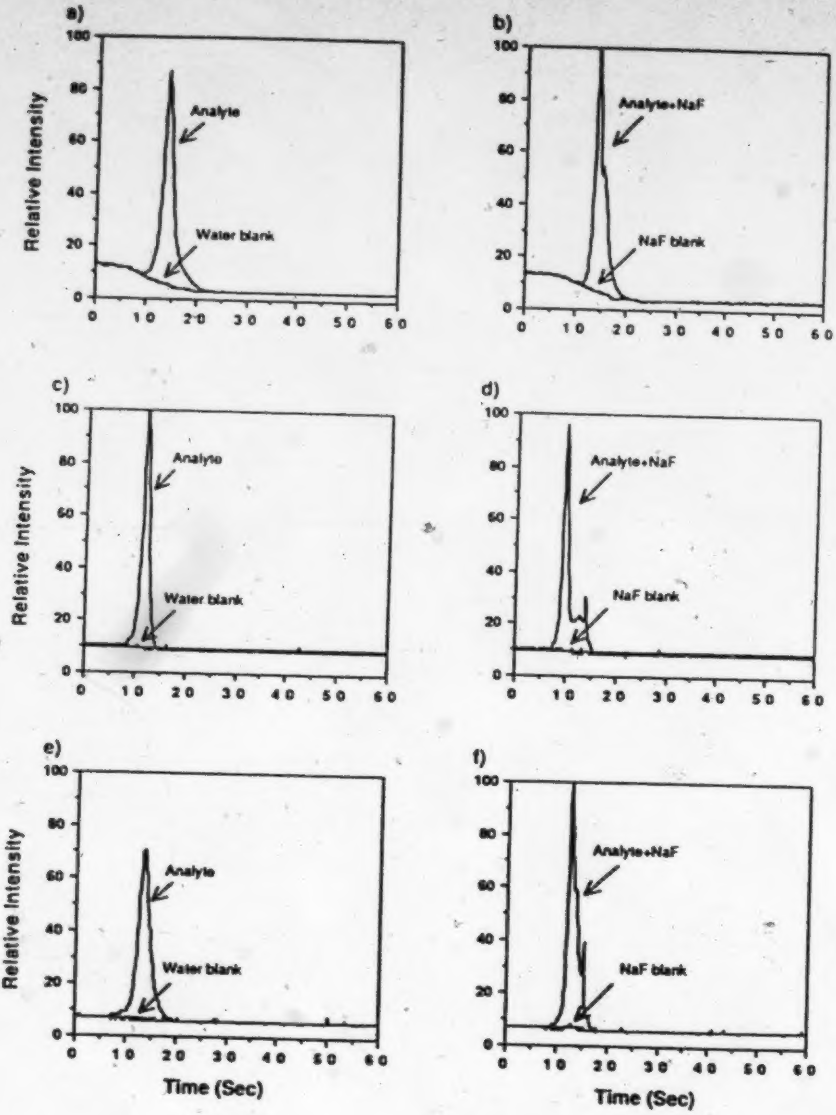

Figure 4-8. The effect of a 10 µl injection of 0.25 M NaF on the temporal emission behavior of Ag, Cd and Zn for: (a) water blank and 10 µl of 0.25 M NaF on 10 ng Ag; (b) 10 µl of 0.25 M NaF blank and 10 µl of 0.25 M NaF on 10 ng Ag; (c) water blank and 10 µl of 0.25 M NaF on 10 ng Cd; (d) 10 µl of 0.25 M NaF blank and 10 µl of 0.25 M NaF on 10 ng Cd; (e) water blank and 10 µl of 0.25 M NaF on 10 ng Zn; (f) 10 µl of 0.25 M NaF blank and 10 µl of 0.25 M NaF on 10 ng Zn;

Calibration curves have also been constructed from multielement solution residues of Al, Ca and Zr with NaF as a volatilization enhancing agent, the results are shown in Figure 4-9. These are linear for over 3-orders for Al and Ca and 2-orders of magnitude for Zr, however, they tend to 'level-off' at high concentrations. Again, similar results have been reported by others [7]. In our case, this is attributed to saturation of the electronics and PMT gains of the corresponding PMT channel. Determinations at higher concentration levels can be made by reducing these gains. On the other hand, an increase in gain is expected to result in an increase in sensitivity and to allow calibration curves to be extended to lower concentration levels. With such an increase, however, peak heights of a considerable intensity (typically a few hundred mV for a 10 V full scale) were observed even for a blank run (i.e., 10 µl of 0.25 M NaF) for the elements tested. These signals are due to impurities found in the NaF utilized in these experiments. Depending on the element, a further increase in electronic and PMT-gains may even saturate the corresponding PMT channel, thus making blank subtraction [1] an impossible feat. Clearly, measurements at concentration levels near or at the detection limit are not possible, due to the low purity of the reagents utilized. In general, for determinations at low concentration levels, 'pure' NaF must be utilized. Others have also experienced similar problems [26] when using

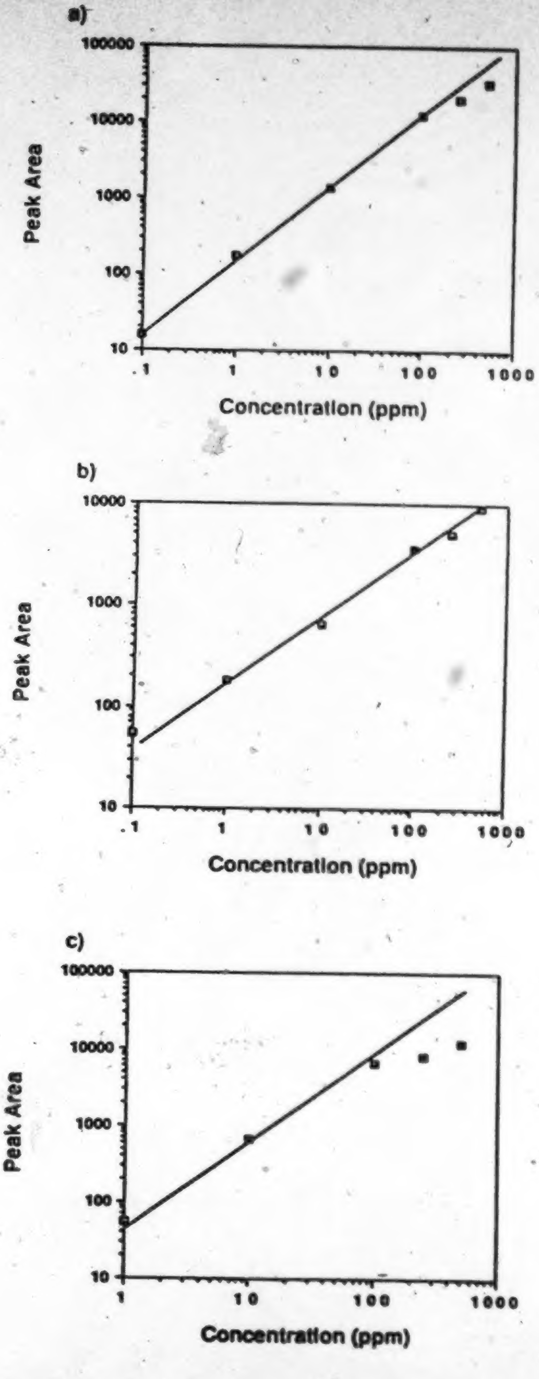

Figure 4-9. Calibration curves from multielement solution residues of Al, Ca and Zr with a 10 µl addition of 0.25 M NaF for (a) Al (slope: 0.96); (d) Ca (slope: 0.96) and (c) Zr (slope: 1.03).

chemical modifiers with the dc arc. It is worth noting that spectroscopically 'pure' NaF was found to contain a considerable amount of impurities, surprisingly, of higher concentration levels for Al, Ca, Sr and Zr, than the analytical reagent grade NaF. Undoubtedly, as sensitivity increases, the question of 'how pure is pure' is becoming increasingly important [27].

The application of NaF chemical modification on multi-element solution residues has been described thus far. However, one of the main goals for the development of a DSID for the ICP is the added capability of handling powdered/solid samples with little or no sample pre-treatment. In order to demonstrate this capability, the determination of B in powdered $CaSO_4$ samples was chosen.

C.2 Powdered Samples

Although Boron can be used as an indicator of mineralization, its use in this capacity *"has been handicapped by the absence of effective analytical methods for geological materials"* [28]. Methodology for the ICP-AES determination of B from such materials has been recently developed [28-30], however, all these methods rely on lengthy sample preparation procedures. Alternatively, taking advantage of the *in situ* sample processing capability offered by the DSID, B can be determined rapidly. Because B is a strong carbide former [23], it could not be determined by the ICP as observed here and reported by others [32], unless NaF is utilized. The amount of NaF required for quantitative conversion of B to the corresponding fluoride was determined by injecting 25 µl of NaF solution on 2 mg of powdered $CaSO_4$ and by measuring the SBR for B, the results are shown in Figure 4-10. From these it can be concluded that the optimum NaF concentration is that of 0.50 M. Linear calibration curves were constructed with two methods: the standard additions method (procedure: 25 µl of 0.5 M NaF were injected into 2 mg of $CaSO_4$ and the sample was brought to dryness, this was followed by a 10 µl injection of standard solution and another drying cycle) as shown in Figure 4-11a; and from synthetic standards (procedure: 2 mg of $CaSO_4$ was mixed with solid H_3BO_3 onto which 10 µl of 0.5 M NaF were injected, followed by a drying cycle) as shown in Figure 4-11b. Equivalent results (within experimental error) were observed by both methods, indicating that in this case there is no need for matrix matched standards. It would be interesting to see the range of matrices that this holds true, thus permitting non-matrix matched standard solutions to be used in calibration [31], or where matrix-matched standards are required [8, 32]. This short application demonstrates that *in situ* sample processing is possible and that rapid determinations from powdered samples with little sample pre-treatment can be realized with the DSID.

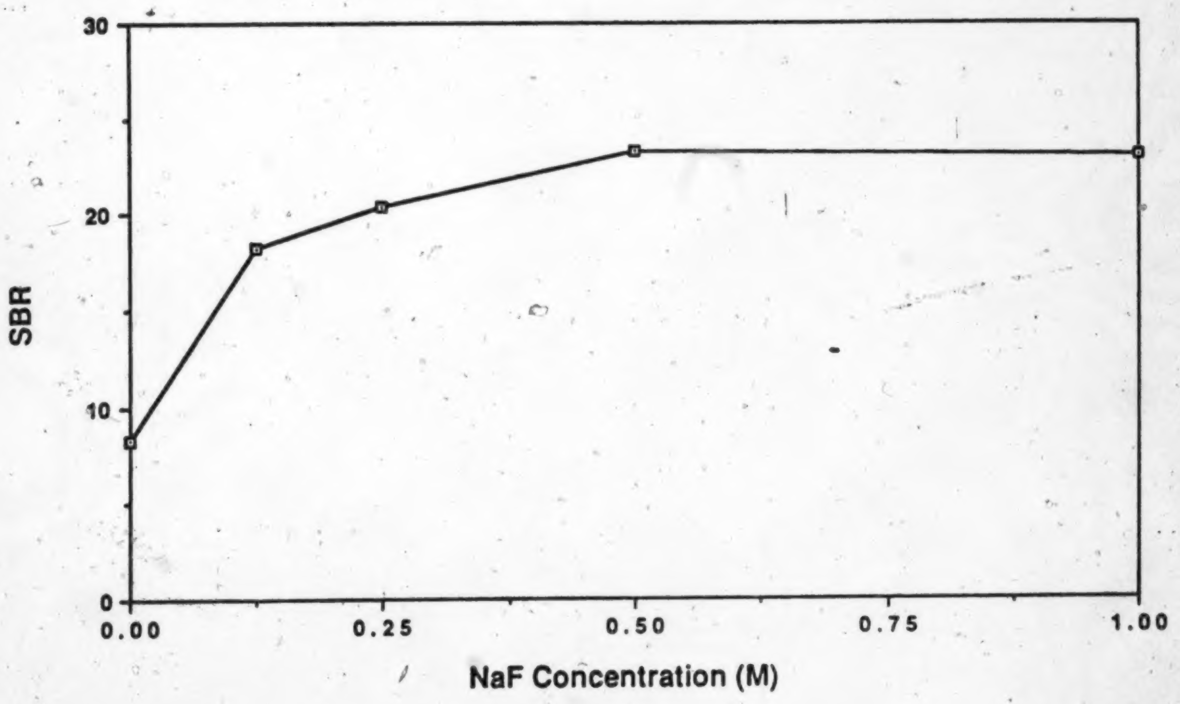

Figure 4-10. The effect of NaF concentration (25 µl injection) on the Signal-to-Background Ratio (SBR) of B in 2 mg $CaSO_4$

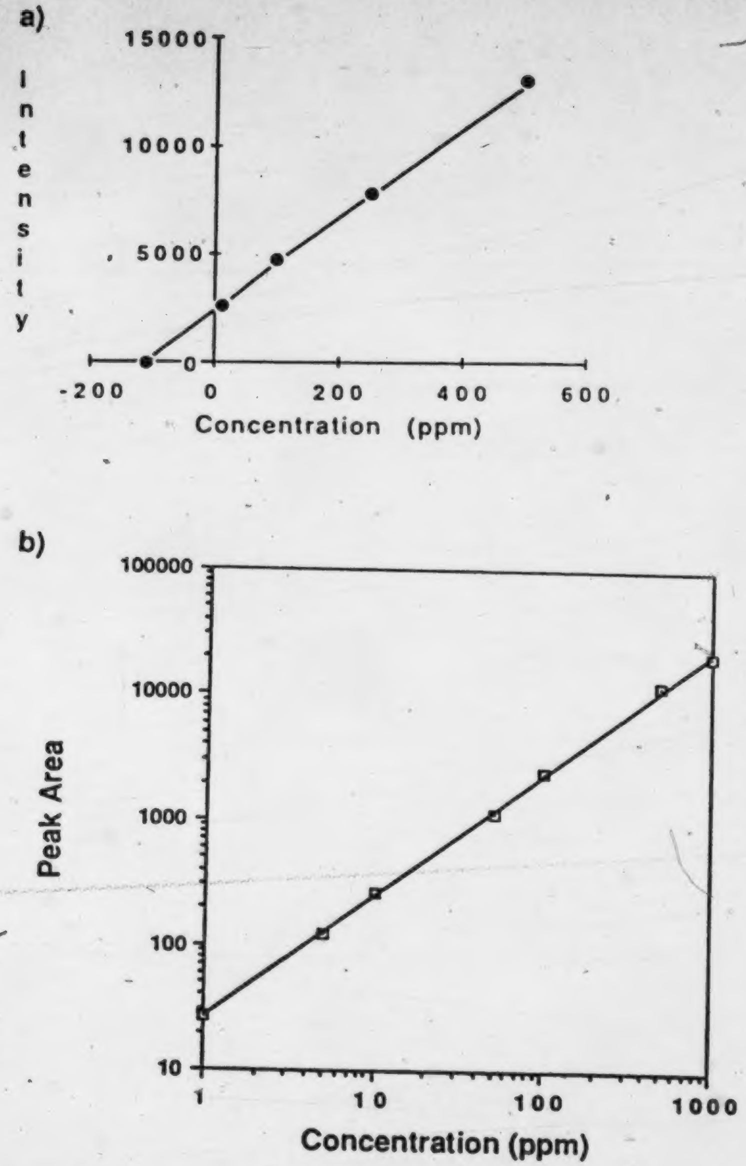

Figure 4-11. Calibration curves for B in 2 mg $CaSO_4$ with a 25 µl injection of 0.5 M NaF: (a) standard additions method; (b) from synthetic standards (slope: 0.98).

D. Conclusions

In spite of the capabilities offered by a fully automated graphite-cup DSID [1, 2], carbide formation was a stumbling block preventing it from attaining its full potential. As it has been shown here and reported by others [4, 7], the problem of incomplete volatilization of difficult-to-volatile elements can be solved via chemical modification. From these results, it can also be concluded that further studies involving chemical modification are warranted in order to define the limits and to demonstrate the full potential of NaF chemical modification. Furthermore, the aim of such studies is not only to solve DSID-related problems but to extend its capabilities, for example, for the direct determination of solids (i.e., metal chips) with little or no sample pre-treatment. In the future, chemical modification may also prove to be an invaluable tool for the analysis of 'exotic' or 'space shuttle-type' materials (i.e., high temperature ceramics, catalysts) that are expected to become a part of every day life. Furthermore, applications involving robot-assisted dispensing of chemical modifiers are not hard to envision [1, 2, 34]. Therefore, the metaphor of the sample carrying cup as a 'crucible' in which *in situ* chemical processing of the samples takes place becomes literal, and the concept of the DSID as a sample processor for the ICP appears to be realizable.

REFERENCES

1. V. Karanassios and G. Horlick, *'A computer-controlled DSID for ICP-AES'*, Spectrochim. Acta, (submitted)

2. V. Karanassios, G. Horlick and M. Abdullah ,*'Characterization of a DSID for ICP-AES'*, Spectrochim. Acta, (submitted)

3. W.E. Pettit and G. Horlick, Spectrochim. Acta, **41B**, 699 (1986)

4. Y. Shao and G. Horlick, Appl. Spectrosc., **40**, 386 (1986)

5. G.F. Kirkbright and S.J. Walton, Analyst, **107**, 276 (1982)

6. M. Abdullah, K. Fuwa and H. Haraguchi, Spectrochim. Acta, **39B**, 1129 (1984)

7. G.F. Kirkbright and Z. Li-Xing, Analyst, **107**, 617 (1982)

8. G. Zaray, P. Burba, J.A.C. Broekaert and F. Leis, Spectrochim. Acta, **43B**, 255 (1988)

9. A.G. Page, K.H. Madraswala, S.V. Godbole, M.J. Kulkarni, V.S. Mallapurkar and B.D. Joshi, Frezenius Z. Anal. Chem., **315**, 38 (1983)

10. A.G. Page, S.V. Godbole, K.H. Madraswala, M.J. Kulkarni, V.S. Mallapurkar and B.D. Joshi, Spectrochim. Acta, **39B**, 551 (1984)

11. R.E. Sturgeon and C.L. Chakrabarti, Prog. Analyt. Atom. Spetrosc., **1**, 5 (1978)

12. H.S. Wahab and C.L. Chakrabarti, Spectrochim. Acta, **36B**, 463 (1981)

13. H. Matusiewicz and R.M. Barnes, Spectrochim. Acta, **40B**, 29 (1985)

14. M.C. Almeida and W.R. Seitz, Appl. Spectrosc., **40**, 4 (1986)

15. G.D. Renshaw, At. Absorption Newslett., **12**, 158 (1973)

16. C.D. Wall, Talanta, **24**, 755 (1977)

17. B.V. L'vov and L.A. Pelieva, Can. J. Spectrosc., **23**, 1 (1978)

18. M.S. Elalfy, M. Mazurkiewicz and H. Nickel, Paper B7.8, Book of abstracts, XXV Colloquium Spectroscopium Internationalle, Toronto, Canada, 1987

19. H. Nickel, M. Reisch and M. Mazurkiewicz, Paper F5.1, Book of abstracts, XXV Colloquium Spectroscopium Internationalle, Toronto, Canada, 1987

20. N.W. Barnett, M.J. Cope, G.F. Kirkbright and A.A.H. Taobi, Spectrochim. Acta, **39B**, 343 (1984)

21. A. Lorber and Z. Goldbart, Analyst, **110**, 155 (1983)

22. F.A. Cotton and G. Willkinson, *'Advanced Inorganic Chemistry'*, Interscience, New York, 1972

23. L.H. Ahrens and S.R. Taylor, *'Spectrochemical Analysis'*, Addison-Wesley, Reading, MA, 1961

24. P.W.J.M. Boumans, *'Theory of Spectrochemical Excitation'*, Hilger and Watts, London, 1966/Plenum, NY, 1966

25. CRC Handbook, 57th Edition, CRC Press, Inc., Boca Raton, Florida, 1979

26. R.W. Dabeka, P. Tymchuk and D.S. Russell, Appl. Spectrosc., **34**, 43 (1980)

27. L.B. Rogers, J. Chem. Ed., **63**, 3 (1986)

28. G.E.M. Hall and J. Pelchat, Analyst, **111**, 1255 (1986)

29. J.C. Mills, Anal. Chim. Acta, **183**, 231 (1986)

30. J.N. Walsh, Analyst, **110**, 959 (1985)

31. C.W. McLeod, P.A. Clarke and D.J. Mowthorpe, Spectrochim. Acta, **41B**, 63 (1986)

32. M. Abdullah and H. Haraguchi, Anal. Chem., **57**, 2059 (1985)

33. ~~M.~~ Umemoto and M. Kubota, Spectrochim. Acta, **42B**, 491 (1987)

34. V. Karanassios and G. Horlick, Appl. Spectrosc., **41**, 360 (1987)

CHAPTER 5

HUMAN PROCESSOR INTERFACE FOR ICP-AES: CONCEPTS AND IMPLEMENTATION

A version of this chapter has been published.
V. Karanassios and G. Horlick, Appl. Spectrosc., **41**, 360-380 (1987)

A. Introduction

The synergy between scientific instrumentation and the various systems, sub-systems, modules and software packages provided by the business/personal computer segment of the computer industry has altered the nature of scientific instrumentation. Such is the impact of personal computers on laboratory instrumentation that it has been said, *"it is probably a mistake to design an instrument on anything else but personal computers"* [1]. However, microcomputer system design is one of the fastest growing domains in the computer industry, with newer and more powerful personal computers being introduced at an accelerated pace. Ironically, this growth can lead to the obsolescence of an instrument well before the expiration of its economic life.

An effective way to counter this trend towards rapid obsolescence is the utilization of distributed intelligence in the design of microcomputer based instrumentation [2]. An implementation involving a moderately coupled, two processor system is shown in Figure 5-1. This instrument is an inductively coupled plasma atomic emission spectrometer. In this instrument, one processor handles data acquisition and instrument control and the second, called the front end processor, handles mass storage, additional number crunching, supports high speed communications channels and provides an effective communications link with the operator through the extensive utilization of human processor interface (HPI) tools. The two processors communicate with each other via a communications bus.

Linking an intelligent instrument to a front end processor as shown in Figure 5-1 eliminates several potential problems associated with instrument obsolescence. The design of the spectrometer and its associated readout system is likely to remain basically the same throughout the life of the instrument while new personal computers with advanced features are continually being developed. By distributing the processing, the data acquisition and control microcomputer and electronics do not have to be re-designed in order to take advantage of the new generation microcomputers at the front end of the instrument.

Besides the distribution of the work load, there are other advantages pertaining to this approach: utilizing a front end processor that implements a powerful user interface makes instruments easier to use, makes facts easier to find and gives the operator more time to think about the data rather than how to collect them. Off loading data acquisition and control tasks onto the controlling microcomputer frees the front end processor for other tasks, such as data base management, communications or data presentation. This way, the operator does not have to waste time 'waiting for the computer to respond' as, for example, during data acquisition.

The question that arises then is : which microcomputers should be chosen for the data acquisition and control function and for the front end processor?

Typical selection criteria are summarized in Table 5-1. Although there is a variety of microcomputer systems currently available [2, 3, 4], the battle lines seem to have been drawn between two of the most important personal computer families: the IBM PC and the Apple Macintosh. In our case, the IBM PC was chosen for control and data acquisition, the Apple Macintosh was selected as a front end processor. The IBM PC communicates its data and control information to the Macintosh via an RS-232 serial port.

The IBM PC family (IBM PC, XT or AT) is well suited for the data acquisition and control microcomputer [4]. Of particular strength is its intelligent motherboard design, with internal slots, for which a plethora of support boards are available. For example, in our system data acquisition and instrument control is handled using a Data Translation DT 2801A board. This data acquisition and control system described in a separate publication [5].

The Apple Macintosh is uniquely suited for the front end processor primarily because of its very effective implementation of modern human processor interface concepts. These concepts will be outlined in the next section and then our implementation of these concepts to the instrument shown in Figure 5-1 will be presented.

Table 5-1. Microcomputer selection criteria.

A. Data acquisition and control microcomputer

1. Expandability
2. Availability of specialized boards and subsystems
3. Processor speed
4. Number crunching capability
5. Memory capacity
6. Popularity

B. Front end processor

1. Ease of use
    - Supports HPI tools
    - Implements an effective user interface
2. Memory capacity
3. Mass storage
4. Communications capability
5. Processor speed
6. Number crunching capability
7. Availability of applications software
8. Availability of AI languages and software
9. Expandability
10. Popularity

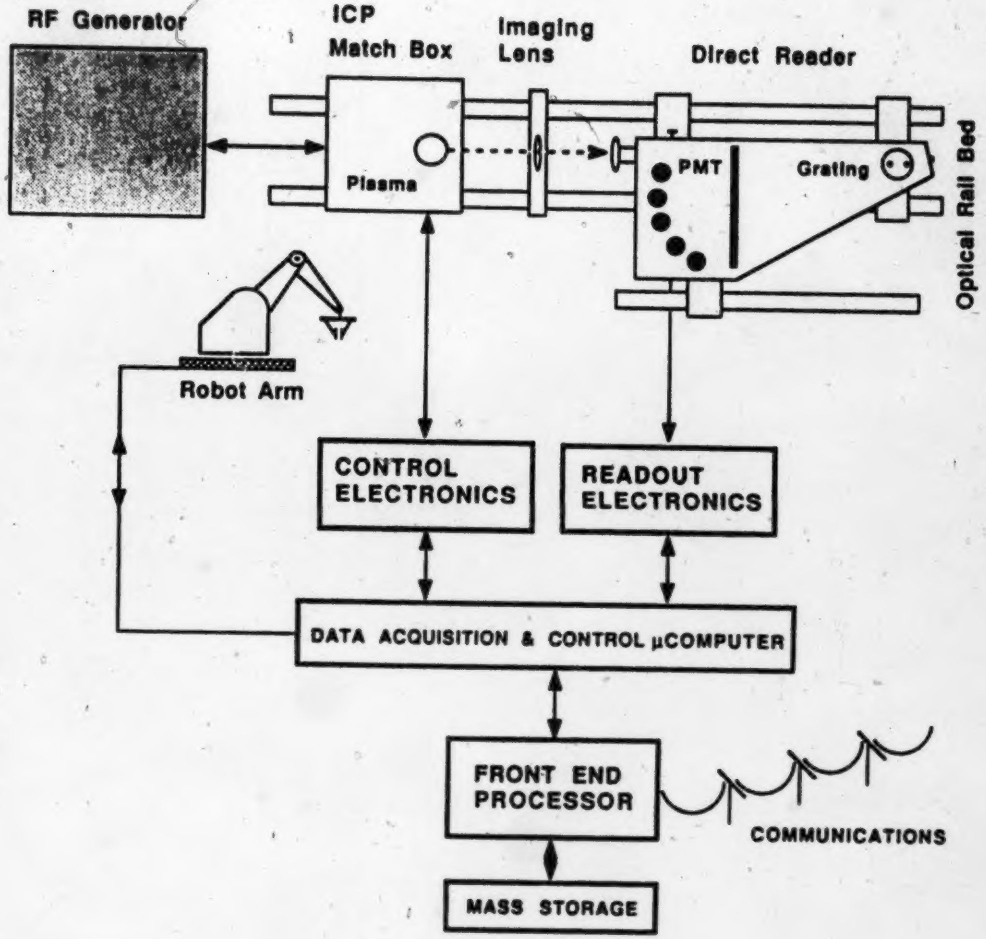
RF Generator
ICP
Match Box
Plasma
Imaging
Lens
Direct Reader
PMT
Grating
Optical Rail Bed
Robot Arm
CONTROL
ELECTRONICS
READOUT
ELECTRONICS
DATA ACQUISITION & CONTROL µCOMPUTER
FRONT END
PROCESSOR
COMMUNICATIONS
MASS STORAGE

Figure 5-1. Block diagram of a dual processor based inductively coupled plasma atomic emission spectrometer (ICP-AES).

B. Human Processor Interface Concepts

Perhaps the most important and revolutionary aspect of all HPIs is the user interface, which is that part of the system that bridges the gap between the user and the operator. Put otherwise, the user interface is a set of rule and conventions that allow the user to communicate with the computer [6, 7]. Central to the design of user interfaces are: high resolution bit mapped graphics; multiple windows; menus; icons; pictures or other graphic objects; and implementation of the desk top metaphor concept; and an easy command of the user interface which operates in conjunction with hardware devices for cursor control. This interface is usually interactive: it promotes a dynamic dialog between the user and the application. In this fashion, the application intercepts and interprets user specified actions and responds accordingly. High resolution graphics hardware and software are the key the design and implementation of such interfaces.

B.1 Graphics

Far too frequently, high resolution graphics implies simply the drawing of charts and spectra. The issue, in reality, is far more complex than that. The question is how to represent data or information on the screen. High resolution graphics and appropriate software allow users to treat the screen as an elaborate drafting table. The ability to place and easily manipulate arbitrary objects on the screen, including text, provides unparalleled flexibility. It also means that computer graphics can now accomplish a great deal more than simply drawing spectra, bar-graphs, pie-charts or scatter plots.

High resolution graphics also increases the effective communications bandwidth between the operator and the computer by displaying pictorial representations of the physical objects themselves rather than textual descriptions of them. The idea behind pictorial symbols or "icons" is quite simple: to convey the maximum amount of information in the least possible time, to avoid confusion by using pictorial representations that the user is already familiar with, and to provide a form of visual rather than textual or audio feedback. To use the old adage, a picture is worth a thousand words, icons convey a message far more effectively than words. Therefore, text-only or low resolution displays are no longer adequate, high resolution bit-mapped graphics are required. Such is the impetus behind bit-mapped graphics, that "*...the IBM PC, in its common monochrome screen form, is probably the last important text based microcomputer*" [8].

Although graphics hardware has become a significant consideration in laboratory computing, graphics software is paramount importance. Furthermore, user interfaces demand graphics software which is part of the architecture of the machines themselves, as opposed to a software package that has been added on as an afterthought. The reason for this is that for some applications and add-on software packages, screen updating becomes *"intolerably"* slow [9]. The need for high-speed built-in graphics software is so crucial to the design of user interfaces, that it has been included on all graphics oriented personal computers.

B.2 The Desk Top Metaphor

The desk top metaphor is a symbolic representation of a desk top and its associated tools (i.e., file folders, calculator, documents) on a computer display. Icons are the typical symbols utilized for these tools. In mapping the desk top onto the screen and by utilizing a *"point-and-click"* syntax, operating a computer becomes an exercise in intuition rather than a memorization test. As a consequence, computer systems become user friendly.

The point-and-click syntax (i.e., pointing a mouse at strategic locations on the screen and pressing its button) that stems from the select-then-choose paradigm (i.e., selecting an object on the screen and then choosing an operation from the menu), is exclusively utilized in most graphics oriented personal computers or software packages. Selecting an object, with no regard to its internal representation or data structure (i.e., text, graphics or spreadsheet cells) on the screen and then choosing an operation from the menu is similar to the way operations on physical objects are performed.

These concepts, derived from Smalltalk and the pioneering work of Alan Kay, were developed at Xerox's PARC (Palo Alto Research Center) and first implemented on the Xerox Star and Apple Lisa. Apple's Macintosh currently offers one of the best examples of a successful implementation of the desk top metaphor that heavily relies on the point-and-click syntax. Currently, the Commodore Amiga and the Atari ST also use these concepts.

B.3 The Apple Macintosh

For quite some time now, the Macintosh has been pointing the way to the future [9, 10]. With its new hardware and software concepts, it has changed the way users work with personal computers and represents both an opportunity and a challenge for use in the laboratory. The real impetus for its utilization is derived from a successful implementation of modern HPI concepts. Such is the impact the Macintosh user interface has already had, that it is expected to affect not only the design but also the design philosophy behind laboratory interfacing and computing.

The success the Macintosh's HPI enjoys is exemplified by its growing list of imitators. And although some users object to the use of a 'Mac-like' HPI, its growing popularity suggests that it has the potential to become the next *de facto* industry standard in much the same way as PC-DOS (and MS-DOS) has become a standard operating system for 8-bit microcomputers.

The most important concepts popularized on the Macintosh are its advanced software concepts and a unique implementation of the user interface, both of which are a crucial part of its architecture. The Macintosh can provide unique solutions to several software related laboratory needs. Of particular significance is the unique capability of Macintosh software to integrate text and graphic information with exceptional ease of interfacing with the operator, a result of its unique HPI. This includes: a mouse as a pointing device for cursor control; bit-mapped graphics that handle both text and graphics; a menu bar in association with pull-down menus for menu selection; multiple overlapping windows that serve as a two-way communications link with the user; icons; pictures; a unique implementation of the desk top metaphor, and an innovative operating system. At the heart of the Macintosh operating system there is the user interface ToolBox, which forms the basis for the implementation of the user interface [6, 7, 11].

The ToolBox can be loosely defined as a collection of routines occupying the entire contents of the Macintosh ROM, including the Operating system, QuickDraw and the User Interface routines. The ToolBox, as its name implies, is a 'box of tools', i.e., procedures and functions that can be used from within most programming languages. Having these tools pre-defined reduces the programming effort required to produce an application, thus alleviating the problem of having to re-invent the wheel. It also promotes software consistence and compatibility, since it enforces a proprietary standard. Having them in ROM, saves RAM space for the application.

A key feature of the Macintosh is its high resolution bit-mapped graphics: at the heart of the user interface, and part of the ToolBox, there is a set of routines called QuickDraw (developed by Apple fellow Bill Atkinson) which is one of the most versatile graphics packages ever developed. QuickDraw routines form the basis of the Macintosh user interface. Everything that appears on the screen, from text, to pictures, to icons, to menus and windows is handled by QuickDraw; the Macintosh does not have a text mode. Even printing is supported by QuickDraw, which is why the 'what you see, is what you get' concept has been so successfully implemented on the Macintosh.

The Macintosh's motherboard deviates from the traditional backplane bus concept that Apple itself helped establish with the introduction of the Apple II family of personal computers [3]. The Macintosh currently utilizes what Apple calls the *"virtual slot"* concept, which is implemented on high speed (up to 1 Mbit/s) RS-422 serial ports utilizing a Zilog Z8535 SCC (Serial Communications

Controller) [12]. The reasoning behind this concept is that, with plummeting hardware prices, peripherals have become smart enough (i.e., include a CPU, RAM, ROM, I/O devices) so that there is no need to tie-up the processor. Indeed, the current trend is to include local intelligence in a wide variety of peripheral devices. This, however, necessitates an efficient communications link between the processor and its peripheral devices. In order to increase the bandwidth of that communications link, the Macintosh Plus also includes an 8-bit parallel interface designed around the SCSI (Small Computer Systems Interface) standard, as described elsewhere [13, 14].

Although the lack of a backplane bus structure may keep the Macintosh from conventional laboratory data acquisition and control tasks, its communications capabilities and its unique HPI definitely give it a place in the laboratory as a front end processor. And, as such, is ideally suited for the development of user interfaces.

C. Instrument User Interface Considerations

The traditional form of an instrument user interface consists of controls, dials, indicators and chart recorders. The introduction of the personal computer in the laboratory has altered the nature of that interface. Two basic categories of instrument user interfaces have emerged. In the first, the instrument incorporates a computer inside it, and the user interacts with it via a control panel which is equipped with a display and a host of switches, controls and indicators. Design and implementation of that interface draws from the control panel concept. In the second category, there are instruments that are either controlled a computer terminal or incorporate a personal computer. In this case, the user deals with a traditional computer user interface rather than an instrument user interface.

Conventional computer based instrument user interfaces are typically keyboard based and therefore textual: characters typed at a keyboard serve as input, output is directed to a terminal or a printer. The basic form of this type of interface consists of a short question/answer period: the user responds to a computer generated prompt. If something goes wrong (i.e., a response that the computer does not 'like'), the computer either beeps, or it displays some form of a cryptic error message, or it wanders into the never-never land (i.e., 'hangs'), or it simply crashes. With the introduction of the IBM PC, cursor control keys, function keys and high resolution color graphics are becoming increasingly popular in laboratory applications. However, the user is still dealing with a computer rather than an instrument oriented user interface.

Recently new approaches have emerged for instrument user interfaces. These new approaches are Mac-like, in that they are window based, menu-driven, mouse-supporting and tend to use intensive graphics in an interactive mode [9, 15-17]. A key goal in the development of these new interfaces is, or should be, to make the front end processor's behavior 'instrument-like' as opposed to making the instrument 'computer-like', that is, to implement an ***instrument metaphor***.

The term instrument metaphor is derived in concept from the desk top metaphor: it is a pictorial representation of the actual instrument mapped onto the computer screen where it appears as a graphic version of the original.

An example of an instrument metaphor is shown in Figure 5-2 for the ICP-AES instrument described earlier and depicted in pictorial form in Figure 5-1 in a more traditional block diagram format. At this point the instrument metaphor appears to be, perhaps, a somewhat cryptic representation of the instrument. However, as will be seen in the next sections, it is actually the base for a powerful menu that allows the instrument operator to control, operate and monitor the instrument from the screen, access extensive knowledge bases about the instruments' operation and technique utilization and exchange data with other applications programs such as spreadsheets and graphics programs.

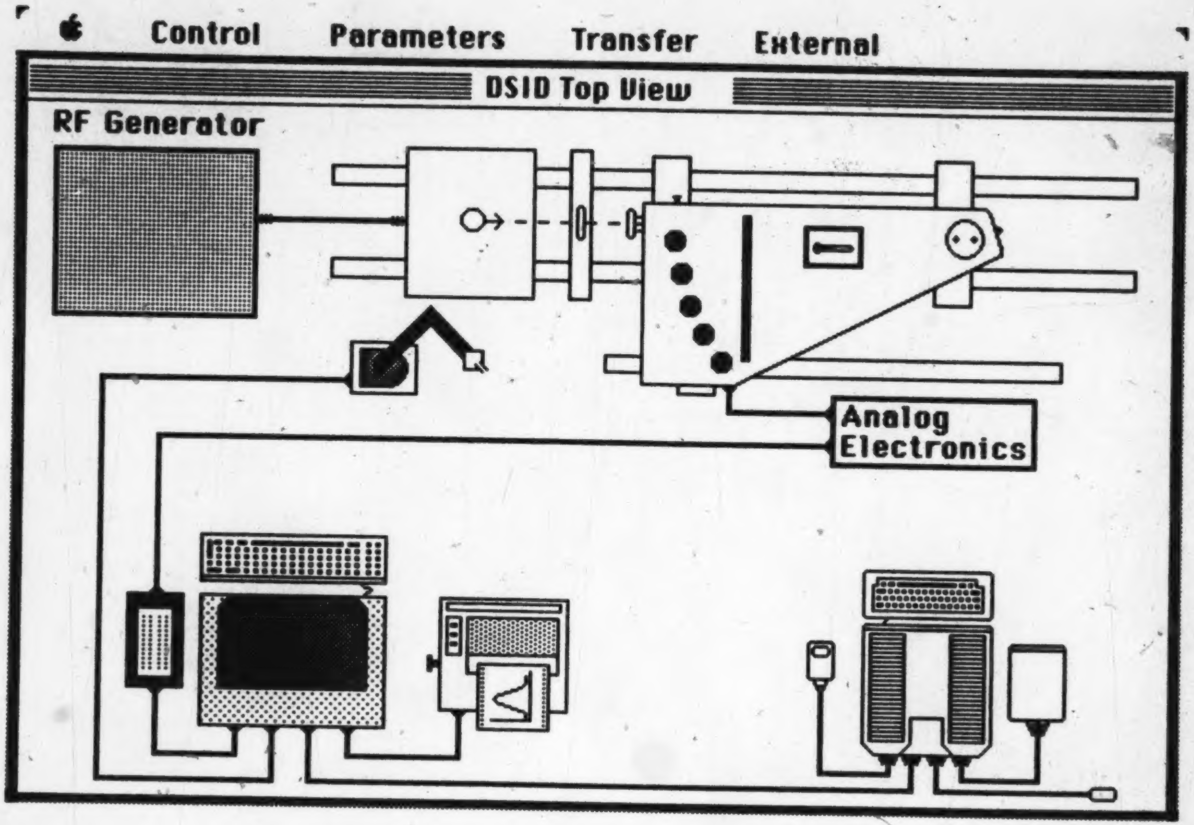
Control
Parameters
Transfer
External
DSID Top View
RF Generator
Analog
Electronics

Figure 5-2. Instrument metaphor for the ICP-AES.

Thus a key aspect of the instrument user interface is the instrument metaphor concept applied as a menu. The power of this approach comes when it is used in conjunction with the point-and-click syntax, multiple overlapping windows and pull-down menus. By clicking at locations on this instrument metaphor, multiple levels of overlapping windows appear on the screen that provide various dimensions of additional graphic and text information about the system.

A window is probably the most powerful means of establishing and maintaining a meaningful dialog between the computer and the operator: the program displays information in it and the user instructs it what the next step will be by clicking at strategic locations on the screen. In other words, the user controls what will take place and in what sequence: this is accomplished by instructing the computer what to do next and not allocating this task to the program or the programmer behind it. In this way, the user does not have to go through a question/answer period in order to get at a particular level: the level of information desired becomes available only when a particular region of the screen is activated, otherwise it remains inactive until is recalled. The number of options available, and, therefore, the number of levels of information that can be made accessible by the user can be increased by taking advantage of pull-down menus. In this way, the type of information presented in a window depends on a pull-down menu selection.

These ideas have been applied to the design of an instrument user interface for ICP-AES which is described in the next section. This program should be regarded as a prototype, illustrating both concepts and implementation.

D. ICP-AES Instrument User Interface

The instrument user interface described in this section was written in Modula-2 [18]. It has been designed around four programs and several 'Help' and 'Explain' files. The software package currently occupies over 700 thousand bytes of disk space and runs on a 512 k Macintosh.

D.1 The Instrument Metaphor

The basic instrument metaphor for this system was introduced in the last section and is shown in Figure 5-2. This graphic representation of the ICP-AES instrument, in combination with the menu bar, is the 'menu' for the system. From it, all system parameters can be controlled, read out and understood.

Most graphic regions representing objects on the screen are active, that is, they can be activated by pressing the mouse button when the arrow cursor is located anywhere within the graphic object displayed on the screen. This operation is often referred to as 'clicking the mouse'. When a region is activated, a new window appears on the screen. This new window usually displays information pertinent to the graphically represented object just clicked. The type of information displayed in window often depends on a menu selection. The active areas on the screen for the main program are shown labeled A through O in Figure 5-3a. A short description of the objects they graphically represent is given in Table 5-2. It should be stressed that the labels shown in Figure 5-3a are _not_ part of the actual display: they have only been added on for the purposes of discussion.

In order to obtain information about any part of the instrument, one simply 'clicks' on the appropriate graphic region. Placing the arrow cursor anywhere within the graphic region labeled A in Figure 5-3a, that is the rectangle ascribed by 'opqr', and by pressing the mouse button at that location, a new window that contains an exploded view of the radio frequency generator appears on the screen, as illustrated in Figure 5-3b. Clicking the mouse anywhere within the rectangle ascribed by 'stvu', a new window that displays the IBM PC is shown on the screen, as shown in Figure 5-3c. Similarly, by clicking the mouse anywhere within the graphic region labeled B in Figure 5-3a, that is within the rectangle ascribed by 'wxyz', a new window that displays the ICP match box appears on the screen, as shown in Figure 5-3d. These windows can be easily dismissed by the user. This is achieved either by

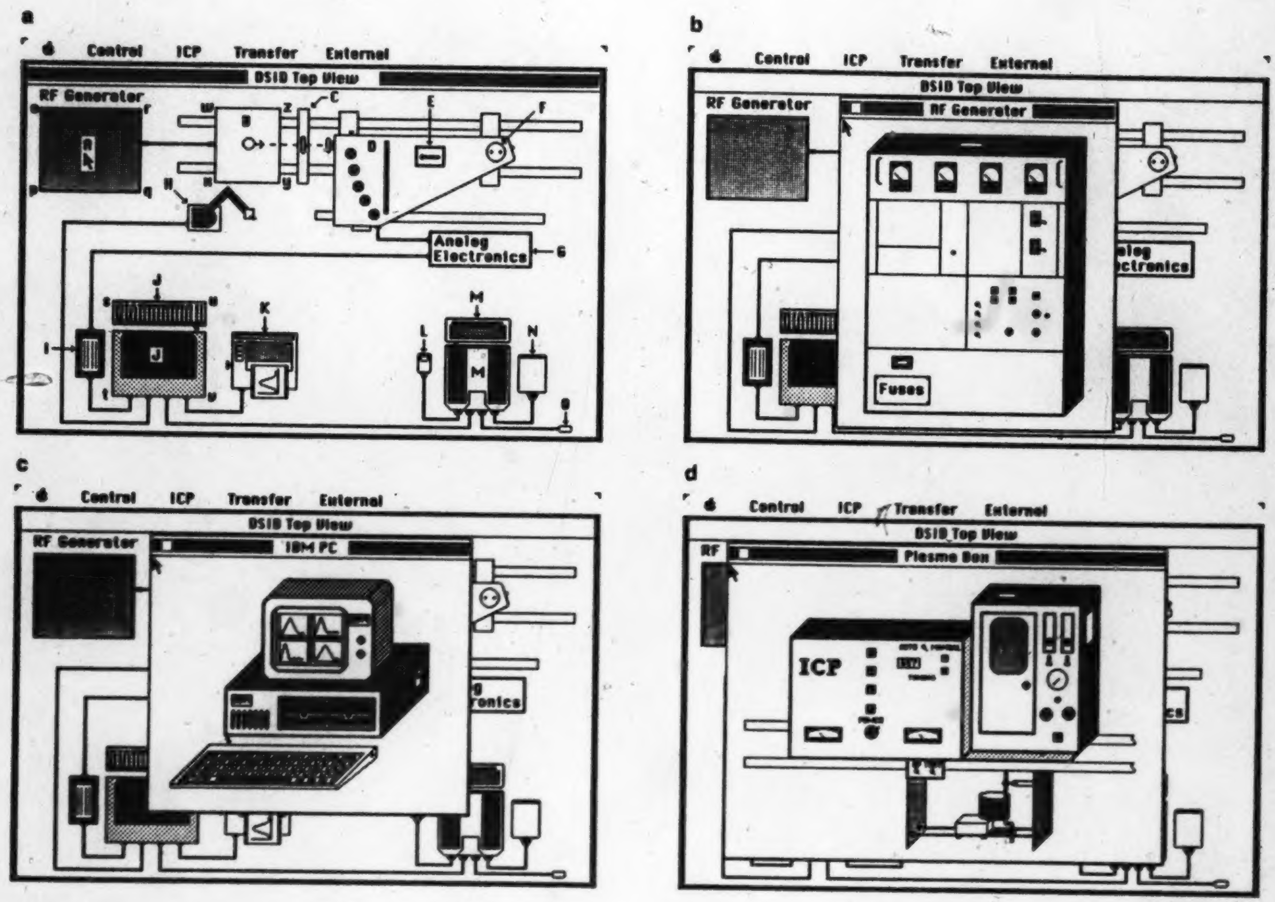
a
Control
ICP
Transfer
External
DSID Top View
RF Generator
Analog Electronics
b
Control
ICP
Transfer
External
DSID Top View
RF Generator
RF Generator
Fuses
c
Control
ICP
Transfer
External
DSID Top View
RF Generator
IBM PC
d
Control
ICP
Transfer
External
DSID Top View
RF
Plasma Box
ICP

Figure 5-3. Examples of first level windows accessible by clicking on the instrument metaphor (a) at location (A) (b), location J (c), and location B (d).

clicking on the window's GoAway box (located in the upper left corner of the window), or by clicking the mouse anywhere outside the window. This first level window is available for all active areas as listed in Table 5-2 and depicted in Figure 5-3a. Thus the instrument operator can quickly 'see' the various parts of the instrument.

The windows shown in Figures 5-3b, 5-3c and 5-3d are clickable in themselves. This is shown in Figure 5-4 for the RF Generator window. Its active regions have been labeled A through G for convenience and are shown in Figure 5-4a. Clicking the mouse on top of the generator (region A) brings up the window shown in Figure 5-4b. This window provides the basic specifications of the RF generator. Similarly, clicking on the control panel (region E) brings up the window shown in Figure 5-4c. Included in this window are an expanded view of the RF Generator control panel and a definition of each knob, control and indicator that appears on it. The final example is the window shown in Figure 5-4d which results from clicking on the on/off switch (region F) of the generator. This window provides details of the complete power-on procedure.

These simple illustrations begin to show the power of this instrument user interface. A great deal of detailed information about the instrument can be quickly accessed by the user on a need to know basis. One does not have to serially work through a conventional printed manual, but in a

Table 5-2. Main program active areas.

A: Radio frequency generator
B: ICP matching box
C: Lens assembly
D: Polychomator channels
E: Temperature sensor
F: Grating assembly
G: Analog electronics
H: Robot arm
I: Custom designed interface
J: IBM PC and keyboard
K: Epson printer
L: Macintosh mouse
M: Macintosh
N: Macintosh external disk drive
O: AppleTalk node

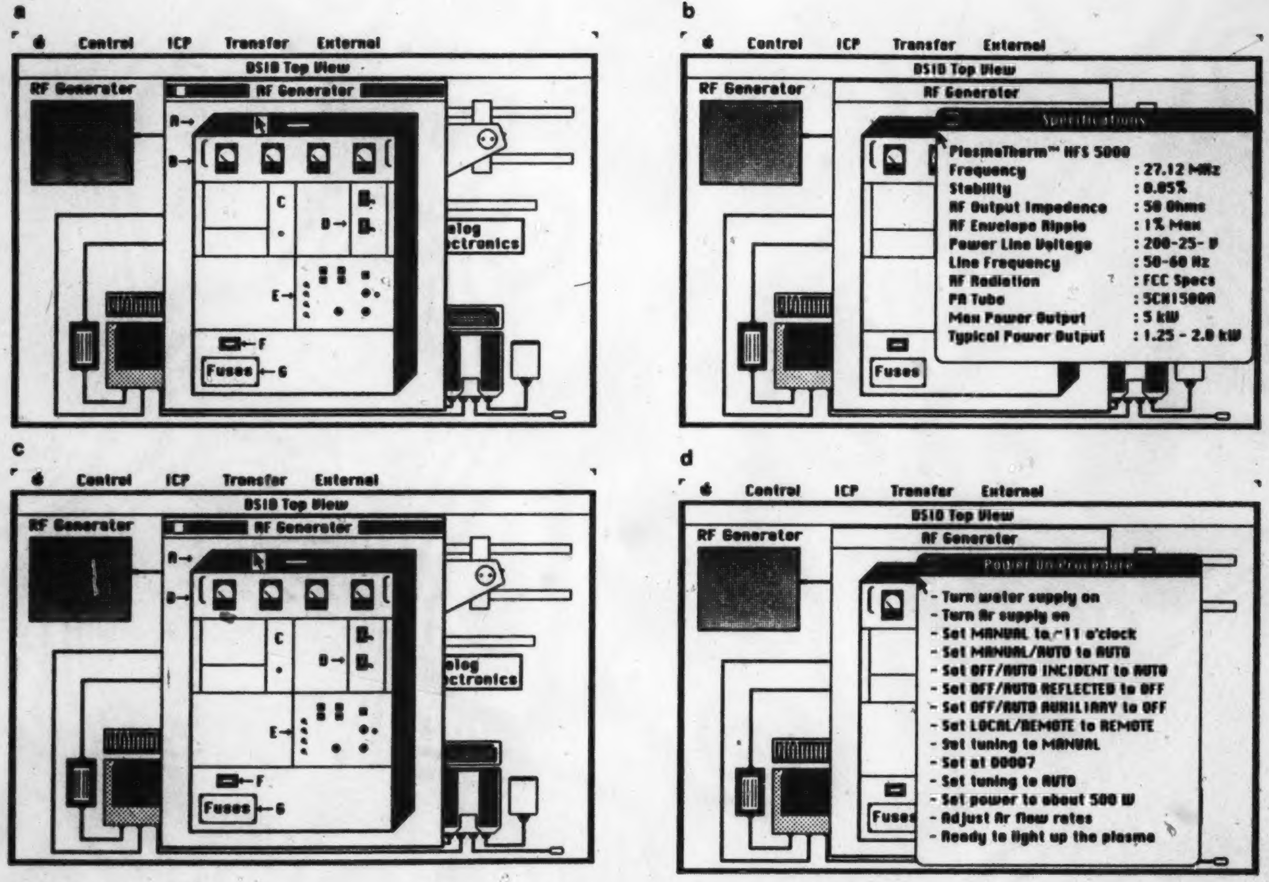
a
Control
ICP
Transfer
External
DSID Top View
RF Generator
RF Generator
A→
B→
C
D→
E→
F
Fuses
G
alog
ctronics
b
Control
ICP
Transfer
External
DSID Top View
RF Generator
RF Generator
Specifications
Fuses
c
Control
ICP
Transfer
External
DSID Top View
RF Generator
RF Generator
A→
B→
C
D→
E→
F
Fuses
G
alog
ctronics
d
Control
ICP
Transfer
External
DSID Top View
RF Generator
RF Generator
Power On Procedure
Fuses

PlasmaTherm™ HFS 5000

Frequency	: 27.12 MHz
Stability	: 0.05%
RF Output Impedence	: 50 Ohms
RF Envelope Ripple	: 1% Max
Power Line Voltage	: 200-25- V
Line Frequency	: 50-60 Hz
RF Radiation	: FCC Specs
PA Tube	: 5CX1500A
Max Power Output	: 5 kW
Typical Power Output	: 1.25 - 2.0 kW

- Turn water supply on
- Turn Ar supply on
- Set MANUAL to ~11 o'clock
- Set MANUAL/AUTO to AUTO
- Set OFF/AUTO INCIDENT to AUTO
- Set OFF/AUTO REFLECTED to OFF
- Set OFF/AUTO AUXILIARY to OFF
- Set LOCAL/REMOTE to REMOTE
- Set tuning to MANUAL
- Set at 00007
- Set tuning to AUTO
- Set power to about 500 W
- Adjust Ar flow rates
- Ready to light up the plasma

Figure 5-4. Examples of second level windows accessible by clicking the RF Generator window (a) at location A (b), location E (c), and location F (d).

highly interactive and parallel fashion, various levels of information can be obtained with a few mouse clicks.

However, the simple point-and-click syntax may not be sufficient to access certain types of information about a part of the instrument. In such cases, information is obtained by a combination of graphic windows and pull-down menu selections. Clicking the mouse on the Macintosh graphic region (region M of Figure 5-3a) brings up the window shown in Figure 5-5a clearly indicating that this system component is a Macintosh personal computer. However, note that at the same time, a new menu specific to this window has been installed on the menu bar.

Also, in order to alert the user, the Macintosh, with its voice output capabilities and through its loudspeaker, informs the user that a new menu has become active. The menu items pertinent to this window are shown in Figure 5-5b. By selecting the "Specifications" item of the "Macintosh" menu a new window (Figure 5-5c) that displays the specifications of the Macintosh appears on the screen. Similarly, by selecting the "Bus Structure" item from the same menu, a block diagram of the bus structure supported by the Macintosh is displayed on a new window (Figure 5-4d) that appears on the screen. Similar behaviour is observed for the other menu items. When the "Macintosh" window is dismissed by the user, the "Macintosh" menu is removed from the menu bar. In this way, while a limited number of menus

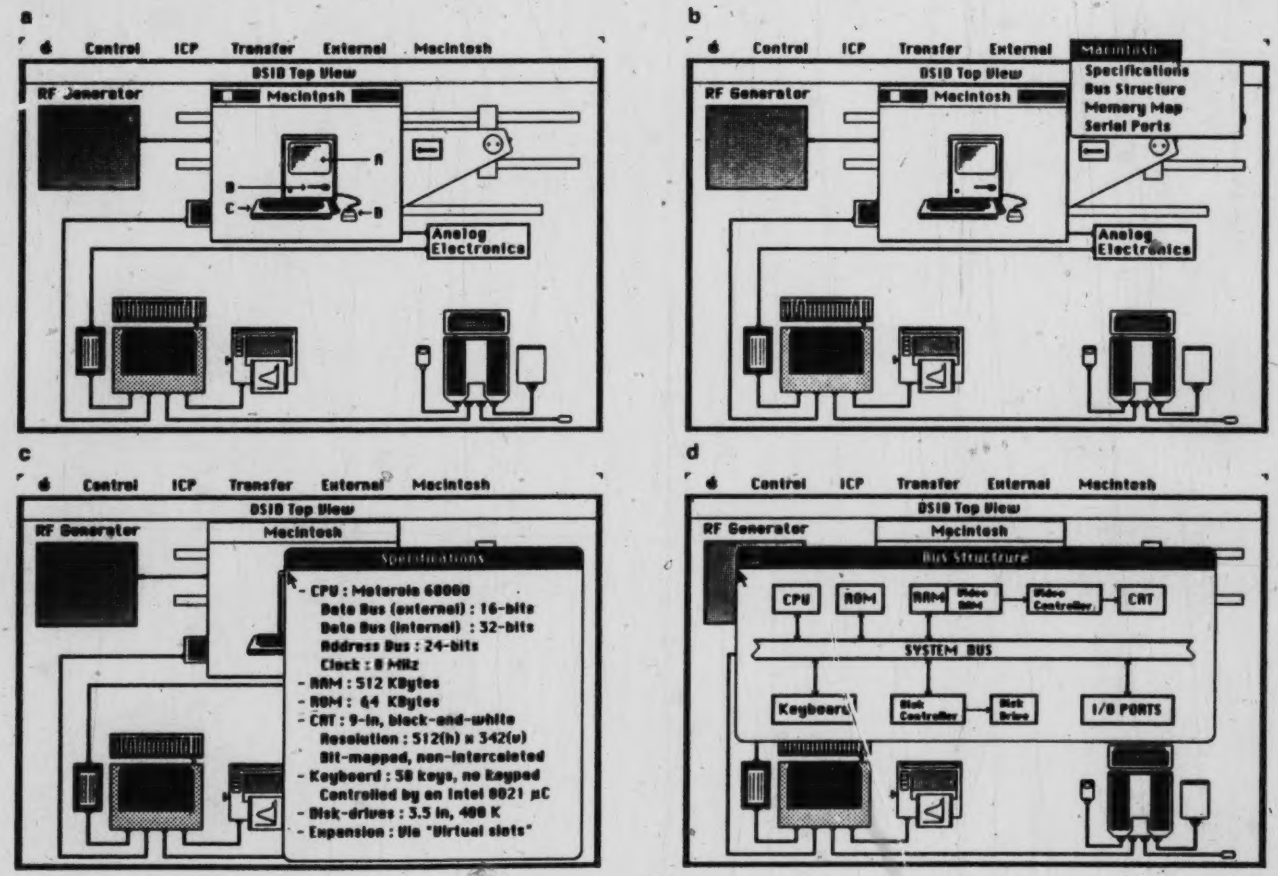
a
Control
ICP
Transfer
External
Macintosh
DSID Top View
RF Generator
Macintosh
A
B
C
D
Analog Electronics
b
Macintosh
Specifications
Bus Structure
Memory Map
Serial Ports
c
Specifications
d
Bus Structure
CPU
ROM
RAM
Video RAM
Video Controller
CRT
SYSTEM BUS
Keyboard
Disk Controller
Disk Drive
I/O PORTS

- CPU : Motorola 68000
  Data Bus (external) : 16-bits
  Data Bus (internal) : 32-bits
  Address Bus : 24-bits
  Clock : 8 MHz
- RAM : 512 KBytes
- ROM : 64 KBytes
- CRT : 9-in, black-and-white
  Resolution : 512(h) x 342(v)
  Bit-mapped, non-intercalated
- Keyboard : 58 keys, no keypad
  Controlled by an Intel 8021 µC
- Disk-drives : 3.5 in, 400 K
- Expansion : Via "Virtual slots"

Figure 5-5. (a) The Macintosh window accessed by clicking on location M of Figure 5-3a, (b) the Macintosh pull down menu, (c) and (d) are secondary windows accessible from the Macintosh pull down menu.

appear on the menu bar at any given time, new information levels can be added by simply placing new items on the menu bar. This combination provides a powerful means for information retrieval and instrument control.

D.2 Parameter Readout and Control

The window for the ICP match box and torch enclosure was shown in Figure 5-3d. This figure is repeated as Figure 5-6a with the active areas labeled A through J for convenience of discussion. The information and course of action for this part of the program is highly dependent on window/menu selections.

The default state of the "ICP" menu items is shown in Figure 5-7a. Some items can assume either of two states: they can be toggled between On and Off, and can be thought of the software equivalent of a toggle switch. This is demonstrated on the "Monitor" and "Power" items with their states shown in Figures 5-7a and 5-7b and Figures 5-7a and 5-7c, respectively. Some of the "ICP" menu items are inter-dependent, as is the case between "Power", "Diagnostics" and "Line Profile": when "Power Off" is selected, these items are disabled, as shown in Figures 5-7a and 5-7b; when "Power On" is selected they become enabled, as shown in Figure 5-7c and Figure 5-7d. Other items, such as "Monitor On", Monitor Off" and "Monitor All" can be set independently.

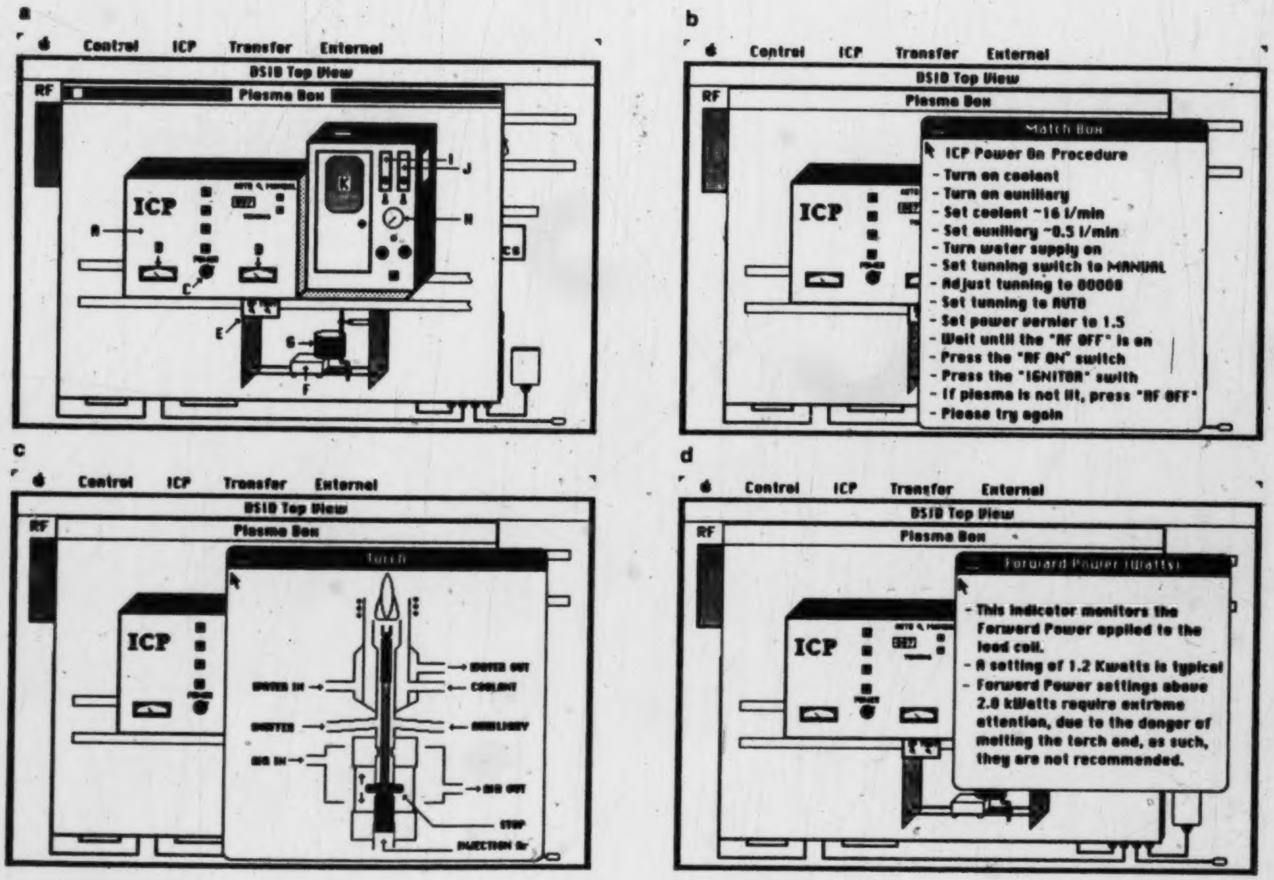
a
b
c
d
Control
ICP
Transfer
External
DSID Top View
RF
Plasma Box
ICP
A
B
C
D
E
F
G
H
I
J
K
CS
Match Box
Torch
WATER IN
IGNITER
AIR IN
WATER OUT
COOLANT
AUXILIARY
AIR OUT
STOP
INJECTION Ar
Forward Power (Watts)

ICP Power On Procedure

- Turn on coolant
- Turn on auxiliary
- Set coolant ~16 l/min
- Set auxiliary ~0.5 l/min
- Turn water supply on
- Set tunning switch to MANUAL
- Adjust tunning to 00000
- Set tunning to AUTO
- Set power vernier to 1.5
- Wait until the "RF OFF" is on
- Press the "RF ON" switch
- Press the "IGNITOR" swith
- If plasma is not lit, press "RF OFF"
- Please try again

- This indicator monitors the Forward Power applied to the load coil.
- A setting of 1.2 Kwatts is typical
- Forward Power settings above 2.0 kWatts require extreme attention, due to the danger of melting the torch end, and, as such, they are not recommended.

Figure 5-6. Examples of second level windows (Monitor Off) accessible by clicking on the Plasma Box window (a) at location A (b), location K (c) and location B (d).

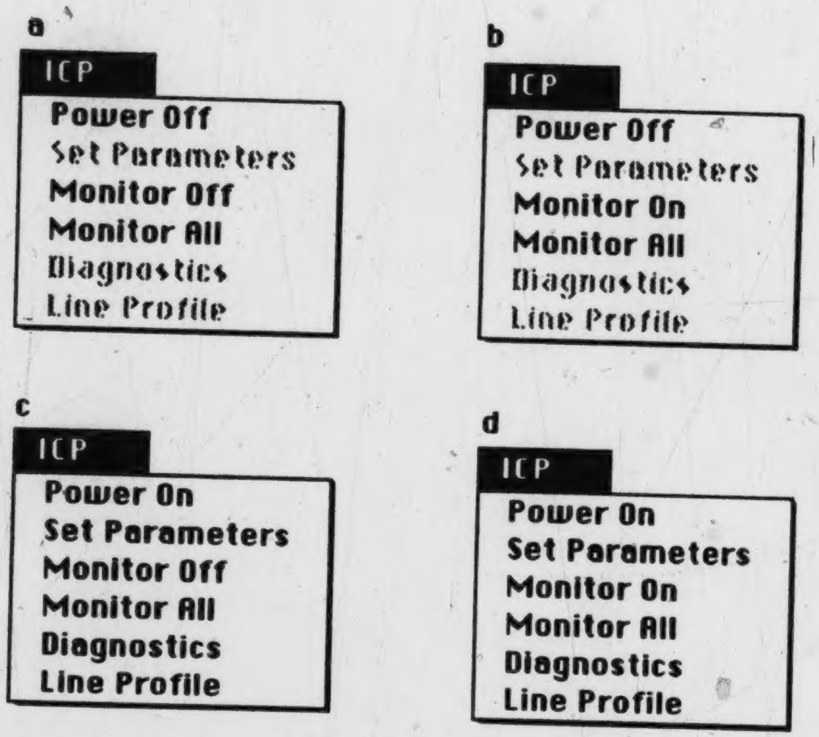
a
ICP
Power Off
Set Parameters
Monitor Off
Monitor All
Diagnostics
Line Profile
b
ICP
Power Off
Set Parameters
Monitor On
Monitor All
Diagnostics
Line Profile
c
ICP
Power On
Set Parameters
Monitor Off
Monitor All
Diagnostics
Line Profile
d
ICP
Power On
Set Parameters
Monitor On
Monitor All
Diagnostics
Line Profile

Figure 5-7. The ICP pull down menu (see text for discussion).

The result of clicking the mouse at selected graphics regions on the ICP plasma box window with the "Monitor Off' menu item selected provides basic information about the selected item. For example, clicking on the match box control panel (region A of Figure 5-6a) brings up the window shown in Figure 5-6b which gives the ~~ICP~~s ignition sequence. Clicking the mouse on the door of the torch box (region K, Figure 5-6a) brings up a graphic window showing the torch configuration for this particular experiment (Figure 5-6c). This is a direct sample insertion system in which a sample carrying cup is pneumatically injected into the plasma. This system has been described in the literature [19, 20]. As a final example, clicking on one of the meters (region B) brings up the window shown in Figure 5-6d, where information about the forward power meter is presented. However, when the "Monitor On" menu item is selected, as shown in Figure 5-7d, a completely different level of information is accessed.

Now, clicking the mouse on the forward power meter (region B of Figure 5-6a) brings up the window shown in Figure 5-8a. As stated in the title of this paper, both implementation and concepts are being discussed and this example is in the realm of concept. Sensors that deliver the actual real time readings to the Macintosh via the IBM PC have not yet been connected. However, it is a conceptual goal that the indicators shown in Figure 5-8a should

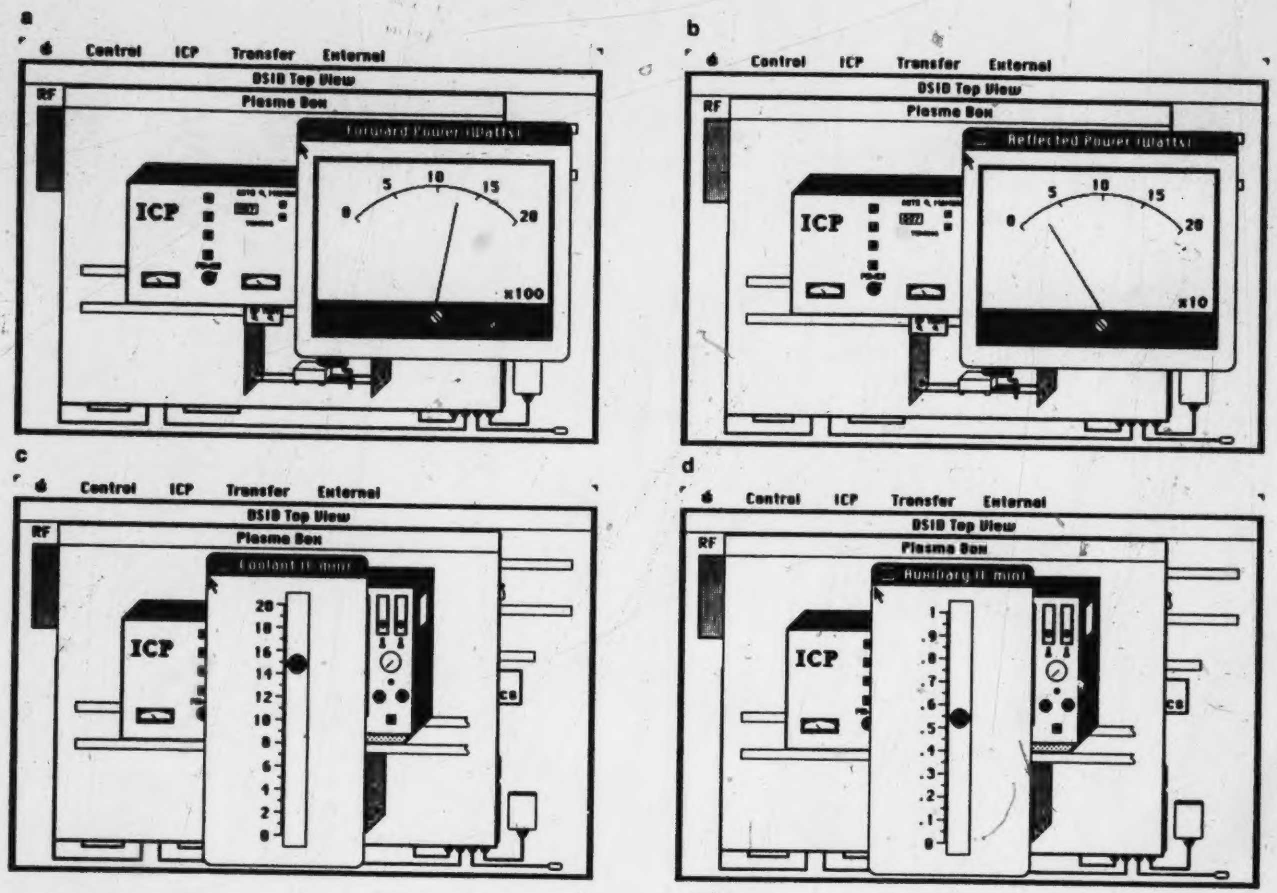
a
Control
ICP
Transfer
External
DSID Top View
RF
Plasma Box
Forward Power (Watts)
ICP
0
5
10
15
20
x100
b
Control
ICP
Transfer
External
DSID Top View
RF
Plasma Box
Reflected Power (Watts)
ICP
0
5
10
15
20
x10
c
Control
ICP
Transfer
External
DSID Top View
RF
Plasma Box
Coolant (l/min)
ICP
20
18
16
14
12
10
8
6
4
2
0
d
Control
ICP
Transfer
External
DSID Top View
RF
Plasma Box
Auxiliary (l/min)
ICP
1
.9
.8
.7
.6
.5
.4
.3
.2
.1
0

Figure 5-8. Examples of second level windows (Monitor On) accessible by clicking on the Plasma Box (window Figure 5-6a) at location B (a), location D (d), location J (c) and location I (d).

provide an actual, animated, real time readout of forward power. Similarly, when the reflected power meter (region I) and auxiliary meter (region D of Figure 5-6a), coolant meter (region I) and auxiliary meter (region J) are clicked, the windows shown in Figures 5-8b, 5-8c and 5-8d are accessed respectively. Again, it is a goal that these would, in fact, all provide active animated real time readout of the selected parameters when sensors are fully interfaced.

There are instances, of course, when the user may wish to view all indicators simultaneously rather than take the reading of one indicator at a time. The "Monitor All" menu item of the "ICP" menu, as shown in Figure 5-7, provides a comprehensive view of the instrument's status by displaying all indicators simultaneously. When selected, the status of all indicators appears on the screen, as shown in Figure 5-9. Furthermore, animation can be included in such a way that whatever changes occur in the ICP parameters, they are immediately represented on the screen can be easily monitored. Even the electrode's movement could be animated, so that the user could follow it on the screen as it is being inserted into the torch. And since the actual indicators are dispersed in different panels of the actual instrument, the ability to bring all indicators together, display them in a single window and monitor them simultaneously, would provide unparalleled flexibility.

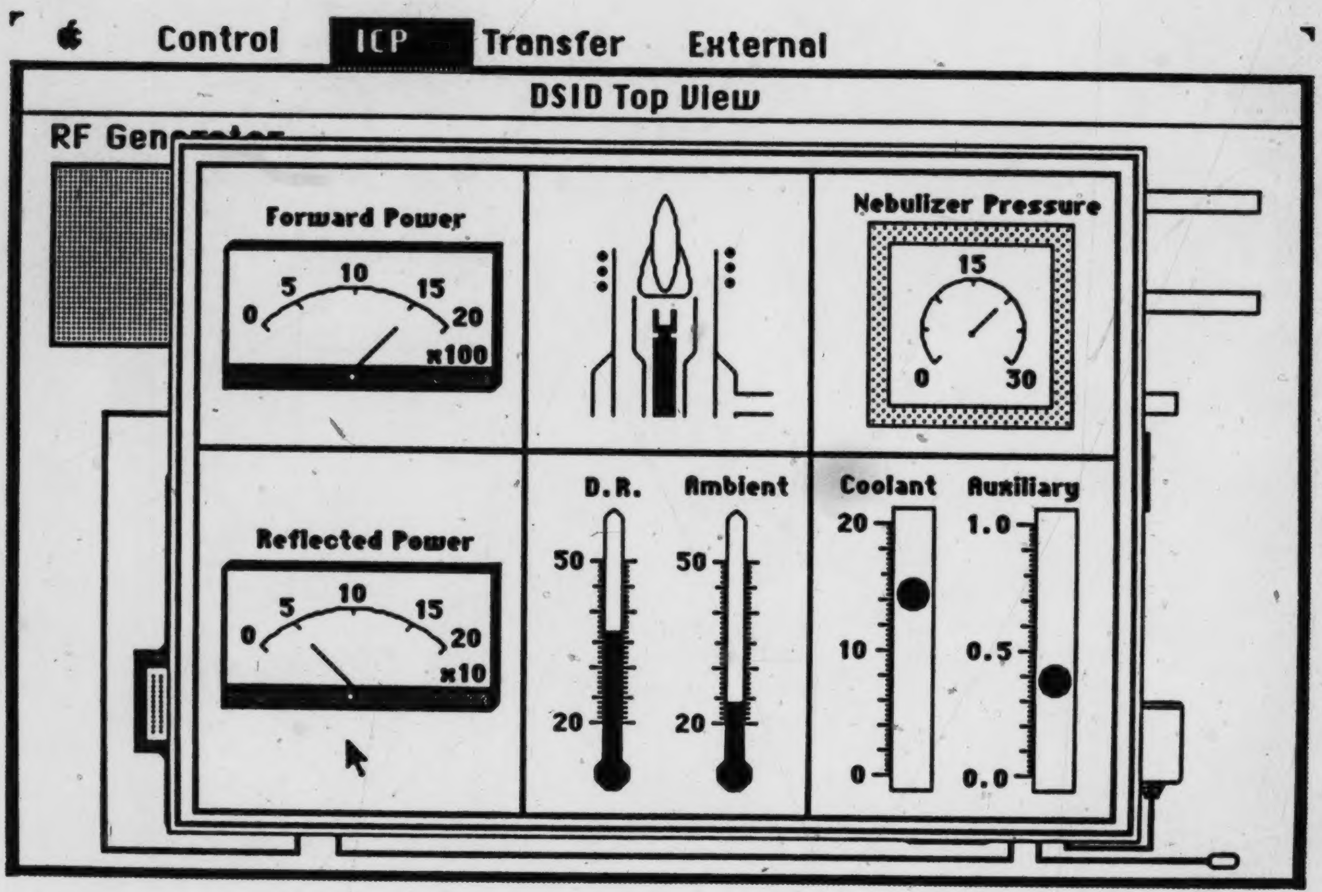
Control
ICP
Transfer
External
DSID Top View
RF Gen
Forward Power
0
5
10
15
20
x100
Nebulizer Pressure
15
0
30
Reflected Power
0
5
10
15
20
x10
D.R.
Ambient
50
20
50
20
Coolant
Auxiliary
20
10
0
1.0
0.5
0.0

Figure 5-9. The window display for "Monitor All" selected from the ICP menu.

Thus far, a one way communications link has been established between the operator and the instrument. However, the ability to manipulate and set ICP parameters is of paramount importance in analytical instrumentation: it allows complete instrument control from the computer's screen. This is the function of the "Set Parameters" item of the "ICP" menu (Figure 5-7). When it is selected, a new program is loaded and executed. And although this program retains the same visual interface as before, as shown in Figure 5-10a, new menus are installed on the menu bar. The "Parameters" menu, shown in Figures 5-10b and 5-10d has two items: one allows the setting of ICP parameters, the other of electrode related parameters. When "Plasma" is selected from the "Parameters" menu, as shown in Figure 5-10b, the menu bar displays the "Plasma" menu as shown in Figure 5-10a, with its menu items shown in Figure 5-10c. When the "Electrode" menu item is selected from the "Parameters" menu, as shown in Figure 5-10d, the menu bar changes to reflect the new parameters. The "Plasma" menu disappears from the menu bar, and the "Electrode" menu, whose items are shown in Figure 5-10e, is installed on the menu bar. Although similar considerations apply for both menus, our focus will be on the "Plasma" menu and its items.

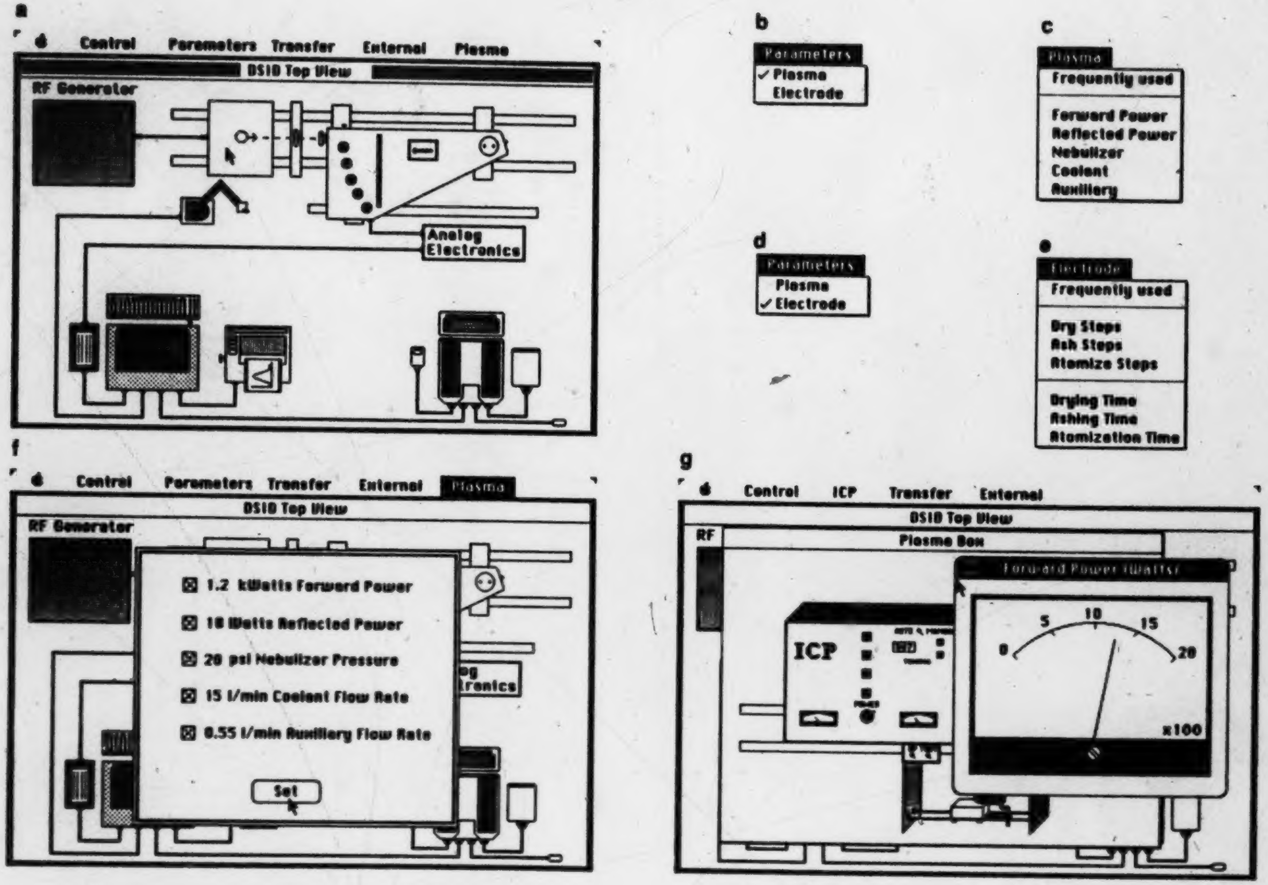
a
Control
Parameters
Transfer
External
Plasma
DSIO Top View
RF Generator
Analog Electronics
b
Parameters
✓ Plasma
Electrode
c
Plasma
Frequently used
Forward Power
Reflected Power
Nebulizer
Coolant
Auxiliary
d
Parameters
Plasma
✓ Electrode
e
Electrode
Frequently used
Dry Steps
Ash Steps
Atomize Steps
Drying Time
Ashing Time
Atomization Time
f
Set
g
ICP
RF
Plasma Box
Forward Power (Watts)
0
5
10
15
20
x100

☒ 1.2 kWatts Forward Power

☒ 18 Watts Reflected Power

☒ 20 psi Nebulizer Pressure

☒ 15 l/min Coolant Flow Rate

☒ 0.55 l/min Auxiliary Flow Rate

Figure 5.10. (a) The main screen display and (b-e) menu bar options and selections when "Set Parameters" is selected from the ICP pull down menu, (f) window display when "Frequently used" is selected form the "Plasma" pull down menu, (g) Plasma Box window for "Set parameters" program.

The various plasma parameters that can be individually set are shown in Figure 5-10c. In certain cases, as in routine analysis, there is little day-to-day variation in the setting of ICP parameters. Furthermore, setting the ICP parameters individually is an error prone and time consuming operation. The "Frequently used" menu item of the "Plasma" menu, shown in Figure 5-10c, has been included to remedy the situation. When selected, a window displaying some of the most frequently used parameters appears on the screen (Figure 5-10f). Any or all parameters can then be set by simply clicking the mouse on the appropriate check box, the user does not have to go through each indicator individually. Setting of ICP parameters on an individual basis can be accomplished either by a menu selection (Figure 5-10c) or by clicking the mouse on selected graphics regions (Figure 5-10g) of the ICP plasma box window.

In this program, when the mouse is clicked on the forward power meter (region A of Figure 5-10g), the window shown in Figure 5-11a appears. This window displays both an analog and a digital readout of the forward power along with a scroll bar. The desired power can be selected by using the up and down arrows of the scroll bar or by moving the scroll box, all easily manipulated using the mouse as on any standard Macintosh scroll bar. Clicking on the "Set" button would actually set the reflected the selected forward power. Similar windows are shown for setting the

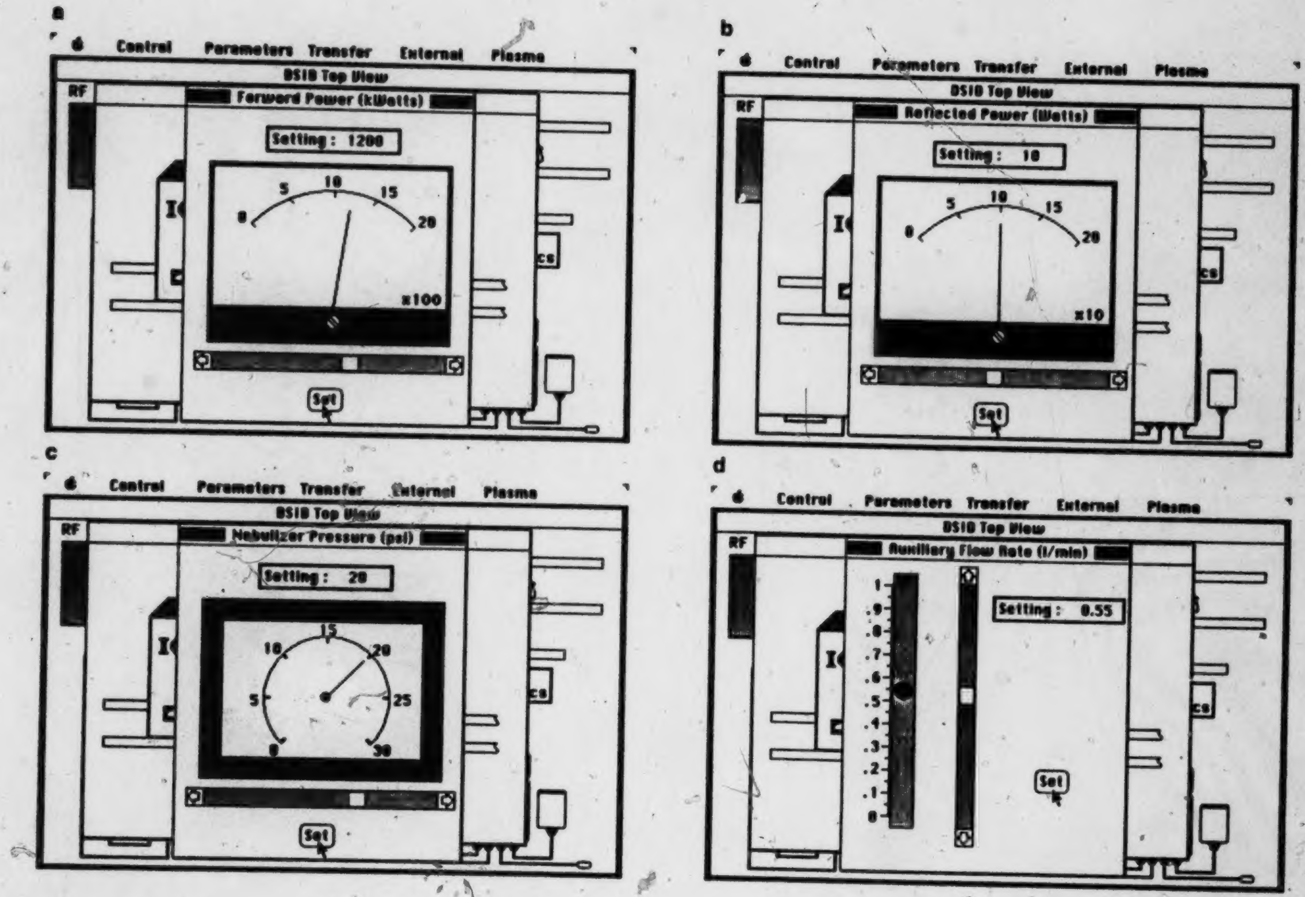
a
Control
Parameters
Transfer
External
Plasma
DSIO Top View
RF
Forward Power (kWatts)
0
5
10
15
20
x100
Set
b
Reflected Power (Watts)
x10
c
Nebulizer Pressure (psi)
0
5
10
15
20
25
30
d
Auxiliary Flow Rate (l/min)
1
.9
.8
.7
.6
.5
.4
.3
.2
.1
0

Setting : 1200

Setting : 10

Setting : 20

Setting : 0.55

Figure 5-11. Examples of secondary windows for the Plasma Box window (Figure 5-10g) of the "Set Parameters" program accessed by clicking locations A (a), B (b), C (c) and E (d).

reflected power threshold, nebulizer pressure and auxiliary flow rate, as shown in Figures 5-11b, 5-11c and 5-11d. Again, it should be emphasized that this is a conceptual illustration. Hardware sensors and controls that actually implement this part of the program are not yet in place.

With the ability of the system to set and monitor ICP parameters it is possible to built-in simple safeguards to help avoid inappropriate settings. For example, assume that normal coolant flow rates used in the laboratory are in the range of 15 l/min and suppose that a new or inexperienced operator set coolant flow rate too low as shown in Figure 5-12b. Clicking the "Why?" button brings up the window shown in Figure 5-12c which provides a brief explanation of the anticipated problem. The "History" button lists the last nine settings so that the new operator can see the normally used settings. In fact, these previous settings are used to control when the alert window is activated. For example, if the new setting is within plus or minus 1 l/min of the average of the last four settings, the alert window never appears on the screen, otherwise is automatically activated. In effect, this is a primitive form of self-learning in which the program decides the flow of information based on previous settings and operator responses.

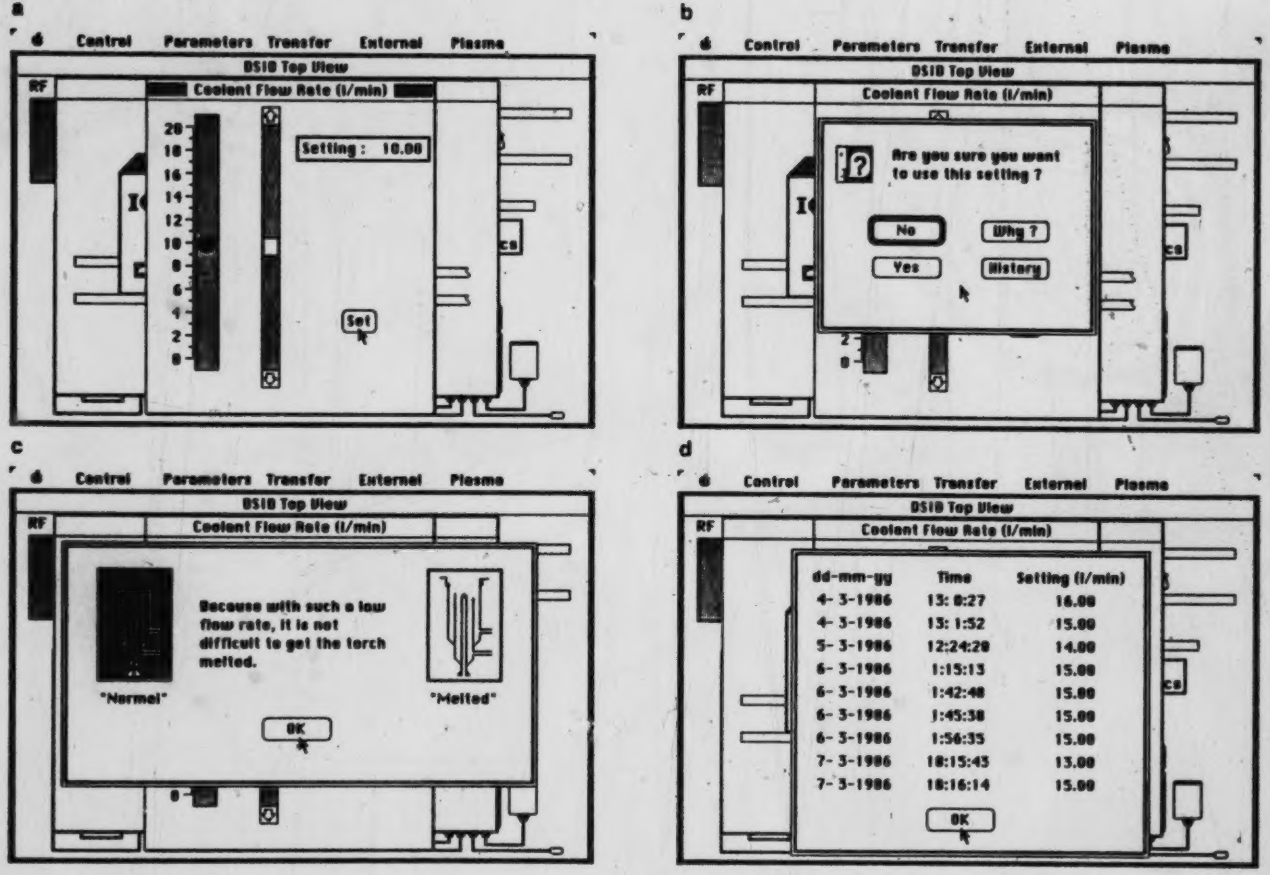
a
Control
Parameters
Transfer
External
Plasma
DSI0 Top View
RF
Coolant Flow Rate (l/min)
20
18
16
14
12
10
8
6
4
2
0
Set
b
No
Yes
Why ?
History
c
"Normal"
"Melted"
OK
d
OK

Setting : 10.00

Are you sure you want to use this setting ?

Because with such a low flow rate, it is not difficult to get the torch melted.

dd-mm-yy	Time	Setting (l/min)
4- 3-1986	13: 0:27	16.00
4- 3-1986	13: 1:52	15.00
5- 3-1986	12:24:20	14.00
6- 3-1986	1:15:13	15.00
6- 3-1986	1:42:40	15.00
6- 3-1986	1:45:38	15.00
6- 3-1986	1:56:35	15.00
7- 3-1986	10:15:43	13.00
7- 3-1986	10:16:14	15.00

Figure 5-12. (a) Secondary window for setting coolant flow rate, (b) Alert window indicating a potential problem and (d) History window giving last 9 settings.

D.3 Spectral Data Base Access and Display

One of the most important data bases associated with ICP-AES is that listing analytical lines, potential spectral interferences and specific operating conditions. This data base is built into the instrument user interface and can be accessed via the direct reader graphics region on the instrument metaphor. The main instrument metaphor is shown in Figure 5-13a along with three information windows associated with the direct reader. Clicking on the grating end of the direct reader (region A) brings up the window shown in Figure 5-13b, which is the basic optical schematic of the direct reader. If the "Monitor On" option on the "ICP" menu is chosen (Figure 5-7), then clicking on the thermometer icon (region B) brings up the window shown in Figure 5-13c. With appropriately interfaced sensors, real time readout of ambient and polychromator temperature could be provided in this window. Finally, if the mouse is clicked on the PMT channel end of the instrument (region C), the window shown in Figure 5-13d appears. Elements shown in bold face text represent channels available on the direct reader. This periodic table also serves as a menu for accessing spectral information. This information is contained in another program, so that when the mouse is first clicked on an element, the alert shown in Figure 5-14a appears, prompting the user to select "Element Info"

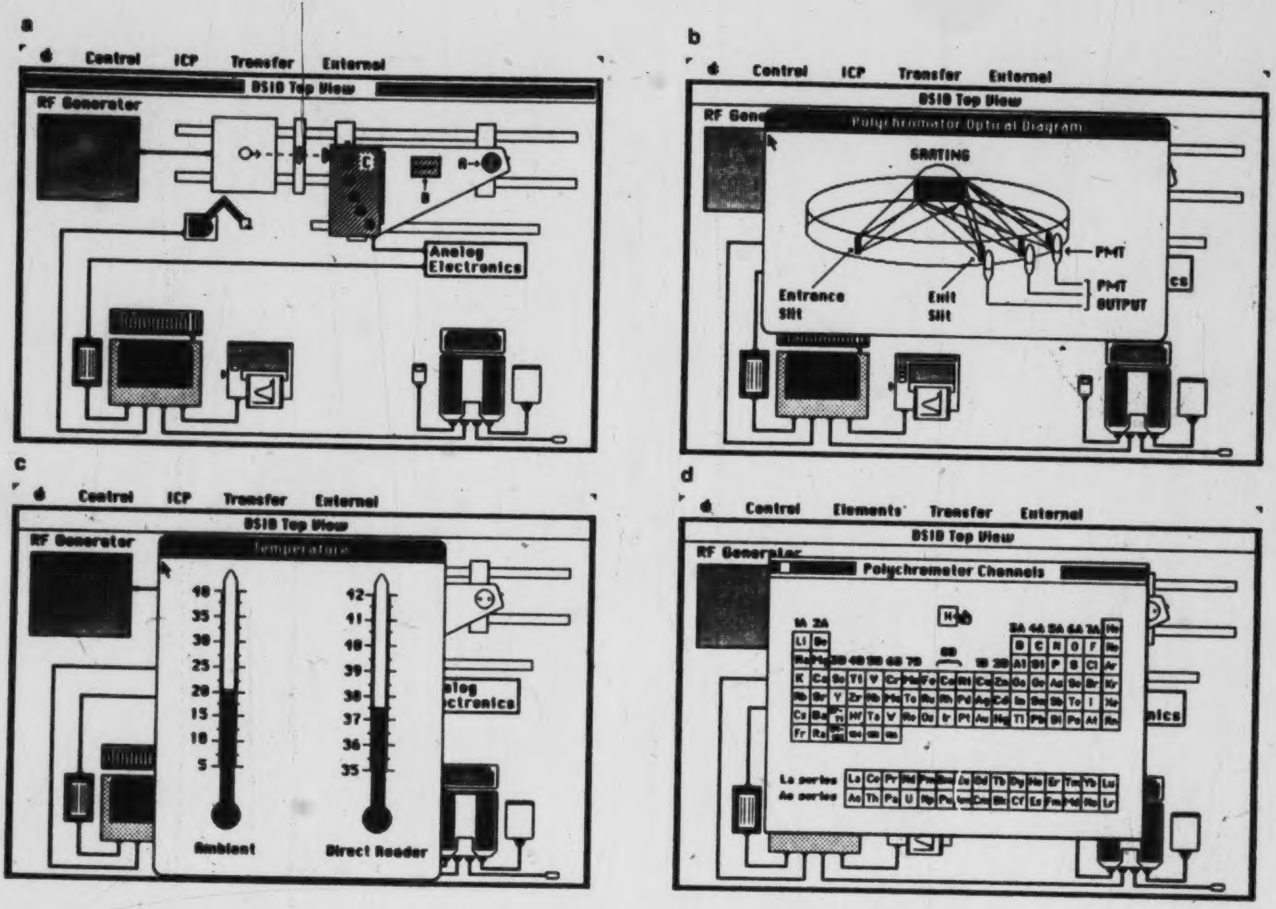
a
Control
ICP
Transfer
External
DSID Top View
RF Generator
A
B
C
Analog Electronics
b
Polychromator Optical Diagram
GRATING
PMT
PMT OUTPUT
Entrance Slit
Exit Slit
c
Temperature
40
35
30
25
20
15
10
5
42
41
40
39
38
37
36
35
Ambient
Direct Reader
d
Elements
Polychromator Channels
La series
Ac series

Figure 5-13. The instrument metaphor (a) with first level windows accessible by clicking the polychromator at locations A (A), B (b) and C (d).

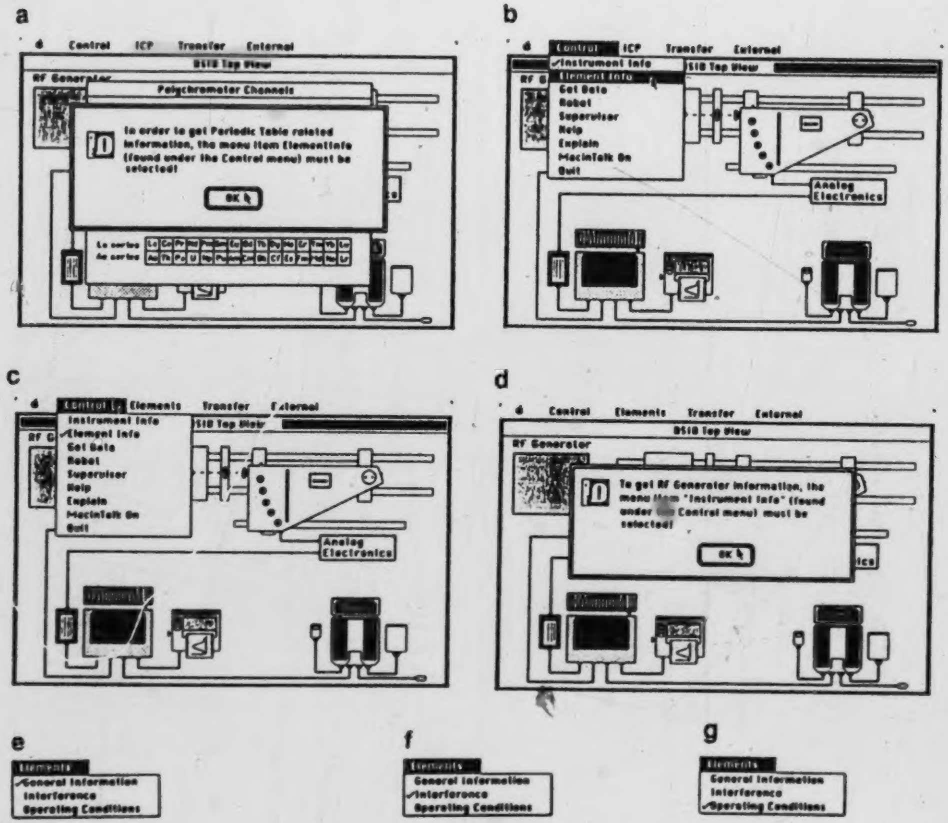
a
b
c
d
e
f
g
Control
ICP
Elements
Transfer
External
DS10 Top View
RF Generator
Polychromator Channels
Instrument Info
Element Info
Get Data
Robot
Supervisor
Help
Explain
MacinTalk On
Quit
Analog Electronics
La series
Ac series
OK
Elements
General Information
Interference
Operating Conditions

In order to get Periodic Table related information, the menu item ElementInfo (found under the Control menu) must be selected!

To get RF Generator information, the menu item "Instrument Info" (found under [illegible] Control menu) must be selected!

Figure 5-14. The alert window (a) telling the user to load the Element Info program (b) in order to access the periodic table data (c). The alert window (d) indicating inactivity of graphic areas under the new program. Selections with the new "Elements" pull down menu associated with the periodic table window (e, f, g).

from the "Control" menu (Figure 5-14b). This launches (i.e., load and executes) a new program that retains the same visual interface but with a new menu item called "Elements" replacing the old "ICP" menu, and with a check mark placed on the "Element Info" item of the "Control" menu (Figure 5-14c). The previously established active regions of the instrument metaphor are no longer active and attempts to access them will result in alerts of the type shown in Figure 5-14d. Although displaying alerts of this type may appear a trivial and unnecessary step, they have been included as a demonstration of the basic philosophy behind the design of this user interface, namely that of simplicity and ease of operation. Furthermore, because the alerts shown promote an interactive environment and can act as a help facility in disguise, they can eliminate frequent references to instruction manuals or they have the potential to replace them altogether.

As mentioned earlier, the difference in the menu bar between this program and the main program resides with the installation of the "Element" menu on the menu bars as shown in Figures 5-14b and 5-14c. The user has the option of selecting: "General Information" (Figure 5-14e), "Interference" information (Figure 5-14f), or "Operating Conditions" (Figure 5-14g). As soon as a menu item is selected, a check mark is placed next to it to indicate that this has become the active item.

Therefore, from the periodic table displayed on the screen, different levels of spectral information about an element can be selected. For example, by clicking the mouse while the cursor is positioned within the rectangle occupied by Zn on the periodic table (Figure 5-15a), a new window appears on the screen. The information displayed in the window depends on the item selected from the "Elements" menu. For example, if "General Information" has been selected, then, general information about Zn is presented (Figure 5-15b). This includes: atomic number, atomic weight, channel number, emission line, spectral order, detection limit and prominent ICP lines as listed in Bouman's line coincidence tables [21]. Provisions for upper linear concentration (ULC) and background equivalent concentration (BEC) data have also been made, although such data have not been included on this version of the program.

When "Interference" is selected from the "Element" menu (Figure 5-14f) and the mouse is clicked on Zn (Figure 5-15a), a new window appears on the screen (Figure 5-15c) displaying possible spectral interference for the Zn 213.86 nm line. The list includes the interfering element and the wavelength of the corresponding emission line. It also includes a suggestion about possible line broadening and stray light effects. Spectral interference data displayed in this window have been taken from the literature [22].

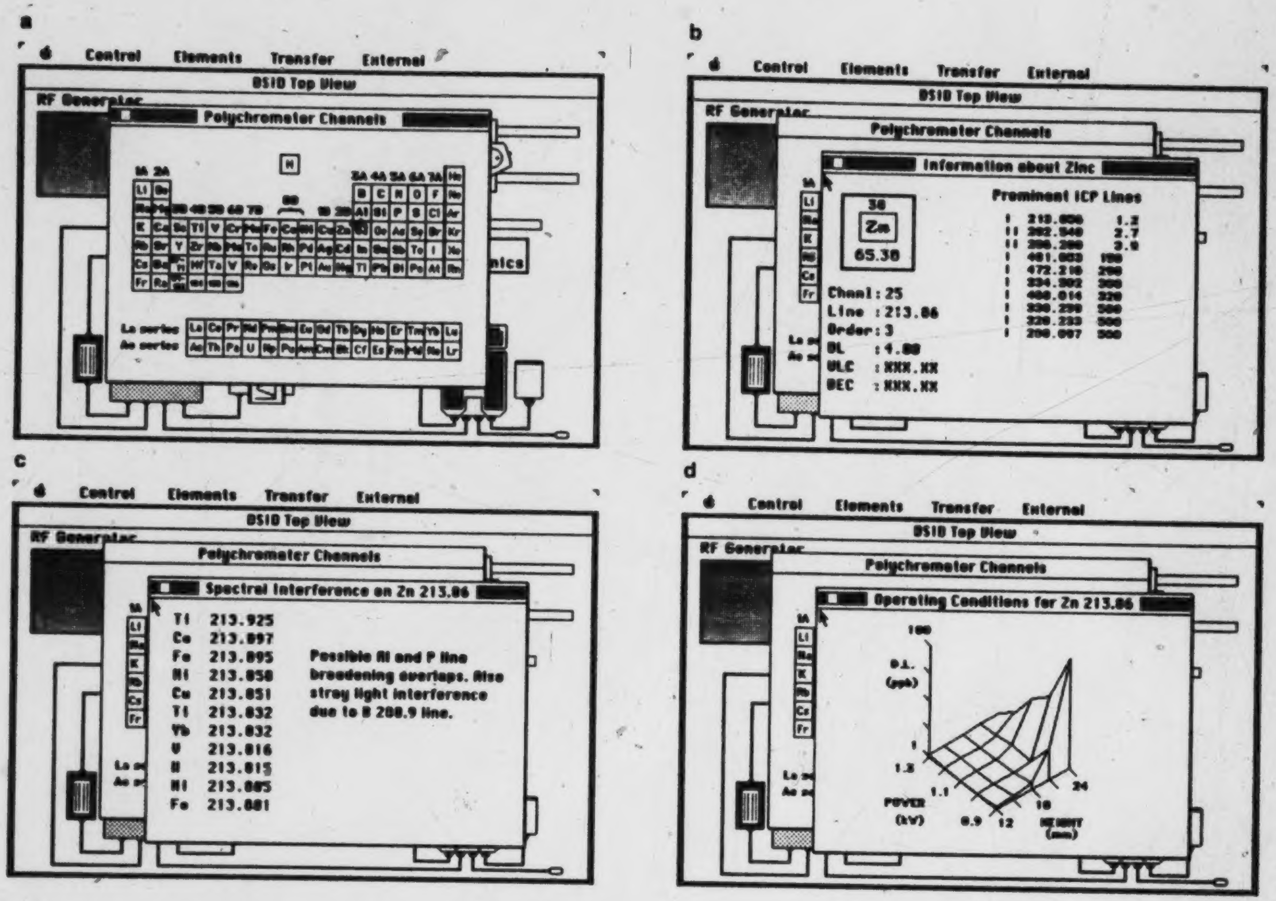
a
b
c
d
Control
Elements
Transfer
External
DSID Top View
RF Generator
Polychromator Channels
1A 2A
3A 4A 5A 6A 7A
La series
Ac series
Information about Zinc
30
Zn
65.38
Spectral Interference on Zn 213.86
Operating Conditions for Zn 213.86
100
D.L.
(ppb)
1
1.3
1.1
POWER
(kW)
0.9
12
18
24
HEIGHT
(mm)

Chanl : 25
Line : 213.86
Order : 3
DL : 4.80
ULC : XXX.XX
DEC : XXX.XX

Prominent ICP Lines

I	213.856	1.2
II	202.548	2.7
II	206.200	3.9
I	481.053	150
I	472.216	290
I	334.502	300
I	468.014	320
I	330.259	500
I	328.233	500
I	280.087	500

Ti	213.925
Co	213.897
Fe	213.895
Ni	213.858
Cu	213.851
Ti	213.832
Yb	213.832
V	213.816
W	213.815
Ni	213.805
Fe	213.801

Possible Al and P line broadening overlaps. Also stray light interference due to B 208.9 line.

Figure 5-15. The periodic table window (a) with General Information, (b) Interference (c) and Operating Conditions (d) windows for Zn.

Finally, if the "Operating Conditions" item of the "Element" menu is selected (Figure 5-14g), and the mouse is clicked on Zn (Figure 5-15a), a new window that offers optimization information appears on the screen (Figure 5-15d). In this particular case, power and observation height are plotted against the detection limit. As depicted in this figure, a combination of a high observation and of a low power can compromise the detection limit by as much as two orders of magnitude.

Similar levels of information are provided for all 29 channels that constitute the channels on the polychromator, that is all elements in bold face text. For example, the three windows accessible by clicking on Cu with the appropriate menu selections are shown in Figure 5-16.

A comparison between Zn and Cu operating conditions, shown in Figures 5-15d and 5-16d respectively, reveals that the best set of operating conditions for the Zn 213.86 nm line compromises the detection limit of the Cu 324.75 nm line by about an order of magnitude. Therefore, for analytical determinations at these wavelengths and for samples containing Zn and Cu near the detection limit, two sets of measurements may be required. A desirable feature would be to have the computer, in an automated fashion, reach this conclusion and recommend or proceed automatically with appropriate measurements.

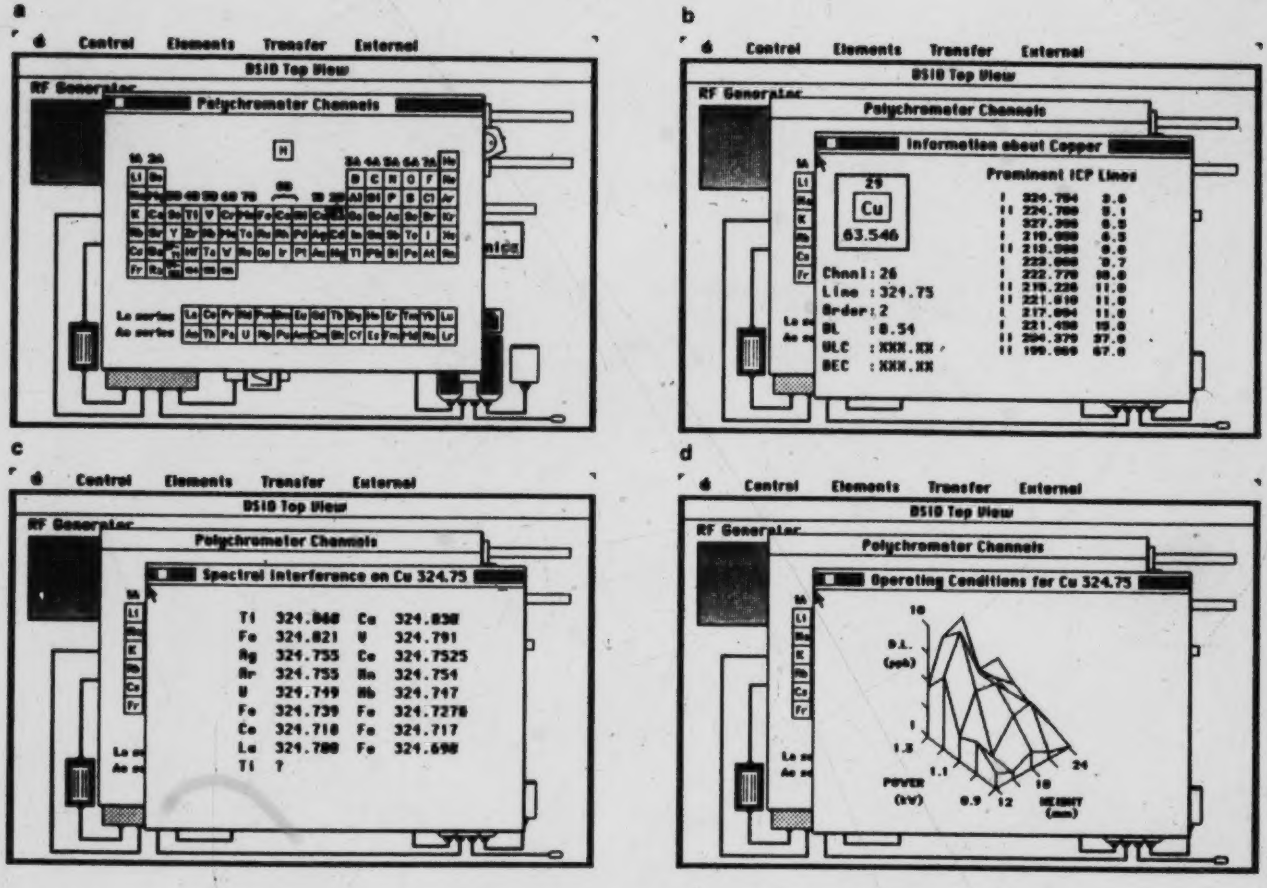
a
b
c
d
Control
Elements
Transfer
External
DSID Top View
RF Generator
Polychromator Channels
La series
Ac series
Information about Copper
Spectral Interference on Cu 324.75
Operating Conditions for Cu 324.75
D.L. (ppb)
POWER (kW)
HEIGHT (mm)

Information about Copper

29
Cu
63.546

Chnnl : 26
Line : 324.75
Order : 2
DL : 8.54
ULC : XXX.XX
BEC : XXX.XX

Prominent ICP Lines

```
I    324.754    3.0
II   224.700    5.1
I    327.396    6.5
I    219.958    6.3
II   213.598    8.0
I    223.008    8.7
I    222.778   10.0
II   219.226   11.0
II   221.810   11.0
I    217.894   11.0
I    221.458   15.0
II   204.379   37.0
II   199.969   67.0
```

Spectral Interference on Cu 324.75

```
Ti  324.860   Ce  324.830
Fe  324.821   V   324.791
Ag  324.755   Ce  324.7525
Ar  324.755   Rh  324.754
U   324.749   Nb  324.747
Fe  324.739   Fe  324.7278
Ce  324.718   Fe  324.717
La  324.700   Fe  324.698
Ti  ?
```

Figure 5-16. The periodic table window with (a) General Information, (b) Interference and (c) Operating Conditions (d) windows for Cu.

A considerable amount of additional spectral information is included in this data base over and above that specific to the polychromator channels. As shown in Figures 5-15b and 5-16b, the general information window for each channels lists several prominent ICP lines for the particular element. This could aid alternative line selection for an N+1 channel or a separate slew-scanning instrument. In addition, spectral line information is available for all elements listed in Bouman's line coincidence tables [21] and is accessible by clicking on the periodic table. For example, if "General Information" is selected on the "Elements" menu and Y or Sb are clicked, the windows shown in Figures 5-17a and 5-17c appear. However, since neither of these elements are polychromator channels, clicking on them with either of the other two menu items checked (Interference or Operating Conditions) results in the windows shown in Figures 5-17b and 5-17d.

Some elements, those that cannot be determined by the ICP, are not listed in Bouman's line coincidence tables. Argon can serve as an example. When "General Information" is selected from from the "Elements" menu and Ar is chosen, as shown in Figure 5-18a, a new window containing its own icon appears on the screen, as shown in Figure 5-18b. In this case, no Ar emission lines are listed. When "Interference" or "Operating Conditions" are selected from "Elements" menu and Ar is chosen from the periodic table

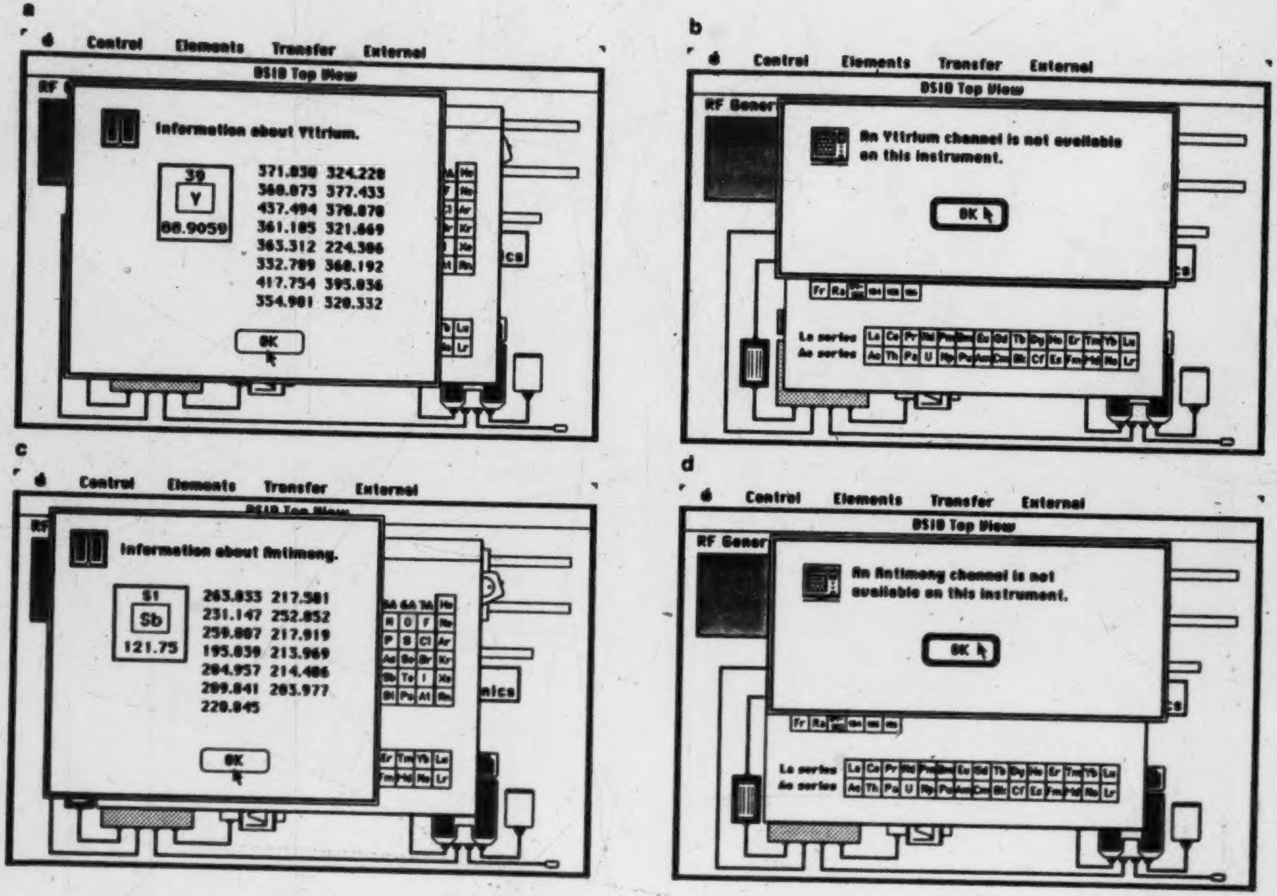
a
b
c
d
Control
Elements
Transfer
External
DSIO Top View
RF Gener
La series
Ac series
OK

(a)

Information about Yttrium.

39
Y
88.9059

371.030 324.228
360.073 377.433
437.494 378.870
361.105 321.669
363.312 224.306
332.789 360.192
417.754 395.036
354.901 320.332

(b)

An Yttrium channel is not available on this instrument.

(c)

Information about Antimony.

51
Sb
121.75

206.833 217.581
231.147 252.852
259.807 217.919
195.039 213.969
204.957 214.486
209.841 203.977
220.845

(d)

An Antimony channel is not available on this instrument.

Figure 5-17. General Information windows for Y (a) and Y (b). The Interference and Operating Conditions windows for Y (b) and Sb (d).

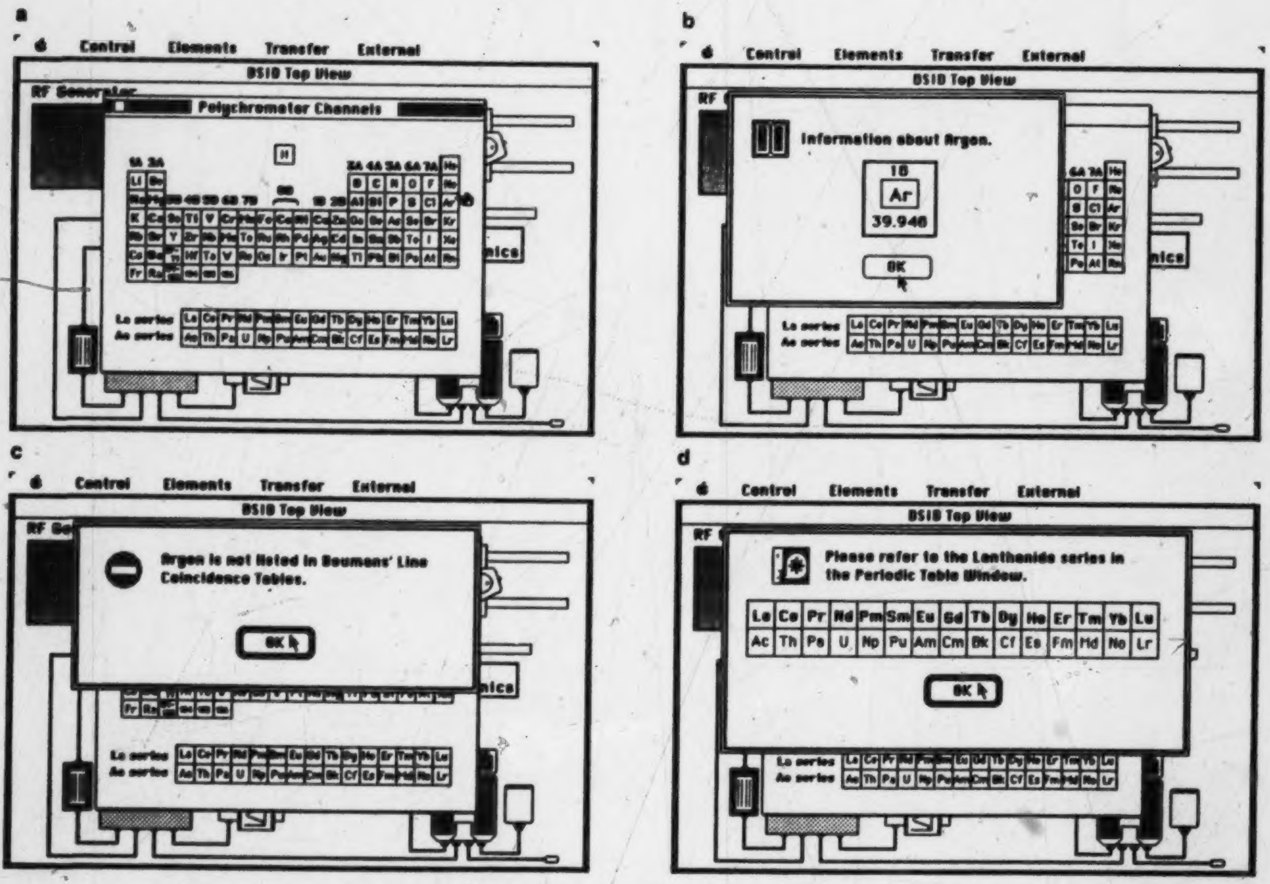
a
Control
Elements
Transfer
External
DSID Top View
RF Generator
Polychromator Channels
La series
Ac series
b
Control
Elements
Transfer
External
DSID Top View
OK
c
Control
Elements
Transfer
External
DSID Top View
OK
d
Control
Elements
Transfer
External
DSID Top View
OK

Information about Argon.

18
Ar
39.948

Argon is not listed in Boumans' Line Coincidence Tables.

Please refer to the Lanthanide series in the Periodic Table Window.

La	Ce	Pr	Nd	Pm	Sm	Eu	Gd	Tb	Dy	Ho	Er	Tm	Yb	Lu
Ac	Th	Pa	U	Np	Pu	Am	Cm	Bk	Cf	Es	Fm	Md	No	Lr

Figure 5-18. (a) The periodic table window, (b) general Information window for Ar, (c) Interference or Operating Conditions window for Ar (d) and window for La (marked 57-71) on the periodic table.

window, another alert appears on the screen, as shown in Figure 5-18c. This alert, also contains its own icon, so that the experienced user can immediately recognize that the element chosen cannot be determined by the ICP.

The entire periodic table is active in this version of the program, that is, it contains information for all elements. This part of the program, then, can be thought of as a data base containing elemental information which is of interest to analytical atomic spectroscopists. In addition, several precautionary steps have been taken in order to simplify the user interface and avoid surprising the user. For example, clicking the mouse within the rectangle occupied by the La series (marked 57-71 on the periodic table) a new window appears on the screen, as shown in Figure 5-18d. The information displayed in this window directs the user to the next step.

Overall, this clickable periodic table with multiple windows and hence depths of information, is a powerful and effective approach to accessing a data base. Other applications in our laboratory have included accessing an ICP-MS spectral data base in a similar fashion [24].

D.4 Help and Explain Files

Throughout the program numerous "Help" and "Explain" files can be accessed in order to support the user. A help facility aids the user in running the instrument or a program more efficiently and without frequent reference to manuals; an explain facility attempts to offer an explanation of the process(es) and measurements involved during operation of the instrument and justify its significance. Put otherwise, a help facility can be thought of as the means to provide an answer to a "how?" question, an explanation facility attempts to provide an answer a "why?" question. By virtue of their design then, such facilities are of tutorial nature.

Explain and Help files are accessed through the "Control" menu. For example, in the "Instrument Info" program, explain files can be accessed as shown in Figure 5-19a. When the "Explain" menu item under the "Control" menu is selected a "Mini Finder", listing all available explain files appears on the screen, as shown in Figure 5-19b. These can be selected and opened as needed. Two examples are shown in Figures 5-19c and 5-19d.

A different set of Help and Explain files are provided in the "Element Info" periodic table program just described. Again, they are selected from the control menu and the help files "Mini Finder" window is shown in Figure 5-20a. These files contain Ar spectral lines [22, 25-27], one window of which is shown in Figure 5-20b. Help with the meaning of the "Elements" menu shown in Figure 5-20c and information on spectral interferences in Figure 5-20d.

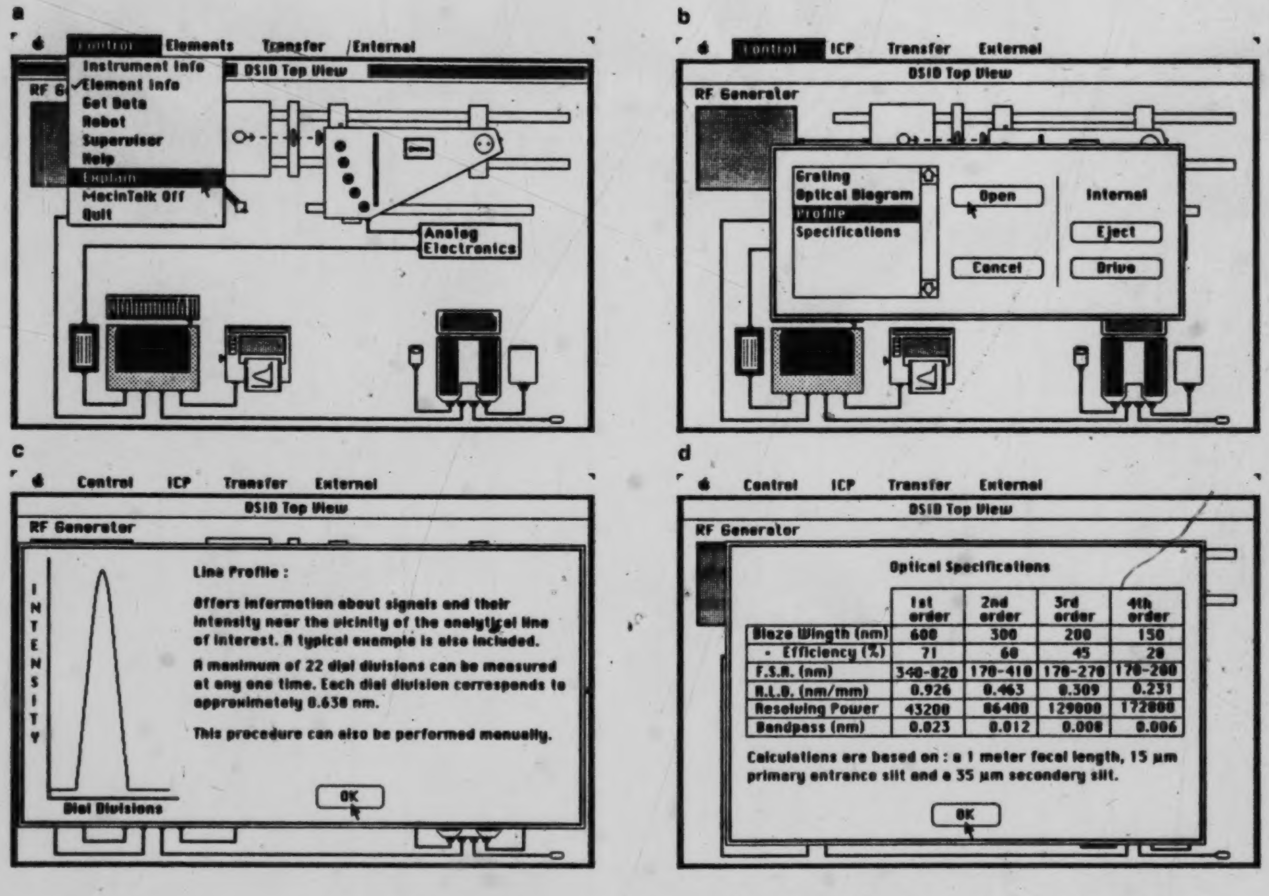
a
Control
Elements
Transfer
External
Instrument Info
✓Element Info
Get Data
Robot
Supervisor
Help
Explain
MacinTalk Off
Quit
DSID Top View
RF G
Analog Electronics
b
Control
ICP
Transfer
External
DSID Top View
RF Generator
Grating
Optical Diagram
Profile
Specifications
Open
Cancel
Internal
Eject
Drive
c
Control
ICP
Transfer
External
DSID Top View
RF Generator
INTENSITY
Dial Divisions
OK
d
Control
ICP
Transfer
External
DSID Top View
RF Generator
OK

Line Profile :

Offers information about signals and their intensity near the vicinity of the analytical line of interest. A typical example is also included.

A maximum of 22 dial divisions can be measured at any one time. Each dial division corresponds to approximately 0.630 nm.

This procedure can also be performed manually.

Optical Specifications

	1st order	2nd order	3rd order	4th order
Blaze Wlngth (nm)	600	300	200	150
• Efficiency (%)	71	60	45	20
F.S.R. (nm)	340-820	170-410	170-270	170-200
R.L.D. (nm/mm)	0.926	0.463	0.309	0.231
Resolving Power	43200	86400	129000	172800
Bandpass (nm)	0.023	0.012	0.008	0.006

Calculations are based on : a 1 meter focal length, 15 µm primary entrance slit and a 35 µm secondary slit.

Figure 5-19. (a) Pull down menu to access Help and Explain files, (b) Explain files "Mini Finder" window for the ICP main program, (c) profile explain file and (d) specifications.

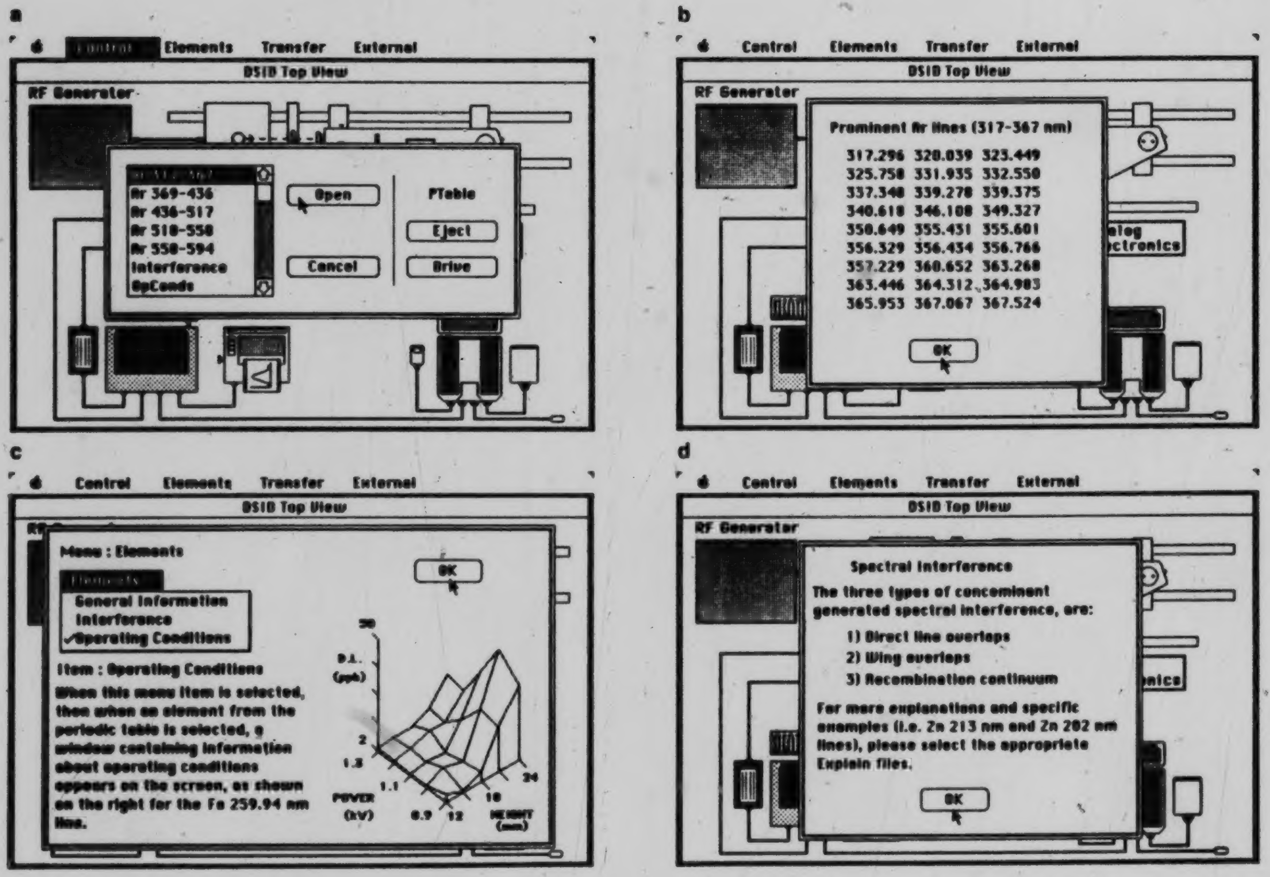
a
Control
Elements
Transfer
External
DSID Top View
RF Generator
Ar 369-436
Ar 436-517
Ar 518-558
Ar 558-594
Interference
OpConds
Open
Cancel
PTable
Eject
Drive
b
c
d
OK
D.L. (ppb)
POWER (kV)
HEIGHT (mm)
30
2
1.3
1.1
0.9
12
18
24
Menu : Elements
Elements
General Information
Interference
✓Operating Conditions
Analog Electronics

Prominent Ar lines (317-367 nm)

317.296	320.039	323.449
325.758	331.935	332.550
337.348	339.278	339.375
340.618	346.108	349.327
350.649	355.431	355.601
356.329	356.434	356.766
357.229	360.652	363.268
363.446	364.312	364.983
365.953	367.067	367.524

Item : Operating Conditions

When this menu item is selected, then when an element from the periodic table is selected, a window containing information about operating conditions appears on the screen, as shown on the right for the Fe 259.94 nm line.

Spectral Interference

The three types of concomitant generated spectral interference, are:

1) Direct line overlaps
2) Wing overlaps
3) Recombination continuum

For more explanations and specific examples (i.e. Zn 213 nm and Zn 202 nm lines), please select the appropriate Explain files.

Figure 5-20. (a) Mini Finder window for Help files of Element Info program, (b) Ar 317-367 help file, (c) Op Conds help file and (d) Interference help file.

This last window directs the user to specific explain files, four of which are shown in Figure 5-21.

Explain files can be accessed by selecting "Explain" from the "Control" menu: a "Mini Finder" window appears on the screen. When the appropriate file is selected, as illustrated before, information about direct spectral overlaps on the Zn 213.856 nm line along with an explanation about spectral overlaps is provided in the window that appears on the screen, as shown in Figure 5-21a. If direct spectral overlaps on the Zn 213 nm line cannot be tolerated, it is reasonable to suggest the use the Zn 202 nm line as an alternative, although, changing lines is not easily accomplished with a direct reading spectrometer. By selecting the appropriate file for the "Mini Finder" window, a comparison between the Zn 213 and the 202 nm line is provided, as shown in Figure 5-21b.

Upon selection of the appropriate file from the "Mini Finder", a short description of recombination continuum along with the effect it has on the Zn 213 nm line is displayed on the screen, as shown in Figure 5-21c. If the effect that Al recombination continuum has on the Zn 213 nm line cannot be tolerated, the Zn 202 nm line can be suggested as an alternative. By selecting the appropriate file, a new window appears on the screen that places both lines side by side, so that can be easily compared, as shown in Figure 5-21d. Although not shown, information

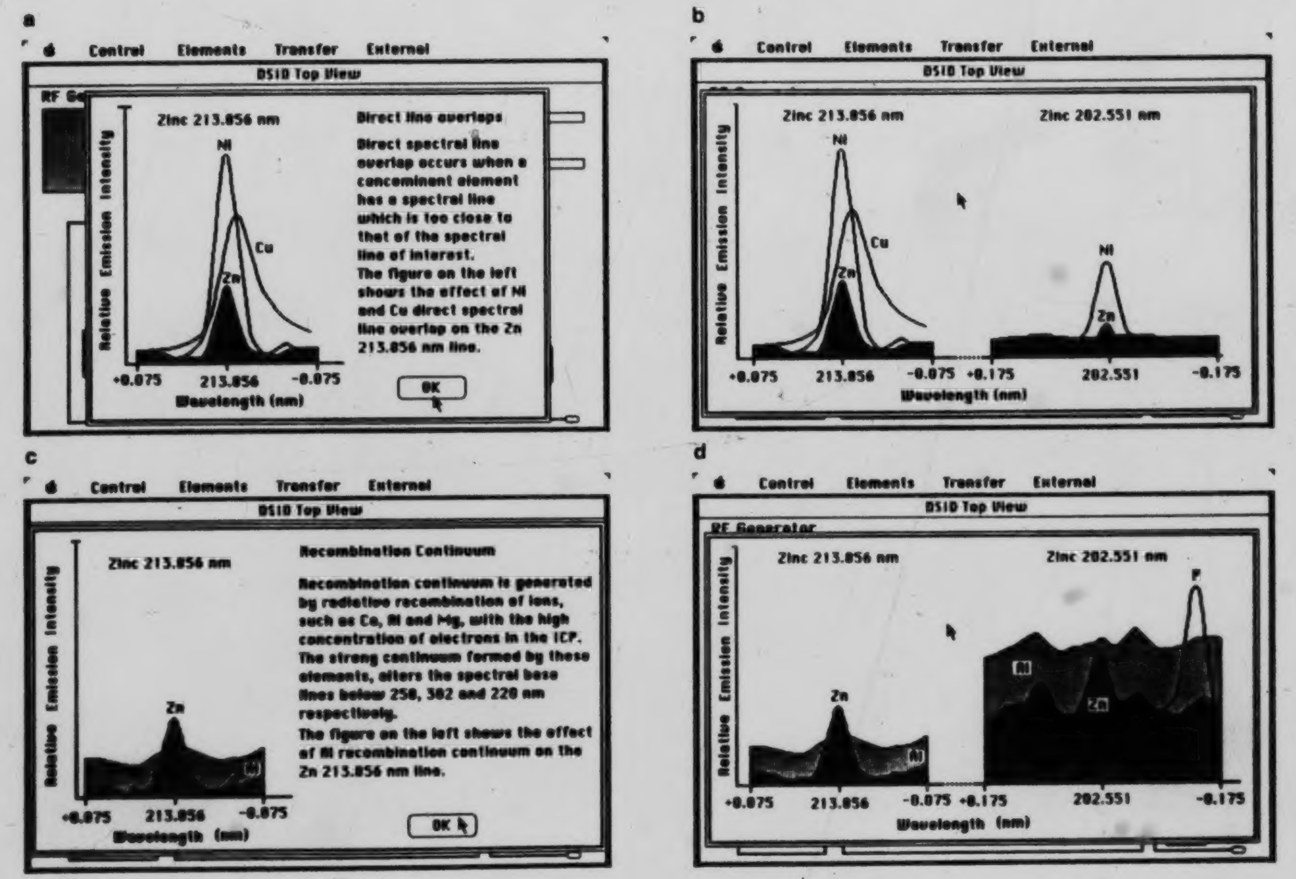
a
Control
Elements
Transfer
External
DSID Top View
RF Ge
Zinc 213.856 nm
Ni
Cu
Zn
Relative Emission Intensity
+0.075
213.856
-0.075
Wavelength (nm)
OK
b
Control
Elements
Transfer
External
DSID Top View
Zinc 213.856 nm
Zinc 202.551 nm
Ni
Cu
Zn
Ni
Zn
Relative Emission Intensity
+0.075
213.856
-0.075
+0.175
202.551
-0.175
Wavelength (nm)
c
Control
Elements
Transfer
External
DSID Top View
Zinc 213.856 nm
Zn
Ni
Relative Emission Intensity
+0.075
213.856
-0.075
Wavelength (nm)
OK
d
Control
Elements
Transfer
External
DSID Top View
RF Generator
Zinc 213.856 nm
Zinc 202.551 nm
Zn
Ni
Ni
Zn
F
Relative Emission Intensity
+0.075
213.856
-0.075
+0.175
202.551
-0.175
Wavelength (nm)

Direct line overlaps

Direct spectral line overlap occurs when a concominant element has a spectral line which is too close to that of the spectral line of interest.
The figure on the left shows the effect of Ni and Cu direct spectral line overlap on the Zn 213.856 nm line.

Recombination Continuum

Recombination continuum is generated by radiative recombination of ions, such as Co, Ni and Mg, with the high concentration of electrons in the ICP. The strong continuum formed by these elements, alters the spectral base lines below 258, 302 and 220 nm respectively.
The figure on the left shows the effect of Ni recombination continuum on the Zn 213.856 nm line.

Figure 5-21. Examples of Explain files available in the Element Info program.

about wing spectral overlaps is on-line and displayed in a similar fashion. And even though this implementation of the explain facility involves only Zn, two of its lines, and three types of spectral interference, it can be easily expanded to include most elements of the periodic table and more than two emission lines. In this way, information crucial to chemical analysis via spectrochemical methods can be made easily accessible to the user.

D.5 Communication to System Support Programs

One of the goals set for the instrument user interface was that the program can communicate its data to commercially available software. This is accomplished through a series of menus which are common to all programs. Common menus and their items are shown in Figure 5-22. The "Apple" menu, as shown in Figure 5-22a, supports desk accessories. Its first item, the "About Program...", always contains information about the currently active program. The other menu items are typical desk accessories. The "Control" menu always remains the same: the check mark is placed on the active item. The menu shown in Figure 5-22c, changes accordingly to correspond with the currently active program. For example, on the main program this is the "ICP" menu, on the periodic table program it is the "Elements" menu and on the program that allows the setting of the parameters it is the "Parameters" menu.

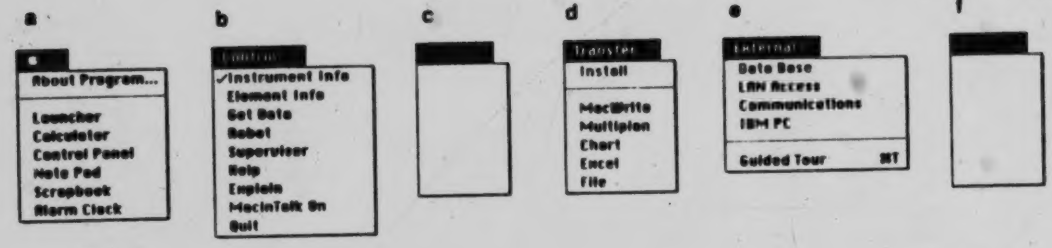
a
About Program...
Launcher
Calculator
Control Panel
Note Pad
Scrapbook
Alarm Clock
b
Control
✓Instrument Info
Element Info
Get Data
Robot
Supervisor
Help
Explain
MacinTalk On
Quit
c
d
Transfer
Install
MacWrite
Multiplan
Chart
Excel
File
e
External
Data Base
LAN Access
Communications
IBM PC
Guided Tour ⌘T
f

Figure 5-22. Pull down structure for the complete user interface.

Menus labeled a, b, d and e shown in Figure 5-22, are common to all programs. The "Transfer" and "External" menus allow the program to interface with commercially available software. For example, the "Install" menu items allow immediate access to any of the following programs: MacWrite, a word processor that can be used for report generation; Multiplan [28], a spreadsheet that can be used for computerized what-if scenarios; Chart [28] that can be utilized for data presentation; Excel [28], a speadsheet with graphics capabilities; and File [28], a data base program that can be used for archival and retrieval purposes. The "External" menu, shown in Figure 5-22, allows the installation of selected commercially available software packages, through a special transfer mechanism. Information on how these menus operate is includes in a series of help and explain files: typical examples are shown in Figures 5-23a and 5-23b.

Although the idea of interfacing a particular program with commercially available software appears to be very appealing, there exists a potential problem: what to do if more advanced software packages become available. In order to circumvent this, the "Launcher" desk accessory was developed. In this particular implementation when "Launcher" is chosen from the "Apple" menu (Figure 5-22a) a new window appears on the screen and a new menus installed on the menu bar, as shown in Figure 5-23c.

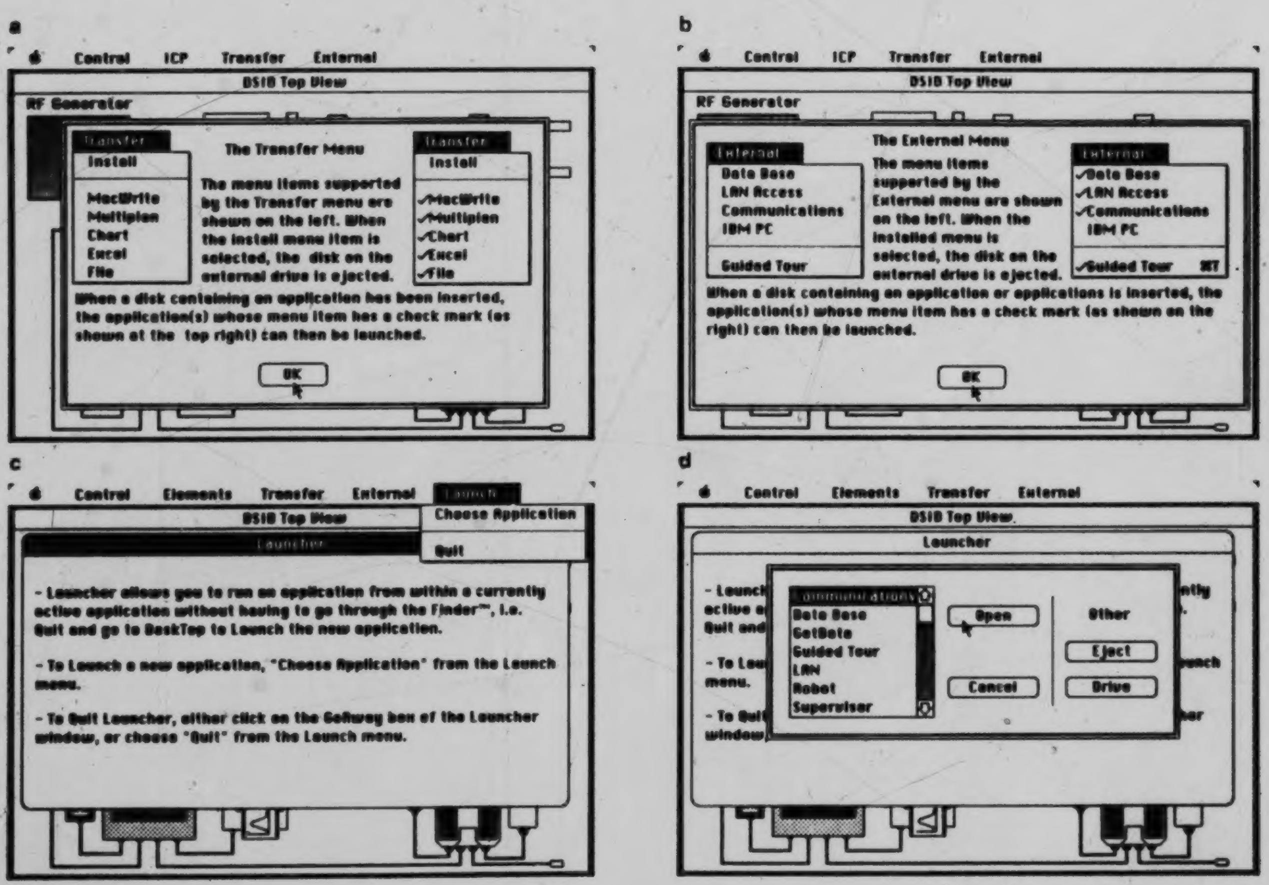
a
Control
ICP
Transfer
External
DSIB Top View
RF Generator
Transfer
Install
MacWrite
Multiplan
Chart
Excel
File
The Transfer Menu
Transfer
Install
✓MacWrite
✓Multiplan
✓Chart
✓Excel
✓File
OK
b
Control
ICP
Transfer
External
DSIB Top View
RF Generator
External
Data Base
LAN Access
Communications
IBM PC
Guided Tour
The External Menu
External
✓Data Base
✓LAN Access
✓Communications
IBM PC
✓Guided Tour ⌘T
OK
c
Control
Elements
Transfer
External
Launch
DSIB Top View
Launcher
Choose Application
Quit
d
Control
Elements
Transfer
External
DSIB Top View.
Launcher
Communications
Data Base
GetData
Guided Tour
LAN
Robot
Supervisor
Open
Cancel
Other
Eject
Drive

The menu items supported by the Transfer menu are shown on the left. When the install menu item is selected, the disk on the external drive is ejected.

When a disk containing an application has been inserted, the application(s) whose menu item has a check mark (as shown at the top right) can then be launched.

The menu items supported by the External menu are shown on the left. When the installed menu is selected, the disk on the external drive is ejected.

When a disk containing an application or applications is inserted, the application(s) whose menu item has a check mark (as shown on the right) can then be launched.

- Launcher allows you to run an application from within a currently active application without having to go through the Finder™, i.e. Quit and go to DeskTop to Launch the new application.

- To Launch a new application, "Choose Application" from the Launch menu.

- To Quit Launcher, either click on the GoAway box of the Launcher window, or choose "Quit" from the Launch menu.

Figure 5-23. (a) The "Transfer" menu help file, (b) the "External" menu help file, (c) Launcher window after chosing "Launcher" from the "Apple" menu (Figure 5-22a) and (d) Mini Finder window for choosing an application to launch.

When the "Choose Application" item is chosen from the "Launch" menu, a "Mini-Finder" window appears on the screen. This allows users to launch (i.e., load and execute) any program thus eliminating the need to continuously update the program in order to take advantage of the latest software generation. This is how the program anticipates future software needs.

E. Conclusions

Hirchfeld in his excellent paper entitled *"Instrumentation in the Next Decade"* [1] indicated that: *"As even more data are generated in progressively faster measurements, the I/O bandwidth of the human observer is being rapidly exceeded".* We feel that the concepts and implementation of the human processor interface presented here provides one approach to addressing this important problem. In addition, the instrument metaphor in association with an extensive, graphically accessible atomic spectroscopy data base, an elaborate help and explain facility, and intelligent software for the control of instrumental parameters, is anticipated to provide a unique shell for artificial intelligence software.

REFERENCES

1. T. Hirschfeld, Science, **230**(4723), 286,1985

2. V. Karanassios and G. Horlick, Talanta, **32**, 583, 1985

3. V. Karanassios and G. Horlick, Talanta, **32**, 601, 1985

4. V. Karanassios and G. Horlick, Talanta, **32**, 615, 1985

5. V. Karanassios and G. Horlick, *'Development of a Computer-Controlled DSID for ICP-AES'*, Spectrochim. Acta, (submitted)

6. S. Chernikoff, *"Macintosh Revealed. Volume One: Unlocking the ToolBox"*, Hayden Book Co., New Jersey, 1985

7. S. Chernikoff, *"Macintosh Revealed. Volume Two: Programming with the ToolBox"*, Hayden Book Co., New Jersey, 1985

8. C. Lu, High Technology, **6**(3), 18 (1986)

9. C. Penyhold, PC Magazine, **5**(4), 110, (1986)

10. D. Burns and S. Venit, PC Magazine **4**(15), 112 (1985)

11. Inside Macintosh, Volumes I, II and III, Addison-Wesley Publishing Co., Menlo Park, CA, 1985

12. "Z8030/Z8530 Serial Communications Controller Technical manual", Zilog Inc., Corporate Publications, 1315 Dell Ave., Cambell, CA 95008

13. S. Ciarcia, Byte, **11**(5), 85, 1986

14. S. Ciarcia, Byte, **11**(6), 107, 1986

15. T.C. O'Haver, Am. Lab., **18**(2), 22,1986

16. M. G. Heaton and L.A. Kutchins, Am. Lab., **18**(5), 128, 1986

17. B. Curry-Koening and C. Seiter, Am. Lab., **18**(5), 70, 1986

18. Modula Corp., 950 N. University Ave., Provo, Utah 84604

19. Pettit W. and Horlick G., Spectrochim. Acta, **41B**, 699 (1986)

20. Y. Shao and G. Horlick, Appl. Spectrosc., **40**, 386, 1986

21. P. W. J. M.Boumans, *"Line Coincidence Tables for Inductively Coupled Plasma Atomic Emission Spectrometry"*, 2nd Edition, Pergamon Press, 1984

22. I. B. Brenner and H. Eldad, ICP Information Newslett., **10**(6), 451, 1984

23. R. L. Dahlquist., ARL report ICP-01-001-0880-MK-E, 1980., ARL., 9545 Wentworth St., Sunland, CA 91040

24. M.A. Vaughan and G. Horlick, Appl. Spectrosc., **41**, 523 (1987)

25. R.K. Winge, V. J. Peterson and V. A. Fassel, Appl. Spectrosc., **33**, 206, (1979)

26. R.K. Winge, V.A. Fassel, V.J. Peterson and M.A. Floyd, Appl. Spectrosc., **36**, 210, 1982

27. R.K Winge, V.J. Peterson and V.A. Fassel, "*Inductively Coupled Plasma-Atomic Emission Spectroscopy: Prominent Lines*", EPA-600/4-79-017, March 1979. USA Environmental Protection Agency, Athens, GA 30605

28. Microsoft Corp., 10700 Northup Way, Box 97200, Bellevue, WA 98009

THE UNIVERSITY OF ALBERTA

DEVELOPMENT AND CHARACTERIZATION OF DIRECT SAMPLE INSERTION DEVICES FOR INDUCTIVELY COUPLED PLASMAS

©

by

VASSILIOS KARANASSIOS of STERGIOS

A THESIS

SUBMITTED TO THE FACULTY OF GRADUATE STUDIES AND RESEARCH

IN PARTIAL FULFILMENT OF THE REQUIREMENTS FOR THE DEGREE

OF DOCTOR OF PHILOSOPHY

DEPARTMENT OF CHEMISTRY

EDMONTON, ALBERTA

FALL 1988

TABLE OF CONTENTS

CHAPTER PAGE

6. DEVELOPMENT OF A COMPUTER-CONTROLLED DIRECT SAMPLE INSERTION DEVICE FOR ICP-MS 328
   A. Introduction 329
   B. Instrumentation 336
      B.1 ICP-MS, Computer Systems and Operating Conditions 336
      B.2 DSID 343
      B.3 Data Acquisition Considerations 361
      B.4 Software 364
         B.4.1 For Serial Transfers and DSID Control 367
         B.4.2 Simulating Virtual Reality 371
   C. Basic Response 373
   D. Conclusions 377
   REFERENCES 383

7. SPECTRAL AND MATRIX INTERFERENCE EFFECTS USING A DSID FOR ICP-MS 387
   A. Introduction 388
   B. Experimental 390
   C. Spectroscopic Interference Effects 391
      C.1 Background Spectral Features of ICP-MS ... 391

C.1.1 Wet and Dry Plasma
Background Spectra 393
C.1.1.1 Distiled Water
Background Spectra 395
C.1.1.2 Dry Plasma
Background Spectra 403
C.1.1.3 Comparison of Background
Spectral Features 416
C.1.1.4 Summary and Conclusions 422
C.1.2 Probe Background Spectra 425
C.1.2.1 Graphite Electrodes 426
C.1.2.2 Mo Cups 430
C.1.2.3 Ta Cups 436
C.1.2.4 W Wire-loop 440
C.1.2.5 Summary and Conclusions 445
C.2 Oxides, Hydroxides
and Doubly-charged Species 449
C.3 Solvent-induced Background Species 459
D. Non-spectroscopic Interference Effects........ 463

E. Conclusions.................................. 468
REFERENCES.................................. 471

8. CONCLUDING REMARKS 473
A. Summary.................................... 474

B. The Concept of Processors in Spectrochemical Instrumentation 479

C. Integration: Imagineering the Next Generation Analytical Instrumentation 483

REFERENCES 488

APPENDIX A. NEW DESIGN CONCEPTS FOR DIRECT READER MEASUREMENT ELECTRONICS 489

APPENDIX B. ICP-MS-DSID BLUEPRINTS 516

APPENDIX C. ICP-MS PARAMETER SET UTILIZED FOR THE ACQUISITION OF TRANSIENT SIGNALS 533

APPENDIX D. SPECTRAL CHARACTERISTICS OF A NEW SPECTROMETER DESIGN FOR ATOMIC EMISSION SPECTROSCOPY 535

APPENDIX E. DEVELOPMENT SYSTEMS AND PROGRAMMING ENVIRONMENTS UTILIZED 569

LIST OF TABLES

TABLE PAGE

6-1. Ion lens voltage settings.................... 342

7-1. Types of interference effects in ICP-MS....... 389

7-2. Typical solvent-induced background species.... 394

7-3. Background species arising from a wet and dry plasma................................ 400

7-4. Background species eliminated from a wet plasma when using a dry plasma and an extended torch................................ 423

7-5. Probe-induced background species............. 446

A-1. Truth table for 74154, 4-line-to-16-line decoder/demultiplexer........................ 509

A-2. Truth table for 74155, 2-line-to-4-line decoder/demultiplexer........................ 511

A-3. Truth table for 74138, 3-~~line-to-8-~~line decoder/demultiplexer........................ 512

C-1. Sciex® Elan parameter set used for the acquisition of transient signals............. 534

D-1. Preliminary technical specifications for the SPS-10 Simultaneous Plasma Spectrometer....... 539

D-2. Mask Specifications.......................... 543

E-1. Development systems and programming environments utilized.. 570

LIST OF FIGURES

FIGURE PAGE

6-1. Block diagram of the experimental set-up of a DSID for ICP-MS 331

6-2. Sample carrying probes employed in this work. (a) long undercut graphite electrode; (b) long undercut graphite electrode fitted with a metal cup; (c) wire-loop 334

6-3. Typical analyte temporal behavior 335

6-4. Schematic illustration of alignment device 338

6-5. Top view of the direct sample insertion device (x, y is the plane of the drawing, the z-axis is perpendicular to the drawing) 340

6-6. Three dimensional view of the DSID (not to scale) 344

6-7. Three dimensional view of the torch support assembly (not to scale) 346

6-8. Schematic illustration of the 'DSID' torch 348

6-9. Top view of the shutter, (a) open and (b) closed 349

6-10. Top view of the sliding platform (x- and y-axis define the plane of the page, the z-axis is perpendicular to the drawing) 351

6-11. Schematic illustration of the probe assembly support, (a) probe assembly positioned vertically; (b) probe assembly positioned horizontally 352

6-12. Front view of sliding platform (probe assembly support is not shown for clarity, dimensions in cm) 353

6-13. Schematic illustration of probe assembly at: (a) home position; (b) an intermediate state and (c) the horizontal position 357

6-14. Schematic illustration of probe insertion 359

6-15. Typical temporal behavior for Cu and Zn (10 ng each) as transferred to the Macintosh at 1200 baud 362

6-16. Pull-down menu structure 365

6-17. An example of a hierarchical menu 369

6-18. Typical temporal behavior for Cu and Zn (10 ng each) as transferred to the Macintosh at 9600 baud 370

6-19. Number of data points per second per number of masses scanned. (a) one mass scanned; (b) two masses; (c) three masses and (d) four masses 375

6-20. The effect of central tube flow rate on intensity as a function of power and sampling depth for: (a) 10 ng Mg; (b) 10 ng Mn; (c) 10 ng Zn 376

6-21. Typical analyte temporal behavior from long undercut graphite electrodes, a 10 mm sampling depth and 1.50 kW power for 1 ng of: (a) Mg; (b) Mn and (c) Zn 378

6-22. Background spectrum for a graphite electrode (low resolution scan, 10 mm sampling depth, 1.25 kW) 379

6-23. Background spectrum for a Mo cup (low resolution scan, 10 mm sampling depth, 1.25 kW) 380

6-24. Background spectrum for a Ta cup (low resolution scan, 10 mm sampling depth, 1.25 kW) 381

6-25. Background spectrum for a W wire-loop (low resolution scan, 10 mm sampling depth, 1.25 kW) 392

7-1. Illustration of the DSID torch with its extension in place............................ 396

7-2. Background spectra for a wet plasma, high resolution scan, sampling depth 15 mm, mass range 1-45 amu................................ 397

7-3. Background spectra for a wet plasma, high resolution scan, sampling depth 15 mm, mass range 40-85 amu 405

7-4. Background spectra for a dry plasma, high resolution scan, sampling depth 15 mm, mass range 10-40 amu 406

7-5. Background spectra for a dry plasma, high resolution scan, sampling depth 15 mm, mass range 40-75 amu 411

7-6. Background spectra for a dry plasma, high resolution scan, sampling depth 10 mm, mass range 10-40 amu 412

7-7. Background spectra for a dry plasma, high resolution scan, sampling depth 10 mm, mass range 40-75 amu 414

7-8. Background spectra for a dry plasma, extended torch, high resolution scan, sampling depth 10 mm, mass range 10-45 amu 415

7-9. Background spectra for a dry plasma, extended torch, high resolution scan, sampling depth 10 mm, mass range 40-75 amu 417

7-10. Background spectra, mass range 10-40 amu for: (a) wet plasma (15 mm); (b) Dry plasma (15 mm);(c) Dry plasma (10 mm); (d) Dry plasma, extended torch.................................. 418

7-11. Background spectra, mass range 40-75 amu for: (a) wet plasma (15 mm); (b) Dry plasma (15 mm); c) Dry plasma (10 mm); (d) Dry plasma, extended torch 420

7-12. Bar graph background spectra, mass range 12-38 amu. (a) Wet plasma, sampling depth 15 mm; (b) Dry plasma, extended torch 421

7-13. Bar graph background spectra, mass range 42-75 amu. (a) Wet plasma, sampling depth 15 mm; (b) Dry plasma, extended torch 424

7-14. Bar graph background spectra (logarithmic scale intensity axis) for the wet plasma (sampling depth 15 mm) and the dry plasma (extended torch) for: (a) mass range 12-42 amu and (b) mass range 42-75 amu 427

7-15. High resolution background spectrum of a 'blank' long undercut graphite electrode, mass range 1-40 amu 428

7-16. High resolution background spectrum of a 'blank' long undercut graphite electrode, mass range 40-85 amu. Note scale expansion in (c) 431

7-17. Low resolution background spectrum for a Mo cup, mass range 1-40 amu 432

7-18. Low resolution background spectrum for a Mo cup, mass range 40-85 amu 433

7-19. Low resolution background spectrum for a Mo cup, mass range 80-140 amu. Note scale expansion 434

7-20. Low resolution background spectrum for a Mo cup,mass range 140-210 amu 437

7-21. Low resolution background spectrum for a Ta cup, mass range 1-40 amu 438

7-22. Low resolution background spectrum for a Ta cup, mass range 40-85 amu 439

7-23. Low resolution background spectrum for a Ta cup. (a) Mass range 80-160 amu, scale expanded; (b) Mass range 160-210 amu; (c) Mass range 160-210, note scale expansion 441

7-24. Low resolution background spectrum for a W wire-loop, mass range 1-40 amu 442

7-25. Low resolution background spectrum for a W wire-loop, mass range 40-85 amu 443

7-26. Low resolution background spectrum for a W wire-loop, mass range 80-140 amu 444

7-27. Low resolution background spectrum for a W wire-loop, mass range 140-205 amu 453

7-28. Temporal behavior arising form 1 µg Ba for: (a) $^{138}Ba^{+}$; (b) $^{138}Ba^{16}O^{+}$; (c) $^{138}Ba^{2+}$; and (d) $^{138}Ba^{16}OH^{+}$ 455

7-29. Temporal behavior after addition of 10 µl of 0.25 M of NaF on the dried solution residue of the previously run electrode (Figure 2-28). (a) $^{138}Ba^+$; (b) $^{138}Ba^{16}O^+$; (c) $^{138}Ba^{2+}$ and (d) $^{138}Ba^{16}OH^+$ 457

7-30. Temporal behavior arising from 10 µl of 0.25 M NaF for: (a) $^{138}Ba^+$; (b) $^{138}Ba^{16}O^+$; (c) $^{138}Ba^{2+}$ and (d) $^{138}Ba^{16}OH^+$ 458

7-31. Temporal behavior arising form 1 µg of Ce, for $^{140}Ce^+$, $^{140}Ce^{16}O^+$ and $^{140}Ce^{2+}$ (a), (c) and (d); and after addition of 10 µl of 0.25 M NaF into a previously inserted electrode and upon re-insertion for $^{140}Ce^+$, $^{140}Ce^{16}O^+$ and $^{140}Ce^{2+}$, (b), (d) and (f) 461

7-32. Effect of $^{35}Cl^{16}O^+$ on $^{51}V^+$ determinations. Blank long undercut graphite electrode, $^{51}V^+$ (a) and $^{35}Cl^+$ (c); 10 µg of NaCl, $^{51}V^+$ (b) and $^{35}Cl^+$ (c) 462

7-33. Effect of $^{35}Cl^{16}O^+$ on $^{51}V^+$ determinations. After injection of 0.1 µg of V, $^{51}V^+$ (a) and $^{35}Cl^+$ (c); after addition of 10 µl of 0.25 M NaF and electrode re-insertion, $^{51}V^+$ (b) and $^{35}Cl^+$ (d) 465

7-34. The effect of Zn on U. 50 ng of Zn, $^{64}Zn^+$ (a) and $^{238}U^+$ (b); 50 ng of Zn and 10 µg of U, $^{64}Zn^+$ (c) and $^{238}U^+$ (d); after addition of 10 µl of 0.25 M NaF and electrode re-insertion, $^{64}Zn^+$ (e) and $^{238}U^+$ (f) 467

7-35. Same as Figure 7-34 without scale expansion..... 491

8-1. Illustration of a proposed 'next generation' DSID for ICP-MS 478

8-2. Block diagram of an atomic spectrochemical measurement system 481

8-3. Concept diagram illustrating a 'next generation' analytical instrumentation 485

8-4. Illustration of a spectrochemical answer machine 486

A-1. Optical configuration of a typical Paschen-Runge mount direct reading spectrometer 491

A-2. Block diagram of a typical readout system for a conventional direct reading spectrometer 492

A-3. Block diagram of a multichannel measurement system for a direct reading spectrometer based on i/f converters and a series of single channel frequency meters 494

A-4. Block diagram of a single measurement channel... 497

A-5. Circuit diagram for a single measurement channel 498

A-6. Simplified circuit diagram for the Microflex 65 bus to single channel system interface logic. LDB is the Local Data Bus, LAD is the Local Address Bus and LCB is the Local Control Bus, see text for discussion 503

A-7. Functional block diagram of the single channel system with the relocatable partial address decoding scheme 505

A-8. Simplified block diagram of the relocatable, switch configurable address decoding scheme 507

A-9. Circuit diagram of the address decoding scheme utilized in the single channel system. DAB is the Decoded Address Bus, see text for discussion 508

A-10. Photograph of the single channel system. The LEDs are Light Emitting Diodes, the 8253s are the programmable timer/counter chips, the 6522 VIA (Versatile Interface Adapter) is a digital I/O integrated circuit, the 74LS138 is a 3-line-to-8-line decoder/demultiplexer, the 74LS155 is a 2-line-to-4-line decoder/demultiplexer, the 74154 is a 4-line-to-16-line decoder/demultiplexer, S-1 is the first switch bank, S-2 is the second switch bank, the 74LS640 is an octal bus transceiver, the 74LS240s are octal buffers/line drivers, and the discrete transistor is a PNP 3393. The dimensions of the card are (LxW):6.5 v 3.9 in (164 v 100 mm) 513

B-1. Top view of DSID-base (see Figure C-2 for more details) 517

B-2. Top view of DSID-base (complements dimensions shown in Figure C-1) 518

B-3. Bottom view of DSID-base 519

B-4. Three-dimensional view of DSID- and of plexiglass-base 520

B-5. Lead screw support 521

B-6. Top view of sliding platform (dimensions in cm) 522

B-7. Top view of plasma box 523

B-8. Top view of plexiglass-base 524

B-9. Top view of plexiglass-base with the torch support in place 525

B-10. Side view of plexiglass-base with the torch support in place 526

B-11. Side view of torch, torch support and shutter... 527

B-12. Three-dimensional illustration of shutter....... 528

B-13. Top view of torch support assembly (with torch and shutter in place) on top of the plasma box 529

B-14. Side view of torch support brace 530

B-15. Front view of torch brace 531

B-16. Top view of torch support assembly on DSID-base 532

D-1. Simplified schematic diagram of the optical design of the SPS-10 Simultaneous Plasma Spectrometer.................................. 540

D-2. Schematic diagram of pre-disperser selection mask.. 542

D-3. Schematic diagram of instrument spectral operation....................................... 545

D-4. Mask-out/mask-in spectra for Cu................ 548

D-5. Mask-out/mask-in spectra for Fe................ 549

D-6. Mask-out/mask-in spectra for Ti................ 551

D-7. Spectra for Mo indicating source of leakage lines (see text for discussion).................. 552

D-8. Spectra for Si indicating sources of leakage lines (see text for discussion.................. 554

D-9. Mask-out/mask-in spectra for multielement solution (10 ppm Al, Cr, Fe, Mo, Ni, Si; 1 ppm Cu, Mg, Ti).................................. 555

D-10. Mask-out single element spectra composite with mask-in multielement spectrum.................. 557

D-11. Multielement bar graph spectrum................ 558

D-12. Mask-out/mask-in spectra for V................. 560

D-13. Superimposition of V and multielement bar graph spectra.................................. 561

D-14. Mask-out/mask-in spectra for Co................. 562

D-15. Superimposition of Co and multielement bar graph spectra.................................. 563

CHAPTER 6

DEVELOPMENT OF A COMPUTER-CONTROLLED DIRECT SAMPLE INSERTION DEVICE FOR ICP-MS

A. Introduction

Since the first description of an inductively coupled plasma-mass spectrometry (ICP-MS) system in 1980 [1], followed by the introduction of a commercial system in 1984, the technique has attracted a great deal of interest and has undergone rapid development. The expanding activity and widespread interest in ICP-MS is exemplified by the growing list of publications (over 120 references are listed in a 1987 literature compilation [2]), the organization of special conferences [3] and the commercial availability of two systems (with the introduction of two more pending). Currently, ICP-MS is widely accepted as a powerful tool for trace and ultra-trace elemental and isotopic analysis.

The wide acceptance of ICP-MS is due to its desirable characteristics. Included in these are [4-7]: routinely attainable low detection limits (which are 1-3 orders of magnitude lower that those achieved by inductively coupled plasma-atomic emission spectrometry (ICP-AES) under comparable operating conditions); spectral simplicity (ICP-MS spectra contain *"a maximum of 250 spectral lines, including virtually all elements, their isotopes, and possible polyatomic species"* [8] as opposed to thousands of lines found in ICP-AES spectra; and rapid isotope ratio measurement capability with moderate precision.

The success ICP-MS enjoys is partly due to the ICP, the plasma discharge is now being widely accepted in its new role as an ion source for mass spectrometry. And although ICP-MS systems maintain all noteworthy features of the ICP, they also inherit its most important current limitation which arises from sample introduction.

Even though the ICP was initially developed using liquid samples (typically pneumatically aspirated into the plasma), gaseous, powdered and solid samples can also be introduced. In principle, any sample introduction method used with ICP-AES can also be used with ICP-MS. For example, electrothermal vaporization [9, 10], laser ablation [11, 12], arc nebulization [13], slurry nebulization [14], flow injection [15, 16], and wire-loop [17] sample introduction systems have been coupled to ICP-MS.

A particularly attractive method involves the use of direct sample insertion devices (DSIDs). In these, the sample is placed into or onto a probe with subsequent introduction of the sample carrying probe, via the central tube of the torch, into the plasma, as shown in Figure 6-1. An extensive review of DSIDs for the ICP has been presented by Karanassios and Horlick [18].

The advantages offered by a DSID for ICP-AES include increased sample introduction efficiency and an inherent ability to handle µl volumes of liquids and mg quantities of powdered/solid samples with little or no sample pretreatment [19-21]. In addition to these, a host of benefits are anticipated to arise from coupling a DSID to

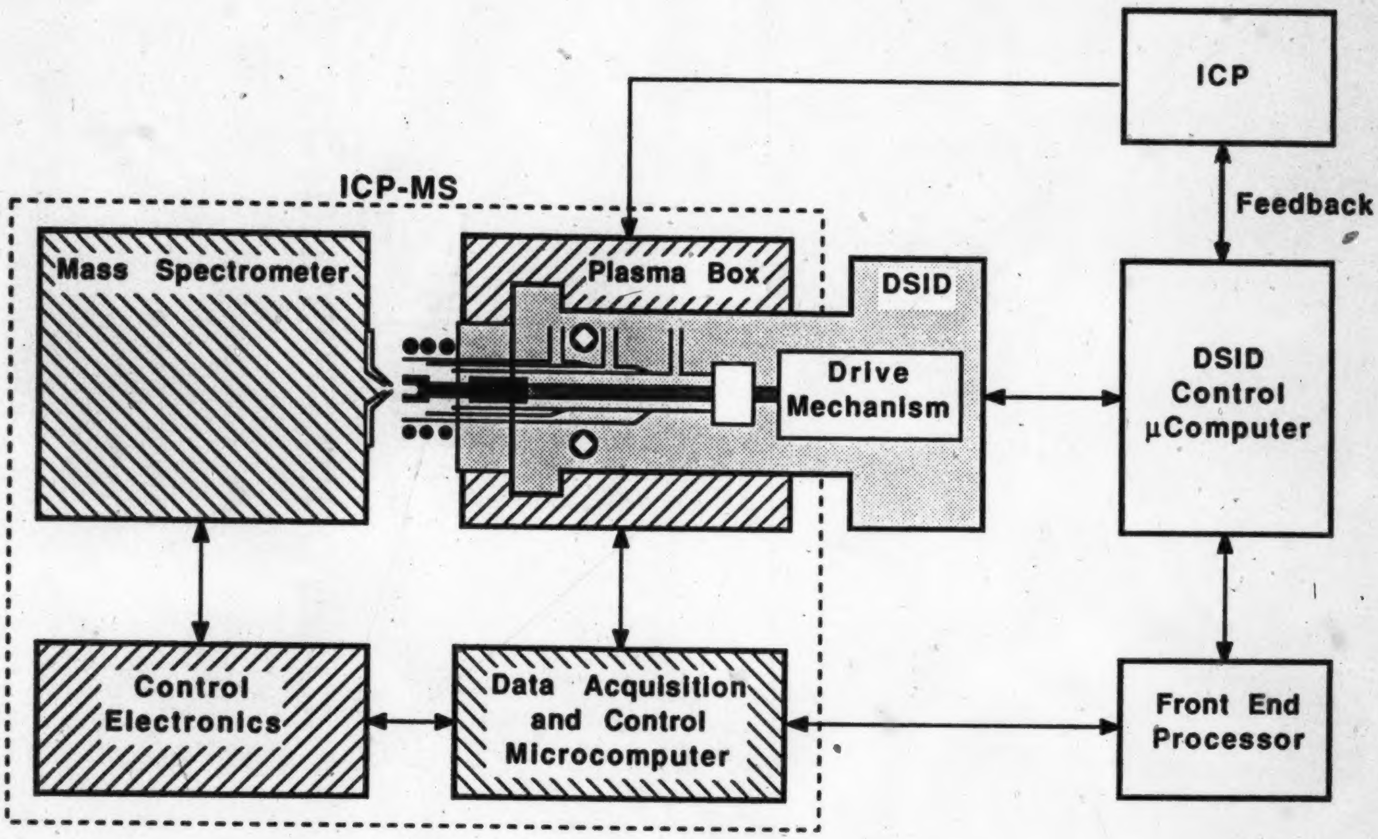
ICP
Feedback
ICP-MS
Mass Spectrometer
Plasma Box
DSID
Drive Mechanism
DSID Control µComputer
Control Electronics
Data Acquisition and Control Microcomputer
Front End Processor

Figure 6-1. Block diagram of the experimental set-up of a DSID for ICP-MS.

ICP-MS. These are expected to originate from the use of a dry plasma (defined as one in which neither sample nor solvent is introduced into the discharge). Among these are reductions in spectroscopic interference, for example, isobaric overlaps [7, 22, 23]), in non-spectroscopic interference, for instance, matrix effects [7, 24], and elimination of solvent loading effects [25-27]. Therefore, due to the advantages of a DSID, the impressive performance characteristics of ICP-MS and the benefits of a dry plasma, an ICP-MS DSID is expected to be a powerful combination and to extend the analytical capability and utility of ICP-MS.

In previous investigations, a 'next generation DSID' [19] and its application as an intelligent sample processor for the ICP have been proposed [19, 20, 28]. The findings of these investigations and the experience gained by using the ICP-AES-DSID will be used as the basis for the development and characterization, discussed both here and elsewhere [29], of a DSID for ICP-MS.

The aim of this study is the development and subsequent characterization of a computer-controlled DSID capable of handling a variety of sample carrying probes and implementing the 'next generation' concepts previously proposed. Because ICP-MS time is at premium in our laboratory, a key design goal for this system was rapid changeover (i.e., less than 5 min) from the conventional pneumatic nebulizer system of the ICP-MS utilized in this work to the DSID.

Because a finite amount of sample is placed into graphite or metal cups (Figures 6-2a and 6-2b) or onto wire-loops (Figure 6-2c), the spectral signals observed with a DSID are peak-like and transient in nature [19-21]. Typical examples of analyte temporal behavior are shown in Figure 6-3. With respect to Figure 6-1, the transient nature of the spectral signals defines a data acquisition mode for simultaneous multielement analysis, it determines the nature of readout electronics, and it defines the software requirements for data acquisition, signal processing, display and DSID control. And much like a DSID for ICP-AES [19], the DSID imposes new constraints on data acquisition and software. These issues will be addressed in detail and the development of new software will be discussed. The preliminary nature of the work reported here and in the following chapter is worth mentioning. Unfortunately, the ICP-MS system installed in our laboratory was not functioning when this work was slated for completion. And although more work remains to be done in order to characterize the DSID, it is felt that the preliminary results presented in the following adequately demonstrate its capabilities.

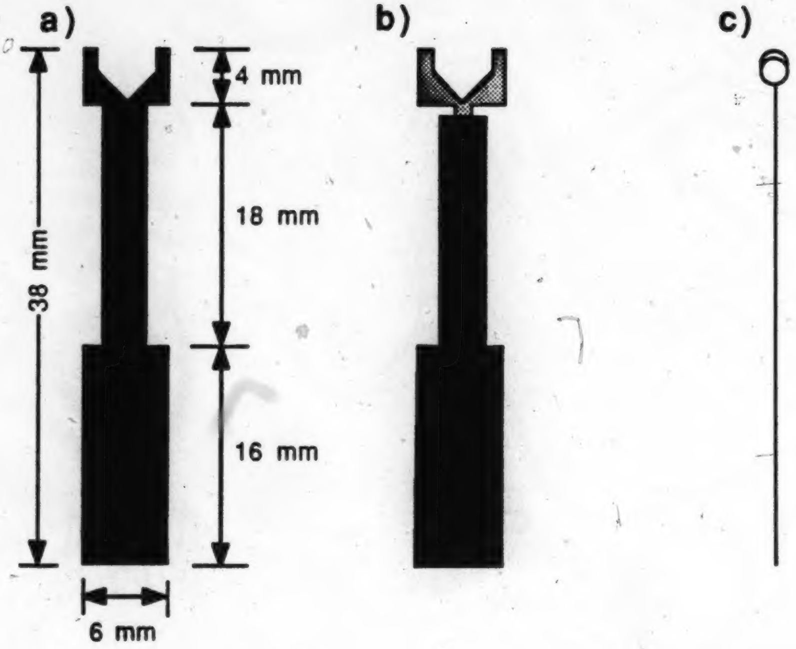
a)
b)
c)
4 mm
18 mm
16 mm
38 mm
6 mm

Figure 6-2. Sample carrying probes utilized in this work. (a) long undercut graphite electrode; (b) long undercut electrode fitted with a metal cup; (c) wire-loop.

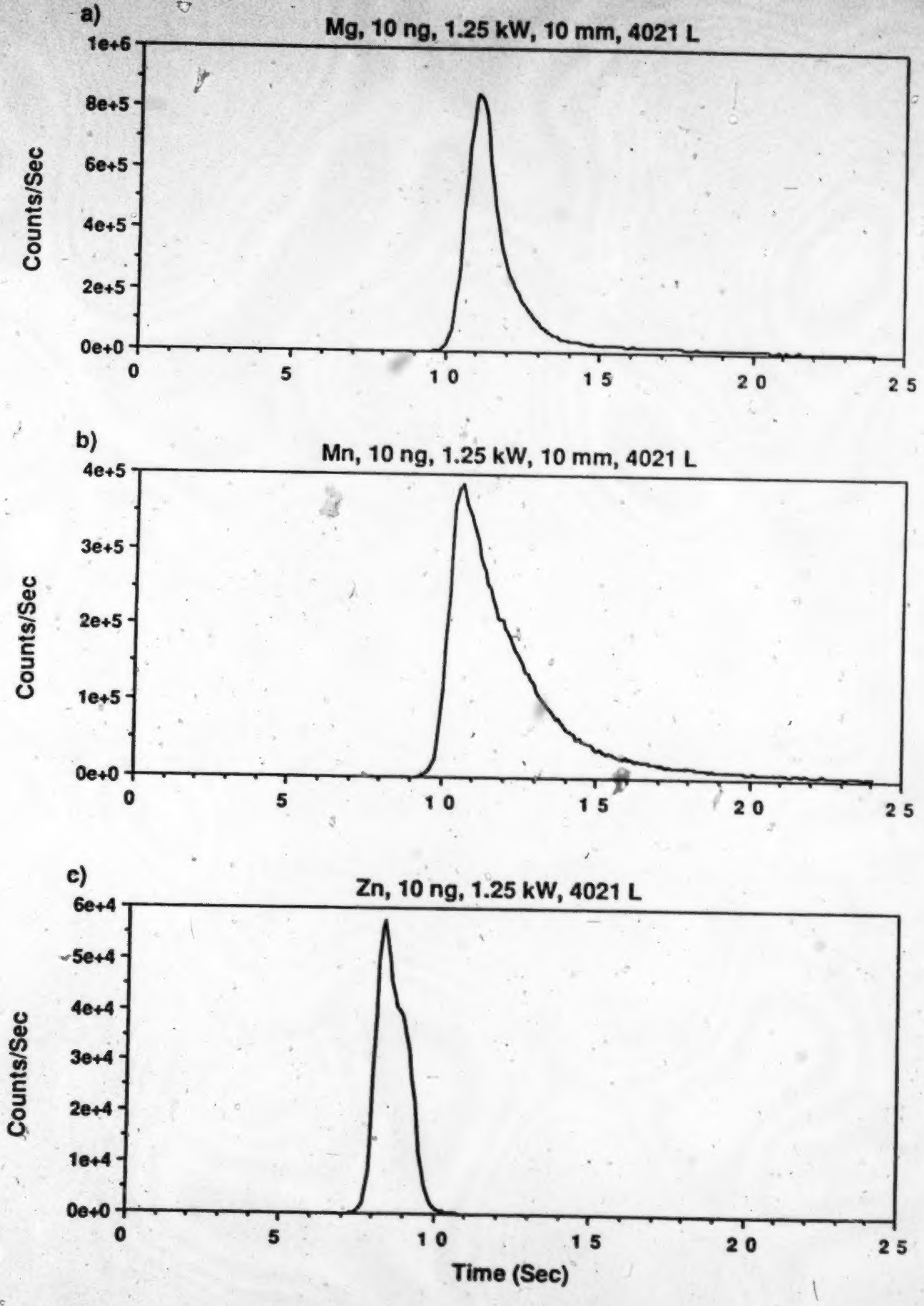

Figure 6-3. Typical analyte temporal behavior.

B. **Instrumentation**

B.1 ICP-MS, Computer Systems and Operating Conditions

The basic components required for a DSID for ICP-MS are shown in Figure 6-1. The horizontally operated DSID described here bolts on top of the plasma box. A Sciex Elan model 250 (Perkin-Elmer/Sciex Instruments, Thornhill, Ontario, Canada) ICP-MS system with vendor-modified ion optics was utilized in this work. Because a key design goal was to operate the device with the Elan instrument cover closed and the RF plasma shield (located on top of the plasma box) in place, the length and the height of the DSID were dictated by the size of the Elan system and the height of the RF shield. Holes were cut in the Elan cover and the RF plasma shield in order to accommodate operation of the DSID with both covers closed.

As mentioned earlier, the signals generated by a DSID are peak-like and transient in nature (Figure 6-3), thus dictating the use of a multichannel spectrometer for simultaneous multielement analysis. However, by virtue of its design, the quadruple-based mass spectrometer utilized by the Elan is sequential in nature. A way to circumvent this limitation is by making intensity measurements at one mass for a given period of time (referred to as a "dwell time") and then rapidly switching (via electronic means) into another mass. This "peak-hopping" mode provides some multielement capability, the extent of which depends upon dwell time, peak widths, analyte volatility and the number of elements/masses scanned. These considerations will be discussed in detail in a later section.

Data acquired by the Elan were serially transferred to the front-end processor for further processing, display and presentation. More specifically, a network of three-computer systems was utilized in this work (Figure 6-1). A Multibus-based microcomputer [30] equipped with an 8086 CPU and installed on the Elan was used for data acquisition and ICP-MS control. An Apple II+ microcomputer [31] equipped with a 6502 CPU and running a menu-driven program was used for DSID control, while an Apple Macintosh Plus microcomputer (68000 CPU) served as a front end processor. Data acquired by the Multibus-based microcomputer were serially transferred to the Macintosh (via its modem port) for further processing and presentation. The Apple II+ (equipped with a super serial card supplied by Apple Computer, Inc.) also communicated serially with the Macintosh (via its printer port).

Data acquisition (t=0 s) was initiated by simultaneously pressing the <Return> key on both the Elan terminal and the Apple II+ microcomputer when the sample carrying probe was in alignment with the central tube of the torch (referred to as the 'reference position' in Figure 6-4).

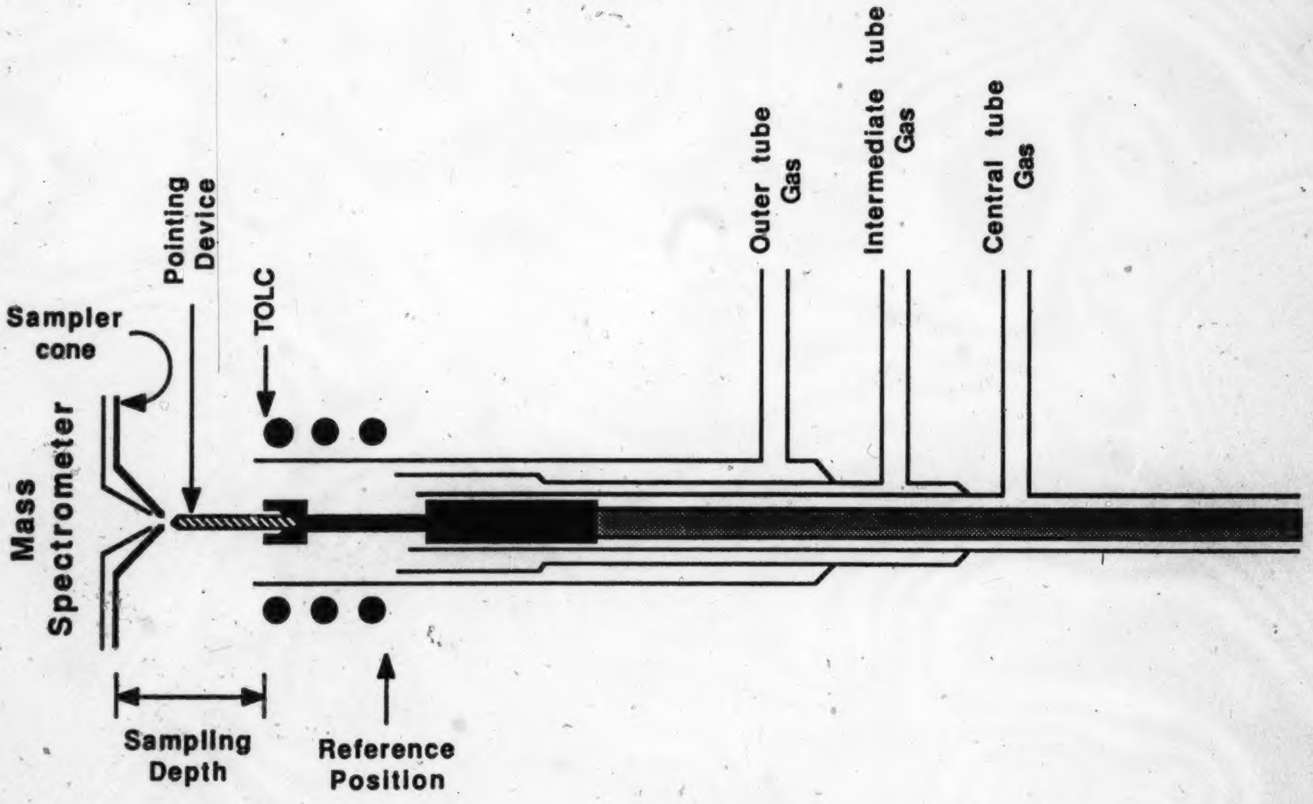
Sampler cone
Pointing Device
TOLC
Outer tube Gas
Intermediate tube Gas
Central tube Gas
Mass Spectrometer
Sampling Depth
Reference Position

Figure 6-4. Schematic illustration of alignment device.

However, due to software overhead and the difference in the time of pressing the <Return> keys, t=0 s varied from run to run and, thus, it cannot be used as a reference point for comparison purposes of analyte emission temporal behavior and of appearance time (defined as the time at which the peak maximum appears). Because the most effective probe insertion position for the ICP-AES-DSID previously described in chapter 2 was found to be that in which the top of the sample carrying probe was in alignment with the top of the load coil (TOLC in Figure 6-4), all measurements were taken with the probe inserted in that position.

The inability to continuously aspirate a solution in order to align the center of the torch with respect to the sampler cone orifice of the mass spectrometer was overcome by utilizing the device shown in Figure 6-4 and by translating the plasma box-DSID combination horizontally (in the +y or -y direction, Figure 6-5). This allowed precise alignment of the probe with the sampler cone orifice which is critical for transient signals. The sampling depth (Figure 6-4) was varied by translating the plasma box-DSID combination horizontally (in the +x or -x direction, Figure 6-5), and except where otherwise indicated, a depth of 10 mm above the load coil was chosen.

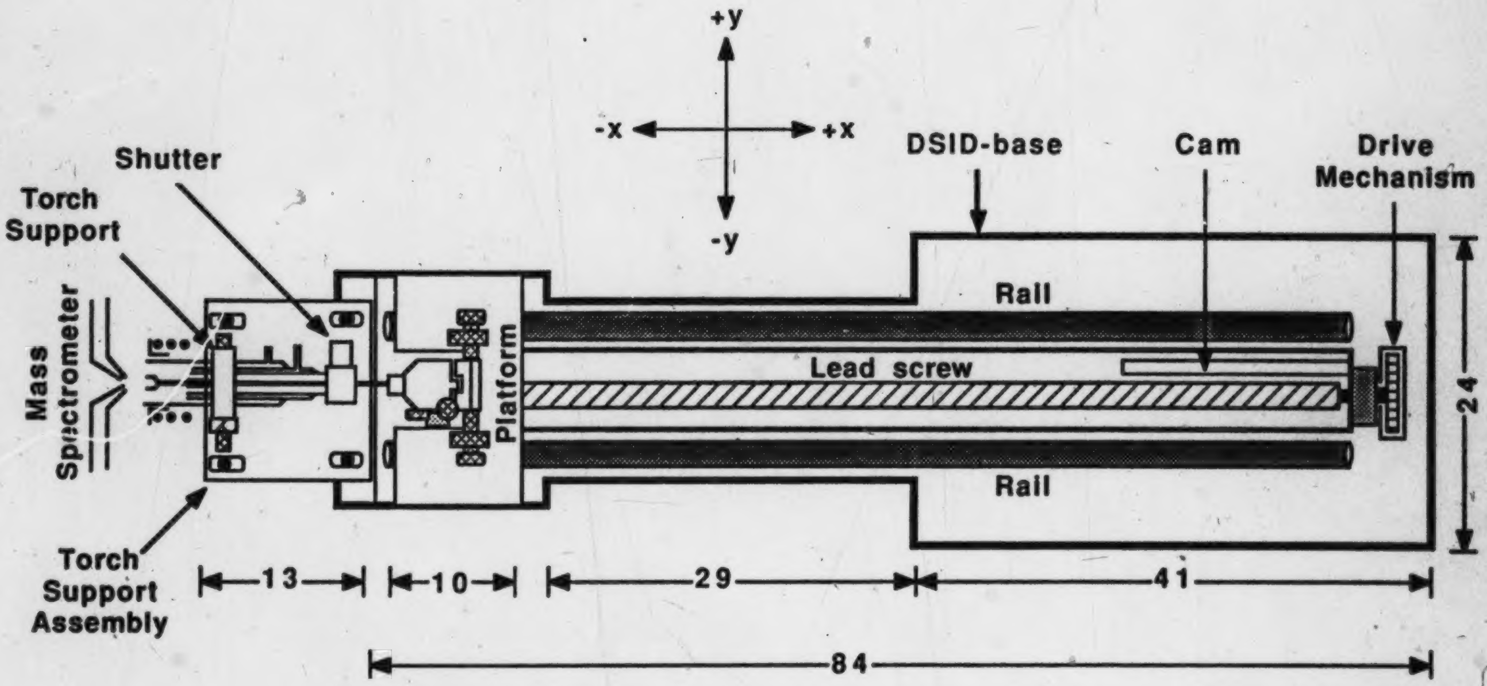
+y
-x
+x
-y
DSID-base
Cam
Drive Mechanism
Shutter
Torch Support
Mass Spectrometer
Platform
Rail
Lead screw
Rail
Torch Support Assembly
24
13
10
29
41
84

Figure 6-5. Top view of the Direct Sample Insertion Device (x, y is the plane of the drawing, the z-axis is perpendicular to the drawing).

Unless otherwise stated, typical operating conditions were: forward power, 1.25 kW; reflected power, less than 5 W; outer tube (coolant) gas (Ar) 14 l/min; intermediate tube (auxiliary) gas (Ar) 1.8 l/min; and central tube (nebulizer) gas (Ar) 0.9 L/min. The ion lens voltages used are listed in Table 6-1. These were established using a pneumatic nebulizer system, by running a 0.1 ppm Cu solution and by maximizing for the Cu signal before installing the DSID.

The long undercut graphite electrodes utilized in this work (shown in Figure 6-2a and often referred to as the 4021 L electrode) were machined in our laboratory out of the corresponding HPND+ 4021 graphite electrode (SPEX Industries, Inc., Edison, NJ or Bay Carbon, Inc., Bay City, MI). Prior to their use, the graphite electrodes were treated as previously described [19]. Metal cups (i.e., Mo and Ta) were machined out of the corresponding metal rod and were placed on top of a long undercut electrode as shown in Figure 6-2b. The wire-loop (Figure 6-2c) consists of a W wire, 8 cm in length and 1 mm in diameter that forms two loops, 5 mm in diameter each. Unless otherwise stated, the use of a long undercut graphite electrode is assumed.

All solutions were prepared by serial dilution with distilled/deionized water of 1000 ppm standard stock solution (standards for plasma emission spectroscopy, SPEX Industries, Inc., Edison, NJ) of the respective element.

Table 6-1. Ion lens voltage settings.

Lens	Setting	Voltage (V)
Bessel Box Barrel (B)	50	5
Bessel Box Plates (P)	30	-18
Einzel Lens (E1)	95	-19
Photon Stop (S2)	40	-8

A 10 µl volume was transferred (i.e., injected) to the sample carrying probe utilizing an Eppendorf micropipette. Solution volumes injected into cups were dried by heating the electrode in an aluminium holder on a hot plate prior to insertion into the plasma. Those applied onto the wire-loop were dried with an IR-lamp.

B.2 DSID

As mentioned earlier, the basic components of a DSID for ICP-MS are shown in Figure 6-1. At the heart of this system is the DSID itself. A top view of the horizontally-operated DSID developed in this work is shown in Figure 6-5 and a three-dimensional view of the system is shown in Figure 6-6. (Detailed drawings of the DSID are included in Appendix B).

The key design constraints for this sample introduction system are revealed by considering the tight mechanical tolerances, the need to reduce ICP-MS down-time, and its intended use for rapid prototyping of probe geometries and torch designs. Furthermore, in order to facilitate a key design goal, namely that of utilizing a variety of sample carrying probes and, because no two torches have identical dimensions, the DSID should be easily and rapidly aligned.

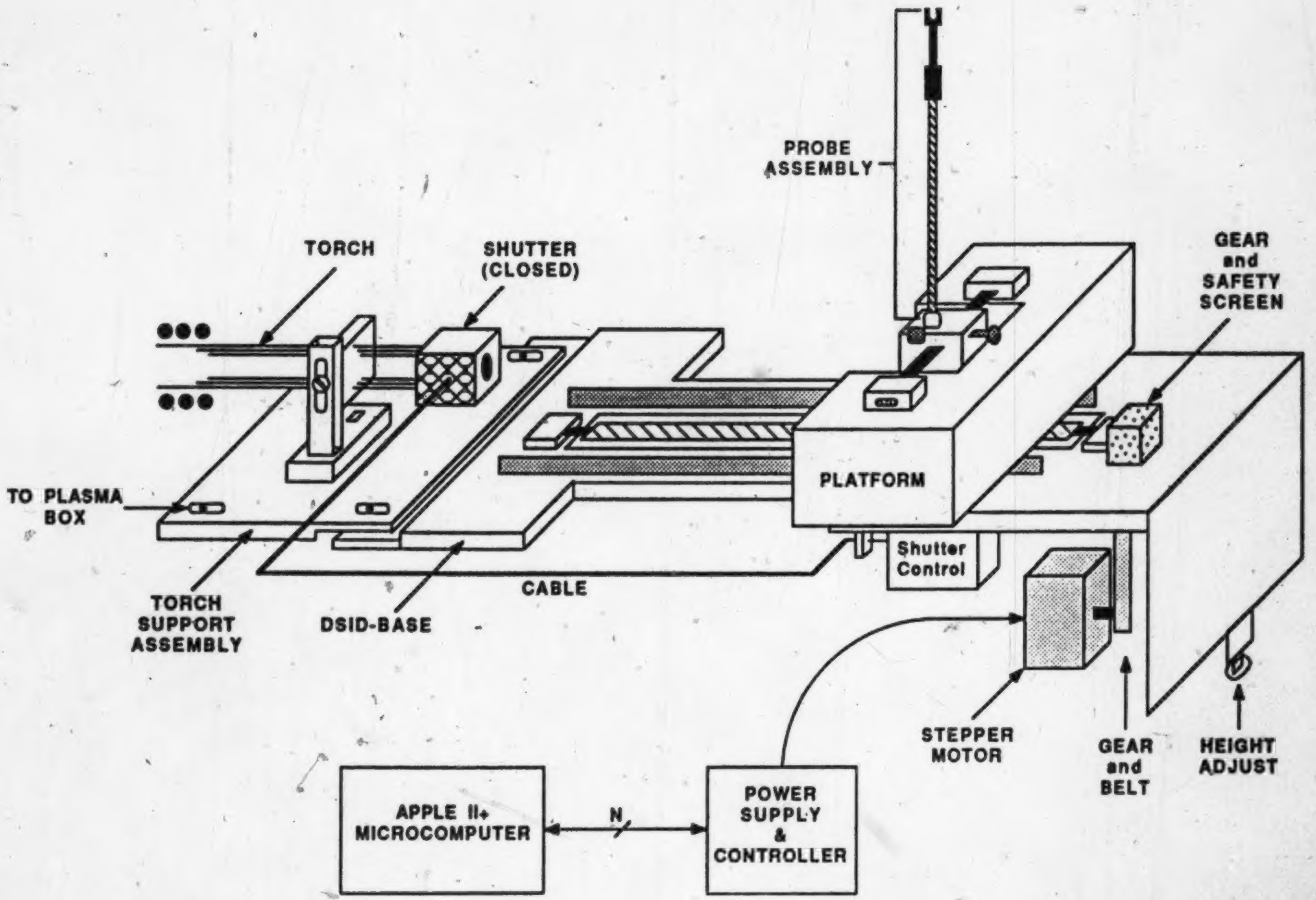
PROBE ASSEMBLY
TORCH
SHUTTER (CLOSED)
GEAR and SAFETY SCREEN
TO PLASMA BOX
PLATFORM
Shutter Control
CABLE
TORCH SUPPORT ASSEMBLY
DSID-BASE
STEPPER MOTOR
GEAR and BELT
HEIGHT ADJUST
APPLE II+ MICROCOMPUTER
N
POWER SUPPLY & CONTROLLER

Figure 6-6. Three dimentional view of the DSID (not to scale).

More specifically, as revealed by close examination of Figures 6-5 and 6-6, it should be easy to align: the torch with respect the load coil; the sample carrying probe with respect to the central tube of the torch; and the center of the sample carrying probe with respect to the mass spectrometer sampler (Figure 6-4). These aspects will be addressed when discussing the appropriate building blocks of the DSID.

Four functional blocks can be distinguished in this DSID design (Figures 6-5 and 6-6). The torch support assembly, the platform carrying the probe assembly, the DSID base and the drive mechanism.

The torch support assembly, a three-dimensional view of which is shown in Figure 6-7, consists of a plexiglass base, the torch support, the torch and the shutter (which is placed directly on the torch). The plexiglass base, which is bolted onto the plasma box on one side and on the DSID-base on the other side (Figures 6-5 and 6-6), can be easily adjusted horizontally in the x-direction. The torch support can be easily adjusted in both the y-direction (e.g., horizontal) and the z-direction (e.g., vertical), thus providing a total of three degrees of freedom. In this way, the torch can be easily positioned and centered within the load coil, and as a consequence, it can be easily aligned with respect to the sampler cone orifice of the mass spectrometer (Figure 6-7).

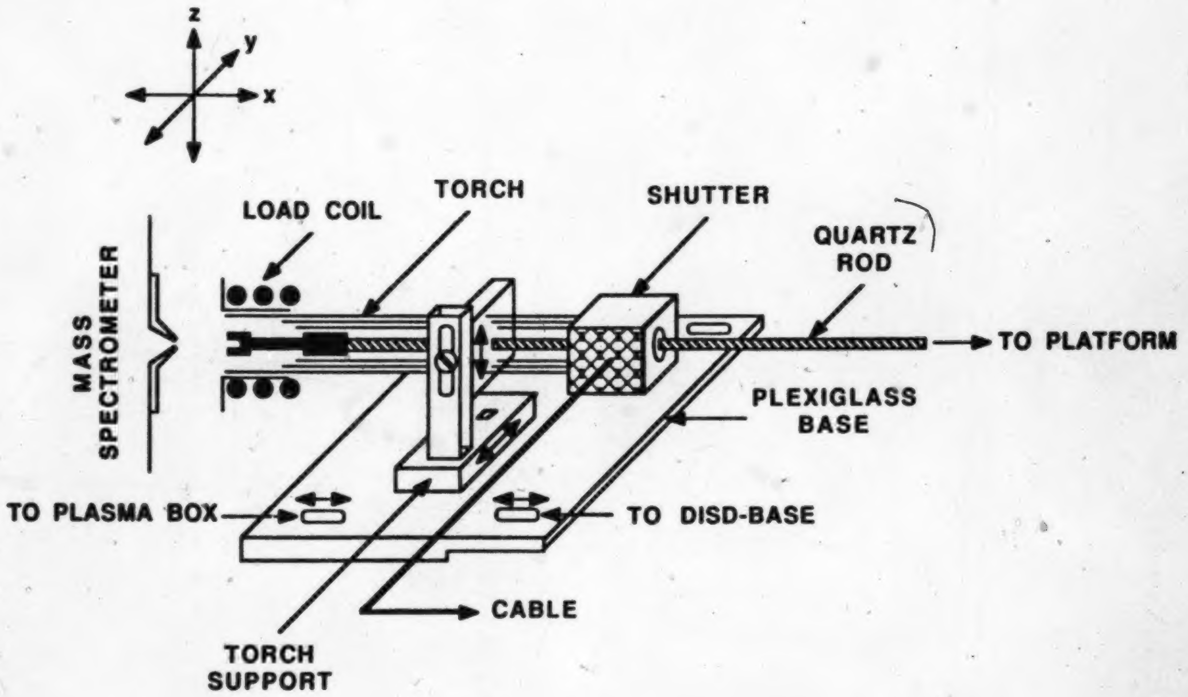
z
y
x
LOAD COIL
TORCH
SHUTTER
QUARTZ ROD
MASS SPECTROMETER
TO PLATFORM
PLEXIGLASS BASE
TO PLASMA BOX
TO DISD-BASE
CABLE
TORCH SUPPORT

Figure 6-7. Three-dimensional view of torch support assembly (not to scale).

At the heart of the torch support assembly is a modified Fassel-type torch. The torch is simply modified, by removing the tip of the central tube and by making the tube wider than the typical 1.5 mm (Figure 6-8). As mentioned earlier, the shutter is placed directly on the torch (Figure 6-7). This feature helped maintain the three degrees of freedom provided by the torch support assembly, it simplified the design and it alleviated the need for unconventional torch designs, as reported in the literature for some DSIDs for ICP-AES [19].

The L-shaped shutter utilized in this work consists of a spring-loaded Teflon plunger, as illustrated in Figure 6-9. The shutter is opened and closed electromechanically. The shutter control mechanism basically consists of a 110 V solenoid which is mounted underneath the DSID (Figure 6-6). The action of the solenoid is transferred to the shutter via a bowden cable (e.g., a typical bicycle brake-cable). In its default state the shutter is closed. And although the plasma can be operated with the bottom of the torch open, when the plasma is operated with an open shutter, the discharge physically moves down and rests upon the inner-tubes of the torch, thus causing overheating of the torch. Though it has not been tested, prolonged operation, for example more than 10 min, with an open shutter may also cause torch melt-down.

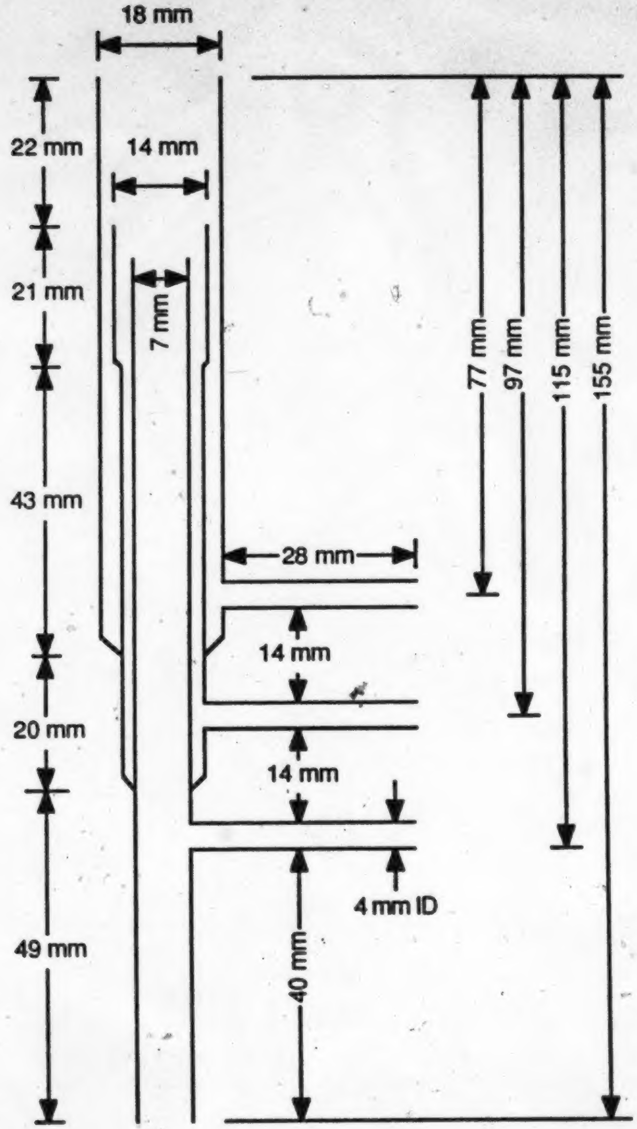
18 mm
22 mm
14 mm
21 mm
7 mm
43 mm
28 mm
14 mm
20 mm
14 mm
49 mm
4 mm ID
40 mm
77 mm
97 mm
115 mm
155 mm

Figure 6-8. Schematic illustration of the 'DSID' torch.

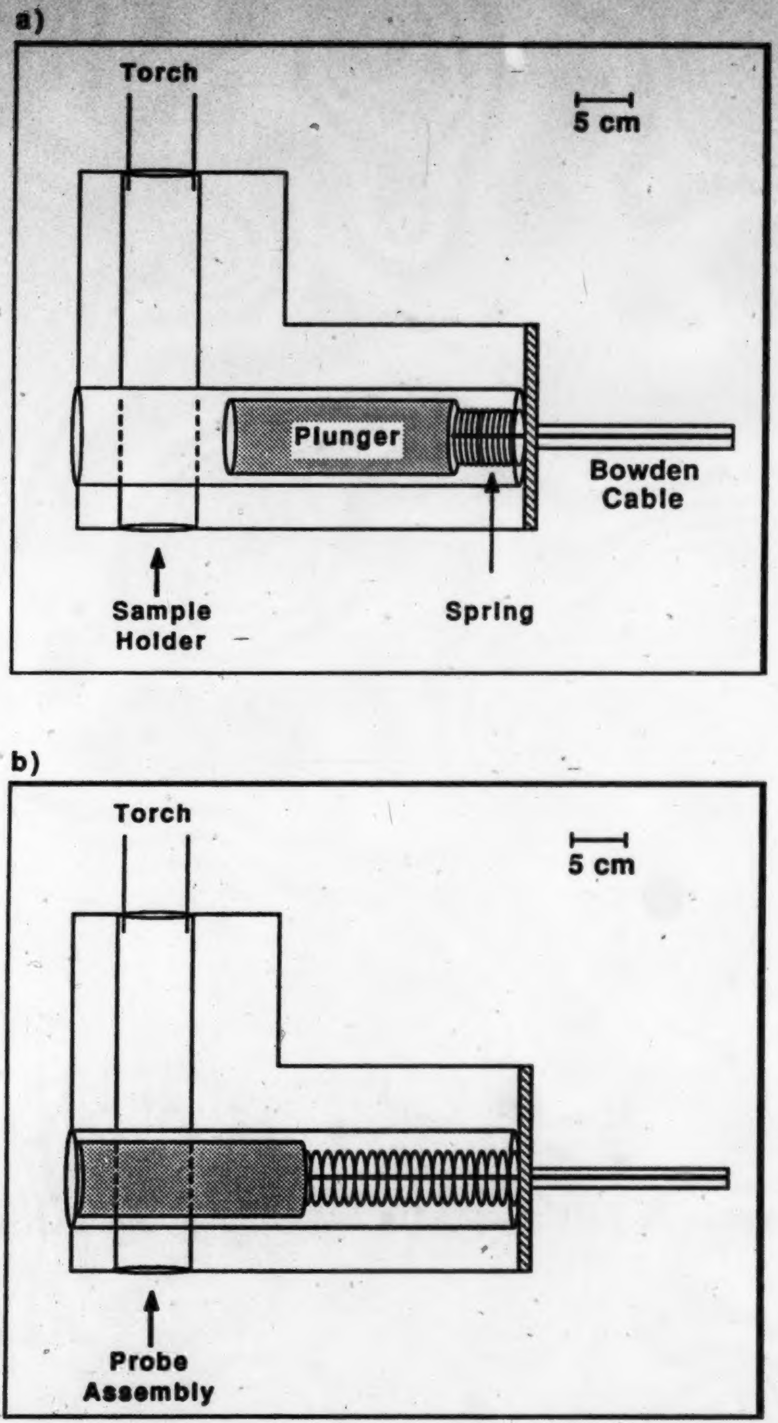
a)
Torch
5 cm
Plunger
Bowden Cable
Sample Holder
Spring
b)
Torch
5 cm
Probe Assembly

Figure 6-9. Top view of the shutter, (a) open and (b) closed.

The sliding platform (a top view of which is shown in Figure 6-10) consists of six main parts: the probe assembly, the probe assembly support, and vertical and horizontal probe assembly position adjusting mechanisms, which are shown in Figure 6-10; and a cam follower (i.e., a wheel attached to the end of a lever, as shown in Figure 6-11), a ball bearing nut (Figure 6-12), and a pillow block bearing system (Figure 6-12) which are mounted underneath the platform.

The probe assembly (Figure 6-10), consists of a quartz rod fitted on one side with the sample carrying probe (a long undercut graphite electrode is shown here) and on the other with a cylindrical Teflon adapter which is mounted inside the probe assembly support and secured (i.e., locked into place) with the aid of a simple nut-and-bolt clamp (identified as the probe adapter clamp in Figure 6-10).

The probe assembly support consists of a stainless steel rotating shaft, a notched block (labeled A in Figures 6-10 and 6-11), a grooved block (labeled B in Figures 6-10 and 6-11), and the cam follower (Figure 6-11). The grooved part is connected to the sliding platform via the rotating shaft and two position adjusting mechanisms (a simple nut-and-bolt design mounted on top of the platform and identified as 'horizontal probe assembly position adjusting mechanism' in Figure 6-10). These are used in tandem to allow the probe assembly to be adjusted horizontally on the

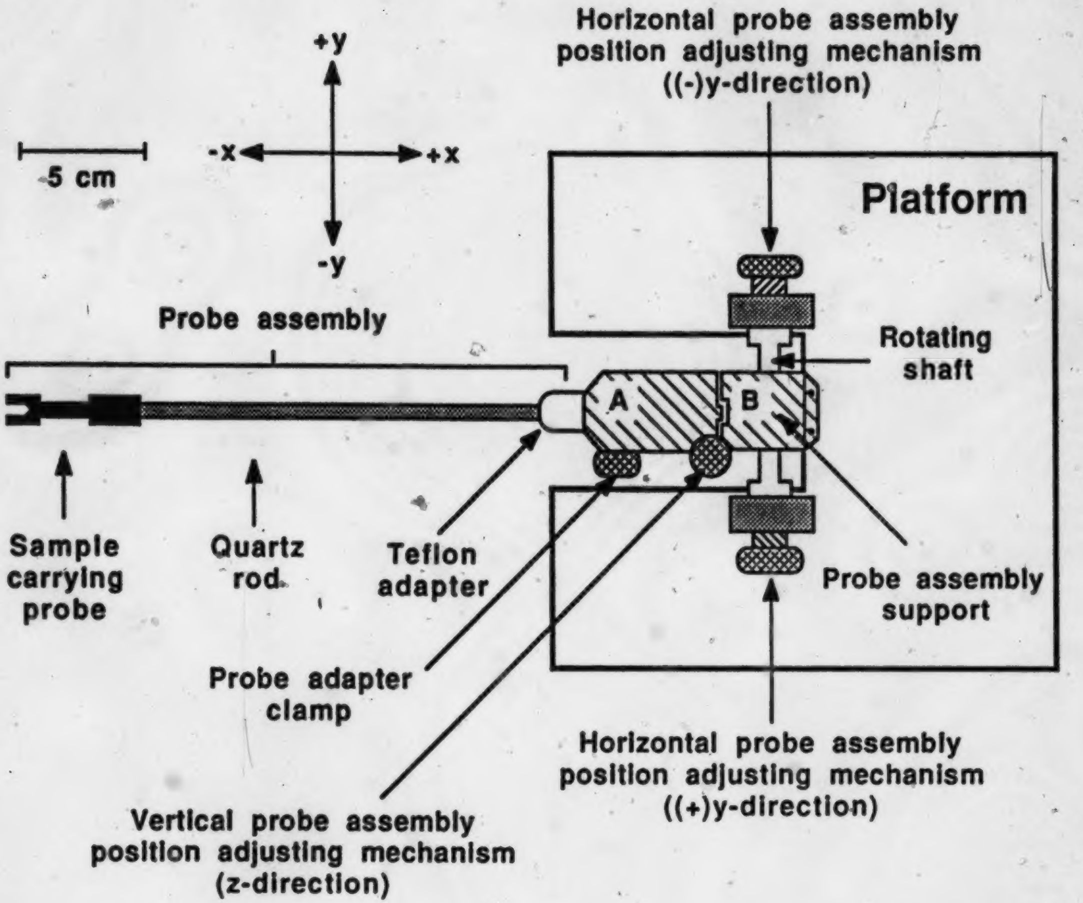
Horizontal probe assembly position adjusting mechanism ((-)y-direction)
+y
-x
+x
-y
5 cm
Platform
Probe assembly
Rotating shaft
A
B
Sample carrying probe
Quartz rod
Teflon adapter
Probe assembly support
Probe adapter clamp
Horizontal probe assembly position adjusting mechanism ((+)y-direction)
Vertical probe assembly position adjusting mechanism (z-direction)

Figure 6-10. Top view of the sliding platform (x- and y-axis define the plane of the page, the z-axis is perpendicular to the drawing).

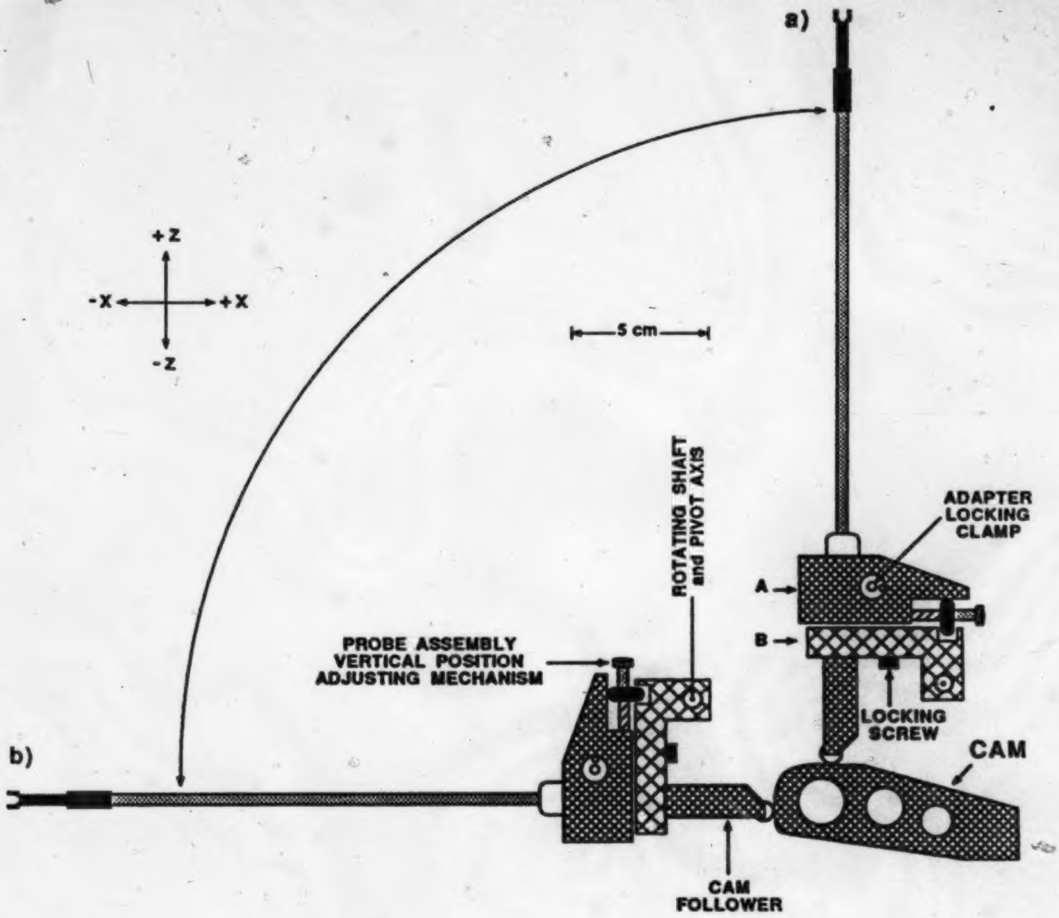
a)
+Z
-X
+X
-Z
5 cm
ADAPTER LOCKING CLAMP
ROTATING SHAFT and PIVOT AXIS
A
B
PROBE ASSEMBLY VERTICAL POSITION ADJUSTING MECHANISM
LOCKING SCREW
CAM
b)
CAM FOLLOWER

Figure 6-11. Schematic illustration of the probe assembly support, (a) probe assembly positioned vertically; (b) probe assembly positioned horizontally.

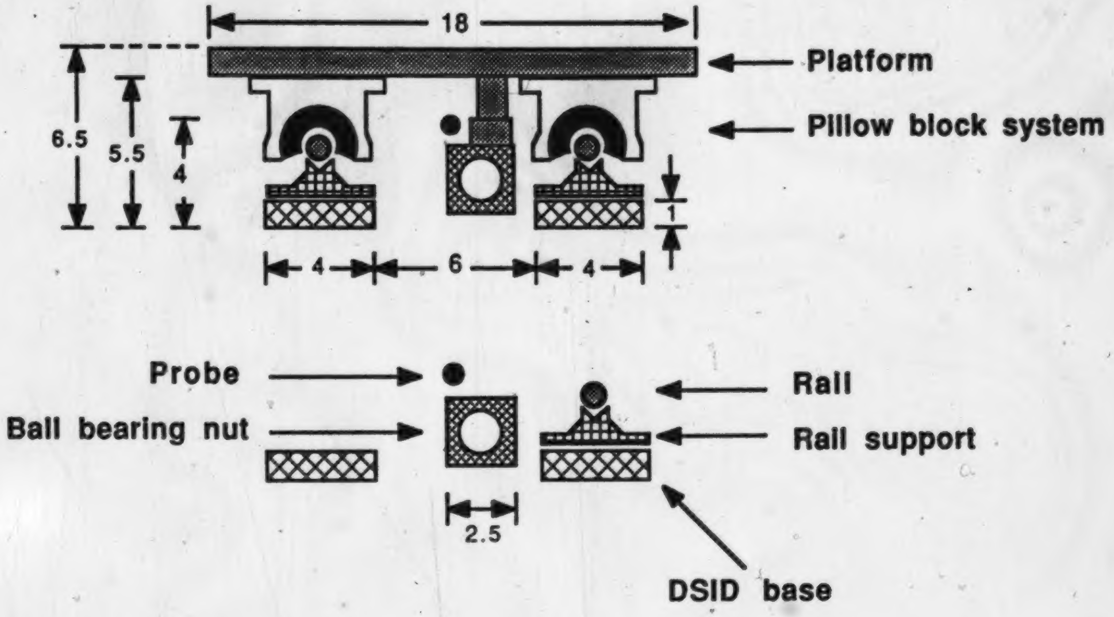
18
Platform
Pillow block system
6.5
5.5
4
1
4
6
4
Probe
Ball bearing nut
Rail
Rail support
2.5
DSID base

Figure 6-12. Front view of sliding platform (probe assembly support not shown for clarity, dimensions in cm).

y-axis (i.e., in the +y or -y direction, Figure 6-10). A second position adjusting mechanism, labeled the 'vertical probe assembly position adjusting mechanism' in Figures 6-10 and 6-11, is sandwiched between the notched and the grooved parts of the probe assembly support (Figures 6-10 and 6-11). This mechanism allows the notched part (and consequently the probe assembly) to be adjusted vertically (i.e., up or down on the z-axis). Once the vertical position has been adjusted, the two parts are bolted together by means of a locking screw (Figure 6-11). In this way, the center of the sample carrying probe can also be easily aligned with the sampler cone orifice (Figure 6-7).

The probe assembly support, which freely rotates on the notched rotating shaft (Figure 6-10), can attain any position between 0° (horizontal, x-axis) and 90° (vertical, z-axis) depending on the position of the cam follower on the cam (Figure 6-11, the cam is bolted on the DSID-base, Figure 6-5). For example, if the sliding platform moves forward (i.e., right-to-left in Figure 6-11 or +x to -x direction in Figure 6-10) from its position in Figure 6-11a, the cam follower (as its name implies) follows the cam. The probe assembly follows an arced trajectory and, as the platform moves forward, it ends up positioned horizontally when the end of the cam travel is reached, as shown in Figure 6-11b. If the direction is reversed (i.e., the sliding platform is moving from left-to-right or -x to +x direction in Figure 6-10), the probe assembly follows the reverse path and the horizontally positioned probe assembly (Figure 6-11b) is raised to the upward (i.e., home) position (Figure 6-11a), thus making probe replacement an easy task. This position was also chosen because it makes robotic manipulation of sample carrying probes a relatively easier task [29], an important consideration in this design.

The platform is bolted onto two pillow block bearings which slide on round rails (12.7 mm in diameter) and which form the basis of a guide-rail bearing system (Figure 6-12). The rails are mounted on a rail support which is bolted onto the DSID-base, thus forming the basis of a 'track' on top of which the platform is sliding. (The rail/rail support system, simply referred to as rails, can be thought of as the equivalent of a train track with the sliding platform serving the function of a trolley). The aluminium DSID-base is hollow in the middle in order to accommodate the lead screw driving the sliding platform and the cam (Figure 6-5).

The ball bearing nut (THK Co., Ltd., 6-4, 3-chome, Kamiosaki, Shinagawa-ku, Tokyo, Japan) is connected (with a vibration absorbing mechanism) to the platform and a lead screw (i.e., a precision, course-threaded, 5 mm-per-revolution, ball-bearing shaft also supplied by THK Co.). The lead screw is, in turn, driven by a microcomputer-controlled stepper motor (Rogers Labs, 2710 South Croddy Way, Santa Ana, CA 92704), the action of the motor is transferred to the lead screw with the aid of a timing belt (Figure 6-6). The stepper motor (Oriental motor, type PH 299-01 supplied by Rogers Labs) was interfaced to an Apple II+ microcomputer via a stepper motor timer/driver board (Rogers Labs, model A6 T/D) and a stepper motor driver board (Rogers Labs, model R2D34). The two external power supplies required were built in our electronics shop. The menu driven stepper motor control software was written in BASIC around a series of machine language subroutines which were provided by Rogers Labs.

Insertion of the sample carrying probe into the torch is accomplished by sending the appropriate data and instructions (via the Apple II+ microcomputer) to the stepper motor. As the platform slides forward from its initial position (i.e., home position, Figure 6-13a), the probe assembly rapidly attains a horizontal position, as depicted in a stepwise fashion in Figures 6-13b and 6-13c, and previously discussed in conjunction with the sliding platform and the cam follower. Because in its default state the shutter is closed, the probe assembly is on a collision course with the shutter (Figure 6-13c). When the top of the probe is a few mm away from the shutter (Figure 6-13c), the probe is stopped and the shutter is opened (currently under manual control) in order to accommodate probe insertion into the torch.

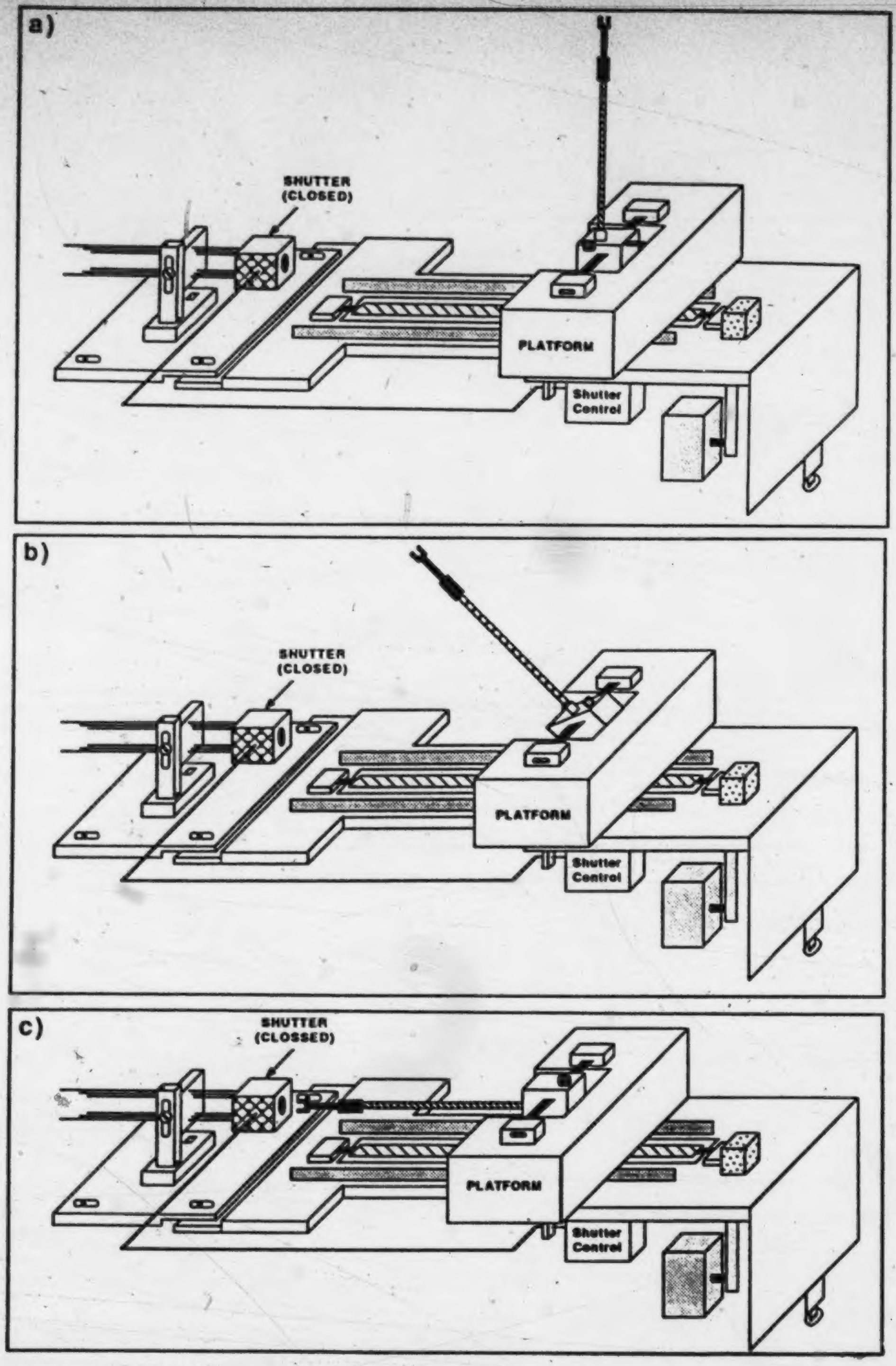
a)
SHUTTER
(CLOSED)
PLATFORM
Shutter
Control
b)
SHUTTER
(CLOSED)
PLATFORM
Shutter
Control
c)
SHUTTER
(CLOSSED)
PLATFORM
Shutter
Control

Figure 6-13. Schematic illustration of probe assembly at: (a) the home position; (b) an intermediate position and (c) the horizontal position..

Upon insertion (Figure 6-14), the sample carrying probe can be stopped below the load coil where, much like a DSID for ICP-AES, drying and ashing can take place *in situ* below the plasma prior to atomization. These steps, which are currently under computer control, are analogous to the dry, ash, and atomize cycles of graphite furnace spectrometry. When these steps have been completed, final insertion to TOLC can be initiated. Because the speed of the final insertion stage (i.e., reference position to TOLC) was found to exert a considerable influence on analyte emission temporal behavior and the analytical performance characteristics of the device [20], it was a major consideration in this design. With this system, it takes a fraction of a second for the sample carrying probe to travel the final ~22 mm (i.e., from the reference position to TOLC). It is worth noting that it takes approximately 5 seconds for the sample carrying probe to cover the distance from the home position (Figure 6-13a) to a few mm away from the shutter (Figure 6-13c).

Retraction is accomplished by simply reversing the direction of the motor. A 3-dimensional view of probe retraction is shown, in a step-by-step fashion, in Figures 6-13c, 6-13b and 6-13a. The shutter is closed as soon as the sample carrying probe exits the torch and after it clears the shutter (Figure 6-13c).

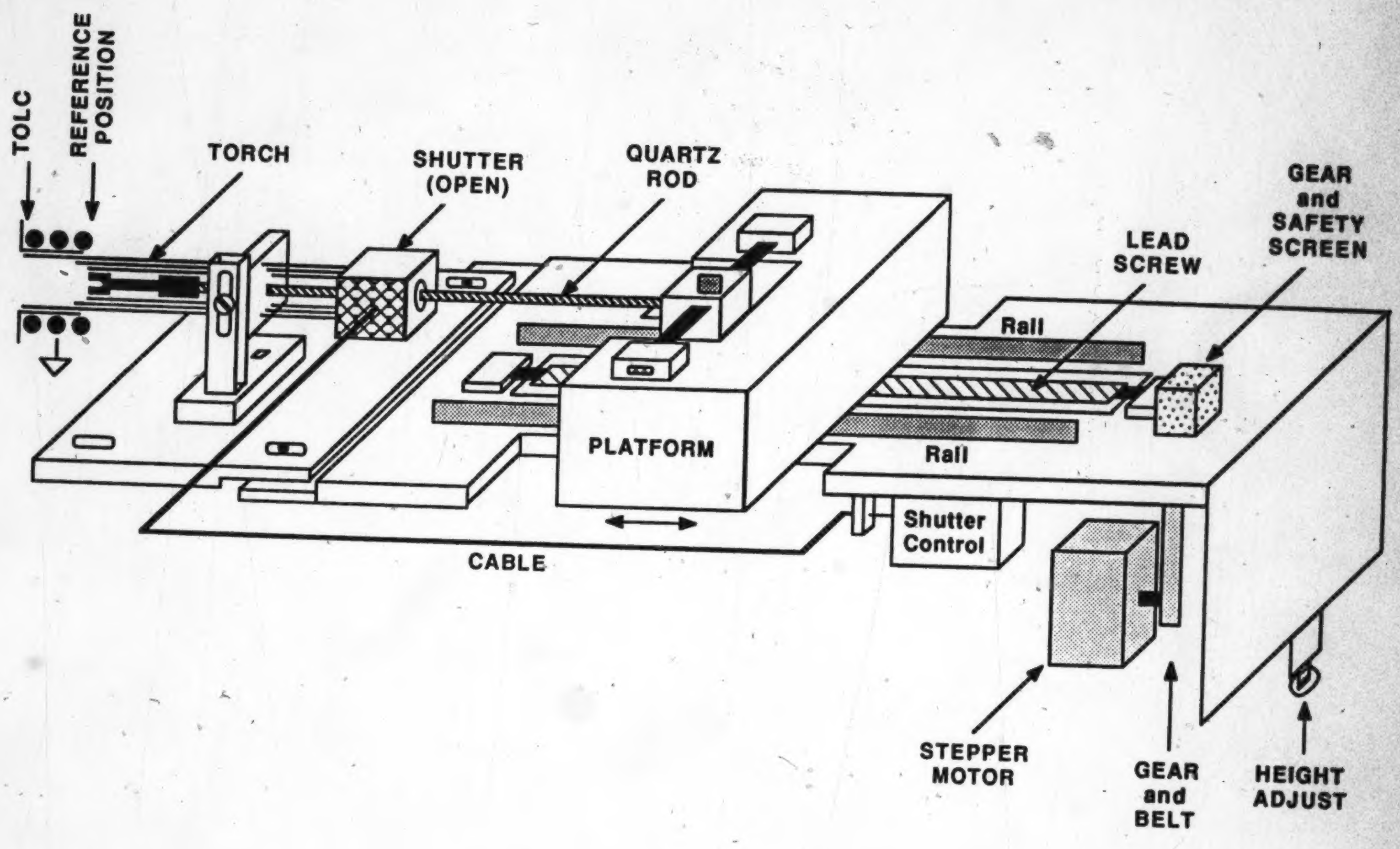
TOLC
REFERENCE POSITION
TORCH
SHUTTER (OPEN)
QUARTZ ROD
LEAD SCREW
GEAR and SAFETY SCREEN
Rail
PLATFORM
Rail
Shutter Control
CABLE
STEPPER MOTOR
GEAR and BELT
HEIGHT ADJUST

Figure 6-14. Schematic illustration of probe insertion.

A

It should be noted that the plasma is only very slightly disturbed upon probe insertion and retraction. In addition, formation of a discharge filament between the plasma and the sample carrying probe upon retraction (a typical occurrence in some DSIDs for ICP-AES [19, 33]) has not been observed here, thus further simplifying design and operation of the device (i.e., there is no need for extra gas manifolds [19, 33] or foreign gases [34] in order to snuff out filament formation). This is possibly due to grounding of the middle load coil of the ICP (frequently referred to as a center-tap ground). The center-tap ground (Figure 6-14) is currently available only on the Elan system. Upon final probe insertion (i.e., to TOLC), the plasma is very stable, more so than the ICP-AES DSIDs utilized in this laboratory [19, 33, 34]. This extra plasma stability can also be attributed to the center tap ground of the load coil.

In summary, in response to the requirements for flexibity and rapid change-over between a conventional pneumatic sample introduction system and the DSID, the computer-controlled device described in this work has been developed. In this design, once the device has been aligned (an operation which is usually done off-line, thus further reducing ICP-MS down-time), change-over is facilitated (in less than 5 min) by simply removing the standard pneumatic nebulizer sample introduction system of the Elan and by replacing it with the DSID. In addition, the ability to easily and rapidly align the torch with respect to the load coil and the sample carrying probe with respect to the center of the torch, were key objectives in this design. These were met as described above.

B.3 Data Acquisition Considerations

As it has been amply demonstrated with DSIDs for ICP-AES, differential vaporization of analyte is an important aspect of the DSIT (direct sample insertion technique). Therefore, due to the temporal behavior displayed by analytes, and much like ICP-AES [19], the resulting peak-like signals must also be acquired as time-varying intensities and be digitized in real-time in ICP-MS. As mentioned earlier, a peak hoping mode was used to provide some multichannel/multielement measurement capability, the success of which depends upon peak widths.

Typical results obtained utilizing a 1.25 kW applied forward power, a long undercut graphite electrode, a two mass (i.e., Cu and Zn) peak-hopping measurement mode, and a 100 ms and 10 ms dwell time are shown in Figure 6-15a and Figure 6-15b. The data acquired by the Elan microcomputer were serially transferred to the Macintosh at 1200 baud for further processing and presentation. And although 10 points/s were expected for a 100 ms dwell time, only 3 to 4 points/s were actually acquired.

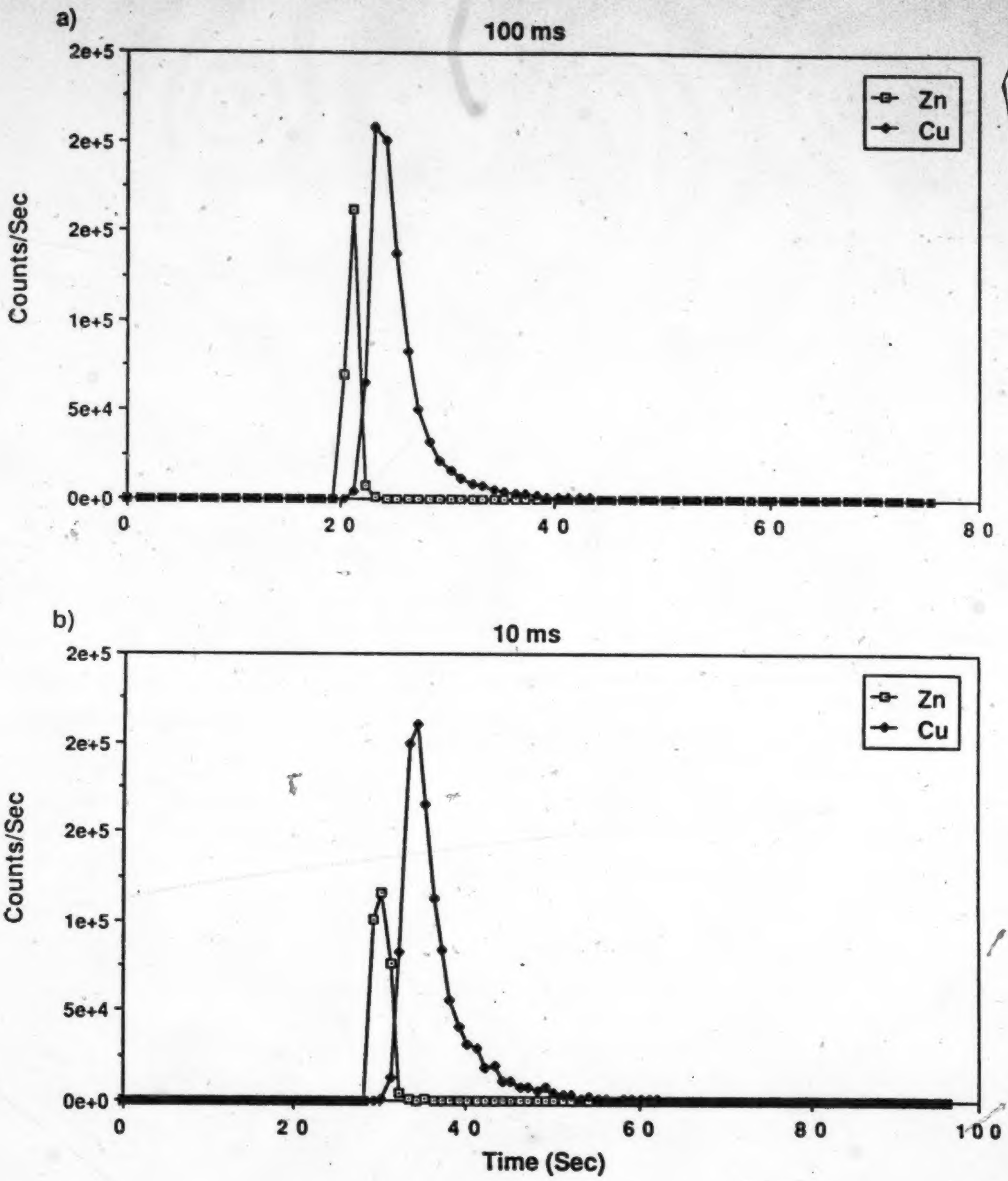

Figure 6-15. Typical temporal behavior for Cu and Zn (10 ng each) as transferred to the Macintosh at 1200 baud.

The situation worsens when a 10 ms dwell time is used, only 4 to 6 data points/s are acquired. The discrepancy between the expected and the acquired nuber of points per second must be due to software overhead imposed by the Elan system. As a consequence, even with a 10 ms dwell time, an inadequate number of data points is acquired in order to define analyte temporal behavior. The situation worsens even further as peak widths decrease by considering, for instance, higher plasma powers (i.e., 2.00 kW), low volatility elements (i.e., Cd), and sample carrying probes with low thermal mass (i.e., a W wire-loop). To illustrate the point, peak widths of a few hundred milliseconds for a wire loop system have been reported for DSIDs for both ICP-AES [18] and ICP-MS [17]. Clearly, a solution to this problem must be found, otherwise software would limit the applicability of the DISD to ICP-MS. It should be noted that the problems encountered here are not unique to the DSID, similar problems have been encountered by others when utilizing sample introduction techniques that generate transient analyte populations, such as electrothermal vaporization devices [35, 36], in conjunction with the Sciex Elan. In response to the afore-mentioned requirements, the parameter set described in Appendix D was used on the Elan and new software developed for the Macintosh.

B.4 Software

The function of this program (written on the Macintosh in LightSpeed Pascal, Think Technologies, Inc., 420 Bedford St., Suite 350, Lexington, MA 02173) is two-fold. First, to facilitate high speed data transfers between the Elan and the Macintosh and to allow the operator to control the DSID from the Macintosh screen. Such an approach is expected to form the foundation for a more complete implementation of a loosely-coupled distributed intelligence network [30], thus giving rise to an overall system design of the concept previously described by Karanassios and Horlick [36]. The second function is to provide a further implementation of some HPI (Human Processor Interface) concepts concepts previously developed for an ICP-AES-DSID [37].

The menu structure of the program developed here is shown in Figure 6-16, the menu items are self-explanatory. And much like the software package developed for data acquisition, control and signal processing and presentation for a DSID for ICP-AES [19], this program also borrows and implements the hierarchical menu concept. A typical example of a hierarchical menu as implemented here is shown in Figure 6-17.

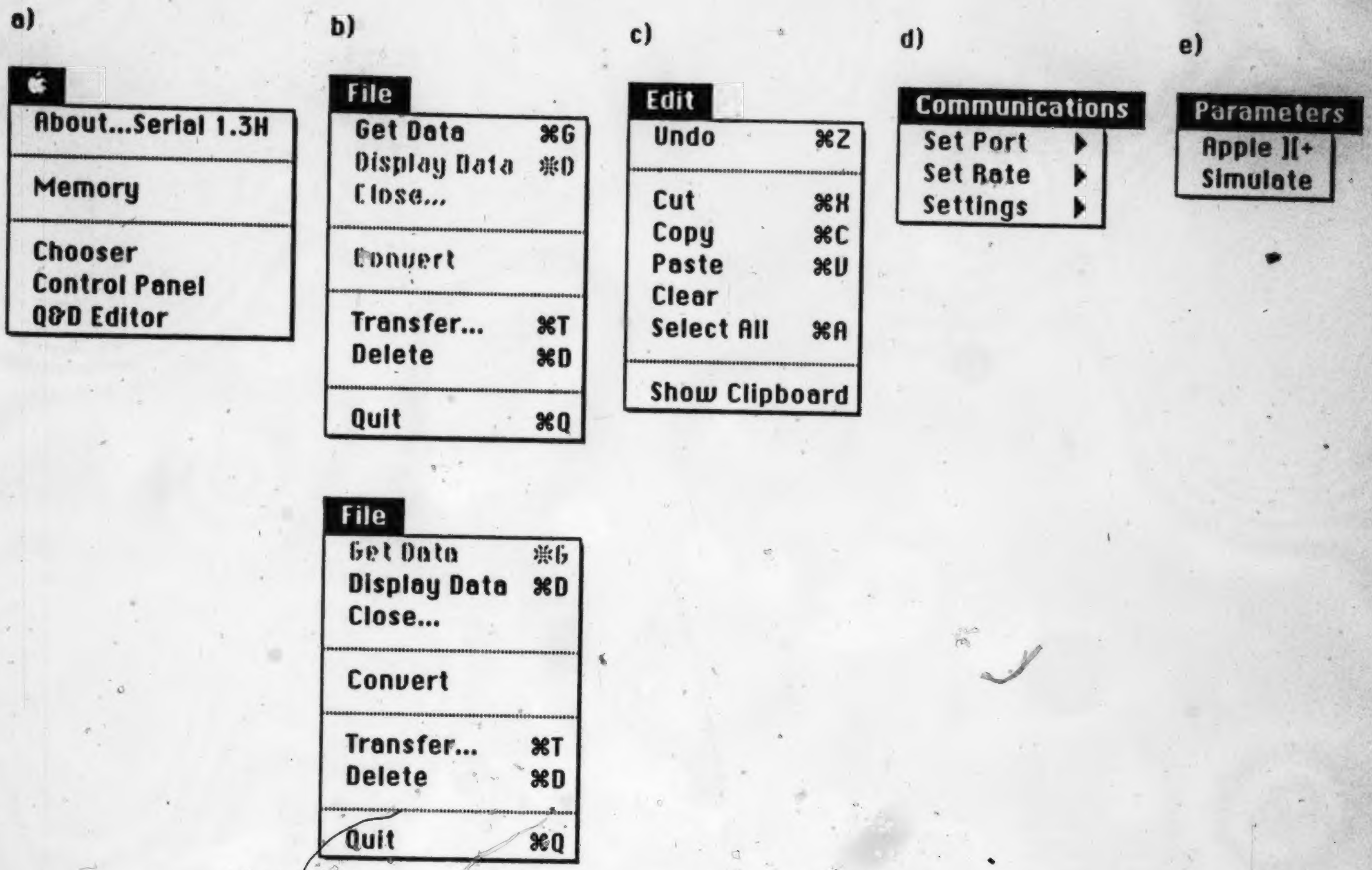
a)
About...Serial 1.3H
Memory
Chooser
Control Panel
Q&D Editor
b)
File
Get Data ⌘G
Display Data ⌘D
Close...
Convert
Transfer... ⌘T
Delete ⌘D
Quit ⌘Q
c)
Edit
Undo ⌘Z
Cut ⌘X
Copy ⌘C
Paste ⌘V
Clear
Select All ⌘A
Show Clipboard
d)
Communications
Set Port
Set Rate
Settings
e)
Parameters
Apple][+
Simulate
File
Get Data ⌘G
Display Data ⌘D
Close...
Convert
Transfer... ⌘T
Delete ⌘D
Quit ⌘Q

Figure 6-16. Pull-down menu structure.

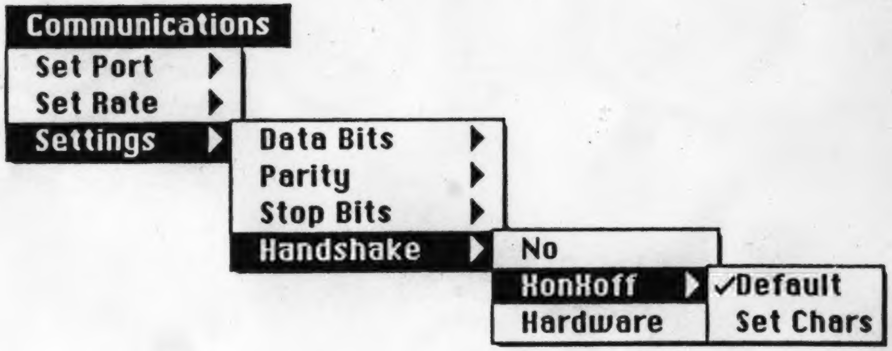
Communications
Set Port ▶
Set Rate ▶
Settings ▶
Data Bits ▶
Parity ▶
Stop Bits ▶
Handshake ▶
No
XonXoff ▶
Hardware
✓Default
Set Chars

Figure 6-17. An example of a hierarchical menu.

B.4.1 For Serial Transfers and DSID Control

Upon selection of menu item "Get Data" of the "File" menu (Figure 6-16b), data acquired by the Elan microcomputer are serially transferred to the Macintosh at 9600 baud with no error checking. The 32 kbyte limit for a serial buffer on the Macintosh (as set by Apple) was bypassed in this work. This allowed blocks of data as large as 400 kbytes (the size of a single-sided, 3.5 inch floppy-disk) to be transferred at that speed. With this software package, a typical 20 kbyte block of data is transferred in about 20 sec. In contrast, it takes about 200 sec (over 3 min) to transfer the same block of data at the typical 1200 baud rate (the maximum data rate that can be utilized when error detection is supported), thus making data transfers an unnecessarily time-consuming operation. Due to the high speed data transfers and the speed of probe insertion and retraction, the mean time between consecutive sample insertions is approximately the same as that required by conventional pneumatic nebulizer systems for consecutive sample runs. This is becoming an increasingly important consideration as operating costs rise and budgets are cut.

Menu item "Apple II+" of the "Parameters" menu (Figure 6-16e) deserves special mention. By selecting it, a new window appears on the screen that allows the user to take complete control of the Apple II+ and to run the DSID from the Macintosh, thus giving rise to the computer network pictorially represented in Figure 6-1.

Typical results obtained with this software package, the parameter set described in Appendix D, a 1.25 kW applied forward power, a long undercut graphite electrode, a two mass (i.e., Cu and Zn) peak-hopping measurement mode, and 100 ms and 10 ms dwell times are shown in Figure 6-18a and Figure 6-18b. From these results, it can be concluded that an adequate number of data points is acquired when a 100 ms dwell time is used (Figure 6-18a), and that the peak-like signals are over-sampled when a 10 ms dwell time is used (Figure 6-18b). The number of points/s acquired is in marked contrast with and a considerable improvement over those shown in Figures 6-15a and 6-15b.

In general, when one mass is 'scanned' and a 100 ms dwell time is used 8 points/s are acquired, with a 10 ms dwell time the number of points/s rises to 75. However, the situation worsens as the number of scanned masses increases. For example, a 100 ms and a 10 ms dwell time yield 5 and 36 points/s for a two mass scan, a 23 and a 1 points/s for a three mass scan and a 23 and 1 point/s for a four mass scan. The results of the effect of the number of masses scanned on the number of acquired points/s when different dwell times are used are summarized in Figure 6-19. From these, it can be concluded that the number of data points/s is dependent on the number of elements/masses

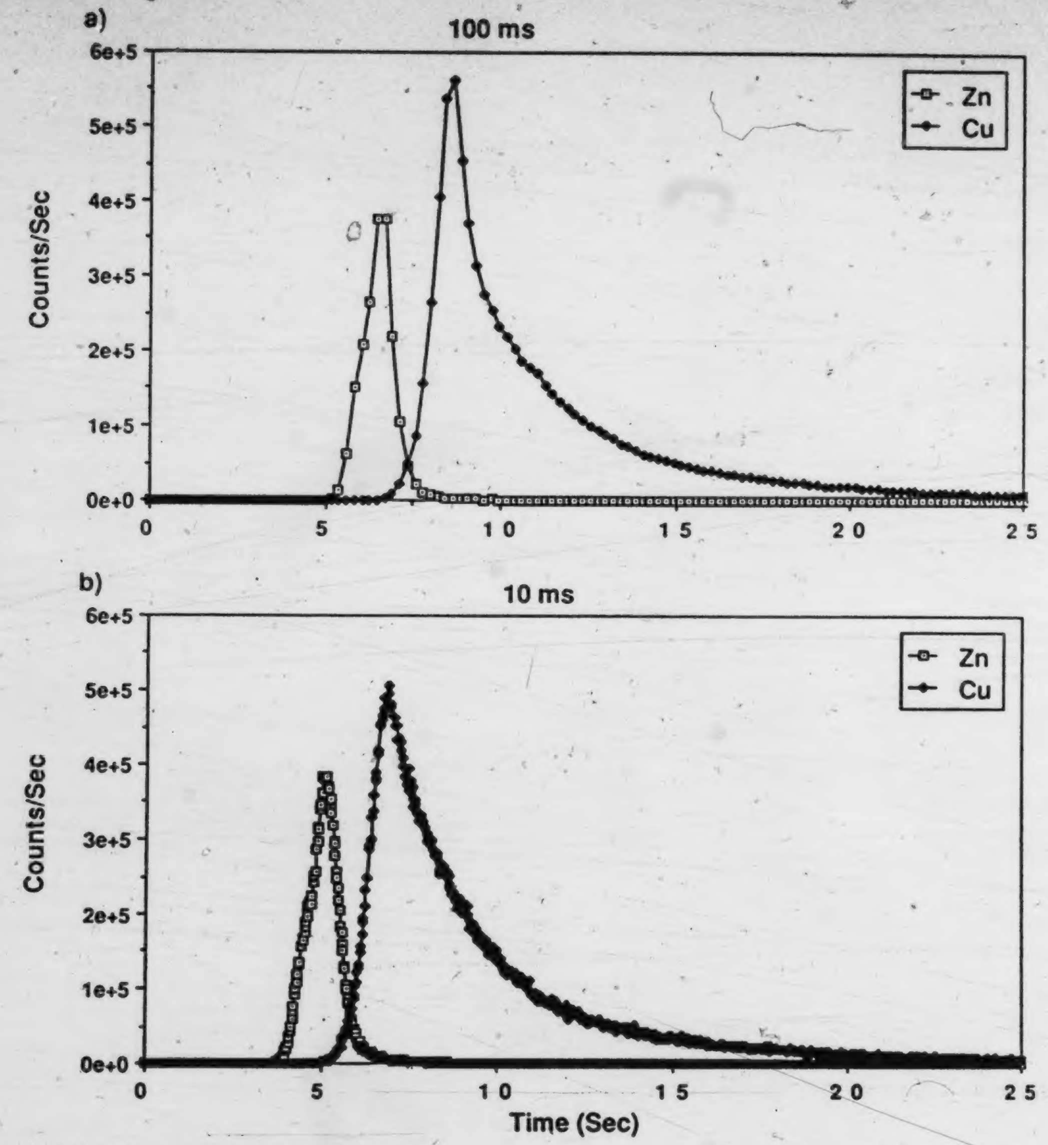

Figure 6-18. Typical temporal behavior for Cu and Zn (10 ng each) as transferred to the Macintosh at 9600 baud.

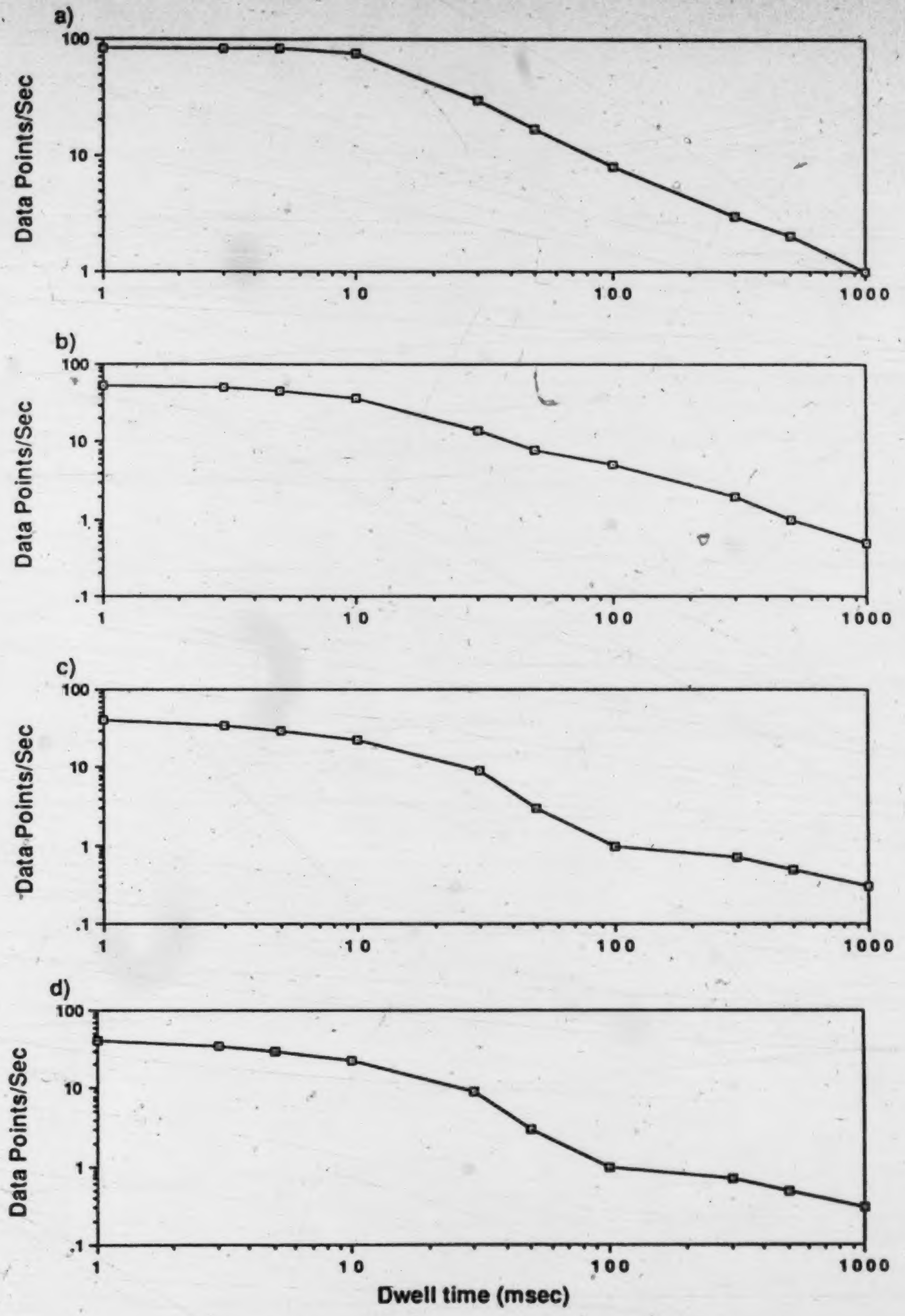

Figure 6-19. Number of data points/second per number of masses scanned. (a) One mass; (b) two masses; (c) three masses and (d) four masses.

scanned for a given dwell time. Similar results have been reported for an ICP-MS/laser ablation system, were the sample rate was inversely proportional to the number of masses scanned [12]. However, as shown in Figure 6-19, a more complex dependence was observed here. From the results shown in Figures 6-18 and 6-19 it can be concluded that in order to simultaneously acquire and to adequately describe analyte temporal behavior, a judicious choice of the dwell time and the number of elements/masses scanned must be made.

In summary, the parameter set used on the Elan and the software described here provide the necessary means to assess analyte behavior in the time domain and offer multielement analysis capabilities.

B.4.2 Simulating Virtual Reality

Recently, the *instrument metaphor* concept was invented, a unique Human Processor Interface (HPI) was developed for an ICP-AES-DSID and was implemented on an Apple Macintosh as described by Karanassios and Horlick [37]. In their work, real-time animation of controls and indicators was suggested but not implemented. *"Even the electrode's movement could be animated, so that the user could follow it on the screen as it is being inserted into the torch"* [37]. Their approach toward animation of controls, dials, indicators and instrument components has presently evolved to that of *simulating virtual reality* (the virtual reality concept was inspired by MITs media lab [38]), and is implemented as described below for the ICP-MS-DSID.

Upon selection (Figure 6-16e) of the menu item "Simulate" (this part of the program currently runs only on an Apple Macintosh II equipped with a color monitor), a window appears on the screen which displays the DSID and animates its movements (i.e., the lead screw rotates as the platform slides forward toward the torch; when the shutter opens, audio is used in conjunction with a visual effect displayed on the screen to indicate opening of the shutter, etc). In addition, color is used to illustrate what happens when the electrode is inserted into the plasma (i.e., upon insertion into the plasma, the electrode becomes red hot in time; this effect is displayed on the screen by painting the top of the electrode bright red). In addition, color-coded analyte emission is displayed on the screen as it would be seen in reality by visually observing the plasma. For example, when a solution sample residue of Yttrium is run using the DSID, a red plume is initially observed low in the plasma (i.e., ~ 10 mm above TOLC); a short time later, a blue plume situated high in the plasma (i.e., ~20 mm above TOLC), is visually observed. These observations are likewise color coded on the Macintosh screen and are separated in time, in much the same way as they actually occur in reality, thus giving rise to the concept of

simulating virtual reality. And although not yet implemented, the ultimate goal is to follow the movement of the sample carrying probe in real-time while simultaneously animating it on the computer screen. This approach is expected to give another dimension on the HPI previously developed for a DSID for ICP-AES.

C. Basic Response

As with any analytical technique, improved analytical performance can be obtained by optimizing the instrumental parameters affecting analytical performance characteristics. The ICP-MS is no exception. A review of the literature reveals that from the large number of ICP-MS instrumental parameters available for optimization [7, 8, 39], nebulizer flow rate (often referred to as injector gas flow rate [7]) and applied forward power most significantly affect analyte signal intensities. Parameter plots (i.e., intensity *versus* nebulizer flow rate at a given power setting) having a mountain peak shape have become a frequent scene in the ICP-MS literature. It was thus decided to carry that experience to the DSID and study the effect of central tube gas flow rate and power on analyte temporal behavior.

In this preliminary study, the central tube gas flow rate (which is equivalent to the nebulizer flow rate of pneumatic nebulizer systems) varied for 0 l/min to 2 l/min, the power varied from 1.25 to 1.50 kW and the sampling depth varied from 15 to 10 mm. The results (reported as peak heights) obtained by running multielement solution residues of Mg, Mn and Zn (10 ng each) are shown in Figure 6-20a, 20b and 20c. From these results, it can be concluded that for the conditions used in this experiment and unlike conventional pneumatic nebulizer systems, the central tube gas flow rate had little effect on the peak heights of the analyte signals. And although not shown, for brevity's sake, it also had little or no effect on analyte temporal behavior and on peak shapes. Perhaps the actual electrode position in the torch (i.e., the exact location of TOLC) may be a more important variable. This, however, was not tested. These results also show that, as expected, power had an effect on peak heights, with an increase in power resulting in an increase in signal intensity. In addition, an increase in power also affected analyte temporal behavior, with the peak-like signals becoming sharper.

Typical results obtained after optimization for Mg, Mn and Zn (1 ng each) at 1.5 kW, 10 mm, are shown in Figure 6-21a, 6-21b and 6-21c. And although detection limits were not determined, these results can be used as an indication of the potential detection capability of the device. (It should be noted that a background intensity of less than 100 counts/sec was observed for most elements tested).

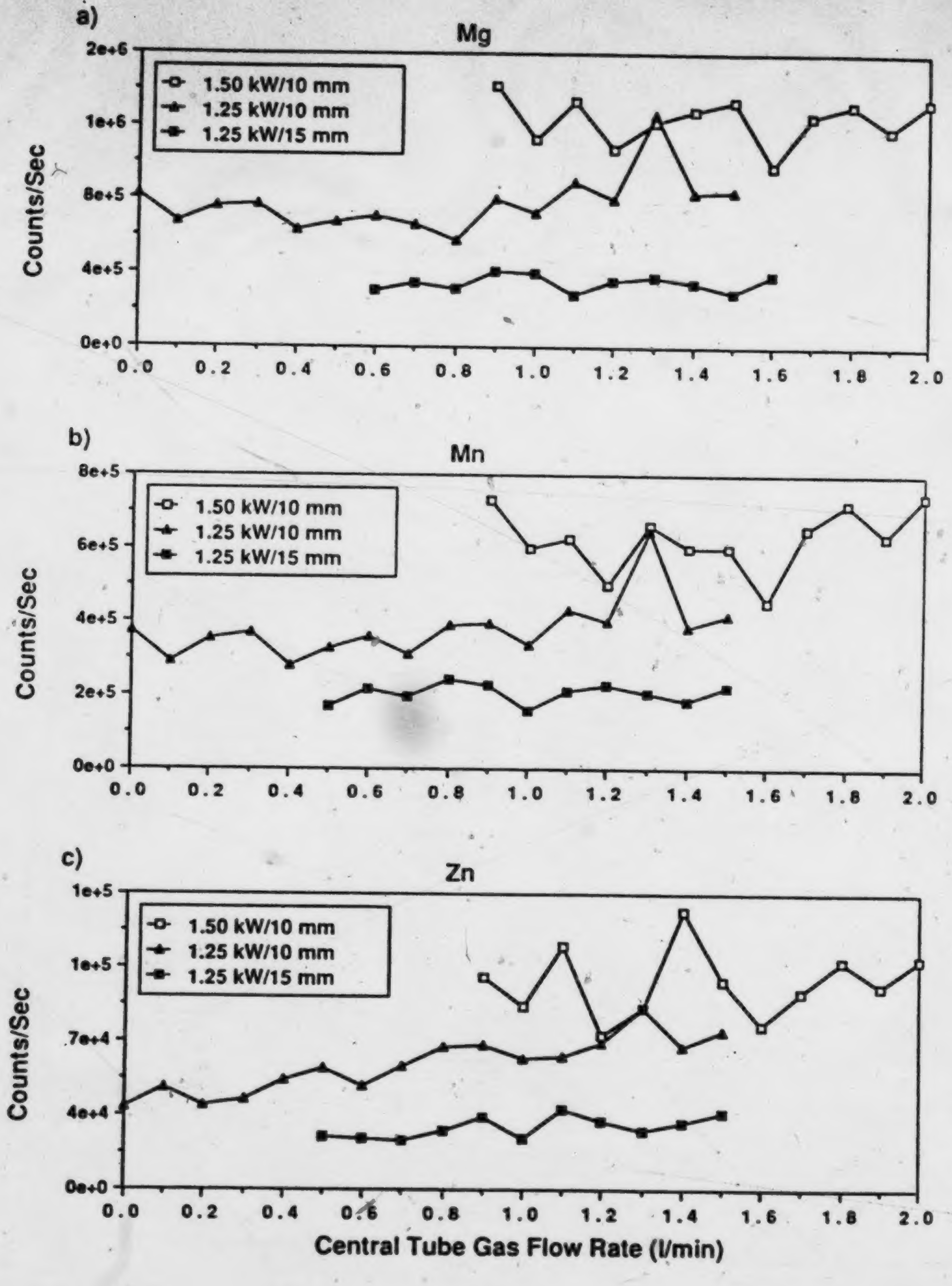

Figure 6-20. The effect of central tube flow rate analyte intensity as a function of power and sampling depth for: (a) 10 ng Mg; (b) 10 ng Mn and (c) 10 ng Zn.

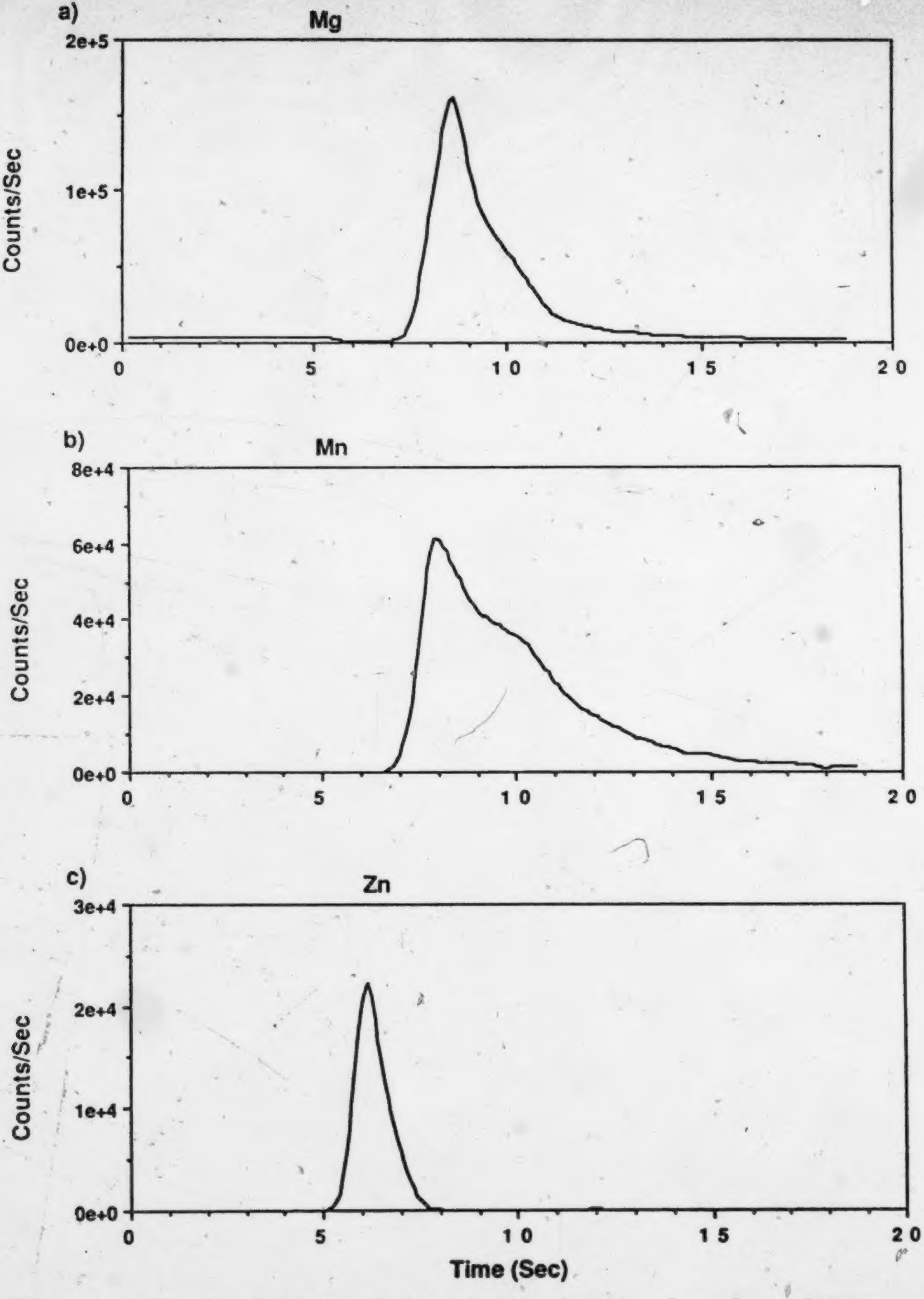

Figure 6-21. Typical analyte temporal behavior from long undercut graphite electrodes, a 10 mm sampling depth and 1.50 kW power for 1 ng of: (a) Mg; (b) 1 Mn and (c) 1 Zn.

However, before proceeding any further in characterizing the DSID and in order to assess potential spectral interference effects, the background spectral features of a DSID for ICP-MS must be determined. Low resolution spectral scans (10 points/peak, 1.0 s/point, 1.25 kW, 10 mm sampling depth) covering the mass range from 1 to 210 amu are shown in Figures 6-22, 6-23, 6-24 and 6-25 for a blank graphite electrodes, a Mo- and a Ta-metal cup and a wire-loop. Perhaps, the most interesting aspect revealed by these spectral scans is the simplicity of the background, especially in comparison to that arising from continuous aspiration of solvent into the plasma [23]. This is further documented in chapter 7.

D. Conclusions

The basic goal of extending the analytical capability and utility ICP-MS by developing a DSID that can easily and rapidly be interfaced to a commercially available ICP-MS system were met as described above. Due to its principles of operation, further automation of the DSID (i.e., via robotics and automated dispensing of chemical modifiers) can be easily accomplished.

From the findings reported here and those of chapter 2 it can be concluded that ICP-AES-DSIDs and ICP-MS-DSIDs share similar data acquisition and results presentation

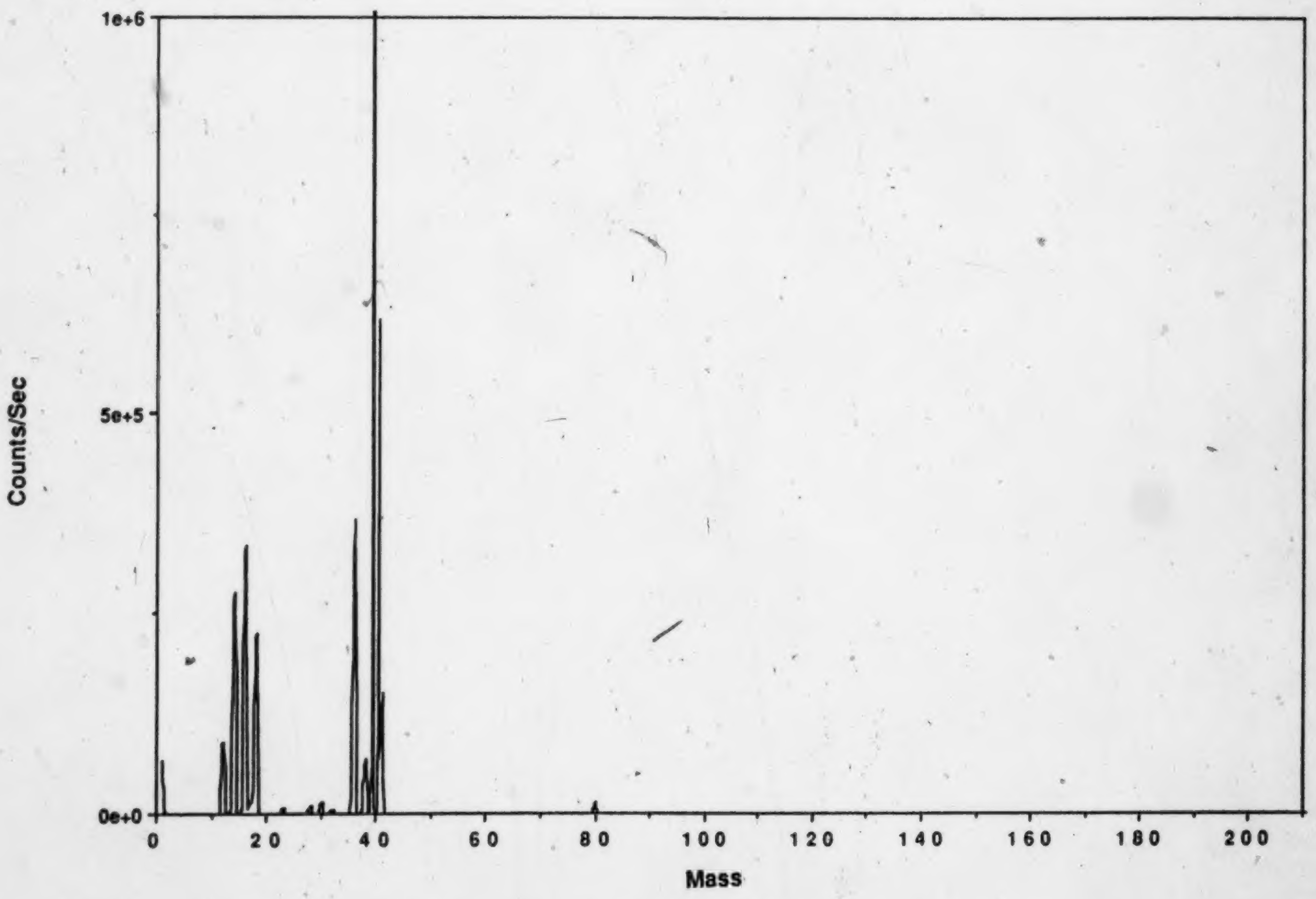

Figure 6-22. Background spectrum for a graphite electrode (low resolution scan, 10 mm sampling depth, 1.25 kW).

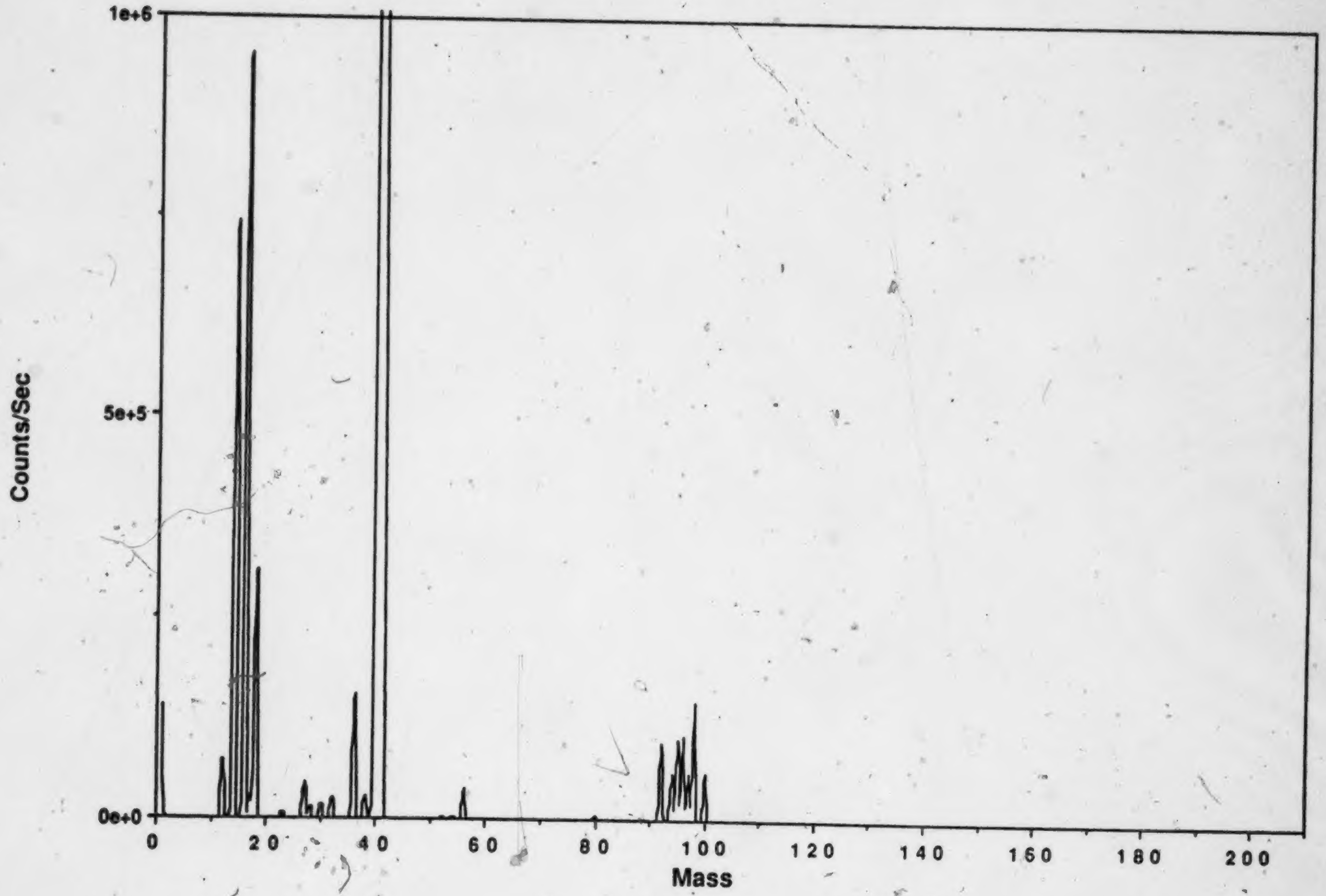

Figure 6-23. Background spectrum for a Mo cup (low resolution scan, 10 mm sampling depth, 1.25 kW).

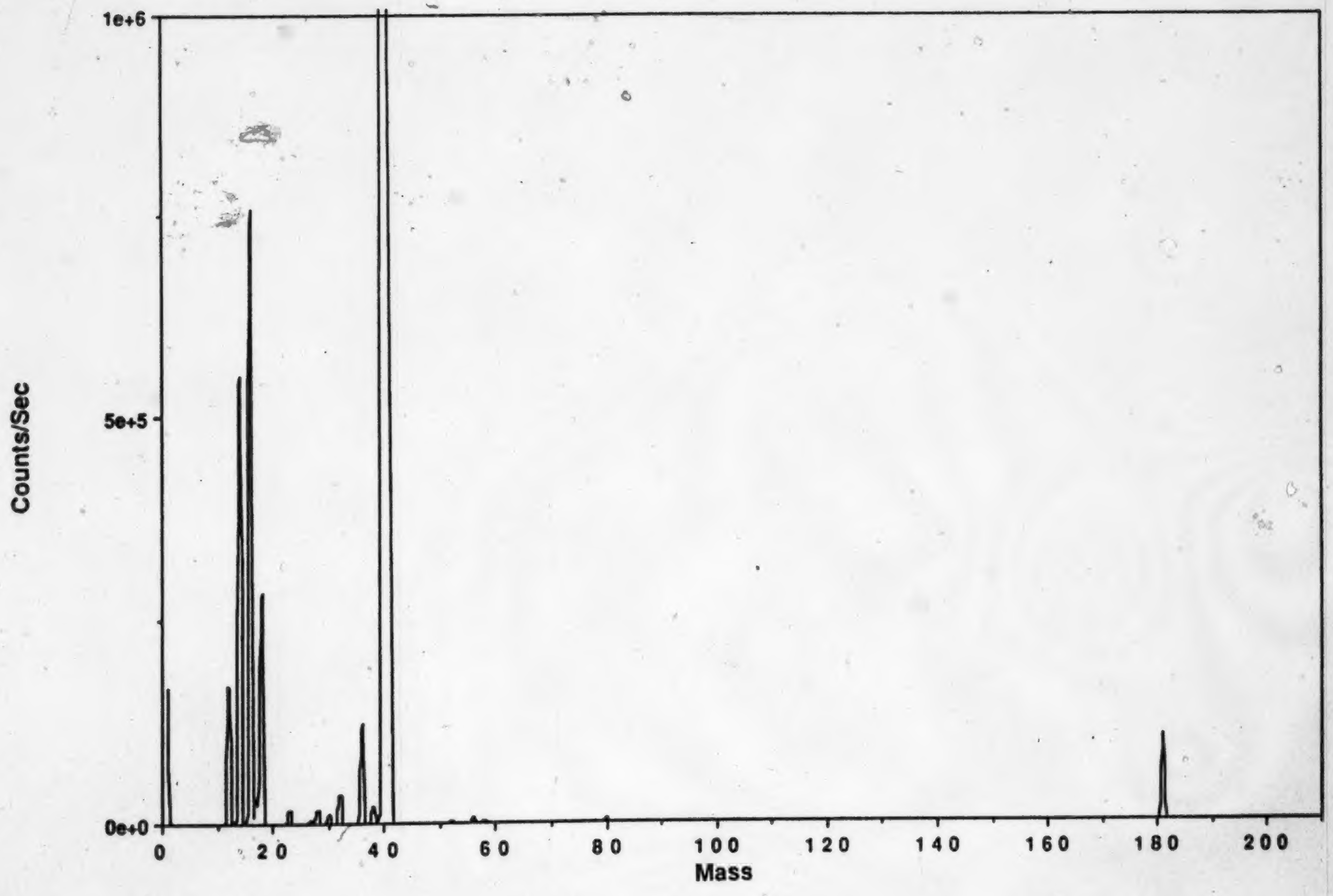

Figure 6-24. Background spectrum for a Ta cup (low resolution scan, 10 mm sampling depth, 1.25 kW).

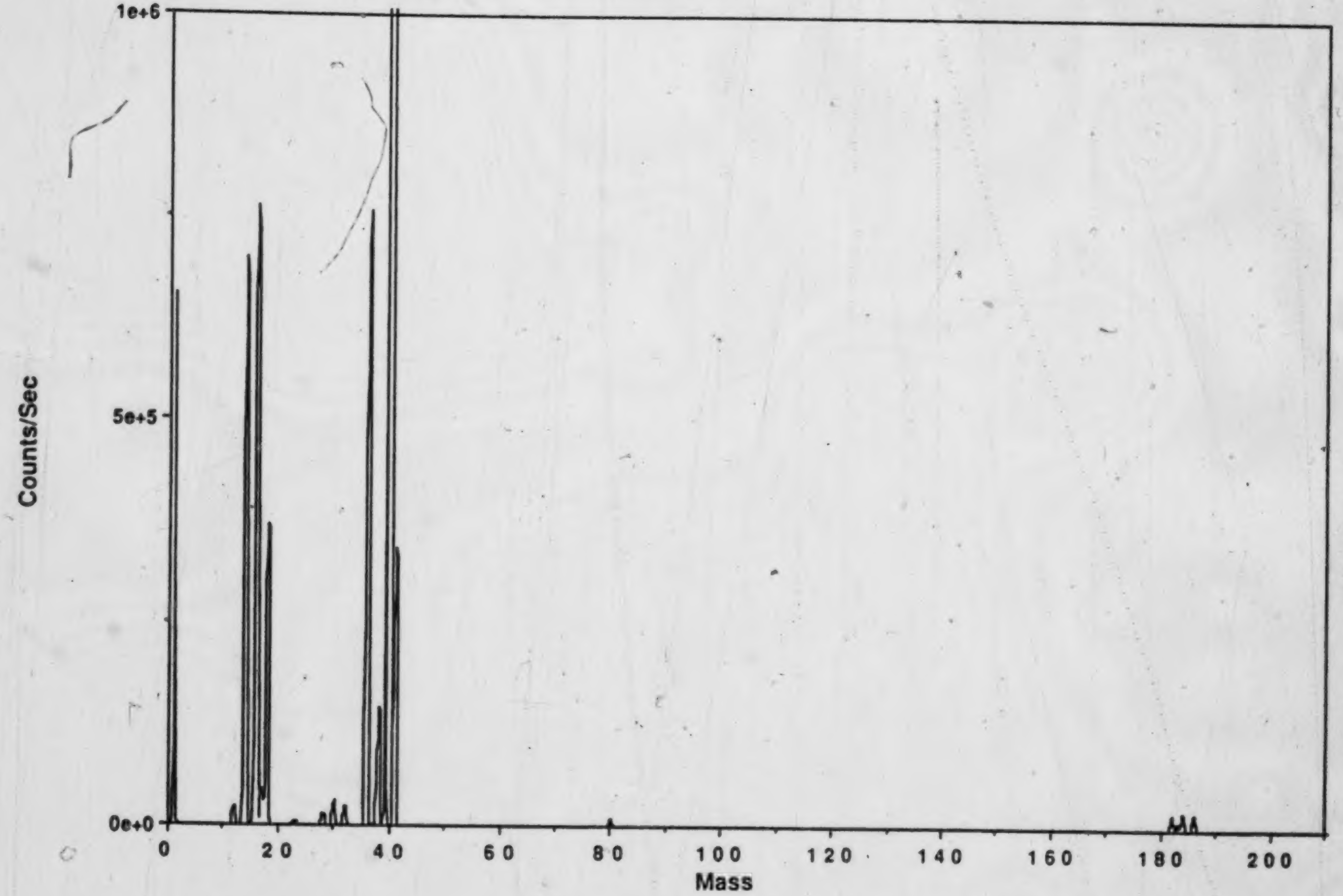

Figure 6-25. Background spectrum for a W wire-loop (low resolution scan, 10 mm sampling depth, 1.25 kW).

constraints. The development of new software on the front-end processor relaxed some of these constraints, it increased the operating speed per sample run and it augmented the utility of the device.

In this preliminary investigation, the potential detection capability of the device was briefly demonstrated for graphite electrodes. The analytical performance characteristics of the device were not established. Metal cups and wire-loops were only used in order to determine the background spectral features of ICP-MS-DSID. Clearly, more remains to be done in order to characterize the DSID and to establish its performance characteristics. For example, calibration curves must be tested for linearity, %RSDs must be determined, detection limits must be established, and complete optimization (i.e., insertion position with respect to TOLC, lens voltages etc) must be performed. In addition, potential applications of the device (especially for determinations in powdered/solid samples) must be considered.

However, before attempting to establish the performance characteristics of ICP-MS-DSID or to proceed with potential applications, the anticipated benefits of a dry plasma, as revealed in the introduction of this report, must be established. This is addressed in yet another preliminary investigation, as detailed in the following chapter.

REFERENCES

1. R.S. Houk, V.A. Fassel, G.D. Flesch, H.J. Svec, A.L. Gray and C.E. Taylor, Spectrochim. Acta, **52**, 2283 (1980)

2. A copy of a an ICP-MS bibliography (compiled R. Edinger) can be obtained from: The Perkin-Elmer Corp., Norwalk, 761 Main Ave., Connecticut, 06859-0082, USA

3. ICP-MS 87: A symposium on ICP-MS, Muskoka Sands, Gravenhurst, Ontario, Canada, June 1987

4. A.L. Gray, Spectrochim. Acta, **40B**, 1525 (1985)

5. D.J. Douglas and R.S. Houk, Prog. Anal. At. Spectrosc., **8**, 1 (1985)

6. R.S. Houk, Anal. Chem., **58**, 97A (1986)

7. G. Horlick, S.H. Tan, M.A. Vaughan and Y. Shao, *"Inductively Coupled Plasma-Mass Spectrometry"*, in *'Inductively Coupled Plasmas in Analytical Atomic Spectrometry'*, A. Montaser and D.W. Golightly, Eds, VCH Publishers, Inc., NY, 1987, pp. 361-398

8. G. Zhu and R.F. Browner, Appl. Spectrosc., **41**, 349 (1987)

9. A.L. Gray and A.R. Date, Analyst, **108**, 1033 (1983)

10. C.J. Park, J.C. Van Loon, P. Arrowsmith and J.B. French, Can. J. Spectrosc., **32**, 29 (1987)

11. A.L. Gray, Analyst, **110**, 551 (1985)

12. P. Arrowsmith, Anal. Chem., **59**, 1437 (1987)

13. S.J. Jiang and R.S. Houk, Anal. Chem., **58**, 1739 (1986)

14. J.G. Williams, A.L. Gray, P. Norman and L. Ebdon, J. Anal. At. Spectrom., **2**, 469 (1987)

15. Thomson, J.J. and R.S. Houk, Anal. Chem., **58**, 2541 (1986)

16. J.R. Dean, L. Ebdon, H.M. Crews and R.C. Massey, J. Anal. At. Spectrom., **3**, 349 (1988)

17. D.W. Boomer, M. Powell, R.L.A. Sing and E.D. Salin, Anal. Chem., **58**, 975 (1986)

18. V. Karanassios and G. Horlick, *'A review of DSID for the ICP'*, (in preparation)

19. V. Karanassios and G. Horlick, *'A computer-controlled direct sample insertion device for ICP-AES'*, Spectrochim. Acta, (sumbmitted)

20. V. Karanassios, G. Horlick and M. Abdullah, *'Characterization of a direct sample insertion device for ICP-AES'*, Spectrochim. Acta, (sumbmitted)

21. V. Karanassios, M. Abdullah and G. Horlick, *'The application of chemical modification to a direct sample insertion device for ICP-AES'*, Spectrochimim. Acta, (sumbitted)

22. M.A. Vaughan and G. Horlick, Appl. Spectrosc., **40**, 434 (1986)

23. S.H. Tan and G. Horlick, Appl. Spectrosc., **40**, 445 (1986)

24. S.H. Tan and G. Horlick, J. Anal. At. Spectrom., **2**, 745 (1987)

25. Y.Q. Tang and C. Tracey, Spectrochim. Acta, **41B**, 143 (1986)

26. A.L. Gray, Spectrochim. Acta, **41B**, 151 (1986)

27. R.C. Hutton and A.N. Eaton, J. Anal. At. Spectrom., **2**, 595 (1987)

28. G. Horlick and V. Karanassios, *'Instrumentation Systems for Atomic Spectrometry'*, chapter monograph on Analytical Atomic Spectrometry, J.A. Holcombe, Ed., (accepted)

29. V. Karanassios and G. Horlick, *'Spectroscopic and Non-spectroscopic Interference Effects in ICP-MS Using a DSID'*, (in preparation)

30. V. Karanassios and G. Horlick, Talanta, **32**, 583 (1985)

31. V. Karanassios and G. Horlick, Talanta, **32**, 601 (1985)

32. W.E. Pettit and G. Horlick, Spectrochim. Acta, **41B**, 699 (1986)

33. Y. Shao and G. Horlick, Appl. Spectrosc., **40**, 386 (1986)

34. C.J. Park and G.E.M. Hall, J. Anal. At. Spectrom., **2**, 473 (1987)

35. D.C. Gregoire, J. Anal. At. Spectrom., **3**, 309 (1988)

36. V. Karanassios and G. Horlick, Appl. Spectrosc., *'New Design Concepts for Direct Reader Measurement Electronics"*, (in press)

37. V. Karanassios and G. Horlick, Appl. Spectrosc., **41**, 360 (1987)

38. S. Brand, *"The Media Lab"*, Viking Penguin, Inc., New York, 1987

39. M.A. Vaughan, G. Horlick and S.H. Tan, J. Anal. At. Spectrom., **2**, 765 (1987)

CHAPTER 7

SPECTRAL AND MATRIX INTERFERENCE EFFECTS IN ICP-MS USING A DSID

91

A. Introduction

During the initial stages of the development of inductively coupled plasma-mass spectrometry (ICP-MS) in the early 1980s, the original claims of its advantages were very impressive. And although the technique has lived up to or out-performed some of these claims, more recent reports indicate that spectral simplicity and lack of interference effects were over-emphasized.

ICP-MS interference effects can be classified as spectroscopic (i.e., direct spectral overlaps) and non-spectroscopic (i.e., matrix induced signal changes), typical examples of spectroscopic interference are given in Table 7-1. In general, spectral interference effects in ICP-MS are not as extensive as in ICP-AES (inductively coupled plasma-atomic emission spectrometry), but non-spectroscopic interference effects are more severe in ICP-MS than in ICP-AES [1].

Spectroscopic interference effects arise from overlaps of: isobaric isotopes of elements; basic plasma background species; matrix induced background species; oxides; hydroxides; doubly charged species; and from overlaps with ArX^+ species.

In non-spectroscopic interference, also referred to as matrix effects, the intensity of an analyte changes due to the presence of a matrix component, both signal enhancements and suppressions have been observed [1, 2].

Table 7-1. Types of spectral interference effects in ICP-MS.

Type	Mass	Species	Element(s) affected[a]
Isobaric isotopes of elements			
- Analyte	138	$^{138}Ce^{+}$	**Ba(71.7)**, La(0.09)
- Matrix (i.e., iron-rich samples)	58	$^{58}Fe^{+}$	**Ni(67.8)**
Basic plasma species			
- Mono-atomic	40	$^{40}Ar^{+}$	**Ca(99.94)**
- Poly-atomic	80	$^{40}Ar_2^{+}$	[b]**Se(49.62)**
Solvent/matrix-induced species			
- Mono-atomic	35	$^{35}Cl^{+}$	**Cl(75.77)**
- Poly-atomic	51	$^{35}Cl^{16}O^{+}$	**V(99.75)**
	75	$^{40}Ar^{35}Cl^{+}$	**As(100)**
- Oxides	56	$^{40}Ar^{16}O^{+}$	**Fe(91.75)**
	152	$^{136}Ba^{16}O^{+}$	**Sm(26.6)**, Gd(0.21)
	153	$^{137}Ba^{16}O^{+}$	**Eu(52.2)**
	154	$^{138}Ba^{16}O^{+}$	Sm(22.4), Gd(2.23)
- Hydroxides	55	$^{38}Ar^{16}OH^{+}$	**Mn(100)**
	59	$^{40}Ar^{16}OH^{+}$	**Co(100)**
	103	$^{87}Sr^{16}OH^{+}$	**Ru(100)**
	152	$^{135}Ba^{16}OH^{+}$	**Sm(26.6)**, Gd(0.21)
	153	$^{136}Ba^{16}OH^{+}$	**Eu(52.2)**
	154	$^{137}Ba^{16}OH^{+}$	Sm(22.4), Gd(2.23)
	155	$^{138}Ba^{16}OH^{+}$	Gd(15.1)
- Doubly-charged species	75	$^{150}Nd^{2+}$, $^{150}Sm^{2+}$, $^{149}Sm^{2+}$, $^{151}Eu^{2+}$	**As(100)**
	69	$^{138}Ba^{2+}$	**Ga(60.2)**
- Argides	63	$^{40}Ar^{23}Na^{+}$	**Cu(69.17)**

a: The major isotopes are shown in bold face text

b: Ar-dimmer isotopic combinations potentially interfere with all isotopes of Se

In general, the degree of matrix effects appears to be dependent on the mass of the matrix and the analyte element, light analytes are more seriously affected than heavy analytes [1].

The justification for the development of a computer-controlled DSID (direct sample insertion device) for ICP-MS, as described in chapter 6, was based on the anticipated advantages it would offer. Among these were reduced spectroscopic and non-spectroscopic interference effects. These are addressed in detail in this study.

B. Experimental

Instrumentation and operating conditions were described previously in chapter 6. The distilled water used was obtained by feeding in-house distilled water into a Millipore Milli-Q water purification system. Two spectra acquisition modes were utilized: a high resolution mode with a peak width of ~0.6 (±0.05) amu at 10% of the peak's height, a scan increment of 0.05 amu (i.e., 20 points/peak) and a measurement time of 1.0 s/point; and a low resolution mode with a peak width of 1.0 (±0.1) amu at 10% of the peak's height, a scan increment of 0.1 amu (i.e., 10 points/peak) and a measurement time of 1.0 s/point.

A wet-aerosol plasma, referred to as 'wet plasma', is one in which a solvent is continuously aspirated into the plasma, a typical example is an ICP equipped with a conventional pneumatic nebulizer sample introduction system. A dry-aerosol plasma, referred to as 'dry plasma', is one in which neither sample nor solvent are introduced into the discharge.

Wet plasma background spectra were acquired using a torch which is the same as that typically used for optical work, those for a dry plasma were acquired using either a DSID torch or a DSID torch fitted with a sleeve, as shown in Figure 7-1. The latter is referred to as an 'extended' torch. Unless otherwise stated, dry plasma background spectra were acquired with the DSID installed, the torch in place and the DSID shutter closed.

C. Spectroscopic Interference Effects

C.1 Background Spectral Features of ICP-MS

Of the various types of spectroscopic interference effects listed in Table 7-1, those arising from background species are the most prevalent. Background species in ICP-MS originate from the plasma gases, from air entrainment, and from the sample and/or the solvent. The background spectral features of ICP-MS, when using a wet plasma, have been the subject of numerous investigations [3-6]. For example, Tan and Horlick [5] show background spectra for distilled water and for three acidic matrices (i.e., 5% aqueous solutions of HCl, HNO_3, H_2SO_4). The spectral complexity depended upon the solvent used and they tabulated a number

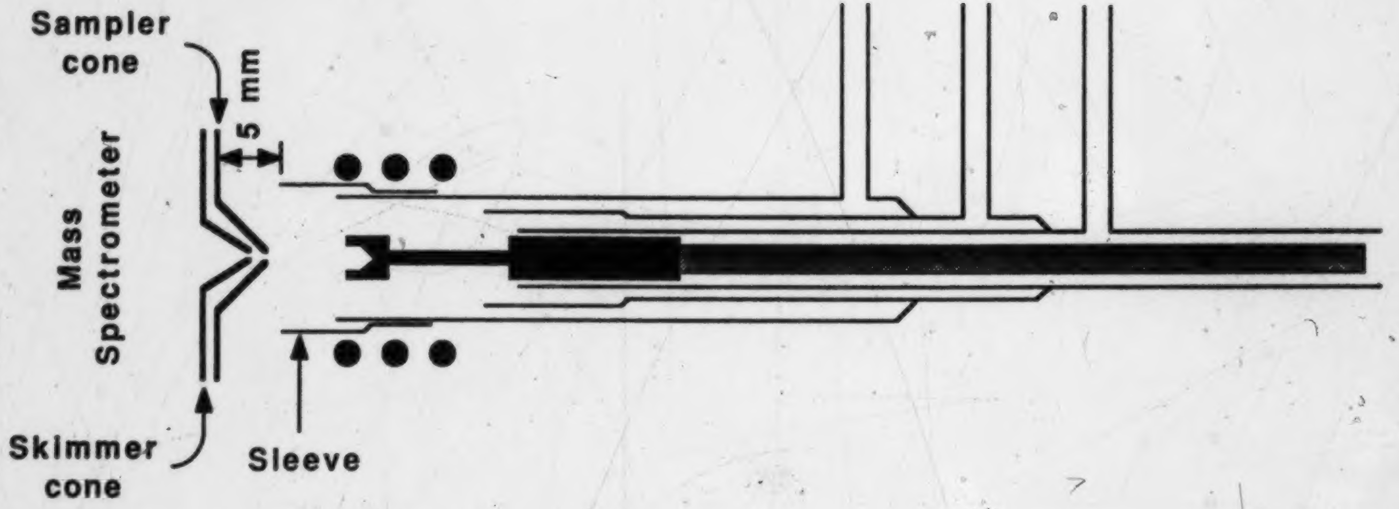
Sampler cone
5 mm
Mass Spectrometer
Skimmer cone
Sleeve

Figure 7-1. Illustration of the DSID torch with its extension in place.

of the isotopic combinations of background species (mono-atomic or poly-atomic) that could potentially interfere with major and minor isotopes of elements. Low-resolution background spectra acquired when aspirating a 5% H_3PO_4 acid solution into the ICP have also been reported and possible interferences have been tabulated in Tan's Ph.D. thesis [6]. To summarize [3-6], wet plasma ICP-MS background spectra are particularly complex below mass 80 and are essentially free of background species above mass 80. Perhaps the most important aspect revealed by these studies is the strong dependence of the background on the mineral acids used for sample dissolution. Typical examples of solvent-induced background species are listed in Table 7-2. In addition, the presence of water solvent is giving rise to sample-induced background species, such as oxides (MO^+) and hydroxides (MOH^+), for example, BaO^+ and $BaOH^+$ (Table 7-1). These are a major source of spectral interference in ICP-MS, there are *"literally hundreds of potential spectral interference problems involving oxides"* [7].

C.1.1 Wet and Dry Plasma Background Spectra

The existence of a solvent-dependent background raises an interesting question, namely, what are the basic spectral features of a 'dry plasma'? By allowing identification of species basic to the plasma discharge, detailed knowledge of the background spectral features of a dry

Table 7-2. Typical solvent-induced background species.

Mass	**Element(s) affected**	**Species**
19	**F(100)**	**$^{16}OH_3^+$**
28	**Si(92.91)**	**$^{14}N^{14}N^+$**
31	**P(100)**	**$^{14}N^{16}OH^+$**
32	**S(95.02)**	**$^{16}O^{16}O^+$**
33	S(0.75)	**$^{16}O^{16}OH^+$**
34	S(4.21)	**$^{18}O^{18}O^+$**
35	**Cl(75.77)**	**$^{18}O^{18}OH^+$**, $^{34}S^+$, $^{33}S^+$
45	**Sc(100)**	**$^{12}C^{16}O^{16}OH^+$**
48	**Ti(73.98)**, Ca(0.11)	**$^{32}S^{16}O^+$**
51	**V(99.76)**	**$^{35}Cl^{16}O^+$**
52	**Cr(83.76)**	**$^{40}Ar^{12}C^+$**, **$^{35}Cl^{16}OH^+$**, $^{36}Ar^{16}O^+$
55	**Mn(100)**	**$^{40}Ar^{14}NH^+$**
56	**Fe(91.66)**	**$^{40}Ar^{16}O^+$**
69	**Ga(60.61)**	$^{37}Cl^{16}O^{16}O^+$
74	Ge(36.56), Se(0.87)	**$^{40}Ar^{32}S^+$**, $^{38}Ar^{38}Ar^+$
75	**As(100)**	**$^{40}Ar^{35}Cl^+$**

Major isotopes are shown in bold face text.

plasma is expected to help devise methods of reducing or eliminating potential spectral interference effects arising from solvent-dependent species observed in a wet plasma and to help assess potential spectral interference effects in dry plasmas.

In addition, because dried solution residues or powdered/solid samples are introduced into the plasma with the DSID, background spectral features, such as oxides and hydroxides, are also expected to be reduced or eliminated. Furthermore, due to differential volatilization, for example, a matrix component volatilizing prior to analyte volatilization, interference from molecular species, such as those listed in Table 7-2, may also be reduced or eliminated. Clearly, further investigation is warranted.

It should be borne in mind that due to the use of dry plasmas with electrothermal atomization and laser ablation sample introduction systems, the relevance of such investigations extends beyond the DSID.

C.1.1.1 Distilled Water Background Spectra

These were acquired (a 15 mm sampling depth was used) in order to provide a reference for comparison purposes. Because no significant spectral features have been reported above mass 84 [5], the mass range covered was from mass 1 to 84. The spectral scans are shown in Figure 7-2 (mass range 1-44) and Figure 7-3 (mass range 42-84).

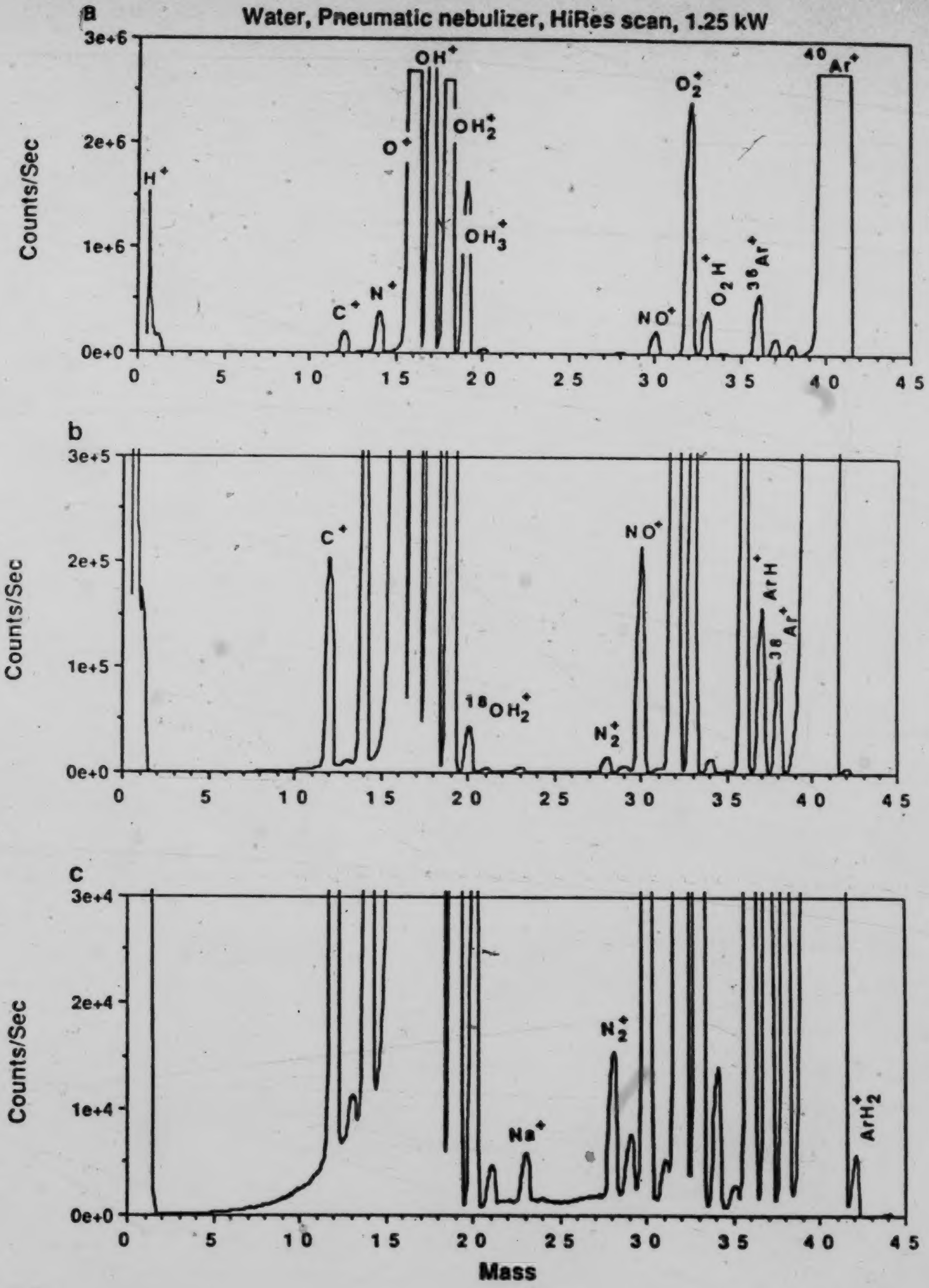

Figure 7-2. Background spectrum for a wet plasma, high resolution scan, sampling depth 15 mm, mass range 1-45 amu.

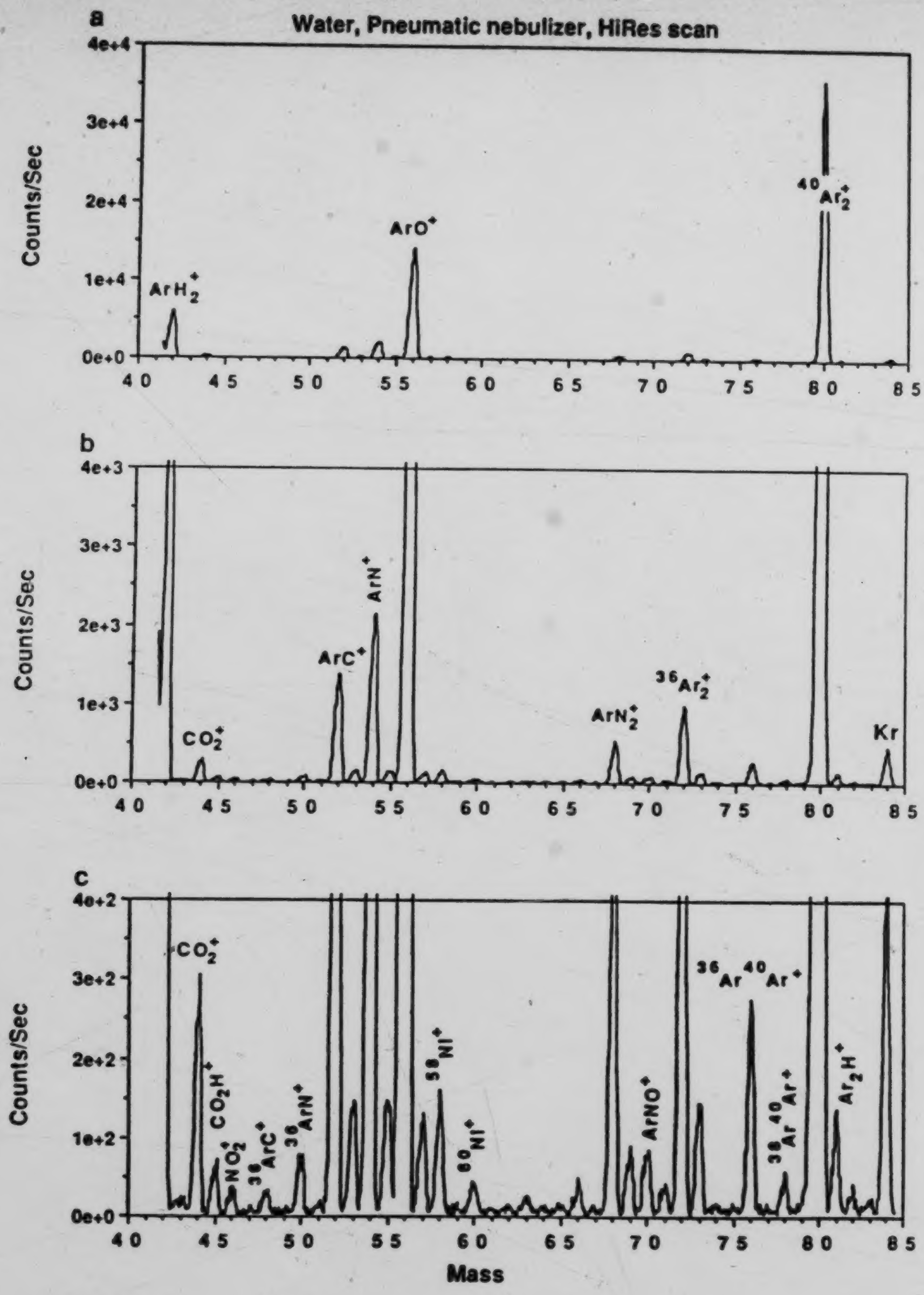

Figure 7-3. Background spectrum for a wet plasma, high resolution scan, sampling depth 15 mm, mass range 40-85 amu.

Shown in the top frame of each figure is the basic spectrum, in the middle frame the intensity axis has been scale-expanded by an order of magnitude and in the bottom frame the intensity axis has been scale-expanded by another order of magnitude. The flat-tops of the peaks at masses 16, 17, 18 and 40 shown in Figure 7-2a have been added on during post-processing to denote detector saturation. Actually, in order to protect the detector from excessive currents which result from highly concentrated species, such as $^{40}Ar^+$, the instrument automatically 'hops over' a mass as it is scanning; thus a gap appears in the spectrum.

A quick visual scan of the data presented in Figures 7-2 and 7-3 reveals that, not surprisingly, argon, oxygen, hydrogen, nitrogen and carbon-containing species are the dominant background ions. There were some surprises too: for example, $^{82}Kr^+$ and $^{84}Kr^+$ which are attributed to impurities found in argon, and $^{23}Na^+$. These ions were also observed by others utilizing a non-commercial instrument [4].

More specifically, the region from mass 16 to 21 is dominated by oxygen and protonated oxygen containing species (i.e., $^{16}O^+$, $^{16}OH^+$, $^{16}OH^{2+}$, $^{16}OH_3^+$), the region from mass 36 to 42 is dominated by argon isotopes and their protonated forms, and the region from 76 to 81 is dominated by argon dimer species and their protonated forms. Carbon and carbon containing species (i.e., $^{12}C^{16}O_2^+$, $^{40}Ar^{12}C^+$) and nitrogen and nitrogen containing species (i.e., $^{14}N^+$, $^{14}N_2^+$,

$^{14}N^{16}O^+$, $^{14}N^{16}O^+$, $^{14}N^{16}O_2^+$, $^{40}Ar^{14}N_2^+$) are also present in significant amounts. The high intensity of the background observed in the region from mass 10-39 is highly unusual, the reason(s) are not known at this stage. The low-intensity Ni peaks observed at mass 58 and 60 (Figure 7-3) are most likely due to the sampling of the Ni-based skimmer (Figure 7-1). The species identified in the water blank spectrum are listed in Table 7-3, the most abundant isotope of an element (the % natural abundance is shown in parentheses) is highlighted in bold face text. Potential spectral interference effects can be identified by consulting Table 7-3.

In general, the results shown in Figures 7-2 and 7-3 and listed in Table 7-3 are very similar (with some minor differences depending on instrumentation and operating conditions) to those reported by others [3-5].

A quick scan of Table 7-3 also reveals the origin of these species and offers an indication of their reduction or elimination. For example, the majority of them are oxygen- and/or hydrogen-containing species arising from continuous aspiration of water solvent. If there is a way to reduce or eliminate water in the plasma, and hence oxygen and hydrogen, it could be speculated that oxides and hydroxides (i.e., ArO^+, $ArOH^+$, MO^+, MOH^+) will also be reduced or eliminated.

Table 7-3. Background species arising from a wet and a dry plasma.

Mass	Wet[a] 15 mm[c]	Dry[b] 15 mm[c]	Dry[b] 10 mm[c]	Dry[b] XTND[d]	Interferes with (abundance)
12	$^{12}C^{+}$	$^{12}C^{+}$	$^{12}C^{+}$	$^{12}C^{+}$	C(98.89)
14	$^{14}N^{+}$	$^{14}N^{+}$	$^{14}N^{+}$	$^{14}N^{+}$	N(99.63)
16	$^{16}O^{+}$	$^{16}O^{+}$	$^{16}O^{+}$	$^{16}O^{+}$	O(99.76)
17	$^{16}OH^{+}$	$^{16}OH^{+}$	$^{16}OH^{+}$	$^{16}OH^{+}$	O(0.04)
18	$^{16}OH_2^{+}$	$^{16}OH_2^{+}$	$^{16}OH_2^{+}$	$^{16}OH_2^{+}$	O(0.20)
19	$^{16}OH_3^{+}$	$^{16}OH_3^{+}$			F(100)
20	$^{18}OH_2^{+}$	$^{18}OH_2^{+}$	$^{18}OH_2^{+}$		Ne(90.92)
21	$^{18}OH_3^{+}$				Ne(0.26)
23	$^{23}Na^{+}$	$^{23}Na^{+}$	$^{23}Na^{+}$	$^{23}Na^{+}$	Na(100)
28	$^{14}N_2^{+}$	$^{14}N_2^{+}$	$^{14}N_2^{+}$	$^{14}N_2^{+}$	Si(92.91)
29	$^{14}N^{14}NH^{+}$	$^{14}N^{14}NH^{+}$			Si(4.7)
30	$^{14}N^{16}O^{+}$	$^{14}N^{16}O^{+}$	$^{14}N^{16}O^{+}$	$^{14}N^{16}O^{+}$	Si(3.09)
31	$^{14}N^{16}OH^{+}$	$^{14}N^{16}OH^{+}$			P(100)
32	$^{16}O_2^{+}$	$^{16}O_2^{+}$	$^{16}O_2^{+}$	$^{16}O_2^{+}$	S(95.02)
33	$^{16}O_2H^{+}$				S(0.75)
34	$^{16}O^{18}O^{+}$				S(4.21)
35	$^{16}O^{18}OH^{+}$				Cl(75.77)
36	$^{36}Ar^{+}$	$^{36}Ar^{+}$	$^{36}Ar^{+}$	$^{36}Ar^{+}$	Ar(0.34), S(0.02)

Table 7-3. Continued.

Wet[a]	**Dry**[b]	**Dry**[b]	**Dry**[b]	**Dry**[b]	**Interferes with**
Mass	15 mm[c]	15 mm[c]	10 mm[c]	XTND[d]	**(abundance)**
37	$^{36}ArH^+$	$^{36}ArH^+$			Cl(24.23)
38	$^{38}Ar^+$	$^{38}Ar^+$	$^{38}Ar^+$	$^{38}Ar^+$	Ar(0.06)
40	$^{40}Ar^+$	$^{40}Ar^+$	$^{40}Ar^+$	$^{40}Ar^+$	Ar(99.6), Ca(96.97), K(0.01)
41	$^{40}ArH^+$	???	???	???	K(6.91)
42	$^{40}ArH_2^+$	$^{40}ArH_2^+$	$^{40}ArH_2^+$	$^{40}ArH_2^+$	Ca(0.64)
44	$^{12}C^{16}O^{16}O^+$	$^{12}C^{16}O^{16}O^+$	$^{12}C^{16}O^{16}O^+$	$^{12}C^{16}O^{16}O^+$	Ca(2.06)
45	$^{12}C^{16}O^{16}OH^+$				Sc(100)
46	$^{14}N^{16}O_2^+$	$^{14}N^{16}O_2^+$	$^{14}N^{16}O_2^+$	$^{14}N^{16}O_2^+$	Ti(7.99), Ca(0.003)
47		$^{14}N^{16}O_2H^+$	$^{14}N^{16}O_2H^+$	$^{14}N^{16}O_2H^+$	Ti(7.32)
48	$^{36}Ar^{12}C^+$	$^{36}Ar^{12}C^+$	$^{36}Ar^{12}C^+$	$^{36}Ar^{12}C^+$	Ti(73.98), Ca(0.19)
50	$^{36}Ar^{14}N^+$	$^{36}Ar^{14}N^+$	$^{36}Ar^{14}N^+$	$^{36}Ar^{14}N^+$	Ti(5.25), Cr(4.35), V(0.24)
52	$^{40}Ar^{12}C^+$, $^{36}Ar^{16}O^+$	$^{40}Ar^{12}C^+$, $^{36}Ar^{16}O^+$	$^{40}Ar^{12}C^+$, $^{36}Ar^{16}O^+$	$^{40}Ar^{12}C^+$	Cr(83.76)
53	$^{36}Ar^{16}OH^+$	$^{36}Ar^{16}OH^+$	$^{36}Ar^{16}OH^+$		Cr(9.51)
54	$^{40}Ar^{14}N^+$	$^{40}Ar^{14}N^+$	$^{40}Ar^{14}N^+$	$^{40}Ar^{14}N^+$	Fe(5.82), Cr(2.83)
55	$^{40}Ar^{14}NH^+$	$^{40}Ar^{14}NH^+$	$^{40}Ar^{14}NH^+$	$^{40}Ar^{14}NH^+$	Mn(100)
56	$^{40}Ar^{16}O^+$	$^{40}Ar^{16}O^+$	$^{40}Ar^{16}O^+$	$^{40}Ar^{16}O^+$	Fe(91.66)
57	$^{40}Ar^{16}OH^+$	$^{40}Ar^{16}OH^+$	$^{40}Ar^{16}OH^+$	$^{40}Ar^{16}OH^+$	Fe(2.19)

Table 7-3. Continued.

Wet^a **Mass**	**Dry^b** 15 mm^c	**Dry^b** 15 mm^c	**Dry^b** 10 mm^c	**Dry^b** XTND^d	**Interferes with** **(abundance)**
58	$^{58}Ni^+$	$^{58}Ni^+$	$^{58}Ni^+$	$^{58}Ni^+$	**Ni(67.77)**, Fe(0.33)
59	**$^{59}Co^+$**	**$^{59}Co^+$**	**$^{59}Co^+$**	**$^{59}Co^+$**	**Co(100)**
60	**$^{60}Ni^+$**	**$^{60}Ni^+$**	**$^{60}Ni^+$**	**$^{60}Ni^+$**	Ni(26.16)
62	????	????	????	????	Ni(3.51)
63		**$^{63}Cu^+$**	**$^{63}Cu^+$**	**$^{63}Cu^+$**	**Cu(69.1)**
65		$^{65}Cu^+$	$^{65}Cu^+$	$^{65}Cu^+$	Cu(30.9)
66	$^{36}Ar^{14}N^{16}O^+$				Zn(27.8)
68	**$^{40}Ar^{14}N^{14}N^+$**	**$^{40}Ar^{14}N^{14}N^+$**	**$^{40}Ar^{14}N^{14}N^+$**	**$^{40}Ar^{14}N^{14}N^+$**	Zn(18.57)
69	**$^{40}Ar^{14}N^{16}N^{16}H^+$**				**Ga(60.16)**
70	**$^{40}Ar^{14}N^{16}O^+$**	**$^{40}Ar^{14}N^{16}O^+$**			Ge(20.51), Zn(0.62)
71	**$^{40}Ar^{14}N^{16}OH^+$**				Ga(39.84)
72	$^{36}Ar_2^+$	$^{36}Ar_2^+$			Ge(27.4)

The major isotopes are shown in bold face text

a: Wet plasma

b: Dry plasma, DSID torch

c: Sampling depth, in mm

d: Dry plasma, extented torch

C.1.1.2 Dry Plasma Background Spectra

Due to the absence of continuous aspiration of water, dry plasma background spectra are anticipated to be simpler, only basic plasma ions are expected to be the prevailing background species. The background spectra for the dry plasma were acquired using the same operating conditions as for the wet plasma, with the exception of the use of the DSID torch. The results presentation format described below will be subsequently used for all background spectral scans presented in this section.

Because no significant species, other than hydrogen, were observed in the mass region 1 to 9 and in order to avoid scanning over mass 40 ($^{40}Ar^+$), only the region from mass 10 to 39 was scanned. Although the region from mass 16 to 21 is not analytically useful, the intensity of the peaks observed in this region serves both as a measure of the oxygen and hydrogen present in the plasma and as an indication of oxide and hydroxide formation. The region from mass 28 to 36 is analytically useful, as an elimination of the peaks present in this region would allow interference free determinations of Si, P, S and Cl (Table 7-3).

Again, because only Ar dimer, Ar-dimer protonated species and Kr impurities were observed above mass 75, only the region from mass 42 to 75 was scanned. This region is analytically useful, for example, elimination of the background spectral features present in this region would allow interference free determinations of Ca, Sc, Ti, Cr, V, Fe, Cu, Zn, Ga, Ge, Se and As (Table 7-3). Because $^{40}Ar^{14}N^+$, $^{40}Ar^{16}O^+$, $^{40}Ar^{16}OH^+$ and their isotopic combinations (i.e., $^{36}Ar^{16}O^+$, $^{36}Ar^{16}OH^+$, $^{36}Ar^{14}N^+$, $^{40}Ar^{15}N^+$) dominate the spectral region from mass 50 to 57, they are a source of potential spectral interference for isotopes of Ti, Cr, V, Fe and Mn (Table 7-3). Due to their significance, the intensity of these species will be closely followed in all subsequent experiments.

In order to facilitate comparisons with the wet plasma, the first set of dry plasma background spectra were acquired at a sampling depth of 15 mm and the other operating conditions were kept as before. The background spectral features of the dry plasma are shown in Figures 7-4 and 7-5. The presentation format is the same as that used in Figures 7-2 and 7-3, except that the bottom frame of Figure 7-5 is only scale-expanded by a factor of four (with respect to the middle frame).

A cursory examination of Figures 7-4 and 7-5 and a quick comparison with the wet plasma background spectra (Figures 7-2 and 7-3) reveals that the dry plasma background spectrum has been considerably simplified. As shown in Figure 7-4a, oxygen and oxygen containing species no longer saturate the detector (mass range from 16 to 21, Figure 7-2a), however, nitrogen has now became the dominant

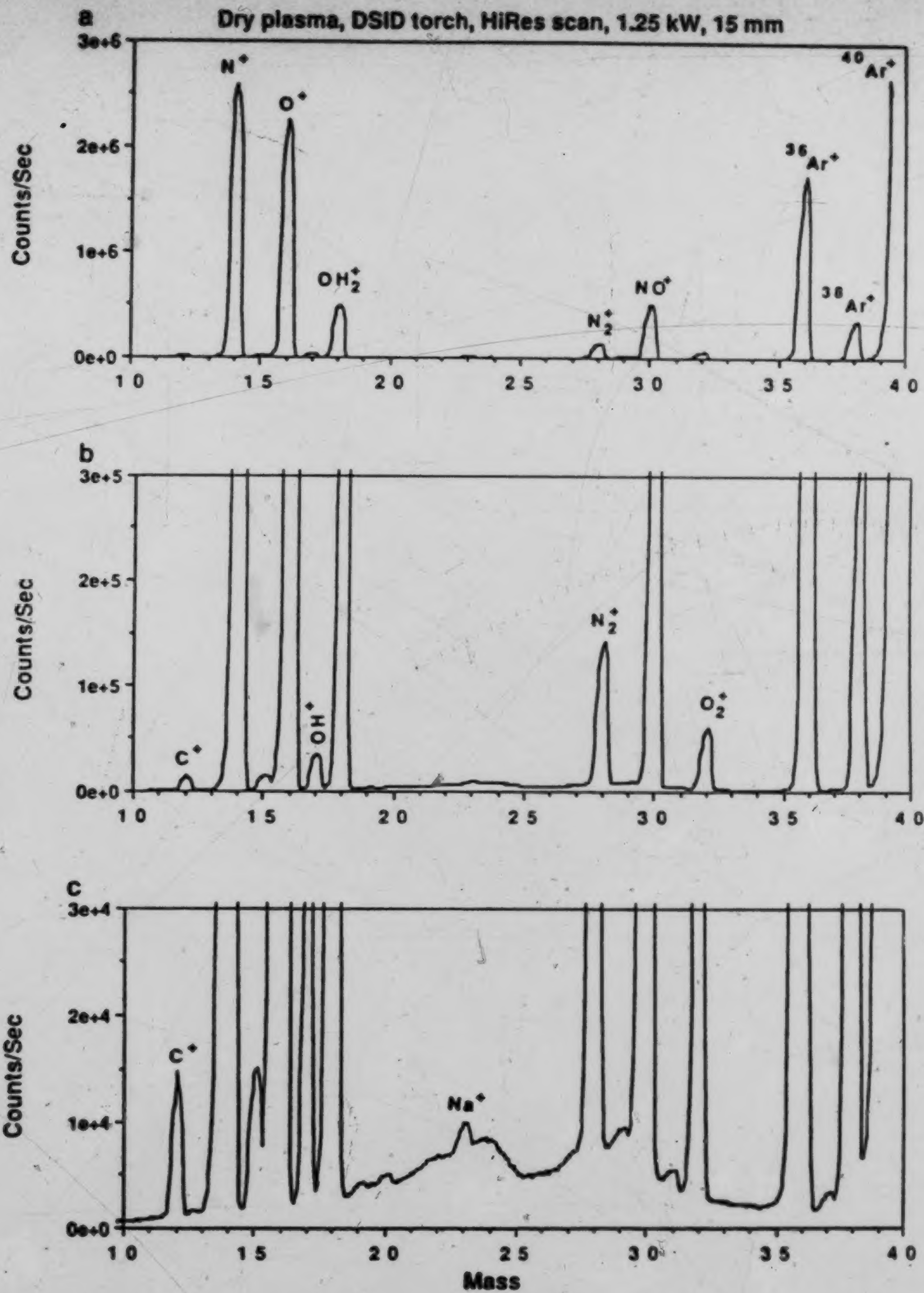

Figure 7-4. Background spectrum for a dry plasma, high resolution scan, sampling depth 15 mm, mass range 10-40 amu.

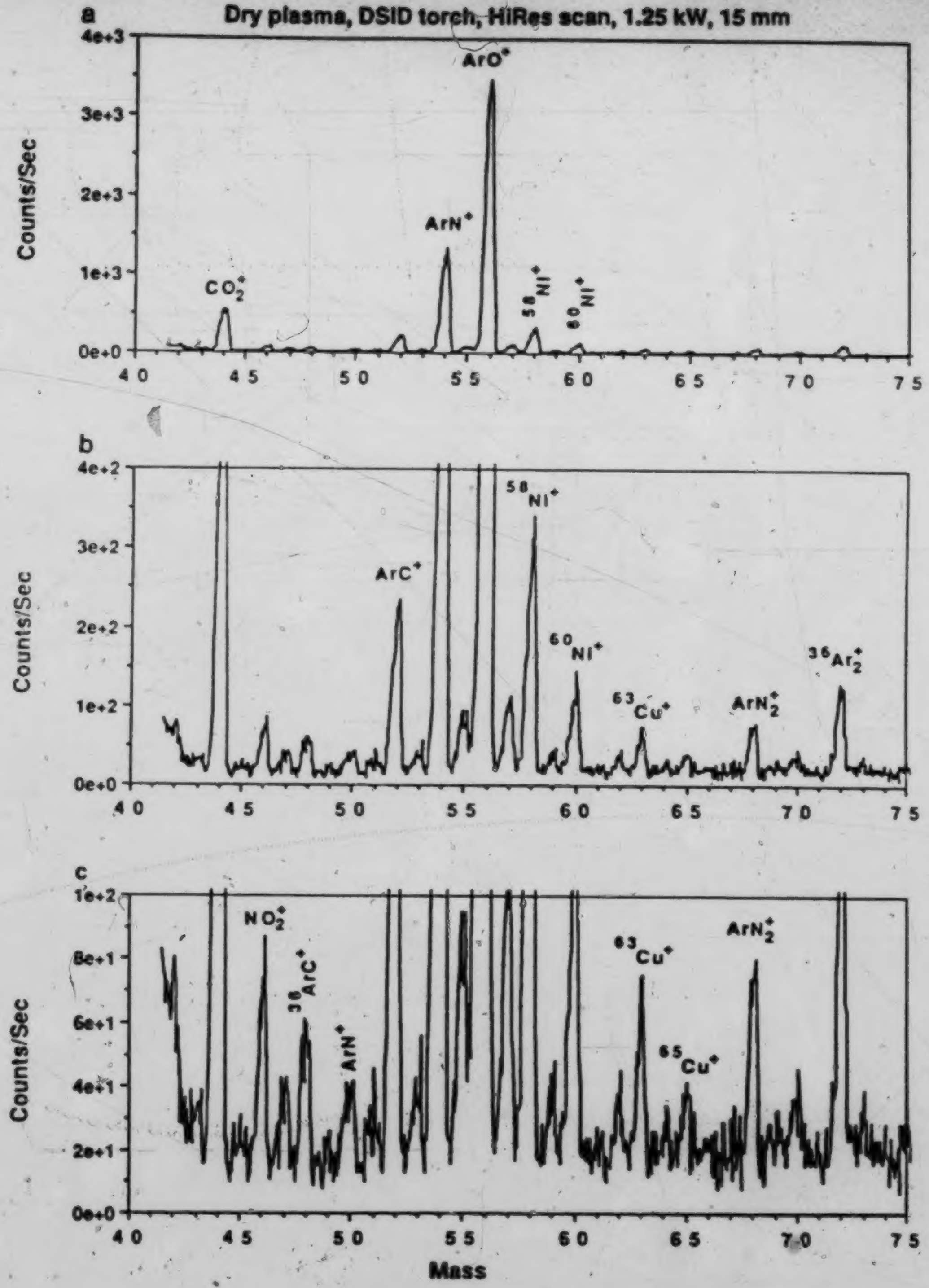

Figure 7-5. Background spectrum for a dry plasma, high resolution scan, sampling depth 15 mm, mass range 40-75 amu.

species. This is tentatively attributed to air entrainment. The increased amount of air entrained is due to a change in the shape and the size of the plasma (a more confined and physically smaller plasma is formed when there is a central channel).

A close examination and a further comparison of wet and dry plasma background reveals that the dry plasma intensities of $^{36}Ar^+$ and of $^{38}Ar^+$ (Figure 7-4) have increased as compared to those observed for the wet plasma (Figure 7-2). This can be explained by considering that an increase in the population of Ar ions (i.e., $^{36}Ar^+$, $^{38}Ar^+$, $^{40}Ar^+$) is caused by the use of a hotter plasma. (In general, a dry plasma is hotter than a wet plasma due to the absence of a cooling effect). In addition, due to the absence of continuous aspiration of water in the plasma, the population of oxygen and hydrogen is considerably reduced as demonstrated by the reduction in the intensity of $^{16}O^+$ and $^{16}OH^+$ peaks (compare Figures 7-2 and 7-4) and the corresponding decrease in the intensity of poly-atomic ions, such as $^{40}ArH_2{}^+$ and $^{40}Ar^{16}O^+$ (compare Figures 7-3 and 7-5). (The residual hydrogen and oxygen observed in the dry plasma background is attributed to water impurities found in nominally pure argon and to air entrainment). A constant population of Ar ions in the plasma (calculated to be about $1.2x10^{15}$ per cm^{-3} [8]) coupled with a decrease in the population of molecular species, and thus of argon ions bound in such species, results in a net increase in the population of unbound argon ions in the plasma, thus accounting for the increase observed in the intensities of $^{36}Ar^+$ and $^{38}Ar^+$.

Observing the spectral region from mass 50 to 70 shows that the intensity of the species present in the dry plasma background spectra (Figure 7-5) is, in general, about 5 times smaller than that observed for the wet plasma background spectra (Figure 7-3). More specifically, the intensities of $^{40}Ar^{14}N^+$, $^{40}Ar^{16}O^+$ and $^{40}Ar^{14}N_2^+$ have been reduced by a factor of 1.5, 5 and 7.5; the intensity of $^{40}Ar^{16}OH^+$ has remained virtually the same. The largest decrease was observed in the intensity of the $^{40}Ar^{14}N_2^+$ peak, which is most likely due to the hotter dry plasma breaking up the tri-atomic $^{40}Ar^{14}N_2^+$. Even in high sensitivity (Figure 7-5c), most spectral features have intensities below 100 counts/s. (Sensitivities of 10^4 counts/s to 10^5 counts/s per ppm of analyte are typically observed for most elements when aspirating solution samples in the ICP). Although the intensity of the $^{12}C^+$ peak has decreased and $^{40}C^{16}O_2H^+$ has been eliminated, the intensity of the $^{40}C^{16}O_2^+$ has increased, possibly due to an increase in the air entrained by the dry plasma.

A further comparison of dry and wet plasma background spectral features in the region from mass 41 to 84 (Figures 7-3 and 7-5, note the difference in the intensity of the spectra shown in Figures 7-3a and 7-5a) shows two peaks (at mass 63 and 65) in the dry plasma spectrum (Figure 7-5c) that were not previously observed in the wet plasma spectrum (Figure 7-3c). These are assigned to copper ($^{63}Cu^+$ and $^{65}Cu^+$) and are most likely due to sampling of the the copper sampler cone orifice used in these experiments (Figure 7-1). The background species identified in Figures 7-4 and 7-5 are summarized in Table 7-3, the lack of an entry in this table indicating the absence of a species. Therefore, interference-free determinations are now possible at these masses/isotopes.

In general, the background spectra are considerably simplified when a dry plasma is used. However, new questions arise, as the origin of carbon, nitrogen and oxygen must now be accounted for. Two possible sources can be identified: impurities in the argon supplies used in this work (typically <2 ppm CO, 4 ppm CO_2, <3 ppm CH_4, <3 ppm halogenated hydrocarbons, <100 ppm N_2 and 4-150 ppm H_2O are reported by the department's spectral services laboratory for the Ar used in these experiments) and air entrainment.

In an attempt to further reduce air entrainment and in order to establish the origin of carbon- and nitrogen-containing species identified in the background spectrum, the torch was translated even closer to the plasma. Measurements were taken at a 10 mm sampling depth and the other operating conditions were kept as before. The results are shown in Figures 7-6 and 7-7. The presentation format is the same as before, except that the bottom frame of Figure 7-7 is only scale-expanded by a factor of three (with respect to the middle frame). The maximum intensity of the spectrum shown in Figure 7-7a, which is exactly an order of magnitude smaller than that shown in Figure 7-5a, should be noted.

The results shown in Figures 7-6 and 7-7 demonstrate that dry plasma background spectra taken at a 10 mm sampling depth are further simplified *vis-á-vis* dry plasma background spectra measured at a 15 mm sampling depth (Figures 7-4 and 7-5). The background species observed in Figures 7-6 and 7-7 are listed in Table 7-3, again, the lack of an entry in this table indicates the elimination of a species.

From the reduction in the intensity of the $^{12}C^+$, $^{14}N^+$ and $^{16}O^+$ peaks (compare Figures 7-4 and 7-6) it can be concluded that a significant amount of these species is present in the plasma due to air entrainment. In addition, the intensities of $^{40}Ar^{14}N^+$, $^{40}Ar^{16}O^+$ and $^{40}Ar^{14}N_2^+$ have been reduced by a factor of 6, 2 and 2; $^{40}Ar^{16}OH^+$ has been eliminated. The largest decrease was observed in the intensity of the $^{40}Ar^{14}N^+$ peak, correlating with the reduction in the intensity of the $^{14}N^+$ peak. In summary, translating the torch closer to the plasma helps reduce air entrained species and further simplifies the background spectrum.

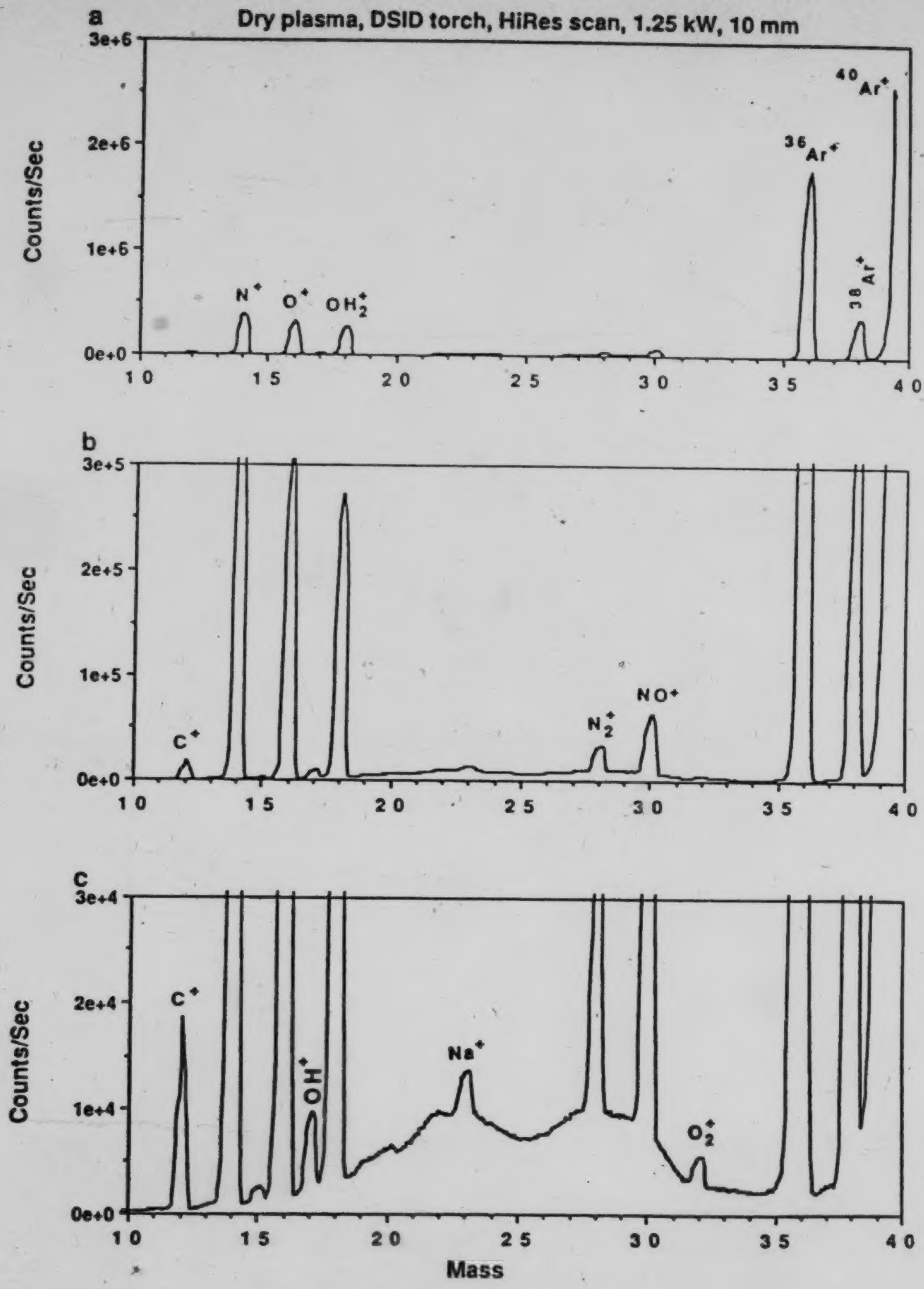

Figure 7-6. Background spectra for a dry plasma, high resolution scan, sampling depth 10 mm, mass range 10-40 amu.

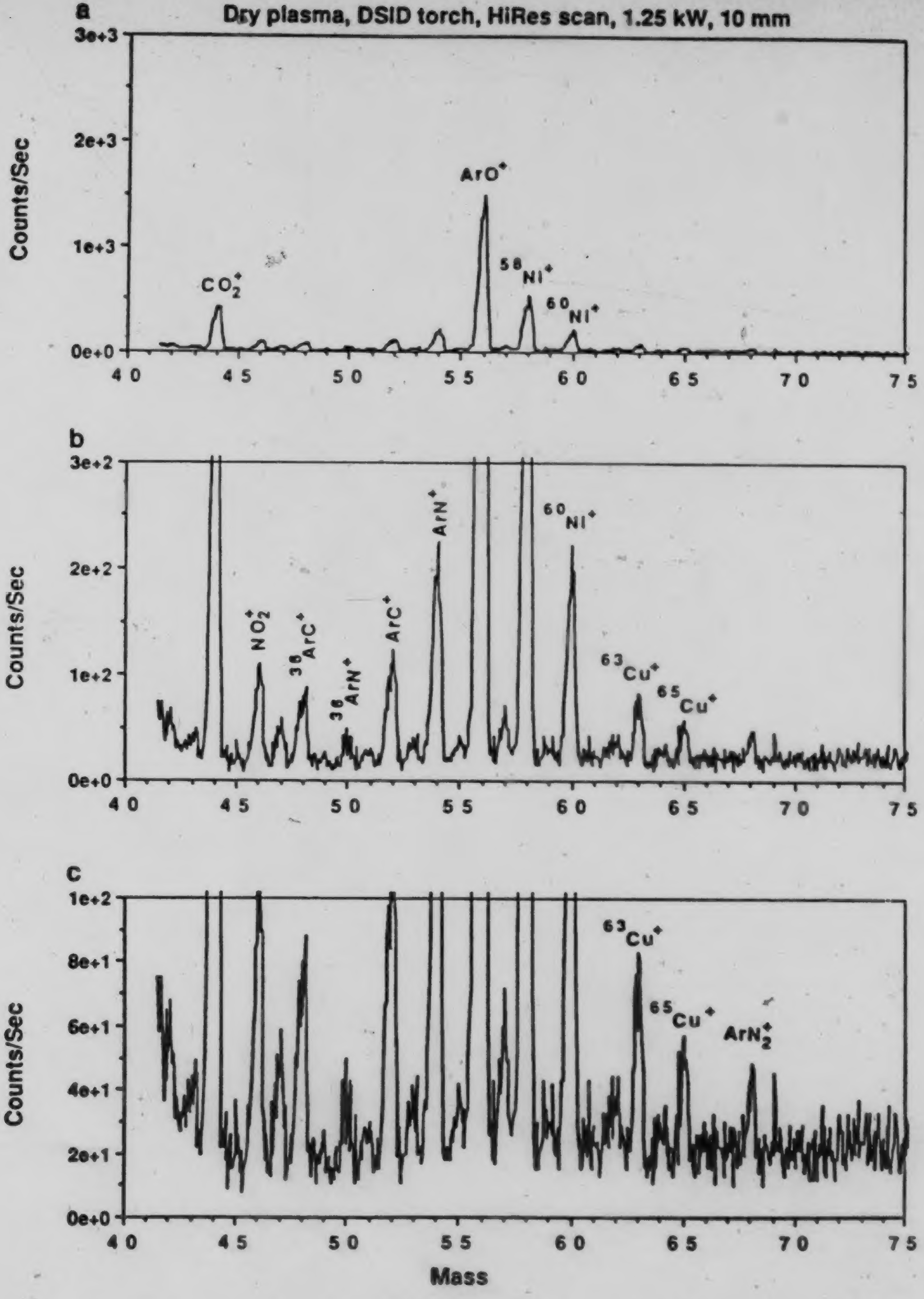

Figure 7-7. Background spectrum for a dry plasma, high resolution scan, sampling depth 10 mm, mass range 40-75 amu.

In an attempt to further reduce air entrained species, thus further simplifying the background spectrum, it was decided to carry the ICP-AES experience (in which a 'long' torch, typically about 20 mm longer than that usually used in optical work is employed in order to reduce N_2-band emission caused by air entrainment [9]) to ICP-MS. It is worth noting that the Elan was originally equipped with such a torch. In this case, instead of designing a new torch, a torch extension (i.e., a sleeve) that fit in the DSID torch was utilized, as shown in Figure 7-1. The background spectra shown in Figures 7-8 and 7-9 were acquired with the extension in place while the other operating conditions were kept as before. In this case, the middle frame of Figure 7-9 is only scale-expanded by a factor of four (with respect to the top frame) and the bottom frame is scale-expanded 2.5 times (with respect to the middle frame). Note that the maximum intensity of the spectrum shown in Figure 7-9a is 10 times smaller than that shown in Figure 7-7a. The background species observed are listed in Table 7-3.

As shown in Figure 7-8a, the spectral region from mass 15 to 20 is further simplified *vis-a-vis* a dry plasma background spectrum measured at a 10 mm sampling depth (Figure 7-6). In addition, the intensities of the $^{12}C^+$, $^{14}N^+$ and $^{16}OH_2^+$ peaks have been greatly reduced (compare Figures 7-8 and 7-6) when the extended torch is utilized.

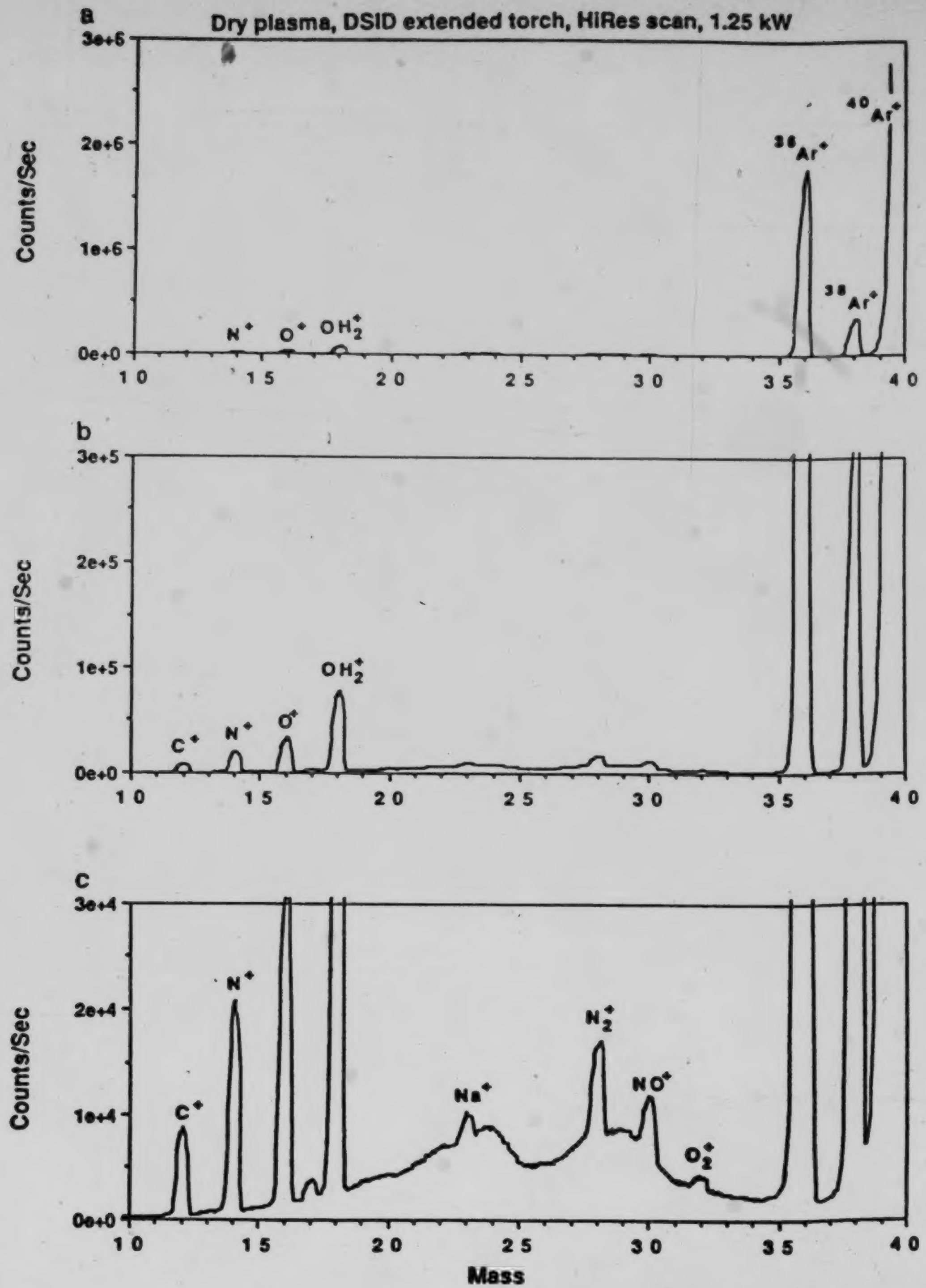

Figure 7-8. Background spectra for a dry plasma, extended torch, high resolution scan, sampling depth 10 mm, mass range 10-45 amu.

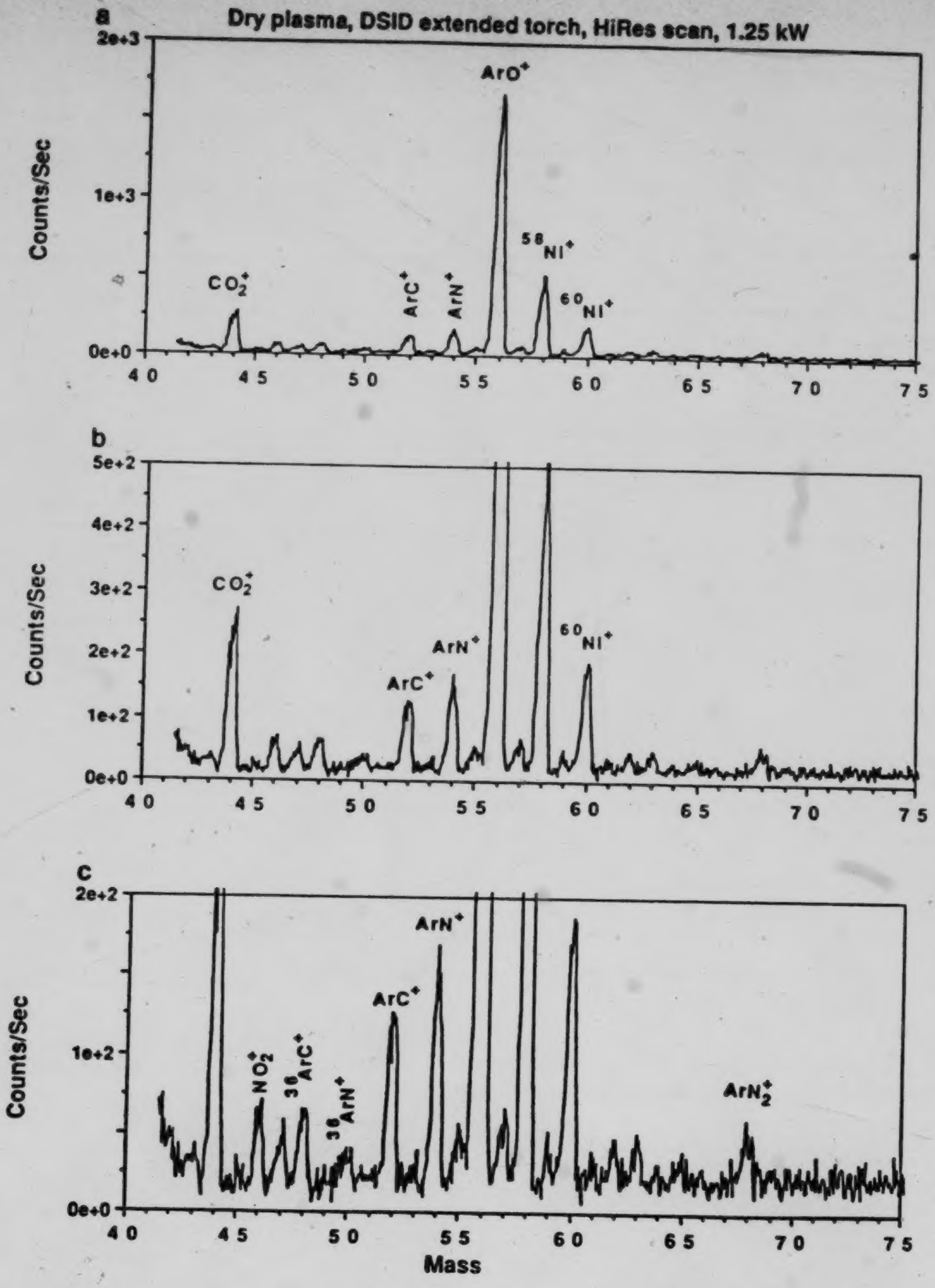

Figure 7-9. Background spectrum for a dry plasma, extended torch, high resolution scan, sampling depth 10 mm, mass range 40-75 amu.

From the results presented in this section it can be concluded that the torch extension was successful in further reducing air entrained species. However, the intensities of $^{40}Ar^{14}N^+$, $^{40}Ar^{16}O^+$ and $^{40}Ar^{14}N_2^+$ have been only slightly reduced; a small peak appeared for $^{40}Ar^{16}OH^+$. These results indicate that, perhaps, a further reduction in the intensity of these species, and as a consequence of MO^+ and MOH^+, can only be realized by reducing the concentration of the water impurities in argon.

In general, the background spectra are simpler when an extended torch is used. However, its effect on signal intensity and analyte temporal behavior must be investigated before it can be used on a routine basis.

C.1.1.3 Comparison of Background Spectral Features

In order to illustrate the differences observed in the background spectral features, spectral data from the previous figures has been grouped together. The background spectral features of the mass region 10 to 40 are shown in Figure 7-10 and those of the mass region from 40 to 75 are shown in Figure 7-11. In Figure 7-10, the top frames of Figures 7-2, 7-4, 7-6 and 7-8 are reproduced, in Figure 7-11 the top frames of Figures 7-3, 7-5, 7-7 and 7-9 are replicated.

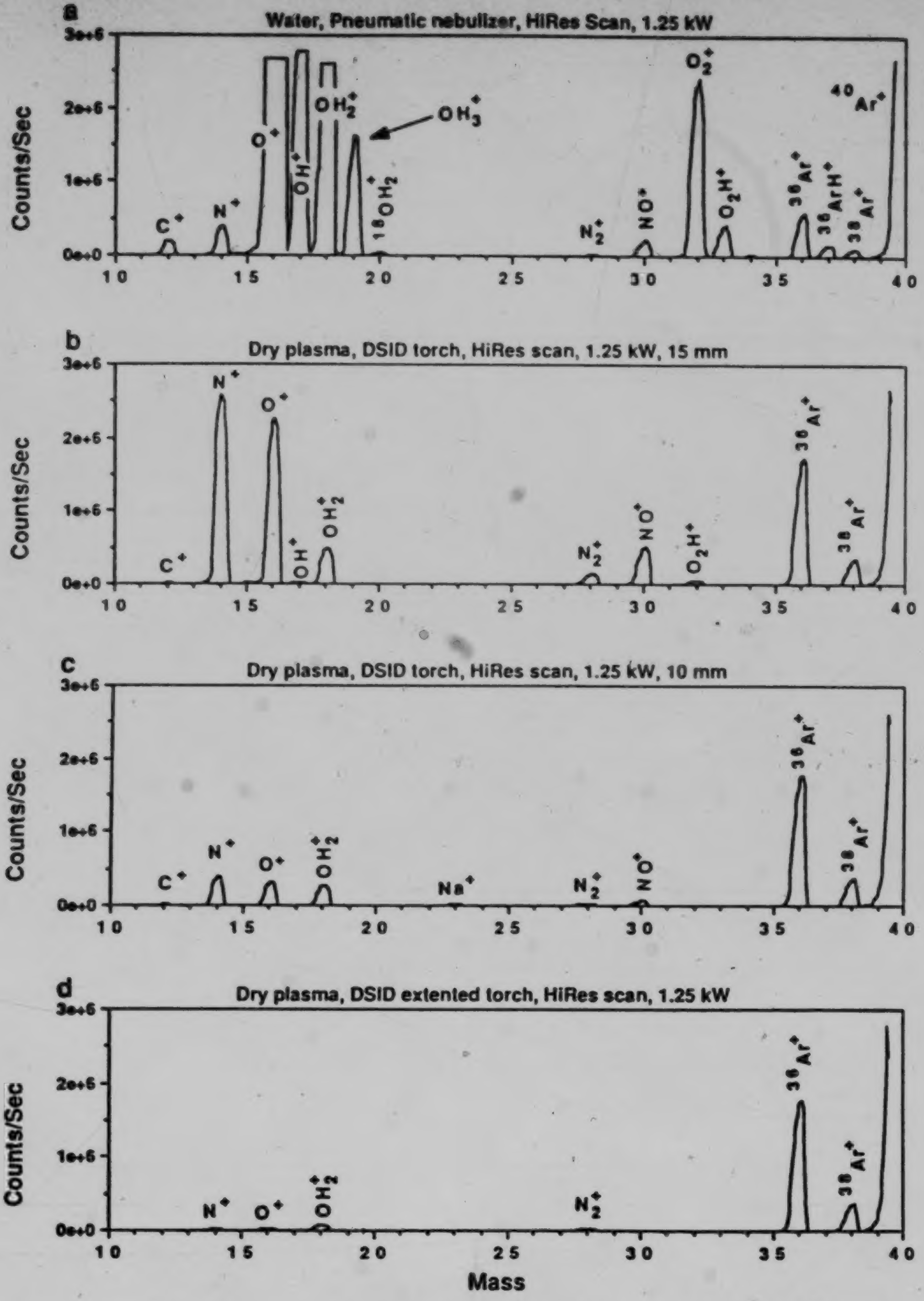

Figure 7-10. Background spectra, mass range 10-40 amu for: (a) wet plasma (15 mm); (b) dry plasma (15 mm); (c) dry plasma (10 mm); (d) dry plasma, extended torch.

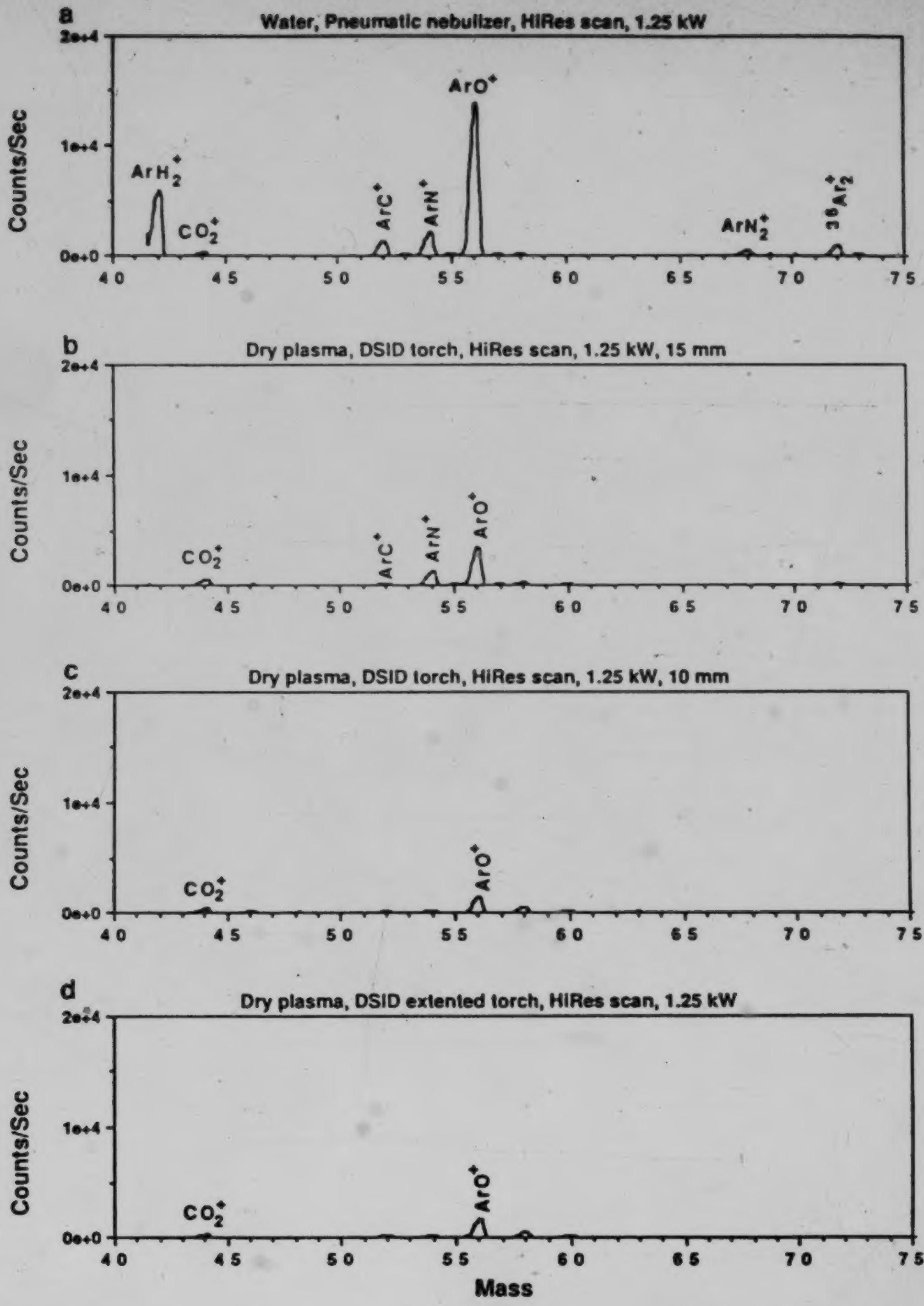

Figure 7-11. Background spectra, mass range 40-75 amu for: (a) wet plasma (15 mm); (b) dry plasma (15 mm); (c) dry plasma (10 mm); (d) dry plasma, extended torch.

From the results shown in Figures 7-10a, 7-10b, 7-10c and those shown in Figures 7-11a, 7-11b, 7-11c it can be concluded that the background spectra are considerably simplified when a dry plasma is utilized. As shown in Figures 7-10d and 7-11d, a further simplification of the background results when the extended torch is employed. From these results it can also be concluded that the key comparison is between two limiting-case plasmas, namely, a wet and a dry plasma with an extended torch.

The advantages of using a dry plasma are perhaps better demonstrated by converting the spectral lines to bars with a width of 1 mass unit and by comparison with a wet plasma, as shown in Figure 7-12 (for mass range from 1-39) and in Figure 7-13 (for mass range from 41 to 84). Shown in the top frame of each figure is a bar graph background spectrum of a wet plasma, the bottom frame refers to a dry plasma background (with the torch extension in place). The spectral simplicity which results from the use of a dry plasma and the extended torch is evident in these figures.

However, due to the wide dynamic range of the observed signals, for instance, about 6 orders of magnitude, detailed information about peaks of smaller intensity is lost when a linear scale is used, as in Figures 7-12 and 7-13.

Information about small peaks becomes available when wet and dry plasma bar graph background spectral features

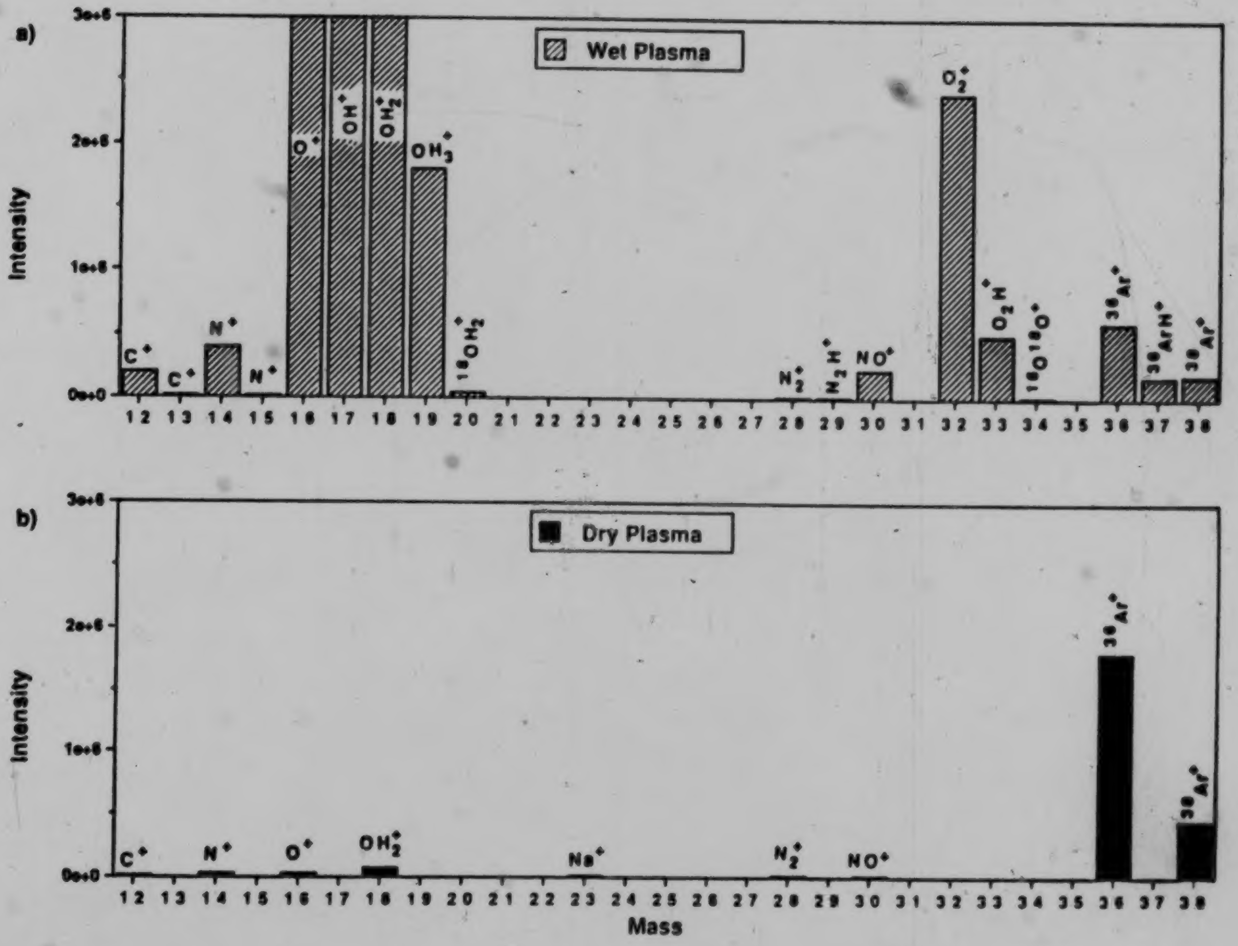

Figure 7-12. Bar graph background spectra, mass range 12-38 amu for: (a) wet plasma, sampling depth 15 mm; (b) dry plasma, extended torch.

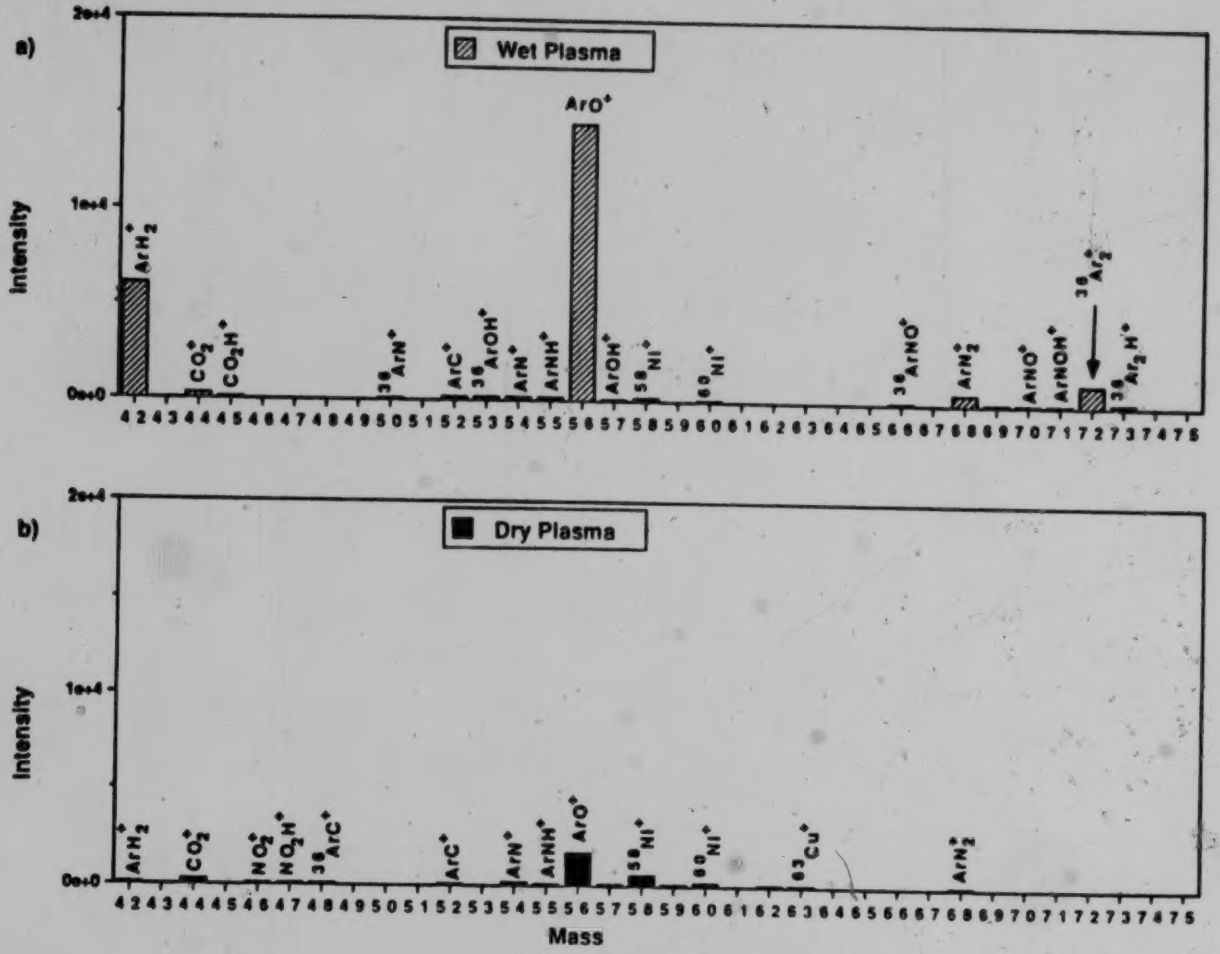

Figure 7-13. Bar graph background spectra, mass range 42-75 amu for: (a) wet plasma, sampling depth 15 mm; (b) dry plasma, extended torch.

are plotted using a logarithmic intensity axis, as shown in Figure 7-14. This presentation format is also useful in assessing spectral interference effects. From the results shown in Figure 7-14 it can be concluded that the peak intensities of some species have been considerably reduced, for example, $^{16}O^+$, $^{16}OH^+$ and $^{16}OH_2{}^+$ have been attenuated by about 2.5, 3 and 2 orders of magnitude whereas others have simply vanished into the background, for instance, $^{16}OH_3{}^+$, $^{18}OH_2{}^+$, $^{18}OH_3{}^+$, $^{14}N_2H^+$, $^{14}N^{16}OH^+$, $^{16}O_2H^+$, $^{16}O^{18}O^+$ and $^{36}ArH^+$. In general, significant reductions in the intensity of the background species has been observed, for example, the intensities of $^{40}Ar^{14}N^+$, $^{40}Ar^{16}O^+$, $^{40}Ar^{16}OH^+$ and $^{40}Ar^{14}N_2{}^+$ have been reduced by factors of 12, 10, 2 and 10.

C.1.1.4 Summary and Conclusions

Looking at the spectra presented thus far and referring to Table 7-3, potential spectral overlaps due to background species can now be assessed. A closer look at Table 7-3 reveals that interference-free determinations that were previously thought to be impossible when a conventional pneumatic nebulizer system is utilized, have now become possible, especially if an extended torch is utilized. The results are summarized in Table 7-4.

The most significant determinations involve the monoisotopic $^{31}P^+$ and $^{45}Sc^+$ and $^{29}Si^+$, $^{32}S^+$, $^{34}S^+$, $^{35}Cl^+$, $^{37}Cl^+$, $^{53}Cr^+$, $^{70}Ge^+$, $^{70}Zn^+$, $^{71}Ga^+$, $^{72}Ge^+$, $^{73}Ge^+$. It should also be

Table 7-4. Background species eliminated from a wet plasma when using a dry plasma and an extended torch.

Mass	Eliminated species	Interferance free determination
19	$^{16}OH_3^+$	F(100)
20	$^{18}OH_2^+$	Ne(90.92)
21	$^{18}OH_3^+$	Ne(0.26)
29	$^{14}N^{14}NH^+$	Si(4.7)
31	$^{14}N^{16}OH^+$	P(100)
33	$^{16}O^{16}OH^+$	S(0.75)
34	$^{16}O^{18}O^+$	S(4.21)
35	$^{16}O^{18}OH^+$	Cl(75.77)
37	$^{36}ArH^+$	Cl(24.23)
45	$^{12}C^{16}O^{16}OH^+$	Sc(100)
53	$^{36}Ar^{16}OH^+$	Cr(9.51)
66	$^{36}Ar^{14}N^{16}O^+$	Zn(27.9)
69	$^{40}Ar^{14}N^{16}OH^+$	Ga(60.16)
70	$^{40}Ar^{14}N^{16}O^+$	Ge(20.51), Zn(0.62)
71	$^{40}Ar^{14}N^{16}OH^+$	Ga(39.84)
72	$^{36}Ar^{36}Ar^+$	Ge(27.4)
73	$^{36}Ar^{36}ArH^+$	Ge(7.76)

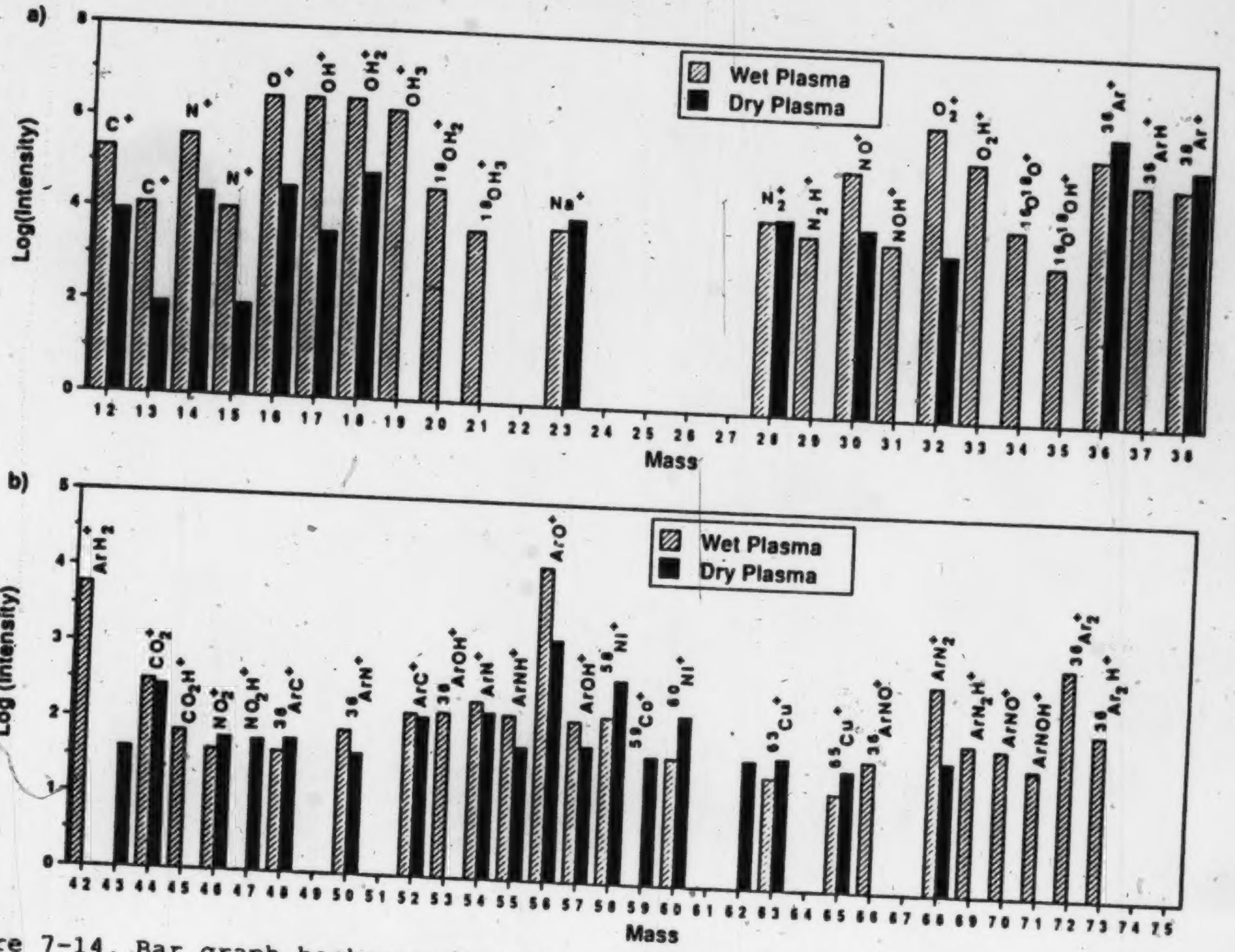

Figure 7-14. Bar graph background spectra (logarithmic scale intensity axis) for a wet plasma (sampling depth 15 mm) and the dry plasma (extended torch) for: (a) mass range 12-42 amu and (b) mass range 42-75 amu.

noted that the intensity of some of the interfering species listed in Table 7-3 is small, for example, mono-isotopic $^{55}Mn^+$ is interfered with by $^{40}Ar^{14}NH^+$ when the extended torch is used, however, $^{40}Ar^{14}NH^+$ count rate is about 30 counts/s with a background of approximately 20 counts/s. This is hardly a problem given the sensitivity of Mn in ICP-MS (about 10^5 counts/s per ppm of aspirated Mn solution).

C.1.2 Probe Background Spectra

From the results presented thus far it can be concluded that spectral simplicity is an important feature of a dry plasma ICP-MS system. However, when a DSID is utilized, a foreign object (i.e., probe) is inserted into the discharge. Therefore, a practical and realistic limiting-case plasma background for an ICP-MS-DSID results when the sample carrying probe is inserted into the discharge. The background spectral features of an ICP-MS-DSID when several types of sample carrying probes are utilized are discussed in detail in what follows.

All spectra reported in this section were taken at a sampling depth of 10 mm; a regular DSID torch; a 1.25 kW applied forward power and, with the exception of the graphite electrode, at low resolution. The other operating conditions were kept as before.

C.1.2.1 Graphite Electrodes

High resolution scans of the mass region 1 to 40 and 42 to 84 for a 'blank' graphite electrode are shown in Figures 7-15 and 7-16. And, as pointed out in chapter 6, no significant spectral features were observed above mass 85.

A quick visual scan of the background spectral features shown in Figures 7-15 reveals their similarity with those of a dry plasma presented thus far. However, there are some note-worthy differences, the most significant being the low intensity of the $^{12}C^+$ peak (which is of the same magnitude as that observed for the wet plasma, as shown in Figure 7-2). Due to its significance, this observation was verified optically by observing the 193.09 nm carbon line when utilizing the DSID for ICP-AES previously described in chapter 2. Therefore, carbon is not expected to plug the mass spectrometer sampler cone orifice (Figure 7-1), excessive carbon deposits are not anticipated in the mass spectrometer itself and intense background spectral features due to carbon containing species should be absent. The $^{12}C^+$, $^{14}N^+$ and $^{16}OH_2^+$ peaks are of the same intensity as those of a dry plasma (at a 10 mm sampling depth, Figure 7-6); in contrast, the intensities of $^{36}Ar^+$ and $^{38}Ar^+$ are considerably lower. This is attributed to a reduction in energy available to the plasma due to energy coupling with the graphite electrode.

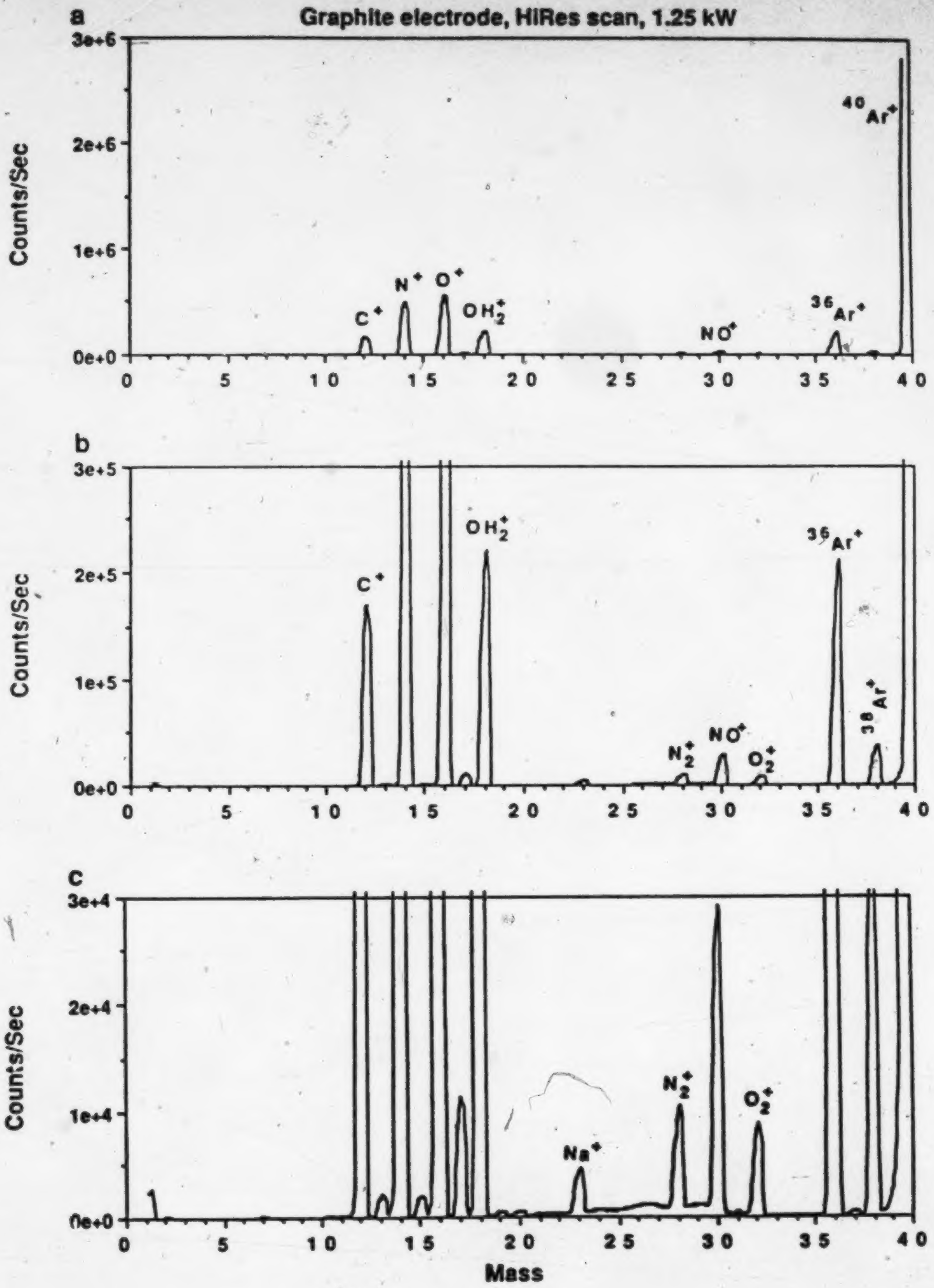

Figure 7-15. High resolution background spectrum of a 'blank' long undercut graphite electrode, mass range 1-40 amu.

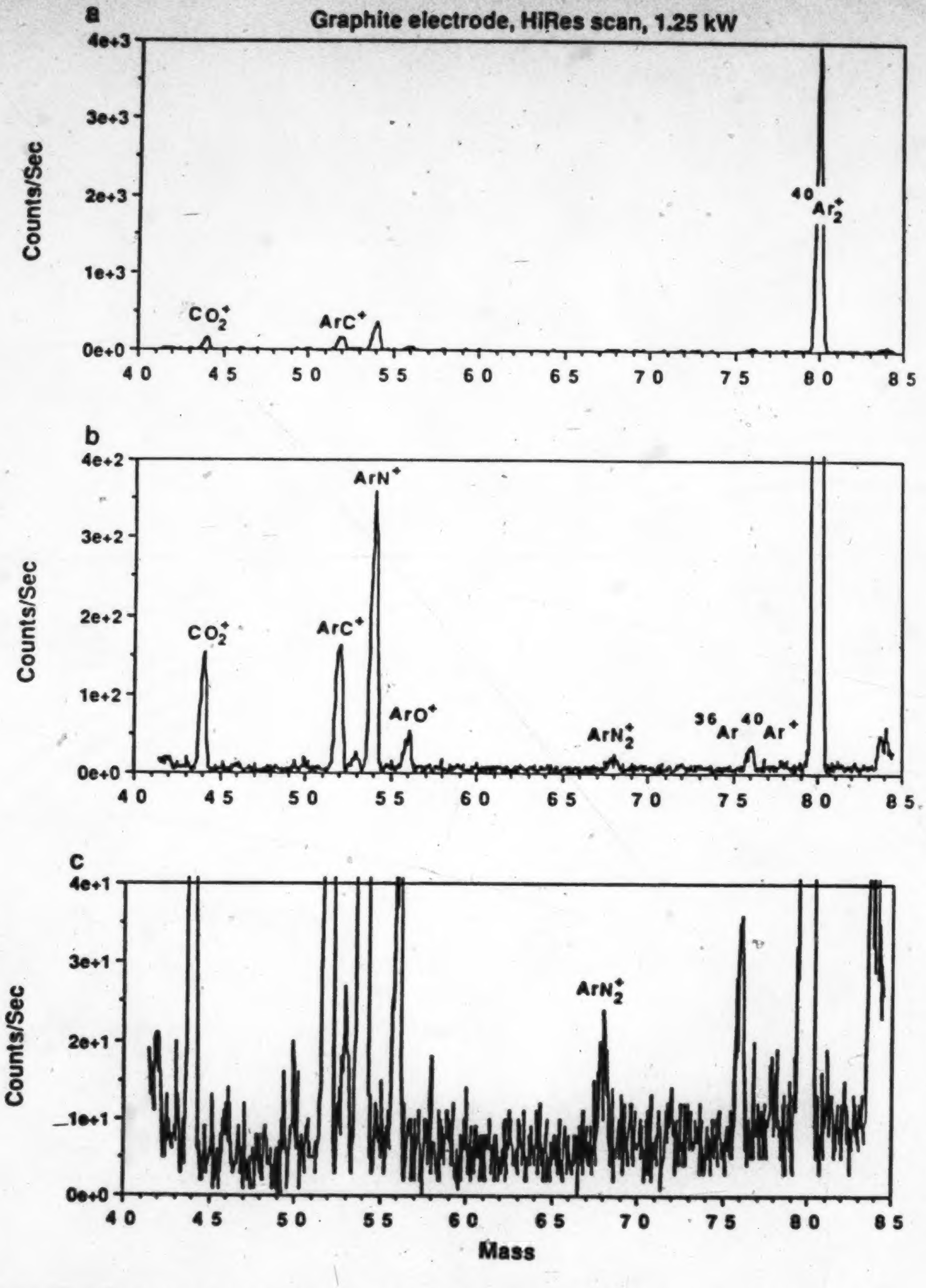

Figure 7-16. High resolution background spectrum of a 'blank' long undercut graphite electrode, mass range 40-85 amu. Note scale expansion in (c).

The region from mass 40 to 85 is interesting from the spectral interference point of view. It is almost featureless as compared to the wet plasma (compare Figure 7-16b with Figure 7-2c) and relatively feature-free, as compared to the dry plasma with an extended torch (compare Figure 7-16b with Figure 7-9b). In general, the intensity of the background spectral features is remarkably low. And in spite of the presence of the graphite electrode, the intensity of the $^{12}C^{16}O_2^+$ peak (at mass 44) is low. It is almost half the size of that observed when the wet plasma (Figure 7-3) or the dry plasma with an extended torch (Figure 7-9) are used. The intensity of the $^{40}Ar^{12}C^+$ peak (at mass 52) has been reduced by as much as an order of magnitude when compared to the wet plasma (Figure 7-3), but it is of the same magnitude as that observed for the dry plasma (extended torch, Figure 7-9). However, the contribution of $^{36}Ar^{16}O^+$ on $^{40}Ar^{12}C^+$ (both present at mass 52) must also be taken into consideration before drawing any further conclusions. The intensity of the $^{40}Ar^{14}N^+$ peak has been reduced by as much as an order of magnitude when compared to the wet plasma background (Figure 7-3). Undoubtedly, the most important reduction in intensity was observed for the $^{40}Ar^{16}O^+$ peak, its intensity (approximately 60 counts/s) is about 250 times lower than that observed when a wet plasma is used (Figure 7-3). Using $^{40}Ar^{16}O^+$ as an example, it can be speculated that M^+/MO^+ and M^+/MOH^+ will also be considerably reduced.

In summary, simple background spectra are observed when a graphite electrode is inserted into the plasma, hence the advantages of a dry plasma appear to be augmented, not just simply maintained, when a graphite electrode is used.

C.1.2.2 Mo Cups

Spectral simplicity is also observed when a blank Mo metal cup is used, as demonstrated by the low resolution background spectra shown in Figures 7-17, 7-18, 7-19 and 7-20. Due to the dissimilarity of the spectral scan modes (i.e., high resolution *versus* low resolution), direct comparisons with the spectra reported thus far are not possible. It is felt, however, that semi-quantitative and qualitative comparisons are still possible. For example, the intensity of the $^{12}C^+$ peak is reduced compared to that of the graphite electrode background, as expected. In contrast, the intensity of the $^{14}N^+$, $^{16}O^+$ and $^{16}OH_2^+$ peaks have slightly increased (Figure 7-15 vs. Figure 7-17). The peak at mass 27 is attributed to aluminium impurities in the Mo cups. No discernible change in the intensity of the $^{36}Ar^+$ and $^{38}Ar^+$ was observed.

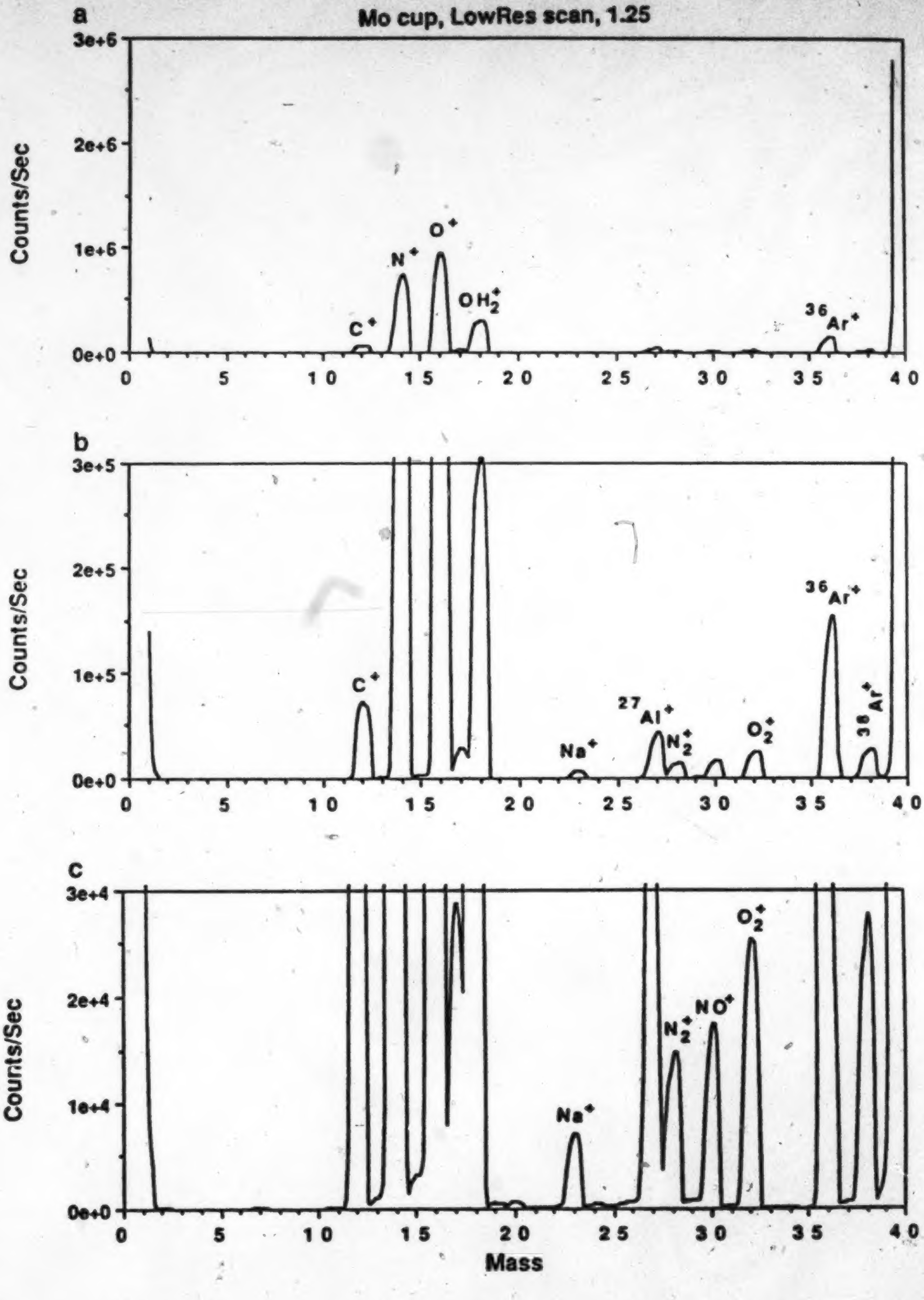

Figure 7-17. Low resolution background spectrum of a Mo cup, mass range 1-40 amu.

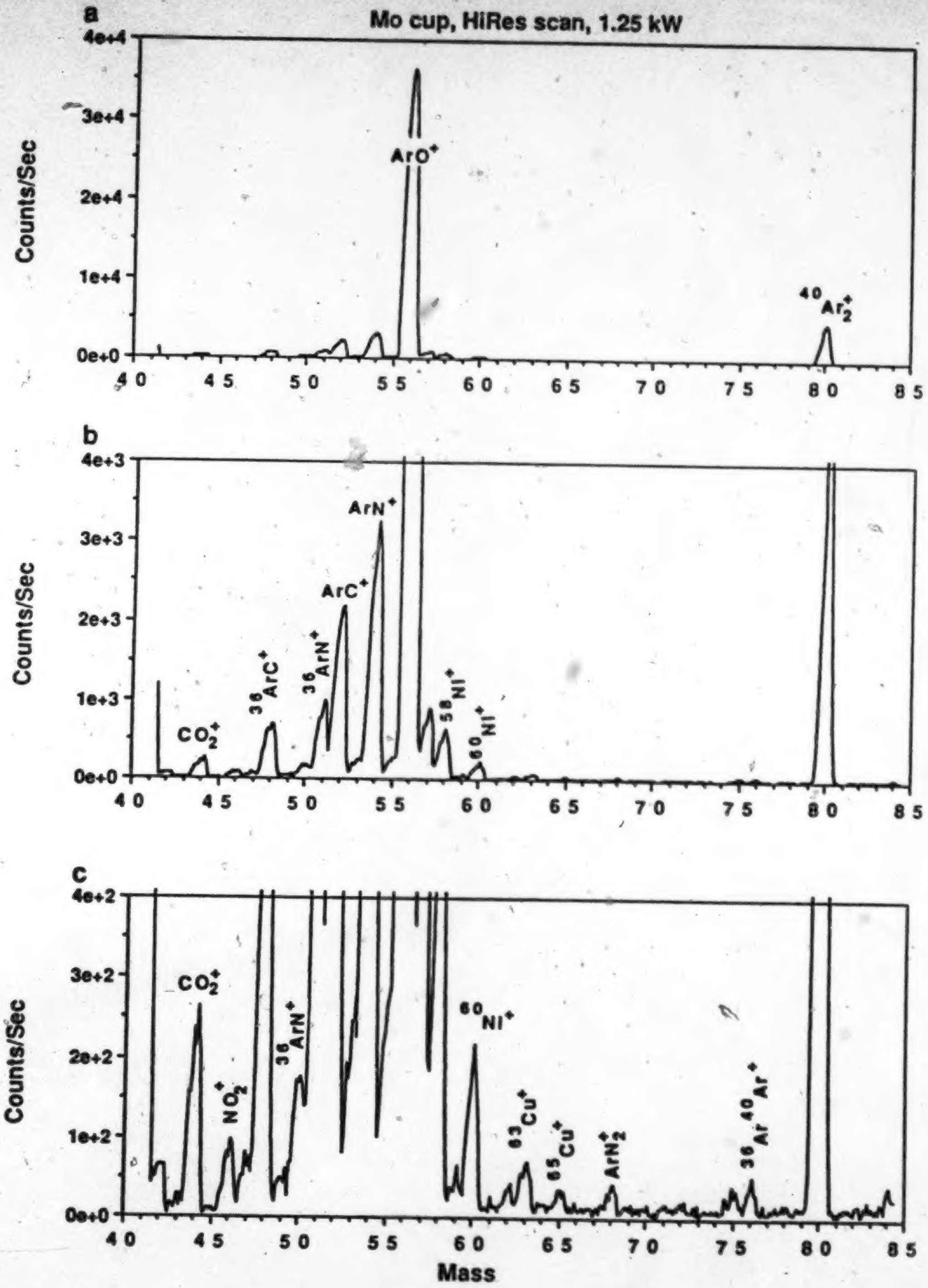

Figure 7-18. Low resolution background spectrum of a Mo cup, mass range 40-85 amu.

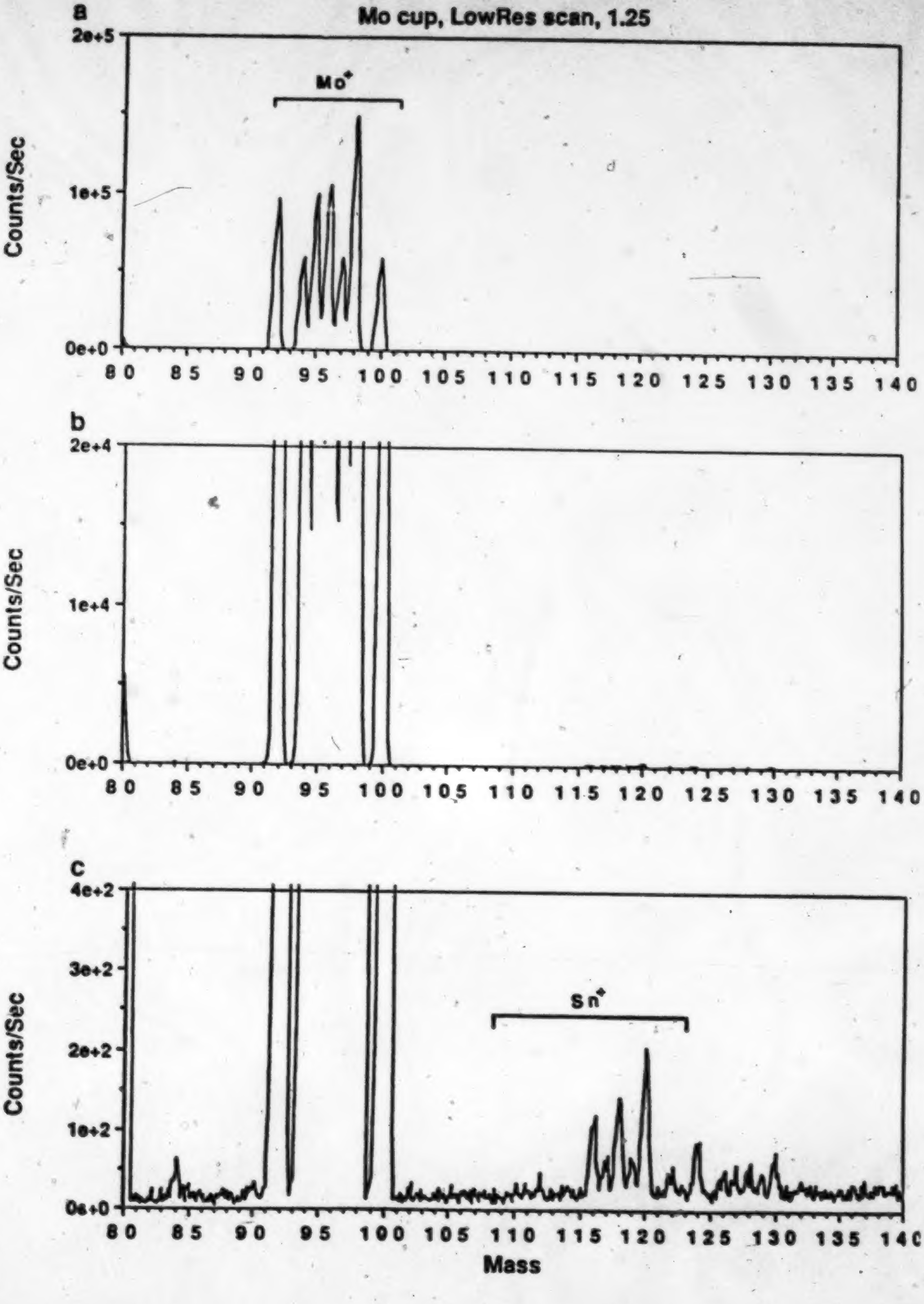

Figure 7-19. Low resolution background spectrum of a Mo cup, mass range 80-140 amu. Note scale expansion.

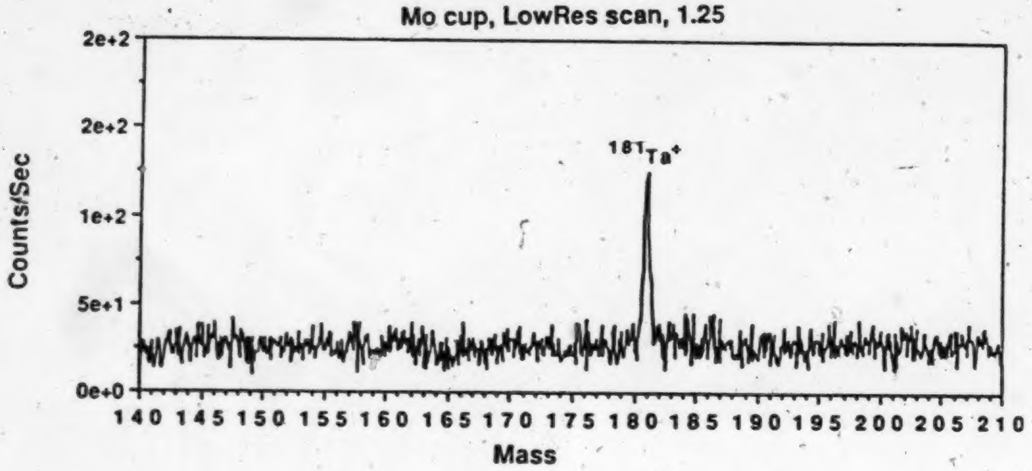

Figure 7-20. Low resolution background spectrum of a Mo cup, mass range 140-210 amu.

More significant changes were observed in the region from mass 46 to 57 (Figure 7-16 *vs.* 7-19). Undoubtedly, analytical determinations in this region will encounter significant interference effects, most notably from ArN^+, ArO^+ and their isotopic combinations. Even $^{40}Ar^{16}OH^+$ is present in significant amounts (i.e., over 900 counts/s). In contrast, $^{40}Ar^{16}OH^+$ was present in insignificant amounts, for example less than 80 counts/s, when a dry plasma was used (10 mm sampling depth, Figure 7-7). The increase in the spectral complexity is possibly due to a change in argon supplies, however, more work remains to be done to verify this claim.

With the exception of the relatively low intensity Mo peaks from mass 92 to 100 (i.e., $^{92}Mo^+$, $^{94}Mo^+$, $^{95}Mo^+$, $^{97}Mo^+$, $^{98}Mo^+$, $^{100}Mo^+$), the region from mass 80 to 140 when viewed at low sensitivity (Figure 7-19a) appears to be free of background spectral features. The peaks appearing from mass 122 to 124 (Figure 7-19c) are assigned to Sn (i.e., $^{114}Sn^+$, $^{115}Sn^+$, $^{116}Sn^+$, $^{117}Sn^+$, $^{118}Sn^+$, $^{119}Sn^+$, $^{120}Sn^+$, $^{122}Sn^+$, $^{124}Sn^+$) and are due to impurities found in the Mo cups. It was not possible to assign the peaks observed in the mass range 125 to 130. A low intensity $^{181}Ta^+$ peak (less than 200 counts/s) is the only species present in the region from mass 140 to 210 (Figure 7-20). This is attributed to impurities in the Mo cups.

C.1.2.3 Ta Cups

Low resolution background spectral scans were also acquired with a Ta cup inserted into the plasma, the results are shown in Figures 7-21, 7-22 and 7-23. No significant differences between the Mo and Ta cups were observed in the mass region from 1 to 39 (Figure 7-17 and 7-21). In the region from mass 50 to 60 (Figure 7-22), the intensity of most species has been reduced by about 5 times with respect to those observed for the Mo cups (Figure 7-18). From the intensity of the Ni peaks ($^{58}Ni^+$, $^{60}Ni^+$, $^{62}Ni^+$ and $^{64}Ni^+$), it can be suggested that Ni is an impurity of the Ta cups. Alternatively, sampling of the aging Ni-skimmer cone (which was subsequently replaced with a new one during the course of this work) could also explain the increased intensity of the nickel peaks. An increase in the intensity of the $^{40}Ar_2^+$ has also been observed (Figure 7-22 *vs.* 7-18), although no explanation can be offered at this time.

No background spectral features were observed in the region from mass 80 to 160 (Figure 7-23a), the small peak appearing at mass 84 is attributed to $^{84}Kr^+$. There were only two peaks in the spectral region from mass 160 to 210 (Figures 7-23b and 7-23c). The relatively low intensity peak at mass 181 is due to $^{181}Ta^+$. Unlike Mo, a peak appeared at mass 197, which is 16 mass units from the main isotope of Ta, indicating oxide formation. (Alternatively, this peak could also be assigned to mono-isotopic Au.

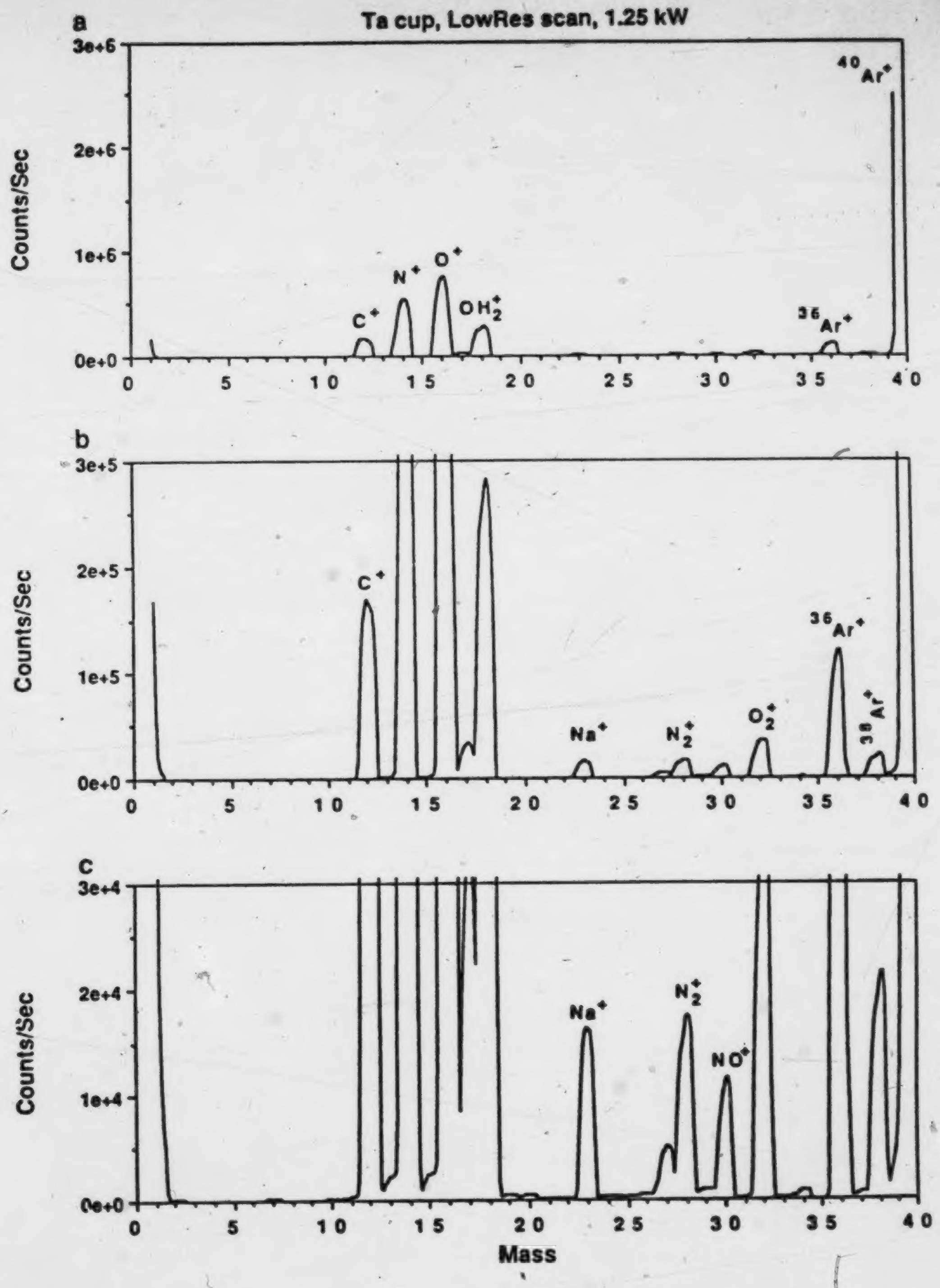

Figure 7-21. Low resolution background spectrum of a Ta cup, mass range 1-40 amu.

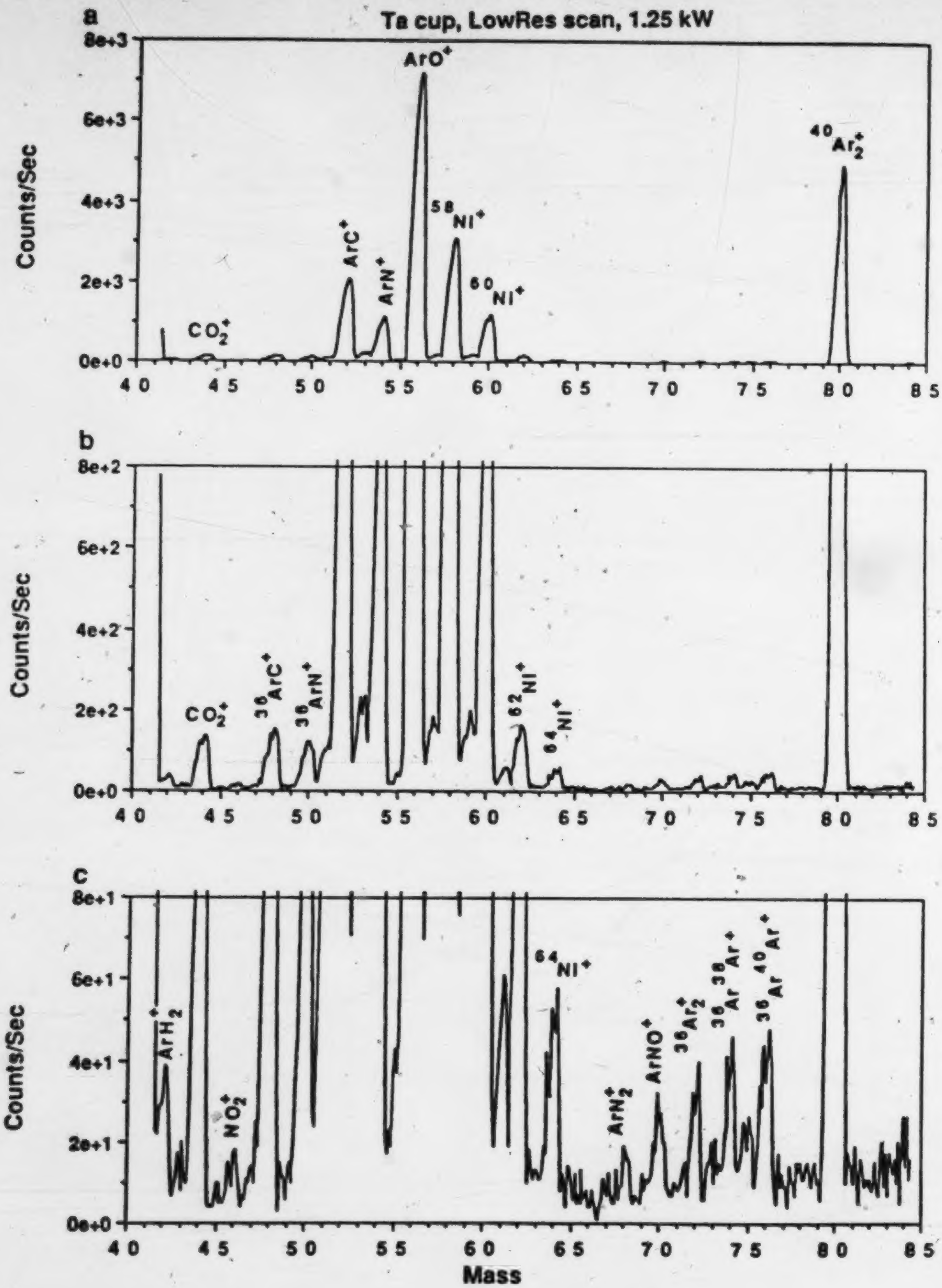

Figure 7-22. Low resolution background spectrum of a Ta cup, mass range 40-85 amu.

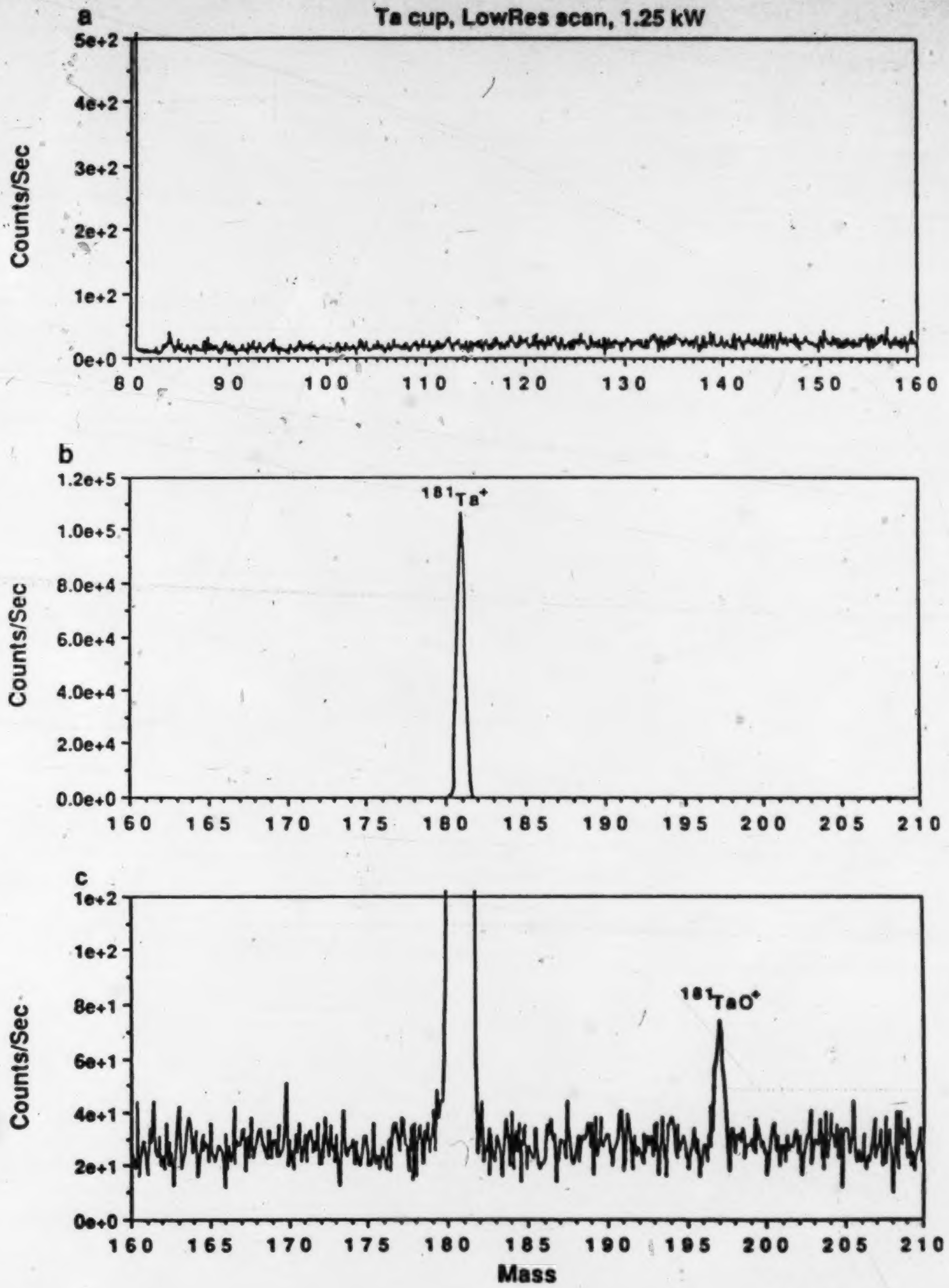

Figure 7-23. Low resolution background spectrum of a Ta cup, for: (a) mass range 80-160, scale expanded; (b) mass range 160-210 amu; (c) mass range 160-210 (note scale expansion).

This, however, is highly unlikely unless it is due to a memory effect arising from a previously run gold solution).

C.1.2.4 W Wire-loop

Low resolution background spectral scans were also acquired with a W wire-loop inserted into the plasma. The results are shown in Figures 7-24, 7-25, 7-26 and 7-27. The intensity of the peak due to $^{12}C^+$ is lower than that observed for the Mo and Ta cups (Figures 7-17, and 7-21). The $^{27}Al^+$ peak previously observed when Mo and Ta metal cups were used is absent. Perhaps the most note-worthy difference between metal (Figure 7-17 and 7-21)) and graphite cups (Figure 7-15) and the wire-loop (Figure 7-24) is the increase in the intensity of the $^{36}Ar^+$ and $^{38}Ar^+$ peaks. This can be explained by considering that, due to the smaller thermal mass of the wire-loop, less energy is lost to the probe (as opposed to graphite or metal cups) thus resulting in a hotter plasma.

The spectral simplicity observed for the graphite cups in the mass region from 41-84 (Figure 7-16) is also observed for the wire-loop (Figure 7-25). When compared to Mo and Ta cups (Figure 7-18 and 7-22), the intensities of most species has been reduced by more than an order of magnitude. The low intensities of, for example, $^{40}Ar^{12}C^+$ (~40 counts/s), $^{40}Ar^{14}N^+$ (~400 counts/s) and $^{40}Ar^{16}O^+$ (~200 counts/s) are worth noting.

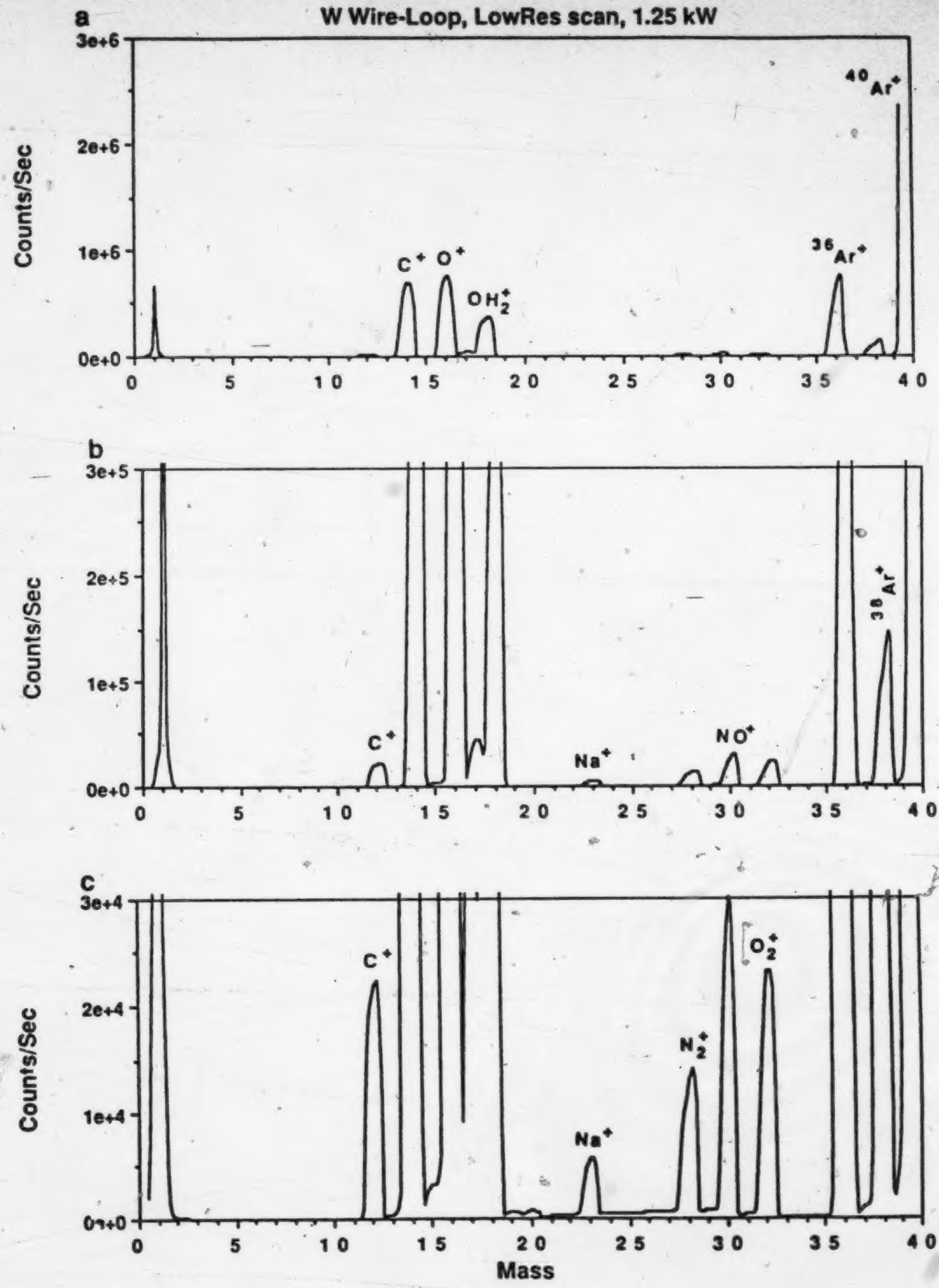

Figure 7-24. Low resolution background spectrum of a W wire-loop, mass range 1-40 amu.

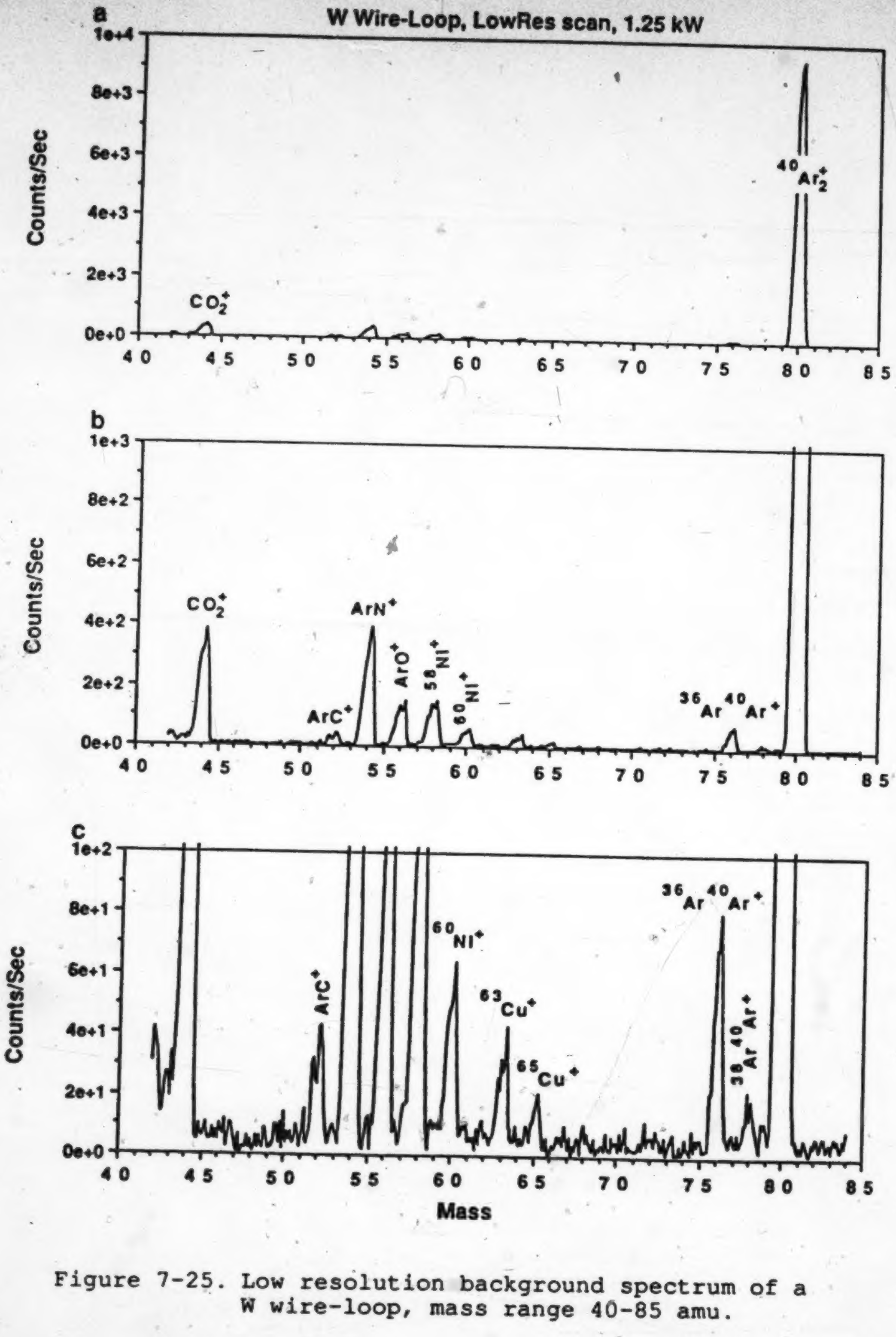

Figure 7-25. Low resolution background spectrum of a W wire-loop, mass range 40-85 amu.

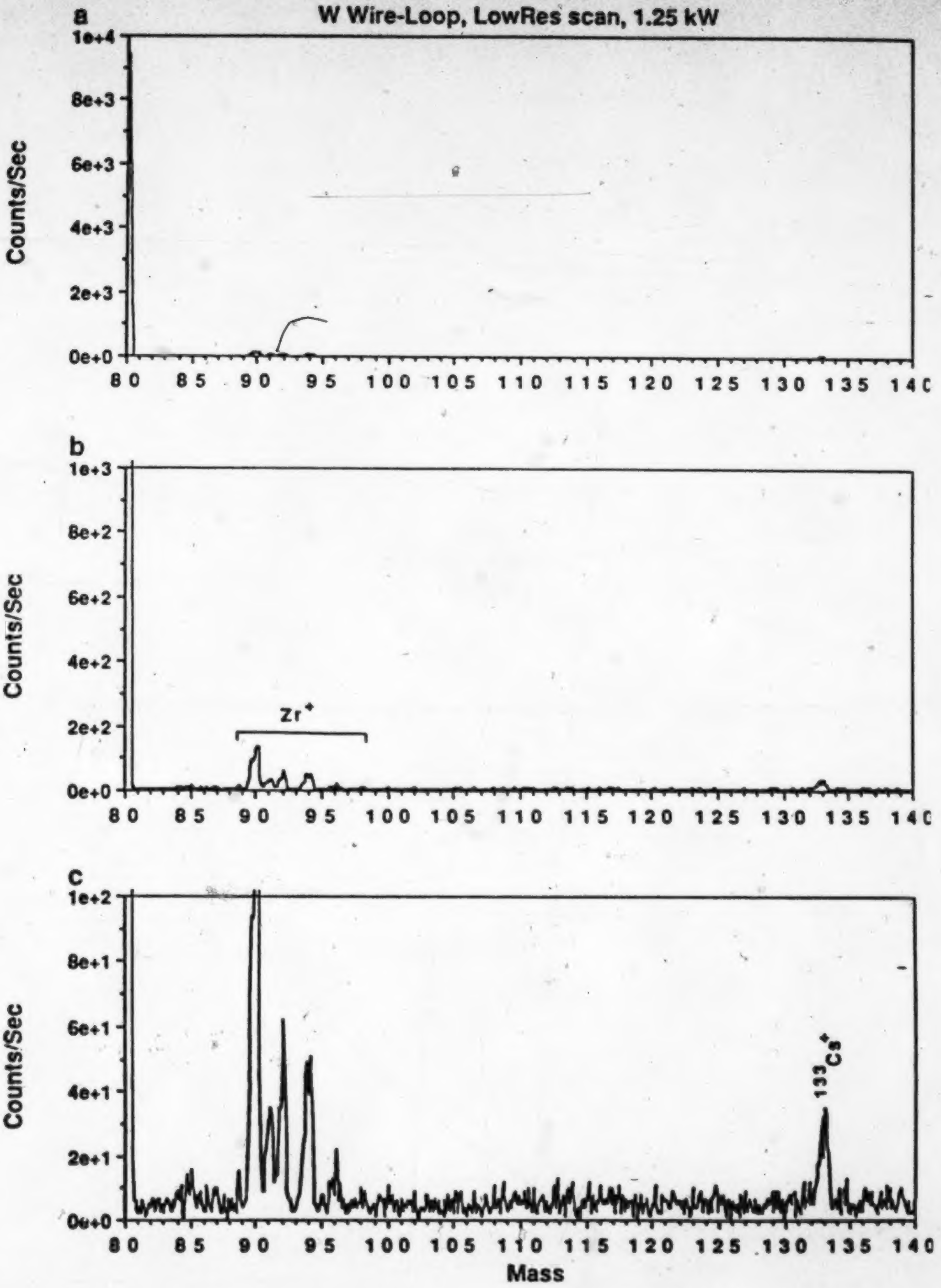

Figure 7-26. Low resolution background spectrum of a W wire-loop, mass range 80-140 amu.

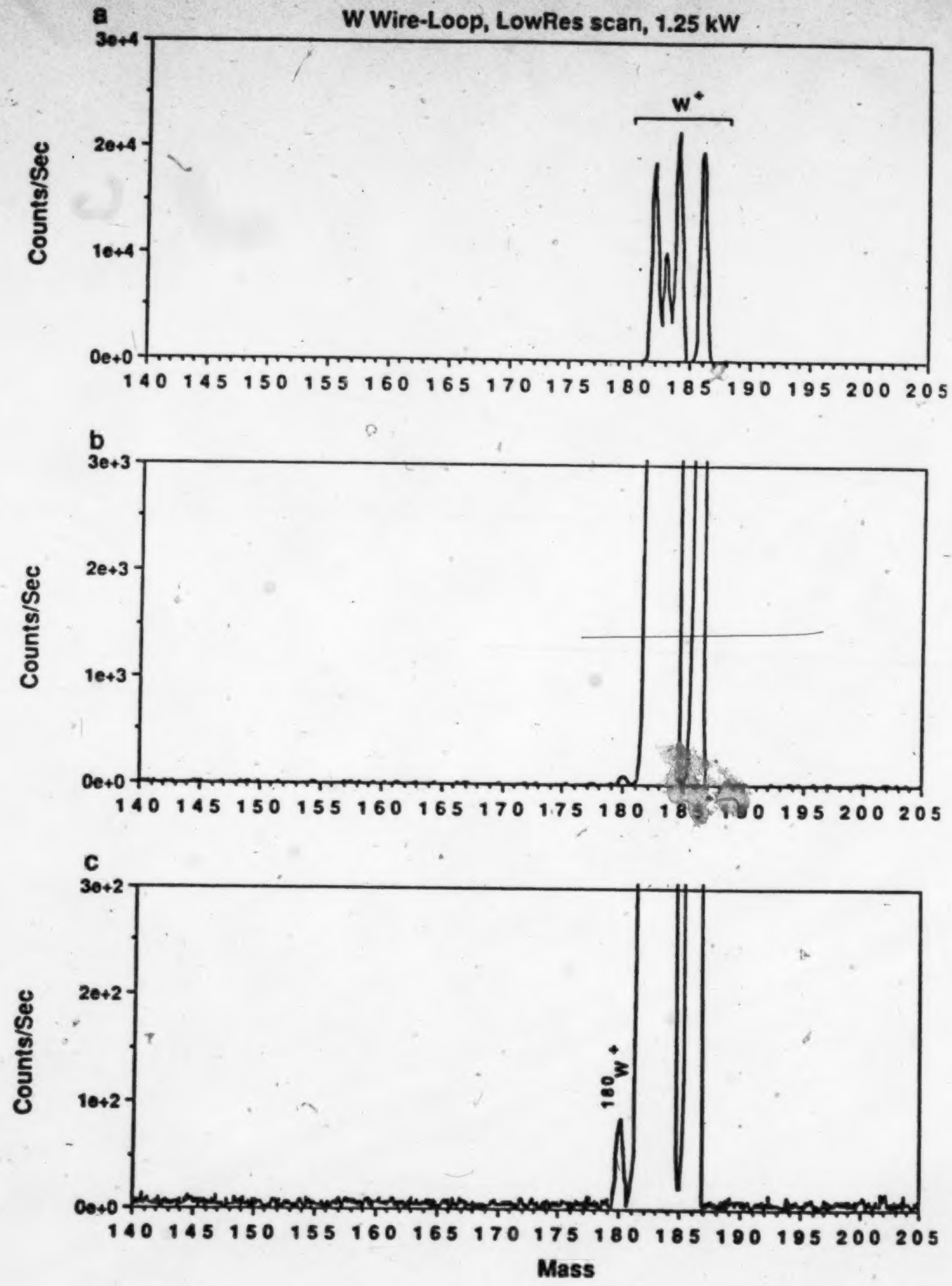

Figure 7-27. Low resolution background spectrum of a W wire-loop, mass range 140-205 amu.

With the exception of the low intensity Zr and Cs peaks ($^{90}Zr^+$, $^{91}Zr^+$, $^{92}Zr^+$, $^{94}Zr^+$, $^{96}Zr^+$ and $^{123}Cs^+$) which are attributed to impurities, no other species were observed in the region from mass 80 to 140 (Figure 7-26). The only species observed in the region from mass 140 to 205 (Figure 7-27) were the relatively low intensity tungsten isotopes (i.e., $^{180}W^+$, $^{182}W^+$, $^{183}W^+$, $^{183}W^+$, $^{184}W^+$, $^{186}W^+$).

C.1.2.5 Summary and Conclusions

In general, and as the results listed in Table 7-5 demonstrate, the sample carrying probe does not introduce significant background spectral features. This is in marked contrast with the wet plasma in which solvent-induced species (i.e., the sample-carrier) dominate the background. In addition, the remarkably low intensities of the C, Mo, Ta and W when graphite-, Mo-, Ta- and W-based probes have been inserted into the plasma are worth pointing out.

It should be noted, however, that because the probes were 'burned' in the plasma for an extended period of time, for example, a high resolution scan from mass 1 to 210 took about 70 min to complete, the results presented here represent an ideal case of impurity-free probes. In a typical run, the probes are pre-burned several times prior to their use (as described in chapter 6) in order to drive-off impurities or eliminate memory effects.

Table 7-5. Probe-induced background species.

Mass	Graphite[a]	Mo Cup[b]	Ta Cup[c]	W wire-loop[d]	Interferes with (Abundance)
27		$^{27}\mathrm{Al}^+$	$^{27}\mathrm{Al}^+$		Al(100)
..					
90				$^{90}\mathrm{Zr}^+$	Zr(51.45)
91				$^{91}\mathrm{Zr}^+$	Zr(11.22)
92		$^{92}\mathrm{Mo}^+$		$^{92}\mathrm{Zr}^+$	Zr(17.15), Mo(14.83)
..					
94		$^{94}\mathrm{Mo}^+$		$^{94}\mathrm{Zr}^+$	Zr(17.38), Mo(9.25)
95		$^{95}\mathrm{Mo}^+$			Mo(15.92)
96		$^{96}\mathrm{Mo}^+$		$^{96}\mathrm{Zr}^+$	Mo(16.67), Zr(2.80)
97		$^{97}\mathrm{Mo}^+$			Mo(9.55)
98		$^{98}\mathrm{Mo}^+$			Mo(24.13)
..					
100		$^{100}\mathrm{Mo}^+$			Mo(9.63)
..					
112		$^{112}\mathrm{Sn}^+$			Sn(0.97)
..					
114		$^{114}\mathrm{Sn}^+$			Sn(0.65)
115		$^{115}\mathrm{Sn}^+$ (?)			Sn(0.36)

Table 7-5. Continued.

Mass	Graphite[a]	Mo Cup[b]	Ta Cup[c]	W wire-loop[d]	Interferes with (Abundance)
116		$^{116}Sn^+$			Sn(14.53)
117		$^{117}Sn^+$			Sn(7.67)
118		$^{118}Sn^+$			Sn(0.97)24.22
119		$^{119}Sn^+$			Sn(8.58)
120		$^{120}Sn^+$			Sn(32.59)
..					
122		$^{122}Sn^+$			Sn(4.63)
..					
124		$^{124}Sn^+$			Sn(5.79)
..					
126		?			Xe(0.09)
127		?			I(100)
128		?			Te(31.69), Xe(1.92)
129		?			Xe(26.44)
130		?			Te(33.8), Xe(4.08), Ba(0.1)
..					
133				$^{133}Cs^+$	Cs(100)

Table 7-5. Continued.

Mass	Graphite^a	Mo Cup^b	Ta Cup^c	W wire-loop^d	Interferes with (Abundance)
..					
180				$^{180}W^+$	Hf(35.1), W(0.12), Ta(0.012)
181		$^{181}Ta^+$	$^{181}Ta^+$		Ta(99.988)
182				$^{182}W^+$	W(26.31)
183				$^{183}W^+$	W(14.28)
184				$^{184}W^+$	W(30.64), Os(0.02)
..					
186				$^{186}W^+$	W(28.64)
..					
197			$^{181}Ta^{16}O^+$, $^{197}Au^+$(?)		Au(100)

a: High resolution scan, mass range 1 to 85 only

b: Low resolution scan, mass range 0 to 210

c: Low resolution scan, mass range 0 to 210

d: Low resolution scan, mass range 0 to 205

C.2 Oxides, Hydroxides and Doubly-charged Species

In addition to the background species discussed thus far, oxides (MO^+), hydroxides (MOH^+) and doubly charged (M^{2+}) species are also observed in ICP-MS. Their presence has been noted in several reports [3, 7, 10-14], comprehensive tables that list all possible isotopic combinations of MO^+, MOH^+ and M^{2+} species that might interfere with isotopes of elements has been presented by Vaughan and Horlick [14]. In addition to decreasing the population levels of singly charged analyte ions in the ICP, the presence of MO^+, MOH^+ and M^{2+} also gives rise to spectroscopic interference. Of the various types of spectroscopic interference effects listed in Table 7-1, MO^+, MOH^+ and M^{2+} species formation are considered to be the most difficult to correct [7].

Three performance rating ratios are typically used to describe the magnitude of the interference caused by these species. The ratio of M^{2+}/M^+, MO^+/M^+ and MOH^+/M^+ are used as a measure of the amount of interfering species formed (i.e., M^{2+}, MO^+ or MOH^+), a smaller ratio indicating reduced interference effects.

Oxide and hydroxide levels observed in ICP-MS when conventional pneumatic sample introduction systems are employed vary according to element, operating conditions and instrumentation used. In general, the MO^+/M^+ ratio ranges from 0.2% to 3%, the MOH^+/M^+ ratio is typically a few percent. Oxides and hydroxides can cause significant interference, especially if they arise from an element which is present at high concentration in a sample and if they overlap with a low concentration sought-for analyte. The significance of oxide interference is best demonstrated by considering that *"the application of ICP-MS to the determination of trace elements in Ni-base alloys was severely limited due to the formation of matrix metal oxide ions of the same nominal mass as the trace metal ions of interest"* [12].

Depending on the second ionization potential of the element under consideration, doubly charged species are also formed to a significant extent, M^{2+}/M^{+} ratios of a few percent are not unusual. To complicate things even further, because an M^{2+} ion occurs at half the mass-to-charge ratio of M^{+}, it typically falls in a mass region which is already crowded with background spectral features.

The strong dependence of MO^{+}, MOH^{+} and M^{2+} levels on instrumentation (substantially different levels are reported depending on instrumentation used) and on operating conditions should also be noted. Their dependence on power, nebulizer flow rate, sampling depth and ion-lens settings has been documented. For example, at 1.3 kW, $^{138}BaO^{+}/^{138}Ba^{+}$ and $^{138}Ba^{2+}/^{138}Ba^{+}$ values ranging from about 18% to a fraction of a percent, and $^{138}BaOH^{+}/^{138}Ba^{+}$ values ranging from a fraction of a percent to 25%, depending on nebulizer flow rate, have been reported for the ICP-MS system utilized in this work [14]. The data published by Vaughan and Horlick [14] will be used for comparison purposes, the MO^+/M^+ and M^{2+}/M^+ ratios determined at 1.3 kW, a 15 mm sampling depth, and a 1.2 l/min nebulizer flow rate will be utilized. These conditions were chosen because they yielded the highest count rate for $^{138}Ba^+$ (ICP-MS systems are typically optimized for the highest M^+ count rate).

As it has been amply demonstrated thus far, the use of a dry plasma results in reduced amounts of ArO^+ and of $ArOH^+$. It has also been speculated that a reduction of the hydrogen and the oxygen content of the plasma will produce a corresponding reduction in MO^+ and MOH^+. This is demonstrated in conjunction with the DSID in what follows. The instrumentation and operating conditions were the same as those previously described in chapter 6. The DSID torch (without the extension), a long undercut graphite electrode and a 10 mm sampling depth were used throughout.

Barium was chosen as the means to demonstrate oxide, hydroxide and doubly-charged species formation. It was chosen because: it has been extensively studied in ICP-MS; it readily forms oxides and hydroxides; and, due to its low second ionization potential, it is the best element with which to demonstrate M^{2+} formation. In addition, because Ba, its isotopes and isotopic combinations of its associated species, such as, Ba^{2+}, BaO^+ and $BaOH^+$, can potentially interfere with 29 isotopes [7].

The results for $^{138}Ba^+$, $^{138}Ba^{16}O^+$, $^{138}Ba^{16}OH^+$ and $^{138}Ba^{2+}$ obtained by running 1 μg of a dried solution residue of Ba are shown in Figure 7-28. From the results shown in Figures 7-28b and 7-28d it can be concluded that $^{138}Ba^{16}O^+$ and $^{138}Ba^{16}OH^+$ are not formed at this concentration level (thus allowing interference free determinations at masses 154 ($^{138}Ba^{16}O^+$) and 155 ($^{138}Ba^{16}OH^+$)). However, $^{138}Ba^{2+}$ (Figure 7-28c) is formed, as expected. The level of doubly charged species has improved over those reported for conventional wet plasma, the 0.9% ratio of $^{138}Ba^{2+}/^{138}Ba^+$ (calculated from peak heights) observed here is a considerable improvement over the 11.7% reported for a laboratory constructed ICP-MS system [14], but it is about equivalent to that reported for the ICP-MS system utilized in this work [14].

From the results presented above it can be concluded that interference free determinations of isotopes, for example, of ^{154}Sm (22.4%), ^{154}Gd (2.23%) and ^{155}Gd (15.1%) are possible, even in the presence of 1 μg Ba. There is a catch, however, as Ba is a carbide former, but, so are Sm and Gd. Chemical modification, as described in chapter 4, was used in order to release Ba from the cup. Following cup retraction, 10 μl of 0.25 M NaF solution were injected into the cup and the resultant solution was brought to dryness (by placing the electrode on an Aluminium hot plate)

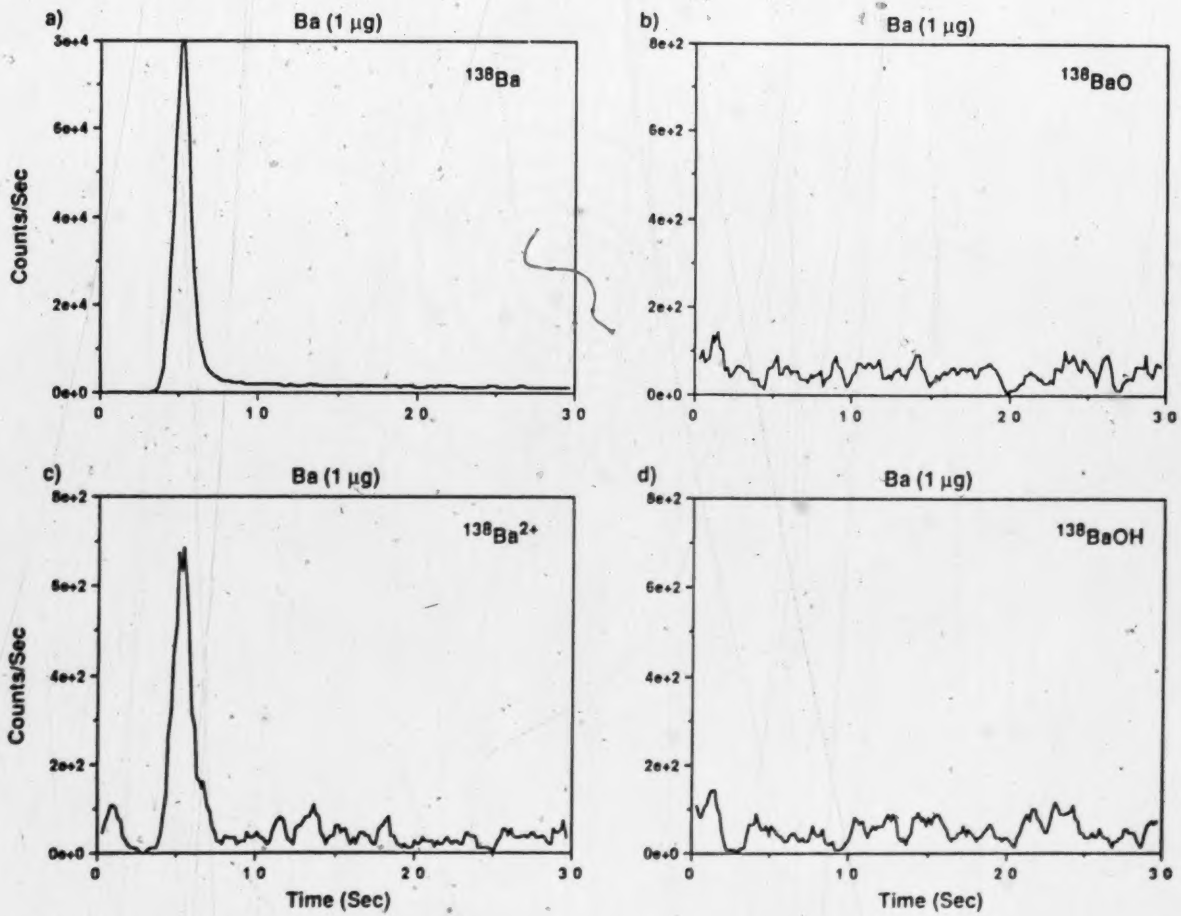

Figure 7-28. Temporal behavior arising from 1 µg Ba for: (a) $^{138}Ba^{+}$; (b) $^{138}Ba^{16}O^{+}$; (c) $^{138}Ba^{2+}$ and (d) $^{138}Ba^{16}OH^{+}$.

prior to re-insertion. Analyte temporal behavior observed upon re-insertion is shown in Figure 7-29. (By considering peak heights, an estimated <0.5% Ba was released when the cup was inserted the first time (Figure 7-28a). The estimate arises from the non-linear response observed when intensities of over 10^6 counts/s are measured with this system.) As Ba is released from the cup, in addition to $^{138}Ba^+$ (Figure 7-29a) and to $^{138}Ba^{2+}$ (Figure 7-29c), $^{138}Ba^{16}O^+$ (Figure 7-29b) and $^{138}Ba^{16}OH^+$ (Figure 7-29d) are also formed. The $^{138}Ba^{16}O^+/^{138}Ba^+$ ratio (peak height determination) is approximately 0.001 (or 0.1%), a considerable improvement over the ~3.8% previously reported for this system [14]. Insignificant amounts of impurities were detected in NaF by running a blank as shown in Figure 7-30. These have been included here as an indication of the background levels observed at these masses.

The results shown thus far indicate that oxide and hydroxide levels have been reduced by about an order of magnitude with respect to those reported for a wet plasma [14]. This correlates rather well with the reduction in ArO^+ resulting in from the use of a dry plasma. By further reducing the amount of Ba injected into the cup (thus also allowing quantitative determinations of Ba), for example, by using 100 ng as opposed to 1 µg, the intensities of the $^{138}Ba^{16}O^+$, $^{136}Ba^{2+}$ and $^{138}Ba^{16}OH^+$ peaks (Figures 7-29b, 7-29c and 7-29d) are expected to be indistinguishable from the

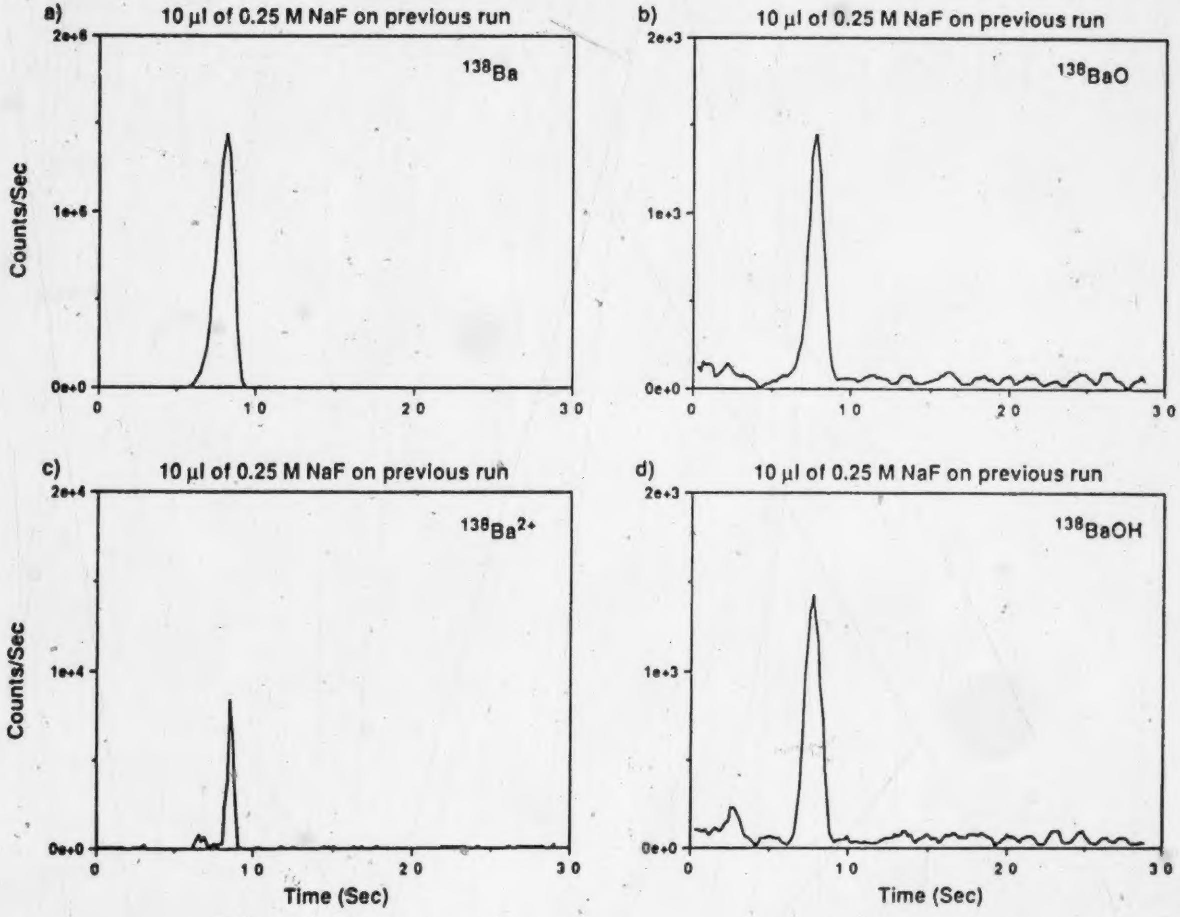

Figure 7-29. Temporal behavior after addition of 10 µl of 0.25 M of NaF on the dried solution residue of the previously run electrode (Fig. 2-28). (a) $^{138}Ba^+$; (b) $^{138}Ba^{16}O^+$; (c) $^{138}Ba^{2+}$ and (d) $^{138}Ba^{16}OH^+$.

background (Figures 7-30b, 7-30c and 7-30d), therefore allowing interference-free determinations at these masses even for carbide forming elements, such as Sm and Gd. Interference-free determinations are also expected when oxides and hydroxides of minor isotopes of Ba, for instance ^{136}Ba (7.81%) and ^{137}Ba (11.32%) interfering with major isotopes of ^{152}Sm (26.6%) and ^{153}Eu (52.2%) are considered. However, the aim here was to get an indication of the MO^+/M^+, MOH^+/M^+ and M^{2+}/M^+ ratios rather than to demonstrate the possibility of interference-free determinations.

The second example involves Ce, which was chosen because it easily forms M^{2+} species, it has been reported to be the 'best' oxide former in the ICP [10], and it represents rare earths, many of which form M^{2+} and MO^+ species. Temporal behavior derived from 1 μg of a dried solution of Ce is shown in Figure 7-31. Because Ce is also a strong carbide former, temporal behavior for $^{140}Ce^+$, $^{140}Ce^{16}O^+$ and $^{140}Ce^{2+}$ was not observed, as shown in Figures 7-31a, 7-31c and 7-31e. Therefore, interference-free determination of $^{70}Ge^+$ (20.7%), which is interfered with by $^{140}Ce^{2+}$ becomes possible. And although no signal was observed for $^{140}Ce^{16}O^+$ (mass 156), thus also permitting interference-free determinations of $^{156}Gd^+$ (20.6%), because Gd is a carbide forming element, it cannot be determined without chemical modification.

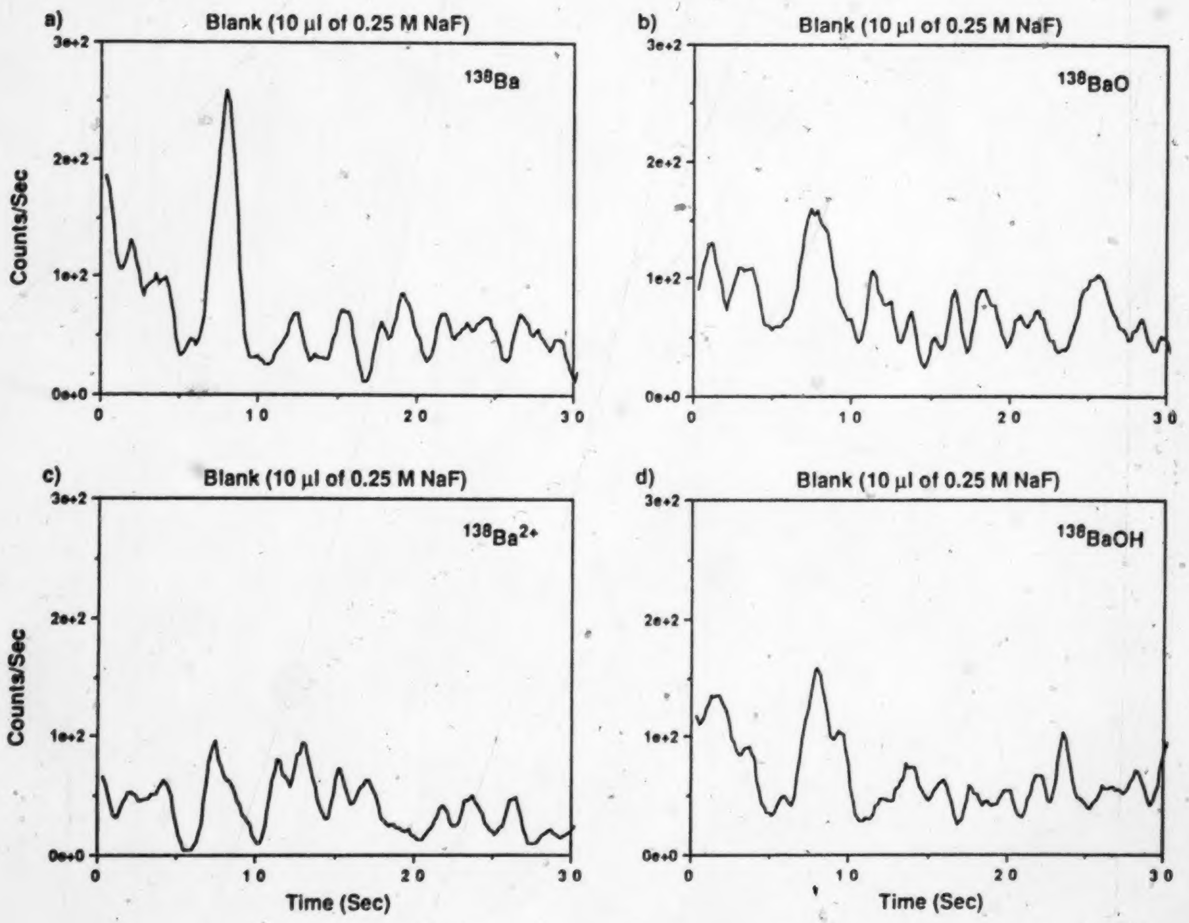

Figure 7-30. Temporal behavior arising from 10 µl of 0.25 M NaF for: (a) $^{138}Ba^+$; (b) $^{138}Ba^{16}O^+$; (c) $^{138}Ba^{2+}$ and (d) $^{138}Ba^{16}OH^+$.

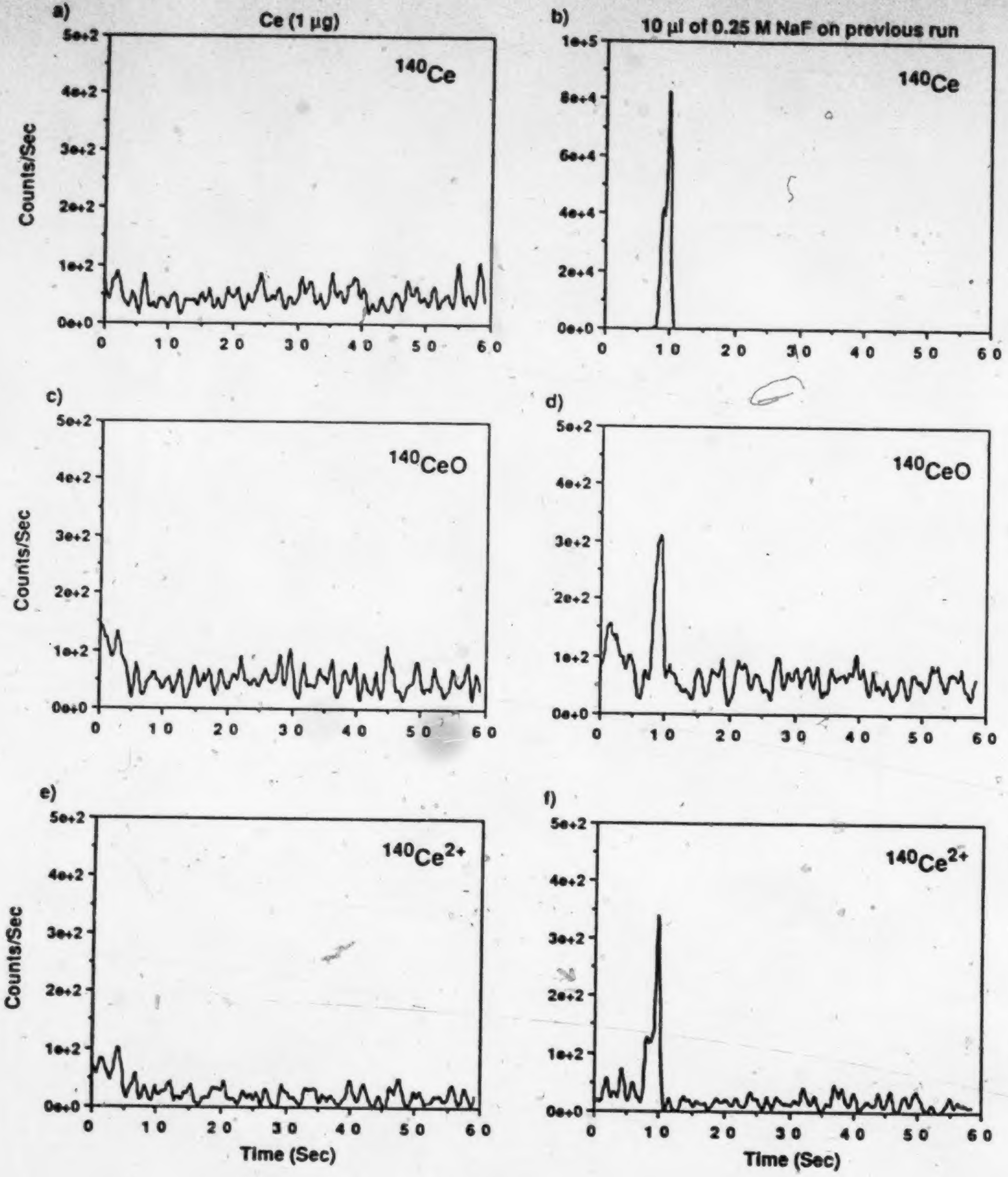

Figure 7-31. Temporal behavior arising from 1 µg of Ce for $^{140}Ce^{+}$ (a), $^{140}Ce^{16}O^{+}$ (c) and $^{140}Ce^{2+}$ (e); and after addition of 10 µl of 0.25 M NaF into a previously inserted electrode and upon re-insertion for $^{140}Ce^{+}$ (b), $^{140}Ce^{16}O^{+}$ (d) and $^{140}Ce^{2+}$ (f);

Cerium was released from the cup using NaF in a manner similar to that for Ba. The observed temporal behavior after the addition of NaF is shown in Figures 7-31b, 7-31d and 7-31f for $^{140}Ce^{+}$, $^{140}Ce^{16}O^{+}$ and $^{140}Ce^{2+}$. The $^{140}Ce^{16}O^{+}/^{140}Ce^{+}$ and $^{140}Ce^{2+}/^{140}Ce^{+}$ are both about 0.4%, which is a considerable achievement considering that the operating conditions were not adjusted so as to minimize the $^{140}Ce^{16}O^{+}/^{140}Ce^{+}$ and $^{140}Ce^{2+}/^{140}Ce^{+}$ ratios, as is typically done with an ICP-MS equipped with a conventional pneumatic nebulizer system.

C.3 Solvent-induced Background Species

As listed in Table 7-2, a major source of spectral interference arises from solvent-induced poly-atomic species. And although these can be easily corrected by blank subtraction, accurate control of the blank levels is not always possible. Admittedly, $^{35}Cl^{16}O^{+}$, which interferes with $^{51}V^{+}$, is the most serious interference arising from molecular species when a 5% HCl solution is aspirated into the plasma, thus making vanadium determinations by ICP-MS nearly impossible if the solution matrix contains chlorine or chlorine-containing compounds [7].

A determination of V from chlorine containing solutions then necessitates elimination of oxygen or chlorine. Because, in a dry plasma, oxygen is considerably reduced, a corresponding decrease in $^{35}Cl^{16}O^{+}$ is also expected. The possibility of determining V from a chlorine matrix with the DSID is demonstrated below.

Analyte temporal behavior for $^{51}V^+$ and $^{35}Cl^+$ derived from 10 μg of NaCl solution sample residue is shown in Figure 7-32b and 7-32d ($^{35}Cl^+$ saturates the detector, hence the nature of the signal shown in Figure 7-32b). From the results shown in Figure 7-32b it can be concluded that even at high salt concentrations (i.e., 0.1% NaCl solution, which is the upper limit for conventional pneumatic nebulizer systems), an insignificant amount $^{35}Cl^{16}O^+$ is formed. This, however, is inconsequential as V, being a carbide forming element, quantitatively remains in the cup whereas the matrix is released from the cup. Vanadium or chlorine impurities were not detected in a blank graphite electrode, as shown in Figures 7-32a and 7-32c. The drop in the signal level shown in Figure 7-32c is due to electrode insertion.

In order to further demonstrate the effect of $^{35}Cl^{16}O^+$ on V determinations, 100 ng of a dried solution residue of V was injected into a graphite cup, the observed temporal behavior of $^{51}V^+$ and $^{35}Cl^+$ is shown in Figures 7-33a and 7-33c. Because V is a carbide former, temporal behavior for $^{51}V^+$ was not observed, as shown in Figure 7-33a.

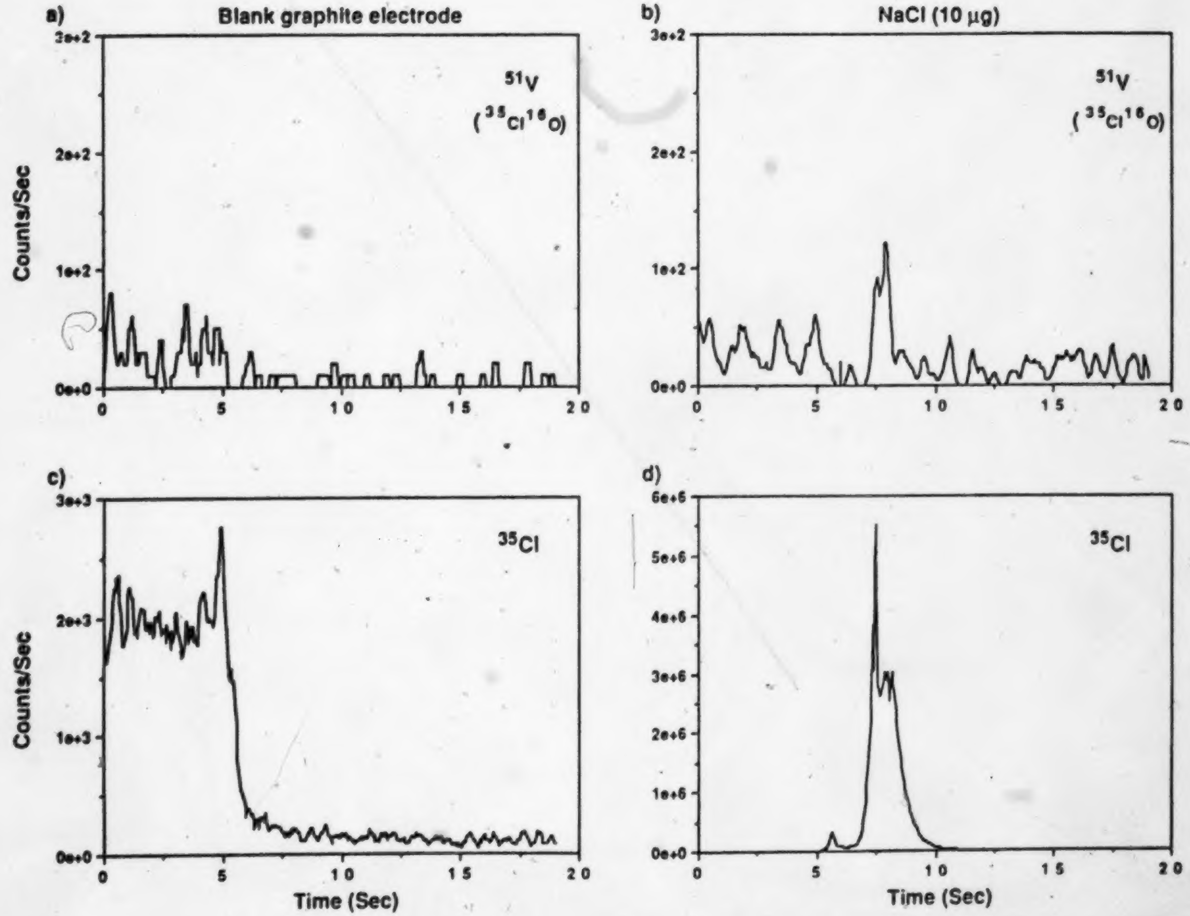

Figure 7-32. The effect of $^{35}Cl^{16}O^+$ on $^{51}V^+$ determinations. Blank long undercut graphite electrode, $^{51}V^+$ (a) and $^{35}Cl^+$ (c); 10 µg of NaCl, $^{51}V^+$ (b) and $^{35}Cl^+$ (d).

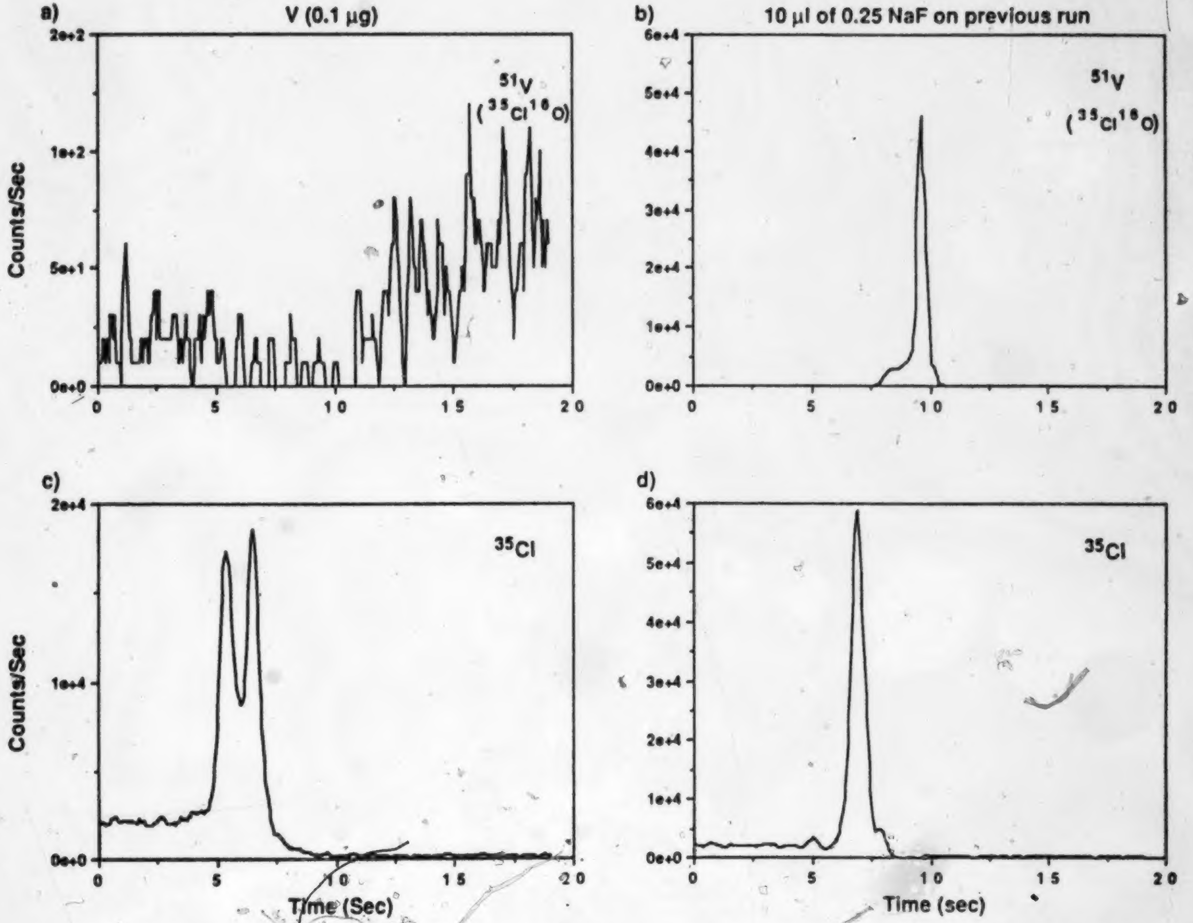

Figure 7-33. The effect of $^{35}Cl^{16}O^+$ on $^{51}v^+$ determinations. After injection of 0.1 µg of V, $^{51}v^+$ (a) and $^{35}Cl^+$ (c); after addition of 10 µl of 0.25 M NaF and electrode re-insertion, $^{51}v^+$ (b) and $^{35}Cl^+$ (d).

The temporal behavior observed for $^{35}Cl^+$ (Figure 7-33c) is partly attributed to residual chloride (the V sample was prepared from a 2% HCl stock solution) and partly to the conversion of vanadium chloride to the corresponding carbide.

Vanadium was released from the cup using NaF in a manner similar to that for Ba. The observed temporal behavior after the addition of NaF is shown in Figures 7-33b and 7-33d for $^{51}V^+$ and $^{35}Cl^+$. The $^{35}Cl^+$ observed (Figure 7-33d) is attributed to chloride impurities in NaF. In summary, determinations of V from chlorine-containing matrices become possible with an ICP-MS when a DSID is utilized.

D. Non-spectroscopic Interference Effects

It is generally agreed that an ICP-MS system is also susceptible to non-spectroscopic inter-element interference effects, often referred to as matrix effects. In these, a high concentration of a concomitant species induces changes in the signal intensity of an analyte [1]. And although mostly suppressions have been reported, signal enhancements have also been observed. Three recent reports [1-3] summarize these findings. Even though their cause has not been firmly established, they are currently under investigation in many laboratories around the world, their origin (or at least part of it) appears to be due to the mass spectrometer interface or the ion optics transfer system.

Whatever their cause, the DSID is not expected to be immune to their effects. However, looking at the symptoms, the most serious matrix effects occur when determinations of low concentrations of a light element are attempted in the presence of a high concentration of a heavy element, an often cited example is that of U on Zn, causing an over 80% suppression of the Zn signal [1].

An interesting scenario arises when studying the effect of U on Zn with the DSID. Consider the following 'thought experiment' involving the determination of low concentration Zn in the presence of a high concentration of U. Because U is a strong carbide former, it should quantitatively remain in the cup. On the other hand, because Zn is a high volatility element, it should quantitatively volatilize. Therefore, matrix effects could be separated in the time domain (much like spectral interferences were separated in the time domain, as described in chapter 2 for an ICP-AES-DSID). This has been verified experimentally and is documented below.

Temporal behavior was simultaneously observed for $^{64}Zn^+$ and $^{238}U^+$: for an electrode containing a dried solution residue of 50 ng Zn (Figures 7-34a and 7-34b for $^{64}Zn^+$ and $^{238}U^+$); for a second electrode containing a dried solution residue containing 50 ng Zn and 10 μg of U (Figures 7-34c and 7-34d for $^{64}Zn^+$ and $^{238}U^+$); and by re-inserting the

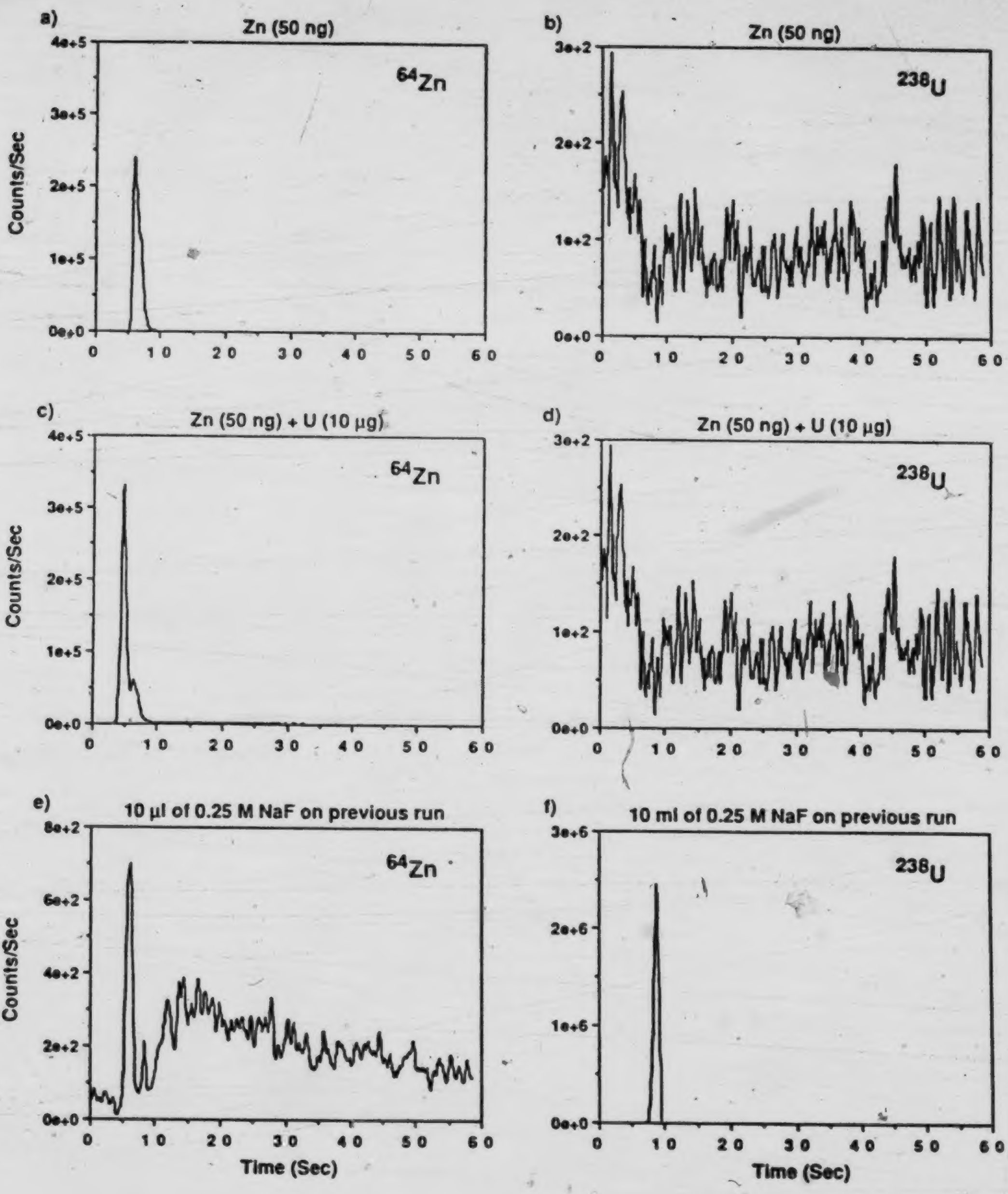

Figure 7-34. The effect of Zn on U. 50 ng Zn, $^{64}Zn^+$ (a) and $^{238}U^+$ (b); 50 ng Zn and 10 µg of U, $^{64}Zn^+$ (c) and $^{238}U^+$ (d); after addition of 10 µl of 0.25 M NaF and electrode re-insertion, $^{64}Zn^+$ (e) and $^{238}U^+$ (f).

second electrode (i.e., the one into which a 50 ng Zn was previously injected) in the plasma after the addition of 10 µl of 0.25 M NaF solution and drying (Figures 7-34e and 7-34f for $^{64}Zn^+$ and $^{238}U^+$). When only 50 ng of Zn is run (Figures 7-34a and 7-34b) temporal behavior for $^{238}U^+$ is not observed, as expected. The slight change in the observed $^{238}U^+$ signal (Figure 7-34b) is due to electrode insertion. When a residue containing 50 ng of Zn and 10 µg of U is run (Figures 7-34c and 7-34d), because U is a strong carbide former, temporal emission of $^{238}U^+$ is also not observed (Figure 7-34d), again, the drop in the signal observed is attributed to electrode insertion. When NaF is added, a weak $^{64}Zn^+$ signal (Figure 7-34e) and a very intense $^{238}U^+$ signal (Figure 7-34f) are observed. The low intensity $^{64}Zn^+$ signal shown in Figure 7-34e is most likely due to a memory effect. Although the peak heights of the $^{64}Zn^+$ signals are different (Figures 7-34a and 7-34c), the corresponding peak areas are within 5% of each other indicating lack of a matrix effect.

The lack of a matrix effect when a DSID is utilized is better demonstrated by re-plotting the data shown in Figure 7-34 without scale expansion. The scale in Figures 7-35a, 7-35c and 7-35e is set by the intensity of the $^{46}Zn^+$ peak (Figure 7-35a); the scale in Figures 7-35b, 7-35d and 7-35f is set by the intensity of the $^{238}U^+$ peak (Figure 7-35f).

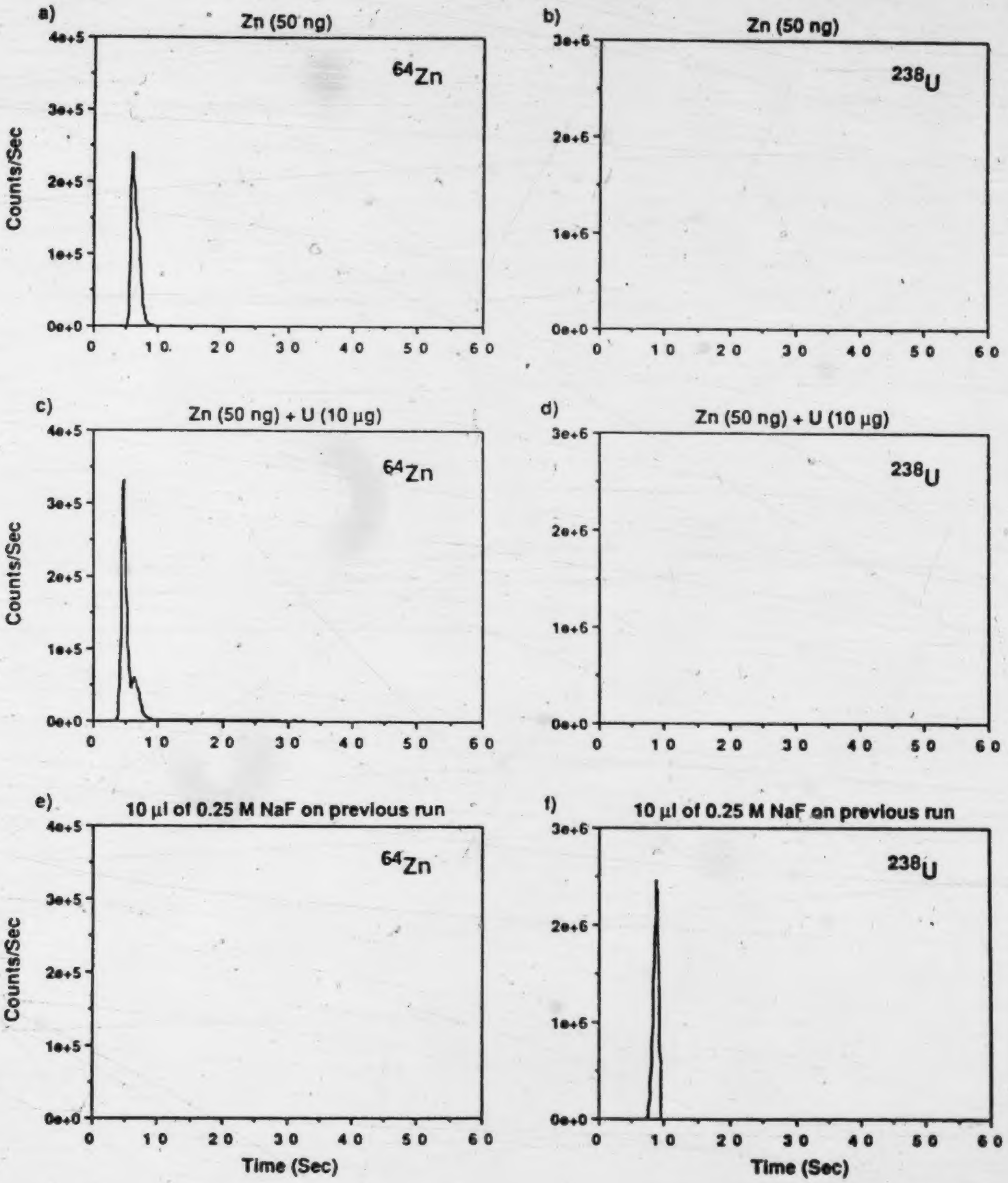

Figure 7-35. Same as Fig. 7-34 without scale expansion.

In conclusion, the separation of the ion signals of Zn and U in time has been successful in eliminating matrix effects. And because a large number of heavy elements (i.e., Lanthanides and Actinides) are strong carbide formers, the example used here is not an isolated one.

E. Conclusions

Lead by the success of the ICP as a source in atomic spectroscopy, a dramatic increase has been seen in the last few years in the use of ICPs as ion sources for mass spectrometry. However, the coupling of ICP to MS is not without its shortcomings. Predominant among these are those that arise from the ICP, such as, sample introduction and those that originate from its coupling to MS, for instance, interference effects. Consequently, it comes as no surprise that a great deal of emphasis is being placed in documenting and understanding these effects and at improving sample introduction into the plasma.

A DSID coupled to an ICP-MS system was perceived as being capable of simultaneously lessening the effects of both of these shortcomings, its development was justified based on this premise. The potential of the DSID to extend the capability and analytical utility of the ICP has been documented in chapters 2, 3 and 4 for ICP-AES and briefly demonstrated in chapter 6 for ICP-MS. From the results presented in this chapter, it can be concluded that the

DSID is also capable of reducing or eliminating some of the interference effects encountered in ICP-MS when utilizing conventional sample introduction systems and wet plasmas.

Due to the use of a dry plasma with an ICP-MS-DSID, spectral simplicity is realized, as it has been demonstrated in this chapter. Therefore, spectral interferences due to background and solvent-induced spectral features are reduced, the potential for the analysis of elements/isotopes previously thought impossible by ICP-MS is realized and the original claims of the spectral simplicity are partly justified. The simple idea that a reduction in the water content of the plasma would also reduce ArO^+, $ArOH^+$, MO^+ and MOH^+ has been verified. However, further studies are needed in order to unequivocally prove interference-free determinations in the presence of oxide forming elements. In addition, it has also been demonstrated that by relying on differential thermal volatilization, non-spectroscopic interference and interference from solvent-induced poly-atomic species have also been reduced or eliminated. The catch, of course, lies in the fact that chemical modification must be utilized. In general, DSIDs and chemical modification appear to be tightly bound, the ideas of automated dispensing of chemical modifiers and of the sample carrying cup as a crucible in which *in situ* sample processing takes place have been discussed in several occasions throughout this thesis.

In the case of an ICP-MS-DSID, however, chemical modification does not only solve DSID-related problems, such as carbide formation, but it also effectively resolves some inherent ICP-MS shortcomings. Therefore, it provides an 'ideal' vehicle for the implementation of an intelligent sample processor for the ICP.

REFERENCES

1. S.H. Tan and G. Horlick, J. Anal. Atom. Spectrom., **2**, 745 (1987)

2. D. Beauchemin, J.W. McLaren and S.S. Berman, Spectrochim. Acta, **42B**, 467 (1987)

3. D.A. Wilson, G.H. Vickers and G.M. Hieftje, Spectrochim. Acta, **42B**, 29 (1987)

4. D.A. Wilson, G.H. Vickers and G.M. Hieftje, J. Anal. Atom. Spectrom., **2**, 365 (1987)

5. S.H. Tan and G.Horlick, Appl. Spectrosc., **40**, 445 (1986)

6. S.H. Tan, Ph.D. Thesis, Univ. of Alberta, 1987

7. G. Horlick, S.H. Tan, M.A. Vaughan and Y. Shao, *"Inductively coupled plasma-mass spectrometry"* in *'Inductively coupled plasmas in analytical atomic spectromety'*, A. Montaser and D.W. Golightly, VCH publishers, 1987, pp. 361-398

8. A.L. Gray, Spectrochim. Acta, **41B**, 151 (1986)

9. J. Davies and C.M. Du, J. Anal. Atom. Spectrom., **3**, 433 (1988)

10. D.J. Douglas and R.S. Houk, Prog. Analyt. Atom. Spectrosc., **8**, 1 (1985)

11. R.S. Houk, Anal. Chem., **58**, 97A (1986)

12. C.W. McLeod, A.R. Date and Y.Y. Cheung, Spectrochim. Acta, **41B**, 169 (1986)

13. A.R. Date, Y.Y. Cheung and M.E. Stuart, Spectrochim. Acta, **42B**, 3 (1987)

14. M.A. Vaughan and G. Horlick, Appl. Spectrosc., **40**, 434 (1986)

CHAPTER 8

CONCLUDING REMARKS

A. Summary

From the results and the arguments presented, it can be concluded that the basic goal of extending the analytical capability and utility of the ICP by developing means of overcoming its key practical limitation with respect to sample introduction has been met by developing DSIDs for the ICP.

The transient nature of the signals generated by the DSID necessitated the development of new hardware and software, as described in chapter 2 for ICP-AES and in chapter 6 for ICP-MS. (Due to their sheer volume, program listings have not been included for brevity's sake.) The systems described in these chapters were subsequently used to characterize the DSID. For example, a number of design attributes, such as insertion speed, position and sequence, were found to exert a considerable influence on background and analyte emission temporal behavior. The results reported in chapter 3 also show that improved analytical performance can be attained by using special electrode geometries. This is not a surprising conclusion, as Boumans in his Ph.D. thesis had suggested similar electrode designs for the dc arc [1].

DSID optimization was only briefly addressed in this work in chapters 3 and 6. It was concluded that optimization should be performed on a next generation DSID proposed in chapter 3. As revealed in chapter 1 (Table 1-4), univariate search methods were mostly used as the means to establish the best set of operating conditions. However, because this optimization method is tedious, time-consuming and labor-intensive, new approaches that lend themselves to automation could be utilized. For example, it can generally be said that, although in most experimental situations there is an imperfect knowledge of the various parameters affecting the performance characteristics, an experienced operator is able to establish an optimum set of operating conditions typically faster than an inexperienced one. In this case, 'tuning' procedures depend on user-developed heuristics (i.e., rules of thumb, inexact knowledge and guessing strategies) that drastically limit the search space for an optimum solution, which is causally referred to as the 'magic touch'. Can the semantics of this magic touch be put under stored program control?

Although rule-based heuristic methods do not always guarantee a solution, let alone an optimum one, the payoffs of computer-controlled heuristic optimization based on AI (artificial intelligence) and expert systems is two-fold. First, the time to search for a solution is reduced, thus providing the capability to optimize the DSID on a batch (i.e., sample type) basis and in an automated fashion. Second, the knowledge, experience and expertise required to optimize an ICP-DSID can be electronically disseminated to a wider group of users. And even though this may appear to be an attempt to 'automate automation', applications of this type are just around the corner. Due to the number of variables that need to be optimized with an ICP-MS-DSID, this system is expected to be an 'ideal' vehicle for the application of rule-based optimization. Furthermore, it is also expected to help establish the merits of such an approach.

With a graphite cup-based DSID poor results are obtained for carbide forming elements. Several chemical modification reagents were tested in order to improve the vaporization characteristics of such analytes and to solve the problem of carbide formation, as detailed in chapter 4. This, however, necessitates a 'zero based design' of sample preparation. In the case of an ICP-MS-DSID, chemical modification does not only solve DSID-related problems but it also effectively resolves some inherent ICP-MS shortcomings, as detailed in chapter 7.

In general, DSIDs and chemical modification appear to be tightly bound. The idea of automated dispensing of chemical modifiers and the concept of a sample carrying cup as a crucible in which *in situ* sample processing takes place have been discussed in several occasions throughout this thesis.

Undoubtedly, the automated DSIDs described in this work can offer high sample throughput, which however, cannot be sustained unless sample and standards preparation is also automated. The proposed solution involves the use of programmable automation in the form of robots, as described in chapter 3 for a DSID for ICP-AES and in chapters 6 and 7 for a DSID for ICP-MS. However, the current generation of robots is deaf, dumb and blind. By exploiting recent advances in sensor technology, robots can acquire powerful sensory inputs. An implementation of the proposed next generation DSID (as illustrated in Figure 3-21 for an ICP-AES-DSID and in Figure 8-1 for a DSID for ICP-MS) would undoubtedly require a synergy between intelligent controllers (for DSID control), sensors, actuators and programmable automation in association with AI tools, concepts and expert systems for intelligent dispensing of chemical modifiers. Therefore, the overall goal of developing an intelligent sample processor for the ICP can be realized, with the ICP-MS-DSID providing an ideal vehicle for such an implementation.

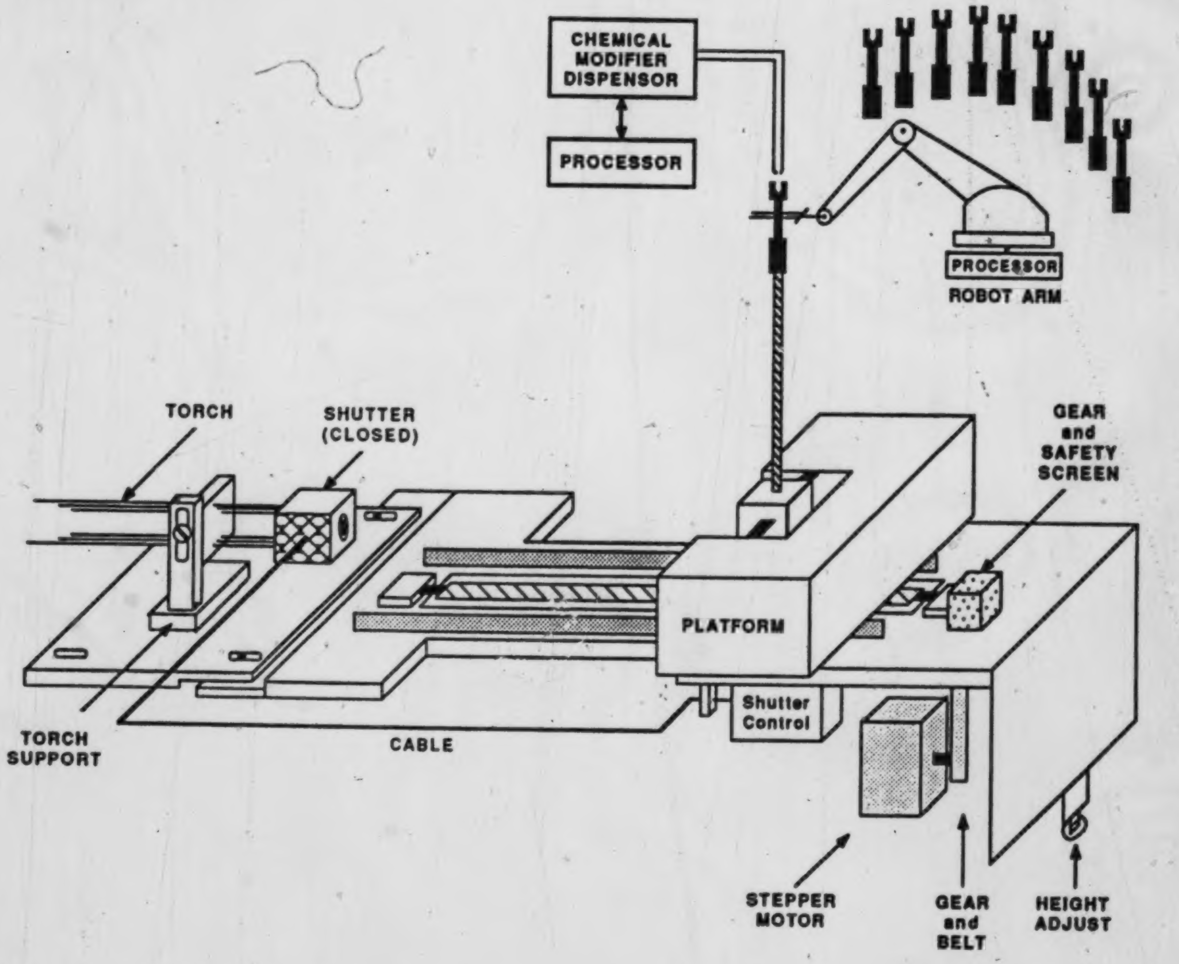
CHEMICAL
MODIFIER
DISPENSOR
PROCESSOR
PROCESSOR
ROBOT ARM
TORCH
SHUTTER
(CLOSED)
GEAR
and
SAFETY
SCREEN
PLATFORM
Shutter
Control
TORCH
SUPPORT
CABLE
STEPPER
MOTOR
GEAR
and
BELT
HEIGHT
ADJUST

Figure 8-1. Illustration of a proposed 'next generation' DSID for ICP-MS.

B. The Concept of Processors in Spectrochemical Instrumentation

In broad sense, a measurement system for analytical atomic spectroscopy consists of four main sub-systems; a sample processor, a signal generator, a signal processor and an information processor, as illustrated in Figure 8-2.

The sample processor involves sampling, sample preparation and sample introduction. Lead by DSIDs, which are assisted by robotic sample and standards preparation and are supported by automated addition of chemical modifiers, the development of a sample processor for the ICP is well underway. The processed sample is subsequently presented to the signal generator where information about the sample is encoded, for instance, in the form of electromagnetic radiation or gas phase atoms and ions. The ICP is expected to be the signal generator of choice for some time to come.

The way analytical information is encoded dictates the nature of the signal processor, for example, a dispersive spectrometer for atomic emission or a mass spectrometer. Undoubtedly, mass spectrometry will have a major influence on the nature of the signal processor. In terms of optical emission spectroscopy, improvements in spectrometer design originating from optical sensors, such as Photodiode Arrays (PDAs) are likely to change the design philosophy behind multielement AES.

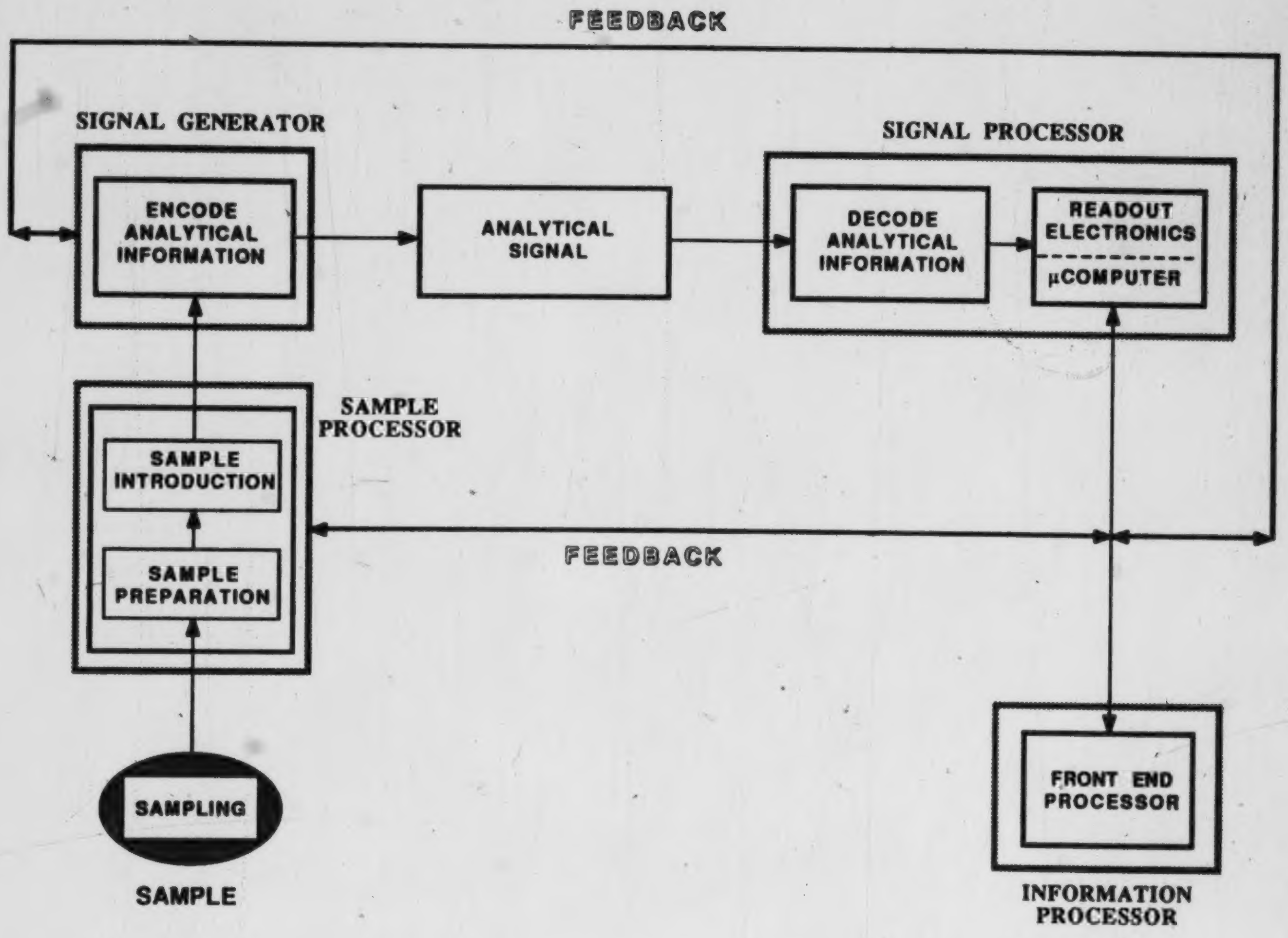
FEEDBACK
SIGNAL GENERATOR
ENCODE ANALYTICAL INFORMATION
ANALYTICAL SIGNAL
SIGNAL PROCESSOR
DECODE ANALYTICAL INFORMATION
READOUT ELECTRONICS
µCOMPUTER
SAMPLE PROCESSOR
SAMPLE INTRODUCTION
SAMPLE PREPARATION
FEEDBACK
SAMPLING
SAMPLE
FRONT END PROCESSOR
INFORMATION PROCESSOR

Figure 8-2. Block diagram of an atomic spectrochemical measurement system.

Because PDAs allow one to take an 'electronic' snapshot of the spectrum, they can be thought of as miniature electronic photographic plates. Carrying this analogy a bit further, a PDA-based spectrometer, such as the field programmable direct reading spectrometer described in Appendix D, front-ended with an ICP which is equipped with a DSID, can be thought of as the present day equivalent of the dc arc. Such an implementation is expected to bring Boumans's analogy of the ICP as a dc arc in a new jacket [2] closer to reality.

Ideally, the signal processor should be capable of automatically acquiring all spectral information about a sample. Because the key goal is not just the automation of the acquisition of spectrochemical data but the acquisition of spectrochemical information, the development of the information processor and of the feedback loops shown in Figure 8-2 becomes of paramount importance. A small step toward this direction has already been taken in chapter 5. In addition to implementing the *instrument metaphor* concept, the HPI developed can be thought of as a graphics-based natural language interface for data base query. (Again, due to its volume, the 57,000-line program and resource listings have not been included here for brevity's sake.)

This concept can be further expanded and a graphics oriented programming language can be developed around it. By displaying virtual robots, beakers and flasks on the computer's screen, complete automation of samples and standards preparation becomes possible. Thus, the robot arm-DSID combination can become an easily accessible front-end processor peripheral device capable of performing complex tasks in the laboratory.

Other considerations also arise. For example, automated spectrochemical systems can generate vast amounts of data in a very short period of time, a fully automated DSID is a case in point. However, as Hirschfeld has indicated *"...the I/O bandwidth of the human observer is being rapidly exceeded"* [3]. This ultimate limit can only be overcome by utilizing multiple processor systems. The question of multiprocessor configurations and of microcomputer systems suitable for the analytical laboratory has been addressed by the author in a series of extensive review articles [4, 5, 6], this work has not been included in this thesis.

However, because the ultimate goal is automation of chemical decisions, the development of the information processor and of the feedback loops shown in Figure 8-2 is of utmost importance. The decisions could take many forms, for example, feedback to dispense NaF or to decrease forward power in order to increase the separation of emission signals in order to resolve spectral interference in the time domain, or to simply monitor a different isotope in order to avoid isobaric overlaps. Higher-level decisions or some form of results interpretation or even answers to an analytical problem could be envisioned. For example, a large number of analyses in the metals industry are performed on problem statements like *"is this alloy within specifications?"* An answer to this question can be displayed on the screen as opposed to elemental composition or to detailed intensity data. An interactive environment which allows the computer to be interrogated by the operator would then provide access to any desired level of information or to the raw data.

Undoubtedly, the next generation of intelligent spectrochemical instrumentation lies in the integration of all steps required for the acquisition of spectrochemical information.

C. Integration: Imagineering the Next Generation Analytical Instrumentation

When the steps involved in the acquisition of spectrochemical information are integrated, the 'next generation analytical instrumentation' becomes possible. This generation is anticipated to be marked by innovation with future instruments becoming information driven. In the meantime, the design philosophy behind traditional measurement systems is changing and the concept of an isolated stand-alone instrument is being gradually replaced by an analytical work station with capabilities never before thought possible. And although it is not yet possible to blueprint this analytical work station, an attempt to describe it is shown in Figure 8-3. Within the context of Figure 8-3 the label 'sensor' is taken beyond its traditional meaning to include an analytical technique which provides complementary information about the sample. This multifunction instrument can be thought of as a network of instrumentation modules with the task of sample and standards preparation assigned to an intelligent sample processor. Within the context of spectrochemical instrumentation, the integrated analytical work station just described can decide, based on results obtained at the early stages of an analytical run, on the best set of operating conditions, chose spectral lines, perform the analysis and comment on the results. It may also provide an answer to a particular spectrochemical problem, which easily leads to the concept of a *spectrochemical answer machine*, as pictorially depicted in Figure 8-4.

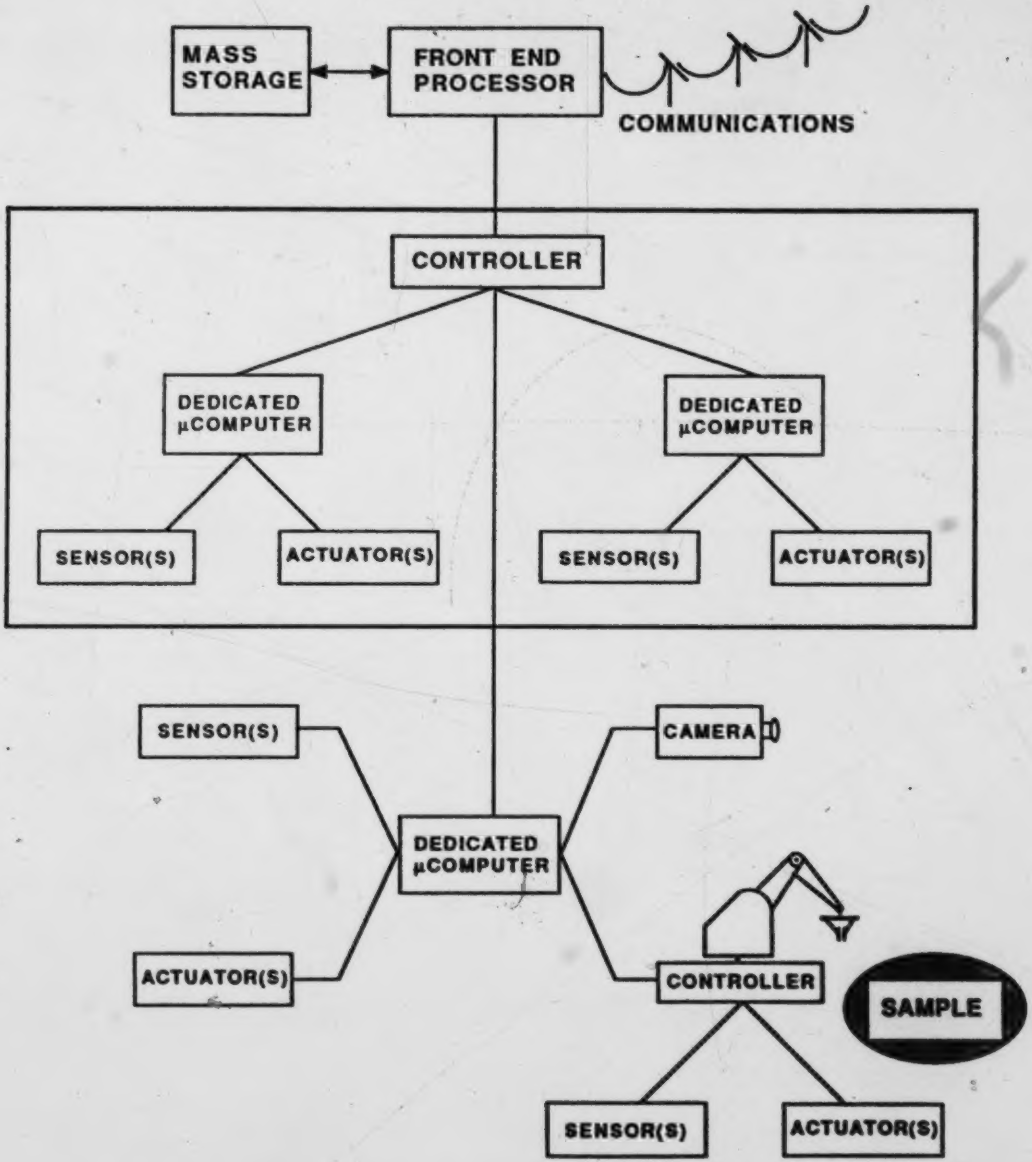
MASS STORAGE
FRONT END PROCESSOR
COMMUNICATIONS
CONTROLLER
DEDICATED µCOMPUTER
SENSOR(S)
ACTUATOR(S)
DEDICATED µCOMPUTER
SENSOR(S)
ACTUATOR(S)
SENSOR(S)
CAMERA
DEDICATED µCOMPUTER
ACTUATOR(S)
CONTROLLER
SAMPLE
SENSOR(S)
ACTUATOR(S)

Figure 8-3. Concept diagram illustrating a 'next generation' analytical instrumentation.

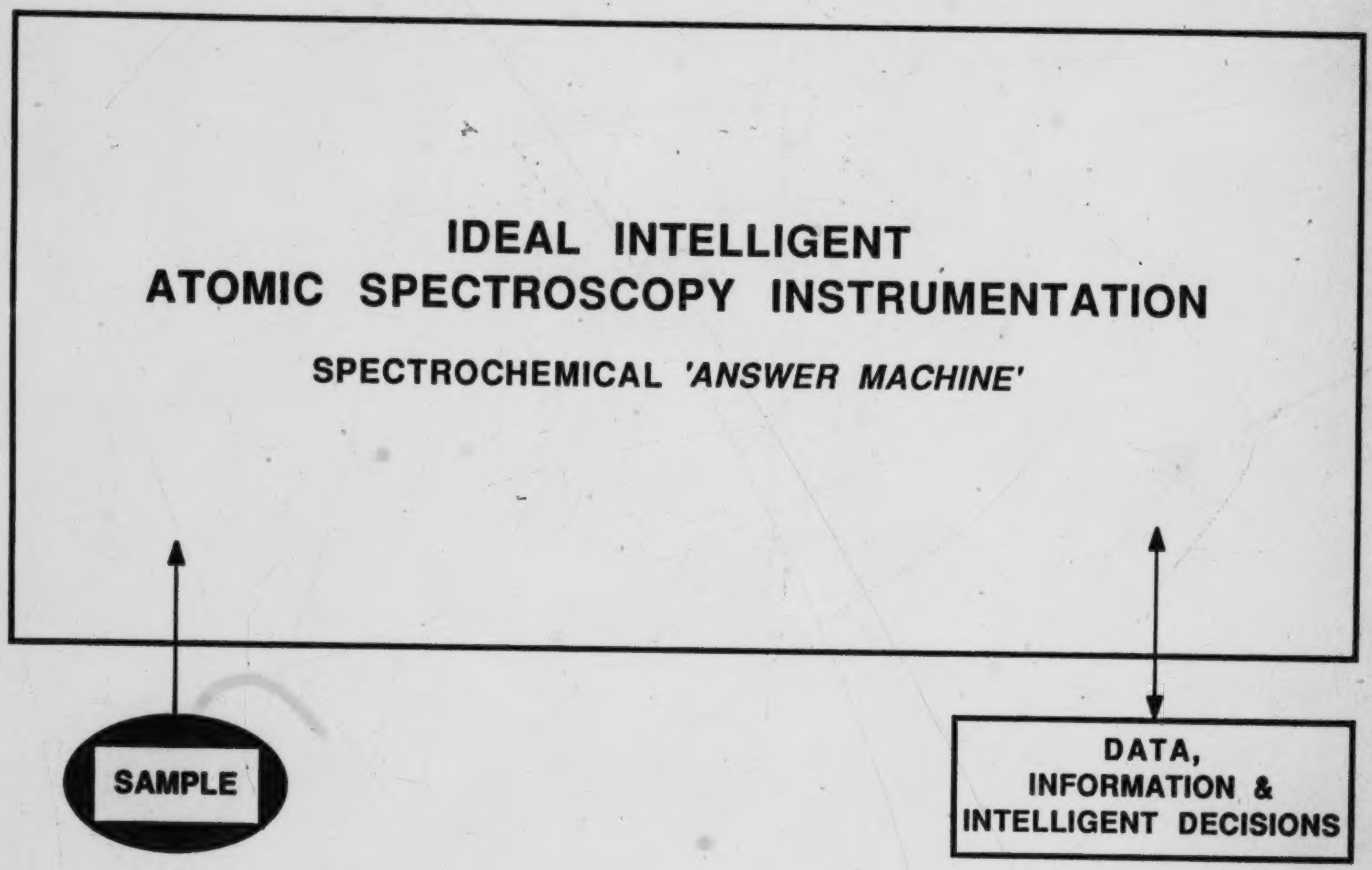
IDEAL INTELLIGENT
ATOMIC SPECTROSCOPY INSTRUMENTATION
SPECTROCHEMICAL *'ANSWER MACHINE'*
SAMPLE
DATA,
INFORMATION &
INTELLIGENT DECISIONS

Fig. 8-4. Illustration of a spectrochemical answer machine.

There is little doubt that modern instrumentation can offer unique solutions to analytical problems of considerable complexity with the ultimate goal and a thrilling challenge of performing reliable qualitative and quantitative ultra-trace chemical analysis of totally unknown samples in real-time. And even though it is inherently dangerous to predict the future in any scientific field, it is tempting to speculate about the nature of the next generation analytical instrumentation. The long-term consequences of the developments mentioned above lead to some interesting thoughts about the very nature of 21^{st} century analytical instrumentation. They can be thought of as 'systems' delivering a great deal of the total physicochemical information content of a sample in real-time and are capable of making decisions based on their findings.

REFERENCES

1. P.W.J.M. Boumans, Personal communication, June 1987
2. P.W.J.M. Boumans, Spectrochim. Acta, **35B**, 57 (1980)
3. T. Hirschfeld, Science, **230**, 286 (1985)
4. V. Karanassios and G. Horlick, Talanta, **35**, 583 (1985)
5. V. Karanassios and G. Horlick, Talanta, **35**, 601 (1985)
6. V. Karanassios and G. Horlick, Talanta, **35**, 615 (1985)

APPENDIX A

NEW DESIGN CONCEPTS FOR DIRECT READER MEASUREMENT ELECTRONICS

A version of this chapter has been published.
V. Karanassios and G. Horlick, Appl. Spectrosc., **42**, 961-972 (1988)

A. Introduction

The direct reading spectrometer (polychromator) is widely used in emission spectrochemical analysis in conjunction with spark sources or inductively coupled plasmas. A simplified optical diagram for a direct reading spectrometer is shown in Figure A-1 and a block diagram of a typical approach for the measurement electronics is shown in Figure A-2. In this measurement system current signals from the photomultiplier tubes are simultaneously integrated with analog integrators, the integrated signals are sequentially multiplexed to an ADC, and the converted values are then read by a computer. Although active integrators are illustrated in Figure A-2, the use of simple, capacitor-based passive integrators is not unusual. Because of the dynamic range limitations of analog integration, and in order to accommodate wide dynamic range signals the integrated values may be read more than once during a typical analytical run, shorting the capacitor each time. A subsequent summation of the converted values then provides the final result. The later approach can place considerable software overhead on the controlling processor. Finally, with most measurement systems, all channels have the same integration time.

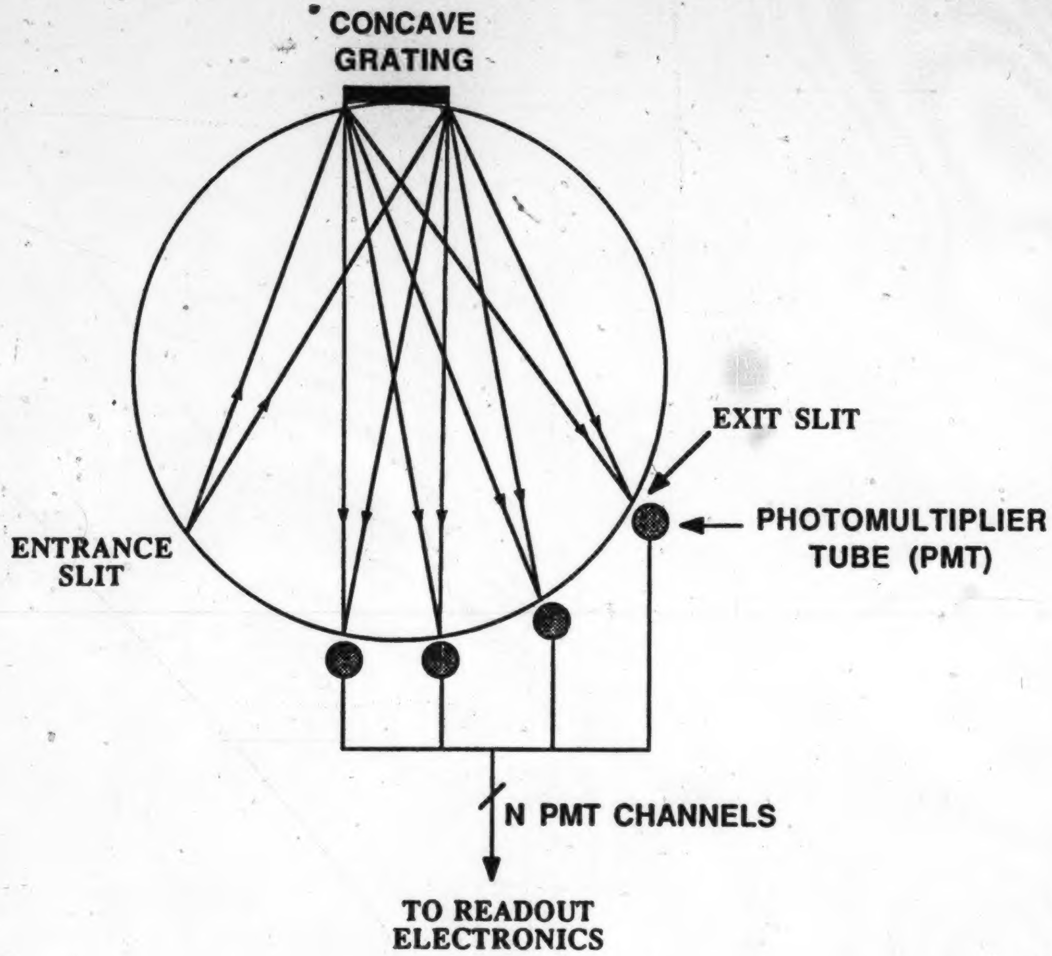
CONCAVE GRATING
EXIT SLIT
PHOTOMULTIPLIER TUBE (PMT)
ENTRANCE SLIT
N PMT CHANNELS
TO READOUT ELECTRONICS

Figure A-1. Optical configuration of a typical Paschen-Runge mount direct reading spectrometer.

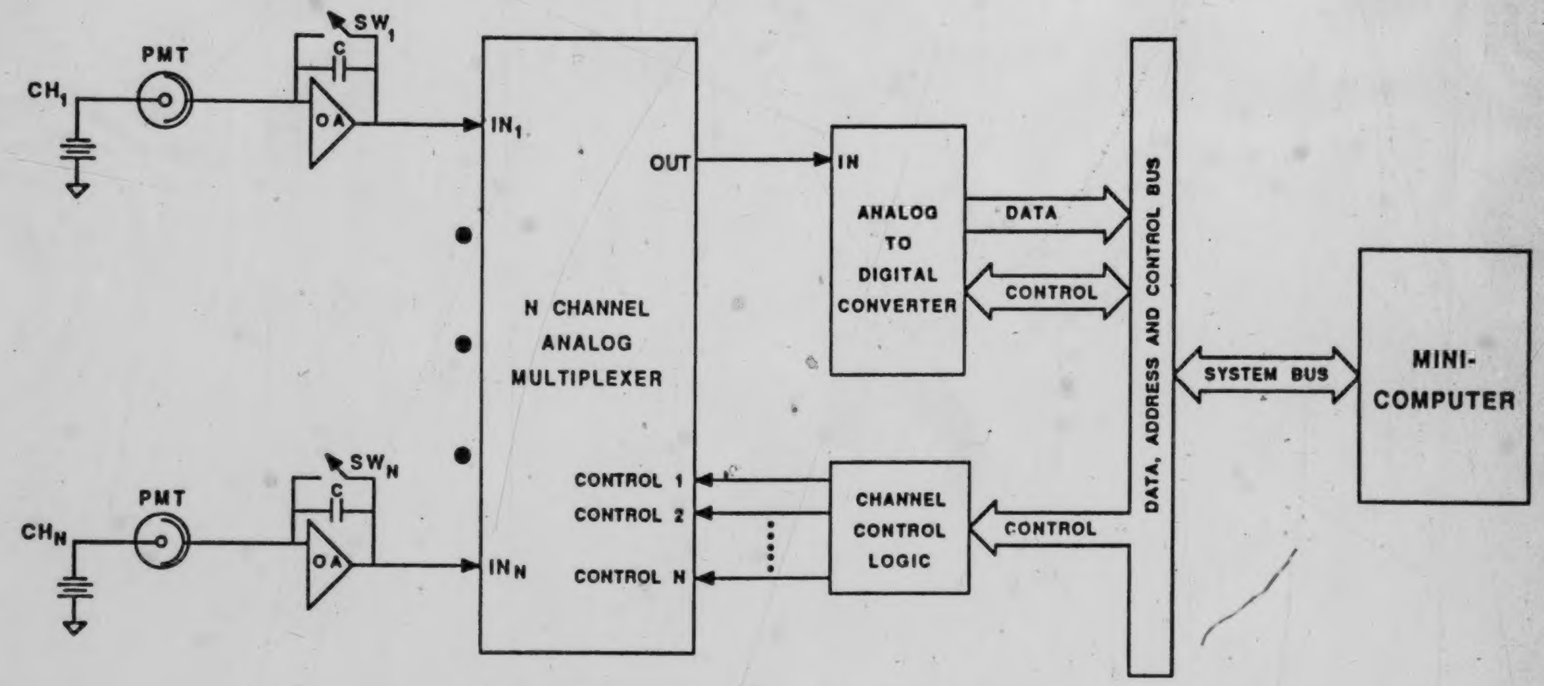
CH$_1$
PMT
SW$_1$
C
OA
IN$_1$
CH$_N$
PMT
SW$_N$
C
OA
IN$_N$
N CHANNEL ANALOG MULTIPLEXER
OUT
CONTROL 1
CONTROL 2
CONTROL N
IN
ANALOG TO DIGITAL CONVERTER
DATA
CONTROL
CHANNEL CONTROL LOGIC
CONTROL
DATA, ADDRESS AND CONTROL BUS
SYSTEM BUS
MINI-COMPUTER

Figure A-2. Block diagram of a typical readout system for a conventional direct reading spectrometer.

Interestingly, outside of the addition of an analog-to-digital converter (ADC) and a computer, the basic design philosophy for the measurement electronics has remained relatively unchanged since the 1940's. In fact, in the last 15 years the computer has gone from a PDP-8 to a PDP-11, to an APPLE II+ to an IBM PC/XT/AT with only minor changes in the rest of the system.

An alternative approach for a direct reader measurement system is shown in Figure A-3 [1]. This approach is based on a more complete utilization of a microprocessor bus architecture throughout the measurement system, programmable support chips, inexpensive data domain conversion ICs (Integrated Circuits), inexpensive microcomputers, and distributed processing. In this system the current signal from the PMT is converted to a frequency using a current-to-frequency (i/f) converter and then digitally integrated using a software programmable counter. Each channel has its own software programmable integration timer. This subsystem provides wide dynamic range digital integration with full independent control of the integration time at each channel of the direct reader. These sub-systems are controlled using a small single board computer dedicated to data acquisition and instrument control. Once programmed, each counter/timer unit requires no processor attention during integration, which minimizes software requirements and hence processor overhead.

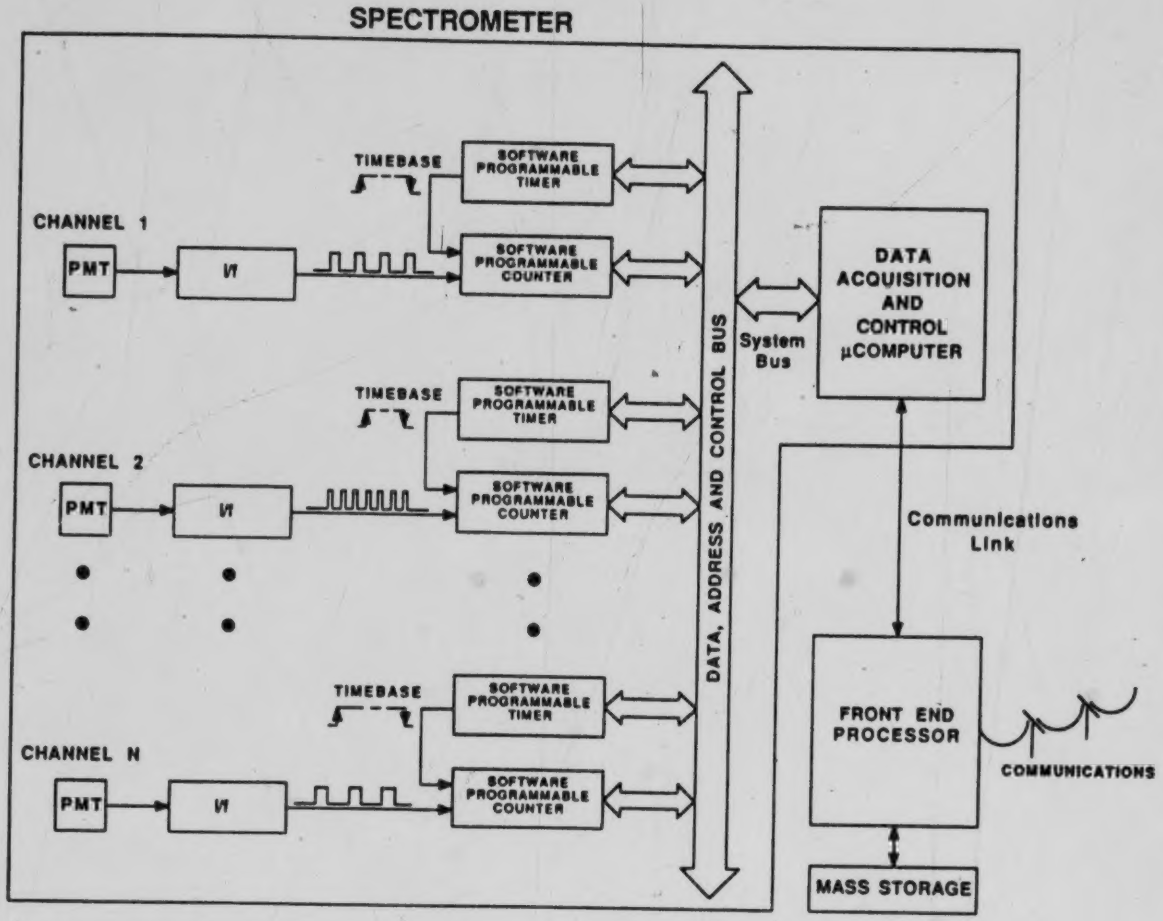
SPECTROMETER
CHANNEL 1
PMT
i/f
TIMEBASE
SOFTWARE PROGRAMMABLE TIMER
SOFTWARE PROGRAMMABLE COUNTER
CHANNEL 2
PMT
i/f
TIMEBASE
SOFTWARE PROGRAMMABLE TIMER
SOFTWARE PROGRAMMABLE COUNTER
CHANNEL N
PMT
i/f
TIMEBASE
SOFTWARE PROGRAMMABLE TIMER
SOFTWARE PROGRAMMABLE COUNTER
DATA, ADDRESS AND CONTROL BUS
System Bus
DATA ACQUISITION AND CONTROL μCOMPUTER
Communications Link
FRONT END PROCESSOR
COMMUNICATIONS
MASS STORAGE

Figure A-3. Block diagram of a multichannel measurement system for a direct reading spectrometer based on i/f converters and a series of single channel frequency meters.

A fully relocatable addressing scheme has been implemented for each counter/timer channel, which provides the overall system with great flexibility with respect to expandability and ease of reconfiguration. This is a key advantage for bus-based addressible channels.

The front end processor is the computer used for data processing, display, management, and communication. The requirements for this processor have been discussed in detail by Karanassios and Horlick [2] and will not be discussed in this presentation. It should be noted, however, that distributing the above tasks and those of data acquisition and control between two computers guards against instrument obsolescence. An instrument can be perceived to be obsolete if it does not have the latest data processing/display/management and/or communication hardware and software but, in fact, may still have a very effective spectrochemical data acquisition unit. Most of the new computer capability comes from the rapid developments occurring in computers that would be used as a front end processor and, with the design shown in Figure A-3, the front end processor can be easily replaced without having to go through a major readout and control electronics redesign. A computer change in the traditional system (Figure A-2) often required major interface electronics redesign and, as such, slowed innovation and utilization of the most recent computing capability.

B. Measurement Channel

A block diagram of a single measurement channel along with its associated control logic is shown in Figure A-4. The current signal from the PMT is converted to a voltage using an operational amplifier (Analog Devices AD545). A 10 MΩ feedback resistor was used in parallel with a 1000 pf capacitor. The output voltage was 1 V for a 10^{-7} amp input current. The voltage was then converted to a frequency with a voltage-to-frequency (v/f) converter. Two types of converters were used for the various PMT channels. One was a low cost v/f (Analog Devices AD537) with a 1 - 10^5 Hz dynamic range and the second was a high precision converter with a 6 order of magnitude (1- 10^6 Hz) dynamic range (Analog Devices AD460). The software programmable timer and counter were based on Intel's 8253 programmable interval timers and digital I/O was provided by MOS Technology 6522 Versatile Interface Adapter (VIA). The overall design of the counter/timer system was based on that described by Blades and Horlick [3] and is shown in Figure A-5. Changes made to this former design include the use of a 6522 rather than an 8255 (Intel programmable peripheral interface) to provide digital I/O and changes in the bus structure because a different single board computer (AIM 65) is used in this application.

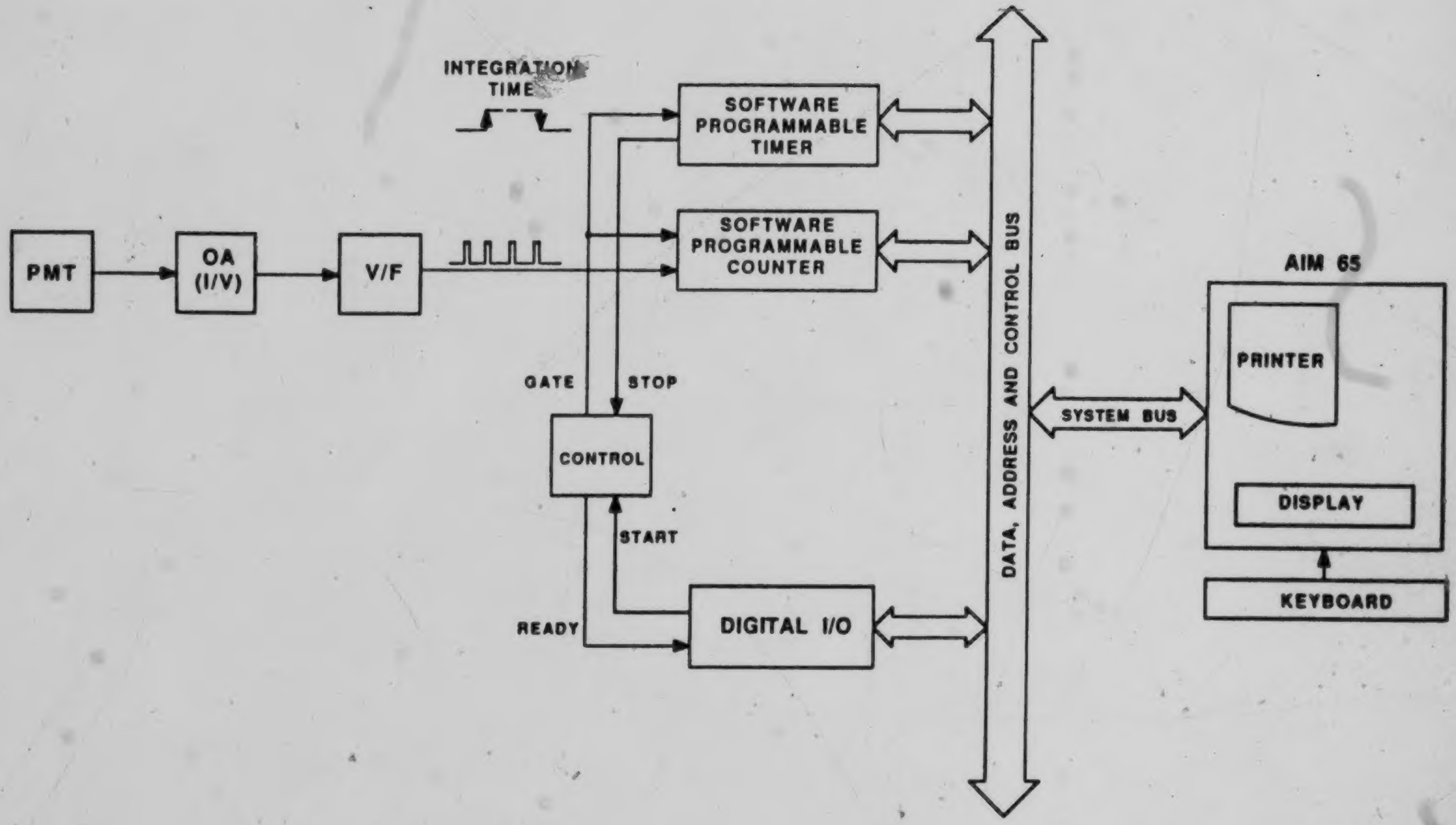
PMT
OA (I/V)
V/F
INTEGRATION TIME
SOFTWARE PROGRAMMABLE TIMER
SOFTWARE PROGRAMMABLE COUNTER
GATE
STOP
CONTROL
START
READY
DIGITAL I/O
DATA, ADDRESS AND CONTROL BUS
SYSTEM BUS
AIM 65
PRINTER
DISPLAY
KEYBOARD

Figure A-4. Block diagram of single channel measurement system.

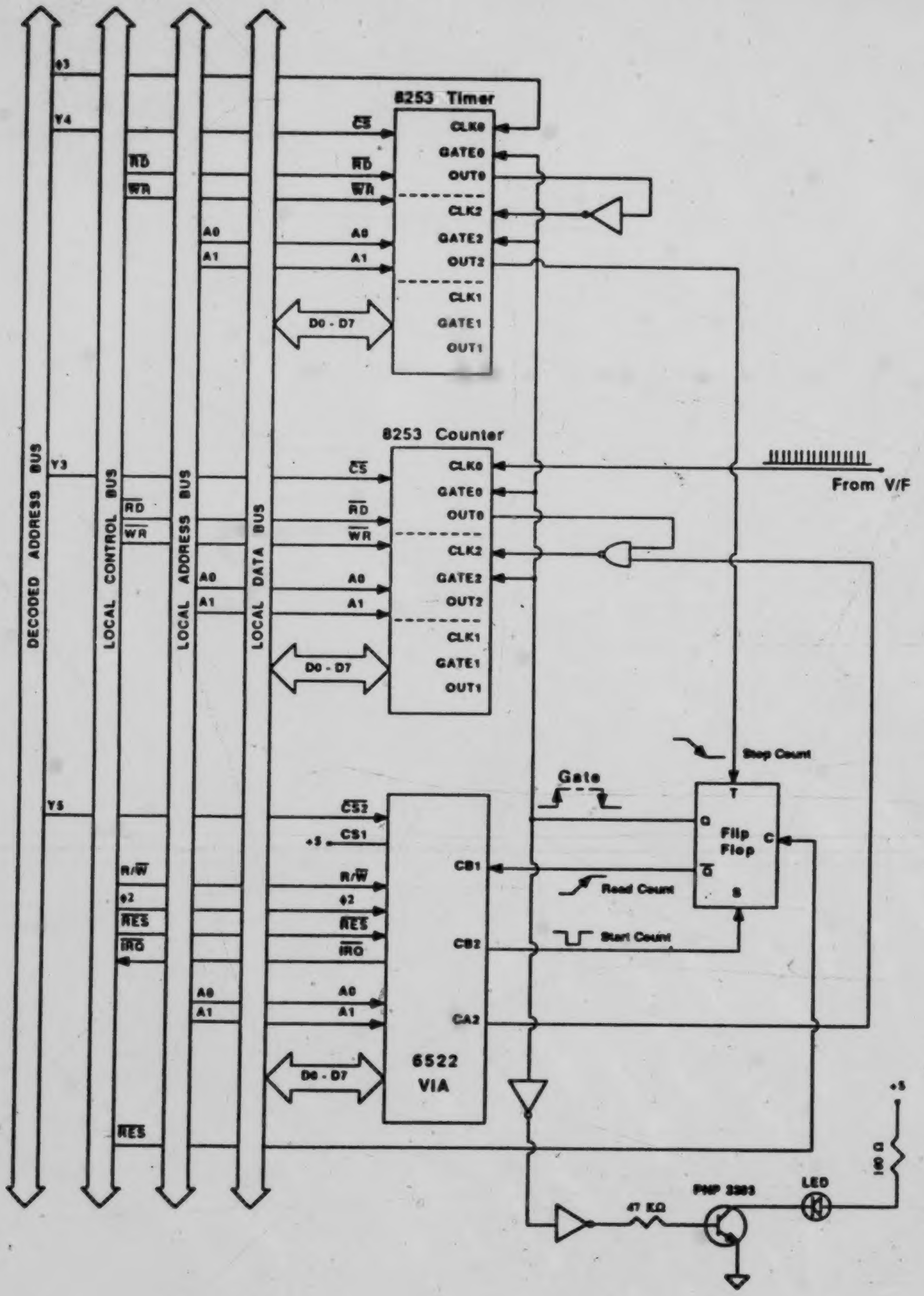
DECODED ADDRESS BUS
LOCAL CONTROL BUS
LOCAL ADDRESS BUS
LOCAL DATA BUS
ϕ3
Y4
RD
WR
A0
A1
8253 Timer
CS
RD
WR
A0
A1
CLK0
GATE0
OUT0
CLK2
GATE2
OUT2
CLK1
GATE1
OUT1
D0 - D7
8253 Counter
Y3
RD
WR
A0
A1
CS
RD
WR
A0
A1
CLK0
GATE0
OUT0
CLK2
GATE2
OUT2
CLK1
GATE1
OUT1
D0 - D7
From V/F
Stop Count
Gate
T
Q
Flip Flop
C
Q̄
S
Read Count
Start Count
Y5
CS2
+5
CS1
R/W
ϕ2
RES
IRQ
A0
A1
R/W
ϕ2
RES
IRQ
A0
A1
CB1
CB2
CA2
6522 VIA
D0 - D7
RES
+5
100 Ω
LED
PNP 3303
47 KΩ

Figure A-5. Circuit diagram for a single measurement channel.

As mentioned above, two 8253 counter/timers and a 6522 digital I/O form the basis of the software programmable counter as shown in Figure A-5. An Intel 8253 is a programmable interval timer [4] consisting of three software programmable 16-bit down counters, a tri-state, bi-directional, 8-bit data bus buffer; read/write logic that determines device operation; a control word register whose contents define the operating mode of each counter; and it operates from a single +5 V power supply. Each counter is individually software programmable in any of six different modes, it sustains a bandwidth from dc to 2 MHz, and can count in either binary or BCD (Binary Coded Decimal).

Two-thirds (i.e. two cascaded 16-bit counters) of one 8253 serve as the integration timer and two-thirds of another 8253 function as the counter. The 1 MHz (0.9997 MHz) crystal controlled clock ($\phi 3$ shown in Figure A-5) is connected to the clock (CLK0) of the integration timer. This counter, operating in mode 2, functions as a software programmable divide by N counter. When loaded with hex 270D (9997 in decimal), it provides an output signal whose frequency is 100 Hz, in other words, it offers a 10 ms timebase. This signal is then routed to the second counter of the same 8253, which also operates in mode 2, where it is counted. The output of this second counter controls the integration time. For example, when this counter is loaded with 100 decimal (hex 64) then 100, 10 ms intervals are counted. When the final count has been reached, its output (OUT2) undergoes a high to low transition signaling the end of a 1 s period. Therefore, by loading the appropriate number in this counter, control of the integration time is provided. The 8253 counters are 16-bits wide, thus a maximum of 65636, 10 ms intervals can be counted, providing a maximum integration time of 655.36 s (or approximately 10 min).

The second 8253 chip shown in Figure A-5 is used as the counter (signal integrator). Because the 8253s counters are 16-bits wide and in order to provide adequate bit resolution, two counters are cascaded to form a 32-bit wide counter using the second 8253. This is required for the measurement of wide dynamic range signals. As they are down counters, they are both loaded with 65535 in decimal (FFFF in hex). In this case, both counters operate in mode 2.

On power on, the reset line undergoes a high to low transition, resetting the computer, the counter, the timer, the 6522 and the flip-flop. Subsequently, both timer and counter are appropriately configured (i.e. mode and pre-set values) as described above. Counting begins by sending a start pulse to the flip-flop, this sets the flip-flop, Q goes high (Q="1") and opens the gates. As the first pulse sent to the 8253 is required to set the counters, a pulse generated by the CA2 line of the 6522 is routed, through a

NAND gate, to CLK2 of the 8253 counter. This pulse is not required for the integration timer as, in mode 2, the output will go low after N-1 pulses have been counted. For the 8253 counter, however, as the full count will not be realized, this first pulse is required. Upon completion of the integration time interval, OUT2 of the integration timer undergoes a high to low transition. This toggles the flip-flop: Q goes low (Q="0"), thus closing the gates, and Q undergoes a low-to-high transition. This rising edge is monitored by the microprocessor and, when it occurs, it indicates the end of the measurement. The Q output of the flip-flop is also connected, through a series of gates and a PNP 3393 transistor, to an LED (Light Emitting Diode) in order to provide a form of visual feedback to the operator.

C. Computer, Buses and Addressing

Although there is quite a variety of microcomputers currently available [5-7], the Rockwell AIM 65 [8] was chosen for this implementation. The features of this single board micro computer have been summarized by Horlick [1]. Cost and microcomputer availability at the time the project was initiated aside, the main reasons for the selection of this microcomputer were the availability of a backplane bus (the Microflex 65 bus), an AIM 65- and Microflex 65 bus-compatible single board microcomputer, and an adequate selection of interface boards and development tools with which to work with. A multichannel system can then be built around the AIM 65/card cage combination, with the AIM 65 serving as the development system. At the end of the development cycle, the AIM 65 can be replaced with a single board microcomputer, placed inside the card cage along with the rest of the readout electronics and be mounted inside the polychromator's enclosure serving as the data acquisition and control computer, as depicted in Figure A-3.

Important aspects of our overall system are the bus structure and address decoding. The Microflex 65 bus is shown in Figure A-6. The address, data and control buses have been buffered, thus generating three additional buses that are local to the counter/timer system (see Figure A-5). Two 74LS240 octal buffers/line drivers are used to buffer the address bus and define the Local Address Bus (LAB) and a 74LS640 octal bus transceiver is used to buffer the data bus and define the Local Data Bus (LDB). Directionality of the data transfers is determined by inverting the buffered $R/\overline{W}$ line ($BR/\overline{W}$) provided by the Microflex 65 bus whereas the 74LS640 is enabled by a signal, labeled A in Figure A-6, generated from address decoders discussed later.

The AIM 65 is a 6502 CPU based computer. Because there is a mix of 6502 family support chips (6522) and 808X family support chips (8253) it is necessary to create a

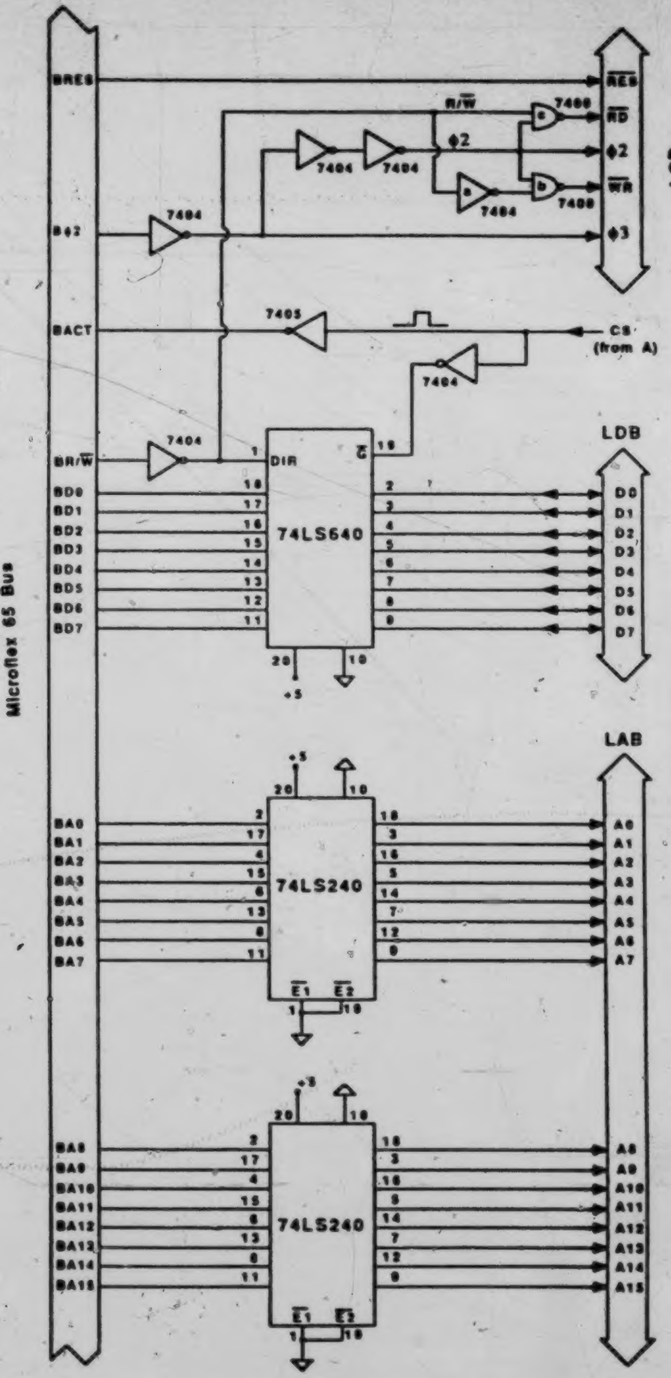
Microflex 65 Bus
BRES
$\overline{RES}$
R/$\overline{W}$
7400
$\overline{RD}$
φ2
$\overline{WR}$
LCB
Bφ2
7404
φ3
BACT
7405
CS
(from A)
BR/$\overline{W}$
DIR
$\overline{G}$
74LS640
LDB
BD0
BD1
BD2
BD3
BD4
BD5
BD6
BD7
D0
D1
D2
D3
D4
D5
D6
D7
+5
LAB
74LS240
BA0
BA1
BA2
BA3
BA4
BA5
BA6
BA7
A0
A1
A2
A3
A4
A5
A6
A7
$\overline{E1}$
$\overline{E2}$
74LS240
BA8
BA9
BA10
BA11
BA12
BA13
BA14
BA15
A8
A9
A10
A11
A12
A13
A14
A15

Figure A-6. Simplified circuit diagram for the Microflex 65 bus to single channel interface logic. LDB is the Local Data Bus, LAD is the Local Address Bus and LCB is the Local Control Bus, see text for discussion.

control bus with "read" and "write" signals that are appropriate to both families. This is the function of gates a, b and c shown in Figure A-6. The $R/\overline{W}$ (6502 family) is inverted (through gate a) and gated (through gate b) with the $\phi 2$ microprocessor clock to produce a $\overline{WR}$ (808X family) signal of about 500 ns in duration. Similarly, a 500 ns $\overline{RD}$ (808X family) signal is generated by gating the $R/\overline{W}$ with the $\phi 2$ microprocessor clock through gate c. These signals are part of a tertiary bus dubbed the Local Control Bus (LCB). The LCB does not include all signals supported by the Microflex 65 bus, whereas it supports some new ones, such as $\overline{RD}$ and $\overline{WR}$.

One of the overall goals for the complete direct reader measurement electronics is to have each channel's electronics as independently addressible components. That is, each channel of the direct reader should be an addressible peripheral device. To provide the most flexibility for system expansion, adaptability and modification; relocatable addressing has been utilized. Each single channel counter/timer unit can be, via switch settings, located at essentially any area of memory.

Partial address decoding is used in this application and is shown in block diagram form in Figure A-7. In this case a series of contiguous memory locations (128 bytes) are assigned to a peripheral device. Although most peripheral devices require fewer memory locations (i.e., four by

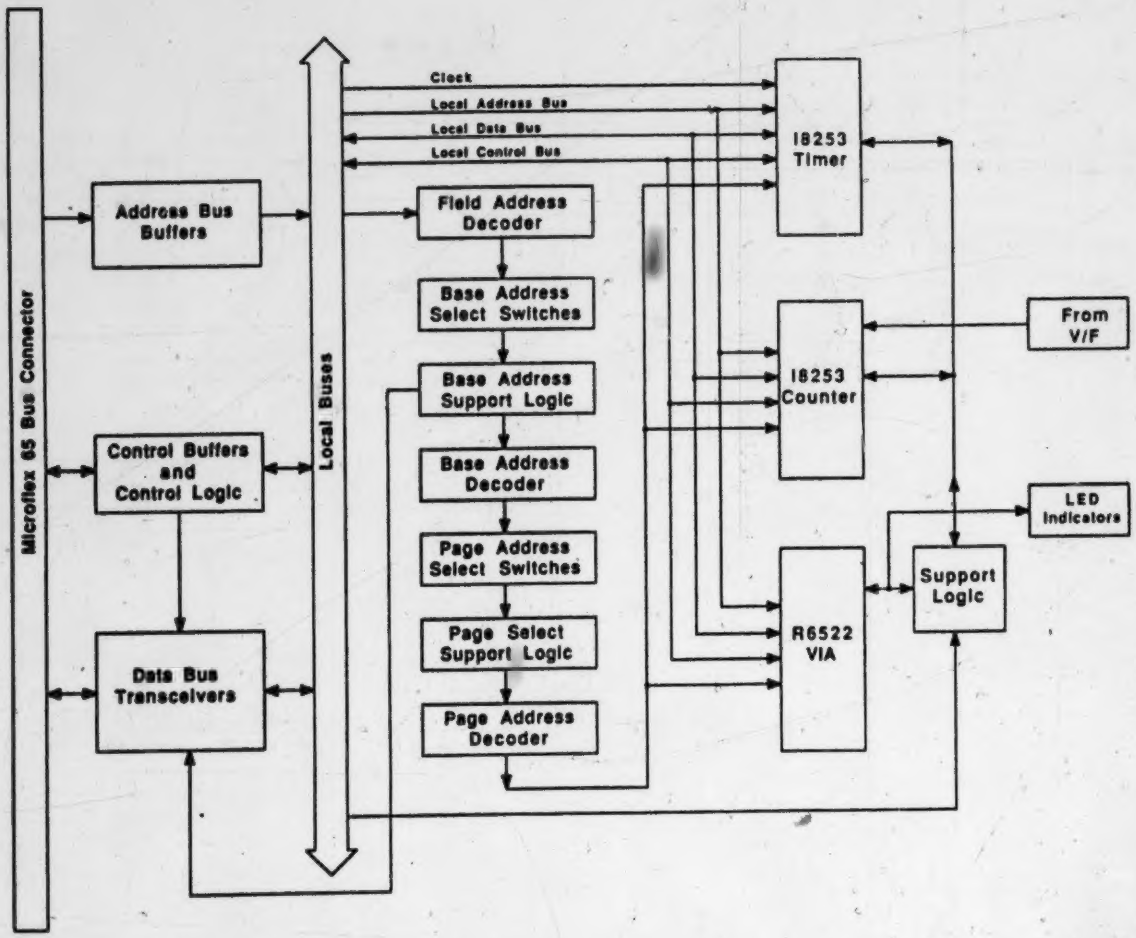
Microflex 65 Bus Connector
Address Bus Buffers
Control Buffers and Control Logic
Data Bus Transceivers
Local Buses
Clock
Local Address Bus
Local Data Bus
Local Control Bus
Field Address Decoder
Base Address Select Switches
Base Address Support Logic
Base Address Decoder
Page Address Select Switches
Page Select Support Logic
Page Address Decoder
I8253 Timer
I8253 Counter
R6522 VIA
From V/F
LED Indicators
Support Logic

Figure A-7. Functional block diagram of the single channel system with the relocatable partial address decoding scheme.

an 8253 and sixteen by a 6522) and therefore memory locations are wasted, it appears to be a good compromise as full address decoding becomes intractably complex. The Field Address Decoder shown in Figure A-8 decodes the entire 64 Kbyte address field into 4 Kbyte blocks. The user, using the switches located on switch bank S1 can then select the base address of any desired 4 Kbyte block. The output signal ($\overline{EN1}$) generated from the support logic of the Field Address Decoder enables another decoder, the Base Address Decoder whose function is to decode the previously selected 4 Kbyte block into four, 1 Kbyte pages. The user, again using switches, this time located on switch bank S2, can select the desired 1 Kbyte page within the selected 4 Kbyte block. The output signals generated from this decoder, $\overline{EN2}$ and $\overline{EN1}$, are used to further enable the Page Decoder which decodes the selected 1 Kbyte page into eight, 128 byte segments. The output of this decoder provides the appropriate chip select signals for the peripheral devices. In this way, an 8253 occupies 128 bytes, although only 4 bytes are required by it.

The actual implementation is shown in Figure A-9. A 74154 4-line-to-16-line decoder/demultiplexer serves as the Field Address Decoder. The user, utilizing switches S1-1 to S1-16 can select the desired base address of any 4 Kbyte block within the 64 Kbyte address field. The truth table for the 74154 is given in Table A-1. The output signal of

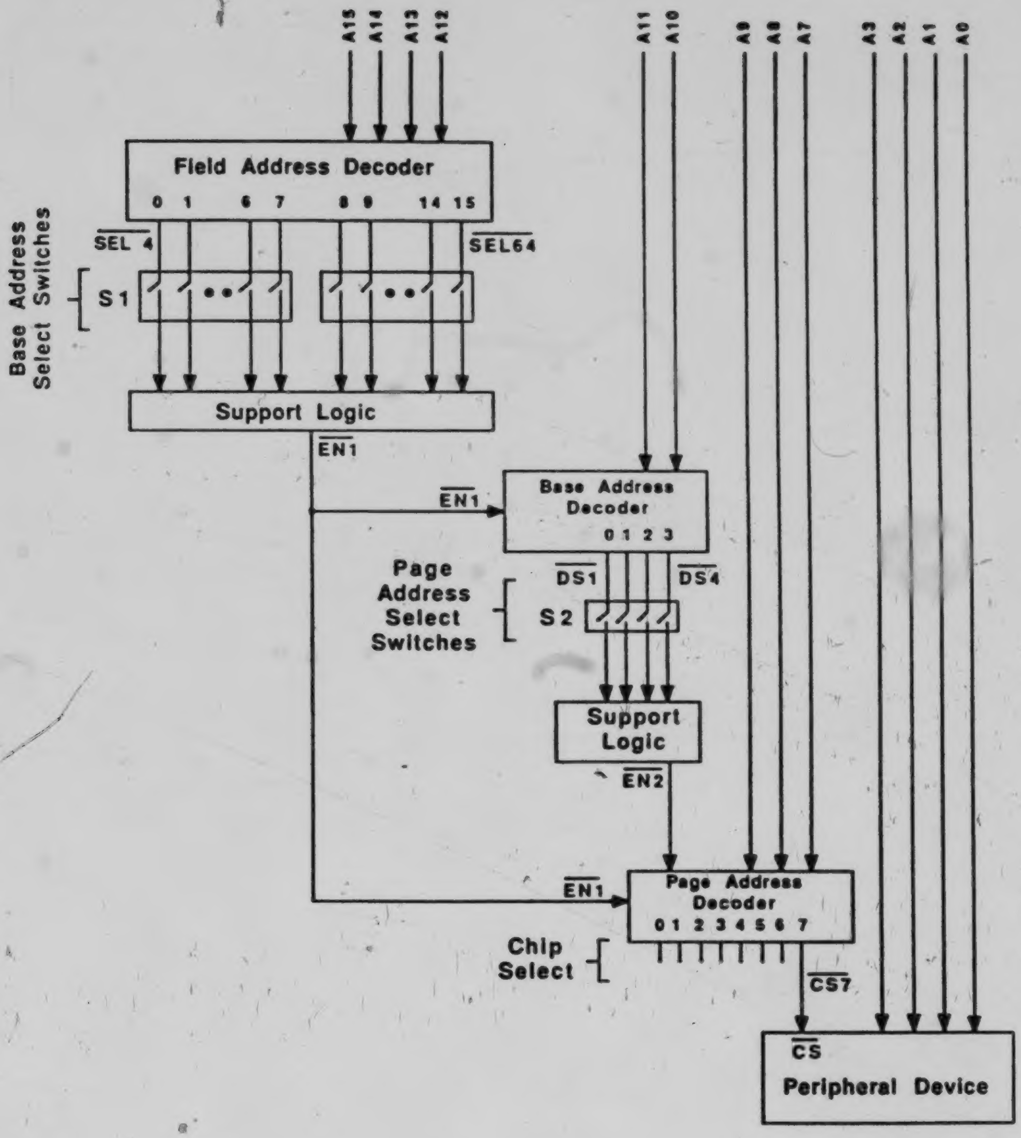
A15
A14
A13
A12
A11
A10
A9
A8
A7
A3
A2
A1
A0
Field Address Decoder
0 1 6 7 8 9 14 15
SEL 4
SEL64
Base Address Select Switches
S1
Support Logic
EN1
EN1
Base Address Decoder
0 1 2 3
DS1
DS4
Page Address Select Switches
S2
Support Logic
EN2
EN1
Page Address Decoder
0 1 2 3 4 5 6 7
Chip Select
CS7
CS
Peripheral Device

Figure A-8. Simplified block diagram of the relocatable, switch configurable address decoding scheme.

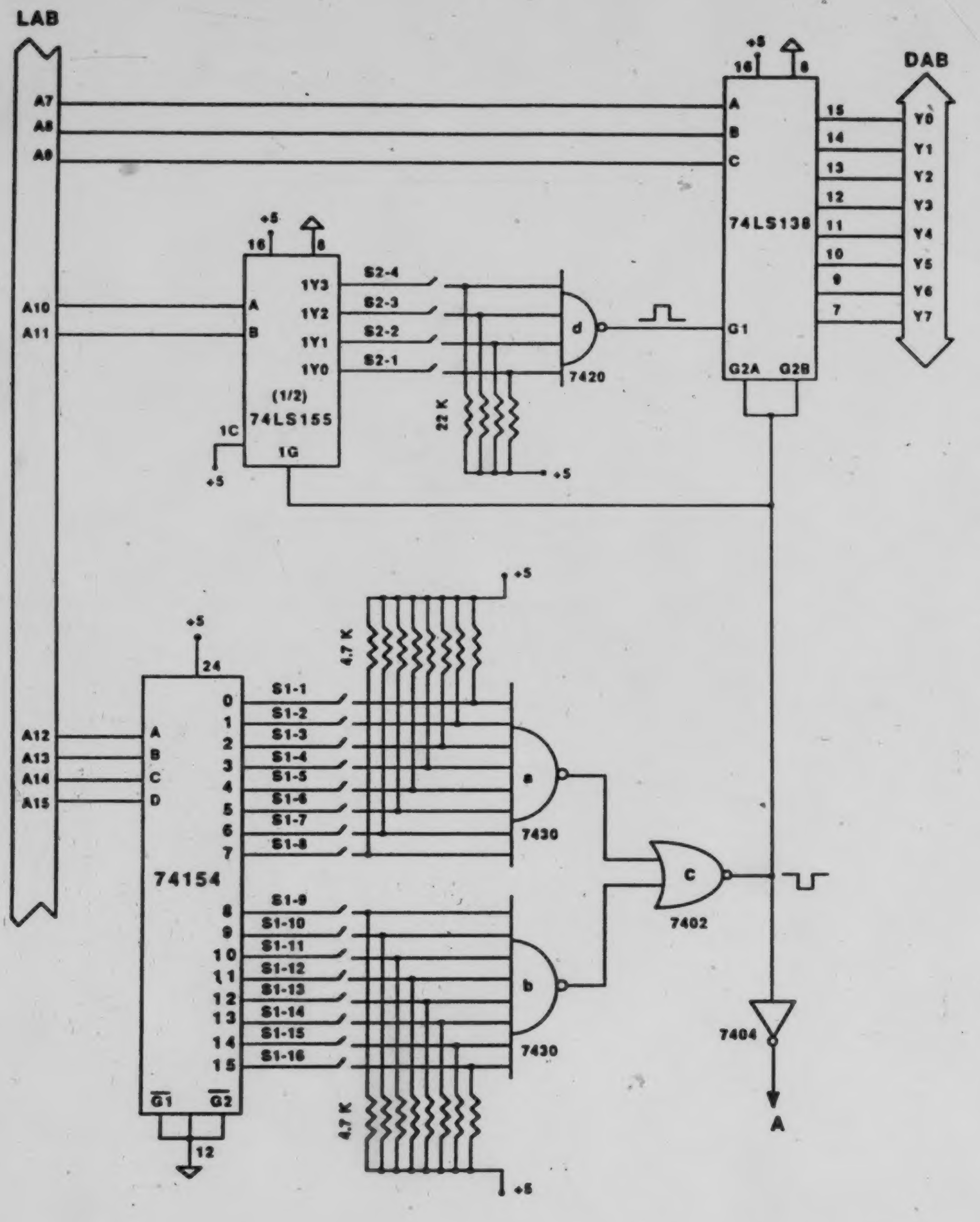
LAB
A7
A8
A9
A10
A11
A12
A13
A14
A15
DAB
74LS138
Y0
Y1
Y2
Y3
Y4
Y5
Y6
Y7
G1
G2A
G2B
(1/2)
74LS155
1Y3
1Y2
1Y1
1Y0
1C
1G
S2-4
S2-3
S2-2
S2-1
22 K
7420
d
+5
74154
S1-1
S1-2
S1-3
S1-4
S1-5
S1-6
S1-7
S1-8
S1-9
S1-10
S1-11
S1-12
S1-13
S1-14
S1-15
S1-16
4.7 K
7430
a
b
c
7402
7404
A
24
12

Figure A-9. Circuit diagram of the address decoding scheme utilized in the single channel system. DAB is the decoded Address Bus, see text for discussion.

Table A-1. Truth table for 74154,4-line-to-16 line decoder/demultiplexer.

INPUTS						OUTPUTS																			
G1	G2	D	C	B	A	0	1	2	3	4	5	6	7	8	9	10	11	12	13	14	15	Signal Name	Address Range (Hex)	Switch Bank 1	Address Upper Bound (Dec)
0	0	0	0	0	0	0	1	1	1	1	1	1	1	1	1	1	1	1	1	1	1	$\overline{\text{SEL 4}}$	0000-0FFF	S1- 1	4 K
0	0	0	0	0	1	1	0	1	1	1	1	1	1	1	1	1	1	1	1	1	1	$\overline{\text{SEL 8}}$	1000-1FFF	S1- 2	8 K
0	0	0	0	1	0	1	1	0	1	1	1	1	1	1	1	1	1	1	1	1	1	$\overline{\text{SEL12}}$	2000-2FFF	S1- 3	12 K
0	0	0	0	1	1	1	1	1	0	1	1	1	1	1	1	1	1	1	1	1	1	$\overline{\text{SEL16}}$	3000-3FFF	S1- 4	16 K
0	0	0	1	0	0	1	1	1	1	0	1	1	1	1	1	1	1	1	1	1	1	$\overline{\text{SEL20}}$	4000-4FFF	S1- 5	20 K
0	0	0	1	0	1	1	1	1	1	1	0	1	1	1	1	1	1	1	1	1	1	$\overline{\text{SEL24}}$	5000-5FFF	S1- 6	24 K
0	0	0	1	1	0	1	1	1	1	1	1	0	1	1	1	1	1	1	1	1	1	$\overline{\text{SEL28}}$	6000-6FFF	S1- 7	28 K
0	0	0	1	1	1	1	1	1	1	1	1	1	0	1	1	1	1	1	1	1	1	$\overline{\text{SEL32}}$	7000-7FFF	S1- 8	32 K
0	0	1	0	0	0	1	1	1	1	1	1	1	1	0	1	1	1	1	1	1	1	$\overline{\text{SEL36}}$	8000-8FFF	S1- 9	36 K
0	0	1	0	0	1	1	1	1	1	1	1	1	1	1	0	1	1	1	1	1	1	$\overline{\text{SEL40}}$	9000-9FFF	S1-10	40 K
0	0	1	0	1	0	1	1	1	1	1	1	1	1	1	1	0	1	1	1	1	1	$\overline{\text{SEL44}}$	A000-AFFF	S1-11	44 K
0	0	1	0	1	1	1	1	1	1	1	1	1	1	1	1	1	0	1	1	1	1	$\overline{\text{SEL48}}$	B000-BFFF	S1-12	48 K
0	0	1	1	0	0	1	1	1	1	1	1	1	1	1	1	1	1	0	1	1	1	$\overline{\text{SEL52}}$	C000-CFFF	S1-13	52 K
0	0	1	1	0	1	1	1	1	1	1	1	1	1	1	1	1	1	1	0	1	1	$\overline{\text{SEL56}}$	D000-DFFF	S1-14	56 K
0	0	1	1	1	0	1	1	1	1	1	1	1	1	1	1	1	1	1	1	0	1	$\overline{\text{SEL60}}$	E000-EFFF	S1-15	60 K
0	0	1	1	1	1	1	1	1	1	1	1	1	1	1	1	1	1	1	1	1	0	$\overline{\text{SEL64}}$	F000-FFFF	S1-16	64 K

G1 is connected to GND

G2 is connected to GND

A is connected to A12

B is connected to A13

C is connected to A14

D is connected to A15

the 74154 is routed, through gates a, b and c shown in Figure A-9, to both the base address decoder and the page decoder. A 74LS155, a 2-line-to-4-line decoder/demultiplexer does base address decoding, the truth table when S1-9 is closed is given in Table A-2. The user, utilizing switches S2-1 to S2-4 selects the desired 1 Kbyte page. The output signal of gate d is routed to a 74LS138, a 3-line-to-8-line decoder/demultiplexer that does page address decoding and generates the actual $\overline{\text{CS}}$ (Chip Select) signals. The truth table when S2-1 is closed is given in Table A-3. The output of this decoder forms the basis of yet another local bus, the Decoded Address Bus (DAB), which provides the $\overline{\text{CS}}$ signals required by the single channel system (see Figure A-5).

A photograph of the complete single channel counter/timer, complete with the bus buffering, the local bus generation logic and the relocatable addressing is shown in Figure A-10. This card plugs into the Microflex 65 bus.

Table A-2. Truth table for 74155, 2-line-to-4-line decoder/demultiplexer.

INPUTS				OUTPUTS								
1C	1G	B	A	1Y0	1Y1	1Y2	1Y3	Signal Name	Switch Bank 2	Logical Address Range (Hex)	Physical Address Range (Hex) *	Physical Address Upper Bound (Dec)
1	0	0	0	0	1	1	1	$\overline{DS1}$	S2-1	X000-X3FF	8000-83FF	37 K
1	0	0	0	1	0	1	1	$\overline{DS2}$	S2-2	X700-X7FF	8400-87FF	38 K
1	0	0	0	1	1	0	1	$\overline{DS3}$	S2-3	XB00-XBFF	8800-8BFF	39 K
1	0	0	0	1	1	1	0	$\overline{DS4}$	S2-4	XF00-XFFF	8C00-8FFF	40 K
X	1	0	0	1	1	1	1					
0	X	0	0	1	1	1	1					

X: Don't Care

* Selected when S1-9 is closed

1C is connected to +5 V

1G is a strobe signal

A is connected to A10

B is connected to A11

Table A-3. Truth table for 74138, 3-line-to-8-line decoder/demultiplexer.

INPUTS					OUTPUTS									
G1	G2*	C	B	A	Y0	Y1	Y2	Y3	Y4	Y5	Y6	Y7	Signal Name	Physical Address Range(Hex)**
1	0	0	0	0	0	1	1	1	1	1	1	1	$\overline{CS1}$	8000-807F
1	0	0	0	1	1	0	1	1	1	1	1	1	$\overline{CS2}$	8080-80FF
1	0	0	1	0	1	1	0	1	1	1	1	1	$\overline{CS3}$	8100-817F
1	0	0	1	1	1	1	1	0	1	1	1	1	$\overline{CS4}$	8180-81FF
1	0	1	0	0	1	1	1	1	0	1	1	1	$\overline{CS5}$	8200-827F
1	0	1	0	1	1	1	1	1	1	0	1	1	$\overline{CS6}$	8280-82FF
1	0	1	1	0	1	1	1	1	1	1	0	1	$\overline{CS7}$	8300-837F
1	0	1	1	1	1	1	1	1	1	1	1	0	$\overline{CS8}$	8380-83FF
1	X	X	X	X	1	1	1	1	1	1	1	1		
X	0	X	X	X	1	1	1	1	1	1	1	1		

X : Don't care

* : G2=G1A+G2A

G2 is active when S1-9 is closed

G1 is active when S1-9 and S2-1 are closed

A is connected to A7

B is connected to A8

C is connected to A9

**: Selected when S1-9 is closed

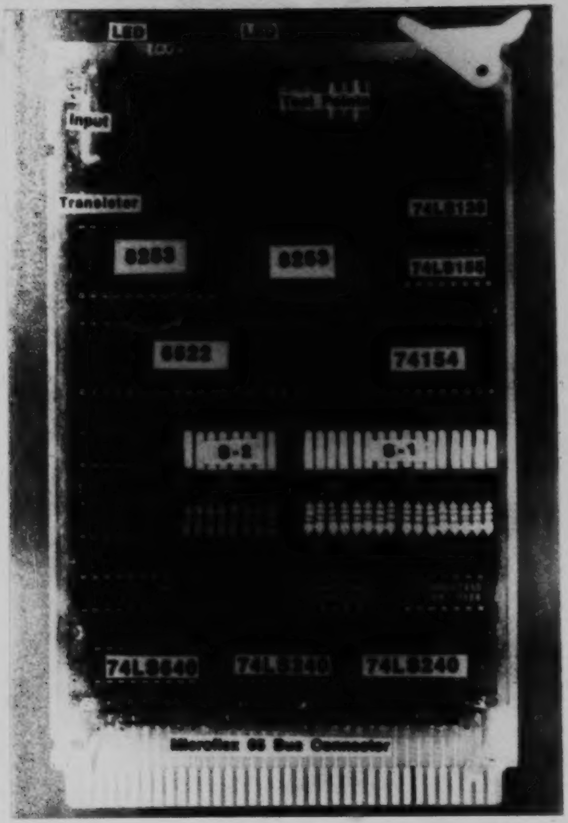
LED
LED
Input
Transistor
74LS138
8253
8253
74LS155
6522
74154
S-2
S-1
74LS640
74LS240
74LS240
Microflex 65 Bus Connector

Figure A-10. Photograph of the single channel system. The LEDs are Light Emitting Diodes, the 8253s are the programmable timer/counter chips, the 6522 VIA (Versatile Interface Adapter) is a digital I/O integrated circuit, the 74LS138 is a 3-line-to-8-line decoder/demultiplexer, the 74LS155 is a 2-line-to-4-line decoder/demultiplexer, the 74154 is a 4-line-to-16-line decoder/demultiplexer, S-1 is the first switch bank, S-2 is the second switch bank, the 74LS640 is an octal bus transceiver, the 74LS240s are octal buffers/line drivers, and the discrete transistor is a PNP 3393. The dimensions of the card are (LxW):6.5 x 3.9 in (164 x 100 mm).

D. Conclusions

We have not yet implemented the complete multichannel system as illustrated in Figure A-3. The primary goal of this work was to illustrate one approach to a 'zero based design' of the measurement end of a direct reading spectrometer utilizing a microprocessor bus architecture, programmable support chips, inexpensive data domain-conversion chips, and inexpensive single board computers. To this end a complete single measurement channel was implemented. A multichannel system could be configured by duplicating the unit shown in Figure A-10 and combining the measurement channels in a Microflex 65 bus card cage along with an AIM 65-compatible single board microcomputer and a serial communications card all of which are available from Rockwell [8]. A smart backplane derived from the IBM PC family of personal computers [7] can also provide a powerful and inexpensive alternative for the design of a multichannel system. Data and control information from the multichannel system can then be serially transferred to a front end processor that would be used for data display, processing, and management giving an overall system of the concept described by Karanassios and Horlick [2].

REFERENCES

1. G. Horlick, Phil. Trans. R. Soc. Lond. A, **305**, 681 (1982)

2. V. Karanassios and G. Horlick, Appl. Spectrosc., **41**, 360 (1987)

3. M.W. Blades and G. Horlick, Talanta, **28**, 534 (1981)

4. G. Horlick, Talanta, **28**, 487 (1981)

5. V. Karanassios and G. Horlick, Talanta, **32**, 583 (1985)

6. V. Karanassios and G. Horlick, Talanta, **32**, 601 (1985)

7. V. Karanassios and G. Horlick, Talanta, **32**, 615 (1985)

8. Rockwell International, Microelectronic Devices Division, 3310 Miraloma Avenue, P.O. Box 3669, Anaheim, CA 92803

APPENDIX B

ICP-MS-DSID BLUEPRINTS

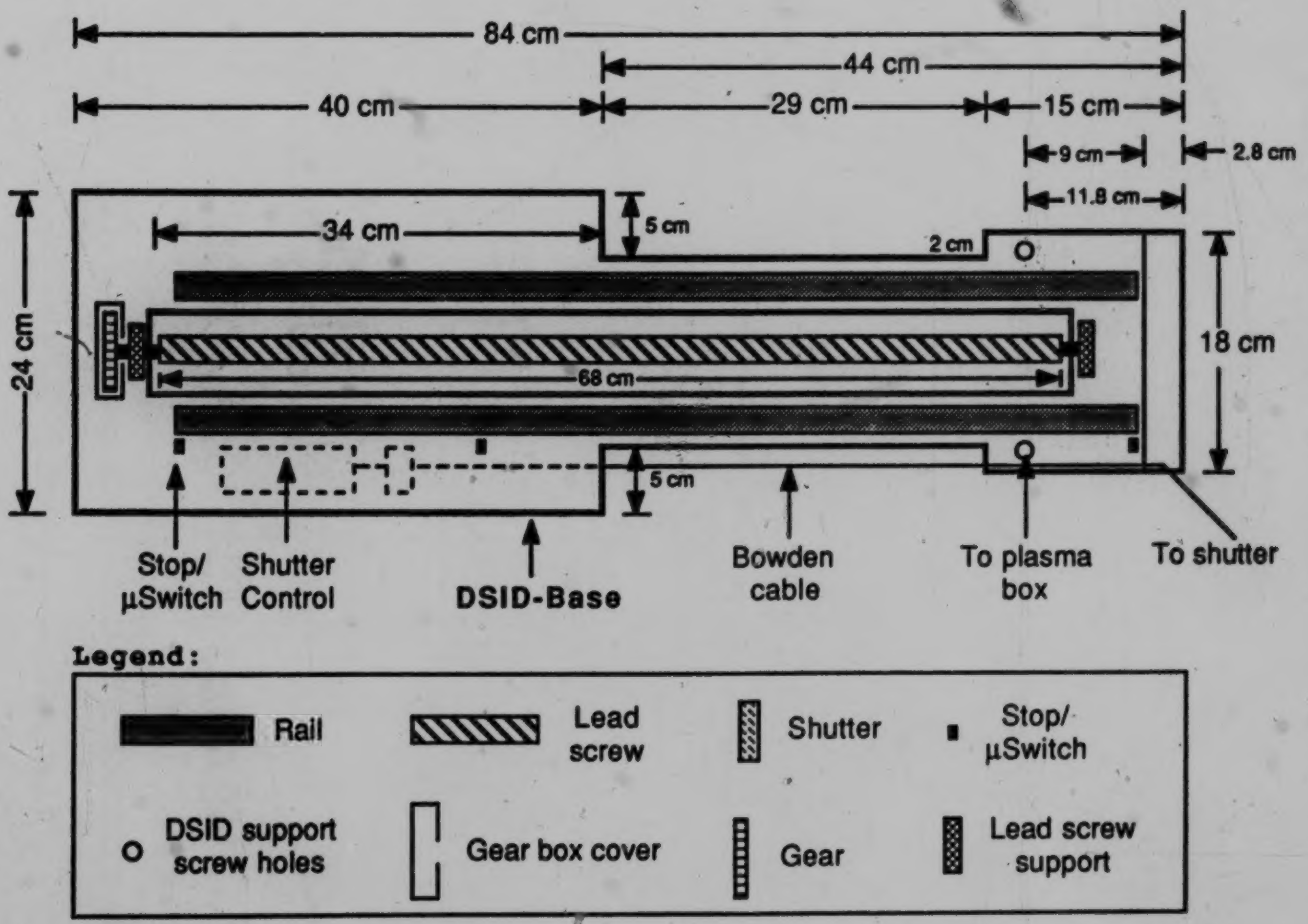
84 cm
44 cm
40 cm
29 cm
15 cm
9 cm
2.8 cm
11.8 cm
24 cm
34 cm
5 cm
2 cm
18 cm
68 cm
5 cm
Stop/
µSwitch
Shutter
Control
DSID-Base
Bowden
cable
To plasma
box
To shutter
Legend:
Rail
Lead
screw
Shutter
Stop/
µSwitch
DSID support
screw holes
Gear box cover
Gear
Lead screw
support

Figure B-1. Top view of DSID-base (see Fig. B-2 for more details).

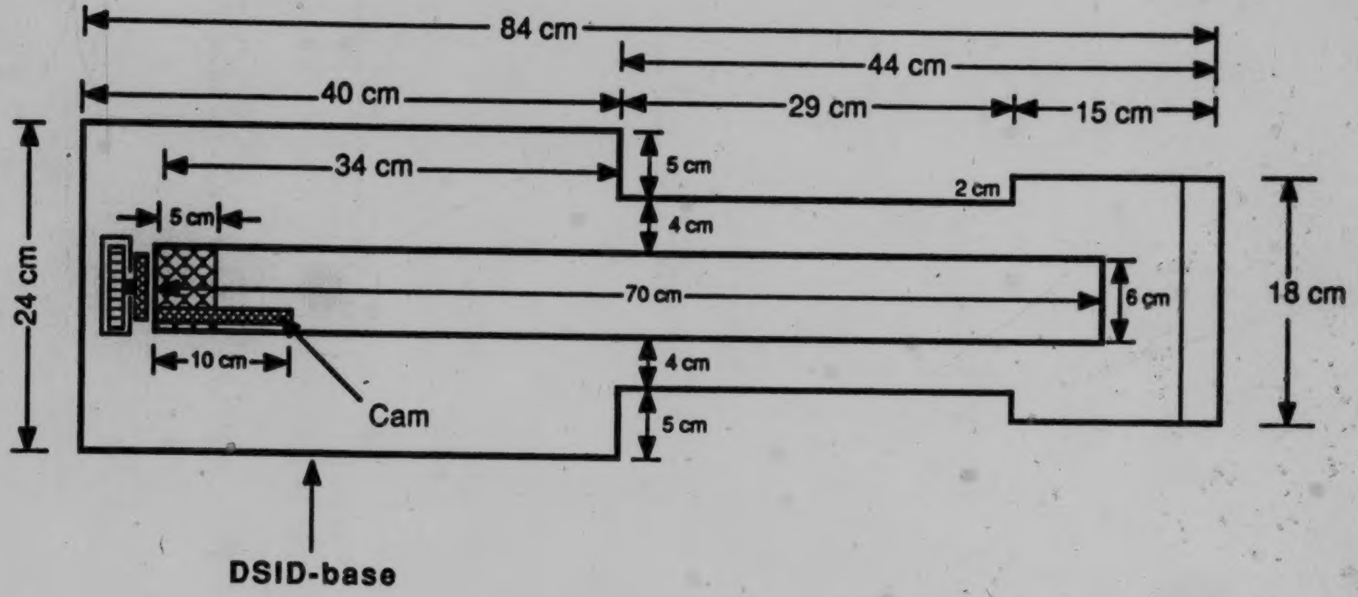
84 cm
44 cm
40 cm
29 cm
15 cm
34 cm
5 cm
2 cm
5 cm
4 cm
24 cm
70 cm
6 cm
18 cm
10 cm
4 cm
5 cm
Cam
DSID-base

Figure B-2. Top view of DSID-base (complements dimensions shown in Fig. B-1).

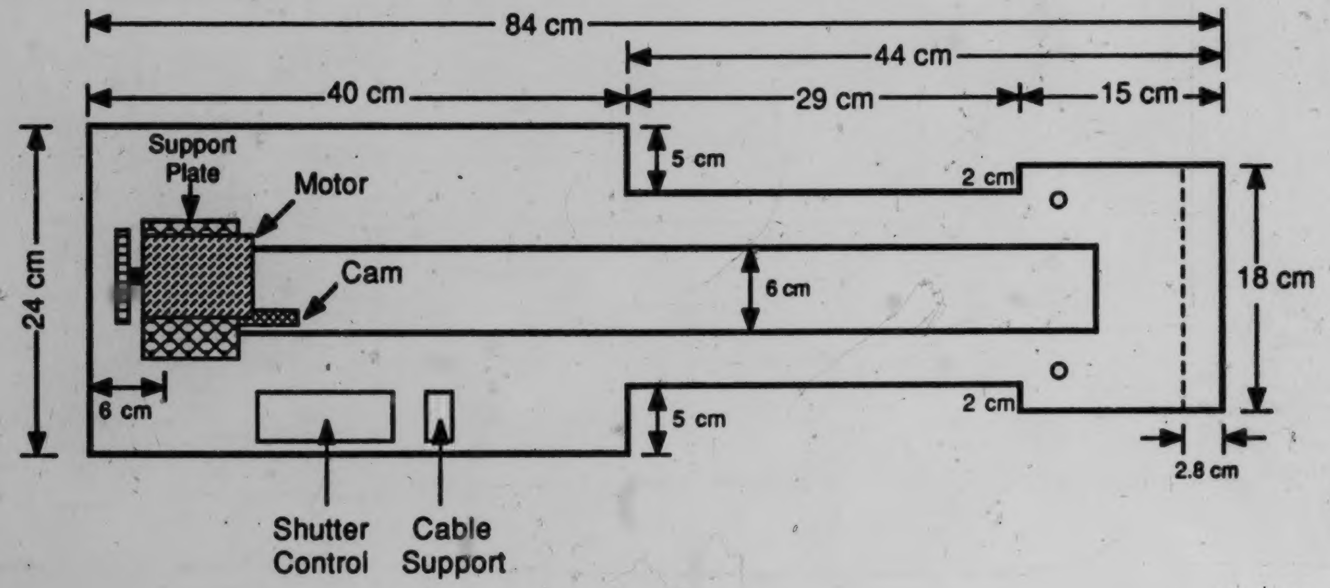
84 cm
44 cm
40 cm
29 cm
15 cm
24 cm
5 cm
2 cm
Support Plate
Motor
Cam
6 cm
18 cm
6 cm
5 cm
2 cm
2.8 cm
Shutter Control
Cable Support

Figure B-3. Bottom view of DSID-base.

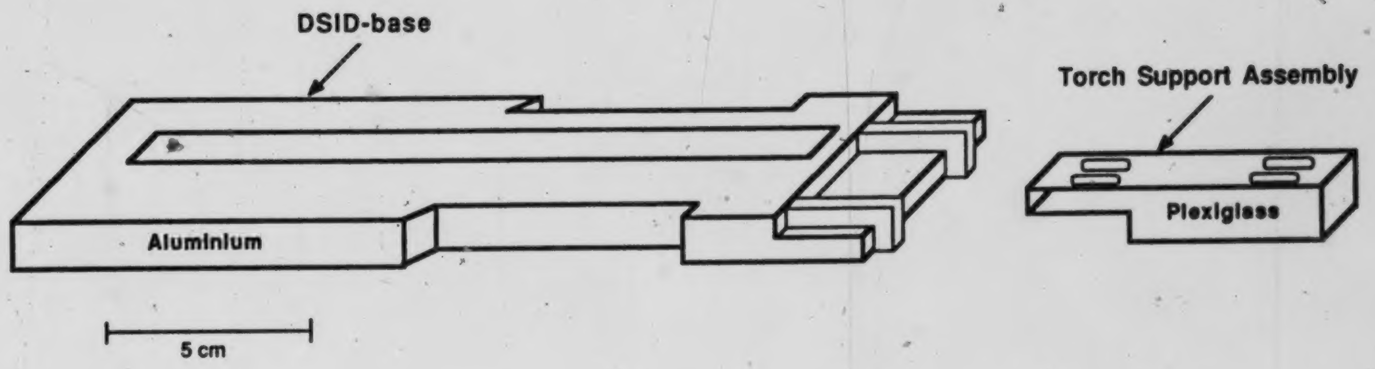
DSID-base
Torch Support Assembly
Aluminium
Plexiglass
5 cm

Figure B-4. Three dimensional view of DSID- and plexiglass-base.

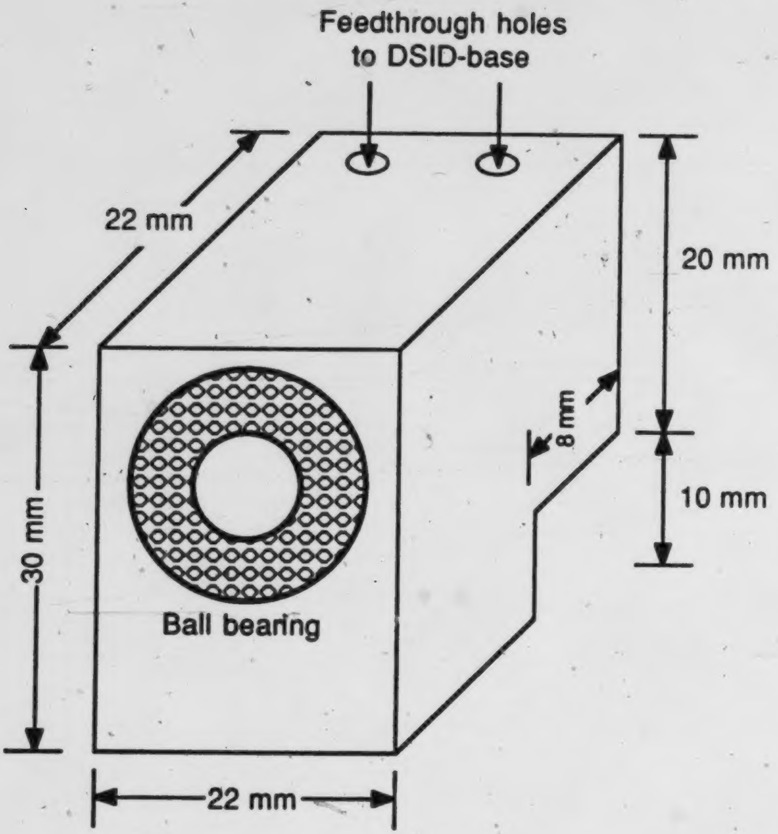
Feedthrough holes
to DSID-base
22 mm
20 mm
8 mm
10 mm
30 mm
Ball bearing
22 mm

Figure B-5. Lead screw support.

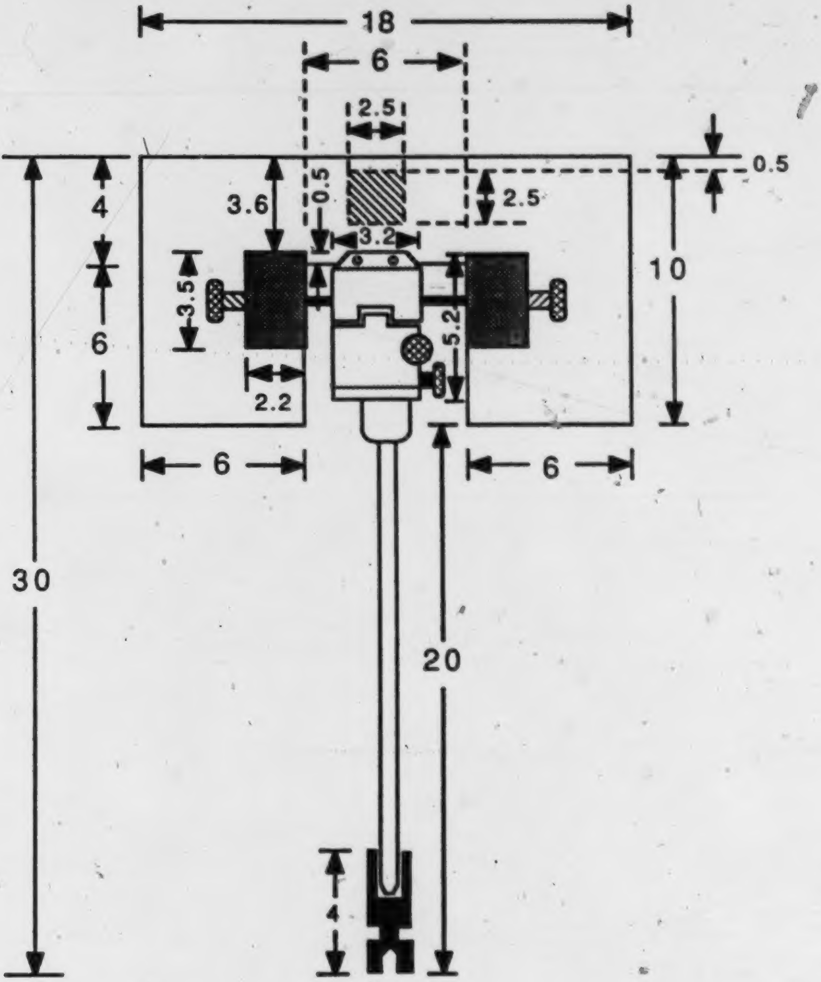
18
6
2.5
0.5
2.5
4
3.6
0.5
3.2
10
3.5
6
5.2
2.2
6
6
30
20
4

Legend:

▨ Ball bearing nut

■ Probe adapter clamp

See Fig. 6.10 and chapter 6 for more details

Figure B-6. Top view of sliding platform (dimensions in cm).

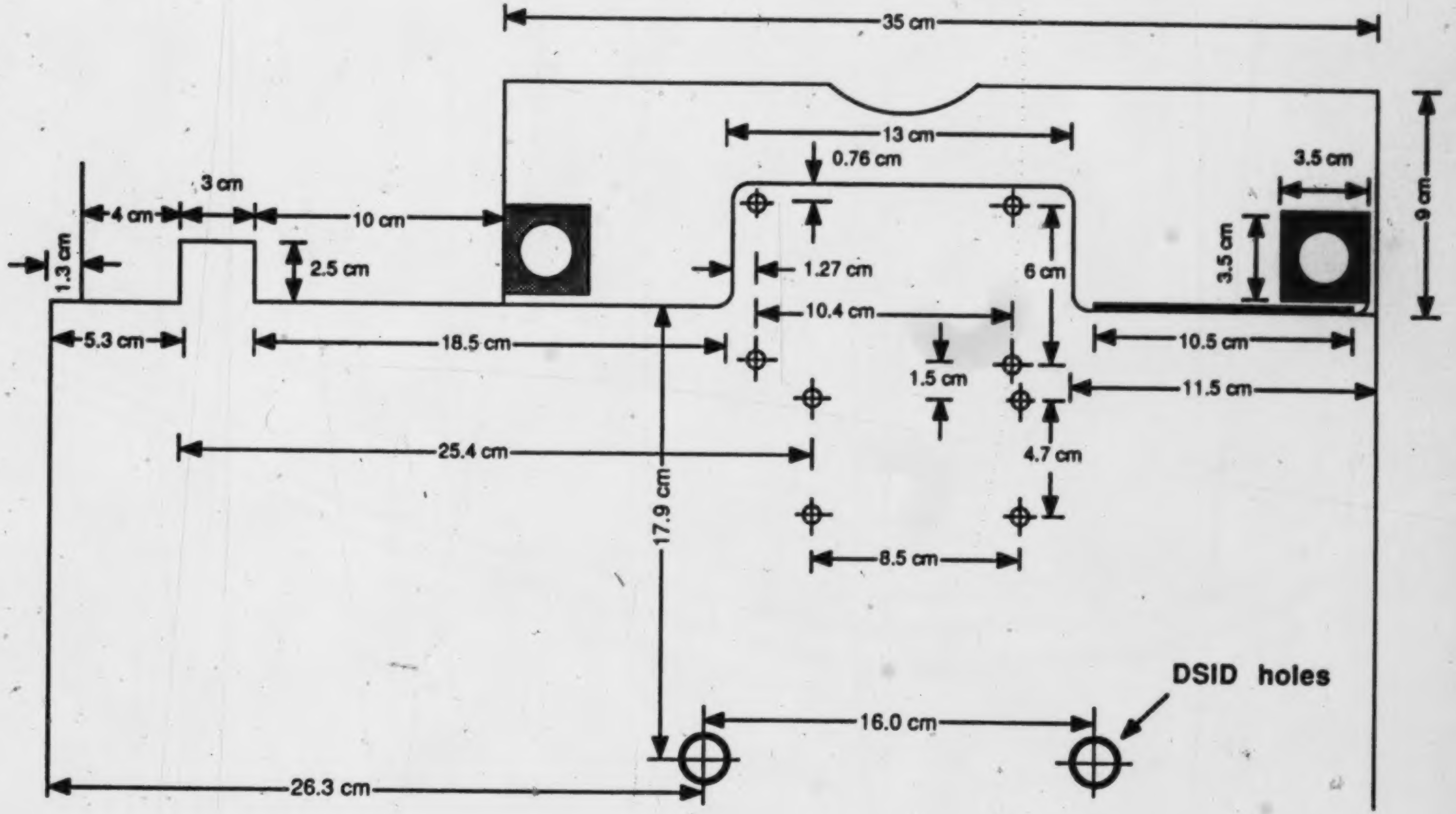
35 cm
9 cm
13 cm
0.76 cm
3 cm
4 cm
10 cm
1.3 cm
2.5 cm
3.5 cm
3.5 cm
1.27 cm
6 cm
10.4 cm
5.3 cm
18.5 cm
10.5 cm
1.5 cm
11.5 cm
25.4 cm
4.7 cm
17.9 cm
8.5 cm
DSID holes
16.0 cm
26.3 cm

Figure B-7. Top view of plasma box.

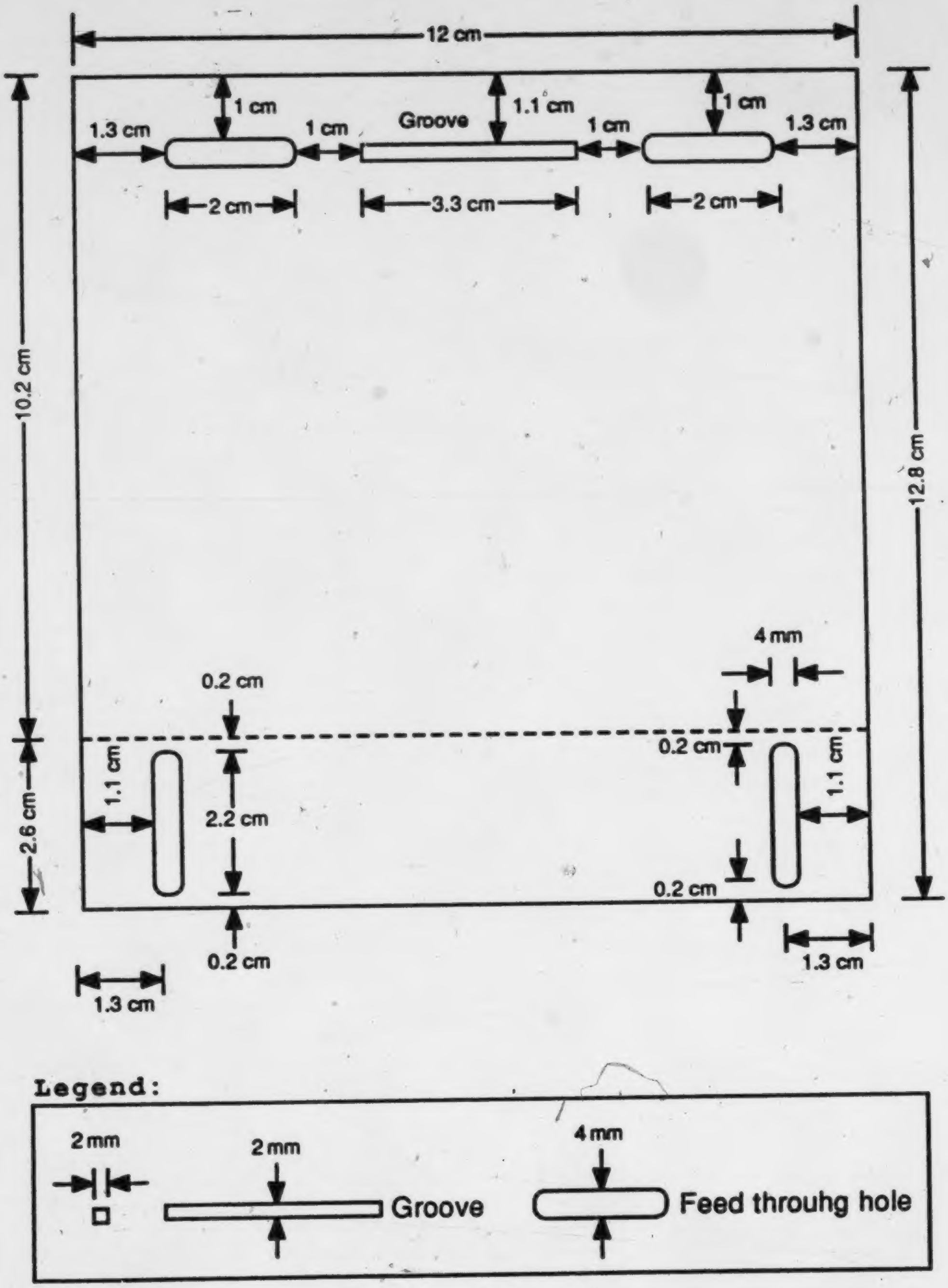
12 cm
1.3 cm
1 cm
1 cm
Groove
1.1 cm
1 cm
1 cm
1.3 cm
2 cm
3.3 cm
2 cm
10.2 cm
12.8 cm
4 mm
0.2 cm
0.2 cm
1.1 cm
2.2 cm
1.1 cm
2.6 cm
0.2 cm
0.2 cm
1.3 cm
1.3 cm
Legend:
2 mm
2 mm
Groove
4 mm
Feed throuhg hole

Figure B-8. Top view of plexiglass-base.

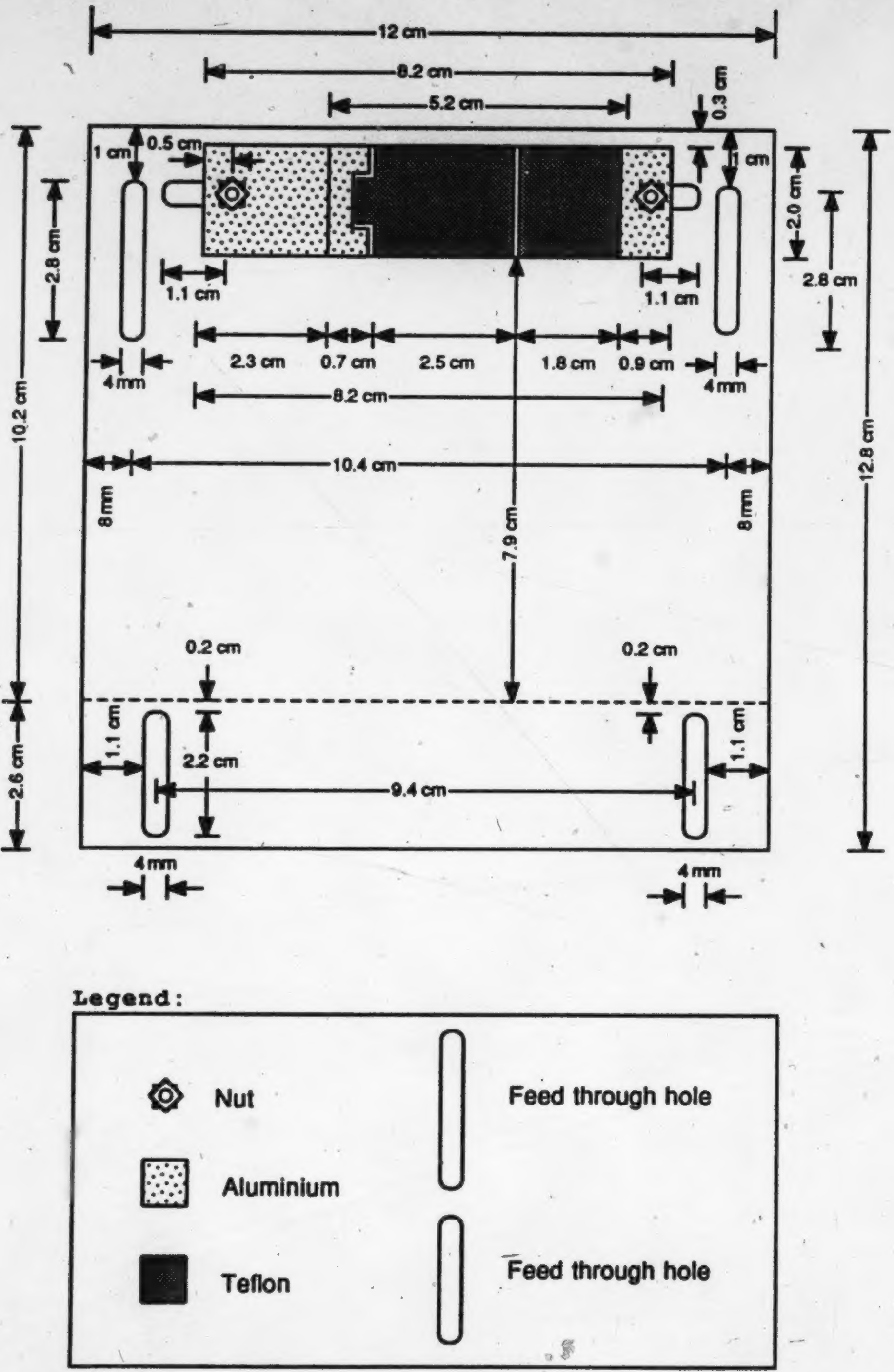
12 cm
8.2 cm
5.2 cm
0.3 cm
1 cm
0.5 cm
1 cm
2.0 cm
2.8 cm
2.8 cm
1.1 cm
1.1 cm
2.3 cm
0.7 cm
2.5 cm
1.8 cm
0.9 cm
4 mm
4 mm
8.2 cm
10.2 cm
12.8 cm
10.4 cm
8 mm
8 mm
7.9 cm
0.2 cm
0.2 cm
1.1 cm
2.2 cm
1.1 cm
2.6 cm
9.4 cm
4 mm
4 mm
Legend:
Nut
Aluminium
Teflon
Feed through hole
Feed through hole

Figure B-9. Top view of plexiglass-base with torch support in place.

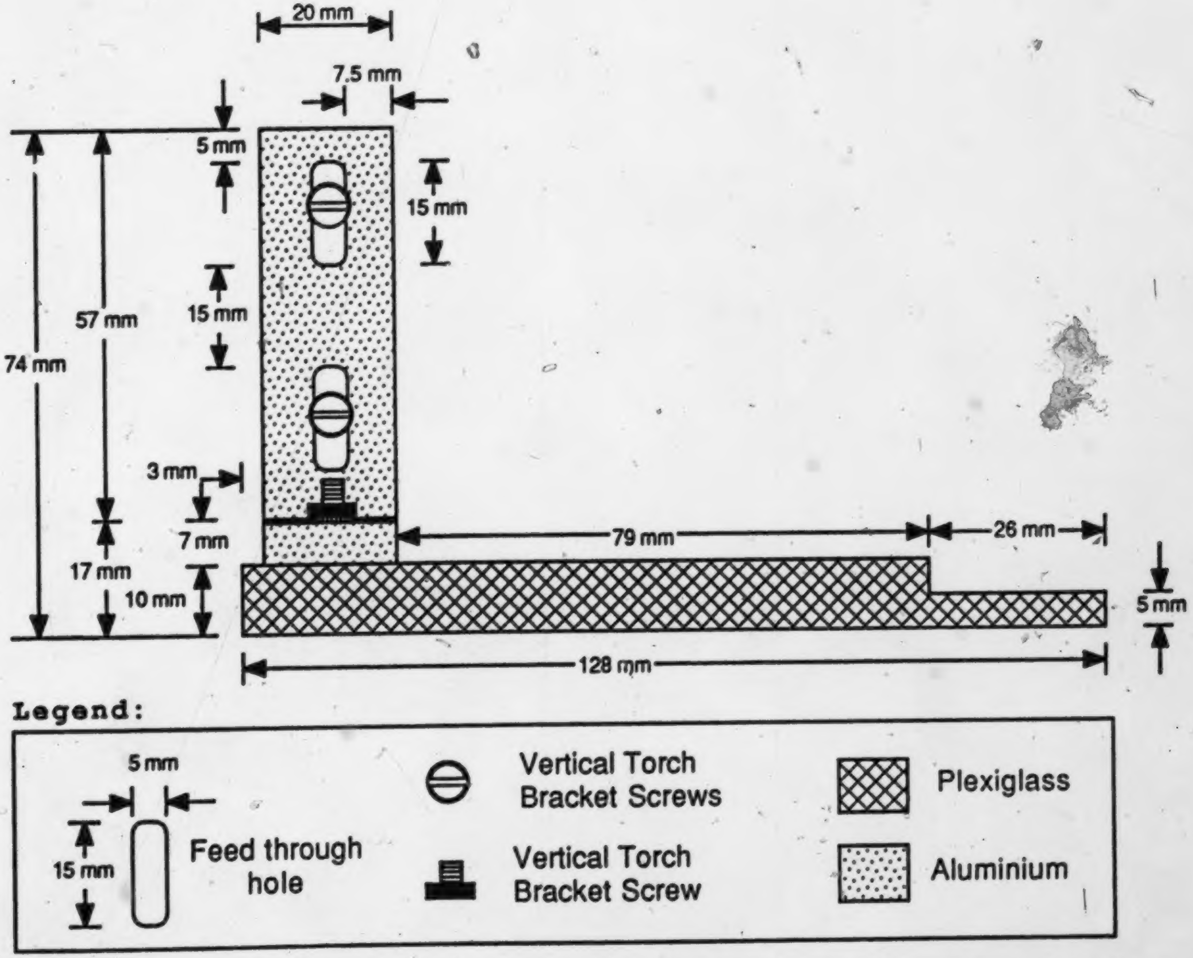
20 mm
7.5 mm
5 mm
15 mm
15 mm
74 mm
57 mm
3 mm
7 mm
17 mm
10 mm
79 mm
26 mm
5 mm
128 mm
Legend:
5 mm
15 mm
Feed through hole
Vertical Torch Bracket Screws
Vertical Torch Bracket Screw
Plexiglass
Aluminium

Figure B-10. Side view of plexiglass-base with the torch support in place.

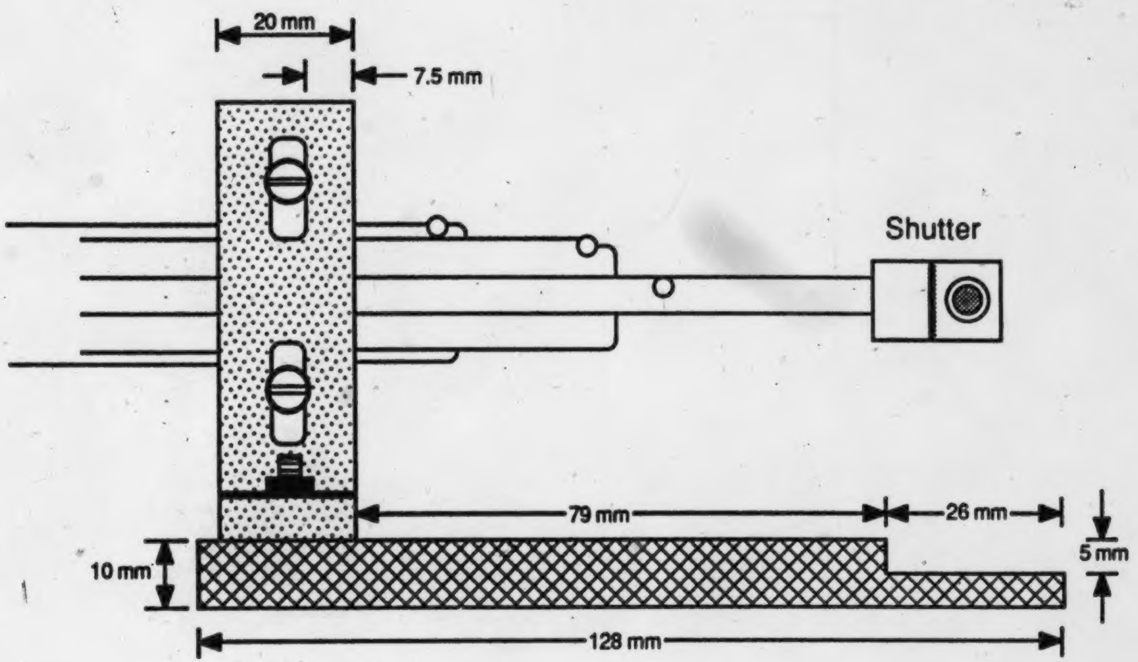
20 mm
7.5 mm
Shutter
79 mm
26 mm
5 mm
10 mm
128 mm

Figure B-11. Side view of torch, torch support and shutter.

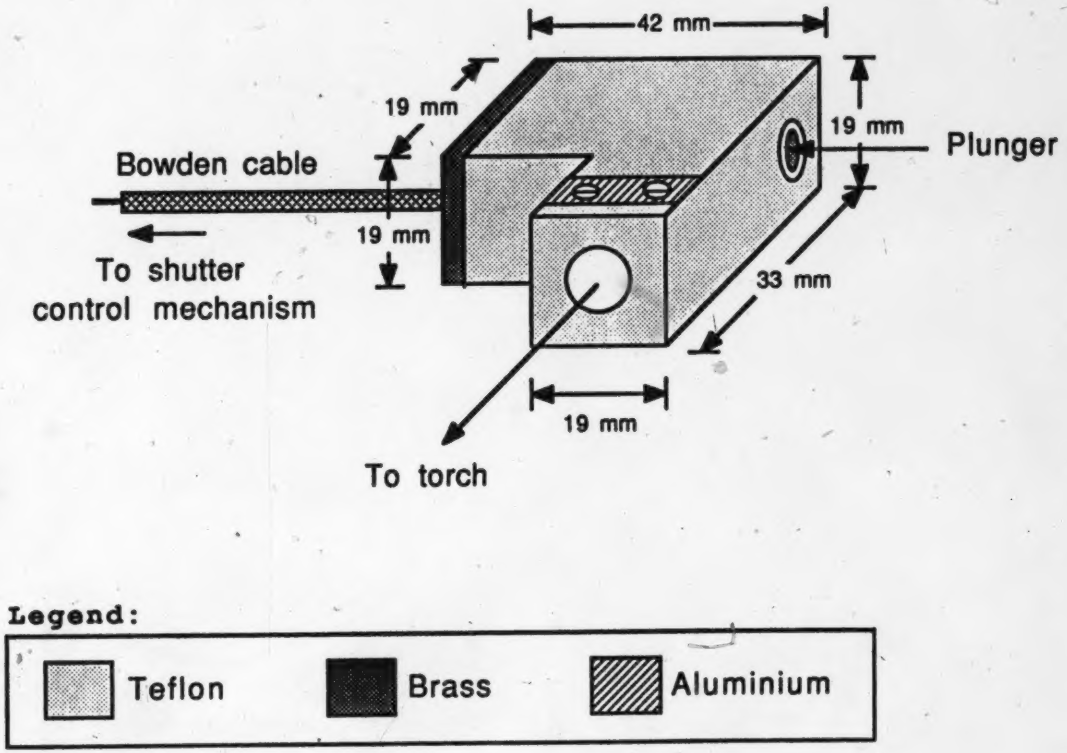
42 mm
19 mm
19 mm
Plunger
Bowden cable
19 mm
To shutter
control mechanism
33 mm
19 mm
To torch
Legend:
Teflon
Brass
Aluminium

Figure B-12. Three-dimensional view of shutter.

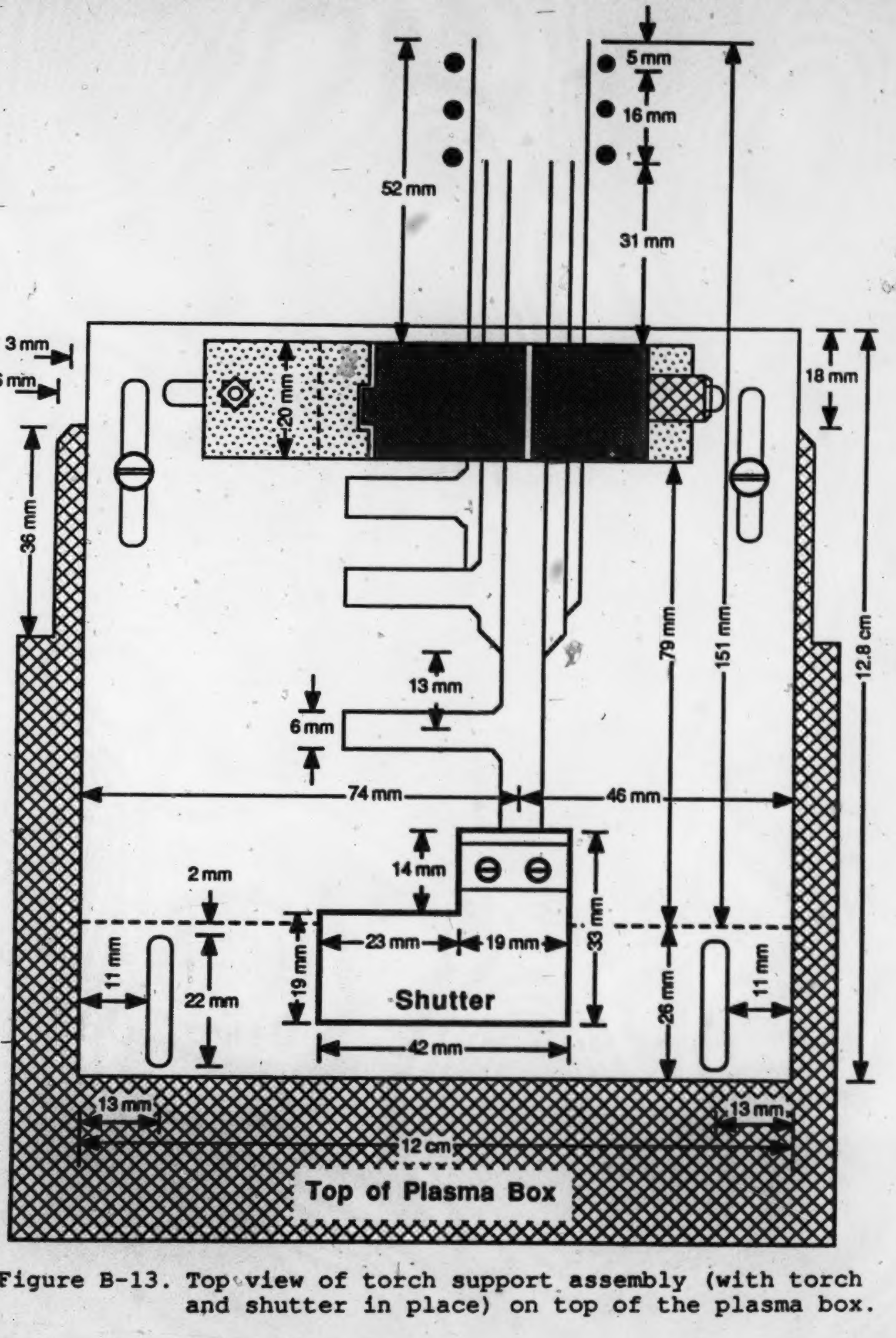
52 mm
5 mm
16 mm
31 mm
3 mm
6 mm
20 mm
18 mm
36 mm
12.8 cm
79 mm
151 mm
13 mm
6 mm
74 mm
46 mm
14 mm
2 mm
33 mm
23 mm
19 mm
19 mm
11 mm
22 mm
Shutter
26 mm
11 mm
42 mm
13 mm
13 mm
12 cm
Top of Plasma Box

Figure B-13. Top view of torch support assembly (with torch and shutter in place) on top of the plasma box.

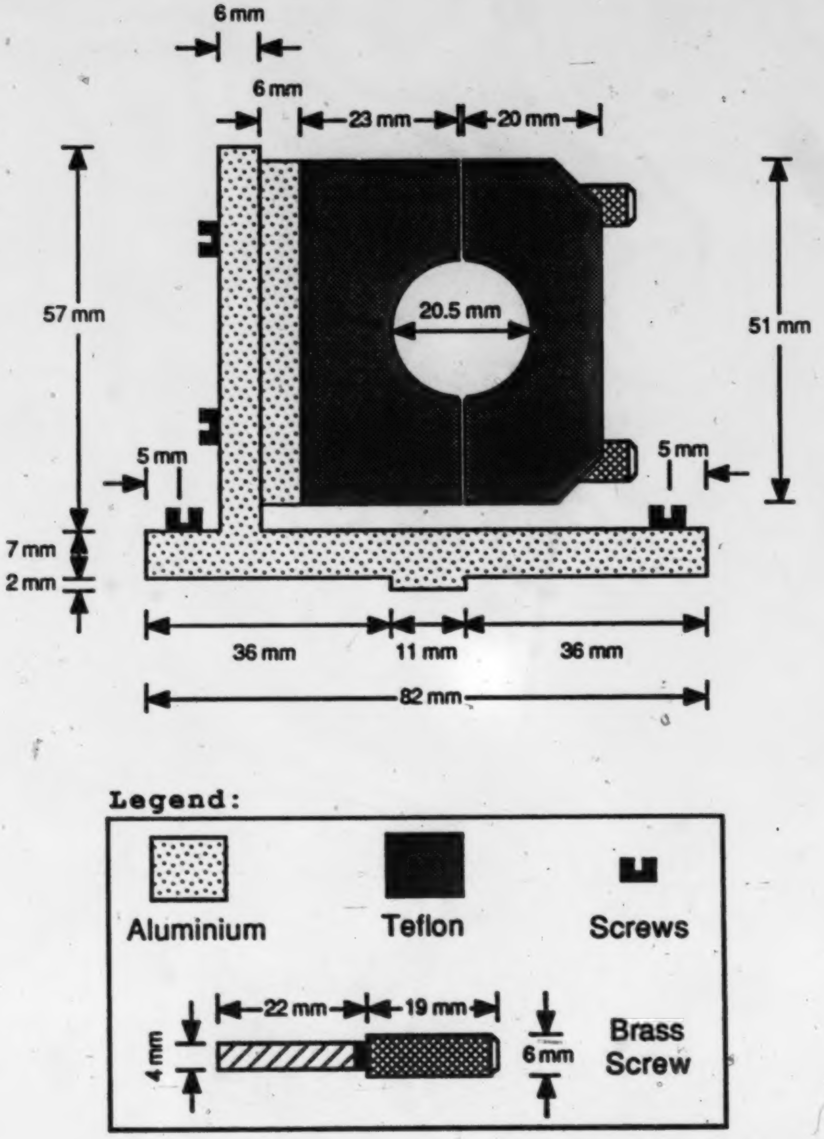
6 mm
6 mm
23 mm
20 mm
57 mm
20.5 mm
51 mm
5 mm
5 mm
7 mm
2 mm
36 mm
11 mm
36 mm
82 mm
Legend:
Aluminium
Teflon
Screws
22 mm
19 mm
4 mm
6 mm
Brass Screw

Figure B-14. Side view of torch support brace.

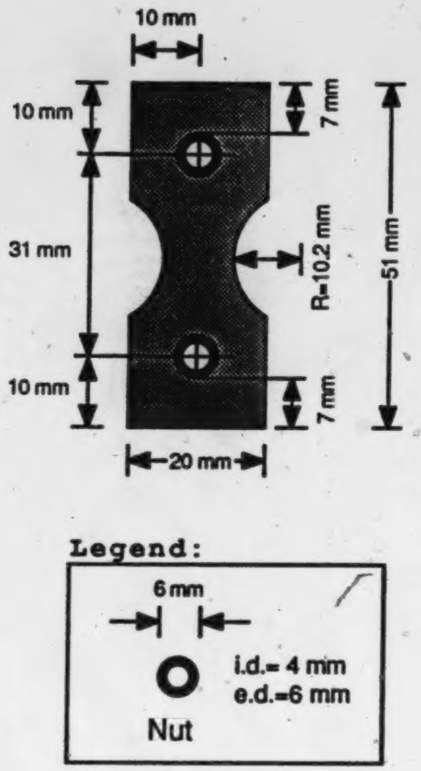
10 mm
10 mm
7 mm
31 mm
R=10.2 mm
51 mm
10 mm
7 mm
20 mm
Legend:
6 mm
i.d.= 4 mm
e.d.=6 mm
Nut

Figure B-15. Front view of torch brace.

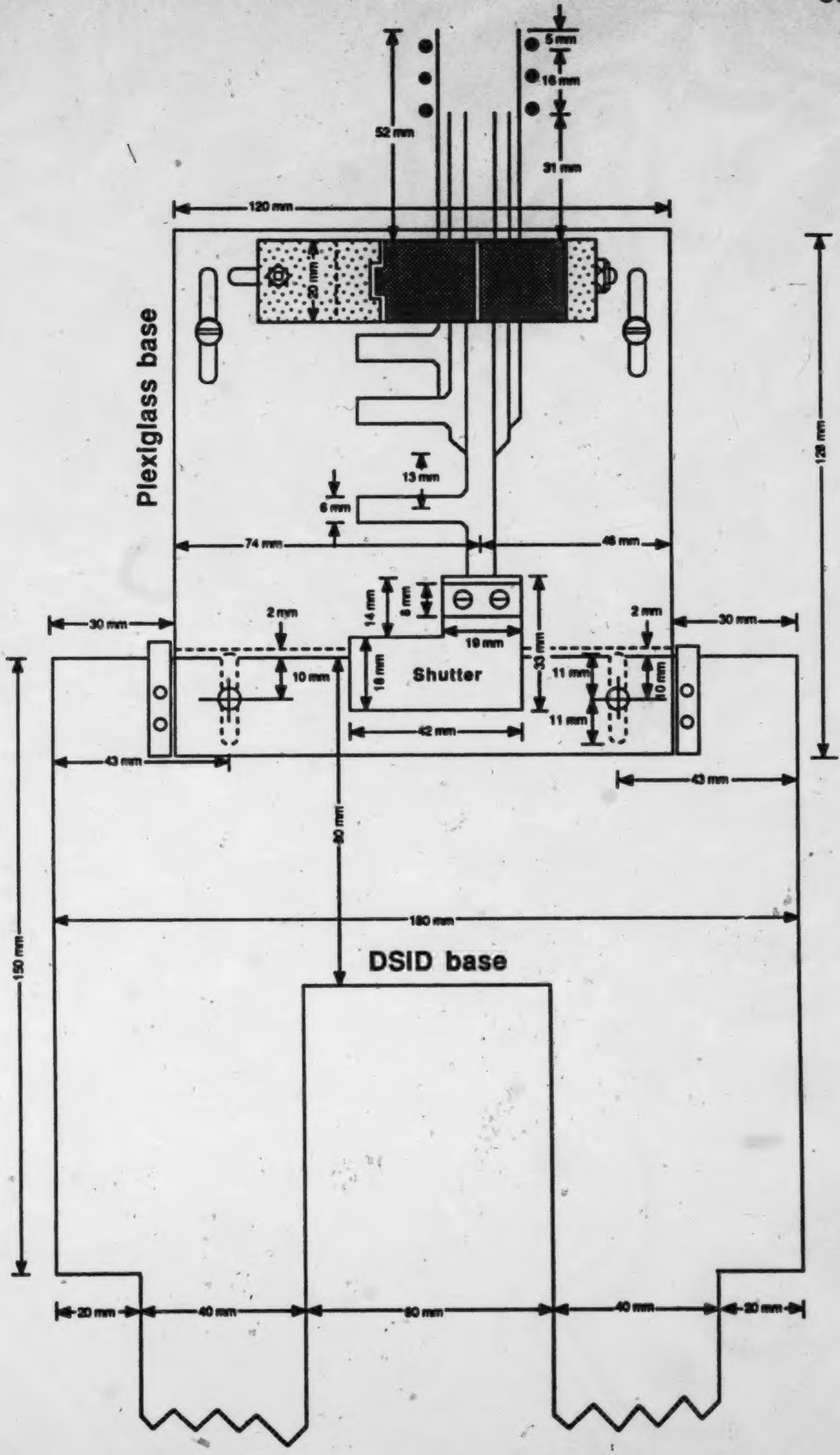
5 mm
16 mm
52 mm
31 mm
120 mm
20 mm
128 mm
Plexiglass base
13 mm
6 mm
74 mm
46 mm
14 mm
8 mm
33 mm
19 mm
2 mm
2 mm
30 mm
30 mm
10 mm
18 mm
Shutter
11 mm
11 mm
10 mm
42 mm
43 mm
43 mm
80 mm
180 mm
DSID base
150 mm
20 mm
40 mm
80 mm
40 mm
20 mm

Figure B-16. Top view of torch support assembly on DSID-base.

APPENDIX C

ICP-MS PARAMETER SET UTILIZED FOR THE ACQUISITION OF TRANSIENT SIGNALS WITH THE SCIEX ELAN ICP-MS SYSTEM

Table C-1. Parameter set used for the acquisition of transient signals.

Resolution		L			
Ion Multiplier	HV	4000			
Rod Offset	Volts	0.0			
Plasma RF Pwr	Watts	1250			
Auxiliary Flow	L/min	1.8			
Plasma Flow	L/min	15.0			
Nebulizer Pressure	psi	30.0			
Sample Flow		0			
Measurements/Peak		1			
Scanning Mode		E			
Measurement Mode		T			
Dwell Time	ms	30			
Preheat Temp	C	0	Time	sec	0.00
Ash Temp	C	0	Time	sec	0.00
Main Heat Temp	C	0	Time	sec	0.00
Initial Measurement	Delay	sec			1.00
Final Measurement	Delay	sec			20.00

Note that:

- Machine configuration must be changed to General Purpose Transient Sample Introduction System.
- Preliminary Transient Scan=Yes
- Data Buffered=Yes (Optional)

APPENDIX D

SPECTRAL CHARACTERISTICS OF A NEW SPECTROMETER DESIGN FOR ATOMIC EMISSION SPECTROSCOPY

A version of this chapter has been published.

V. Karanassios and G. Horlick, Appl. Spectrosc., 40, 813-821 (1986)

A. Introduction

For well over a decade, linear photodiode arrays have been used as detectors for spectrochemical measurements. While linear photodiode array (PDA) based UV-visible molecular absorption spectrometers are commercially available from several manufacturers, a definitive optical configuration for an atomic emission spectrometer utilizing linear photodiode arrays remains elusive. In the simplest configuration, that in which a single PDA is mounted in the exit focal plane of a conventional dispersive spectrometer, the basic problem is that it is impossible to achieve complete simultaneous wavelength coverage at ~~a spectral~~ resolution that is acceptable for atomic spectroscopy given the current size of 1024 and even 4096 element PDA's. Several alternative designs and approaches have been suggested for utilizing linear PDA's for atomic spectrochemical measurements. One approach can be classified as a window-slew-scanning spectrometer in which a single linear PDA is used in conjunction with a slew-scanning spectrometer to sequentially measure a series of narrow spectral windows. This basic type of PDA spectrometer has been used in our own laboratory for a number of years [1] and a vidicon based spectrometer of this type has also been described [2]. Another approach is to use a number of PDA's in a direct reading spectrometer configuration to effect the simultaneous measurement of a number of spectral windows [3, 4]. PDA spectrometers could also be designed around the unique multiple entrance slit spectrometers described by Busch and his co-workers [5, 6].

Over the years, it has also been suggested that electronic image sensors be coupled to echelle spectrometers for atomic spectroscopy applications. While most systems in the literature have focused on coupling area type image sensors to echelle spectrometers designed with cross-dispersion [7, 8], linear sensors can be used with an echelle spectrometer without cross- dispersion if they are coupled to a front end order selecting predisperser. This system could be programmed to present an order at a time to an echelle-PDA spectrometer (without cross-dispersion).

Recently, a new spectrometer design has been described [9] that combines a linear photodiode array detector and an echelle spectrometer (without cross-dispersion) with a very unique dispersion/selection/recombination line selector. This system has the potential to become the definitive optical configuration for an atomic emission PDA spectrometer. In this system, light from a source such as an ICP is first pre-dispersed using a low resolution (0.5 meter) concave grating polychromator. Desired narrow wavelength regions are selected using a slotted mask in the focal plane of the polychromator. The selected wavelengths transmitted by this mask are then recombined into a parallel quasi-white beam using a concave mirror and a second grating. This collimated quasi-white beam is then directed to an echelle grating and the output spectrum from the echelle is finally focussed on a linear photodiode array detector. The optical configuration and characteristics of this instrument will be presented along with spectra obtained using an ICP source illustrating its spectral characteristics for atomic emission spectrometry.

B. Experimental

The SPS-10 Simultaneous Plasma Spectrometer used for this study was developed at PRA International Inc. (London, Ontario, Canada). Preliminary technical specifications are listed in Table D-1. The unit used for this work was a pre-production prototype. A simplified optical diagram of the instrument is shown in Figure D-1. The actual optical layout is a more compact over/under arrangement of the echelle spectrometer and the predispersion/recombination subsystems. However, the operation of the spectrometer is best explained using the "exploded" layout shown in Figure D-1.

At the bottom of Figure D-1, the entrance slit, concave grating G1, and the mask constitute the 0.5 meter

Table D-1. Preliminary Technical Specifications for the SPS-10 Simultaneous Plasma Spectrometer.

Spectrometer

- predispersion spectrometer (concave grating, 590 L/mm) has a 0.5 m focal length with a reciprocal linear dispersion of 3.3 nm/mm.

- recombination system, 1 m concave mirror, plane grating 590 L/mm.

- the high resolution echelle spectrometer has a 1 m focal length and uses a B&L echelle grating (31.6

- wavelength coverage:
  - 0.0015 nm at 200 nm
  - 0.0022 nm at 300 nm
  - 0.0030 nm at 400 nm

Source

- inductively coupled plasma, Plasma Therm 2500

Detector

- 1024 element linear PDA (Reticon)
- camera, Tracor Northern

Computer

- IBM-XT

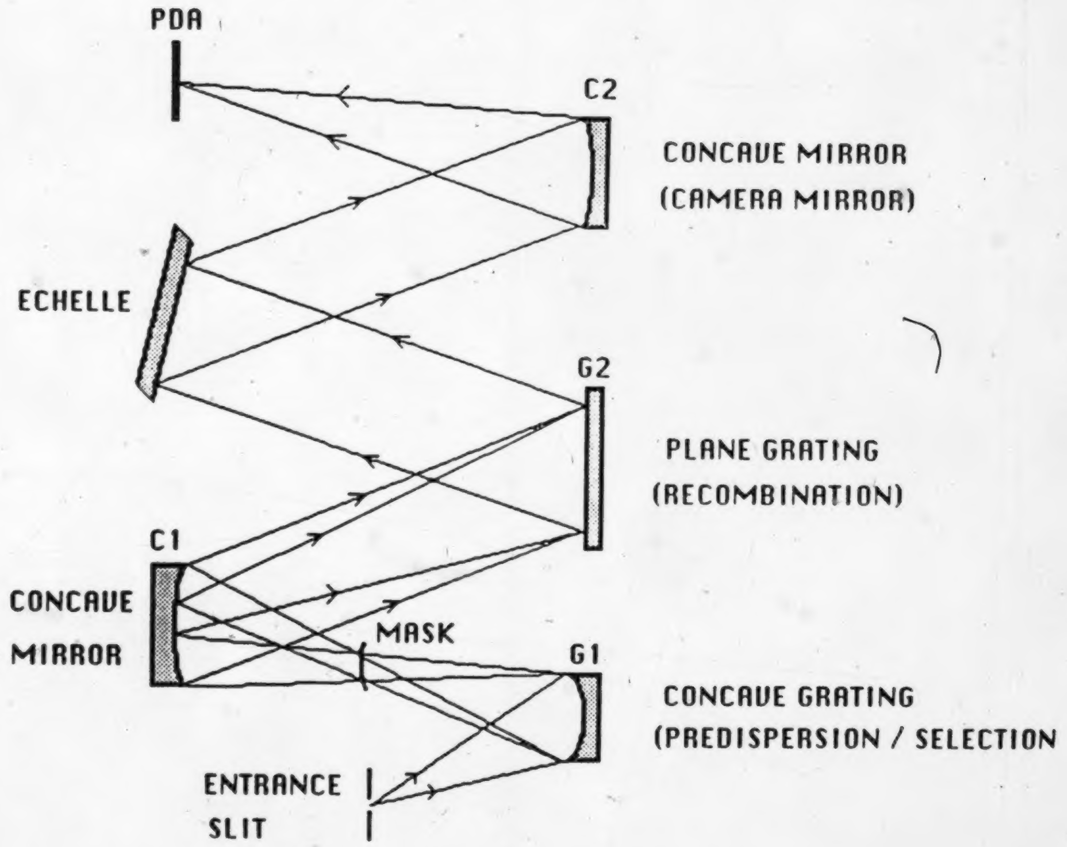
PDA
C2
CONCAVE MIRROR
(CAMERA MIRROR)
ECHELLE
G2
PLANE GRATING
(RECOMBINATION)
C1
CONCAVE
MIRROR
MASK
G1
CONCAVE GRATING
(PREDISPERSION / SELECTION
ENTRANCE
SLIT

Figure D-1. Simplified schematic diagram of the optical design of the SPS-10 Simultaneous Plasma Spectrometer.

predispersion/selection polychromator. The mask, shown schematically in Figure D-2, is simply a curved thin metal plate that is positioned in the exit focal plane of this predispersion polychromator. Slots are cut (machined) in the mask at appropriate positions to allow light from preselected narrow wavelength regions to pass through the mask to concave mirror C1. The slot positions are normally centered on spectral lines of interest and the mask used in this work was set-up for lines of the ten elements listed in Table D-2. The entrance slit width was 50 µm and the mask slot widths were 150 µm and both were about 1 cm high. Although the slots in the mask have slit like dimensions, it is important to bear in mind that a small wavelength window (~5Å) is actually transmitted by each slot and not just a single spectral line.

The narrow wavelength regions transmitted by the mask are recombined into a parallel quasi-white beam by concave mirror C1 and plane grating G2. A good way to think of this recombination part of the optical design is as 'going through a polychromator backwards'. The resulting collimated beam is directed to a 1 M echelle spectrometer and the final spectrum is measured in the exit focal plane of the echelle spectrometer with a 1024 element linear PDA. In the instrument used for this work the PDA system was a Tracor Northern camera containing a Reticon RL1024S array.

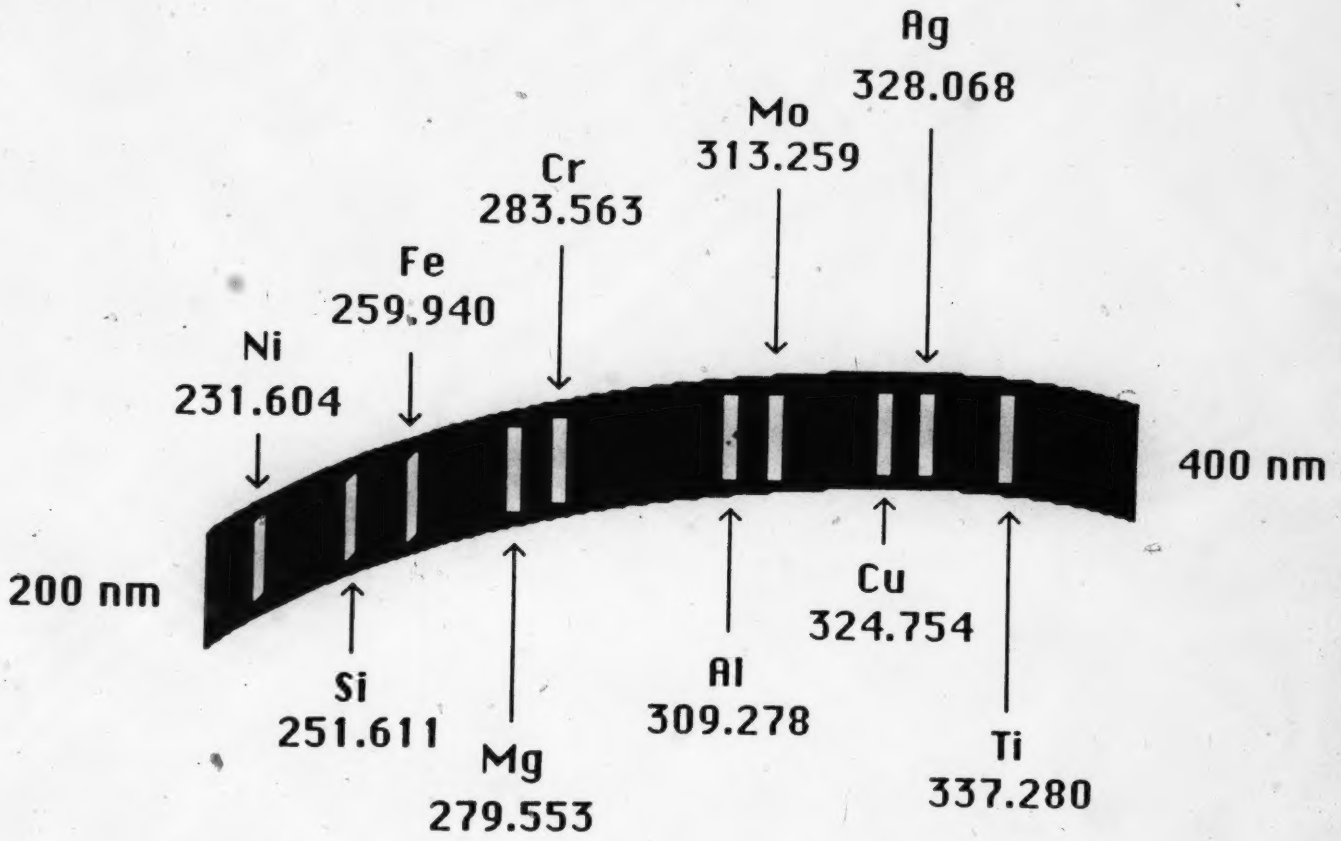
Ag
328.068
Mo
313.259
Cr
283.563
Fe
259.940
Ni
231.604
200 nm
400 nm
Si
251.611
Mg
279.553
Al
309.278
Cu
324.754
Ti
337.280

Figure D-2. Schematic diagram of pre-disperser selection mask.

Table D-2. Mask Specifications.

Element	Spectral Line	Echelle Order
Ni	II 231.6 nm	242
Si	I 251.6 nm	223
Fe	II 259.9 nm	216
Mg	II 279.5 nm	201
Cr	II 283.5 nm	198
Al	I 309.2 nm	181
Mo	I 313.2 nm	179
Cu	I 324.7 nm	173

In this PDA the sensor elements are on 25.4 µm centers and are 2.5 mm high. With 1024 pixels, the sensor is about 2.54 cm long. A quartz cylindrical lens was used to reduce the slit height image down to the size of the pixel height.

As can be seen from the preliminary specifications listed in Table D-1, the spectrometer has excellent resolution. At 200 nm the dispersion is 0.0015 nm per pixel and at 400 nm it is 0.0030 nm per pixel. For a 25 µm entrance slit, width of a spectral line at half-height covers about 5 pixels, consequently the resolution ranges from about 0.0075 nm to 0.0150 nm.

Conceptually, this instrument is a high resolution echelle spectrometer with a random access predisperser. A set of small wavelength regions can be chosen, essentially at random, with an appropriate mask. The spectral information in these selected regions can then be measured under high resolution while still being packed into a short focal plane format. This process is illustrated schematically in Figure D-3. The predisperser focal plane and mask are depicted in the upper part of Figure D-3. In this example, eight spectral lines are present in the predisperser focal plane. To simplify matters, the mask has only four slots, which are positioned to select lines a, d, e, g and h. Line a can be thought of as being at the 200 nm end of the predisperser focal plane and line h at the 400 nm end.

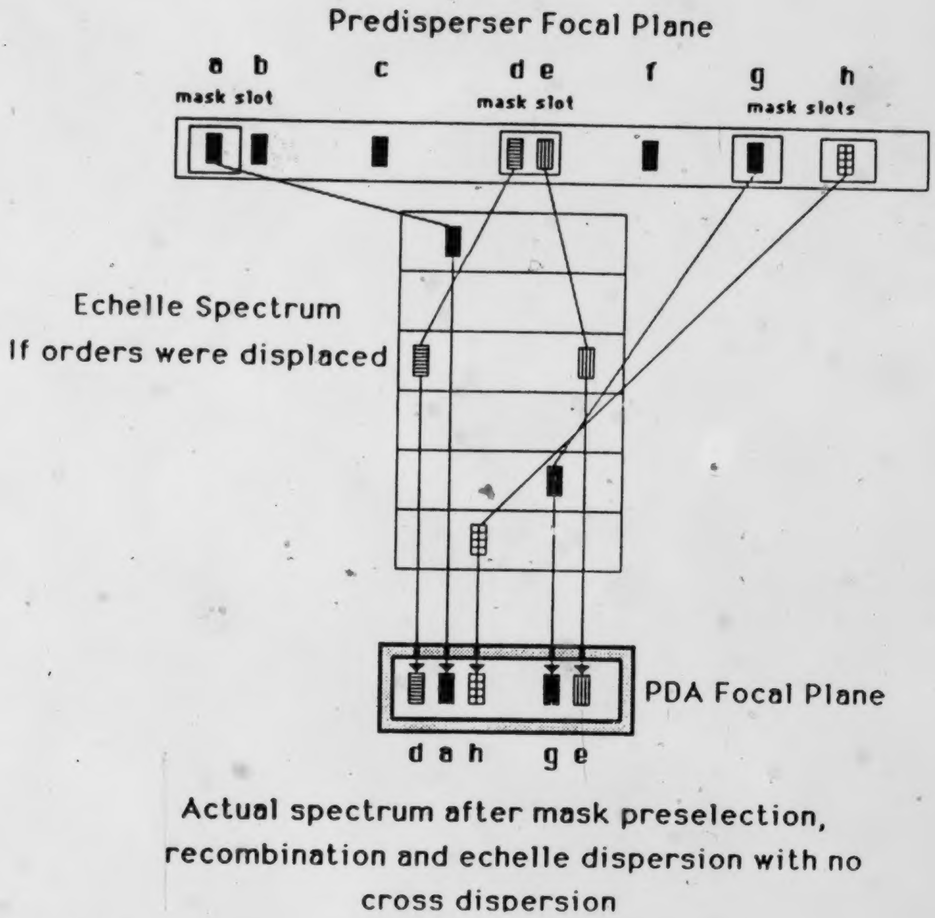
Predisperser Focal Plane
a b
mask slot
c
d e
mask slot
f
g h
mask slots
Echelle Spectrum
If orders were displaced
PDA Focal Plane
d a h g e
Actual spectrum after mask preselection,
recombination and echelle dispersion with no
cross dispersion

Figure D-3. Schematic diagram of instrument spectral operation.

In this example then, lines a, d, e, g and h and spectral background adjacent to these lines, are all transmitted through to the recombination optics and the echelle-PDA spectrometer. The remaining lines (b, d and f) and spectral background get blocked off by the mask. The mask can be thought of as functionally equivalent to an optical filter that lets only the spectral information of interest through.

Although no cross dispersion is involved in this echelle spectrometer it is useful, at this stage, to think of the echelle spectrometer as if the orders were displaced. This is schematically represented in the central part of Figure D-3, with 200 nm orders at the top and 400 nm orders at the bottom. Note that even though a mask slot may pass more than one spectral line, as depicted for the middle lines (d and e), the lines will often be well resolved by the echelle spectrometer.

Since there is no cross dispersion, the orders are not displaced and the 'spectrum' as measured by the PDA in the echelle spectrometer focal plane appears as shown at the bottom of Figure D-3. Note that the PDA spectral axis cannot easily be defined in terms of wavelength because the lines are scrambled with respect to their true wavelength order. As will be seen in the next section, the PDA axis is best thought of as an element axis with certain elements falling at certain pixels, not unlike channels of a direct reading spectrometer.

The direct reader analogy can be carried even further: line selection is provided by the mask and well resolved element channels are formed on the PDA. But more importantly, this direct reader is easily reprogrammable. A new set of lines and or elements can be put in the spectrometer simply by replacing the mask, an operation that literally takes only seconds.

B.1 Single Element Spectra

The basic spectral characteristics of this spectrometer can be illustrated with a series of mask-out/mask-in measurements for single element solutions. In the upper part of Figure D-4 a single element spectrum is shown for Cu (1000 ppm) with no mask present in the predisperser focal plane. With the 10 element mask in place and all slots open a single Cu line is selected. As discussed above, the assignment of a wavelength axis to the PDA axis is not realistic: it is best to think of the selected Cu line as a direct reader channel for Cu centered at diode #385, rather than a wavelength of 324.7 nm as selected by the mask (see Table D-2).

The analogous spectra measured for Fe (1000 ppm) are shown in Figure D-5. The 'spectrum' for Fe with the mask removed is a mess of spectral order overlaps. However, with the mask in place, a very simple Fe 'spectrum' or pattern is measured. Ideally, the function of the mask is to select a

Cu - No Mask

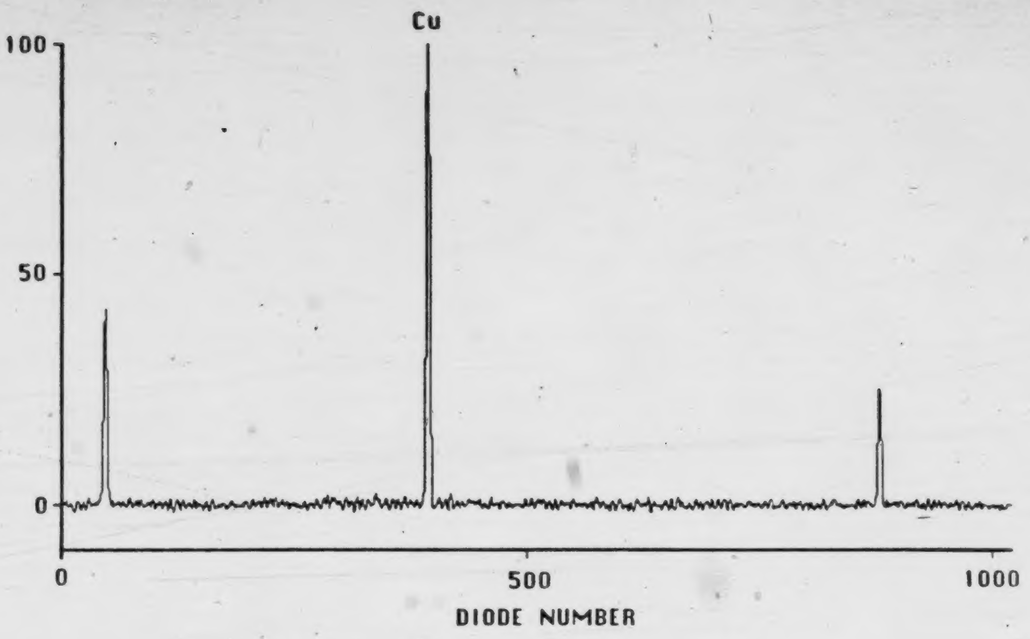

Cu - Mask in, no slot(s) covered

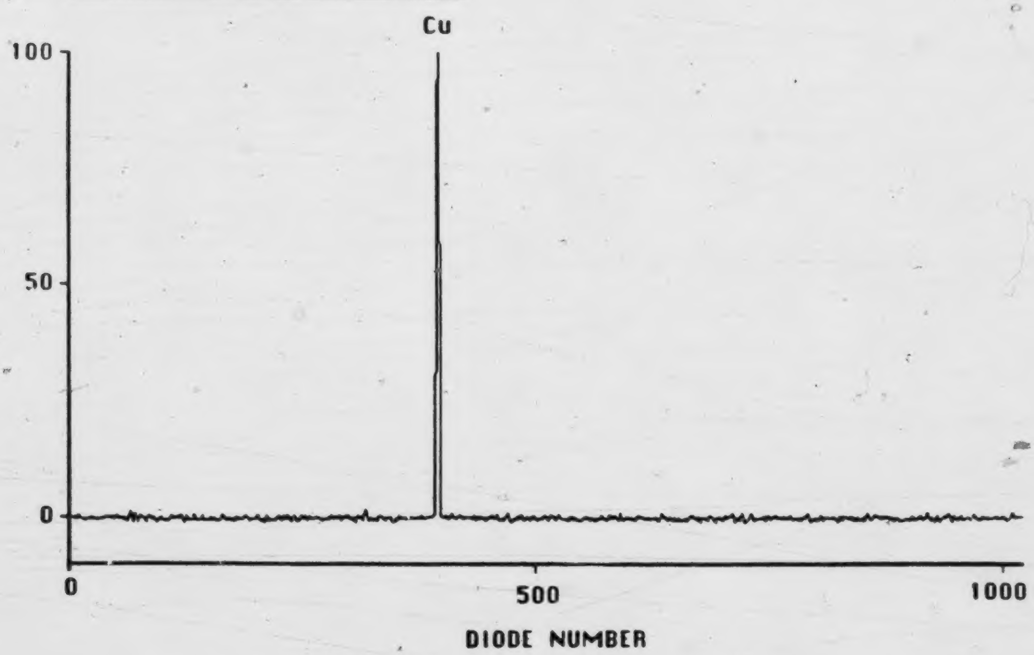

Figure D-4. Mask-out/mask-in spectra for Cu.

Fe - No Mask

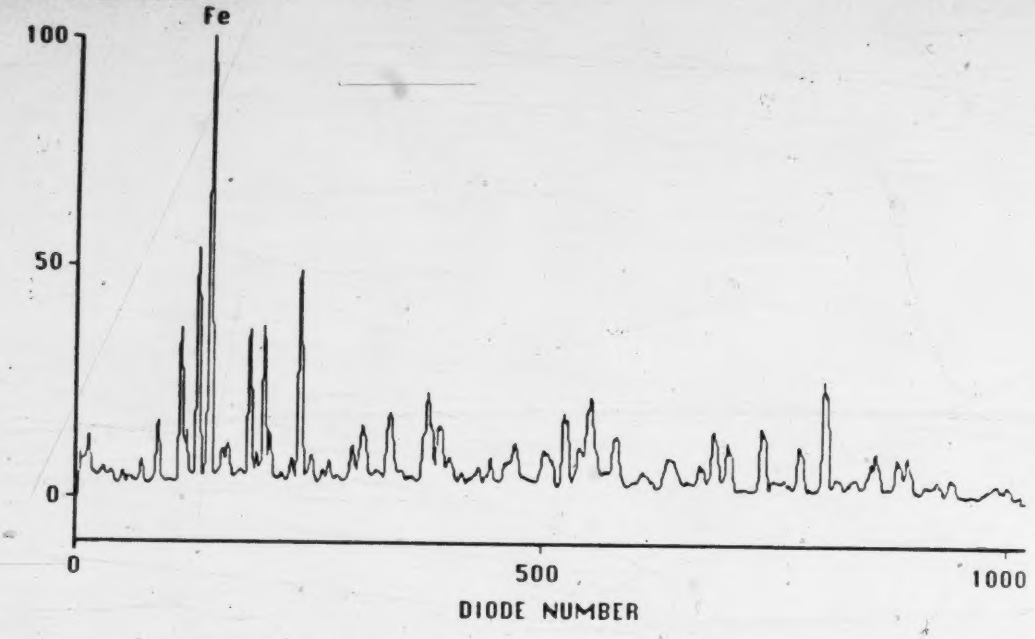

Fe - Mask in, no slot(s) covered

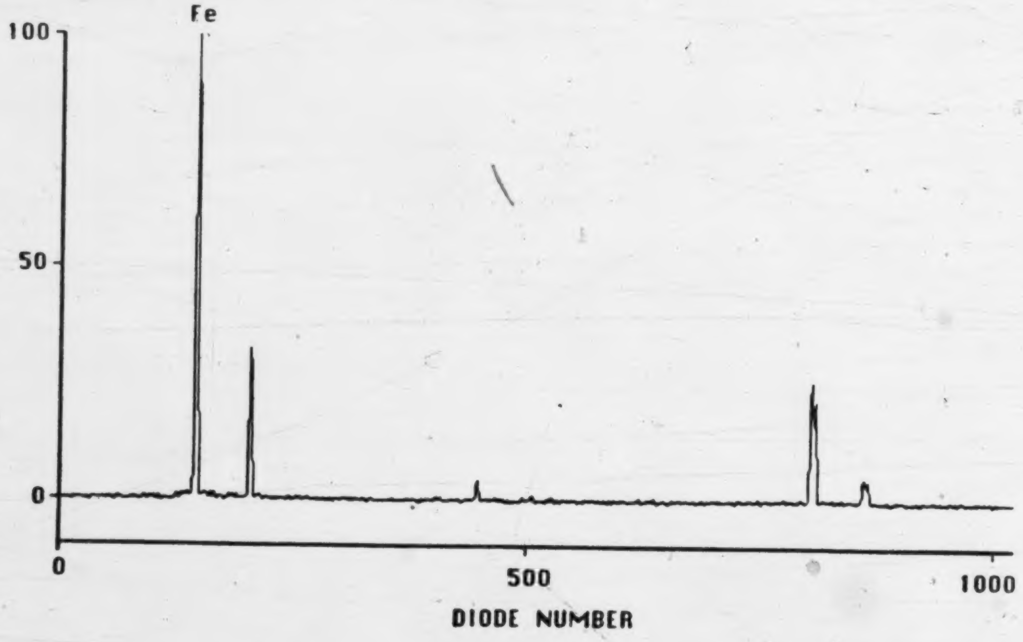

Figure D-5. Mask-out/mask-in spectra for Fe.

single line: this time, however, a single line of the element is not selected. These extra lines will be designated as leakage. There are two sources of leakage. The extra lines could be Fe lines that, in the predisperser focal plane, fall at slot positions designated for the other 9 elements; or they could be other Fe lines passing through the designated Fe slot, as it does have a bandpass of about 5Å; or both. Similarly, the mask-out/mask-in spectra for Ti (1000 ppm) in Figure D-6 indicate that the mask is quite effective in selecting the designated Ti line but, once again, some leakage also occurs.

The source of the extra lines can be established by carrying out two additional measurements. This is illustrated for Mo (1000 ppm) in Figure D-7. Mask-out and mask-in spectra, as before, are shown on the left side of the figure. In addition, a mask-in spectrum for which all the other element slots were covered except the Mo slot is shown along with a spectrum for which the Mo slot was covered and all others were left open. These two spectra are shown on the right side of Figure D-7. Note that in order to establish the extent of leakage, the integration time utilized to acquire the latter Mo spectrum was 10 times that used for the acquisition of the former Mo spectrum. These two spectra show that the designated Mo slot uniquely selects a single line and that the leakage is from Mo lines

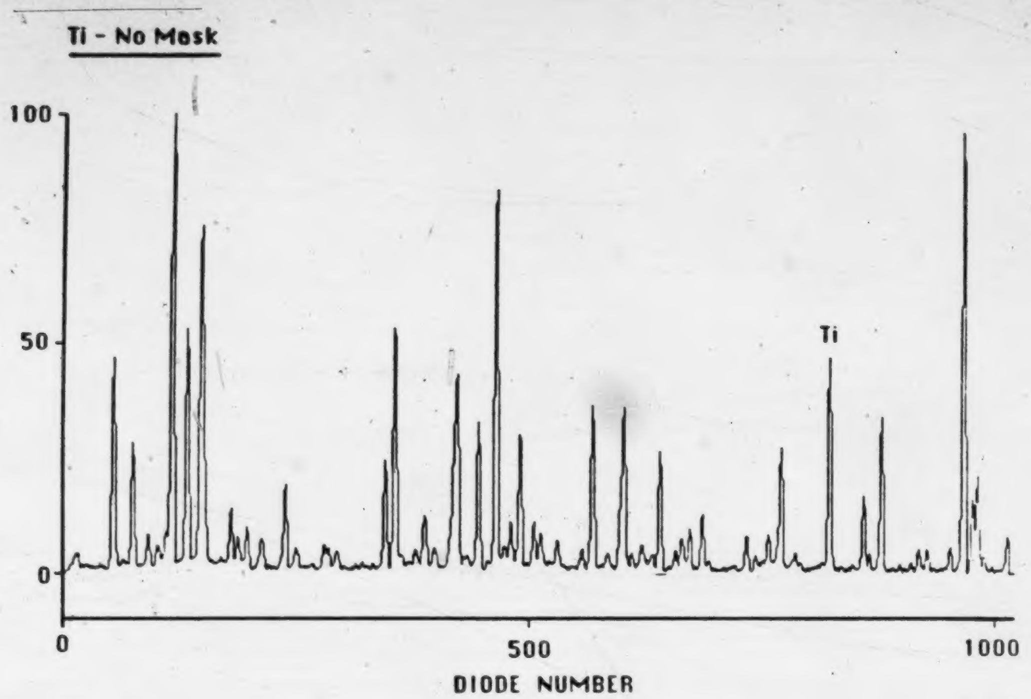

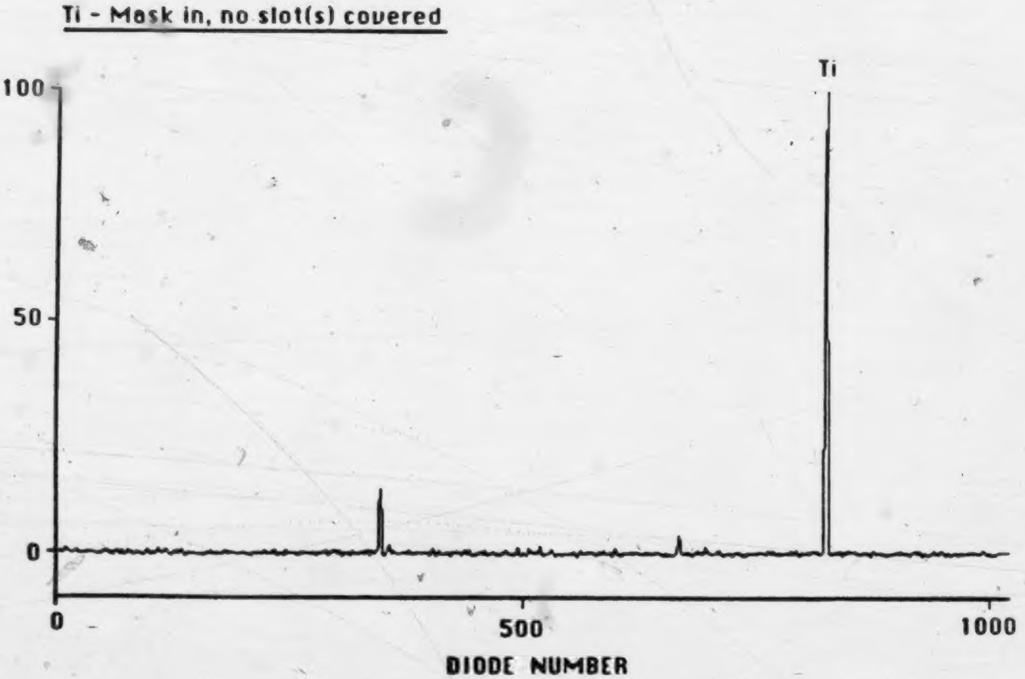

Figure D-6. Mask-out/mask-in spectra for Ti.

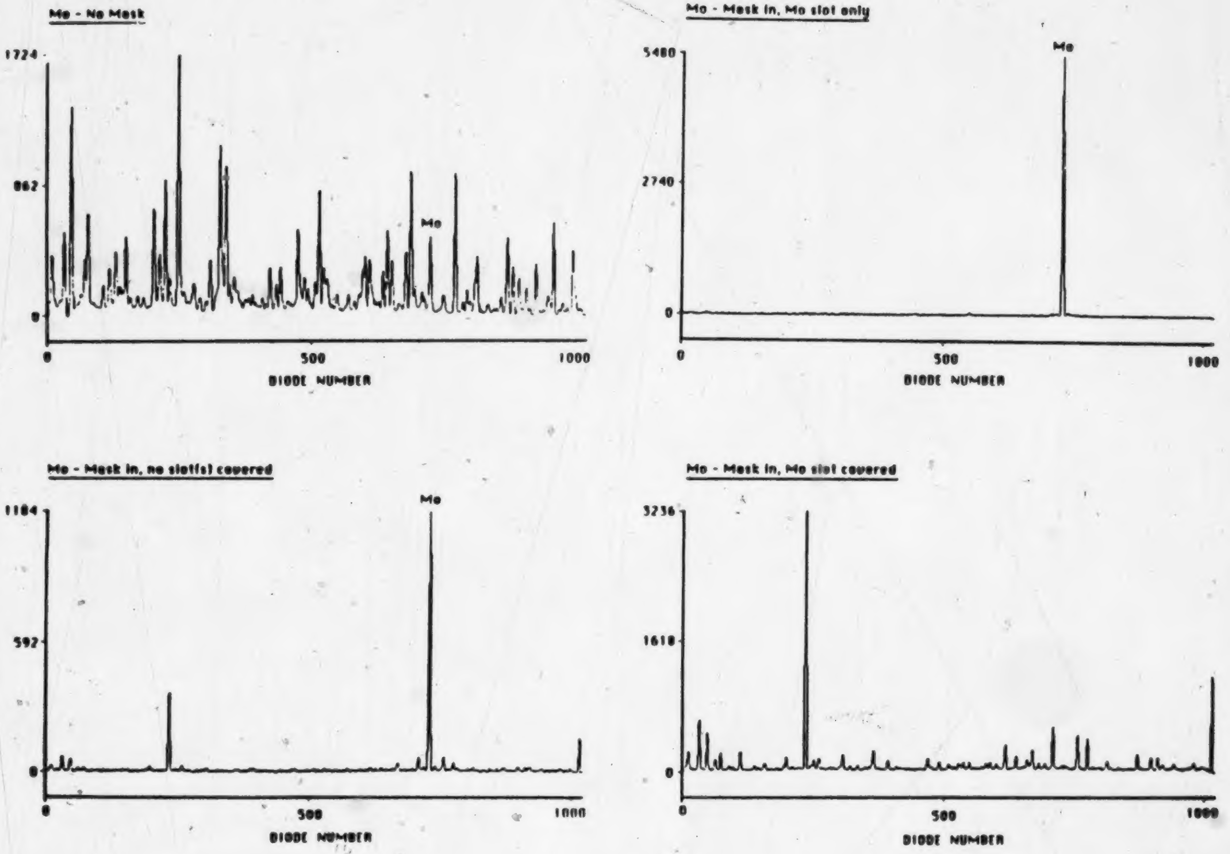

Figure D-7. Spectra for Mo indicating source of leakage lines (see text for discussion).

which have passed through the slots designated for the other 9 elements. An analogous set of spectra are shown in Figure D-8 for Si. Even though the integration time utilized for the acquisition of the spectrum with the Si slot covered is about 7 times that used for the spectrum with the Si slot open, only one very weak line is observed. In this case, then, it can be concluded that the extra lines observed are all the result of leakage through the Si slot. The lines resulting from leakage do not necessarily result in spectral overlap problems unless they fall exactly on another element diode array channel. This point will be specifically illustrated later.

B.2 Multielement Spectra

A multielement no mask spectrum is shown in the upper part of Figure D-9. The 9 element solution contained 10 ppm of Al, Cr, Fe, Mo, Ni and Si and 1 ppm of Cu, Mg and Ti. This measured 'spectrum' is clearly a mess. However, a spectrum of the same sample with the element mask in place (lower part of Figure D-9) illustrates the measurement power of the spectrometer. A unique channel (diode array location) can be established for each element. The instrument has become a 9 element direct reader. The line selection capability of the mask is also illustrated in Figure D-10. In this figure, mask-out single element spectra for 8 of the elements (no room to show Mg) are shown

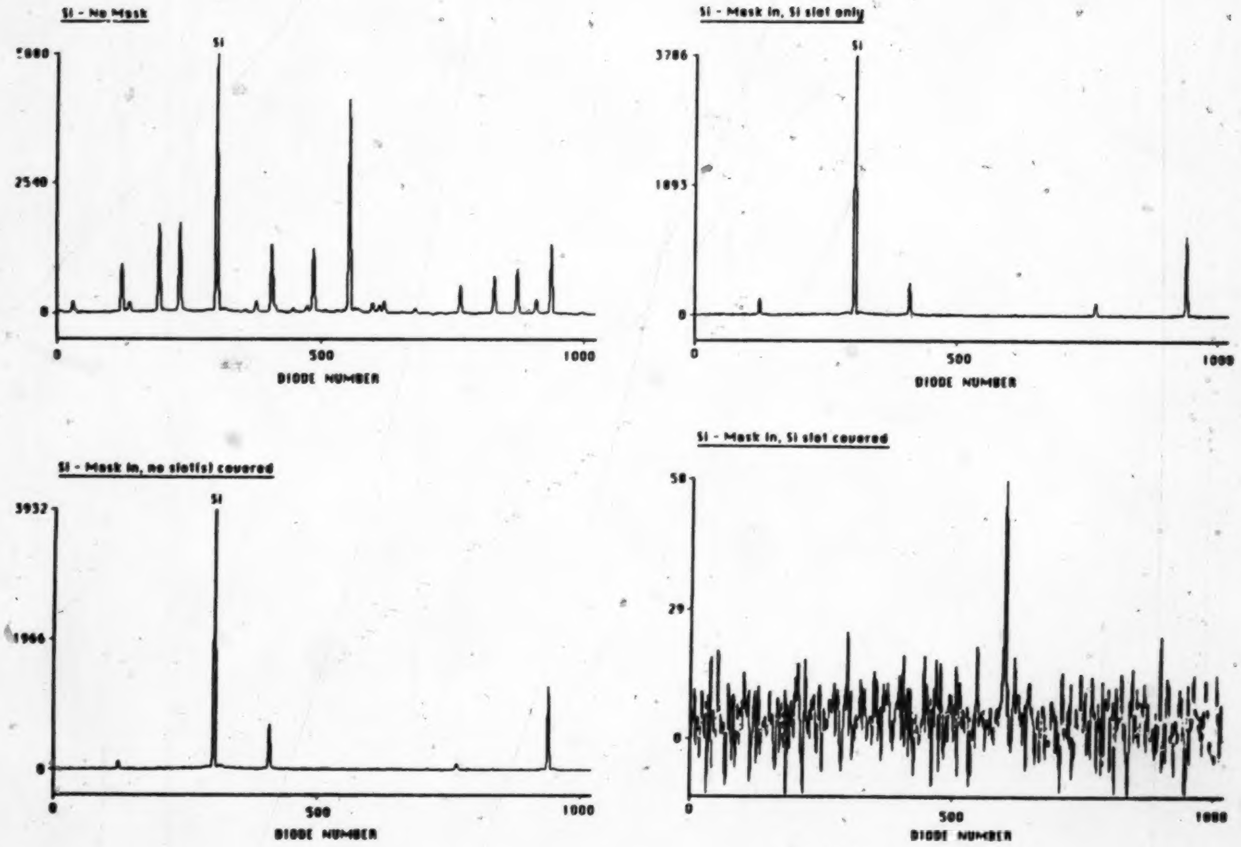

Figure D-8. Spectra for Si indicating source of leakage lines (see text for discussion).

Multielement - No Mask

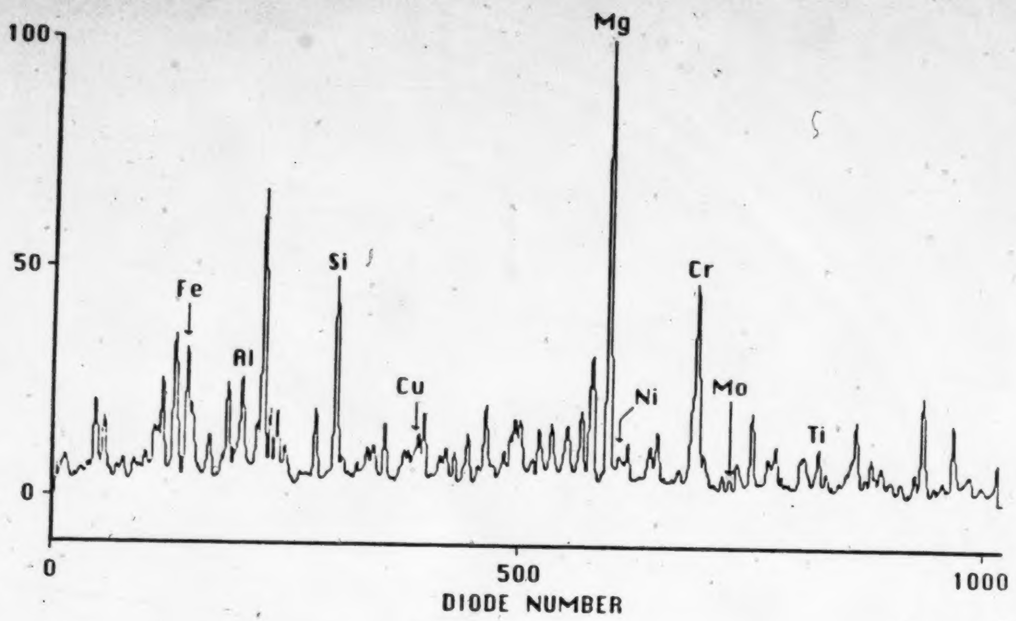

Multielement - Mask in

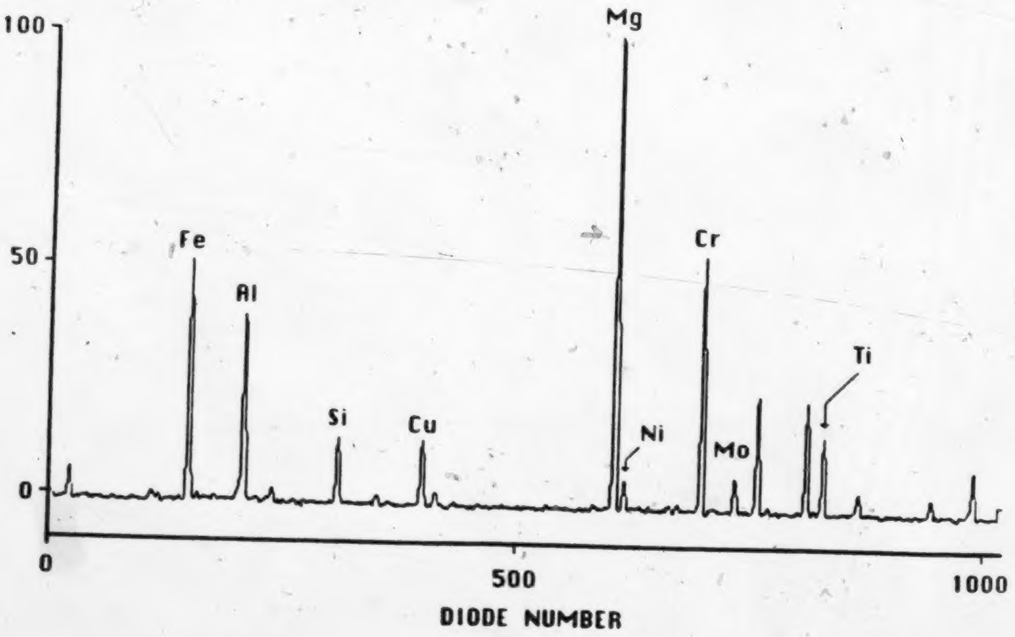

Figure D-9. Mask-out/mask-in spectra for multielement solution (10 ppm Al, Cr, Fe, Mo, Ni, Si; 1 ppm Cu, Mg, Ti).

surrounding the mask-in 9 component multielement spectrum. Despite the complexity of the mask-out ICP spectra, Figure D-10 demonstrates the ability of the mask to discriminate against any unwanted spectral information, while selecting all relevant spectral lines. A useful display format that emphasizes the element channel aspect of the PDA axis is to convert the element lines to bars, each with a width of 7 pixels. This is shown in Figure D-11. This format is also useful when assessing spectral interferences and will be used in the next section.

B.3 Spectral Interference Considerations

As discussed earlier in conjunction with the single element spectral characteristics of this instrument, the mask does not always select a single line for each designated element. For example, the mask-in single element spectra for Fe (Figure D-5), Ti (Figure D-6), Mo (Figure D-7) and Si (Figure D-8) all have more than one line. These extra lines, earlier designated as leakage, could cause spectral interference problems if they fall on a diode location corresponding to a designated analyte channel. For example, if one of the extra Si lines falls on diode #385 and hence interferes with the Cu channel, an interelement correction factor could be established for the determination of Cu in the presence of Si. Thus, interelement background correction procedures could be implemented as has been done

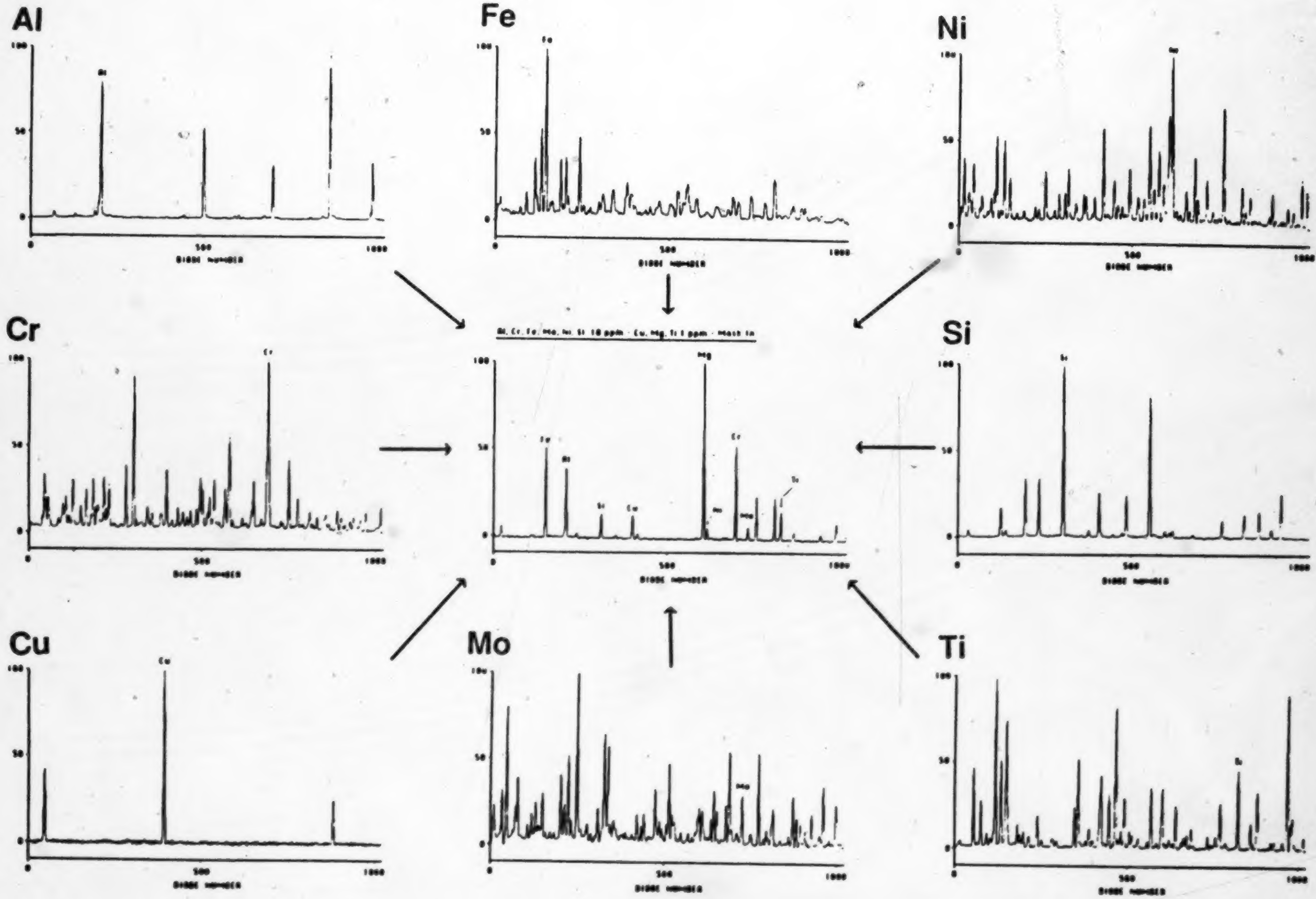

Figure D-10. Mask-out single element spectra composite with mask-in multielement spectrum.

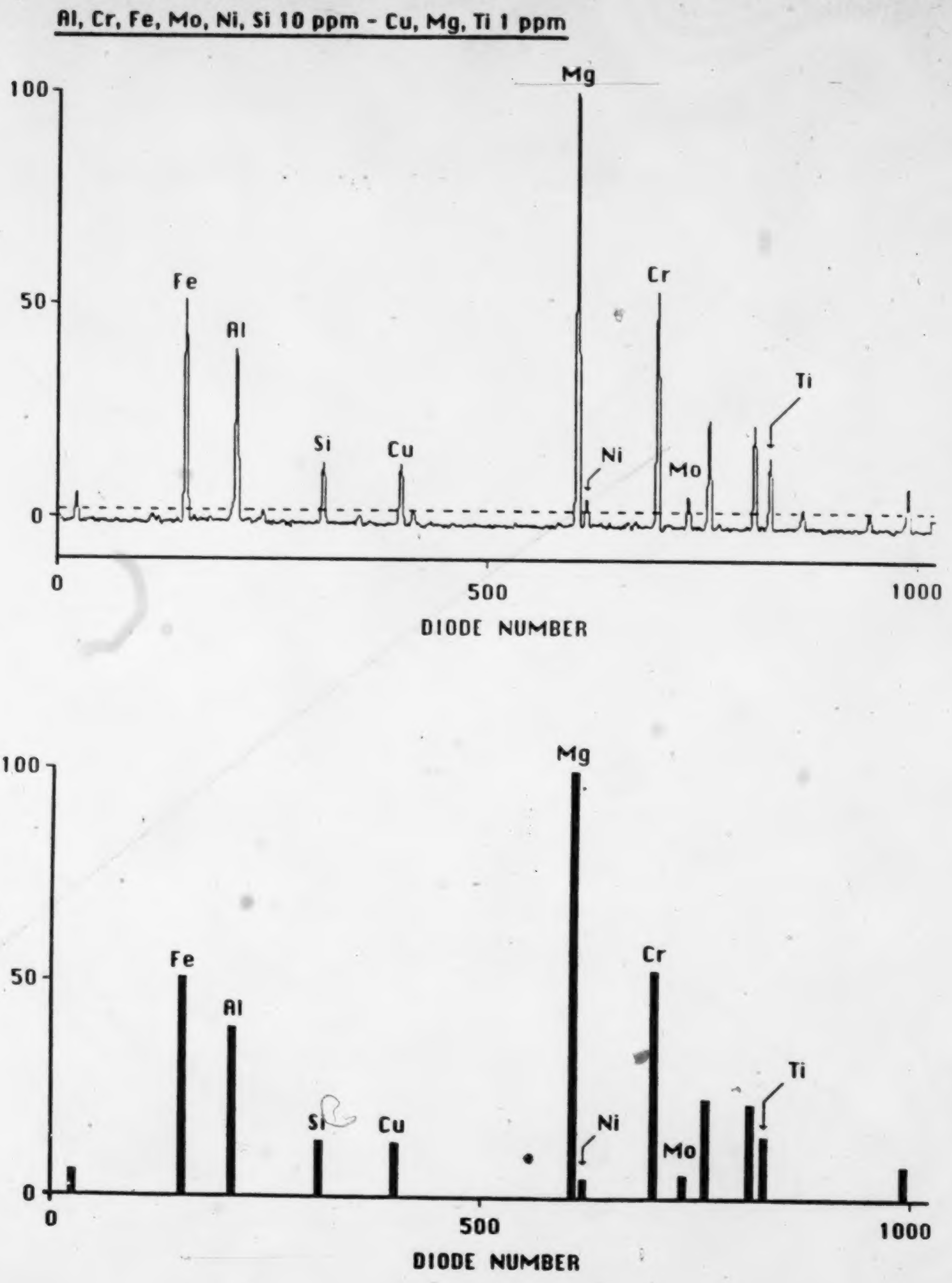

Figure D-11. Multielement bar graph spectrum.

now for several years with conventional direct reading spectrometers.

One also has to recognize that elements present in a sample other than those for which the mask is designed can be a source of spectral interference. This is illustrated in Figures D-12 and D-13. Mask-out and mask-in spectra are shown for V in Figure D-12. While there is no designated slot on this mask for V, spectral lines from V do appear in the final spectrum as some V lines fall on mask slots of the other elements. However, as can be seen by superimposition of analyte channel and V bar graph spectra (Figure D-13) only one of the V lines actually coincides with an element channel on the diode array axis. The Cr channel is subject to a V spectral interference and another line comes close to the Ti channel. Thus, if these two elements were to be determined in a sample matrix containing V as a major component, a new mask would have to be cut that would select different Cr and Ti lines and hence reposition these channels on the PDA axis or background correction factors for these channels would have to be applied.

A second example is shown for Co in Figures D-14 and D-15 and in this case the problem is more serious. A sample matrix containing Co as a major element will result in spectral interference problems at the Fe, Al and Mo channels. Again, appropriate mask design or appropriate background correction procedures could eliminate this specific

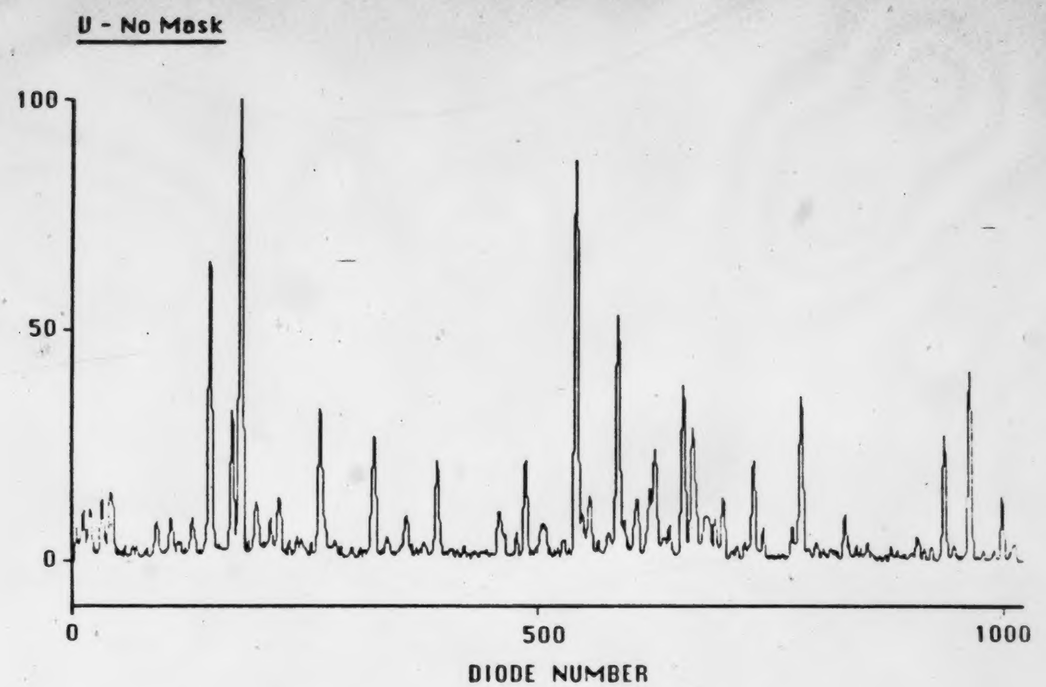

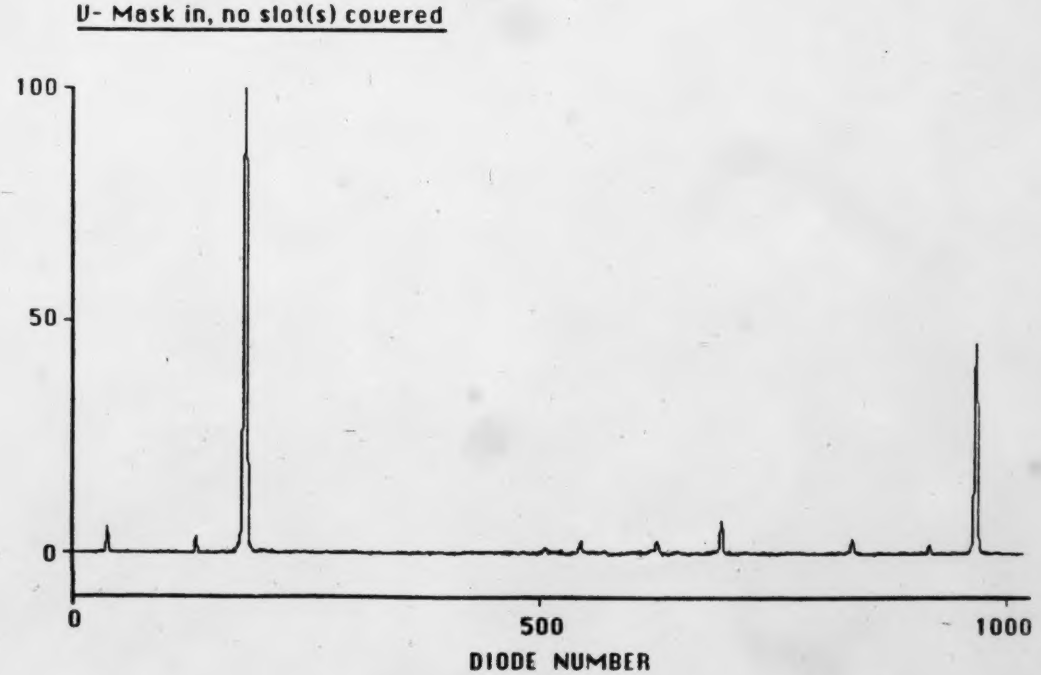

Figure D-12. Mask-out/mask-in spectra for V.

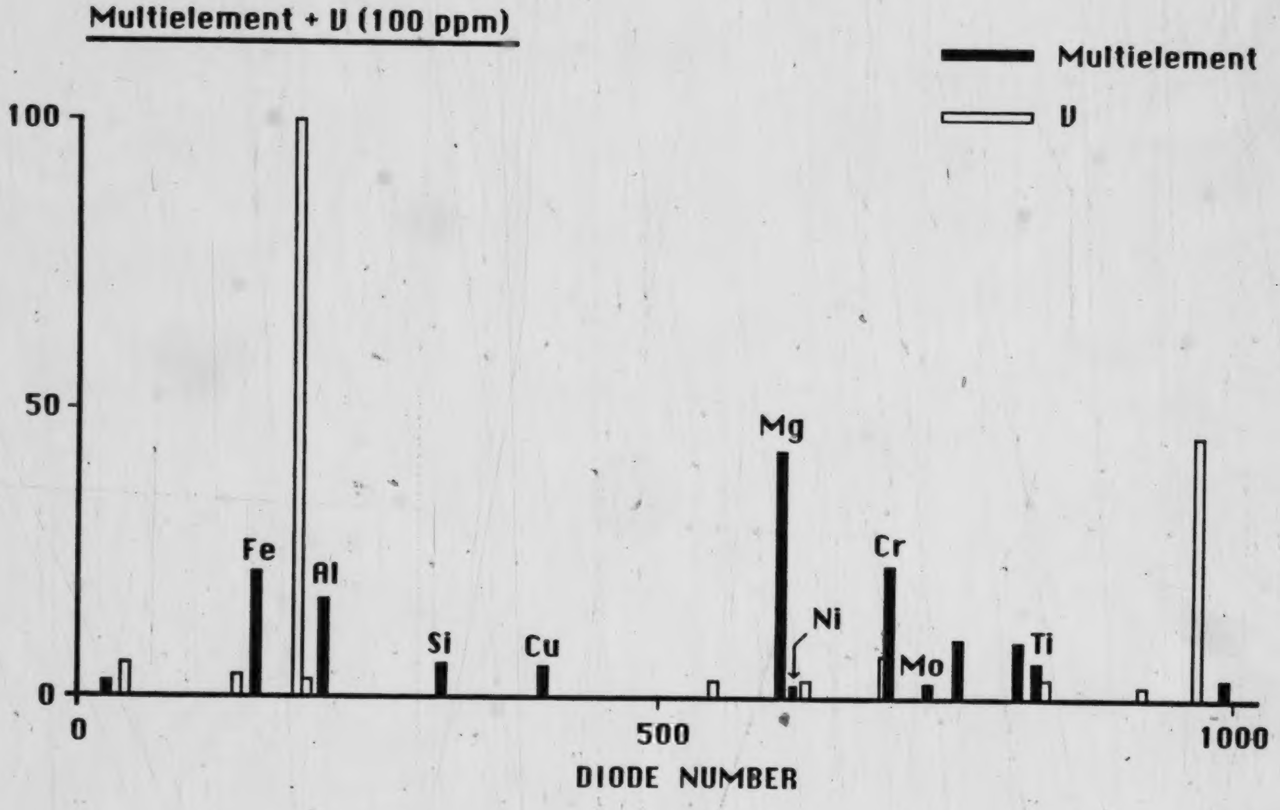

Figure D-13. Superimposition of V and multielement bar graph spectra.

Co - No Mask

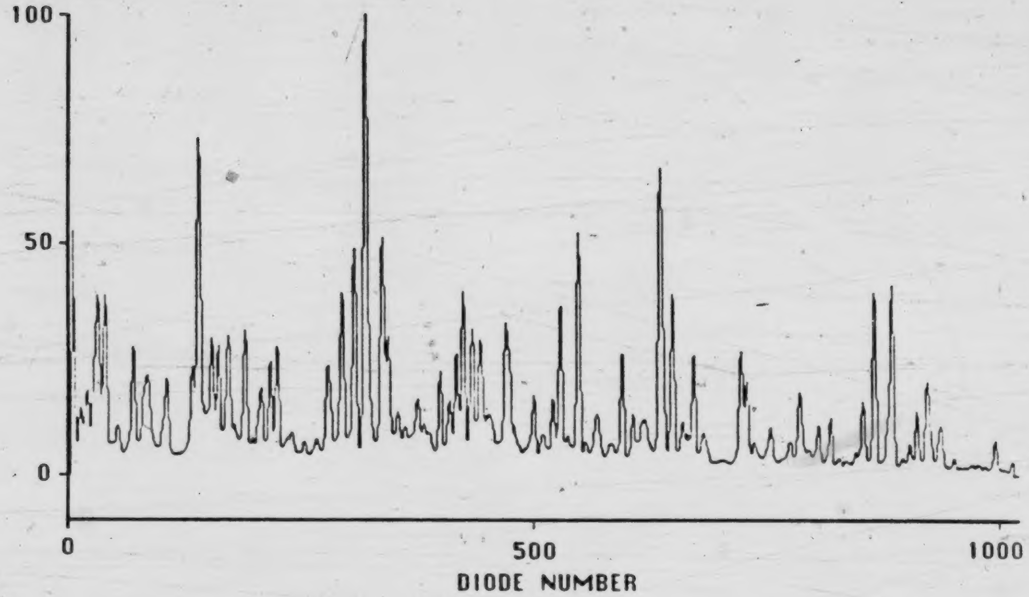

Co - Mask in, no slot(s) covered

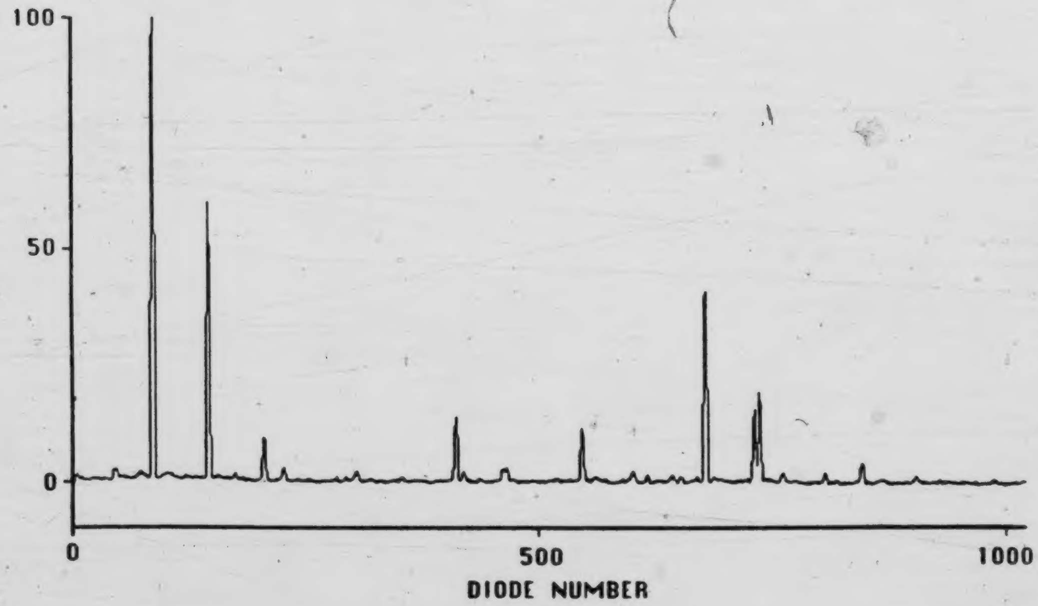

Figure D-14. Mask-out/mask-in spectra for Co.

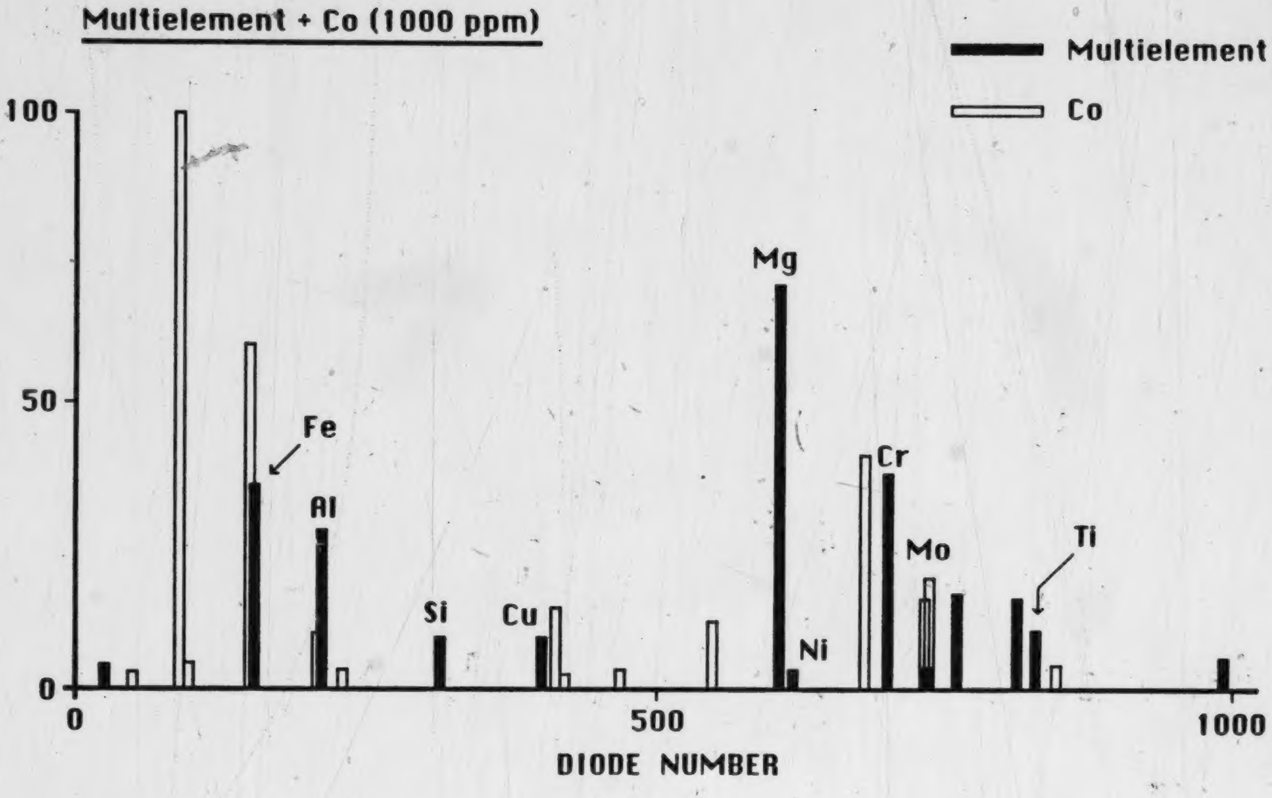

Figure D-15. Superimposition of Co and multielement bar graph spectra.

problem. Of the 12 elements tested for which there are no slots available on the mask, a mask-in spectrum for Ba, Be, Ca, Cd and P was not observed, possibly due to the simplicity of their respective mask-out spectra. Although some lines were observed for Pb and Zn, they did not pose spectral interference problems. However, as the complexity of the mask-out spectra increases, the possibility for spectral interference similarly increases. Therefore, careful assessment of spectral overlaps is required with this instrument, not unlike that required with any direct reading spectrometer.

B.4 Quantitative Performance

The quantitative performance of the instrument was only briefly evaluated. Some detection limits (2σ) established were 0.1 ppb for Mg, 0.2 ppb for Ca, 14 ppb for Cd and 35 ppb for Zn. These are similar to the detection limits measured by Salin and Horlick [10] for another ICP-PDA spectrometer. In general, PDA detection limits will not match PMT detection limits in the far-UV, i.e. near 200 nm. In a detailed analysis McGeorge and Salin [11,12] indicated that in the region 200 to 450 nm, PDA systems can be designed that will match PMT-ICP detection limits above about 230 nm, and that below this wavelength detection limits degrade until at 200 nm they are about a factor of 10 inferior to PMT based measurements. This seems reasonable as on a direct reading spectrometer in our laboratory (ARL 34000), the detection limits for Cd and Zn are 2-4 ppb, about an order of magnitude better than those measured above for the PDA based system.

C. Conclusions

This new spectrometer provides an interesting alternative for the utilization of linear PDA's for atomic emission spectrochemical measurements. Functionally, the spectrometer is a field re-programmable direct reader. As such, it is a uniquely versatile spectrometer for simultaneous multielement analysis applications where a variety of sample matrices and types must be analyzed. Such versatility is not present in current direct reading spectrometers where focal plane line selection is often customized with a single sample type and matrix in mind and cannot easily be altered in the field. Slew scanning spectrometer based instruments are versatile but lack simultaneous multielement measurement capability.

In addition, interesting measurement scenarios can be thought of for an instrument of this type. The easily interchangeable masks lead to the concept of a spectrochemical answer machine. A bank of masks could be developed for a range of analytical problems. In conjunction with the right software, simply dropping in the appropriate mask will provide an instrument customized to answer a particular spectrochemical problem, i.e. What alloy is it? Even go/nogo decisions could be automated based on the presence or absence of a certain group of elements at a particular set of relative concentrations. Another measurement mode could be qualitative analysis. Mask-out spectral patterns on the PDA, while essentially uninterpretable in the normal sense, are nevertheless, characteristic patterns. Correlation techniques [13] and regression analysis [14] could be used to provide automatic pattern recognition for certain analyses.

D. Recent Developments

The following summarizes the developments which have occured since this paper was first written. A version of the SPS-10 research prototype utilized in this work has recently become commercially available (Leco Instruments Ltd., 5151 Everest Drive, Mississauga, Ontario, L4W 2R2). In addition, the optical characteristics of the "Plasmarray" spectrometer (formerly the SPS-10) has been described in detail by Levy et al. [15].

REFERENCES

1. G. Horlick, Appl. Spectrosc., **30**, 113 (1976)

2. N. Furuta, C.W. McLeod, H. Haraguchi and K. Fuwa, Bull. Chem. Soc. Japan, **52**, 2913 (1979)

3. R.G. Evans and G. Horlick, Pittsburgh Conference, Atlantic City, 1982; Paper No. 441

4. R.G. Evans, Ph.D. Thesis, University of Alberta, 1983

5. K.W. Busch and B. Malloy, Anal. Chem., **51**, 670 (1979)

6. K.W. Busch and L.D. Benton, FACSS, Philadelphia 1985; Paper No. 73

7. H.L. Felkel, Jr. and H.L. Pardue, *"Simultaneous Multielement Determinations by Atomic Absorption and Atomic Emission with a Computerized Echelle Spectrometer/Imaging Detector System"* in *'Multichannel Image Detectors'*, Yair Talmi, Editor ACS Symposium Series 102, ACS, Washington, DC, 1979

8. M.B. Denton and G.R. Sims, *"Multielement Emission Spectroscopy Using a Charge Injection Device"* in *'Multichannel Image Detectors'*, Vol. 2, Yair Talmi, Editor, ACS Symposium Series No. 236, ACS, Washington, DC, 1983

9. G.M. Levy, A. Quaglia and R. Lazure, Pittsburgh Conference, New Orleans, 1985; Paper No. 749

10. E.D. Salin and G. Horlick, Anal. Chem., **52**, 1578 (1980)

11. S.W. McGeorge and E.D. Salin, Spectrochim. Acta, **40B**, 435 (1985)

12. S.W. McGeorge and E.D. Salin, Spectrochim. Acta, **40B**, 447 (1985)

13. R.C.L. Ng and G. Horlick, Spectrochim. Acta, **36B**, 543 (1981)

14. D. Wirsz and M.W. Blades, Pittsburgh Conference, New Orleans, 1985; Paper No. 1230

15. G.M. Levy, A. Quaglia, R.E. Lazure and S.W. McGeorge, Spectrochim. Acta, **42B**, 341 (1987)

APPENDIX E

DEVELOPMENT SYSTEMS AND PROGRAMMING ENVIRONMENTS UTILIZED

Table E-1. Development systems and programming environments utilized.

Chapter	**System**	**Language**
Chapter 2	IBM PC	BASICA
Chapter 3	IBM PC Apple Macintosh	BASICA BASIC, TML Pascal
Chapter 4	IBM PC Apple Macintosh	BASICA BASIC, TML Pascal
Chapter 5	Apple Macintosh	Modula-2; MacPascal, TML Pascal, 68000 Assembly
Chapter 6	Apple II+ Apple Macintosh	Applesoft BASIC LightSpeed Pascal, C
Chapter 7	Apple II+ Apple Macintosh	Applesoft BASIC LightSpeed Pascal
Appendix A	Rockwell AIM-65	6502 Assembly
Appendix D	PRA, 6800 CPU IBM PC Apple Macintosh	FORTRAN BASICA Microsoft BASIC, MacPascal